Alexander G. Volkov (Editor)

Plant Electrophysiology

Theory and Methods

Springer

Plant Electrophysiology

Alexander G. Volkov (Ed.)

Plant Electrophysiology

Theory and Methods

With 142 Figures, 26 in Color, and 4 Tables

Springer

Prof. Dr. Alexander G. Volkov
Department of Chemistry
Oakwood College
7000 Adventist Boulevard
Huntsville, AL 35896, USA
e-mail: agvolkov@yahoo.com

Library of Congress Control Number: 2006925966

ISBN-10 3-540-32717-7 Springer Berlin Heidelberg New York
ISBN-13 978-3-540-32717-2 Springer Berlin Heidelberg New York

Springer is a part of Springer Science+Business Media

springer.com

Printed in The Netherlands

Cover design: Design & Production GmbH, Heidelberg, Germany
Typesetting and production: SPi

Printed on acid-free paper SPIN 11392699 149/3100/SPi 5 4 3 2 1 0

Preface

Plants continually gather information about their environment. Environmental changes elicit various biological responses. The cells, tissues, and organs of plants possess the ability to become excited under the influence of environmental factors. Plants synchronize their normal biological functions with their responses to the environment. The synchronization of internal functions, based on external events, is linked with the phenomenon of excitability in plant cells. The conduction of bioelectrochemical excitation is a fundamental property of living organisms.

The conduction of bioelectrochemical excitation is a rapid method of long distance signal transmission between plant tissues and organs. Plants promptly respond to changes in luminous intensity, osmotic pressure, temperature, cutting, mechanical stimulation, water availability, wounding, and chemical compounds such as herbicides, plant growth stimulants, salts, and water potential. Once initiated, electrical impulses can propagate to adjacent excitable cells. The bioelectrochemical system in plants not only regulates stress responses, but photosynthetic processes as well. The generation of electrical gradients is a fundamental aspect of signal transduction.

This book consists of a historical introduction to plant electrophysiology, and two parts. The first one deals with the methods in plant electrophysiology. Seven chapters present methods of measuring the membrane potentials, ion fluxes, transmembrane ion gradients, ion-selective microelectrode measurements, patch-clamp technique, magnetic measurements, new solid state microsensors and electrochemical sensors. The second part deals with experimental results and theoretical interpretation. All chapters are comprehensively referenced throughout.

Green plants are a unique canvas for studying signal transduction. Plant electrophysiology is the foundation for discovering and improving biosensors for monitoring the environment; detecting effects of pollutants, pesticides, and defoliants; monitoring climate changes; plant-insect interactions; agriculture; and directing and fast controlling of conditions influencing the harvest.

I am grateful to my colleagues for their valuable contribution to this book. We thank the authors for the time they spent on this project and for teaching us about their work. I would like to thank our Acquisition Editor, Dr. Christina Eckey, and our Production Editor, Ursula Gramm, for their friendly and courteous assistance.

Alexander George Volkov

Contents

List of Contributors

Jolana T. P. Albrechtová
University of Freiburg, Institute of Biology II, Schänzlestr. 1, Freiburg, D-79104, Germany

Mary J. Beilby
Department of Biophysics, School of Physics, The University of New South Wales, Sydney 2052, Australia

Mary A. Bisson
Department of Biological Sciences, University at Buffalo, Buffalo, NY 14260, USA

Simone Bossi
Department of Plant Biology, Centre of Excellence CEBIOVEM, University of Turin, 25 Viale P.A. Mattioli, Turin 10125, Italy

Courtney Brown
Department of Chemistry, Oakwood College, 7000 Adventist Blvd., Huntsville, AL 35896, USA

Sofia Cordeiro
Centro de Biologia do Desenvolvimento, Instituto Gulbenkian de Ciencia, PT-2780-156 Oeiras, Portugal

Tracey A. Cuin
School of Agricultural Science, University of Tasmania, Private Bag 54, Hobart, Tas 7001, Australia

Eric Davies
North Carolina State University, Department of Botany, 1231 Gardner Hall, Raleigh, NC 27695-7612, USA

Vadim Demidchik
Department of Plant Sciences, University of Cambridge, Downing Street, CB23EA, Cambridge, UK

José Feijó
Universidade de Lisboa, Fac. Ciências, Dept. Biologia Vegetal, Campo Grande C2, 1749-016 Lisboa, Portugal and Centro de Biologia do Desenvolvimento, Instituto Gulbenkian Ciência, PT-2780-156 Oeiras, Portugal

Jörg Fromm
Wood Biology, Technical University of Munich, Winzererstrasse 45, 80797 Munich, Germany

Andrew Goldsworthy
6 Sandall Road, London W5 1JD, UK

Vojko Jazbinsek
Department of Physics, IMFM, University of Ljubljana, Jadranska 19, 1000 Ljubljana, Slovenia

Joseph G. Kunkel
Department of Biology, University of Massachusetts Amherst, MA 01003-5810, USA

Lars Lehner
University of Freiburg, Institute of Biology II, Schänzlestr. 1, Freiburg, D-79104, Germany

Roger R. Lew
Department of Biology, York University, Toronto, Ontario M3J 1P3, Canada

Massimo Maffei
Department of Plant Biology, Centre of Excellence CEBIOVEM, University of Turin, 25 Viale P.A. Mattioli, Turin 10125, Italy

Stefano Mancuso
Department of Horticulture, University of Firenze, Viale delle Idee 30, 50019 Sesto Fiorentino, Italy

Anna Maria Marras
Department of Pharmaceutical Science, Polo Scientifico, Universita di Firence, via Ugo Schiff 6, 50019 Sesto Fiorentino, Italy

Mark A. Messerli
BioCurrents Research Center, Program in Molecular Physiology, Marine Biological Laboratory, 7 MBL Street, Woods Hole, MA 02543, USA

Anthony J. Miller
CPI Division, Rothamsted Research, Harpenden, Hertfordshire, AL5 2JQ, UK

Johanes Normann
University of Freiburg, Institute of Biology II, Schänzlestr. 1, Freiburg, D-79104, Germany

Kenneth R. Robinson
Department of Biological Sciences, Purdue University, West Lafayette, IN 47907, USA

Sergey Shabala
School of Agricultural Science, University of Tasmania, Private Bag 54, Hobart, Tas 7001, Australia

Virginia A. Shepherd
Department of Biological Sciences, University at Buffalo, Buffalo, NY 14260, USA

Teruo Shimmen
Department of Life Science, Graduate School of Science, Himeji Institute of Technology Harima Science Park City, Hyogo, 658-1297 Japan

Alan M. Shipley
Applicable Electronics Inc., Forestdale, MA 02644, USA

Peter J. S. Smith
Director, BioCurrents Research Center, Program in Molecular Physiology, Marine Biological Laboratory, 7 MBL Street, Woods Hole, MA 02543, USA

Anatoly Sokolik
Laboratory of Plant Cell Physiology, Biological Faculty, Belarusian State University, 4 Skaryna Avenue, 220050, Minsk, Belarus

Roger Spanswick
Department of Biological and Environmental Engineering, Cornell University, 316 Riley-Robb Hall, Ithaca, NY 14853-5701, USA

Rainer Stahlberg
University of Washington, POB 355325, Seattle WA 98195, USA

Bratislav Stanković
Brinks Hofer Gilson & Lione, 455 N. Cityfront Plaza Drive, Chicago, Illinois 60611, USA

Tsutomu Takamura
Department of Applied Chemistry, Harbin Institute of Technology, Harbin, China; Permanent address: 3-31-16, Azamino, Aobaku, Yokohama 225-0011, Japan

Gerhard Thiel
Institute of Botany, Plant Biophysics, Darmstadt University of Technology, D-64287, Darmstadt, Germany

Zvonko Trontelj
Department of Physics, IMFM, University of Ljubljana, Jadranska 19, 1000 Ljubljana, Slovenia

Justyna Veit
University of Freiburg, Institute of Biology II, Schänzlestr. 1, Freiburg, D-79104, Germany

Marco Vervliet-Scheebaum
University of Freiburg, Institute of Biology II, Schänzlestr. 1, Freiburg, D-79104, Germany

Alexander G. Volkov
Department of Chemistry, Oakwood College, 7000 Adventist Blvd., Huntsville, AL 35896, USA

Edgar Wagner
University of Freiburg, Institute of Biology II, Schänzlestr. 1, Freiburg, D-79104, Germany

Darren M. Wells
CPI Division, Rothamsted Research, Harpenden, Hertfordshire, AL5 2JQ, UK

Yue (Jeff) Xu
Department of Biology, University of Massachusetts at Amherst, MA 01003-5810, USA

Vladimir Yurin
Department of Physiology and Biochemistry of Plants, Biological Faculty, Belarusian State University, 4 Skaryna Avenue, 220050, Minsk, Belarus

PART I METHODS OF PLANT ELECTROPHYSIOLOGY

1 Historical Introduction to Plant Electrophysiology

RAINER STAHLBERG

It is hardly conceivable that reflex responses, memory and brain activity were once explained without consideration of the electrical activity in nerves and muscles. One must remember that electricity was only known then either as lightning or as the repelling/attracting charges that certain substances (such as amber, the Greek word for which is electron) accumulate when rubbed against wool or other textiles. Among the first people who thought about electrical phenomena and their possible biological consequences were de Sauvages (1706–1767), S. Hales (1677–1761), J.A. Nollet (1700–1770) and most importantly the prior Pierre Bertholon de St Lazare (1742–1791), who proposed to improve agriculture with a novel electroculture of crops (Bertholon 1783). This idea was repeatedly revived, e.g. by Lemstrom (1902), who attempted to demonstrate stimulating effects of natural electrostatic fields by growing plants outside and under Faraday cages. Effects of electrical fields on plants and animals continue to be a flourishing field of serious study and some controversy (see Chapter 11).

The birth of the larger field of experimental electrophysiology, however, is inseparably intertwined with the discovery of useable forms of electricity itself. The well-known common starting point was Luigi Galvani's discovery of "animal electricity" or his observing the contraction of isolated frog legs suspended between copper hooks and the iron grit of his balcony (Galvani 1791). Aside from stimulating dubious medical treatments such as "galvanism" and "mesmerism", this momentous event established electrophysiology as a major discipline of biology (Galvani's work was continued by the studies of A. Matteucci, E. Du Bois-Reymond and many others, see below) and stimulated A. Volta to develop the first practical batteries (the existence of batteries in ancient Egypt has been suggested, but cannot be reliably confirmed). These portable sources of electricity were called galvanic elements. Based on the different redox potentials of metals and non-metals, they provided reliable sources of various fixed voltages. This invention not only laid the foundations of electricity as a novel discipline of the physical sciences but also turned electricity into useable reality that would later serve as the basis for at least two industrial revolutions. Electrical currents, voltages, resistances and fields

University of Washington, POB 355325; Seattle, WA 98195, USA (e-mail: raista@u.washington.edu)

Plant Electrophysiology – Theory & Methods (ed. by Volkov)

could now be experimentally studied and applied to wires and wire networks as well as to animals and plants. The physical understanding of batteries itself also served well as a model to explain some fundamental phenomena of electrophysiology such as the stunning of prey by electrically hunting fishes from the new world (Du Bois-Reymond 1848). As reflected in this book, electrophysiology became to encompass not only the development of methods and instruments for the actual measurement of electrical signals but also the study of physiological effects deriving from electric and electromagnetic currents and fields.

It soon became clear that the role of the electric current in the contraction of frog legs was not to provide the energy for the movement, but to simulate a stimulus that existed naturally in the form of directionally transmitted electrical potentials. Frog legs had just been first and serendipitous current-recording devices to indicate the flow of electrical current in the moment they touched the iron grit of the balcony and their violent jerks were supposedly visible enough to scare Mrs. Galvani, the observant wife of the great scientist. In follow-up studies both Matteucci and Du Bois-Reymond then recognized that wounding of nerve strands generated the appearance of a large voltage difference (called wound potential) between the wounded (internal) and intact (external) site of nerves. This wound potential was the first, crude measurement of what later became known and understood as membrane or resting potential of nerve and other cells. Importantly, this potential could be measured and it was soon found that electrical or mechanical stimulation of the nerve reduced its size (in today's terms: these stimuli caused a depolarization). To describe the phenomenon, novel terms such as action potential (AP) and action current were created (Du Bois-Reymond 1848). After plasmolysis experiments in plant cells suggested that all living cells are surrounded by semi-permeable membranes (Pfeffer 1873, 1906, 1921), it did not take long until W. Nernst (1889) and J. Bernstein (1912) proposed an updated understanding of existing potentials and AP-mediated excitations on the basis of the existence and collapse of K^+ ion gradients across the plasma membrane. It was also recognized that nerves propagate such excitations instantly or with very high speed. In 1850, H. von Helmholtz succeeded in actually measuring this speed in the *Nervus ischiadicus* of frogs and Hermann (1868) developed the "Strömchen" theory to explain the speed and efficiency of AP propagation in nerves in analogy with a leaky wire cable. Until about 1930, this seemed to be all that was to know about nervous signals. However, clever experiments showed surprisingly that signaling between nerve cells through their dendritic connections does not occur by way of a continuation of the electrical action current but by the release of chemical signals diffusing through an intercellular cleft. Following the anatomical work of S. Ramon y Cajal, the biochemical studies of O. Loewi and the terminology of Sir Charles Sherrington, the phenomenon of synaptic transmission was recognized and this meant a gigantic step towards the understanding of nervous integration (Eccles 1964). With these events, the full range of modern electrophysiology

was established and the following examples are added to remind us that this progress was not confined to the academic field but inspired many practical improvements in medical and psychological diagnosis. In 1895, electrocardiography (EEC) was tested and introduced by W. Einthoven and in 1934 H. Berger developed a related method for brain responses in the form of electro-encephalography (EEG; Grey Walter 1954; Brazier 1962). The discovery of piezo-electricity in bones led the way to novel electro-therapeutic treatments for accelerated healing of fractures (Basset 1965). The realization that diaphoretic and alternative changes in skin resistance closely relate the emotional state of individuals turned into another important tool of diagnosis for psychological tests and criminal investigations; the lie detector.

1.1 Intracellular recording of membrane potentials and other improvements

For many years, the application of external electrodes to the surface of plant and animal organs was the only available technique for measuring potentials. The only way to deduce the internal potential of cells was through measuring "wound potentials" in the manner described above (Beutner 1920). Rather than relying on such indirect methods, the membrane theory (Bernstein 1912) made it desirable to measure directly the value of cell membrane potentials. This was facilitated by the introduction of microelectrodes (KCl-filled glass micropipettes with a tip diameter small enough to be inserted into living cells; Montenegro et al. 1991) to record intracellular, i.e. real, membrane potentials (V_m). This technique was first adopted for giant cells from axons of cephalopods such as *Loligo* and *Sepia* (see Keynes 1958) and charophytic algae such as *Chara* and *Nitella*. Early attempts to insert microelectrodes into charophytic cells resulted in long-term damage and were reflected in very low V_m values around −30 mV (Brooks and Gelfan 1928). Improved talent, glass needles, incubation procedures and micromanipulators led to a rapid (i.e. within 1–4 min) return of the initially depolarized V_m of *Nitella* cells to values between −100 and −170 mV (Umrath 1930, 1932; Osterhout 1936). Aside from making the first reliable measurements of V_m values in plant cells, the work of Umrath and Osterhout shows the first intracellular recordings of plant APs as well. When this new technique was complemented with precise electronic amplifiers and voltage clamp circuits in the 1940 s, it permitted measurement of ion currents instead of voltages, and with it monitoring of the activity of ion channels. The smart application of these techniques led to a new, highly detailed understanding of the ionic species and mechanisms involved in V_m changes, especially APs (Hodgkin et al. 1949). Now it could be seen that the depolarization during an AP went beyond zero and well into the range of positive voltages, indicating that other ions in addition to K^+ must participate in the AP. Voltage clamp was introduced to demonstrate the contribution of

various ion currents involved in the AP in nerve cells (Hodgkin et al. 1949; Hille 1992) as well as *Chara* cells (Lunevsky et al. 1983; Wayne 1994). Whereas the depolarizing spike in animal nerve cells is driven by an increased influx of Na^+ ions, plant APs were found to involve influx of Ca^{2+} and/or efflux of Cl^- ions (Sibaoka 1969, 1991). To this day, charophytic algae have served as important models and stepping-stones on the way to the investigation of higher plant cells (see Chapter 16).

Parallel voltage (V) and current (I) measurements allowed I-V-curves to be plotted and so permitted to differentiate between the action of an ion channel (ohmic or parallel changes in I and V) or ion pump (non-ohmic relation between V and I changes; Higinbotham 1973). These new recording techniques led to the recognition of another important difference between plant and animal cells. Whereas most animal cells in their resting stage are very close to the Nernst potential for K^+ ions (as first suggested by Nernst 1889), plant cells can obtain much higher values due to the operation of an electrogenic H^+-ATPase-driven pumps (up to a record V_m value of –296 mV reported by R. Spanswick in *Elodea canadensis*; Higinbotham 1973; see also Chapter 10). As a next step to improve recording possibilities, the patch clamp technique was invented. By going from single cells to isolated membrane patches, one can record the current of as small a unit as a single channel (Neher and Sakmann 1976). Developed for animal cells, this technique was rapidly adopted for plant cells as well (e.g. Hedrich and Schroeder 1989).

1.2 Plant action potentials

The first known recording of a plant AP was done on leaves of the Venus flytrap (*Dionea muscipula* Ellis) in 1873 by the medical physiologist Sir John Burdon-Sanderson in England. This event was organized by C. Darwin, who had found *Dionea* a "most animal-like plant" that showed analogy to the animal nerve reflex (Darwin 1875,1896). Burdon-Sanderson measured the voltage difference between adaxial and abaxial surfaces of a *Dionea* leaf half while he stimulated the other half mechanically by touching the hairs (Burdon-Sanderson 1873, 1899). Ever since then, the trap closure in *Dionea* has been considered as a model case that shows comparable roles of APs in plants and nerve–muscle preparations of animals (e.g. Simons 1992). However, this was and is not a generally accepted view. Reminding his readers that Burdon-Sanderson measured the APs in leaves that were prevented from closure by a plaster harness, Stern (1924), in a first consolidating monograph on plant electrophysiology, concluded that APs had no proven direct connection with the closure movement and that APs produced before and after trap closure do not seem to differ (see similar results by Hodick and Sievers 1988). However, Stern noted that while in resting *Dionea* leaves the upper site is positive relative to the lower one, this relation gets inverted with stimulation.

Other objects of investigation were sensitive plants in the genus *Mimosa,* where the folding movement of the leaflets actually makes the propagating wave of excitation visible. After the wounding of a leaflet action spikes were found to arise in parallel with the visible leaflet movements (Kunkel 1878; Haberlandt 1890; Biedermann 1895; Bose 1906, 1926). However, it was Dutrochet and Pfeffer (1873, 1906) who found that an experimental interruption of the vascular bundles by incision prevented the excitation from propagating beyond the cut. While they concluded that the stimulus moved through the woody or hadrome part of the bundles (in modern terms the xylem), Haberlandt cut or steam-killed the external, non-woody part of the vascular bundles (the leptom, i.e. in modern terms the phloem) and emphasized that not the xylem but the phloem strands were the pathways to conduct the excitation signals in plants. "The effects of incision show that stimuli are actually propagated in this system of highly turgescent tubes and that the mode of transmission is a hydrodynamic one" (Haberlandt 1914). However, this hypothesis was difficult to prove (Tinz-Fruchtmeyer and Gradmann 1990) and up to this day we do not know much about pressure propagation in the phloem except that pressure gradients are considered vital and the driving force of mass flow and net solute transport (Lee 1981; van Bel 2003).

It was namely for that reason that Ricca (1916) and Snow (1924) suggested an alternative mechanism in which an excitation substance is released into the xylem and moved by the transpiration flow is the ultimate cause for the propagating excitation. The most convincing experiment in favor of a chemical substance was to cut through a *Mimosa* stem and then reconnect the two pieces with a water-filled tube. Flame-stimulation of leaves connected to the lower part of the stem frequently caused an excitation response in the upper shoot. It is often forgotten, however, that other researcher could not confirm these results (e.g. Koketsu 1923; Bose 1925, 1926). Observing both leaflet movement and electrical signals, Bose (1926) finally proposed that vascular bundles act analogous to nerves by enabling the propagation of an excitation that moved from cell to cell.

Ignoring Haberlandt's and Bose's results, Houwinck (1935) proposed that wound excitation in Mimosa can be propagated by a chemical wound signal (called Ricca's factor) in the xylem which then could be translated into an AP via the mediation of a new type of electric signal, which he called variation potential. One cannot help noticing that the conversion of a chemical into an electrical signal is a process with striking parallels to post-synaptic events in animals. Houwinck's idea circumvented the existing controversy by including both chemical and electrical signals in the transmission mechanism for the excitation signal in *Mimosa*. In spite of Houwinck's diplomatic proposal, the conflict between chemical and electrical propagation persists to this day Cheeseman and Pickard 1977; Schildknecht 1984). A recent modification in the controversy is the recognition that massive wounding causes a large and propagating pressure increase at the wound site. These wound-induced increases in xylem pressure cannot only temporarily reverse the direction of

the transpiration-driven xylem flow (Malone 1996) but are also sufficient cause for a large depolarization in the form of a slow wave potential (Stahlberg and Cosgrove 1996, 1997). Accordingly, the hydrodynamic propagation of electrical signals proposed by Kunkel (1878) and Haberlandt (1914) has been found to occur less in the phloem (Tinz-Fruchtmeyer and Gradmann 1990) than in the xylem, where it provides the major mechanism for the propagation of a propagating signal called slow wave potentials (Stahlberg et al. 2006).

The majority of recent studies in *Mimosa* and other plant species confirmed Haberlandt's suggestion of the phloem being the pathway of excitation. APs have their largest amplitude near and in the phloem and there again in the sieve cells (Sibaoka 1969; Opritov 1978; Fromm and Eschrich 1988; Fromm and Bauer 1994; Rhodes et el. 1996; Dziubinska et al. 2001). Other studies found that AP-like signals propagate with equal rate and amplitude through all cells of the vascular bundle (Herde et al. 1998). Bose (1907, 1913, 1926) went one huge step ahead when he started studies with isolated vascular bundles (e.g. in the fern *Adiantum)*. Comparing the amplitudes, he found the response to heat in the isolated vascular bundles to be much stronger than in the intact stem. Bose found a series of interesting results; among them an increase in amplitude of heat-induced spikes by repeated stimulation (tetanisation) and by incubation of the strands in 0.5% solution of sodium carbonate and other salts. This daring advance has yet to be repeated and confirmed by other labs. Since the recorded behavior of the isolated vascular strands was comparable to that of isolated frog nerves, Bose felt justified in referring to them as plant nerves.

1.3 "Plants have no nerves!?"

Although Burdon-Sanderson described APs in in *Dionea* plants as early as 1873 and Bose described APs in *Mimosa* as early as 1906, the scientific community was slow to respond with experimental and theoretical follow-up. This lack of enthusiasm was at least in part conditioned by the reiterated belief that plants have no nerves and muscles, that the APs were not involved in activities of primary relevance for plant life such as, e.g. photosynthesis. And yet for some, the existence of APs in *Dionea* and *Mimosa* plus the discovery of plant mechanoreceptors not only in *Dionea*, but also at tendrils and surfaces of common plants (Haberlandt 1890, 1906) was sufficient stimulation to look for structures that could facilitate the rapid propagation of signals. Around 1900, several researchers started took a closer look at plasma strands that run across the lumen of many plant cells, continue over several cells and might possibly serve as excitation-conducting structures similar as nerves. Strands were shown to occur and likely to be involved in the traumatotropic responses of several plant roots (Nemec 1901), but were also seen in the leaves of insectivorous butterworts of the genus *Pinguicula* where they

connect the mucous glue-containing hair tips with the more basal peptidase-producing glands (France 1909, pictured in France 1911). Haberlandt reinvestigated these views and suggested later that the only potential nerve-like structures of plants were the vascular bundles, and in particular the phloem (Haberlandt 1914; but see also recent re-evaluation by Baluska and Hlavacka 2005).

From then on and often to this day papers and textbooks reiterate the statement that "plants have no nerves". This unproductive expression ignores the work of Darwin, Pfeffer, Haberlandt and Bose, together with the result that nerves and vascular bundles share the analog function of conducting electrical signals. Similar anatomical and functional differences were never seen as an obstacle to stating that both plants and animals consist of cells. The mechanistic similarity of excitations in plant and nerve cells were elegantly demonstrated by direct comparison of action potentials in *Nitella* and the giant axon of squids (Cole and Curtis 1938, 1939). Today, the consideration of nerve-like structures in plants involves an increasing number of further f aspects of comparison. We know that many plants can efficiently propagate action potentials and hydraulo-electric signals in the form of slow wave potentials (variation potentials) and that the long-distance propagation of these signals proceeds in the vascular bundles. We also know that plants like *Dionea* can propagate APs with high efficiency and speed without the use of vascular bundles because their cells are electrically coupled through plasmodesmata. Other analogies with neurobiology include vesicle-operated intercellular clefts in axial root tissues (the so-called plant synapses; Baluska et al. 2005) as well as the existence and operation of substances like neurotransmitters and synaptotagmins in plant cells (e.g. Wipf et al. 2002). Such similarities were recently the focus of studies presented at the First Symposium on Neurobiology of Plants in 2005 (Baluska et al 2006).

For a long time, plants were thought to be living organisms whose limited ability to move and respond was appropriately matched by limited abilities of sensing (Trewawas 2003). Exceptions to this rule were made only for plants with rapid and/or purposeful movements such as *Mimosa pudica (*also called *the* sensitive plant*)*, *Drosera (sundews), Dionea muscipula* (flytraps) and tendrils of climbing plants. These sensitive plants attracted the attention of outstanding pioneer researchers such as Burdon-Sanderson (1873, 1899), Pfeffer (1873), Haberlandt (1890, 1906, 1914), Darwin (1896) and Bose (1926). They found them not only to be equipped with various mechanoreceptors that exceeded the sensitivity of a human fingerbut also to trigger action potentials (APs) that implemented these movements.

Although at the time a hardly noticed event, the discovery that normal plants such as pumpkins had propagating APs just as the esoteric "sensitive" plants (Gunar and Sinykhin 1962, 1963; Karmanov et al. 1972) was a scientific breakthrough with important consequences. First, it corrected the long-held belief that normal plants are less sensitive and responsive than so-called "sensitive plants." Second, it led to a new, eagerly pursued belief that such

widely distributed electric signals were not random fluctuations but indeed carried important messages with a broader relevance than the established induction of organ movements in "sensitive plants." In different laboratories around the world, this anticipation became the driving force for a renewed quest for the meaning of the electrical signals (Pickard 1973; Pyatygin 2003).

The ensuing studies made considerable progress in linking electrical signals with respiration and photosynthesis (Gunar and Sinykhin 1963; Koziolek et al. 2003), pollination (Sinykhin and Britikov 1967; Spanjers 1981), phloem transport (Opritov 1978; Fromm and Eschrich 1988; Fromm and Bauer 1994) and the rapid, plant-wide deployment of plant defenses (Wildon et al. 1992; Malone et al. 1994; Herde et al. 1995, 1996; Volkov and Haak 1995; Stankovic and Davies 1996, 1998; Volkov 2000).

1.4 The photoelectric response of green leaves

From the view of many botanists, it was probably equally or more important to decipher the mechanism of action potentials as it was to find the particularities in electric behavior that derive from photosynthetic activity in green plant cells. The first to address this question was Haake (1892). Using leaves of various species, he established that relative to the midvein, the mesophyll had a positive voltage in the dark that turned negative under illumination (in modern understanding and assuming that the midvein potential did not change, this result can be interpreted as a light-induced hyperpolarization of the mesophyll). The further steps in deciphering of the photoelectric response have been described by Higinbotham (1973), Rybin (1977) and also by Lüttge and Higinbotham (1979). Jeschke (1970) and Spanswick (1974) found that illumination of *Elodea* and *Nitella* cells caused them to hyperpolarize by 50–130 mV (in *Elodea canadensis* up to a record V_m value of –296 mV) due to the increased activity of the P-type H^+ ATPase.

For the photoelectric response of higher land plants, it was most revealing to compare green and chlorophyll-free cells within the same variegated leaf. Such a comparison identified a rapid light-induced depolarization as the major photosynthetic contribution to the photoelectric response of mesophyll cells from leaves of higher plants (Stahlberg et al. 2000). The depolarization is associated with and can be simulated by the reduction of inter- and intracellular levels of carbon dioxide (Stahlberg et al. 2001). It is inhibited by the electron-transport blocker DCMU (3–3′-4′-dichloropphenyl-1,1-dimethylurea) and may involve K^+, Ca^{2+} and/or Cl^- currents (Spalding et al. 1992; Elzenga et al. 1995; see also Chapter 10). This transient depolarization response differs from the light-induced hyperpolarizations reported as the major photosynthetic light responses in *Elodea* and *Nitella* cells. A delayed hyperpolarization associated with the P-type H^+ ATPase is also present in leaf cells of higher land plants. It occurs in response to photosynthetic and other factors in a way that

remains unresolved to this day (Stahlberg and Van Volkenburgh 1999). Plants also generate other, non-photosynthetic types of intracellular and intercellular electrical events in response to light. Recently, it was found that the irradiation of soybean plants at 450±50 nm induced APs and that their suppression by ion channels blockers inhibited the phototropic response of these plants (see Chapter 19).

By studying the particularities of photosynthesis, plant transporters, plant membrane potentials, action potentials, slow wave potentials and their coupled responses, electrophysiological studies contributed much to the understanding of the living world and one of its central questions: the defining similarities and differences between animals and plants. Details of these and other contributions can be found in the following chapters.

References

Baluska F, Hlavacka A (2005) Plant formins come of age: something special about cross-walls.- New Phytologist 168: 499–503

Baluska F, Volkmann D, Menzel D (2005) Plant synapses: actin-based domains for cell-to-cell communication. Trends Plant Sci 10:106–111

Baluska F, Mancuso S, Volkmann D (2006) Communications in plants. Neuronal aspects of plant life. Springer, Berlin Heidelberg New York

Basset AL (1965) Electrical effects in bone. Sci Am 213:18–25

Bernstein J (1912) Elektrobiologie. Thieme, Braunschweig

Bertholon (1783) De l'eléctricite des vegetaux. Paris

Beutner R (1920) Die Entstehung elektrischer Ströme in lebenden Geweben. Fischer, Stuttgart

Biedermann W (1895) Elektrophysiologie. Fischer, Jena

Bose JC (1906) Plant response as a means of physiological investigation. Longman Green, London

Bose JC (1913) Researches on the irritability of plants. Longman Green, London

Bose JC (1925) Physiological and anatomical investigations on *Mimosa pudica*. Proc R Soc Ser B 98:280–299

Bose JC (1926) The nervous mechanism of plants. Longman Green, London

Brazier MAB (1962) The analysis of brain waves. Sci Am 206:142–153

Brooks SC, Gelfan S (1928) Bioelectric potentials in *Nitella*. Protoplasma 5:86–96

Burdon-Sanderson J (1873) Note on the electrical phenomena which accompany stimulation of leaf of *Dionea muscipula*. Proc R Soc 21:495–496

Burdon-Sanderson J (1899) On the relation of motion in anima/ls and palnts to the electrical phenomena which are associated with it. Proc R Soc 65:37–64

Cheeseman JM, Pickard BG (1977) Depolarization of cell membranes in leaves of *Lycopersicon* by extract containing Ricca's factor. Can J Bot 55:511–519

Cole KS, Curtis HJ (1938) Electric impedance of *Nitella* during activity. J Gen Physiol 22:37–64

Cole KS, Curtis HJ (1939) Electric impedance of the squid giant axon during activity. J Gen Physiol 22:37–64

Darwin C (1896) The power of movements in plants. Appleton, New York

Darwin C (1875) Insectivorous plants. Murray, London

Du Bois-Reymond (1848) Untersuchungen über thierische Elektrizität. Reimer, Berlin

Dziubinska H, Trebasz K, Zawadzki T (2001) Transmission route for action potentials and variation potentials in *Helianthus annuus* L. J Plant Physiol 158:1167–1172

Eccles JC Sir (1964) The physiology of synapses. Springer, Berlin Heidelberg New York

Elzenga JTM, Prins HBA, van Volkenburgh E (1995) Light-induced membrane potential changes of epidermal and mesophyll cells in growing leaves of *Pisum sativum*. Planta 197:127–134
France RH (1909) Pflanzenpsychologie als Arbeitshypothese der Pflanznephysiologie. Kosmos, Stuttgart
France RH (1911) Pflanzenkunde für jedermann. Ullstein, Berlin
Fromm J, Bauer T (1994) Action potentials in maize sieve tubes change phloem translocation. J Exp Bot 273:463–469
Fromm J, Eschrich W (1988) Transport processes in stimulated and non-stimulated leaves of *Mimosa pudica*. Trees 2:7–24
Galvani L (1791) De viribus electricitatis in motu musculari commentaries. Bononiae Instituti Scientiarum, Bologna
Gunar II, Sinykhin AM (1962) A spreading wave of excitation in higher plants. Proc Acad Sci USSR (Bot) 142:214–215
Gunar II, Sinykhin AM (1963) Functional significance of action currents affecting the gas exchange of higher plants. Soviet Plant Physiol 10:219–226
Grey WF (1954) The electrical activity of the brain. Sci Am 190:54–63
Haake O (1892) Über die Ursachen elektrischer Ströme in Pflanzen. Flora 75:455–487
Haberlandt G (1890) Das reizleitende Gewebesystem der Sinnpflanze. Engelmann, Leipzig Haberlandt G (1906) Sinnesorgane im Pflanzenreich zur Perzeption mechanischer Reize. Engelmann, Leipzig
Haberlandt G (1914) Physiological plant anatomy. Macmillan, London
Hedrich R, Schroeder JI (1989) The physiology of ion channels and electrogenic pumps in higher plants. Annu Rev Physiol Plant Mol Biol 40:539–569
Herde O, Fuss H, Pena-Cortes H, Fisahn J (1995) Proteinase inhibitor II gene expression induced by electrical stimulation and control of photosynthetic activity in tomato plants. Plant Cell Physiol 36:737–742
Herde O, Atzorn R, Fisahn J, Wasternak C, Willmitzer L, Pena-Cortes H (1996) Localized wounding by heat initiates the accumulation of proteinase inhibitor II in abscisic acid deficient tomato plants by triggering jasmonic acid biosynthesis. Plant Physiol 112:853–860
Herde O, Fuss H, Pena-Cortes H, Willmitzer L, Fisahn J (1998) Remote stimulation by heat induces characteristic membrane-potential responses in the veins of wild-type and abscisic acid-deficient tomato plants. Planta 206:146–153
Hermann L (1868) Untersuchungen zur Physiologie der Muskeln und Nerven. Hirschwald, Berlin
Higinbotham N (1973) Electropotentials of plant cells. Annu Rev Plant Physiol 24:25–46
Hille B (1992) Ionic channels of excitable membranes. Sinauer Associates, Sunderland, Massachusetts
Hodgkin AL, Huxley AF, Katz B (1949) Ionic currents underlying activity in the giant axon of the squid. Arch Sci Physiol 3:129–150
Hodick D, Sievers A (1988) The action potential of *Dionea muscipula* Ellis. Planta 174:8–18
Houwinck AL (1935) The conduction of excitation in *Mimosa pudica*. Receuil Traverse Bot Neerlandais 32:51–91
Jeschke WD (1970) Lichtabhangige Veränderungen des Membranpotentials bei Blattzellen von *Elodea densa*. Z Pflanzenphysiol 62:158–172
Karmanov VG, Lyalin OO, Mamulashvili GG (1972) The form of action potentials and cooperativeness of the excited elements in stems of winter squash. Soviet Plant Physiol 19:354–420
Keynes RD (1958) The nerve impulse and the squid. Sci Am 199:83–90
Koketsu R (1923) Journal of the Department of Agriculture of the Kyashu Imperial University 1:55 (cited according to Bose 1926)
Koziolek C, Grams TE, Schreiber U, Matyssek R, Fromm J (2003) Transient knockout of photosynthesis mediated by electrical signals. New Phytologist 161:715–722
Kunkel KAJ (1878) Über elektromotorische Wirkungen an unverletzten lebenden Pflanzenteilen. Arbeiten Botan Institut Würzburg 2:1–17
Lee DR (1981) Synchronous pressure-potential changes in the phloem of *Fraxinus americana*. Planta 151:304–308

Lemstrom S (1902) Elektrokultur. Springer, Berlin Heidelberg New York
Lunevsky VZ, Zherelova OM, Vostrikov IY, Berestovsky GN (1983) Excitation of *Characeae* cell membranes as a result of the activation of calcium and chloride channels. J Membr Biol 72:43–58
Lüttge U, Higinbotham N (1979) Transport in plants. Springer, Berlin Heidelberg New York
Malone M (1996) Rapid, long-distance signal transmission in higher plants. Adv Bot Res 22:163–228
Malone M, Palumbo L, Boari F, Monteleone M, Jones HG (1994) The relationship between wound-induced proteinase inhibitors and hydraulic signals in tomato seedlings. Plant Cell Environ 17:81–87
Montenegro MI, Queiros MA, Daschbach JL (1991) Microelectrodes: theory and applications. Kluwer Academic, Dordrecht
Neher E, Sakmann B (1976) Single-channel currents recorded from membrane of denervated frog muscle fibers. Nature 260:779–802
Nemec B (1901) Die Reizleitung und reizleitende Strukturen bei den Pflanzen. Fischer, Jena
Nernst W (1889) Die elektromotorische Wirksamkeit der Ionen. Z Phys Chem 4:129–181
Opritov VA (1978) Propagating excitation and assimilate transport in the phloem. Soviet Plant Physiol 25:1042–1048
Osterhout WJV (1936) Electrical phenomena in large plant cells. Physiol Rev 16:216–237
Pfeffer W (1873) Physiologische Untersuchungen. Engelmann, Leipzig
Pfeffer W (1906) The physiology of plants, a treatise upon the metabolism and sources of energy in plants. Clarendon Press, Oxford
Pfeffer W (1921) Osmotische Untersuchungen; Studien zur Zellmechanik. Engelmann, Leipzig
Pickard BG (1973) Action potentials in higher plants. Bot Rev 39:172–201
Pyatygin SS (2003) Electrogenesis of plant cells under stress (in Russian). Prog Mod Biol (Moscow) 123:552–562
Rhodes JD, Thain JF, Wildon DC (1996) The pathway for systemic electrical signal conduction in the wounded tomato plant. Planta 200:50–57
Ricca U (1916) Soluzione d'un problema di fisiologia: la propagazione di stimulo nella *Mimosa*. Nuovo G Bot Ital 23:51–170
Rybin IA (1977) The history of concepts on the light-induced bio-electrical responses of plant leaves (in Russian). In: Rybin IA, Mikheeva SA, Birukova EG (eds) The light-induced bio-electrical activity of plant leaves. Uralsk State University Press, Uralsk (Russia)
Schildknecht H (1984) Turgorins—new chemical messengers for plant behavior. Endeavour NS 8:113–117
Sibaoka T (1969) Physiology of rapid movements in higher plants. Annu Rev Plant Physiol 20:165–184
Sibaoka T (1991) Rapid plant movements triggered by action potentials. Bot Mag (Tokyo) 104:73–95
Simons P (1992) The action plant. Movement and nervous behavior in plants. Blackwell, Oxford
Sinyukhin AM, Britikov EA (1967) Action potentials in the reproductive system of plants. Nature 215:1278–1280
Snow R (1924) Conduction and excitation in stem and leaf of *Mimosa pudica*. Proc R Soc Lond Ser B 96:344–360
Spalding EP, Slayman CL, Goldsmith MHM, Gradmann D, Bertl A (1992) Ion channels in *Arabidopsis* plasma membrane. Transport characteristics and involvement in light-induced voltage changes. Plant Physiol 99:96–102
Spanjers AW (1981) Biolelectric potential changes in the style of *Lilium longiflorum* Thunb. after self- and cross-pollination of the stigma. Planta 153:1–5
Spanswick RM (1974) Evidence for an electrogenic pump in *Nitella translucens*. I. Control of the light-stimulated component of the membrane potential. Biochim Biophys Acta 332:387–398
Stahlberg R, Cosgrove DJ (1996) Induction and ionic basis of slow wave potentials in seedlings of *Pisum sativum* L. Planta 200:416–425
Stahlberg R, Cosgrove DJ (1997) The propagation of slow wave potentials in pea epicotyls. Plant Physiol 113:209–217

Stahlberg R, van Volkenburgh E (1999) The effect of light on membrane potential, apoplastic pH and cell expansion in leaves of *Pisum sativum* L. var. *Argenteum*. Planta 208:188–195
Stahlberg R, van Volkenburgh E, Cleland RE (2000) Chlorophyll is not the primary photoreceptor for the stimulation of P-type H^+ pump and growth in variegated leaves of *Coleus x hybridus*. Planta 212:1–8
Stahlberg R, van Volkenburgh E, Cleland RE (2001) Long-distance signaling within *Coleus x hybridus* leaves; mediated by changes in intra-leaf CO_2? Planta 213:342–351
Stahlberg R, Cleland RE, Van Volkenburgh E (2006) Slow wave potentials—a propagating electrical signal unique to higher plants. In: Baluska F, Mancuso S, Volkmann D (eds) Communications in plants. Neuronal aspects of plant life. Springer, Berlin Heidelberg New York
Stankovic B, Davies E (1996) Both action potentials and variation potentials induce proteinase inhibitor gene expression in tomato. FEBS Lett 390:275–279
Stankovic B, Davies E (1998) The wound response in tomato involves rapid growth and electric responses, systemically up-regulated transcription of proteinase inhibitor and calmodulin and down-regulated translation. Plant Cell Physiol 39:268–274
Stern K (1924) Elektrophysiologie der Pflanzen. Springer, Berlin Heidelberg New York
Tinz-Fruchtmeyer A, Gradmann D (1990) Laser-interferometric re-examination of rapid conductance of excitation in *Mimosa pudica*. J Exp Bot 41:15–19
Trewawas A (2003) Aspects of plant intelligence. Ann Bot 92:1–20
Umrath K (1930) Untersuchungen über Plasma und Plasamstromung a Characeen. IV. Potentialmessungen an *Nitella mucronata* mit besonderer Berücksichtigung der Erregungserscheinungen. Protoplasma 9:576–597
Umrath K (1932) Der Erregungsvorgang bei *Nitella mucronata*. Protplasma 17:258–300
Van Bel AJE (2003) The phloem, a miracle of ingenuity. Plant Cell Environm 26:125–149
Volkov AG (2000) Green plants: electrochemical interfaces. J Electroanal Chem 483:150–156
Volkov AG, Haack RA (1995) Insect induced bioelectrochemical signals in potato plants. Bioelectrochem Bioenerg 35:55–60
Wayne R (1994) The excitability of plant cells: with a special emphasis on *Characeae* internode cells. Bot Rev 60:265–367
Wildon DC, Thain JF, Minchin PEH, Gubb IR Reilly AJ, Skipper YD, Doherty HM, O'Donnell PJ, Bowles DJ (1992) Electrical signaling and systemic proteinase inhibitor induction in the wounded plant. Nature 360:62–65
Wipf D, Ludewig U, Teqeder M, Rentsch D, Koch W, Frommer WB (2002) Conservation of amino acid transporters in fungi, plants and animals. Trends Biochem Sci 27:139–147

2 Electrochemical Methods and Measuring Transmembrane Ion Gradients

ANTHONY J. MILLER, DARREN M. WELLS

2.1 Methods for electrical recordings from plants

2.1.1 Making contact

The measurement of a voltage requires a complete electrical circuit or ring that includes the measuring device, a voltmeter or electrometer. The electrical contact to the biological material is provided by an electrode. This interface between the biological specimen and electrometer is very important, as ideally it should provide a low electrical resistance pathway that does not interfere with the cells or tissues being measured. The word *microelectrode* is commonly used to describe a glass micropipette which is pulled into a fine tip at one end and filled with an aqueous salt solution. The junction between the salt solution inside the microelectrode and the input to the electrometer amplifier is provided by a half-cell. There are different types of half-cell, but usually the metal contact is AgCl-coated Ag wire and the salt solution is 0.1 M KCl (e.g. World Precision Instruments, Sarasota, Fla., USA: http://www.wpiinc.com/). The micropipette provides a salt bridge between the inside of a living cell and the metal contact in the half-cell. The simplest microelectrodes measure voltage and when inserted into cells measure the membrane potential, in mV, between the inside and outside of the cell. The metal contact can be made directly to the cell or tissue surface, but this type of electrode can be subject to various types of interference as the surface can be coated by plant material that will influence the stability and size of the electrical potential reported. This problem is much less likely to occur when the tip is constructed from glass that has been heated and pulled into a small fine tipped microelectrode. A small tip also provides less intrusion and interference for the biological tissue or cells being examined.

An *ion-selective* microelectrode contains an ion-selective membrane in the tip of the glass micropipette and is responsive both to the membrane potential and the activity (not concentration) of the ion sensed by the selective membrane. To make intracellular measurements, it is necessary to also simultaneously measure the membrane potential either by insertion of a

Crop Performance and Improvement Division, Rothamsted Research, Harpenden, Hertfordshire, AL5 2JQ, UK

Plant Electrophysiology – Theory & Methods (ed. by Volkov)

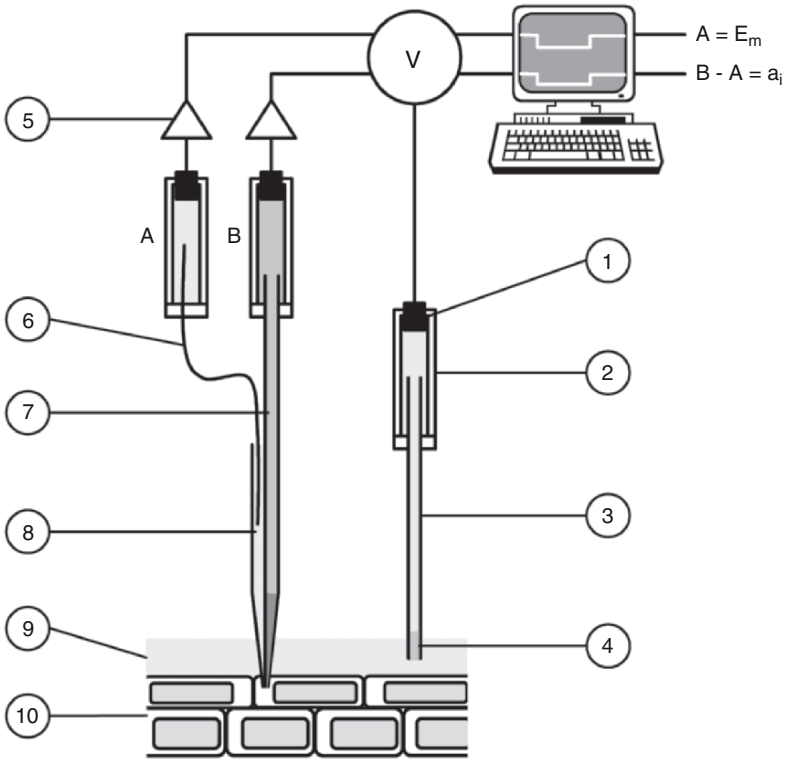

Fig. 2.1. Diagrammatic representation of a double-barreled ion-selective microelectrode. *1* Ag/AgCl chloride coated pellet, *2* half-cell, *3* salt bridge, *4* porous glass frit or agar plug, *5* headstage signal amplifier, *6* Ag/AgCl coated Ag wire, *7* ion-selective barrel with sensor plug in the tip, *8* cell membrane potential barrel filled with 0.1 M KCl, *9* nutrient solution bathing plant, *10* plant tissue with microelectrode tip in a cell (cytoplasm)

second electrode or, for small cells, by combining the ion-selective and voltage-measuring electrodes into a *double-barreled microelectrode* (see Fig. 2.1). In order to be able to measure several different ions, it may be necessary to combine together several different electrodes to make multi-barreled electrodes (e.g. Walker et al. 1995).

Solid metal electrodes have been used to directly report from plant material and for some types of specialist uses such as measurements of electrical current in oxygen electrodes. Metal electrodes are usually made from Ag or platinum and these solid state electrodes have been used to make ion-selective microelectrodes (see section 2.2). Metal electrodes have also been used for direct recording from the surface of plants to measure extracellular transient electrical signals such as those elicited by external signals, e.g. wounding. The interface between the plant material and a metal recording electrode may also

be made by a salt bridge using a wick electrode (e.g. Wildon et al. 1992). The wick can be made of fiber, for example paper or cotton thread soaked in salt solution.

2.1.2 Recording from plants

Electrophysiology recordings from plants require very solid anchoring of the plant material, while at the same time preserving the normal state of the material as far as possible. It is best to avoid dissecting the plant material as this is likely to lead to local wounding that is known to have major effects on gene expression (Delessert et al. 2004). Plants grown in hydroponic culture can be easily transferred to the microscope stage for electrode impalements of either root or leaf tissue. The hydroponic environment for roots is easily maintained on the stage of a microscope but leaves are more difficult, requiring some wet contact between the tissue and the bathing solution. Microelectrode impalements are usually made under a microscope using long working distance objectives that allow sufficient space for microelectrode access. Although they are generally used for patch-clamp experiments, inverted microscopes are not so suitable for this type of work. Dissecting microscopes can be used for microelectrode impalements, but they usually do not have sufficient magnification to see individual cells. They can be used for impalements by letting the electrical recording show when tissue contact has been made and a successful impalement can be gauged by the size of the membrane potential measured. Microelectrodes are mounted on micromanipulators for cellular impalement, to allow the delicate movement of the tip into a cell. There are a range of different types, and hand control of tip movement is achieved by either joystick or rotational manipulation. The size and fine movement axis should be chosen so that the micromanipulator can be conveniently positioned alongside the microscope stage for tissue impalement.

Plant tissue is usually mounted in a purpose built chamber for microelectrode impalements. The chamber is usually made from Plexiglas and is constructed so that the tissue can be perfused with nutrient solution throughout the experiment. This perfusion through the chamber helps prevent large local concentration gradients (unstirred layers) of ions developing around cells. Treatments can be applied to the tissue during a recording by changing the composition of the nutrient solution bathing the tissue. The chamber design is very important, and it is worth investing time in this aspect of the experimental system. If the tissue is not well anchored in position, it is impossible to achieve good electrical recordings. Each type of tissue usually requires a purpose built chamber but published work often does not report the details of this key aspect of the experimental system. The general principles of chamber construction have been reviewed previously (see Blatt 1991) and a chamber for leaf measurements has been described (Miller et al. 2001).

Some of the equipment required for microelectrode recording is shown in Fig. 2.1 but a more complete list is as follows:

- Voltmeter (also known as an electrometer)
- Microscope (with long working distance objectives)
- Micromanipulator
- Tissue chamber (for holding and perfusion)
- Data logging system (e.g. computer or chart recorder)
- Vibration free table (for microscope and micromanipulator to avoid interference from external vibration sources)
- Faraday cage (electrical screening around the microscope and micromanipulator especially necessary for high resistance electrodes)
- Oscilloscope (not essential but useful for fixing recording noise problems)

2.2 Manufacture and use of ion-selective electrodes

Ion-selective microelectrodes are used to measure ion gradients across membranes. These measurements can be made outside and inside cells. For example, ion fluxes at the surface of roots can be measured directly using ion-selective microelectrodes (Henriksen et al. 1990) or by using an ion-selective vibrating probe (Kochian et al. 1992; see Chapter 3 by Sergey Shabala). Intracellular measurements have been used to give important information on the compartmentation of nutrients, dynamics of cellular ion activities (e.g. in intracellular signaling) and transport mechanisms, particularly the energy gradients for ion transport. The main criticism of intracellular measurements made with microelectrodes is that they report the ion activity at a single point within the cell. This will result in incomplete information if there are significant ion gradients within the cytoplasm of a single cell as may occur in some situations. Overall, the chief advantages of using ion-selective microelectrodes are that:

- They offer a non-destructive method of measuring ions within cells
- They do not change the activity of the ion being measured
- They permit simultaneous measurement of the electrical and chemical gradients across membranes
- They are relatively cheap when compared to other methods for measuring intracellular ions and once purchased the same equipment can be used to measure a range of different ions.

2.2.1 Theory of ISEs

The theoretical background has already been described by many authors (e.g. Ammann 1986, and references therein) and will only be outlined here. The properties of an ion-selective microelectrode are defined by several characteristics:

- Detection limit
- Selectivity
- Slope
- Response time

The ideal relationship between electrode output (mV) and the activity (a_i) of the ion of interest (i) is log-linear and is described mathematically by the Nernst equation. Calibration of the electrode against a range of standard solutions should ideally yield a slope (s) of 59 mV (at 25 °C) per decade change in the activity of a monovalent ion. In practice, however, the situation is more complicated than this because no ion-selective electrode (ISE) has ideal selectivity for one particular ion and under most conditions there is more than one ion present in the sample solution. Hence contributions to the overall electromotive force (EMF) made by each interfering ion, j, must be taken into account. In this situation, the Nicolsky–Eisenman equation, a modified Nernst equation, describes the EMF:

$$EMF = E + s \cdot \log\left[a_i + K_{ij}^{pot}\left(a_j\right)^{zi/zj}\right] \quad (1)$$

where K_{ij}^{pot} is the selectivity coefficient of the electrode for the ion i with respect to ion j. This term expresses, on a molar basis, the relative contribution of ions i and j to the measured potential.

The parameters s and K_{ij}^{pot} are the two main characteristics defining any type of ion-selective electrode. The slope should be a near ideal Nernstian response when an electrode is calibrated against ion activity, but s is temperature sensitive (see section 2.4). The selectivity coefficient measures the preference of the sensor for the detected ion i relative to the interfering ion, j. It can be determined by the separate solution method, the fixed interference method or the fixed primary ion method. For ideally-selective membranes, or for samples containing no other ions with the same net charge as the ion in question, K_{ij}^{pot} must be zero. A log selectivity coefficient <1 indicates a preference for the measuring ion i relative to the interfering ion j, and vice versa for a selectivity coefficient >1. The K_{ij}^{pot} values should not be considered to be constant parameters that characterize membrane selectivity under all conditions; the values are dependent on both the method used for determination, and on the conditions under which the calibrations are made. The fixed interference method is most commonly used to calculate the selectivity coefficient and it is the method recommended by the International Union of Pure and Applied Chemistry (Inczédy et al. 1998). Whichever type of method is chosen, the one used should always be quoted.

A schematic representation showing an ideal ion-selective microelectrode calibration curve is given in Fig 2.2. The slope s, is the change in EMF per decade change in activity of a monovalent anion i, which is equivalent to 59.2 mV at 25 °C; the limit of detection is defined as described in the text and is also indicated.

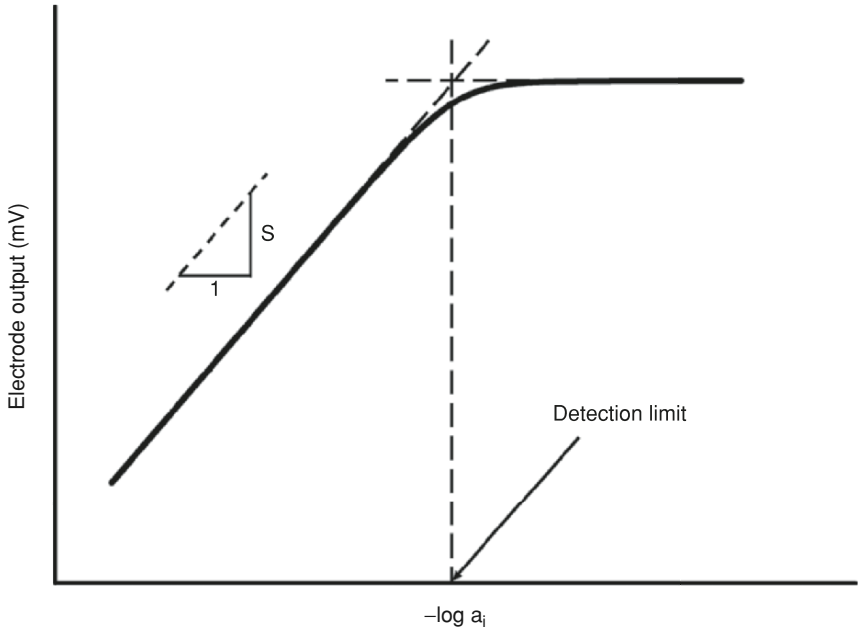

Fig. 2.2. Calibration of an ion-selective microelectrode to show detection limit and how it is calculated

Another important parameter of an ion-selective microelectrode is the detection limit, which is the lowest ion activity that can be detected with confidence and is defined by the intercept of the two asymptotes of the Nicolsky response curve (see Fig. 2.2). In practice, the detection limit seems to depend on the tip geometry and composition of the microelectrode's ion-selective membrane. Finer or smaller diameter tips have higher detection limits; while composition affects detection in ways that can only be determined experimentally (see section 2.4). The presence of interfering ions alters the detection limit (e.g. chloride for nitrate-selective microelectrodes, see Miller and Zhen 1991). Electrodes provide no useful information below their detection limits and for maximum benefit should be used in the linear portion of their calibration curves. The response time of ISEs can be important when measuring changes in ion activities. This microelectrode parameter is dependent on many factors, including tip geometry, membrane composition and resistance. Response time can be measured during the calibration as the time taken for the voltage to adjust when ion activity at the tip is changed.

2.2.2 Types of ISEs

There are three major types of ISE, all of which can be miniaturized for use in plant cells. These are solid state, glass, and liquid (or fluid) membrane

electrodes. Solid-state microelectrodes have been used to measure pH or Cl^- inside plants cells (e.g. Coster 1966) and recessed tip glass microelectrodes have been made using pH-selective glass (Sanders and Slayman 1982). These two types of microelectrode have largely been superseded for intracellular measurements by liquid-membrane electrodes, so only the latter will be described here. Liquid ion-selective membranes are composed of the sensor molecule dissolved in a plasticizer (membrane solvent). The membrane may also contain a lipophilic additive and a matrix. Liquid membrane sensors are commercially available for a wide range of ions (e.g. see Sigma; http://www.sigmaaldrich.com/).

To make an ion-selective microelectrode, the tip of the electrode is filled with an ion-sensing chemical cocktail which gives a voltage output of different values when placed in solutions containing different activities of the ion. Therefore when an electrode is inserted into a cell, the voltage measured gives a direct indication of the intracellular ion activity. This situation is complicated by the voltage across the cell membrane; the ion-selective electrode will sense this in addition to voltage due to the activity of the ion of interest. To obtain the output for the ion alone, the cell membrane potential must be subtracted. This is done by using either two single electrodes or a double-barreled electrode in which the ion-sensing electrode is combined with a cell-voltage-measuring electrode (see Fig. 2.1). Both output voltages are measured against a reference ground electrode in the external solution. The ion activity is determined from the calibration curve after subtracting the membrane potential.

2.2.3 Making ISEs

The preparation of ion-selective microelectrodes can be divided into four main stages:

A. Pulling of glass micropipettes
B. Silanization of the inside of surface of the ion-selective electrode or barrel
C. Backfilling
D. Calibration

The preparation of a nitrate-selective cocktail for backfilling microelectrodes is described by Miller and Zhen (1991) and a generalized method which is suitable for all different types of ion-selective microelectrode has been described previously (Miller 1995). The background to each stage is described here.

2.2.3.1 Pulling of glass micropipettes

Microelectrodes should be prepared to give dimensions suitable for impaling the target cell type. Double-barreled microelectrodes can be prepared by

twisting together two single pieces of filamented glass tubing or using glass which is already fused. Filamented glass has a glass fiber attached to the inner wall; this fiber assists backfilling by providing a hydraulic conduit along which the solution can flow by capillarity. Twisting is done using an electrode puller which both heats the glass and pulls it in a way pre-determined by the operator. The heating is paused for the two barrels to be twisted around one another and then the heating and pulling continues. There are various different types of microelectrode puller and the most important feature is reproducibility; this ensures that when an optimum microelectrode shape for a particular cell type has been prepared, it can be exactly duplicated many times. Before or after pulling, glue or heat shrink tubing can be used to provide support and additional strength to hold together the two or three pieces of glass.

Microelectrodes are usually made from borosilicate glass although the harder aluminosilicate glass is sometimes used. Multi-barreled glass of varying dimensions can be purchased from suppliers (e.g. Hilgenberg; http://www.hilgenberg-gmbh.de/). This type of glass seems to be the best for ion-selective microelectrode work. An alternative type of double-barreled glass called "theta" glass can be used; this has a single thin glass wall between the two pre-formed barrels. Adjacent ion-selective barrels may mutually interfere because the thin glass walls at the electrode tip have electrical impedance that may be as low as the impedances of the liquid ion-exchangers so that the measured potential depends on the potential across the glass as well as the potential across the liquid ion-exchanger. This problem is more acute when "theta" glass is used because the final glass partition in the tip is much thinner. Both barrels of glass should have an internal filament to assist with backfilling. Identification of the different barrels can be done by using different diameter glass, marking with a pen, cutting to various lengths or bending the blunt end of one barrel to give an obvious angle. The advantage of each of the latter two methods is that they make it easier to insert Ag wire (see Fig. 2.1). Wear safety glasses at all times when pulling and breaking glass.

Before preparing the ion-selective microelectrode it is important to determine that glass microelectrodes filled with 0.1 M KCl can be used to impale cells and measure stable resting membrane potentials sensitive to metabolic inhibitors (in the usual range for the cell type, in the bathing solution used). An estimate of the tip geometry of the microelectrode is provided by measuring its electrical resistance when filled with KCl, larger tips having lower resistances. For tips of 2–0.1 μm diameter the electrical resistances of ion-selective microelectrodes are usually in the GΩ range, while microelectrodes filled with 0.1 M KCl have 10^3 smaller resistances in the MΩ range. Electrical resistance does depend on the salt concentration of the backfilling solution. The dimensions of the microelectrodes are usually a compromise between obtaining a stable membrane potential and a good calibration response (detection limit).

2.2.3.2 Silanization of glass surface

The inside of the glass micropipettes must be given a hydrophobic coating to allow the formation of a high resistance seal between the glass and the hydrophobic ion-selective membrane. The barrel designated to be ion-selective is heat dried, then silanized by placing a few drops of a solution of 2% (w/v) silanizing agent in chloroform on its blunt open end. There are a range of different silanizing agents which can be used at this concentration but dimethyldichlorosilane or tributylchlorosilane are most common. Care must be taken to ensure that the reagent does not enter the membrane potential-measuring barrel. Beware: silanizing agents are highly corrosive and toxic, protective glasses and gloves must be worn and glass must be treated in a fume hood. The microelectrode is then placed under a heating lamp giving a temperature of 140 °C at the micropipette surface. After 30 min drying the silanizing solution is added and quickly vaporizes, giving the ion-selective barrel a hydrophobic coating. There should be no visible residue remaining in the microelectrode tip before the next step, backfilling.

2.2.3.3 Backfilling

There are actually two steps to backfilling; the first uses a cocktail to form the ion-selective membrane in the microelectrode tip and the second step, usually a minimum of 48 h later, uses an aqueous salt solution to provide contact between this membrane and the Ag/AgCl metal electrode (in the base of the microelectrode holder). Both steps are made much simpler by using filamented glass to make the microelectrodes and can be achieved using a syringe and fine all metal needle.

Electrodes are back-filled with a sensor cocktail containing several different components:

- An ion-selective molecule, sensor or exchanger
- Membrane solvent or plasticizer
- Additives, e.g. lipophilic cation/anion
- A membrane matrix to solidify the ion-selective membrane. This is essential for measurements in cells possessing turgor.

For many ions, the membrane cocktail can be purchased already mixed and it is advisable to start by using the commercial mixture. However, preparing the cocktail from the individual components is cheaper and these can be bought from chemical suppliers. For commercially available liquid membrane cocktails the membrane matrix is not normally included. A matrix is needed if microelectrodes are to be used in plant cells because turgor will displace a liquid membrane from the electrode tip, thereby changing or eliminating the sensitivity to the measuring ion (Miller 1995). The matrix

used is normally a high molecular weight poly(vinyl chloride) (PVC) polymer, but can also include nitrocellulose for additional strength.

2.2.3.4 Cocktail components

The various components of an ion-selective membrane are mixed together to form a sensor cocktail. Commercial cocktails are available pre-mixed for many ions (e.g. the Selectophore® range from Fluka now sold by Sigma; http://www.sigmaaldrich.com/). If a matrix is present, the cocktail is usually dissolved in a solvent such as tetrahydrofuran. If the cocktail does not include a solvent, it can be introduced to the tip of a micropipette for immediate use. Membranes formed from solubilized cocktails are produced by solvent-casting. The mixture is introduced into a micropipette and the solvent is allowed to slowly evaporate to leave a solid or semi-solid membrane at the micropipette tip. The choice and relative proportions of the components of a cocktail determine the properties of the ion-selective membrane. Cocktails are optimized by a process of informed experimental trial and error, adjusting components and proportions until the desired properties are achieved.

Of all of the components, the ion-selective sensor is the main factor determining electrode characteristics (e.g. slope, selectivity, limit of detection); however the plasticizer can alter properties such as lifetime, stability and selectivity. Additionally, membrane additives, such as lipophilic ions, can be used to improve the performance of microelectrodes. Sometimes these additives can introduce changes in ion selectivity, for example the plasticizer can introduce nitrate sensitivity (Cuin et al. 1999). The final optimum cocktail is found by varying the composition of each component to find electrodes with the best performance. Good electrodes should have a low detection limit, a near ideal slope, and a small selectivity coefficient for physiologically important interfering ions. The roles played by each cocktail component are now described in more detail.

Ion-selective sensor. The sensor is the most important component of the membrane in determining electrode characteristics (Miller 1995). Sensor molecules employed in ion-selective membranes may be ion exchangers or neutral or charged carriers. The discovery of the ion-selective ionophores has lead to the development of a large range of sensors for ion-selective microelectrodes. Sensors are now available for a wide-range of cations and anions (see Miller 1995) and improved sensors are always being reported (e.g. for Na^+, Carden et al. 2001).

Plasticizer. The plasticizer forms the bulk of an ion-selective membrane (typically 60–90 wt %), and can substantially influence membrane properties such as selectivity and lifetime (Ammann 1986). The main function of the plasticizer is to solubilize the ion-selective sensor and any lipophilic additives.

Other important properties include lipophilicity, viscosity, and the ability to plasticize the matrix material (if any). Commonly used plasticizers include: dibutyl sebacate, bis(2-ethylhexyl) sebacate and 2-nitrophenyl octyl ether.

Additives. The performance of most cation-selective neutral carrier membranes can be enhanced by the addition of lipophilic additives. The most common additives are alkali metal salts of lipophilic anions such as sodium tetraphenylborate and potassium tetrakis(4-chlorophenyl) borate. These additives introduce mobile cation-exchange sites into the membrane which can produce many useful effects. They reduce or remove any interference from lipophilic anions in the sample, reduce electrode response time, lower the electrical membrane resistance, and improve cation sensitivity and selectivity (Ammann 1986). A lipophilic cation (methyltriphenylphosphonium bromide) has been used to improve the properties of an anion-selective membrane based on a charged carrier (Miller and Zhen 1991).

Matrix. The membrane matrix provides mechanical stability to a liquid membrane. The most widely used matrix is poly(vinyl chloride), but many other compounds have been used, including: silicone rubber, polyurethane, polystyrene, poly(methyl methacrylate), and nitrocellulose. If a microelectrode is to be used for recording from a cell with turgor, the inclusion of a matrix in the membrane is essential.

2.2.4 Calibration and storage

Ion-selective microelectrodes can be calibrated using concentration or activity, although they actually respond to changes in activity (see section 1.2). Furthermore, activity is actually the important parameter for all biochemical reactions. Calibrating with ion activity gives a microelectrode output which can be used directly without any assumptions of the intracellular activity coefficient for the ion. For these reasons the calibration of microelectrodes generally uses solutions which resemble the intracellular environment in terms of interfering ions, and ionic strength. Calibration of pH microelectrodes is easy because standard pH buffers can be used and simply checked with a pH meter. For other types of ion-selective microelectrode, the calibration solutions may need to contain a pH buffer and a background salt solution to give an ionic strength approximately equivalent to that inside the cell. Care must be taken in the choice of these additional ions; they must not give significant interference over the range of measurements. In other words, the microelectrodes must have very small selectivity coefficients for these background ions. Calibration solutions are usually chosen to be approximately 0.14 M ionic strength. There are very few examples of detailed whole cell sap analysis to suggest what an appropriate figure might be, but for giant algal cells this value would seem reasonable (Okihara and Kiyosawa 1988). The use of computer

programs to calculate ion activity and the availability of a wide range of ion-selective macroelectrodes make it easier to prepare calibration solutions for all types of ion-selective microelectrodes. Furthermore, calibration solution recipes have been published for some ion-selective microelectrodes, (Ca^{2+}, Tsien and Rink 1981; Mg^{2+}, Blatter and McGuigan 1988; Na^{+} Carden et al. 2001; NO_3^-; Miller and Zhen 1991). Some calibration solutions use concentration not activity, and also the term "free" ion usually means concentration of unbound ion and not activity, particularly for Ca^{2+} and Mg^{2+}. The calibration of calcium-selective microelectrodes for intracellular measurements requires the use of calcium buffering agents such as EGTA because of the very low concentrations being measured (Tsien and Rink 1981).

Ion-selective microelectrodes can be calibrated in the microscope chamber where intracellular measurements will be made or in a U-shaped glass funnel alongside the microscope. The slope of the calibration curve is temperature sensitive and both calibrations and intracellular measurements should be done at the same temperature. If the temperature of the calibration solutions is 4 °C and the cell is at 20 °C, the slope of the electrode calibration for a monovalent ion will be 55 mV per decade change in activity, not the 58 mV expected at 20 °C.

Curve fitting software such as the Marquardt curve-fitting algorithm within Sigmaplot (SPSS; http://www.spss.com/) can be used to fit the experimental data to an equation of the form:

$$\mathrm{EMF} = \mathrm{P1} + \mathrm{P2} \cdot \log\left(a_i + \mathrm{P3}\right) \tag{2}$$

where P1, P2 and P3 are constants. Equation (1) can be simplified to (2) and it is then apparent that P2 represents the Nernstian slope, s, and that P3 represents $K_{ij}^{pot} \cdot (a_j)^{zi/zj}$. The term K_{ij}^{pot} is defined as $a_i'/(a_j)^{zi/zj}$ and therefore P3 is equivalent to a_i', the activity at the intersection of the two linear portions of the response curve in Fig. 2.2—the IUPAC definition of detection limit (Inczédy et al. 1998). Constants P2 and P3 from Equation (2) can thus be used to determine the slope, detection limit, and selectivity coefficient (if a_j is known) of ion-selective microelectrodes without recourse to graphical techniques.

Ideally, the detection limits for ion-selective microelectrodes should be calculated using calibration solutions approximating to the cytosolic composition. In practice this is not so easy, because our knowledge of the ionic environment within a cell is very limited, although we do have some information on sap collected from giant algal cells (e.g. Okihara and Kiyosawa 1988). The detection limit of some macroelectrodes is very small, with values of around only 10^{-9} M for some types of ion (Bakker and Pretsch 2005). These limits are quoted by chemists developing new types of sensor molecules but the practical limits for microelectrodes are likely to be several orders of magnitude greater because values depend on the tip diameter and interfering ion concentrations. This means that lower detection limits are possible for extracellular measurements where larger tip diameters can be used.

For long-term storage, ion-selective microelectrodes should be stored without backfilling, in a silica-gel dried sealed container in the dark. This can be done in a screw-cap glass jar containing dry silica gel, with the microelectrodes attached to the inner wall using plasticine or Blu-tack (Bostik, Stafford, UK). Some types of ion-selective microelectrodes can be stored this way for several years and will still give a reasonable performance when back-filled.

2.3 Data analysis, interpretation and presentation

The high electrical resistance of ion-selective microelectrodes requires the use of a high input impedance ($>10^{15}$ Ω) electrometer to measure electrode voltages. In contrast, the electrometer output is of much lower impedance and can thus be monitored and recorded using less specialized equipment. The simplest method is to use a chart recorder, but this requires laborious subsequent processing and it is more convenient to collect data via an analogue to digital (A/D) converter connected to a personal computer. Most modern A/D converters are compatible with software that allows real-time display of the recorded data, reproducing the functionality of a chart recorder whilst storing the raw data in a format that can be easily exported to statistical and graphing software. A useful feature of any data collection software is the ability to fit calibration curves and use the fitted parameters to display real-time ion activities as the data are being collected.

Ion-selective macroelectrodes have a lower resistance and can be used with lower input impedance ($\sim 10^{12}$ Ω) devices such as benchtop pH/mV meters. The output from such meters can again be recorded using an A/D converter and PC or alternatively a simple data logger may be used. Connecting a battery-powered amplifier to a data logger creates a portable system. Portable macroelectrodes can be used for extracellular measurements in the field (Miller et al. 2003) and allow uptake studies to be made in controlled-environment conditions rather than the laboratory.

One point regarding statistical analysis of data concerns the calculation of mean values. These should be calculated using the data which is distributed normally, that is using the log activity or output voltages not the actual activities (Fry et al. 1990). Therefore, when mean activity value is used it can only be expressed within 95% confidence limits, whereas –log [activity] can be given standard errors or standard deviations.

When measuring changes in intracellular ion concentrations, artifacts can be caused by the differential response times of the two barrels; the ion-selective barrel usually has a slower response time than the membrane potential-sensing barrel. Response of the membrane-potential barrel is almost instantaneous whilst that of the ion-selective is usually in the order of 5–20 s depending on the measured activity (Fluka 1996). As ion activity is calculated from the voltage difference between the two barrels, an incorrect activity can

be reported for this time, limiting detection of rapid changes in ion activity. This can be corrected for when the response time of the electrode is known (Sanders and Slayman 1982).

2.4 Finding problems with ion-selective microelectrodes and a comparison with other methods

2.4.1 Troubleshooting guide

The best approach is to solve problems by a process of elimination. Firstly, establish whether a problem occurs in the circuitry or is specific to the ion-selective microelectrodes. The circuitry can be tested by putting a broken-tipped KCl-filled microelectrode in place of the ion-selective microelectrode. The broken-tipped should give a stable zero output. It may be necessary to recoat Ag/AgCl contact in the half-cell or there may be a wiring problem. Noisy recordings can be caused by poor earthing or air bubbles in backfilling solutions. If the circuitry has no problems then the ion-selective microelectrode must be the cause. When the ion-selective microelectrode does not respond to the calibration solutions then the membrane can be checked by deliberately breaking the tip to expose a larger area of ion-selective membrane. Breaking the tip can displace the ion-selective membrane from the tip so it is important to measure the resistance to check it is still in the GΩ range. If the broken tip gives a good response to changes in ion activity then the problem is independent of the composition of the membrane. When the microelectrode tip diameter becomes too fine the output from the ion-selective electrode will no longer respond to changes in ion activity.

Several criteria for acceptable measurements can be defined. After impalement the ion-selective microelectrode should be recalibrated and should give a very similar response to that shown before the cell impalement particularly at activities similar to those measured in vivo. Sometimes the detection limit of the ion-selective microelectrode has changed but provided the measurement was on the linear response range of the electrode calibration curve this is not usually a reason to disregard the result. The performance of the ion selective microelectrode can even improve with the detection limit actually becoming lower. For this reason, it may be best to quickly impale a cell with a new tip before calibrating prior to measuring the activity in the cell. A comparison between the electrical resistance of the ion-selective microelectrode before and after impalement provides a good indicator of whether the tip will recalibrate. If the resistance decreases below 1 GΩ, the ion-selective membrane has probably been displaced during impalement and the electrode will not recalibrate. Throughout the recording the state of the cell can be assessed by monitoring the membrane potential (which should remain stable unless deliberately perturbed) or processes such as cytoplasmic streaming.

In plant cells, identifying in which internal cell compartment (cytoplasm or vacuole) the microelectrode tip is located can be a problem for some ions and it may be necessary to grow the plant under conditions in which two populations of measurements can be identified. Alternatively, a triple-barreled microelectrode can be used where one barrel is pH or Ca^{2+} selective. Large gradients of these two ions are known to exist across the tonoplast, with the cytoplasm maintained at relatively constant values (pH 7.2, Ca^{2+} 100 nM) so compartment identification is possible. Another approach is to use tissues where the two major cell compartments can be identified under the microscope, e.g. root hairs, or cell cultures which have no large vacuole. However, identifying which compartment the electrode is in can still be problematic, particularly if the electrode indents the tonoplast but does not penetrate it.

Leakage of salts from the tip of the membrane potential-sensing barrel has been reported (Blatt and Slayman 1983), and this may particularly be a problem in small cells. Diffusion of ions from the membrane potential-sensing barrel could give high local gradients of ions at the tip of a double-barreled microelectrode. It may be important to try measurements where different types of backfilling solution are used in the reference barrel. Large leaks should affect membrane potential and monitoring this should indicate possible problems.

The Ag/AgCl junctions of electrodes have been found to respond directly to light (Janz 1961) and problems with obtaining stable recordings can result from a poor chloride coating on the Ag of the half-cell. For stable recording, both the metal electrode part of half-cells and the Ag wire contacts (see Fig. 2.1) require regular re-coating with AgCl.

A further possible problem can arise when using ion-selective microelectrodes with inhibitors. Some inhibitor chemicals are highly lipophilic and will readily dissolve in the ion-selective membrane. These chemicals can poison the membrane but this will be demonstrated during the recalibration of the ion-selective microelectrode.

A few practical points:

- Handle microelectrodes with forceps.
- When dispensing THF pour a few ml from the stock bottle into a clean glass beaker, after first rinsing the beaker with a little freshly-dispensed THF. Cover the beaker with Parafilm, then dispense further THF using a glass syringe and needle by piercing the film cover with the needle, this helps to reduce solvent vapor and prevents contamination of THF.
- If more than one type of cocktail is used, employ a different syringe for each type of cocktail. It is best to dedicate a syringe for one particular cocktail only, and thus avoid any contamination by other ion sensors.
- Calibrate starting with the highest concentration, and calibrate only in the range in which you expect to be working. There is no point in exposing electrodes unnecessarily to low ion concentrations as most types of ion-selective membrane respond badly to long exposures at very low concentrations.

2.4.2 Comparison with other methods

No method is ideal for measuring transmembrane ion gradients as all involve some perturbation of the tissue that may directly influence the parameters being measured. Extracellular measurements and biological samples can use ISEs. A recent review of various analytical methods for measuring trace elements in biological samples compared potentiometry (ISEs), voltammetry, atomic spectrometry (e.g. ICP-MS, inductively coupled plasma mass spectrometry) and nuclear techniques (Brown and Milton 2005). For example, ICP-MS and ISE measurement of lead concentrations in the same samples gave excellent agreement. The authors reported that ISEs compared well and provided moderate throughput at a low cost but the detection limits were higher than most other methods, typically 10^{-9} M compared with 10^{-11} M.

There are several different non-destructive methods for measuring transmembrane ion gradients. Ion-selective microelectrodes have an advantage over most other methods because they can be used to report the ion activities in single cells and within the vacuole and cytoplasm. Compartmental tracer ion efflux analysis has frequently been used to measure the cytoplasmic concentrations of ions within living cells (MacRobbie 1971). This technique depends on the fact that the labeled ion or compound is in equilibrium with the unlabelled form in all parts of the cell. The method treats all the different tissues of an organ like the root as a single entity even though the transport properties of each may be different. For the calculation of the intracellular ion concentrations, it is necessary to make assumptions about the volume of each cellular compartment (see Miller and Smith 1996). Dyes can be used to measure intracellular ion concentrations or activities but they first require some method for introducing the dye into the cell. Microinjection, ionophoresis (using electrical current flow to carry charged molecules) and in some cases the cell's transport systems can be used to take up ion reporter dyes into cells (Negulescu and Machen 1990). Once inside the cell, dyes are usually used to monitor ion concentrations in the cytoplasm. The presence of the dye in the cell may influence normal cell processes. In addition, the dyes themselves must bind the ion being detected to function as a reporter and may therefore be influencing the parameter that they are measuring. Nuclear magnetic resonance can also be used to measure transmembrane ion gradients of some ions (e.g. pH and phosphate), but is more commonly used for metabolite molecules (reviewed by Ratcliffe and Shachar-Hill 2001).

Plants can be genetically engineered to express foreign proteins that are sensitive to changes in the local ion environment and these can be used to measure in both the apoplast and the cytoplasm (e.g. Gao et al. 2004). The quantitative use of these reporter proteins requires in vitro calibration and to obtain sufficient signal for the detection system expression is driven by a strong promoter (e.g. CaMV 35S). The use of this promoter gives expression of the reporter protein in many different types of tissue. These proteins, like

the dyes, require physical interaction with the ion and their presence in the cell may cause modifications to normal cellular function.

Energy dispersive X-ray microanalysis (EDAX) is a destructive method for measuring intracellular ion concentrations and the method requires chemical fixation of the tissue prior to the measurement. This treatment may lead to changes in transmembrane ion gradients before the fixation is complete. The precise area of tissue sampled for this analysis is difficult to control and so compartmental assignment of the measurement can be difficult. The method gives total elemental analysis of the tissue and for many ions this figure may be very different from the more biologically relevant value, the ion activity. Another example of a destructive technique is cell fractionation; this involves breaking the tissue into protoplasts and then vacuoles and measuring the concentrations of ions in each fraction. Unfortunately, the preparation of the cell fractions requires incubation for several hours in tissue degrading enzymes that might lead to changes in transmembrane ion gradients.

There are very few comparisons of techniques for intracellular measurements. Intracellular ion-selective microelectrode measurements of vacuolar nitrate have been compared with whole tissue analysis and single cell sap sampling methods (Zhen et al. 1991). In a more recent paper, nitrate-selective microelectrode measurements of cytosolic nitrate were compared with values obtained using NMR on the same tissue (Radcliffe et al. 2005). In both these examples, there was good agreement between the different methods employed. The best approach to making intracellular measurements of ion concentrations is to use several different methods to obtain a consensus value.

2.5 Transport and transmembrane ion gradients

Ion-selective microelectrode data give information as to both intracellular activities and the electrical gradients across the plasma membrane and tonoplast. This information on the intracellular electrochemical gradients can be used to determine the likely mechanisms of transport across cell membranes. One example is the use of pH and nitrate-selective microelectrode measurements to determine the thermodynamics of nitrate transport systems across the plasma membrane (Miller and Smith 1996) and tonoplast (Miller and Smith 1992). Compartmental measurements of the transmembrane ion gradients of NO_3^- and H^+ enabled the energetic feasibility of different co-transporter stoichiometries to be calculated. This type of measurement can also be used to show the activity of proton-coupled transport systems at the plasma membrane as an acidification of cytosolic pH can be measured when nitrate is supplied outside the cell.

Figure 2.3 shows the distribution of NH_4^+ in an internodal cell of the freshwater alga *Chara corallina* measured using NH_4^+-selective microelectrodes (Wells and Miller 2000). Published data for vacuolar and cytoplasmic pH

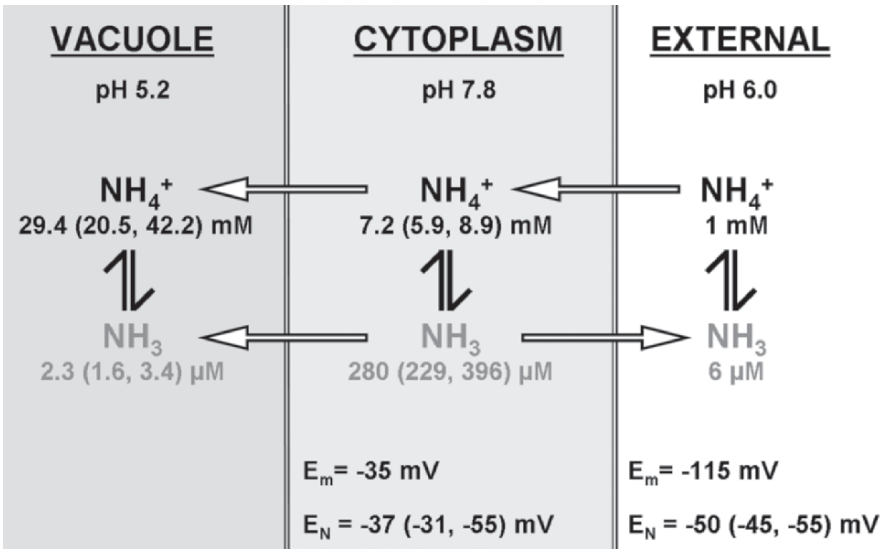

Fig. 2.3. Diagrammatic representation of the transmembrane pH, NH_3 and NH_4^+ gradients in an internodal cell of *Chara corallina*. E_N is the Nernstian equilibrium voltage for the measured NH_4^+ distribution. *Arrows* show direction of the chemical gradient for NH_3 and the electrochemical gradient for NH_4^+. Microelectrode and derived data are given as means (1 SD range). Data from Wells and Miller (2000 and unpublished)

allows a calculation of the compartmental concentrations of NH_3 using the Henderson–Hasselbalch equation. Microelectrodes also measure the transtonoplast and plasma membrane potentials, allowing the mechanism of transport of the two forms of ammonium to be modeled. The Nernstian equilibrium voltage for the observed distribution of NH_4^+ across the plasma membrane is –50 mV, lower than the –115 mV measured, suggesting the passive uptake of NH_4^+ at this external concentration. Similarly, the observed vacuolar levels of NH_4^+ may be explained by passive transport driven by the transtonoplast potential. Calculated NH_3 concentration based on the experimental data is higher in the cytoplasm than either the vacuole or the external solution. NH_3 is freely diffusible across biological membranes and passive diffusion of NH_3 along this concentration gradient will thus be out of the cytoplasm into both the vacuole and the external solution.

Ion-selective microelectrodes can be used to directly measure the ion concentrations in other biological situations such as depletion from a nutrient solution for net uptake studies or on very small samples such as plant exudates. Micro- and macro-electrodes can also be used directly in soil where they provide a direct measure of the nutrient concentration that is available at the surface of plant roots and allow mapping of spatial and temporal nutrient heterogeneity. Soil electrode data can also be used to shed light on important soil

processes such as N mineralization, which can be quantified by the simultaneous use of nitrate- and ammonium-selective electrodes. Combining such field data with laboratory measurement of apoplastic and intracellular ion concentrations allows models of transport to be developed.

Acknowledgements. The authors were funded by the Department of Environment Food and Rural Affairs (AR0910) and the EU (HPRN-CT-2002–00247) and wish to thank Susan Smith for her help with the manuscript. Rothamsted Research is grant-aided by the Biotechnology and Biological Sciences Research Council (BBSRC) of the UK.

References

Ammann D (1986) Ion-selective microelectrodes, principles, design and application. Springer, Berlin Heidelberg New York

Bakker E, Pretsch E (2005) Potentiometric sensors for trace level analysis. Trends Anal Chem 24:199–207

Blatt MR (1991) A primer in plant electrophysiological methods. In: Dey PM, Harbourne JB (eds) Methods in plant biochemistry, vol 6. Academic Press, San Diego, pp 281–356

Blatt MR, Slayman CL (1983) KCl leakage from microelectrodes and its impact on the membrane parameters of a non-excitable cell. J Memb Biol 72:223–234

Blatter LA, McGuigan JAS (1988) Estimation of the upper limit of the free magnesium concentration measured with Mg-sensitive microelectrodes in ferret ventricular muscle: (1) use of the Nicolsky–Eisenmann equation and (2) in calibrating solutions of the appropriate concentrations. Magnesium 7:154–165

Brown RJC, Milton MJT (2005) Analytical techniques for trace element analysis: an overview. Trends Anal Chem 24:266–274

Carden DE, Diamond D, Miller AJ (2001) An improved Na^+-selective microelectrode for intracellular measurements in plant cells. J Exp Bot 52:1353–1359

Coster HGL (1966) Chloride in cells of *Chara australis*. Aust J Biol Sci 19:545–554

Cuin TA, Miller AJ, Laurie SA, Leigh RA (1999) Nitrate interference with potassium-selective microelectrodes. J Exp Bot 50:1709–1712

Delessert C, Wilson IW, van der Straeten D, Dennis ES, Dolferus R (2004) Spatial and temporal analysis of the local response to wounding in *Arabidopsis* leaves. Plant Mol Biol 55:165–181

Fluka Chemicals (1996) Selectophore® Catalogue: 152

Fry CH, Hall SK, Blatter LA, McGuigan JAS (1990) Analysis and presentation of intracellular measurements obtained with ion-selective microelectrodes. Exp Physiol 75:187–198

Gao D, Knight MR, Trewavas AJ, Sattelmacher B, Plieth C (2004) Self-reporting *Arabidopsis* expressing pH and $[Ca^{2+}]$ indicators unveil ion dynamics in the cytoplasm and in the apoplast under abiotic stress. Plant Physiol 134:898–908

Henriksen GH, Bloom AJ, Spanswick RM (1990) Measurement of net fluxes of ammonium and nitrate at the surface of barely roots using ion-selective microelectrodes. Plant Physiol 93:271–280

Inczédy J, Lengyel Y, Ure AM (1998) Compendium of analytical nomenclature: definitive rules 1997, 3rd edn. Blackwell Science, Oxford

Janz GJ (1961) Silver-silver halide electrodes. In: Ives DJG, Janz GJ (eds) Reference electrodes: theory and practice. Academic Press, New York, pp 218–220

Kochian LV, Shaff JE, Kuhtrieber WM, Jaffe L, Lucas WJ (1992) Use of extracellular, ion-selective, vibrating microelectrode system for the quantification of K^+, H^+ and Ca^{2+} fluxes in maize roots and maize suspension cells. Planta 188:601–610

MacRobbie EAC (1971) Fluxes and compartmentation in plant cells. Annu Rev Plant Physiol 22:75–96

Miller AJ (1995) Ion-selective microelectrodes for measurement of intracellular ion concentrations. Methods Plant Cell Biol 49:273–289

Miller AJ, Smith SJ (1992) The mechanism of nitrate transport across the tonoplast of barley root cells. Planta 187:554–557

Miller AJ, Smith SJ (1996) Nitrate transport and compartmentation in cereal root cells. J Exp Bot 47:843–854

Miller AJ, Zhen R-G (1991) Measurement of intracellular nitrate concentration in *Chara* using nitrate-selective microelectrodes. Planta 184:47–52

Miller AJ, Cookson SJ, Smith SJ, Wells DM (2001) The use of microelectrodes to investigate compartmentation and the transport of metabolized inorganic ions in plants. J Exp Bot 52:541–549

Miller AJ, Wells DM, Braven J, Ebdon L, Le Goff T, Clark LJ, Whalley WR, Gowing DJG, Leeds-Harrison PB (2003) Novel sensors for measuring soil nitrogen, water availability and strength. Proceedings of the British Society for Crop Protection International Congress, Glasgow, pp 1107–1114

Negulescu PA, Machen TE (1990) Intracellular ion activities and membrane transport in parietal cells measured with fluorescent dyes. In: Fleischer S, Fleischer B (eds) Methods in enzymology, vol 192. Academic Press, San Diego, pp 38–81

Okihara K, Kiyosawa K (1988) Ion composition of the Chara internode. Plant Cell Physiol 29:21–25

Radcliffe SA, Miller AJ, Ratcliffe RG (2005) Microelectrode and ^{133}Cs NMR evidence for variable cytosolic and cytoplasmic nitrate pools in maize root tips. Plant Cell Environ 28: 1379–1387

Ratcliffe RG, Shachar-Hill Y (2001) Probing plant metabolism with NMR. Annu Rev Plant Physiol Plant Mol Biol 52:499–526

Sanders D, Slayman CL (1982) Control of intracellular pH. Predominant role of oxidative metabolism, not proton transport, in the eukaryotic microorganism *Neurospora*. J Gen Physiol 80:377–402

Tsien RY, Rink TJ (1981) Ca^{2+} selective electrodes: a novel PVC-gelled neutral carrier mixture compared with other currently available sensors. J Neurosci Meth 4:73–86

Walker DJ, Smith SJ, Miller AJ (1995) Simultaneous measurement of intracellular pH and K^+ or NO_3^- in barley root cells using triple-barreled, ion-selective microelectrodes. Plant Physiol 108:743–751

Wells D, Miller AJ (2000) Intracellular measurement of ammonium in *Chara corallina* using ion-selective microelectrodes. Plant Soil 221:105–108

Wildon DC, Thain JF, Minchin PEH, Gubb IR, Reilly AJ, Skipper YD Doherty HM, O'Donnell PJ, Bowles DJ (1992) Electrical signalling and systemic proteinase inhibitor induction in the wounded plant. Nature 360:62–65

Zhen R-G, Koyro H-W, Leigh RA, Tomos AD, Miller AJ (1991) Compartmental nitrate concentrations in barley root cells measured with nitrate-selective microelectrodes and by single-cell sap sampling. Planta 185:356–361

3 Non-Invasive Microelectrode Ion Flux Measurements In Plant Stress Physiology

Sergey Shabala

3.1 Introduction: membranes and plant stress responses

Plant membranes underlie many essential cell biological processes including nutrient acquisition and compartmentation, pH and ionic homeostasis, turgor generation, metabolite distribution and waste excretion, energy transduction and signaling. According to Ward (2001), 43% of over 25,000 protein sequences in the *Arabidopsis* genome have at least one transmembrane spanning (TMS) domain, with 18% proteins having ≥ 2 TMS domains and thus associated with cellular membranes. Recent progress in electrophysiology and molecular genetics has revealed the crucial role of plasma membrane transporters in perception and signaling in response to virtually every known environmental factor (Zimmermann et al. 1999). Changes in plasma membrane potential or modulation of ion flux are amongst the earliest cellular events in response to light, temperature, osmotic stress, salinity, hormonal stimuli, elicitors and mechanical stimulation in many organisms (Blumwald et al. 1998; Sanders et al. 1999; Zimmermann et al. 1999; Spalding 2000; Knight and Knight 2001). For many, if not all the stresses mentioned above, the receptors involved were suggested to be located at one of the cellular membranes.

In addition to hosting various receptors mediating plant–environment interactions, membrane transporters always act as the ultimate effectors, enabling plant adaptive responses. In the case of salt tolerance, this may be by excluding toxic Na^+ from the cytosol via either the SOS1 plasma membrane Na^+/H^+ antiporter (Zhu 2003) or by compartmentalizing it into the vacuole by the NHX tonoplast Na^+/H^+ antiporter (Apse et al. 1999). In the case of Al^{3+} toxicity, the adaptive response includes activation of anion channels responsible for malate efflux and changes in the rhizosphere pH (Ryan et al. 2001). Osmotic adjustment includes rapid increase in the uptake of inorganic ions (Shabala and Lew 2002), while plant adaptive responses to low temperature include dramatic changes in membrane fluidity (Murata and Los 1997). Such a central role of plant membranes and membrane transport processes in plant adaptive responses to environmental conditions makes them important targets for genetic manipulations aimed to improve tolerance to a particular

School of Agricultural Science, University of Tasmania, Private Bag 54, Hobart, Tasmania 7001, Australia (e-mail: Sergey.Shabala@utas.edu.au)

Plant Electrophysiology – Theory & Methods (ed. by Volkov)

stress. To enable this, causal links between membrane-transport processes and other metabolic or physiological processes in the cell need to be understood.

Gaining such an understanding is not an easy task. It is complicated not only by the large number of transporters involved (for cations, 46 unique families are known, containing approximately 880 members in *Arabidopsis*; Maser et al. 2001), but also by the myriad of interactions and cross-talk between various transporters and signaling components. Over the last 2 decades, various state-of-the-art molecular and biophysical techniques (such as patch-clamp or fluorescence imaging) have been used to reveal some of these interactions. These techniques have been the subject of many comprehensive reviews and thus are mentioned only briefly here. However, at the same time, the inevitable consequence of such "in-depth" approaches was a decrease in the physiological reality of the transporters' environment (Tester 1997). There are many reports (some of which are discussed in section 4) showing that activity of a particular transporter differs dramatically when expressed in a heterologous system compared with in planta conditions. This makes it very difficult (and often even impossible) to transfer the results obtained by these advanced techniques to *real* plants in their natural habitats. The more advanced our study, the bigger is the gap between physiologists/molecular biologists and the agronomists interested in plant behavior in the field.

Since the mid-1990s our laboratory has pioneered application of non-invasive ion flux measuring (the MIFE) technique in plant stress physiology. As shown in the following sections, this technique provides a unique possibility to link genetic/genomic data to cellular physiological behavior. Some of its key features (e.g. non-invasiveness, high spatial and temporal resolution) allow us to establish and quantify causal links between membrane-transport processes and other metabolic or physiological processes in the cell in almost natural conditions. In this context, the MIFE technique may be considered as a "bridging element" between molecular biologists and whole plant physiologists or agronomists.

The aim of this review is to show that in situ measurements of net ion fluxes from plant cells and tissues using the MIFE technique can provide insights into the functional genomics of plants and will significantly increase our understanding of the function of specific genes mediating plant adaptive responses to the environment.

3.2 Basic techniques for studying membrane transport in plants

3.2.1 Comparative analysis of basic techniques

A large number of techniques are available to study ionic relations and transport of nutrients and ions across cell membranes. They range from whole-plant methods (depletion experiments, radioactive tracers) to those applicable

at cellular (fluorescence microscopy; intracellular microelectrode measurements) or molecular (patch-clamp studies on single channels) levels. Their pros and cons are briefly summarized below.

1. *Destructive sampling.* At the whole-plant level, basic chemical analysis of the elemental content in plant samples is still the most popular and widely used method. An appropriate plant sample is collected, dried, ground and digested in a strong acid (Handson and Shelley 1993). Then the elemental content of plant sample is analyzed using an appropriate technique (such as ICP-AES or AA spectroscopy; X-ray fluorescence spectroscopy, flame photometry). The advantage of this method is its simplicity. The major problem is a very low time resolution (usually several days or more), as there is an obvious limit on how often the samples may be taken. As a result, this method is mostly used to address some basic agronomical issues, rather than for fundamental physiological research.
2. *Depletion experiments.* This is another basic method used for many decades for studies on plant nutrition. Plants are grown hydroponically, and the rate of nutrient uptake is determined by periodically taking small volumes of the growth solution for chemical analysis (as above). Once again, the method has very low time resolution. The latter may be partially resolved by using conventional ion-selective electrodes placed in the growth solution to monitor concentration changes. Even then, however, the sensitivity of the method is rather low.
3. *Radioactive tracers.* Various radioisotopes have been successfully used to study membrane-transport processes in plants (Abbott and Fraley 1991; Tester and Davenport 2003). The method is relatively straightforward and allows quantification of the unidirectional flux of a specific ion. The main limitation is the spatial resolution of the method, as well as a relatively limited number of ions which can be studied.
4. *Nuclear magnetic resonance spectroscopy.* NMR spectroscopy is a non-destructive tool enabling quantitative analysis of metabolites from cell suspensions, tissues and whole plants (Ratcliffe 1997). As NMR detects atoms with magnetic moments only, not every nutrient can be studied. Taking nitrogen metabolism as an example, ^{14}N is naturally abundant (99.6%) but not useful for NMR studies due to extremely broad signals for almost all nitrogenous metabolites (Mesnard and Ratcliffe 2005). Therefore, plant samples have to be enriched with ^{15}N before analysis, which significantly complicates the procedure. Again, a low time resolution (several hours) is a problem.
5. *Fluorescence microscopy.* Ion imaging by fluorescence microscopy is based on fluorescence probes that accumulate inside cells and change their fluorescence properties when bound to distinct ions (Roos 2000). There is a relatively wide range of commercially available probes (both ratiometric and single-wavelength), enabling quantification and kinetic studies of changes in H^+, Ca^{2+} and, to lesser extent, K^+ and Mg^{2+} in plant cells. The method has high temporal and spatial (especially when confocal microscopy is used)

resolution and, being non-invasive, has a great potential for studying cellular adaptive responses to the environment. Major pitfalls include probe loading, photobleaching, interaction of ion probes with cell metabolism, difficulties of calibration, poor discrimination of some probes (e.g. between K^+ and Na^+) and the limited range of ions that can be measured by this technique (Roos 2000).

6. *Single cell sampling.* This technique has been developed by D. Tomos and co-workers as an extension of pressure-probe measurements at the single cell level (Tomos and Leigh 1999). By using a fine oil-filled glass microcapillary mounted on a micromanipulator, the cell sap is sampled from individual plant cells. Ion concentrations in these samples can then be analyzed using a range of physical and chemical methods such as X-ray microdroplet analysis or capillary electrophoresis (Tomos and Leigh 1999). The method has very high spatial resolution. Two main obstacles limiting its application are (i) the issue of mixing of vacuolar and cytosolic content and (ii) impossibility of kinetics study by this method.
7. *Patch-clamp.* The patch-clamp technique is the most advanced method of studying ion-transport processes at the molecular level (Tester 1997) and can provide comprehensive information about the kinetics and properties of specific transport proteins at cell membranes. The method is based on a tight attachment of a plasma membrane patch to a microelectrode glass pipette, thus establishing a so-called "giga seal" (with up to 10^9 Ω resistance), enabling measurements of very low (pA range) currents through the prepared isolated plasma membrane patch in response to a series of voltage clamps. Ultimately, membrane ion channels may be characterized with respect to the ion they conduct (and their specificity for that ion), the conductance value of their open state, their gating properties, and their sensitivity to various pharmacological agents (Garrill and Davies 1994). However, patch clamp is rather sophisticated method that requires high level technical and data interpretation skills. Quite often, conditions that enable seal formation are rather non-physiological (e.g. high amount of Ca^{2+} in the pipette). As a result, it is not always possible to extrapolate patch-clamp data onto ion channel behavior in *planta*.
8. *Impaled microelectrodes.* Traditionally, microelectrode impalement has been applied to measure plasma membrane potential (MP). Significant membrane depolarization is observed in response to various environmental stresses such as salinity (Shabala et al. 2003), chilling (Clarkson et al. 1988), acidity (Babourina et al. 2001) and hypoxia (Zhang et al. 1992). As transport of all nutrients is directly or indirectly linked to MP values, the more substantial is the membrane depolarization, the more severe is the disturbance to cell ionic homeostasis. A more sophisticated method involves a microelectrode tip being filled with a specific ionophore, sensitive to a particular ion (Miller et al. 2001). As the reference MP electrode also has to be impaled alongside the ion-selective microelectrode, multibarreled electrodes are often used for these purposes (Carden et al. 2003).

This technique thus makes it possible to monitor changes in cytosolic ion homeostasis and therefore provide answers to some fundamental questions about ionic mechanisms underlying stress tolerance in plant cells. However, this technique is extremely technically and skill demanding, and thus not likely to be used routinely.

3.2.2 Non-invasive ion flux measurements

In recent years, non-invasive microelectrode ion flux measurements have become a popular tool in studying adaptive responses of plant cells and tissues to a large number of abiotic stresses. A couple of dozen laboratories around the world employ this technique, and their number is growing.

The idea of using slowly vibrating ion-selective microprobe to measure non-invasively net ion fluxes was first proposed by B. Lucas (Lucas and Kochian 1986). The microelectrodes were proposed to measure ion concentration *gradients* (strictly, electrochemical potential differences), between two positions in solution outside the organism tissues, and to use those gradients to calculate the *net fluxes* of ions in question crossing the membrane. The first rigorous test of the theory was performed on corn roots to measure the stoichiometry of H^+ and K^+ fluxes (Newman et al. 1987). The National Vibrating Probe Facility at Woods Hole, Mass., USA adapted the vibrating probe to include ion flux measuring capability (Smith 1995). An alternative system, named MIFE (*M*icroelectrode *I*on *F*lux *E*stimation), was developed, at about the same time, by I. Newman at the University of Tasmania in Australia (Newman 2001). Since the mid 1990s, MIFE has been successfully applied to the study of various aspects of membrane-transport processes in plants and protoplasts derived from plant tissue (Newman's and Shabala's groups) resulting in nearly 50 publications. Recently, the MIFE technique was successfully used to measure kinetics of ion fluxes from bacterial membranes (Shabala et al. 2001a). Several alternative systems have been also designed elsewhere (e.g. Shipley and Feijo 1999); some of them being commercially available. Several papers in this book provide further specific details on some of these systems.

There are at least five major features that, taken together, provide a significant advantage of the MIFE approach over other methods for ion flux measurements. These include:

1. *Non-destructiveness.* In contrast to many other methods, the MIFE (or other similar) technique allows in-situ measurements of net ion fluxes, in physiologically "realistic" conditions.
2. *High spatial resolution.* The electrode tip is several (typically 2–3) μm in diameter, which makes it possible to measure net ion fluxes from single cells (Babourina et al. 2000; Shabala et al. 2001b) or protoplasts derived from plant cells (Shabala et al. 1998; Tyerman et al. 2001). Moreover, for some ionophores with high signal-to-noise ratio (such as H^+), the electrode

tip diameter can be further reduced to 0.8–1.0 μm. As a result, the cell surface can be "mapped" (Shabala et al. 1998; Tegg et al. 2005), providing information about spatial distribution and functional expression of specific ion transporters.

3. *High temporal resolution.* The "default" MIFE settings assume electrode movement with 10 s period. This could be further reduced without difficulty to 2 or 3 s in some cases. Such high temporal resolution is especially crucial in studying rapid signaling events at plant membranes. Most other non-invasive techniques operate on a time scale at least 1 order of magnitude slower. This gives the MIFE technique a unique opportunity to provide insights into very early (and fast) events associated with plant responses to environmental changes.
4. *Duration of measurements.* As the technique is non-invasive, its application is limited essentially only by the lifetime of the ion-selective electrode (typically 15–20 h). Moreover, electrodes may be easily replaced, and measurements resumed after only a few minutes break. None of the other techniques of the same time resolution (e.g. patch-clamp or fluorescence imaging) provide this opportunity.
5. *Simultaneous measurements of several ions.* The possibility of measuring kinetics of fluxes of several ions simultaneously, and essentially at the same spot, is important in understanding the underlying ionic mechanisms of cell adaptive responses. By assessing stoichiometry ratios between various ions, valuable information about the membrane transporters involved can be gained.

3.3 MIFE technique for non-invasive ion flux measurements

3.3.1 Theory

The theory of non-invasive MIFE ion flux measurements was reviewed in detail by Newman (2001). In this section, I will only reiterate some of its basic principles.

Briefly, if an ion is taken up by living cells, its concentration in the proximity of the cell surface will be lower than that further away. Vice versa, if the ion is extruded across the plasma membrane, there will be a pronounced electrochemical potential gradient directed away from the cell or tissue surface (Fig. 3.1). The principle of the MIFE technique is in measuring this electrochemical potential gradient by slow square-wave movement of ion-selective electrode probes between two positions, close to (position 1), and distant from (position 2) the sample surface (Fig. 3.1). At each position, electrode voltage is recorded and then converted into approximate concentration using the calibrated Nernst slope of the electrode. It is assumed that convection and water uptake are negligibly small and unstirred layer conditions are met (Newman 2001).

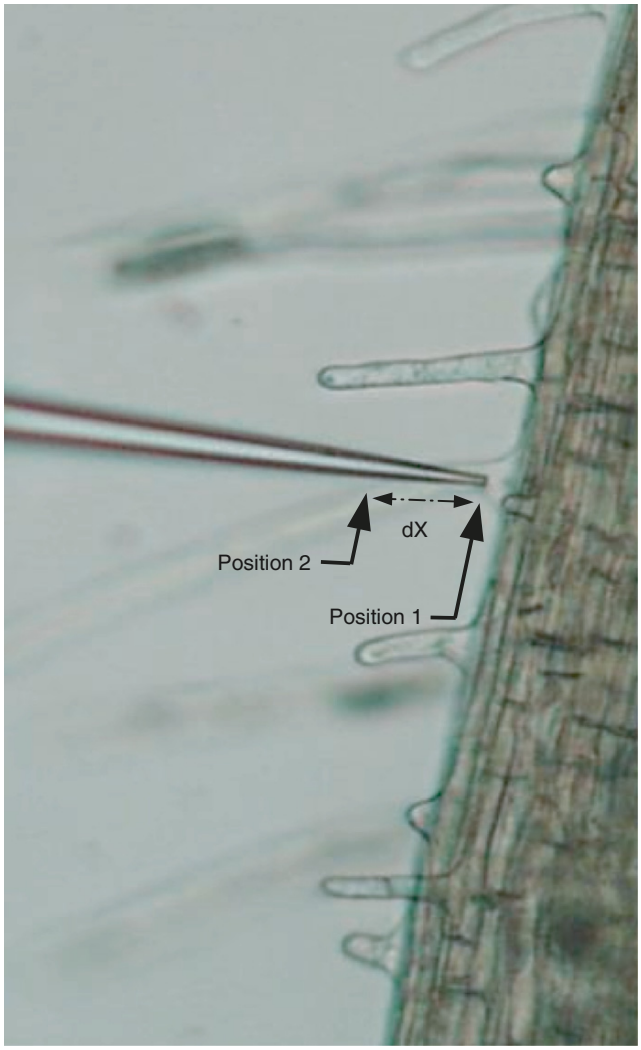

Fig. 3.1. Basic principles of the MIFE ion flux measurement. The ion-selective microelectrode is moved in a square-wave manner between two positions near the root surface. A voltage gradient (dV) is measured by the electrometer between two positions over the travel range dX

Net fluxes of specific ions (mmol m^{-2} s^{-1}) can then be calculated from the measured voltage gradient near the surface. The magnitude of the flux is strongly dependent on the tissue geometry, determining ion diffusion profiles. In the simplest case of planar diffusion (such as from plain leaf surface), the following equation is used (Newman 2001):

$$J = cuz\,Fg\,(dV/dx),$$

where c is ion concentration (mol m^{-3}); u is the ion mobility (m s^{-1} per Newton mol^{-1}); z is the ion's valence; F is the Faraday number (96,500 °C mol^{-1});

g is a factor found from the measured Nernst slope for the electrode during calibration; dV is the voltage difference measured by the electrometer between the two positions (V); dx is the distance between two positions (m).

For cylindrical geometry (e.g. root surface) the radius of the cylinder (r) should be taken into account. This is done by replacing dx in the implementation of the equation above by

$$dx = r^2\left[1/(r + x) - 1/(r + x + dx)\right].$$

For spherical geometry (e.g. protoplast)

$$dx = r \ln\left[(r + x + dx)/(r + x)\right].$$

3.3.2 MIFE hardware

The MIFE setup is built around the microscope system with long distance objectives. There are several basic configurations of the MIFE system used in our laboratory. When fluxes are to be measured from small specimens (such as single cells; protoplasts; bacterial monolayers), an inverted microscope is used. The ion-selective electrodes are mounted on a multi-manipulator providing 3-dimensional fine positioning of the electrode tips near the specimen surface. The manipulator is attached to the stepper motor-driven 3-dimensional hydraulic micromanipulator, enabling the square-wave electrode movement to measure the electrochemical potential of the ions at two positions in solution close to a tissue surface.

The measured specimen is immobilized at the bottom of the open type experimental chamber. The chamber is placed on the microscope stand, and electrode holders are positioned at an angle of 30° to the microscope stand plane. The standard non-polarizing Ag/AgCl reference electrode is positioned in the chamber. The electrodes oscillate (usually at 0.1 Hz), between two positions, close (usually 10–20 μm) and more distant (40–50 μm) from the cells, driven by the computer-controlled stepper motor. The voltage output from the electrodes is amplified by the MIFE electrometer and digitized using an analogue-to-digital interface card on an IBM-compatible PC. The card also controls the stepper motor of the manipulator and is used for offset adjustment of the four-channel electrometer.

The DOS-operated CHART (University of Tasmania, Hobart, Australia) software allows automated and interactive real-time control of the amplifier configuration and the micromanipulator while the data is being collected and written to disk (Shabala et al. 1997). The recorded voltage traces are displayed on the screen in a real time scale (Fig. 3.2), with a possibility of expanding or contracting some selected data segment without interrupting the measurements. More details are available at http://www.mife.com.

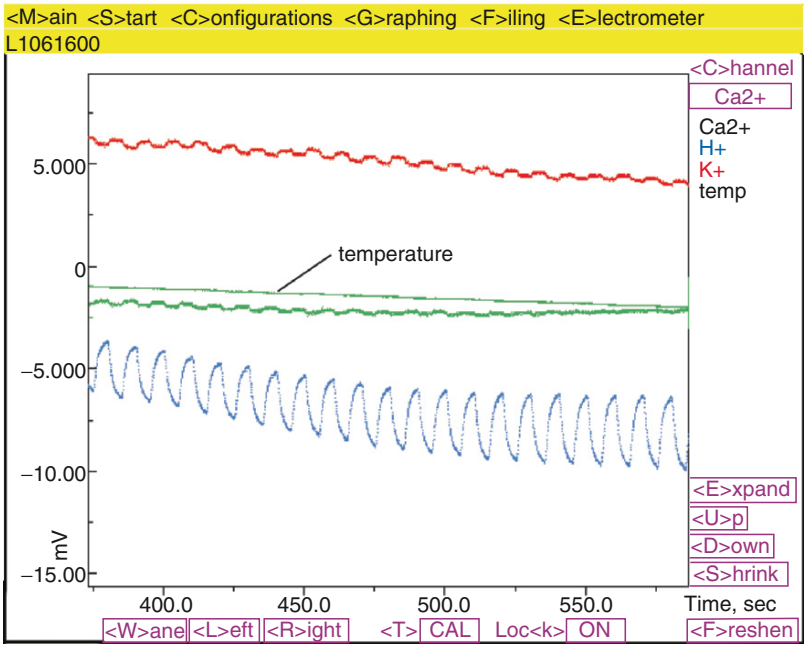

Fig. 3.2. Computer screen display of the MIFE recordings (courtesy Dr. L.Shabala). A (reverse colour) screen is pictured showing four concurrent voltage records for Ca^{2+}, H^+, K^+, and temperature. Fluxes of ions were calculated from the voltage (ΔV) using recorded concentration values. H^+ and K^+ concentrations are decreasing slowly. K^+ and H^+ fluxes are steady, while Ca^{2+} flux decreases to zero. Temperature (reversed scale) increases slowly

Flux calculations are performed automatically by the MIFEFLUX software (University of Tasmania, Hobart, Australia) from the data and log files. Calculated ion fluxes (in nmol m^{-2} s^{-1}) and concentrations are exported into an ASCII-format spreadsheet and saved onto computer disk, alongside the raw (mV records) data.

For ion flux measurements from root or leaf surface, a more "user-friendly" arrangement is used. In this case, the MIFE setup is built around the standard stereomicroscope. The microscope is rotated by 90°, so that the optical axis is horizontal. The measuring chamber is mounted on the computer-driven 3-dimensional hydraulics micromanipulator, while microelectrodes are held by the MMT-5 manipulator. Under such an arrangement, the electrodes are steady, and it is a slow movement of the measuring chamber that enables flux measurement. The main advantage of this arrangement is the convenience of electrode positioning (much further from the chamber's bottom—thus, less danger for electrodes to be broken). For more details, refer to Shabala and Newman (1997).

3.3.3 Methodological issues

Liquid membrane type ion-selective microelectrodes are used for MIFE measurements. Specific details of their fabrication and calibration are given in our publications (e.g. Shabala et al. 1997, 2005a; Shabala and Shabala 2002). Briefly, electrodes are pulled from non-filamentous borosilicate glass capillaries to tip diameter ~1 μm. Electrode blanks are then silanized with tributylchlorosilane (90796; Fluka Chemicals) to make their surface hydrophobic. Dried and cooled electrode blanks are stored under cover and may be used over several weeks. To make the electrode, the electrode tip is first broken slightly to achieve the required diameter (typically 2–3 μm). It is then backfilled with an appropriate solution (see Shabala and Shabala 2002 for more details) and finally front-filled with the appropriate liquid ion exchanger (LIX). Immediately after filling, electrodes are immersed in solution and kept there until use (up to 8–10 h).

In our laboratory, we routinely use the MIFE system to measure net fluxes of H^+, Ca^{2+}, K^+, Na^+, Cl^-, Mg^{2+}, NH_4^+, NO_3^-, and Cd^{2+} from various systems: higher plant tissues and protoplasts; animal tissues (e.g. muscles); fungi; algae; protists; yeasts; bacterial monolayers and biofilms. Several more ions (e.g. Zn^{2+}, Cu^{2+}, Cs^+, Pb^{3+}, SO_4^{-2}) also can be measured using commercially available ionophores.

Despite the same principle being used for measurements of fluxes of each of these ions, there are some "specific features", related to fabrication, calibration, and use of ion-selective microelectrodes to measure fluxes of a specific ion. The full coverage of these issues is beyond the scope of this paper. Some of these issues are also covered in detail in previous reviews on MIFE (Newman 2001; Shabala et al. 2005a). In this paper, only the crucial issues are mentioned.

1. *Basic electrode characteristics.* As a rule, for most physiological conditions, electrode characteristics are expected to be linear. Accordingly, each electrode is calibrated in a set of three known standards, covering the range of concentrations expected to be found in the experiment. The average responses of electrodes are about 53–54 mV/decade for monovalent ions, and 27–28 mV/decade for divalent ions, with a correlation R>0.999. If measurements are made at very low concentrations, non-linearity requires that more than 3 standards should be used.
2. *Electrode "conditioning".* Most of the prepared microelectrodes can be used immediately after preparation, while others (e.g. H^+ and Cl^-) need some conditioning time (~1 h) to ensure a stable response.
3. *Responsiveness.* During MIFE measurements, the electrodes are moved back and forth at 5-s intervals. For accurate flux calculations, the LIX must "settle" at each position. From practical experience, settling achieved quicker if the LIX column length is relatively short. However, in this case there is a danger of a gradual leak of LIX out of the tip and electrode loosing its

selectivity. The compromise is achieved by optimizing the amount of silane used for electrode fabrication and the amount of LIX used for electrode filling.

4. *Effect of ionic strength.* Variations in ionic strength of solutions might significantly affect characteristics of ion selective electrodes and result in inaccurate estimates of ionic concentrations and, ultimately, net ion fluxes. The actual concentration (and, thus, flux) is overestimated for solutions with ionic strength lower than that of the standard, and is underestimated vice versa. For many ions, such a difference may be as big as a factor of 2 in a physiologically relevant range of concentrations (e.g. Na^+ levels 200 mM). More details are available in Shabala et al. (2005a).
5. *Temperature.* Although the theory shows that the Nernst slope is proportional to the Kelvin temperature. However, our experiments in the 4–40 °C range suggested that in all cases, the Nernst slope remained > 50 mV/decade, and the maximum inaccuracy in flux calculation did not exceed 6% (Shabala et al. 2005a). Thus, for practical purposes, the effects of temperature on electrodes may be ignored. However at temperatures above 32 °C, the LIX often became very "noisy" affecting the signal to noise ratio. This should be kept in mind when planning experiments.
6. *Signal to noise ratio.* Due to the thermal electron noise in electrodes, there is some theoretical "lower limit" on the magnitude of the flux that can be measured against the background noise (Ryan et al. 1990). There are two practical measures to overcome this problem and to improve the sensitivity of the flux measurements. One is to increase the travel range of the electrode (making voltage changes larger), and another one is to increase electrode tip diameter. For more details, see Shabala et al. (2005a).
7. *Confounding effect of inhibitors.* Pharmacological experiments are frequent in plant electrophysiology. However, many of the channel blockers and metabolic inhibitors routinely used in patch-clamp experiments may significantly affect LIX characteristics. For example, even micromolar concentrations of CCCP completely "killed" Ca^{2+} LIX, reducing electrode slope from 27 to < 3 mV/decade. Therefore, a rigorous test of LIX performance in the presence of inhibitors should be undertaken first.

3.4 Application of ion-selective microelectrodes to study plant adaptive responses to environmental conditions

3.4.1 Nutritional disorders

A large bulk of literature is available dealing with the application of ion selective microelectrodes to study various aspects of nitrogen (both NH_4^+ and NO_3^-; Henriksen et al. 1990, 1992; Colmer and Bloom 1998; Garnett et al. 2001, 2003) and potassium (Newman et al. 1987; Ryan et al. 1990; Jones et al. 1995) nutrition

and transport in plant roots. These studies revealed a complex heterogenous nature of nutrient acquisition along the root axis, with some pronounced differences between functional root regions. Most of these issues have been comprehensively reviewed by Newman (2001), so are not discussed here. The only aspect I would like to comment on here is the possibility of measuring ion fluxes from root hairs. Root hair growth appears to be linked intimately to the cytosolic free Ca^{2+} concentrations in the apex (Gilroy and Jones 2000). High spatial resolution of the microelectrode ion flux measuring technique allowed fine-scale quantification ("mapping") of ion fluxes from the growing root hair (Jones et al. 1995). These authors reported tip-localized influx of H^+ and Ca^{2+}, with relatively uniform K^+ influx along the length of the root hair.

The ion flux measuring technique is also widely applicable for the study of mechanisms of uptake and translocation of micronutrients in various plant tissues. Studies in Kochian's lab showed the potential for the application of Cd^{2+}-selective microelectrodes to study heavy-metal ion transport in roots (Pineros et al. 1998). Several more LIX are commercially available from Fluka (e.g. Cu^{2+}, Zn^{2+}, Pb^{2+}, Cs^+). Being combined with molecular tools, their use may greatly advance engineering of varieties with higher nutrient efficiency, as well as helping in phytoremediation of metal-contaminated soils.

3.4.2 Salinity

Salt tolerance in non-halophytes is conferred by a large number of adaptive mechanisms, most of which are related to membrane-transport processes. Recently, this topic has been the subject of a large number of comprehensive reviews (e.g. Maathuis and Amtmann 1999; Hasegawa et al. 2000; Zhu 2002, 2003; Tester and Davenport 2003). Also, molecular and ionic mechanisms involved in the regulation of K^+ homeostasis and maintaining an optimal K^+/Na^+ ratio (critical to salt tolerance) in salinized plant tissues are discussed in detail in another review by Cuin and Shabala in this book. Here, I want to discuss only a few specific aspects of the application of the MIFE technique to study mechanisms of salt tolerance in plants.

3.4.2.1 Specific and non-specific components of salt stress

Two principal adverse effects of salinity in non-tolerant plants are osmotic stress and specific ion (Na^+ or Cl^-) toxicity (Munns 2002; Zhu 2003; Tester and Davenport 2003). The intriguing question is: how do plants distinguish between these two?

The above issue was addressed by measuring net ion flux responses to isotonic NaCl and mannitol solutions from various leaf (Shabala 2000) and root (Chen et al. 2005) tissues. While NaCl promoted a net K^+ efflux, isotonic mannitol treatment induced a gradual increase in the net K^+ uptake from both leaf and root tissues, indicating that different ionic mechanisms are

involved in perception of "ionic" and "osmotic" components of the salt stress. Pharmacological and patch-clamp experiments suggested that NaCl-induced K^+ efflux is mediated essentially by depolarization-activated K^+ outward-rectifying channels (DAPC), while inward-rectifying K^+ channels are involved in K^+ uptake in response to mannitol treatment. Overall, our results showed that K^+ fluxes from plant cells under salt conditions are driven by two oppositely directed signals: (i) K^+ efflux resulting from NaCl-induced plasma membrane depolarization and (ii) K^+ uptake resulting from some elusive "osmosensing mechanism" (see section 4.3 for details). Under mild salinities, the latter component dominates, while higher NaCl treatments result in overall net K^+ efflux from salinized tissues.

3.4.2.2 Delineating the role of the plasma membrane H^+-pump in salt stress responses

The other important issue concerns the involvement of the plasma membrane ATP-dependent electrogenic H^+-pump in cellular responses to salt stress. A NaCl-induced increase in plasma membrane H^+-ATPase activity has been reported for many halophytic species (Ayala et al. 1996; Vera-Estrella et al. 1999). It was suggested that the stimulation of H^+-ATPases by salt stress may provide a driving force for a plasma membrane Na^+/H^+ exchanger to move Na^+ from the cytoplasm into the apoplast, thereby providing a significant contribution to the salt adaptation of plant cells (Ayala et al. 1996). However, Serrano et al. (1999b) concluded that cells confronted with toxic cations such as Na^+ temporarily down-regulate their H^+-pump to escape stress. To shed more light on this issue, H^+ fluxes were measured from the mesophyll tissue of salt-sensitive broad bean species (Shabala 2000) in response to NaCl treatment. Our results showed a significant increase in NaCl-induced net H^+ efflux. Leaf pre-treatment with CCCP (a protonophore) and orthovanadate (a specific inhibitor of the plasma membrane H^+ pump) did not prevent the initial "instantaneous drop" towards net H^+ efflux, but did completely arrest the subsequent continuous drift towards larger efflux (Shabala 2000). It was concluded that there are at least two components of the observed H^+ flux: one is "vanadate-sensitive" (suppressed by both vanadate and CCCP), and another is "vanadate-insensitive". Their origin is a matter for further investigation.

3.4.2.3 K^+ homeostasis as a key feature of salt tolerance

The ability of a plant to prevent accumulation of excessive amounts of Na^+ in the cytosol has always been considered as a key feature of salt tolerance (Munns 2002; Zhu 2003; Tester and Davenport 2003). This may be achieved either by preventing Na^+ uptake, or by active Na^+ extrusion from cytosol into the apoplast (via plasma membrane SOS1 Na^+/H^+ antiporter) or into the

vacuole (via tonoplast NHX antiporter) (Blumwald et al. 2000; Hasegawa et al. 2000; Tester and Davenport 2003; Zhu 2003). Accordingly, plant breeding for salt tolerance was traditionally aimed to improve one of those features (Blumwald et al. 2000; Munns 2002; Zhu 2003). However, it appears that it is K^+/Na^+ *ratio* in the cytosol rather than Na^+ concentration per se that is critical to salt tolerance (Maathuis and Amtmann 1999). Direct evidence for this is surprisingly rare (Carden et al. 2003), most likely due to technical difficulties associated with measuring cytosolic Na^+ and K^+ concentrations.

Use of the MIFE technique offers an excellent opportunity to look at mechanisms underlying K^+ homeostasis in salinized plant tissues. Recently, we have made a rigorous comparison of physiological responses of seven barley cultivars contrasting in their salt tolerance (Chen et al. 2005). A very strong correlation ($R>0.8$) was shown to exist between net K^+ fluxes measured from the surface of 3-day-old barley roots after 40 min of treatment in various concentrations of NaCl and plant physiological responses (growth rate, biomass, net CO_2 assimilation, chlorophyll fluorescence, root and leaf elemental and water content) after a month of NaCl treatment in a glasshouse. The difference between NaCl-induced K^+ efflux between tolerant and sensitive cultivars was 3-fold, with much higher K^+ efflux measured from sensitive varieties (Chen et al. 2005). Importantly, this feature was heritable, as shown in experiments on F1 and F2 back-crosses. These findings not only suggest that K^+ homeostasis is a key feature for plant salt tolerance, but also offer a convenient non-destructive screening tool for plant breeders.

3.4.2.4 Ameliorative effects of Ca^{2+}

It is also known that the application of external Ca^{2+} may significantly ameliorate salinity stress symptoms in many species (Cramer et al. 1987; Rengel 1992; Reid and Smith 2000). It was traditionally believed that the dominating mechanism of such amelioration was in Ca^{2+} restriction of Na^+ uptake via non-selective cation channels (NSCC) which are believed to be a major pathway for Na^+ uptake into the cell under conditions of high salinity (Tyerman et al. 1997; Demidchik and Tester 2002; Tester and Davenport 2003). Recent studies provided some evidence that not only Ca^{2+} but also other divalent cations may be important for controlling Na^+ transport across the plasma membrane in saline conditions (Elphick et al. 2001; Demidchik and Tester 2002). Until recently, it remained unclear whether NSCC blockage by elevated $[Ca^{2+}]$ was the only mechanism involved. MIFE experiments on both root (Shabala et al. 2003) and leaf (Shabala 2000; Shabala et al. 2005b) tissues of various species showed that supplemental Ca^{2+} efficiently reduces, or even completely prevents, NaCl-induced K^+ efflux from the cell. Other divalent cations (Mg^{2+}, Ba^{2+}, Zn^{2+}) were also efficient in preventing K^+ leakage in response to salinity (Shabala et al. 2005b). Patch-clamp experiments on *Arabidopsis* leaf and root cells implicated DAPC involvement (S. Shabala, V. Demidchik and J. Davies, submitted).

Overall, our results suggest that, in addition to their known ability to block NSCC, divalent cations also control the activity or gating properties of K^+ transporters at the cell plasma membrane, thereby assisting to maintain the high K^+/Na^+ ratio required for optimal plant growth and leaf photosynthesis.

3.4.3 Osmotic stress

Improving crop resistance to osmotic stresses has always been a focus of breeding programs. Over the last 2 decades, the major emphasis was on molecular engineering of transgenic species, which overexpress genes responsible for biosynthesis of various compatible solutes (Bohnert et al. 1995; Bajaj et al. 1999; Bohnert and Shen 1999; Serrano et al. 1999a). It is traditionally believed that de novo synthesis of such compatible solutes is involved in re-adjustment of cell osmotic potential and prevention of water losses. However, it recently became evident that the functions of compatible solutes are not likely to be limited to conventional osmoprotection. Instead, a regulatory role for compatible solutes in adjustment of metabolic pathways to altered environmental conditions, was postulated (Bohnert and Sheveleva 1998; Serrano et al. 1999b). An important component of such adjustment might be control over activity of membrane ion transporters also involved in cell osmotic adjustment.

It has long been suggested that changes in ion fluxes in response to osmotic stress provide quick (within a few minutes) osmotic adjustment and maintain normal turgor (Wyn Jones and Pritchard 1989; Bohnert et al. 1995; Lew 1996). However, until recently, no direct evidence was provided. Using a non-invasive ion flux measuring technique, we showed that bean mesophyll cells responded to hyperosmotic stress by increased uptake of K^+ and Cl^- (Shabala et al. 2000). This is consistent with other reports obtained using different experimental techniques (Okazaki et al. 1984; Teodoro et al. 1998). Our model calculations estimated that up to 85 % of the changes in the cell turgor may be compensated by uptake of these two inorganic ions within 1 h after stress onset. These calculations were validated in direct concurrent measurements of net ion fluxes and cell turgor changes (the pressure-probe technique) in osmotically stressed *Arabidopsis thaliana* epidermal root cells (Shabala and Lew 2002). Our results showed that > 90% of the cell turgor was recovered by inorganic ion uptake within 40 min after onset of hyperosmotic stress.

There are at least two major advantages in using inorganic ions for cell osmotic adjustment. One of them is the rapidity of turgor recovery (minutes versus. hours or days for de novo synthesis of compatible solutes). This may give an adaptive advantage to plants which experience acute water stress in natural conditions throughout ontogeny (such as with a shallow root system). Another advantage is the energetics of osmotic adjustment. According to Raven (1985), the ATP requirements for synthesis of compatible solutes is approximately 10 times higher than that for active ion transport across membranes.

Specific ionic mechanisms involved in osmotic stress perception are still elusive. Lew (1996) suggested that *Arabidopsis* root hair cells possess an osmosensing but not a turgor-sensing mechanism. At least two mechanisms, namely (i) mechanosensitive (or stretch-activated) channels and (ii) putative intracellular osmosensing mechanisms, have been suggested by Brownlee et al. (1999). However, most reported evidence of SAC was obtained by using the patch-clamp technique; there is thus a need for more experimental observations of SAC effects at the tissue or organ level. Appearance of the additional 2-min oscillatory component in ion flux oscillations measured from hyperosmotically stressed plant roots (Shabala and Newman 1998) may provide such evidence.

A ubiquitous component of osmotic adjustment in higher plants is modulation of the proton-pumping activity (Reinhold et al. 1984; Li and Delrot 1987; Reuveni et al. 1987). Palmgren (1991) suggested that the relaxation of the stretched status of the membrane might directly activate the plasma membrane H^+-ATPase, as the activity of this enzyme is strictly dependent on the lipid environment. Passive H^+ transport is also affected (Bisson and Gutknecht 1977; Lew 1996) implying a multicomponent osmo-regulatory system. It remains to be answered whether the plasma membrane H^+-pump is a primary target (a receptor) of osmotic stress (Reinhold et al. 1984), or merely a component of the complex signaling network controlling the activity of the plasma membrane transporters for other ions (Kinraide and Wyse 1986; Li and Delrot 1987). Supporting evidence for the former hypothesis includes reports of significant osmotic-induced acidification of the bathing medium (Kinraide and Wyse 1986; Reuveni et al. 1987) and direct measurements of net H^+ extrusion (Lew 1998; Shabala and Newman 1998; Shabala et al. 2000).

At the same time, some authors ruled out direct effects of osmoticum on the H^+ pump, suggesting instead that the primary targets in the osmosensory mechanism are stretch-activated Cl^- channels inactivated by hyperosmotic stress (Teodoro et al. 1998; Zingarelli et al. 1999). In our experiments, K^+ uptake kinetics in hyperosmotically stressed mesophyll tissue was not affected when 500 μM vanadate (a known inhibitor of the H^+-ATPase) or 50 μM CCCP (a protonophore) were added (Shabala et al. 2000). At the same time, when K^+ uptake was suppressed by 20 mM TEA, neither K^+ nor H^+ flux changes were evident in response to mannitol treatment. This finding suggests that direct control of K^+ uptake is an important part of the process of osmoregulation. Earlier Liu and Luan (1998) suggested voltage-dependent K^+ and Cl^- channels being potential targets of osmosensing in stomatal guard cells. Direct modification of the turgor activated ionic conductance for K^+ and Cl^- was also shown in *Chara* (Kourie and Findlay 1991). The exact mechanism of this modulation, however, remains unclear.

Enhanced H^+ extrusion (Reinhold et al. 1984; Li and Delrot 1987; Reuveni et al. 1987) is expected to cause significant membrane hyperpolarization. This is indeed the case (Reid et al. 1984; Kinraide and Wyse 1986; Reuveni et al. 1987; Teodoro et al. 1998; Zingarelli et al. 1999; Shabala and Lew 2002). Such

hyperpolarization may enhance K^+ uptake via voltage-gated K^+ inward-rectifying channels or, alternatively, reduce K^+ efflux through outward K^+ channels (Lew 1996; Zingarelli et al. 1999). Both these types of channels are known to show strong voltage dependence (Very and Sentenac 2002; Shabala 2003), and the possibility that voltage clamp of the plasma membrane directly affects net K^+ fluxes into and out of the cell was shown in direct experiments combining the voltage-clamp and MIFE techniques (Shabala and Lew 2002).

3.4.4 Temperature extremes

Low ambient temperatures have a significant impact on agricultural production not only of many species of tropical or subtropical origin grown in temperate regions around the world, but also within a normal plant's habitat (Lyons 1973). Genetic manipulation of chilling-sensitive species for achieving better growth and higher crop yield depends on an understanding of mechanisms of chilling responses and tolerance.

There are numerous papers reporting significant perturbations in root ion uptake and transport under chilling stress (Bravo-F and Uribe 1981; White et al. 1987; Pritchard et al. 1990; Petterson 1995). Results are often controversial. Strong temperature dependence for uptake of potassium and phosphorous was reported for corn roots (Bravo-F and Uribe 1981), while Petterson (1995) found no effect of low root zone temperature on net uptake or transport of these ions in barley. Wang et al. (1993) have reported that high and low affinity transport systems for NH_4^+ in rice roots had very different Q_{10} (2.6 and 1.5, respectively). However, no attempts to directly measure the temperature dependence of fluxes of different nutrients in situ at the cellular level have been undertaken until recently.

Using the unique advantages of the MIFE technique, we showed that critical temperatures, under which the recovery of the activity of plasma membrane transporters took place, was the same for all ions measured (H^+, Ca^{2+}, K^+, Na^+, NH_4^+, and Cl^-; Shabala and Shabala 2002) and very close to the critical temperature of plasma membrane phase transition expected to be found for the measured species (Lyons 1973). We also showed, at the same time, that the apparent difference in ion flux kinetics measured in a traditional way may be misleading, due to different rates of recovery for different transporters (Shabala and Newman 1997).

The primary sites of the chilling effect appear to be plant membranes (Lyons 1973; DuPont 1989; Yoshida 1991). The role of membrane fluidity in temperature perception and transduction of the chilling signal now seems to be indisputable (Marschner 1995; Murata and Los 1997). Chilling temperatures may directly affect the structure and function of the plasma membrane transport enzymes. Changes in lipid composition, carrier activity, permeability, and ultrastructure have been shown to occur at the membrane level (Hällgren and Öquist 1990 and references within). However, specific mechanisms underlying

the effects of membrane phase transition on activities of plasma membrane transporters remain to be elucidated.

Several possibilities have been suggested, including conformational changes of transport proteins (changing affinity), or indirect effects due to modification of the physical properties of the lipid environment (Clarkson et al. 1988). As most membrane transporters are coupled via MP, conformational changes in one transport protein will most likely have a domino effect on the activity of others. Our experiments (Shabala and Shabala 2002) suggest that two transporters of ions are primary "suspects" for such a role.

Plasma membrane H^+-pump. There is much evidence in the literature that active H^+ transporters are among the most sensitive to temperature stress in chilling-sensitive species (DuPont 1989; Yoshida 1991). In our experiments, both vanadate and CCCP caused an 80% reduction in the magnitude of H^+ flux temperature responses (Shabala and Shabala 2002). Observed changes in the activity of other transporters could be explained by the dramatic depolarization of the plasma membrane (Clarkson et al. 1988). A resultant shift in the values for the Nernst potential would enhance the passive cation leak from the cells (Clarkson et al. 1988; Hällgren and Öquist 1990; Wang et al. 1993; Macduff and Dhanoa 1996; Shabala and Shabala 2002).

Cold induced inactivation of the H^+-ATPase may have been due to a structural alteration in the enzyme complex, including a modification of the intermolecular association of the subunits and the uncoupling of ATP hydrolysis and H^+ transport activity (Yoshida 1991). When the principal processes generating ATP temporarily collapse under chilling conditions, the ATP-driven efflux of H^+ will decrease (Clarkson et al. 1988). This is exactly what was observed when measuring net H^+ fluxes in chilled root and leaf tissues (Shabala and Newman 1997).

Ca^{2+} transporters may play a central role in mediation of low-temperature effects on cell nutrient uptake. All tested metabolic inhibitors (La^{3+}, vanadate and TEA) caused dramatic reduction (>90%) in the magnitude of Ca^{2+} flux responses to chilling recovery (Shabala and Shabala 2002). As some of these inhibitors are not Ca^{2+}-specific, it indicates a likely signaling role of Ca^{2+} flux changes (Knight et al. 1996; Murata and Los 1997). According to some models, Ca^{2+} channels open at low temperatures upon a decrease in membrane fluidity, and the entering Ca^{2+} ions activate a signal transduction pathway for up-regulation of the expression of low-temperature-inducible genes (Monroy and Dhindsa 1995). Validation of this model and elucidation of a mysterious putative sensor at the plasma membrane remains a priority for future research.

3.4.5 Soil pH

Soil acidity severely limits plant production worldwide. Among the major constraints, Al^{3+} toxicity is the most important (Marschner 1995), with even micromolar concentrations of Al^{3+} in the soil solution inhibiting the root

growth of many species (Kochian 1995; Ryan et al. 2001). The mechanisms of Al^{3+} toxicity are complex and may include interactions that occur both in the symplast and apoplast (Kochian 1995).

The ability of many species to maintain root growth at low soil pH is associated with the release of weak organic acids (such as malate), chelating Al^{3+} to form non-toxic complexes (Ryan et al. 2001). The *ALMT1* gene, encoding a membrane protein that facilitates an Al^{3+}-activated malate efflux when expressed in tobacco, rice, barley and *Xenopus* oocytes (Delhaize et al. 2004; Sasaki et al. 2004), has been isolated recently. However, the action spectrum of Al^{3+} appears to be much broader than just activation of anion channels responsible for malate efflux. Al^{3+} has the potential to affect membrane potential significantly by directly interacting with the membrane to alter its structure and fluidity (Chen et al. 1991), by blocking Ca^{2+} and K^+ channels (Ding et al. 1993; Gassmann and Schroeder 1994) or by inhibiting the H^+-ATPase in the plasma membrane (Ahn et al. 2002). These changes in membrane potential will inevitably affect cellular ionic homeostasis.

Al^{3+} has been shown to block inward-rectifying K^+ channels (KIR) in root hairs (Gassmann and Schroeder 1994) and guard cells (Schroeder et al. 1994), reducing the open probability and changing the activation kinetics of the channel through some internal membrane-delimited mechanism (Liu and Luan 2001). Therefore, it was suggested that K^+ deficiency in acid soils can be correlated with the inhibitory effect of Al^{3+} on KIR in roots (Gassmann and Schroeder 1994). However, it has also been shown that Al^{3+} has no effect on K^+ accumulation at the whole-plant level (Marschner 1995). Alternatively, Zsoldos et al. (2001) reported that Al^{3+} stimulated K^+ (^{86}Rb) influx in short-term (up to 6 h) experiments. This controversy might be resolved if the effect of Al^{3+} on channel gating and activation kinetics is rather different in situ than when expressed in heterologous conditions (Liu and Luan 2001). It is worth mentioning that the pH-sensitivity of SKT1 (K^+ inward-rectifying channel from potato) was rather different when expressed in insect cells versus *Xenopus* oocytes, indicating that the heterologous expression system influences the functional behavior of the channel (Hartje et al. 2000). From this point of view, non-invasive ion flux measurements are ideal to study effects of Al^{3+} on ion transport across membranes.

Several studies have now demonstrated that the Al^{3+}-activated malate efflux is accompanied by K^+ efflux and it has been proposed that this can account for electroneutrality (Ryan et al. 1995). However, all these studies used excised root apices and relatively short treatment times and it remains unclear whether a similar response operates in intact roots and if it is sustained over long periods of Al^{3+} exposure. In our recent work we used near-isogenic wheat lines that differ in Al^{3+} tolerance (ET8 and ES8) to investigate the effects of Al^{3+} on root-cell membrane potential and ion flux kinetics in intact roots (Wherrett et al. 2005). We showed that addition of 50 μM $AlCl_3$ to the bathing solution stimulated an increase in K^+ efflux and H^+ influx in ET8 but not in ES8. The differences between the genotypes were sustained for

24 h and were observed only at the elongating zone and not the meristematic zone (Wherrett et al. 2005). These results provide new temporal and spatial information on the Al^{3+}-activated efflux of K^+ from intact wheat plants. Based on our MIFE data, we also concluded that a previously proposed model (Olivetti et al. 1995) to explain the Al^{3+}-dependent depolarization in snapbean (blockage of K^+ outward rectifying (KOR) channel by Al^{3+}) is unlikely to be occurring in wheat because the depolarization in ET8 are associated with a transient increase in K^+ efflux, not a decrease as would be predicted from that model. Instead, our data suggested no direct interaction between Al^{3+} and K^+ channels and implied that the stimulation of K^+ efflux is triggered by the membrane depolarization caused by organic anion efflux. Aluminum also caused significant changes in the net H^+ and Ca^{2+} fluxes (Wherrett et al. 2005). The physiological role of these changes is the subject of further investigation.

As mentioned above, no Al^{3+} effect on K^+ accumulation was observed at the whole-plant level (Marschner 1995). That points to the possibility that the soil (or apoplastic) pH per se may influence K^+ uptake. It is known that Shaker-type K^+ channels are controlled (at post-transcriptional level) by both pH_i and pH_0 (Marten et al. 1999; Lacombe et al. 2000).

The most studied channels are K^+ channels in guard cells. Both apoplasmic (Roelfsema and Hedrich 2002) and cytosolic (Dietrich et al. 2001) acidification lead to the activation of inward K^+ currents in guard cells. The effect is voltage-dependent (Roelfsema and Hedrich 2002). Strong pH-dependence of KIR channels was also reported for root (tomato LKT1 channel; Hartje et al. 2000), pulvini (Yu et al. 2001) and mesophyll (Keunecke and Hansen 2000) cells. Results are rather controversial. While LCT1 channel behavior was similar to KIR in guard cells, the pulvinar KIR channels were inhibited by external acidification, with reversible decline of the maximum conductance and an irreversible shift of the voltage dependence of channel gating (Yu et al. 2001), in contrast to their acidification-promoted counterparts in guard cells. In leaf tissues, acidification stimulated K^+ conductance in bundle sheath cells, whereas a decrease was found for mesophyll channels (Keunecke and Hansen 2000). Also, extracellular acidification decreased the macroscopic currents through the AKT3 channel (weakly voltage-dependent channel predominantly expressed in the phloem) by reducing the single-channel conductance (Marten et al. 1999).

Equally controversial are data on pH regulation of KOR channels. Reports range from strong inhibition (Ilan et al. 1994; Lacombe et al. 2000) to insensitivity (Fan et al. 2003). There is also no agreement on the above mechanisms of pH control of K^+ channels. Hoth et al. (2001) showed that essential elements for external pH regulation are located within the channel pore. At the same time, no evidence for pH effects on single channel conductance was reported (Ilan et al. 1994; Lacombe et al. 2000).

The fact that external protons can show opposite effects on different members of the same gene family is hardly surprising as most of the results originate from experiments with heterologously expressed K^+ channels. Amtmann et al. (1999) provided the first *in planta* characterization of the effects of

apoplastic pH on KIR channels in roots, showing that a decrease in external pH shifted the half-activation potential to more positive voltages and increased the limit conductance, resulting in enhancement of the KIR current. Increased probability of the KIR opening was also shown in patch-clamp experiments by Hartje et al. (2000). This is opposite to what would be expected if K^+ deficiency in roots grown at low pH is due to direct regulation of KIR channels by protons. More likely, K^+ acquisition is under the strict control of the plasma membrane potential which, in turn, is pH-sensitive. Indeed, acidifying bathing media to pH 4 leads to significant H^+ influx into the plant tissue (Shabala et al. 1997), which can potentially explain cytoplasmic acidification observed in *Riccia* rhizoids (Felle 1988) and in protoplasts from wheat roots (Lindberg and Strid 1997). At the same time, most K^+ channels in the plant plasma membrane (with the only exception of AKT2/3) show strong potential dependence (Very and Sentenac 2002; Shabala 2003).

The above hypothesis that K^+ deficiency at low pH may result from direct control over K^+ transport by the depolarized MP was confirmed in experiments, when net K^+ and H^+ fluxes near *Arabidopsis* root hairs were measured under voltage clamped conditions and in a range of different external pH and KCl concentrations (Babourina et al. 2001), providing strong evidence that K^+ acquisition by root hairs is under strict voltage control and supporting the above hypothesis on mediation by membrane potential of soil pH effects on K^+ acquisition.

3.4.6 Oxygen deprivation

Many agricultural regions around the world are subject to waterlogging, caused either by natural factors or as a result of excessive irrigation (Gibbs and Greenway 2003). In waterlogged soils, air is displaced from the pore spaces, and oxygen is rapidly depleted, which changes the root chemical environment and affects root growth and causes a decline in acquisition of major nutrients such as N, P, K and Ca (Atwell and Steer 1990; Boem et al. 1996; Barrett-Lennard et al. 1999). Low oxygen levels in the rhizosphere and an associated significant (up to 97%; Gibbs and Greenway 2003) reduction in the rate of energy production are believed to be the main reason for that decline. In addition, long-term waterlogging reduces soil redox potential, causing dramatic increase in the levels of free Fe^{2+} and Mn^{2+}, leading to toxicity of these nutrients for root metabolism (Marschner 1995).

It has frequently been suggested that anoxia decreases membrane selectivity. For example, Armstrong and Drew (2002) showed that low concentration of oxygen in the rooting medium decreases the selectivity of K^+/Na^+ uptake in favor of Na^+ and retards the transport of K^+ to the shoots. This may lead to a several fold increase in Na^+ content in leaf tissues compared with normoxic plants (Smethurst and Shabala 2003). A so called "memory effect", when enhanced shoot transport of Na^+ remains present for many days even after

short-term (1 h) oxygen deficiency, is known from the literature (Brauer et al. 1987). The precise ionic mechanisms involved remain to be elucidated. It also remains unknown whether this decreased selectivity is due to an increased permeability of the lipid bilayer or is caused by leakage of ions through some specific channels or carriers (Greenway and Gibbs 2003).

Despite maintenance of membrane integrity being considered as a key factor in survival of plant cells under anoxia (Rawyler et al. 1999), surprisingly little is known about processes that maintain membrane integrity under anoxic conditions. Non-specific loss of K^+ was reported soon after onset of anoxia (Greenway et al. 1992; Colmer et al. 2001), presumably as a result of plasma membrane depolarization leading to KOR opening (Zhang et al. 1992; Zhang and Greenway 1995). It was speculated that cells direct their limited amounts of energy to the transport of solutes involved in pH regulation and of sugars required for anaerobic carbohydrate catabolism (Greenway and Gibbs 2003). As a result, net uptake of other nutrients (K^+, PO_4^{-3}, Cl^-, and NH_4^+) is strongly inhibited (Petraglia and Poole 1980; Colmer et al. 2001).

Elucidating the signaling cascade of plant responses to anoxia remains one of the great challenges. It was suggested that cytosolic acidification is the primary signal of an O_2 deficit (Ratcliffe 1997; Gibbs and Greenway 2003). Xia and Roberts (1996) provided the evidence that plasma membrane H^+-ATPase can operate under anoxia and that net H^+ extrusion increases when cytosolic pH falls. However, Felle (1996) concluded that changes in pump activity do not affect cytoplasmic pH under anoxic conditions. Changes in $[Ca^{2+}]_{cyt}$ are also thought to be part of the signal transduction pathway (Subbaiah et al. 1998).

Greenway and Gibbs (2003) proposed that in anoxia-tolerant tissues, energy flow during anoxia must be directed towards essential nutrient transport. No direct evidence has been provided though. From this point of view, non-invasive ion flux measurements give an excellent opportunity to look at underlying mechanisms associated with membrane responses to O_2 deprivation. Results of recent studies in our laboratory have revealed that functionally different barley root zones have rather different O_2 requirements (as measured with vibrating O_2 microelectrode) and that oxygen deprivation has qualitatively different effects on the activity of plasma membrane ion transporters in mature and elongation zones. Based on pharmacological data, we suggest that hypoxia-induced K^+ flux responses are mediated by both KIR and NSCC channels in the elongation zone, while in the mature zone KOR channels are likely to be the key (J. Pang and S. Shabala, in preparation). The ion flux "signatures" in response to hypoxia were rather different between cultivars contrasting in waterlogging tolerance, suggesting that the latter was mediated not only by anatomical (e.g. aerenchyma formation) but also physiological mechanisms.

3.4.7 Oxidative stress

Reactive oxygen species (ROS) are produced as a by-product of cellular metabolic pathways and function as a critical second messenger in a variety of

intracellular signaling pathways in animal tissues (Kourie 1998). Plants also respond to both biotic (elicitors) and abiotic (salinity, drought, chilling) stresses by the production of reactive oxygen species such as the superoxide anion radical ($O_2^{\bullet -}$), hydrogen peroxide (H_2O_2) or hydroxyl radical ($OH^{\bullet}$) (Bowler and Fluhr 2000; Smirnoff and Wheeler 2000). It is traditionally believed that increased ROS production has detrimental effects on cell ionic homeostasis, causing lipid peroxidation and impairing membrane integrity (Santos et al. 2001; Lee et al. 2004). However, there is growing evidence that, in addition to having detrimental effects, ROS can also be important signaling and regulatory agents. Examples are numerous and include ROS involvement in plant signal transduction (Pei et al. 2000; Schroeder et al. 2001; Zhang et al. 2001), development (Shorning et al. 2000), and programmed cell death (Hoeberichts and Woltering 2003; Casolo et al. 2005).

Most evidence on the signaling role of ROS comes from experiments on guard cells. ROS have been proposed to function as second messengers in ABA signaling in guard cells (Kwak et al. 2003; Jiang and Zhang 2003). It is believed that in such a signaling cascade, ROS are produced by NAD(P)H oxidases (Jiang and Zhang 2003; Kwak et al. 2003), and this process is preceded by cytoplasmic alkalization (Suhita et al. 2004). The intracellular signaling pathway is rather complex and involves activation of a heterotrimeric G protein, H_2O_2 generation, and changes in $[Ca^{2+}]_{cyt}$ in the regulation of stomatal movements (Chen et al. 2004). However, Kohler et al. (2003) showed that physiological concentrations of H_2O_2 strongly inhibited K^+ outward rectifiers in *Vicia* guard cells. These findings question the role of H_2O_2 as a critical second messenger regulating guard cell ion channels in response to ABA. Obviously, the signaling network is more complex than initially believed, and may include a variety of different types of membrane transporters and second messengers. To understand their orchestrated functions remains a great challenge.

By using the non-invasive MIFE technique we showed, for the first time, that free hydroxyl radicals ($OH^{\bullet}$) caused rapid Ca^{2+} influx and K^+ efflux across the plasma membrane of *Arabidopsis* root cells (Demidchik et al. 2003). Patch-clamp and luminometry experiments suggested that this effect is mediated by ROS control upon the activity of at least two different types of plasma membrane channels. ROS-induced increase in cytosolic Ca^{2+} was mediated by a novel population of NSCC that differ in selectivity and pharmacology from those involved in toxic Na^+ influx (Demidchik and Tester 2002), while ROS-induced K^+ efflux was due to $OH^{\bullet}$ stimulation of a KOR. This is the first characterization of the channel-mediated K^+ efflux mechanism of plant stress responses and is in contrast to H_2O_2 data. Experiments with *abi1* mutant suggested that the phosphorylation state is critical to such KOR activation (Demidchik et al. 2003).

Interaction between ROS and $[Ca^{2+}]_{cyt}$ appears to be critical in mediating plant stress responses (Bowler and Fluhr 2000; Coelho et al. 2002). Modulation of Ca^{2+} permeable channels by H_2O_2 in guard cells, leading to stomatal closure, has been reported widely (Pei et al. 2000; Murata et al. 2001;

Schroeder et al. 2001; Zhang et al. 2001; Kwak et al. 2003). It was shown that this process requires the presence of NAD(P)H in the cytosol (Murata et al. 2001). However, little is known about the subcellular spatio–temporal patterns of ROS production or their significance for downstream responses (Coelho et al. 2002).

Effects of ROS on K^+ channels are well documented in both animal and plant literature. Most studies deal with either mitochondrial K^+-ATP channels (Trono et al. 2004; Casolo et al. 2005) or with K^+ permeable channels in guard cell plasma membranes (Zhang et al. 2001; Kohler et al. 2003). Both of these were suggested to play a role as defense systems under environmental stress. Mitochondrial K^+-ATP channels were activated under stress conditions (salinity and osmotic stress) and were able to control mitochondrial superoxide anion production (Trono et al. 2004).

Potassium efflux is known to be one of the earliest events observed in response to a variety of stresses such as salinity (Shabala 2000; Babourina et al. 2001; Shabala et al. 2003) and acidity (Babourina et al. 2001). Traditionally, these effects were attributed to membrane depolarization (Shabala et al. 2003). Our study of K^+ efflux from plant roots in response to oxidative stress (Demidchik et al. 2003) demonstrated that stress-induced K^+ efflux can be mediated by a previously unknown mechanism—activation of KOR by $OH^\bullet$. In fact, this is hardly surprising. K^+ channels harbor reactive groups and thus are expected to be sensitive to ROS (Kohler et al. 2003). Importantly, flux amplitude and the time-course of K^+ flux response to ROS treatment varied between species, suggesting species-specific "flux signatures" in response to $OH^\bullet$. This also suggests that H_2O_2 is not the sole oxygen-derived species capable of signaling and regulation in plants. The response to $OH^\bullet$ was tissue-specific and stronger in cells which directly interact with the environment (e.g. root epidermis versus pericycle). Based on the above results, two major functions for ROS activation of cation channels were proposed: initialization/amplification of stress signals and control of cell elongation in root growth (Demidchik et al. 2003).

3.4.8 Biotic stresses

Plants respond to attack from pathogens by activating a variety of defense mechanisms, including synthesis of phytoalexins and hypersensitive cell death, which restricts growth of pathogens at the site of infection (Kadota et al. 2004). These responses are preceded by the interaction between pathogen-associated molecules (elicitors) and putative plant receptors (Vera-Estrella et al. 1994; Blumwald et al. 1998). Some of the earliest detectable signaling events in plant defense responses include plasma membrane depolarization and transmembrane ion fluxes, followed by production of ROS (Zimmermann et al. 1998; Clough et al. 2000). These are sequentially followed by defense gene activation and phytoalexin accumulation (Jabs et al. 1997). Most papers

suggest elicitor-induced Ca^{2+} and H^+ influx and effluxes of Cl^- and K^+ (Nurnberger et al. 1994; Jabs et al. 1997; Kadota et al. 2004).

Of particular importance in early recognition between the host and pathogen is the role of Ca^{2+} as a second messenger that triggers a downstream cascade of defense responses (Blumwald et al. 1998; Zimmermann et al. 1999). Fungal elicitors rapidly enhanced expression of the plasma membrane Ca^{2+} pump in soybean (Chung et al. 2000). Ca^{2+} influx and the transient increase in $[Ca^{2+}]_{cyt}$ levels after elicitor treatment have been shown to be necessary and sufficient for the induction of an oxidative burst and thus, plant defense responses (Clough et al. 2000). The important role of Ca^{2+} signaling in response to pathogen infection was observed in a wide range of species (Bach et al. 1993; Nurnberger et al. 1994; Jabs et al. 1997; Blume et al. 2000; Lecourieux et al. 2002; Kadota et al. 2004). Surprisingly, despite the great bulk of literature reporting the critical role of Ca^{2+} in the early recognition between the host and pathogen, direct measurements of Ca^{2+} flux into a single infected cell in vivo are lacking. This is largely due to the lack of appropriate techniques used (as explained below).

Most of above conclusions were derived from either $^{45}Ca^{2+}$ uptake experiments (Bach et al. 1993; Nurnberger et al. 1994) or from experiments with various Ca^{2+} channel blockers (Atkinson et al. 1990; Nurnberger et al. 1997). The above pharmacological data do not provide direct evidence that specific plasma membrane Ca^{2+} channels mediate an elicitor-induced Ca^{2+} influx, because the high (millimolar) concentrations of La^{3+} or Gd^{3+} used to block Ca^{2+} influx may enter the cell and affect the plasma membrane Ca^{2+}-ATPase (Blume et al. 2000). As for the $^{45}Ca^{2+}$ uptake technique, it has a relatively low time resolution and is only capable of measuring cell-associated (not localized) Ca^{2+} uptake (Grant et al. 2000), precluding accurate quantification of Ca^{2+} influx into the cell and adequate resolution of the fast kinetics associated with early signaling events at the plasma membrane.

Another popular technique is the use of aequorin technology, with a large number of papers published on kinetics of $[Ca^{2+}]_{cyt}$ changes in many plant species in response to various elicitors and phytotoxins (Blume et al. 2000; Grant et al. 2000; Lecourieux et al. 2002). The main problem with this method is, however, that it cannot distinguish between transient $[Ca^{2+}]_{cyt}$ changes occurring as a result of increased Ca^{2+} uptake from the external medium (i.e. plasma membrane mediated) and changes resulting from Ca^{2+} release from internal store (such as vacuole or ER). Thus, the use of aequorin technology does not allow location of the specific elicitor target(s) in plant cells.

Direct electrophysiological evidence of elicitor-induced activation of plasma membrane Ca^{2+} permeable channels is scarce (Gelli et al. 1997; Zimmermann et al. 1997) and is usually obtained from patch-clamp experiments. However, as protoplasts are highly artificial systems, it is unclear to what extent these results are applicable to cellular responses in vivo (e.g. Mathieu et al. 1991 versus Zimmerman et al. 1999). Several explanations are possible including (i) indirect regulation of channel activity by an elicitor,

(ii) the loss of responsiveness of the enzymatically isolated protoplasts, and (iii) the end target of toxin being in the cell wall. In each of these cases, the use of the MIFE technique will not be prone to these problems.

In a recent study, we applied the MIFE technique to characterize early signaling events associated with thaxtomin A (a dipeptide phytotoxin produced by all plant pathogenic *Streptomyces* sp. responsible for common scab disease) toxicity in *Arabidopsis* and tomato roots and pollen tubes. Our results indicate that thaxtomin A treatment causes Ca^{2+}-channel-mediated rapid Ca^{2+} influx across the plasma membrane, triggering further Ca^{2+}-induced Ca^{2+} release from some internal store (Tegg et al. 2005). We also showed that thaxtomin A was more effective in young, physiologically active tissues, suggesting higher density of toxin-binding sites in these regions, as well as suggesting a possible interaction between thaxtomin A and plasma membrane auxin receptors, as revealed from experiments on the auxin sensitive *ucu2–2/gi2 Arabidopsis* mutant (Tegg et al. 2005).

Not only Ca^{2+} but fluxes of other ions such as H^+, K^+ and Cl^- are also affected by pathogens (Zimmermann et al. 1999; Clough et al. 2000; Lecourieux et al. 2002; Kadota et al. 2004) and have been implicated in early pathogen recognition. In contrast to Ca^{2+}, effects of elicitors on H^+ flux activity across the plasma membrane are more variable and often controversial. Generally, extracellular alkalinization occurs when plant cells are treated with an elicitor (Atkinson et al. 1990; Nurnberger et al. 1994). However, some papers report significant (up to 4-fold) activation of the plasma membrane H^+-ATPase (Vera-Estrella et al. 1994; Blumwald et al. 1998). This controversy may be explained by the lack of direct measurements of elicitor-induced H^+ fluxes, as most conclusions were derived from observed pH changes in the cell medium.

It remains to be answered what specific membrane proteins mediate elicitor perception and signaling in plants. Various K^+ permeable inward- and outward rectifying channels have been named as potential targets (Blatt et al. 1999; Ivashikina et al. 2001). A series of recent publications using *dnd* (Clough et al. 2000) and *hlm* (Balague et al. 2003) *Arabidopsis* mutants pointed to the involvement of the cyclic nucleotide-gated non-selective ion channels (CNG). Such CNG channels are known to be permeable to all physiologically relevant cations and thus, might mediate the observed elicitor-induced Ca^{2+} and K^+ flux changes. This hypothesis can be easily tested in MIFE experiments on these mutants.

In addition to plant-pathogenic interactions, early electrophysiological events at the plasma membrane are also critical for root nodulation (Felle et al. 1995; Ehrhardt et al. 1996; Zimmermann et al. 1999). Membrane potential changes and ion fluxes were both shown to be of importance for Nod signal perception and transduction (Zimmermann et al. 1999). Specific details of this process remain to be elucidated. It was shown that adding nodulation signaling protein NodO to a planar lipid bilayer causes formation of cation-selective channels that allow K^+ and Na^+ fluxes across the membrane (Sutton

et al. 1994). The full details of this process, as well as the overall role of ion channels during the establishment of symbiosis, remain to be answered (Zimmermann et al. 1999). Non-invasive ion flux measurements might be an excellent tool for doing this.

3.5 Prospects and conclusions

As shown above, key features of the MIFE technique (such as non-invasiveness, high spatial and temporal resolution, and possibility of concurrent measurements of fluxes of several ions) make it a very useful tool to study membrane-transport processes in response to literally every known environmental stress. As ion fluxes are measured in situ, a direct extrapolation of the results to a variety of "natural" situations (e.g. plant stress response in the field) becomes possible.

The power of the MIFE technique is enhanced many fold when used in combination with other advanced experimental tools. One such example is a combination of the MIFE and patch-clamp techniques (Tyerman et al. 2001; Demidchik et al. 2003). Such a combination facilitates better identification of membrane currents and makes it possible to determine stoichiometries of transporter reactions. Another example is a combination of MIFE and fluorescence imaging techniques. Shabala et al. (2002) used such an approach to monitor H^+ flux kinetics across the plasma membrane of *Listeria* bacterial cells in relation to observed intracellular pH_i changes. These authors showed that pH_i and H^+ flux responses were complimentary and reflected the key role of active H^+ extrusion in bacterial adaptation to acid stress. There is no doubt that similar measurements can also be performed on plant tissues, using a variety of dyes to monitor kinetics of the same ion on both side of the plasma membrane. Alternatively, impaled ion-selective microelectrodes may be used in combination with MIFE for these purposes. Earlier we used a similar approach to measure net ion fluxes concurrently with membrane potential changes from leaf epidermal and mesophyll cells in response to light (Shabala and Newman 1999). Combination of the MIFE technique with voltage-clamp (Babourina et al. 2001; Shabala and Lew 2002) or pressure-probe (Shabala and Lew 2002) techniques also gave a significant conceptual advance in our knowledge of the ion-transport processes underlying plant adaptive responses to pH and osmotic stresses.

Most importantly, the MIFE technique is ideal for functional genomics studies. Its application to *Arabidopsis phot* mutants led to the discovery of an important role of plasma membrane Ca^{2+} fluxes in mediating blue light induced phototropic responses (Babourina et al. 2002). Altered ion flux patterns were also reported for newly described *mtr-1* pea mutant with modified tropic responses (Platten et al. 2004) or from *Arabidopsis sos* mutants in response to salt stress (Shabala et al. 2005c). Several more projects are currently at various

stages of completion in our lab, using genetically modified material. Results appear to be very promising.

To summarize, I believe that non-invasive ion flux measurements have a unique role in filling the gap between fundamental membrane-transport studies at the molecular levels and the needs of agronomists, aiming to improve plant performance in the field under stress conditions. Although not perfect, such a technique can probably claim the "best value for money" title in its area. Time will judge if this claim is fully justified.

Acknowledgements. I thank Drs. Tracey Cuin and Ian Newman for critical reading of the manuscript. This work was supported by an Australian Research Council grant to S.S.

References

Abbott ML, Fraley L (1991) Radiotracer methods to determine root distribution—a review. Environ Exp Bot 31:1–10

Ahn SJ, Sivaguru M, Chung GC, Rengel Z, Matsumoto H (2002) Aluminium-induced growth inhibition is associated with impaired efflux and influx of H^+ across the plasma membrane in root apices of squash (*Cucurbita pepo*). J Exp Bot 53:1959–1966

Amtmann A, Jelitto TC, Sanders D (1999) K^+-selective inward-rectifying channels and apoplastic pH in barley roots. Plant Physiol 120:331–338

Apse MP, Aharon GS, Snedden WA, Blumwald E (1999) Salt tolerance conferred by overexpression of a vacuolar Na^+/H^+ antiport in *Arabidopsis*. Science 285:1256–1258

Armstrong W, Drew MC (2002) Root growth and metabolism under oxygen deficiency. In: Waisel Y, Eshel A, Kafkafi U (eds) Plant roots: the hidden half. Dekker, New York, pp 729–761

Atkinson MM, Keppler LD, Orlandi EW, Baker CJ, Mischke CF (1990) Involvement of plasma membrane calcium influx in bacterial induction of the K^+/H^+ and hypersensitive responses in tobacco. Plant Physiol 92:215–221

Atwell BJ, Steer BT (1990) The effect of oxygen deficiency on uptake and distribution of nutrients in maize plants. Plant Soil 122:1–8

Ayala F, Oleary JW, Schumaker KS (1996) Increased vacuolar and plasma membrane H^+-ATPase activities in *Salicornia bigelovii* Torr in response to NaCl. J Exp Bot 47:25–32

Babourina O, Leonova T, Shabala S, Newman I (2000) Effect of sudden salt stress on ion fluxes in intact wheat suspension cells. Ann Bot 85:759–767

Babourina O, Hawkins B, Lew RR, Newman I, Shabala S (2001) K^+ transport by *Arabidopsis* root hairs at low pH. Austral J Plant Physiol 28:635–641

Babourina O, Newman I, Shabala S (2002) Blue light-induced kinetics of H^+ and Ca^{2+} fluxes in etiolated wild-type and phototropin-mutant *Arabidopsis* seedlings. Proc Natl Acad Sci USA 99:2433–2438

Bach M, Schnitzler J-P, Seitz HU (1993) Elicitor-induced changes in Ca^{2+} influx, K^+ efflux, and 4-hydroxybenzoic acid synthesis in protoplasts of *Daucus carota* L. Plant Physiol 103:407–412

Bajaj S, Targolli J, Liu LF, Ho THD, Wu R (1999) Transgenic approaches to increase dehydration-stress tolerance in plants. Mol Breeding 5:493–503

Balague C, Lin B, Alcon C, Flottes G, Malmstrom S, Kohler C, Neuhaus G, Pelletier G, Gaymard F, Roby D (2003) HLM1, an essential signalling component in the hypersensitive response, is a member of the cyclic nucleotide-gated channel ion channel family. Plant Cell 15:365–379

Barrett-Lennard EG, Ratingen PV, Mathie MH (1999) The developing pattern of damage in wheat (*Triticum aestivum* L.) due to the combined stresses of salinity and hypoxia:

experiments under controlled conditions suggest a methodology for plant selection. Aust J Agricult Res 50:129–136
Bisson MA, Gutknecht J (1977) Osmotic regulation in the marine alga, *Codium decorticatum*. II. Active chloride influx exerts negative feedback control on the turgor pressure. J Membrane Biol 37:85–98
Blatt MR, Grabov A, Brearley J, Hammond-Kosack K, Jones JDG (1999) K^+ channels of Cf-9 transgenic tobacco guard cells as targets for *Cladosporium fulvum* Avr9 elicitor-dependent signal transduction. Plant J 19:453–462
Blume B, Nürnberger T, Nass N, Scheel D (2000) Receptor-mediated increase in cytoplasmic free calcium required for activation of pathogen defense in parsley. Plant Cell 12:1425–1440
Blumwald E, Aharon GS, Lam C-H (1998) Early signal transduction pathways in plant-pathogen interactions. Trends Plant Sci 3:342–346
Blumwald E, Aharon GS, Apse MP (2000) Sodium transport in plant cells. Biochim Biophys Acta 1465:140–151
Boem FHG, Lavado RS, Porcelli CA (1996) Note on the effects of winter and spring waterlogging on growth, chemical composition and yield of rapeseed. Field Crop Res 47:175–179
Bohnert HJ, Shen B (1999) Transformation and compatible solutes. Sci Hort 78:237–260
Bohnert HJ, Sheveleva E (1998) Plant stress adaptations—making metabolism move. Curr Opin Plant Biol 1:267–274
Bohnert HJ, Nelson DE, Jensen RG (1995) Adaptation to environmental stresses. Plant Cell 7:1099–1111
Bowler C, Fluhr R (2000) The role of calcium and activated oxygen as signals for controlling cross-tolerance. Trend Plant Sci 5:241–246
Brauer D, Leggett JE, Egli DB (1987) Changes in K, Rb and Na transport to shoots after anoxia. Plant Physiol 83:219–224
Bravo-F P, Uribe EG (1981) An analysis of the relationship between respiration and the transmembrane potential in corn roots. Plant Physiol 67:809–814
Brownlee C, Goddard H, Hetherington AM, Peake L-A (1999) Specificity and integration of responses: Ca^{2+} as a signal in polarity and osmotic regulation. J Exp Bot 50:1001–1011
Carden DE, Walker DJ, Flowers TJ, Miller AJ (2003) Single-cell measurements of the contributions of cytosolic Na^+ and K^+ to salt tolerance. Plant Physiol 131:676–683
Casolo V, Petrussa E, Krajnakova J, Macri F, Vianello A (2005) Involvement of the mitochondrial K^+-ATP channel in H_2O_2- or NO-induced programmed death of soybean suspension cell cultures. J Exp Bot 56:997–1006
Chen J, Sucoff EI, Stadelmann EJ (1991) Aluminum and temperature alteration of cell membrane permeability of *Quercus rubra*. Plant Physiol 96:644–649
Chen YL, Huang RF, Xiao YM, Lu P, Chen J, Wang XC (2004) Extracellular calmodulin-induced stomatal closure is mediated by heterotrimeric G protein and H_2O_2. Plant Physiol 136:4096–4103
Chen Z, Newman I, Zhou M, Mendham N, Zhang G, Shabala S (2005) Screening plants for salt tolerance by measuring K^+ flux: a case study for barley. Plant Cell Environ 28:1230–1246
Chung WS, Lee SH, Kim JC, Heo WD, Kim MC, Park CY, Park HC, Lim CO, Kim WB, Harper JF, Cho MJ (2000) Identification of a calmodulin-regulated soybean Ca^{2+}-ATPase (SCA1) that is located in the plasma membrane. Plant Cell 12:1393–1407
Clarkson DT, Earnshow MJ, White PJ, Cooper HD (1988) Temperature dependent factors influencing nutrient uptake: an analysis of responses at different levels of organization. Plants and temperature. Society for Experimental Botany, Cambridge, pp 281–309
Clough SJ, Fengler KA, Yu IC, Lippok B, Smith RK, Bent AF (2000) The *Arabidopsis* dnd1 "defense, no death" gene encodes a mutated cyclic nucleotide-gated ion channel. Proc Natl Acad Sci USA 97:9323–9328
Coelho SM, Taylor AR, Ryan KP, Sousa-Pinto I, Brown MT, Brownlee C (2002) Spatiotemporal patterning of reactive oxygen production and Ca^{2+} wave propagation in fucus rhizoid cells. Plant Cell 14:2369–2381

Colmer TD, Bloom AJ (1998) A comparison of NH_4^+ and NO_3^- net fluxes along roots of rice and maize. Plant Cell Environ 21:240–246

Colmer TD, Huang SB, Greenway H (2001) Evidence for down-regulation of ethanolic fermentation and K^+ effluxes in the coleoptile of rice seedlings during prolonged anoxia. J Exp Bot 52:1507–1517

Cramer GR, Lynch J, Lauchli A, Epstein E (1987) Influx of Na^+, K^+, and Ca^{2+} into roots of salt-stressed cotton seedlings. Effects of supplemental Ca^{2+}. Plant Physiol 83:510–516

Delhaize E, Ryan PR, Hebb DM, Yamamoto Y, Sasaki T, Matsumoto H (2004) Engineering high-level aluminum tolerance in barley with the ALMT1 gene. Proc Natl Acad Sci USA 101:15249–15254

Demidchik V, Tester M (2002) Sodium fluxes through nonselective cation channels in the plasma membrane of protoplasts from *Arabidopsis* roots. Plant Physiol 128:379–387

Demidchik V, Shabala SN, Coutts KB, Tester MA, Davies JM (2003) Free oxygen radicals regulate plasma membrane Ca^{2+} and K^+-permeable channels in plant root cells. J Cell Sci 116:81–88

Dietrich P, Sanders D, Hedrich R (2001) The role of ion channels in light-dependent stomatal opening. J Exp Bot 52:1959–1967

Ding JP, Badot PM, Pickard BG (1993) Aluminium and hydrogen ions inhibit a mechanosensory calcium-selective cation channel. Aust J Plant Physiol 20:771–778

DuPont FM (1989) Effect of temperature on the plasma membrane and tonoplast ATPases of barley roots. Plant Physiol 89:1401–1412

Ehrhardt DW, Wais R, Long SR (1996) Calcium spiking in plant root hairs responding to rhizobium nodulation signals. Cell 85:673–681

Elphick CH, Sanders D, Maathuis FJM (2001) Critical role of divalent cations and Na^+ efflux in *Arabidopsis thaliana* salt tolerance. Plant Cell Environ 24:733–740

Fan LM, Wang YF, Wu WH (2003) Outward K^+ channels in *Brassica chinensis* pollen protoplasts are regulated by external and internal pH. Protoplasma 220:143–152

Felle HH (1988) Short-term pH regulation in plants. Physiol Plant 74:583–591

Felle HH (1996) Control of cytoplasmic pH under anoxic conditions and its implication for plasma membrane proton transport in *Medicago sativa* root hairs. J Exp Bot 47:967–973

Felle HH, Kondorosi E, Kondorosi A, Schultze M (1995) Nod signal-induced plasma-membrane potential changes in alfalfa root hairs are differentially sensitive to structural modifications of the lipochitooligosaccharide. Plant J 7:939–947

Garnett TP, Shabala SN, Smethurst PJ, Newman IA (2001) Simultaneous measurement of ammonium, nitrate and proton fluxes along the length of eucalypt roots. Plant Soil 236:55–62

Garnett TP, Shabala SN, Smethurst PJ, Newman IA (2003) Kinetics of ammonium and nitrate uptake by eucalypt roots and associated proton fluxes measured using ion selective microelectrodes. Funct Plant Biol 30:1165–1176

Garril A, Davies JM (1994) Patch clamping fungal membranes: new perspectives on ion transport. Micol Res 98:257–263

Gassmann W, Schroeder JI (1994) Inward-rectifying K^+ channels in root hairs of wheat—a mechanism for aluminum-sensitive low-affinity K^+ uptake and membrane potential control. Plant Physiol 105:1399–1408

Gelli A, Higgins VJ, Blumwald E (1997) Activation of plant plasma membrane Ca^{2+}-permeable channels by race-specific fungal elicitors. Plant Physiol 113:269–279

Gibbs J, Greenway H (2003) Mechanisms of anoxia tolerance in plants. I. Growth, survival and anaerobic catabolism. Funct Plant Biol 30:1–47

Gilroy S, Jones DL (2000) Through form to function: root hair development and nutrient uptake. Trend Plant Sci 5:56–60

Grant M, Brown I, Adams S, Knight M, Ainslie A, Mansfield J (2000) The *RPM1* plant disease resistance gene facilitates a rapid and sustained increase in cytosolic calcium that is necessary for the oxidative burst and hypersensitive cell death. Plant J 23:441–450

Greenway H, Gibbs J (2003) Mechanisms of anoxia tolerance in plants. II. Energy requirements for maintenance and energy distribution to essential processes. Funct Plant Biol 30:999–1036

Greenway H, Waters I, Newsome J (1992) Effects of anoxia on uptake and loss of solutes in roots of wheat. Aust J Plant Physiol 19:233–247

Hällgren J-E, Öquist G (1990) Adaptation to low temperatures. In: Alscher RG, Cumming JR (eds) Stress responses in plants: adaptation and acclimation mechanisms. Wiley-Liss, New York, pp 265–293

Handson PD, Shelley BC (1993) A review of plant analysis in Australia. Aust J Exp Agricult 33:1029–1038

Hartje S, Zimmermann S, Klonus D, Mueller-Roeber B (2000) Functional characterisation of LKT1, a K^+ uptake channel from tomato root hairs, and comparison with the closely related potato inwardly rectifying K^+ channel SKT1 after expression in *Xenopus oocytes*. Planta 210:723–731

Hasegawa PM, Bressan RA, Zhu JK, Bohnert HJ (2000) Plant cellular and molecular responses to high salinity. Annu Rev Plant Physiol Plant Mol Biol 51:463–499

Henriksen GH, Bloom AJ, Spanswick RM (1990) Measurement of net fluxes of ammonium and nitrate at the surface of barley roots using ion-selective microelectrodes. Plant Physiol 93:271–280

Henriksen GH, Raman DR, Walker LP, Spanswick RM (1992) Measurement of net fluxes of ammonium and nitrate at the surface of barley roots using ion-selective microelectrodes. 2. Patterns of uptake along the root axis and evaluation of the microelectrode flux estimation technique. Plant Physiol 99:734–747

Hoeberichts FA, Woltering EJ (2003) Multiple mediators of plant programmed cell death: interplay of conserved cell death mechanisms and plant-specific regulators. Bioessays 25:47–57

Hoth S, Geiger D, Becker D, Hedrich R (2001) The pore of plant K^+ channels is involved in voltage and pH sensing: domain-swapping between different K^+ channel alpha-subunits. Plant Cell 13:943–952

Ilan N, Schwartz A, Moran N (1994) External pH effects on the depolarization-activated K^+-channels in guard-cell protoplasts of *Vicia faba*. J Gen Physiol 103:807–831

Ivashikina N, Becker D, Ache P, Meyerhoff O, Felle HH, Hedrich R (2001) K^+ channel profile and electrical properties of *Arabidopsis* root hairs. FEBS Lett 508:463–469

Jabs T, Tschope M, Colling C, Hahlbrock K, Scheel D (1997) Elicitor-stimulated ion fluxes and O_2^- from the oxidative burst are essential components in triggering defense gene activation and phytoalexin synthesis in parsley. Proc Natl Acad Sci USA 94:4800–4805

Jiang M, Zhang J (2003) Cross-talk between calcium and reactive oxygen species originated from NADPH oxidase in abscisic acid-induced antioxidant defence in leaves of maize seedlings. Plant Cell Environ 26:929–939

Jones DL, Shaff JE, Kochian LV (1995) Role of calcium and other ions in directing root hair tip growth in *Limnobium stoloniferum*. 1. Inhibition of tip growth by aluminum. Planta 197:672–680

Kadota Y, Goh T, Tomatsu H, Tamauchi R, Higashi K, Muto S, Kuchitsu K (2004) Cryptogein-induced initial events in tobacco BY-2 cells: Pharmacological characterization of molecular relationship among cytosolic Ca^{2+} transients, anion efflux and production of reactive oxygen species. Plant Cell Physiol 45:160–170

Keunecke M, Hansen UP (2000) Different pH-dependences of K^+ channel activity in bundle sheath and mesophyll cells of maize leaves. Planta 210:792–800

Kinraide TB, Wyse RE (1986) Electrical evidence for turgor inhibition of proton extrusion in sugar beet taproot. Plant Physiol 82:1148–1150

Knight H, Knight MR (2001) Abiotic stress signalling pathways: specificity and cross-talk. Trend Plant Sci 6:262–267

Knight H, Trewavas AJ, Knight MR (1996) Cold calcium signalling in *Arabidopsis* involves two cellular pools and a change in calcium signature after acclimation. Plant Cell 8:489–503

Kochian LV (1995) Cellular mechanisms of aluminum toxicity and resistance in plants. Annu Rev Plant Physiol 46:237–260

Kohler B, Hills A, Blatt MR (2003) Control of guard cell ion channels by hydrogen peroxide and abscisic acid indicates their action through alternate signalling pathways. Plant Physiol 131:385–388

Kourie JI (1998) Interaction of reactive oxygen species with ion transport mechanisms. Am J Physiol 44:1–24

Kourie JI, Findlay GP (1991) Ionic currents across the plasmalemma of *Chara inflata* cells. III. Water-relations parameters and their correlation with membrane electrical properties. J Exp Bot 42:151–158

Kwak JM, Mori IC, Pei ZM, Leonhardt N, Torres MA, Dangl JL, Bloom RE, Bodde S, Jones JDG, Schroeder JI (2003) NADPH oxidase AtrbohD and AtrbohF genes function in ROS-dependent ABA signalling in *Arabidopsis*. EMBO J 22:2623–2633

Lacombe B, Pilot G, Gaymard F, Sentenac H, Thibaud JB (2000) pH control of the plant outwardly-rectifying potassium channel SKOR. FEBS Lett 466:351–354

Lecourieux D, Mazars C, Pauly N, Ranjeva R, Pugin A (2002) Analysis and effects of cytosolic free calcium increases in response to elicitors in *Nicotiana plumbaginifolia* cells. Plant Cell 14:2627–2641

Lee SH, Singh AP, Chung GC (2004) Rapid accumulation of hydrogen peroxide in cucumber roots due to exposure to low temperature appears to mediate decreases in water transport. J Exp Bot 55:1733–1741

Lew RR (1996) Pressure regulation of the electrical properties of growing *Arabidopsis thaliana* L root hairs. Plant Physiol 112:1089–1100

Lew RR (1998) Immediate and steady state extracellular ionic fluxes of growing *Arabidopsis thaliana* root hairs under hyperosmotic and hypoosmotic conditions. Physiol Plant 104:397–404

Li Z-S, Delrot S (1987) Osmotic dependence of the transmembrane potential difference of broad bean mesocarp cells. Plant Physiol 84:895–899

Lindberg S, Strid H (1997) Aluminium induces rapid changes in the cytosolic pH and free calcium and potassium concentrations in root protoplasts of wheat (*Triticum aestivum*). Physiol Plant 99:404–414

Liu K, Luan S (1998) Voltage-dependent K^+ channels as targets of osmosensing in guard cells. Plant Cell 10:1957–1970

Liu K, Luan S (2001) Internal aluminum block of plant inward K^+ channels. Plant Cell 13:1453–1465

Lucas WJ, Kochian LV (1986) Ion transport processes in corn roots: An approach utilizing microelectrode techniques. In: Gensler WG (ed) Advanced agricultural instrumentation: design and use. Nijhoff, Dordrecht, pp 402–425

Lyons JM (1973) Chilling injury in plants. Annu Rev Plant Physiol 24:445–466

Maathuis FJM, Amtmann A (1999) K^+ nutrition and Na^+ toxicity: the basis of cellular K^+/Na^+ ratios. Ann Bot 84:123–133

Macduff JH, Dhanoa MS (1996) Diurnal and ultradian rhythms in K^+ uptake by *Trifolium repens* under natural light patterns—evidence for segmentation at different root temperatures. Physiol Plant 98:298–308

Marschner H (1995) Mineral nutrition of higher plants. Academic Press, London, 889 pp

Marten I, Hoth S, Deeken R, Ache P, Ketchum KA, Hoshi T, Hedrich R (1999) AKT3, a phloem-localized K^+ channel, is blocked by protons. Proc Natl Acad Sci USA 96:7581–7586

Maser P, Thomine S, Schroeder JI, Ward JM, Hirschi K, Sze H, Talke IN, Amtmann A, Maathuis FJM, Sanders D, Harper JF, Tchieu J, Gribskov M, Persans MW, Salt DE, Kim SA, Guerinot ML (2001) Phylogenetic relationships within cation transporter families of *Arabidopsis*. Plant Physiol 126:1646–1667

Mathieu Y, Kurkdjian A, Xia H, Guern J, Koller A, Spiro MD, Oneill M, Albersheim P, Darvill A (1991) Membrane responses induced by oligogalacturonides in suspension-cultured tobacco cells. Plant J 1:333–343

Mesnard F, Ratcliffe RG (2005) NMR analysis of plant nitrogen metabolism. Photosynth Res 83:163–180

Miller AJ, Cookson SJ, Smith SJ, Wells DM (2001) The use of microelectrodes to investigate compartmentation and the transport of metabolized inorganic ions in plants. J Exp Bot 52:541–549

Monroy AF, Dhindsa RS (1995) Low-temperature signal transduction: induction of cold acclimation-specific genes of alfalfa by calcium at 25°C. Plant Cell 7:321–331

Munns R (2002) Comparative physiology of salt and water stress. Plant Cell Environ 25:239–250

Murata N, Los DA (1997) Membrane fluidity and temperature perception. Plant Physiol 115:875–879

Murata Y, Pei ZM, Mori IC, Schroeder J (2001) Abscisic acid activation of plasma membrane Ca^{2+} channels in guard cells requires cytosolic NAD(P)H and is differentially disrupted upstream and downstream of reactive oxygen species production in *abi1–1* and *abi2–1* protein phosphatase 2C mutants. Plant Cell 13:2513–2523

Newman IA (2001) Ion transport in roots: measurement of fluxes using ion-selective microelectrodes to characterize transporter function. Plant Cell Environ 24:1–14

Newman IA, Kochian LV, Grusak MA, Lucas WJ (1987) Fluxes of H^+ and K^+ in corn roots. Characterisation and stoichiometries using ion-selective microelectrodes. Plant Physiol 84:1177–1184

Nurnberger T, Nennsteil D, Jabs T, Sacks WR, Hahlbrock K, Scheel D (1994) High affinity binding of a fungal oligopeptide elicitor to parsley plasma membranes triggers multiple defence responses. Cell 78:449–460

Nurnberger T, Wirtz W, Nennstiel D, Hahlbrock K, Jabs T, Zimmermann S, Scheel D (1997) Signal perception and intracellular signal transduction in plant pathogen defence. J Recept Signal Transd Res 17:127–136

Okazaki Y, Shimmen T, Tazawa M (1984) Turgor regulation in a brackish Charophyte, *Lamprothamnium succinctum*. II. Changes in K^+, Na^+ and Cl^- concentrations, membrane potential and membrane resistance during turgor regulation. Plant Cell Physiol 25:573–581

Olivetti GP, Cumming JR, Etherton B (1995) Membrane-potential depolarization of root cap cells precedes aluminum tolerance in snapbean. Plant Physiol 109:123–129

Palmgren MG (1991) Regulation of plasma membrane H^+-ATPase activity. Physiol Plant 83:314–323

Pei ZM, Murata Y, Benning G, Thomine S, Klusener B, Allen GJ, Grill E, Schroeder JI (2000) Calcium channels activated by hydrogen peroxide mediate abscisic acid signalling in guard cells. Nature 406:731–734

Petraglia T, Poole RJ (1980) Effect of anoxia on ATP levels and ion transport rates in red beet. Plant Physiol 65:973–974

Pettersson S (1995) Low root zone temperature effects on net mineral nutrient uptake and distribution in barley (*Hordeum vulgare*). J Plant Physiol 145:459–464

Pineros MA, Shaff JE, Kochian V (1998) Development, characterization, and application of a cadmium-selective microelectrode for the measurement of cadmium fluxes in roots of *Thlaspi species* and wheat. Plant Physiol 116:1393–1401

Platten JD, Shabala SN, Elliott RC, Reid JB (2004) A novel mutant with modified tropic responses in *Pisum sativum* L. Planta 220:222–229

Pritchard J, Barlow PW, Adams JS, Tomos AD (1990) Biophysics of the inhibition of the growth of maize roots by lowered temperature. Plant Physiol 93:220–230

Ratcliffe RG (1997) In vivo NMR studies of the metabolic response of plant tissues to anoxia. Ann Bot 79:39–48

Raven JA (1985) Regulation of pH and generation of osmolarity in vascular plants: a cost-benefit analysis in relation to efficiency of use of energy, nitrogen and water. New Phytol 101:25–77

Rawyler A, Pavelic D, Gianinazzi C, Oberson J, Braendle R (1999) Membrane lipid integrity relies on a threshold of ATP production rate in potato cell cultures submitted to anoxia. Plant Physiol 120:293–300

Reid RJ, Smith FA (2000) The limits of sodium/calcium interactions in plant growth. Aust J Plant Physiol 27:709–715

Reid RJ, Jefferies RL, Pitman MG (1984) *Lamprothamnium*, a euryhaline charophyte. J Exp Bot 35:925–937

Reinhold L, Seiden A, Volokita M (1984) Is modulation of the rate of proton pumping a key event in osmoregulation? Plant Physiol 75:846–849

Rengel Z (1992) The role of calcium in salt toxicity. Plant Cell Environ 15:625–632
Reuveni M, Colombo R, Lerner HR, Pradet A, Polyakoff-Mayber A (1987) Osmotically induced proton extrusion from carrot cells in suspension culture. Plant Physiol 85:383–388
Roelfsema MRG, Hedrich R (2002) Studying guard cells in the intact plant: modulation of stomatal movement by apoplastic factors. New Phytol 153:425–431
Roos W (2000) Ion mapping in plant cells—methods and applications in signal transduction research. Planta 210:347–370
Ryan PR, Newman IA, Shields B (1990) Ion fluxes in corn roots measured by microelectrodes with ion-specific liquid membranes. J Membrane Sci 53:59–69
Ryan PR, Delhaize E, Randall PJ (1995) Characterization of Al-stimulated efflux of malate from the apices of Al-tolerant wheat roots. Planta 196:103–110
Ryan PR, Delhaize E, Jones DL (2001) Function and mechanism of organic anion exudation from plant roots. Annu Rev Plant Physiol Plant Mol Biol 52:527–560
Sanders D, Brownlee C, Harper JF (1999) Communicating with calcium. Plant Cell 11:691–706
Santos CLV, Campos A, Azevedo H, Caldeira G (2001) In situ and in vitro senescence induced by KCl stress: nutritional imbalance, lipid peroxidation and antioxidant metabolism. J Exp Bot 52:351–360
Sasaki T, Yamamoto Y, Ezaki B, Katsuhara M, Ahn SJ, Ryan PR, Delhaize E, Matsumoto H (2004) A wheat gene encoding an aluminum-activated malate transporter. Plant J 37:645–653
Schroeder JI, Ward JM, Gassmann W (1994) Perspectives on the physiology and structure of inward-rectifying K^+ channels in higher plants—biophysical implications for K^+ uptake. Annu Rev Biophys Biomol Struct 23:441–471
Schroeder JI, Kwak JM, Allen GJ (2001) Guard cell abscisic acid signalling and engineering drought hardiness in plants. Nature 410:327–330
Serrano R, Culianz-Macia FA, Moreno V (1999a) Genetic engineering of salt and drought tolerance with yeast regulatory genes. Sci Hort 78:261–269
Serrano R, Mulet JM, Rios G, Marquez JA, de Larrinoa IF, Leube MP, Mendizabal I, Pascual-Ahuir A, Proft M, Ros R, Montesinos C (1999b) A glimpse of the mechanism of ion homeostasis during salt stress. J Exp Bot 50:1023–1036
Shabala S (2000) Ionic and osmotic components of salt stress specifically modulate net ion fluxes from bean leaf mesophyll. Plant Cell Environ 23:825–837
Shabala S (2003) Regulation of potassium transport in leaves: from molecular to tissue level. Ann Bot 92:627–634
Shabala S, Lew RR (2002) Turgor regulation in osmotically stressed *Arabidopsis* epidermal root cells. Direct support for the role of inorganic ion uptake as revealed by concurrent flux and cell turgor measurements. Plant Physiol 129:290–299
Shabala S, Newman IA (1997) H^+ flux kinetics around plant roots after short-term exposure to low temperature—identifying critical temperatures for plant chilling tolerance. Plant Cell Environ 20:1401–1410
Shabala S, Newman IA (1998) Osmotic sensitivity of Ca^{2+} and H^+ transporters in corn roots—effect on fluxes and their oscillations in the elongation region. J Membrane Biol 161:45–54
Shabala S, Newman IA (1999) Light-induced changes in hydrogen, calcium, potassium, and chloride ion fluxes and concentrations from the mesophyll and epidermal tissues of bean leaves. Understanding the ionic basis of light-induced bioelectrogenesis. Plant Physiol 119:1115–1124
Shabala S, Shabala L (2002) Kinetics of net H^+, Ca^{2+}, K^+, Na^+, NH_4^+, and Cl^- fluxes associated with post-chilling recovery of plasma membrane transporters in *Zea mays* leaf and root tissues. Physiol Plant 114:47–56
Shabala S, Newman IA, Morris J (1997) Oscillations in H^+ and Ca^{2+} ion fluxes around the elongation region of corn roots and effects of external pH. Plant Physiol 113:111–118
Shabala S, Newman I, Whittington J, Juswono U (1998) Protoplast ion fluxes: their measurement and variation with time, position and osmoticum. Planta 204:146–152
Shabala S, Babourina O, Newman I (2000) Ion-specific mechanisms of osmoregulation in bean mesophyll cells. J Exp Bot 51:1243–1253

Shabala L, Ross T, Newman I, McMeekin T, Shabala S (2001a) Measurements of net fluxes and extracellular changes of H^+, Ca^{2+}, K^+, and NH_4^+ in *Escherichia coli* using ion-selective microelectrodes. J Microbiol Method 46:119–129

Shabala L, Shabala S, Ross T, McMeekin T (2001b) Membrane transport activity and ultradian ion flux oscillations associated with cell cycle of *Thraustochytrium sp*. Aust J Plant Physiol 28:87–99

Shabala L, Budde B, Ross T, Siegumfeldt H, Jakobsen M, McMeekin T (2002) Responses of *Listeria monocytogenes* to acid stress and glucose availability revealed by a novel combination of fluorescence microscopy and microelectrode ion-selective techniques. Appl Environ Microbiol 68:1794–1802

Shabala S, Shabala L, van Volkenburgh E (2003) Effect of calcium on root development and root ion fluxes in salinised barley seedlings. Funct Plant Biol 30:507–514

Shabala L, Ross T, McMeekin T, Shabala S (2005a) Non-invasive microelectrode ion flux measurements to study adaptive responses of surface associated microorganisms to the environment. FEMS Microbial Rev (in press)

Shabala S, Shabala L, van Volkenburgh E, Newman I (2005b) Effect of divalent cations on ion fluxes and leaf photochemistry in salinised barley leaves. J Exp Botany 56:1369–1378

Shabala L, Cuin TA, Newman I, Shabala S (2005c) Salinity-induced ion flux patterns from the excised roots of *Arabidopsis sos* mutants. Planta (published on-line first DOI: 10.1007/s00425–005–0074–2)

Shipley AM, Feijo JA (1999) The use of the vibrating probe technique to study steady extracellular currents during pollen germination and tube growth. In: Cresti M, Cai G, Moscatelli A (eds) Fertilization in higher plants: molecular and cytological aspects. Springer, Berlin Heidelberg New York, pp 235–250

Shorning BY, Smirnova EG, Yaguzhinsky LS, Vanyushin BF (2000) Necessity of superoxide production for development of etiolated wheat seedlings. Biochemistry (Moscow) 65:1357–1361

Smethurst CF, Shabala S (2003) Screening methods for waterlogging tolerance in lucerne: comparative analysis of waterlogging effects on chlorophyll fluorescence, photosynthesis, biomass and chlorophyll content. Funct Plant Biol 30:335–343

Smirnoff N, Wheeler GL (2000) Ascorbic acid in plants: biosynthesis and function. Crit Rev Plant Sci 19:267–290

Smith PJS (1995) Non-invasive ion probes—tools for measuring transmembrane ion flux. Nature 378:645–646

Spalding EP (2000) Ion channels and the transduction of light signals. Plant Cell Environ 23:665–674

Subbaiah CC, Bush DS, Sachs MM (1998) Mitochondrial contribution to the anoxic Ca^{2+} signal in maize suspension-cultured cells. Plant Physiol 118:759–771

Suhita D, Raghavendra AS, Kwak JM, Vavasseur A (2004) Cytoplasmic alkalization precedes reactive oxygen species production during methyl jasmonate- and abscisic acid-induced stomatal closure. Plant Physiol 134:1536–1545

Sutton JM, Lea EJA, Downie JA (1994) The nodulation-signaling protein *nodo* from *Rhizobium leguminosarum* biovar *viciae* forms ion channels in membranes. Proc Natl Acad Sci USA 91:9990–9994

Tegg RS, Melian L, Wilson CR, Shabala S (2005) Plant cell growth and ion flux responses to the *Streptomycete* phytotoxin thaxtomin-A: calcium and hydrogen flux patterns revealed by the non-invasive MIFE technique. Plant Cell Physiol 46:638–648

Teodoro AE, Zingarelli L, Lado P (1998) Early changes of Cl^- efflux and H^+ extrusion induced by osmotic stress in *Arabidopsis thaliana* cells. Physiol Plant 102:29–37

Tester M (1997) Techniques for studying ion channels: an introduction. J Exp Bot 48:353–359

Tester M, Davenport R (2003) Na^+ tolerance and Na^+ transport in higher plants. Ann Bot 91:503–527

Tomos AD, Leigh RA (1999) The pressure probe: a versatile tool in plant cell physiology. Annu Rev Plant Physiol Plant Mol Biol 50:447–472

Trono D, Flagella Z, Laus MN, Di Fonzo N, Pastore D (2004) The uncoupling protein and the potassium channel are activated by hyperosmotic stress in mitochondria from durum wheat seedlings. Plant Cell Environ 27:437–448

Tyerman SD, Skerrett M, Garrill A, Findlay GP, Leigh RA (1997) Pathways for the permeation of Na^+ and Cl^- into protoplasts derived from the cortex of wheat roots. J Exp Bot 48:459–480

Tyerman SD, Beilby M, Whittington J, Juswono U, Newman I, Shabala S (2001) Oscillations in proton transport revealed from simultaneous measurements of net current and net proton fluxes from isolated root protoplasts: MIFE meets patch-clamp. Aust J Plant Physiol 28:591–604

Vera-Estrella R, Barkla BJ, Higgins VJ, Blumwald E (1994) Plant defence response to fungal pathogens. Activation of host-plasma membrane H^+-ATPase by elicitor-induced enzyme dephosphorylation. Plant Physiol 104:209–215

Vera-Estrella R, Barkla BJ, Bohnert HJ, Pantoja O (1999) Salt stress in *Mesembryanthemum crystallinum* L cell suspensions activates adaptive mechanisms similar to those observed in the whole plant. Planta 207: 426–435

Very AA, Sentenac H (2002) Cation channels in the *Arabidopsis* plasma membrane. Trend Plant Sci 7:168–175

Wang MY, Siddiqi MY, Ruth TJ, Glass ADM (1993) Ammonium uptake by rice roots. II. Kinetics of $^{13}NH_4^+$ influx across the plasmalemma. Plant Physiol 103:1259–1267

Ward JM (2001) Identification of novel families of membrane proteins from the model plant *Arabidopsis thaliana*. Bioinformatics 17:560–563

Wherrett T, Ryan P, Delhaize E, Shabala S (2005) Effect of aluminium on membrane potential and ion fluxes at the apices of wheat roots. Funct Plant Biol 32:199–208

White PJ, Clarkson DT, Earnshaw MJ (1987) Acclimation of potassium influx in rye (*Secale cereale*) at low root temperatures. Planta 171:377–385

Wyn Jones RG, Pritchard J (1989) Stresses, membranes and cell walls. In: Jones HG, Flowers TJ, Jones MB (eds) Plants under stress: biochemistry, physiology, and ecology and their application to plant improvement. Cambridge University Press, Cambridge, pp 95–114

Xia JH, Roberts JKM (1996) Regulation of H^+ extrusion and cytoplasmic pH in maize root tips acclimated to a low-oxygen environment. Plant Physiol 111:227–233

Yoshida S (1991) Chilling-induced inactivation and its recovery of tonoplast H^+-ATPase in mung bean cell suspension cultures. Plant Physiol 95:456–460

Yu L, Moshelion M, Moran N (2001) Extracellular protons inhibit the activity of inward-rectifying potassium channels in the motor cells of *Samanea saman* pulvini. Plant Physiol 127:1310–1322

Zhang Q, Greenway H (1995) Membrane transport in anoxic rice coleoptiles and storage tissues of beetroot. Aust J Plant Physiol 22:965–975

Zhang Q, Lauchli A, Greenway H (1992) Effects of anoxia on solute loss from beetroot storage tissue. J Exp Bot 43:897–905

Zhang X, Miao YC, An GY, Zhou Y, Shangguan ZP, Gao JF, Song CP (2001) K^+ channels inhibited by hydrogen peroxide mediate abscisic acid signaling in *Vicia* guard cells. Cell Res 11:195–202

Zhu JK (2002) Salt and drought stress signal transduction in plants. Annu Rev Plant Biol 53:247–273

Zhu JK (2003) Regulation of ion homeostasis under salt stress. Curr Opin Plant Biol 6:441–445

Zimmermann S, Nürnberger T, Frachisse JM, Wirtz W, Guern J, Hedrich R, Scheel D (1997) Receptor-mediated activation of a plant Ca^{2+}-permeable ion channel involved in pathogen defence. Proc Natl Acad Sci USA 94:2751–2755

Zimmermann S, Frachisse JM, Thomine S, Barbier-Brygoo H, Guern J (1998) Elicitor-induced chloride efflux and anion channels in tobacco cell suspensions. Plant Physiol Biochem 36:665–674

Zimmermann S, Ehrhardt T, Plesch G, Muller-Rober B (1999) Ion channels in plant signalling. Cell Mol Life Sci 55:183–203

Zingarelli L, Marre MT, Massardi F, Lado P (1999) Effects of hyper-osmotic stress on K^+ fluxes, H^+ extrusion, transmembrane electric potential difference and comparison with the effects of fusicoccin. Physiol Plant 106:287–295

Zsoldos F, Vashegyi A, Pecsvaradi A, Bona L (2001) Growth and potassium transport in common and durum wheat as affected by aluminum and nitrite stress. J Plant Nutr 24:345–356

4 Electrochemical Sensor Applications to the Study of Molecular Physiology and Analyte Flux in Plants

MARK A. MESSERLI,[1] KENNETH R. ROBINSON,[2] PETER J.S. SMITH[1]

4.1 Introduction

Electrophysiological studies on plants have always been challenging. Cell walls and turgor pressure have made it difficult to apply many standard approaches used on animal cells. For these reasons, plant physiologists have long sought and developed novel methods for examining cellular physiology via non-invasive approaches. This review covers one such example, an electrochemical method that evolved out of a series of capacitively coupled techniques using a modulation approach. The first, for biological applications, was published by Blüh and Scott (1950) using an aerial probe. Although sparse on results, the authors claim preliminary data mapping surface potentials from various plant materials. Further development was reported in a series of papers by Grahm (1964) and Grahm and Hertz (1962, 1964) with data on the geoelectric and auxin-induced effects from coleoptiles using parallel plate capacitors. Recently, a more refined device, termed the bioKelvin probe, measured light-induced field changes originating from subsurface currents of a single corn coleoptile (Baikie et al. 1999). This device incorporated positional feedback and improved spatial resolution. Sanger et al. (1990) published a preliminary report using a similar approach.

The biggest breakthrough in the design of an instrument for monitoring external voltage fields, as related to the transmembrane passage of ions, came with the full development of the vibrating voltage probe by Jaffe and Nuccitelli (1974). Davies (1966) briefly described a similar device applied to muscle fibers. While subsequent studies by Jaffe, colleagues, and others are too numerous to mention, the vibrating probe was put to good use by plant physiologists as a method for monitoring ion transport (reviewed by Nuccitelli 1991).

Although a powerful tool, used to great effect on studies involving patterning and tip growth, the voltage probe has the limitation of not being chemically selective. An approach was needed where identification of the transported ion(s) that generated the current could be achieved. The first example was published by Gow et al. (1984), measuring H^+ gradients over the

[1] BioCurrents Research Center, Program in Molecular Physiology, Marine Biological Laboratory, 7 MBL Street, Woods Hole, MA 02543, USA

[2] Department of Biological Sciences, Purdue University, West Lafayette, IN 47907, USA

Plant Electrophysiology – Theory & Methods (ed. by Volkov)

surface of growing hyphae, with the landmark paper by Jaffe and Levy (1987) automating the process for Ca^{2+} measurement. The full description was published by Kühtreiber and Jaffe (1990), with diversification to K^+, H^+, and Ca^{2+} fluxes in maize roots and maize suspension cells by Kochian et al. (1992). Around the same time further plant applications were being explored by Newman and colleagues (Arif and Newman 1993). The use of ion-selective electrodes (ISEs) in this configuration is termed self-referencing by the authors (Smith et al. 1999). Over the approximately 20 years since its development there have been numerous successful applications and diversification to include other liquid membrane sensors, Cd^{2+} for example (Pineros et al. 1998) and Cl^- (Shabala and Newman 1998; Shabala et al. 2000). Cl^- detection is of particular interest to this review, and will be considered below as detection with the available Cl^--selective solvents is problematic, as recognized by Doughty and Langton (2001), Messerli et al. (2004), and Garber et al. (2005). The use of these sensors highlights the problems and pitfalls that can befall the unwary investigator in applying any electrochemical sensor.

Following the potentiometric ISEs came the self-referencing amperometric design, first applied to oxygen detection (Land et al. 1999; Mancuso et al. 2000). These solid-state redox-based sensors have so far seen a broader application in the animal sciences, but the potential to measure nitric oxide flux (Kumar et al. 2001; Porterfield et al. 2001) or H_2O_2 efflux (Twig et al. 2001, 2005) offers a clear application in plants. Modification through enzyme incorporation has also been demonstrated (Jung et al. 2001).

Electrochemical sensors, when used correctly on biological systems, offer a huge experimental return, particularly in the plant sciences where more conventional electrophysiological approaches are difficult. The self-referencing approach enhances this return by providing flux data and powerful signal analysis, refining sensitivity and selectivity. This review aims to introduce the reader to both the strengths and the weaknesses of this technique, which, although now 2 decades old, may still be unfamiliar to many.

4.2 Electrochemical detection with microelectrodes

4.2.1 Properties of electrochemical sensors

Self-referencing with electrochemical sensors is a modulation technique where a single sensor is used to measure the activity/ concentration of an analyte at different points in space and time. As micron-sized electrochemical sensors are the basis for self-referencing, we will discuss some physical properties of these sensors before discussing their use in a self-referencing mode.

The two fundamental types of micro-electrochemical sensors used with self-referencing to date are the potentiometric, ion-selective electrodes (ISEs), and the amperometric microelectrodes. The ISEs are based on an ion-selective

solvent or liquid membrane, immobilized in the tip of a micropipette with tip diameters of 1–4 μm. For an ideal electrode the measured voltage is related to the activity of the ion by the Nernst equation

$$E = E_O + S \log a_i \quad (1)$$

where 'E_O' is the offset (reference) potential, 'S' is the Nernstian slope$= \frac{2.3RT}{z_i F}$ and 'a_i' is the activity of the primary ion. The offset potential is comprised of the many boundary potential and liquid junction potential differences that exist across the circuit comprising the reference and measuring electrodes. Through calibration of each ISE we perform an empirical determination of the slope of the line describing the voltage output for the change in ionic activity. Since ionic activity is directly proportional to ion concentration, via the activity coefficient, and the changes that occur to the activity coefficient due to changes in ionic strength are usually negligible during self-referencing, we will use concentration in place of activity for ISEs.

The amperometric sensors are solid-state sensors with usually a metal, platinum or gold, or carbon as the electrolytic surface. The amperometric sensors used in combination with self-referencing, have only been used in constant-potential mode, where the sensors are voltage-clamped to a known potential, relative to the bath potential, that is sufficient to electrolyze the analyte. It is one of the amperometric methods that provides sub-second temporal resolution, but by itself cannot identify the electroactive analyte (Phillips and Wightman 2003). The electrodes are built in a manner that diffusion of the analyte to the electrolytic surface is rate limiting, creating a current that is dependent on the concentration of the analyte

$$I = I_O + S \cdot C \quad (2)$$

'I_O' is a current offset, 'S' is the slope of the calibration curve with units of Ampere/ Molar, and 'C' is the concentration of the analyte. In special cases of enzyme-based sensors, an electroactive product of the enzyme is measured. The concentration of that product is proportional to the concentration of the non-electroactive substrate of the enzyme (Jung et al. 2001) and thus the concentration of that substrate can be determined.

4.2.2 Response time

General properties of micron-sized sensors (<10 μm) are that they reach equilibrium relatively quickly, have greater spatial resolution, and are much less disturbing to the local chemical environment compared to macroelectrodes. The response times of ion-selective microelectrodes can be so fast that the electronics of the system slow the measured response (Ammann 1986). For example, the response time of potentiometric electrodes will depend on their ability to supply enough charge to the voltage-sensing node in order for

it to reach its steady state value. Low input impedance of the amplifier and stray capacitances in the circuit will draw more charge than an ideal system therefore slowing the response time of the system. Micron-sized, ion-selective sensors have been characterized with high resistances, 1–20 GΩ (Ammann 1986). Amplifier input impedances of 10^5–10^6 GΩ are typically used to minimize current and allow sampling of the ion concentration without dramatically changing it. With an ideal amplifier, why are the electrodes so fast? Diffusion through the stagnant aqueous layer at the surface of the electrode defines the response time of the sensors when the ion-selective membrane is equilibrated with the salt of an ion to which the electrode responds (Bakker et al. 1997). A brief theoretical analysis will put this in perspective. In a diffusion-limited system, how quickly will an analyte diffuse from the edge to the center of the microelectrode? For a 4 μm diameter sensor, K^+, for example, would require only 0.3 ms ($t=L^2/6D$ for diffusion in 3 dimensions, $D_{K+}= 2.0\times10^{-5}$ cm/s). For comparison, it would take 21 s to diffuse from the edge to the center of a 1 mm diameter sensor. Most analytes that have been measured with self-referencing systems have diffusion coefficients in the range of 10^{-4}–10^{-6} cm^2/s indicating that the electronics will be the primary factor limiting the response time of the measurement under relatively ideal conditions.

The response time of ISEs is governed by the ability to provide charge to the sensing node. This involves the availability of charge carriers at the surface of the electrode tip. Therefore, surface area of the ion-selective solvent, proportional to the square of the tip diameter, will affect response time. The presence of interferents will also slow response times. We have characterized the response times of micro electrochemical sensors with our system with different tip diameters, column lengths, and in the presence of an interferent. Figure 4.1A shows an example of the response times for a K^+-selective electrode in a simple solution (100 mM HEPES pH 7 with 0.1, 1 and 10 mM KCl). Figure 4.1B shows an enlargement of the response time from 1 to 0.1 mM K^+, indicated in Fig. 4.1A, and an overlay under the same conditions with the addition of Na^+, a known, albeit poor interferent. These 2–3 μm K^+-selective electrodes respond to 95% of their new steady state value ($t_{95\%}$) in 41–77 ms, depending on the change in concentration (line 3, Table 4.1). The electrode possesses $10^{3.9}$ selectivity for K^+ over Na^+, indicating that a lot of Na^+ must be present to interfere with K^+ detection. In the presence of 450 mM Na^+ (seawater levels) not only does the response time increase nearly 3-fold but the Nernstian response also decreases by 8% (Fig. 4.1B). Both of these features are classic indications of an interferent (Fleet et al. 1974; Bakker et al. 1997). In Table 4.1 we give a listing of the response times of three of the potentiometric sensors and one of the amperometric sensors in defined media. Simple solutions were used in media 1 and 3 to show the effects on response time with changes in tip size and column length. The sensors remained stationary during the experiment, while two to three adjacent streams of media (1 ml/min) were rapidly positioned in front of the measuring electrode. The rapid exchange system was able to exchange streams in front of the measuring electrodes in less than 8 ms ($t_{95\%}$). These measurements describe the response time of the entire measuring system

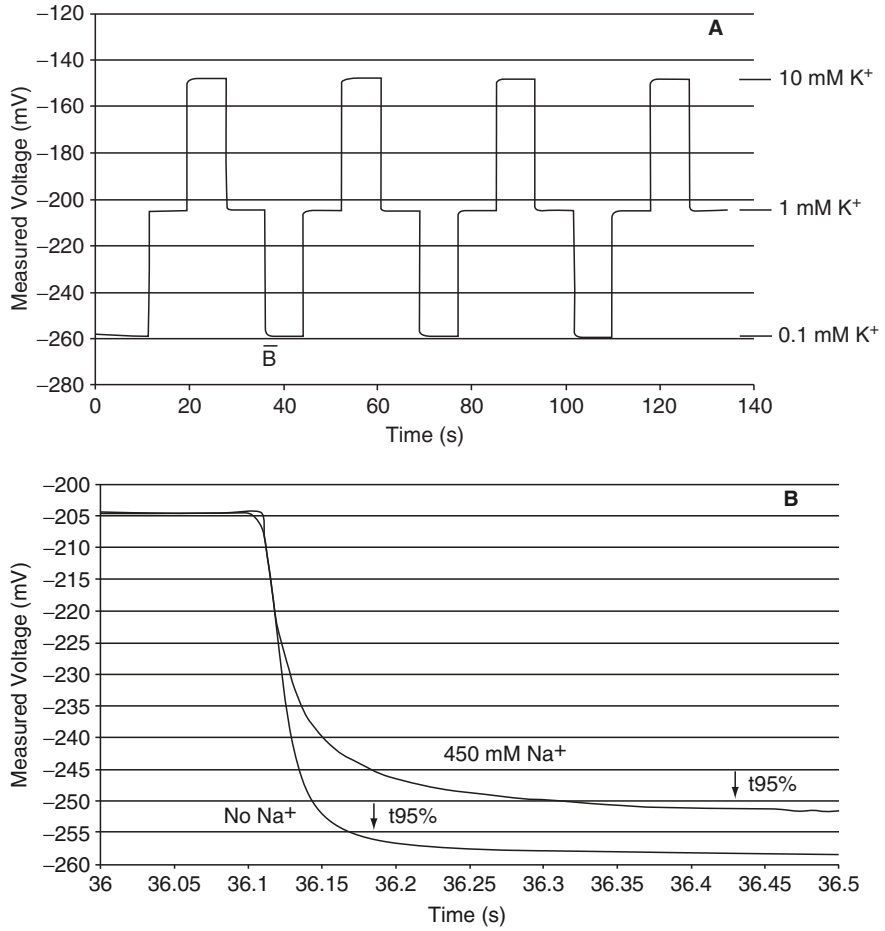

Fig. 4.1. Voltage response of a K^+-selective electrode to step changes in K^+ concentration. **A** The voltage response recorded by a K^+-selective electrode as a simple medium containing 100 mM HEPES (pH 7.0) with 0.1, 1 or 10 mM KCl was passed over the tip with a rapid exchange flow system. **B** An overlay of the magnified voltage response from 1 to 0.1 mM KCl, marked in **A** with a response under similar conditions in the presence of 450 mM NaCl. Na^+ is a characterized interferent of the K^+-selective electrode used here. In the presence of Na^+, the response time is nearly 3 times longer and causes the electrode to respond to this change in K^+ concentration 8% lower than optimal

from the sensor through the electronics for four electrodes of each type. The response times are generally faster than 200 ms for electrodes with tips greater than 1 µm. A few trends can be distinguished:

1) Longer column lengths give rise to longer response times;
2) 2–3 µm diameter pipette tips are faster than 1 µm diameter tips;
3) Longer response times occur when measuring in lower concentrations of the primary ion.

Table 4.1. Response times determined for a variety of electrochemical microsensors under different conditions.

Electrode	Column length	Tip size	Medium	Response times ($t_{95\%}$ ms) for concentration ranges			
K^+				10–1 mM	1–0.1 mM	0.1–1 mM	1–10 mM
	100 µm	~1 µm	1	195 ± 59	376 ± 86	165 ± 41	114 ± 26
	1000 µm	~1 µm	1	369 ± 91	516 ± 86	247 ± 54	191 ± 46
	100 µm	2–3 µm	1	41 ± 3	77 ± 4	53 ± 4	44 ± 3
w/ 450 mM Na+	100 µm	2–3 µm	2	64 ± 9	225 ± 6	91 ± 8	69 ± 15
H^+				pH 6–7	pH 7–8	pH 8–7	pH 7–6
	30 µm	~1 µm	3	209 ± 12	220 ± 15	214 ± 27	202 ± 13
	300 µm	~1 µm	3	251 ± 21	269 ± 14	245 ± 11	244 ± 17
	30 µm	2–3 µm	3	135 ± 23	130 ± 32	126 ± 30	124 ± 35
Ca^{2+}				10–1 mM	1–0.1 mM	0.1–1 mM	1–10 mM
	30 µm		4	58 ± 9	81 ± 10	48 ± 7	53 ± 10
O_2				Air – N_2 saturated		N_2 – Air saturated	
	n.a.	2–3 µm	4	21.8 ± 2.8		24.3 ± 2.6	
H^+ Messerli et al. (1999)	30 µm	1–2 µm	5	pH 5.5–6.0 223 ± 37	pH 6.0–6.5 252 ± 22	pH 6.5–6.0 214 ± 23	pH 6.0–5.5 223 ± 22
H^+ Feijó et al. (1999)	10–15 µm	1–2 µm	6	727 ± 59	664 ± 69	572 ± 27	738 ± 71

Medium 1. 100 mM HEPES (pH 7.0) with 0.1, 1.0 or 10 mM KCl
Medium 2. Medium 1 with 450 mM NaCl
Medium 3. 100 mM MES (pH 6), 100 mM HEPES (pH 7.8) set with KOH
Medium 4. in mM, 120 NaCl, 5 KCl, 2 $CaCl_2$, 2 $MgCl_2$ 10 HEPES (pH 7.4)
Medium 5. in mM, 0.16 H_3BO_3, 0.127 $Ca(NO_3)_2$, 1.0 KNO_3, 5.0 MES, 292 sucrose, pH 5.5 with KOH (Messerli et al. 1999)
Medium 6. in mM 1.6 H_3BO_3, 0.05 $CaCl_2$, 1.0 KCl, 0.05 MES, 146 sucrose (Feijó et al. 1999)

The response times of the H^+ electrodes do not vary as much as the K^+ or Ca^{2+} electrodes and are not as dependent on column length as the K^+. This may be a result of the H^+ buffer present in solution. The response time of the O_2 electrode is very fast as predicted by Schneiderman and Goldstick (1976).

4.2.3 Spatial resolution

The other useful feature of micron-sized sensors is their spatial resolution. The spatial resolution of potentiometric electrodes is defined by the surface area of the ion-selective solvent. As long as bulk movement of analyte does

not occur, the depth of sensing from the surface of a potentiometric electrode is considered negligible compared to the diameter of the ion-selective solvent itself, usually 1–4 μm. For example, if an electrode was being used to measure ionic concentration at a point near the surface of the cell, a 1–4 μm diameter electrode placed with the surface of the tip orthogonal to the cell surface will report the average concentration over the 1–4 μm tip diameter. Amperometric sensors used in constant potential mode, on the other hand, possess a sensing field that extends out into the medium away from the electrolytic surface. Take for example the O_2-sensing electrode. The electrode generates current by reducing O_2 at its sensing surface. Reduction of O_2 consumes O_2 in the region immediately in front of the tip creating an O_2 depleted zone. These O_2 depleted fields have been modeled for both macro and microelectrodes with recessed and/ or coated tips (Schneiderman and Goldstick 1976, 1978). Carefully constructed electrodes with recessed electrolytic surfaces and/ or coatings will limit the extent of this O_2 depleted field keeping the depletion zone restricted close to the tip. A well-constructed electrode can have virtually the entire O_2 depleted zone located within the membrane at its tip. Therefore, the choice of design and construction of amperometric electrodes will have the greatest influence defining the sensing zone.

In summary, electrochemical detection with microelectrodes under relatively ideal conditions can relay a concentration measurement quickly from a spatially restricted domain.

4.2.4 Electrode types

4.2.4.1 Potentiometric: construction

The manufacturing of micron-sized ISEs used in biological systems has changed little in 2 decades. Briefly, our method involves pulling borosilicate glass capillaries to the appropriate taper and tip size, 1–4 μm, drying the glass at >200 °C, making the glass hydrophobic by exposing it to the vapor of N,N-dimethyltrimethylsilylamine, backfilling with an appropriate electrolyte (some are listed in Table 4.1) and then tip filling with a hydrophobic, ion-selective cocktail to the appropriate length, listed in Table 4.1 for the examples given (for more details, see Smith et al. 1999). The column length was chosen empirically, primarily for stability of the ion-selective solvent in the pipette tip and the response time of the electrode. For the examples given in Table 4.1, the H^+ and Ca^{2+} electrodes are made with a 30 μm column of ion-selective solvent, while the K^+ electrode is made with a 100–150 μm column length. More stable K^+ electrodes can be made with smaller diameter tips. The reason for these differences in stability is probably dependent on the physical properties of the solvents used in the ion-selective cocktail. The solvent used in the H^+ (Sigma-Aldrich/Fluka cat #95293–1EA) and Ca^{2+} (Sigma-Aldrich /Fluka cat # 21048–1EA) cocktails is o-nitrophenyl-n-octyl ether,

which is 3.9 times more viscous and nearly 3 orders of magnitude less soluble in water than 2,3-dimethyl-nitrobenzene (Ammann 1986) that is used as the solvent in the K^+-selective solvent (Sigma-Aldrich/ Fluka cat # 60398–1EA-F). There is certainly flexibility in the column length of the electrodes. Based on resistance changes that occur with increased column lengths (Kühtreiber and Jaffe 1990), it was thought that significant increases in response times would occur as column length increases. The response times for shorter columns, such as 10–30 µm used for the H^+ and Ca^{2+} electrodes change more linearly with column length while the response times for longer column lengths increase in a logarithmic manner with increasing column length. In practice, a slight deviation from the expected length does not change the response time very much, at least when considering the use of these electrodes in the self-referencing application.

The back filling solution is used to provide electrical contact between the back surface of the ion-selective solvent and the voltage-sensing node, via a Ag/AgCl wire. Usually a 100 mM solution of the ion being measured is used as the backfill in order to ensure that the ionic concentration between the back of the ion-selective solvent and the backfilling solution does not change. If large amounts of the ion being monitored enter the ion-selective solvent and pass through to the backfilling solution, the voltage recorded by the amplifier will be dependent on both changes. The backfilling solution should also be closely matched osmotically to the bath solution. Osmotic gradients across the ion-selective solvent can lead to movement of ion-selective solvent into or out of the electrode tip, either causing the electrode to fail or increase noise.

4.2.4.2 Potentiometric: selectivity

Selectivity of the electrode is the single most critical factor when performing measurements in complex media. How well does a particular electrode sense the primary ion of interest versus all other ions in solution? While the manufacturer lists many interfering ions there are also many other commonly present ions that may cause interference, which have not been tested. Figure 4.2 shows how an interfering ion will reduce the sensitivity of an ISE for its primary ion. Figure 4.2 compares the relationship of voltage to primary ion concentration for a relatively ideal electrode determined with the modified Nernst equation (solid) to the voltage of the primary ion concentration in the presence of different levels of an interfering ion (dashed) determined with the modified Nicolsky–Eisenman equation. The Nicolsky–Eisenman equation in the upper left of Fig. 4.2 has the addition of the concentration of the interfering ion (C_j) and the selectivity factor K_{ij}, compared to the Nernst equation in the lower right. The Nicolsky–Eisenman equation assumes that the response of the electrode is Nernstian for the interfering ion. For this comparison both primary and interfering ions are monovalent and only one interfering ion is present even though the equation can be used to accommodate many

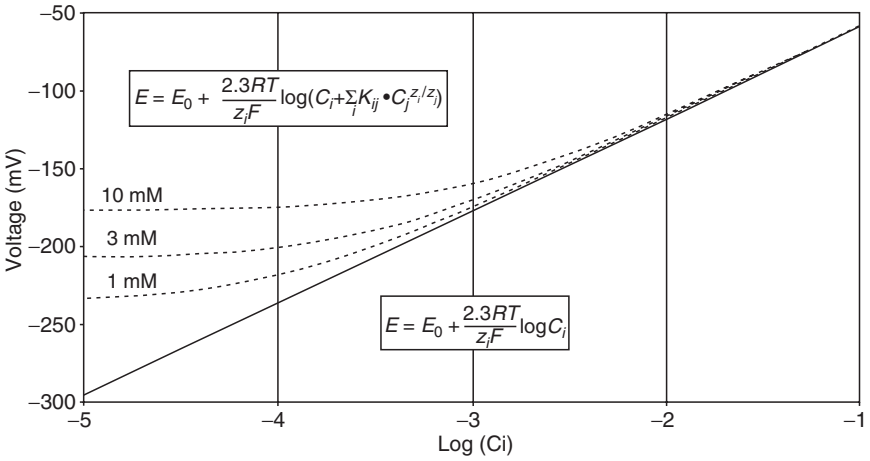

Fig. 4.2. Predicted voltage response for changes in primary ion concentration for a monovalent cation in the absence and presence of different concentrations of a monovalent cation interferent. A modified Nernst equation, listed in the lower right, was used to model the voltage response under ideal conditions for changes in the primary ion concentration (*bold*). A modified Nicolsky–Eisenman equation, listed in the upper left, was used to predict the voltage response for changes in the primary ion concentration in the presence of an interfering ion. The interfering ion concentrations are listed above their respective curves. The selectivity coefficient, K_{ij}, used for this model was 0.1, i.e. the solvent is 10 times more selective for the primary ion than the interfering ion

interfering ions. By comparing the responses of an ideal electrode to one that senses an interfering ion, it can be shown that under circumstances where $K_{ij} \cdot C_j$ is small compared to C_i, the slope approaches the Nernstian value and will remain relatively constant over small differences in primary ion concentration. However, in circumstances where $K_{ij} \cdot C_j$ is large compared to C_i, the slope approaches zero, yielding an electrode that is insensitive to changes in the primary ion concentration. Interfering ions not only reduce the electrode's voltage response to the primary ion but they also slow the response time of the electrode as shown in Fig. 4.1B. This point is particularly important when using the electrodes in self-referencing mode where a temporal component is part of the modulation approach. This will be addressed below.

In biological applications, it is critical for the investigator to empirically test the voltage response and response time of an ISE in the medium in which the experiments are to be performed. Simple solutions of the primary ion are not sufficient. If cellular poisons are to be added, then the electrode must be tested in the presence of those poisons as well. Considering the application of Cl^- sensors provides an example of some problems encountered for one of the ion-selective solvents with poor selectivity. Recently, Zonia et al. (2002) made the rather startling discovery that large Cl^- fluxes were an integral component of pollen tube extension (see "Self-referencing as applied to plants" below). They

used a commercially available Cl^--selective exchanger (Sigma-Aldrich/Fluka cat. #24899). Measurements were performed in the presence of two interferents that were not identified. Sulfonates are listed as interferents for this Cl^--selective cocktail which has less than 1 order of magnitude selectivity for Cl^- over methylsulfonate (Fluka Chemical Corp. 1996; Messerli et al. 2004). However, it may not be so apparent that most of the Good Buffers, specifically 2-(N-Morpholino)ethanesulfonic acid (MES), contain sulfonates and that the Cl^- channel blocker, 4,4′-diisothiocyanatostilbene-2,2′disulfonic acid disodium (DIDS) contains sulfonates. Both compounds were used in the Zonia et al. (2002) studies. It was later determined that the Cl^- electrode had only 2.4-fold selectivity for Cl^- over the anionic form of MES, indicating that the Cl^- electrode can indirectly monitor pH gradients (Messerli et al. 2004). Another Cl^--selective cocktail (Sigma-Aldrich/Fluka cat. 24902) is directly sensitive to pH at low Cl^- (Garber et al. 2005). Consideration of the previously characterized H^+ fluxes in lily pollen grains and tubes (Feijó et al. 1999; Messerli et al. 1999) as well as the poor anion selectivity of the Cl^- electrode, indicates that the putative Cl^- fluxes are in fact changes in the anionic concentration of the buffer due to H^+ gradients and not changes in Cl^- concentration (Messerli et al. 2004). It was also found that in the presence of 100 μM DIDS the electrodes responses to Cl^- drop by 63% on average between 0.1 and 1 mM Cl^- (Messerli et al. 2004). Zonia et al. (2002) measured an 80% drop in Cl^- efflux from a tobacco pollen tube in the presence of 80 μM DIDS and a background Cl^- concentration of 0.4 mM. The decrease in the Cl^- flux measurement can be accounted for by the decreased sensitivity of the electrode with the added interferent. Many of these problems remain in the methodology described in Chapter 5 of this volume.

It should be clear from the examples discussed above that careful testing must be performed in order to determine how an ISE will perform in complex media and in the presence of reagents used to modify cellular activity.

4.2.4.3 Potentiometric: positional artifacts

The positioning of ISEs near surfaces can generate artifacts. Of particular relevance is the current driven and zero-current ion flux emanating from the tip of the sensor. Although our tip sizes are small and the static boundary layer limited in size, ions escaping to the bulk could accumulate between the probe tip and the target cell or tissue. Abnormal, apparent, biological fluxes have been seen for Ca^{2+} when Ca^{2+}-selective electrodes are brought within 1–2 μm of a membrane or an insulating surface when the background Ca^{2+} concentration is <1 mM. The source of this artifact is a combination of current leakage from the electronics supplying charge to the ion-selective solvent and zero-current (electroneutral) ion exchange of the primary ion for an interfering ion. This phenomenon has been shown for K^+ and Ca^{2+}-selective solvents (Mathison and Bakker 1998; Lindner et al. 1999). The artifacts are most apparent in solutions of low background primary ion. Reducing the concentration

of the primary ion in the backfilling solution has been one method of reducing the ion leak (Mathison and Bakker 1998). Additionally, an applied current can control the flux across the membrane counteracting the spontaneous zero-current ion flux (Lindner et al. 1999). Pergel et al. (2001) used a current to compensate for the zero current phenomenon discussed with Pb^{2+} detection. By reducing, if not eliminating the leakage of Pb^{2+} out of the electrode tip, the authors were able to maintain a Nernstian response down to 3 pM.

4.2.4.4 Amperometric: construction

A number of solid-state amperometric microelectrodes have been used in the self-referencing mode. Two different metal electrode configurations have been used. These include gold-plated Woods metal (Diamond General Co., Ann Arbor, Mich., USA) for the detection of O_2, and a platinum disk microelectrode for the measurement of O_2 (Jung et al. 2000a,b) and H_2O_2 (Twig et al. 2001, 2005). Carbon fiber-based microelectrodes have been used for the detection of nitric oxide (NO) (Kumar et al. 2001; Porterfield et al. 2001) and ascorbic acid (Pepperell et al. 2003). More complex enzyme-based microelectrodes have been fashioned to measure gradients of glucose (Jung et al. 2001) and glutamate (Bogorff et al. 2003). We will briefly discuss the fabrication of the first three types of electrodes.

The gold-plated Woods metal microelectrode dates back to the early days of O_2 microelectrodes (Whalen et al. 1967). The low melting temperature Woods metal is heated above melting, forced to the tip of the pulled micropipette by back pressure, etched back into the glass pipette and then electroplated with gold or gold and then platinum to build a recessed electrolytic surface for the reduction of O_2. The recessed tip creates an O_2 diffusion-limited sensor and prevents the O_2 depleted field from extending away from the sensor tip out into the bulk medium (Schniederman and Goldstick 1976, 1978). When the electrode is built such that the O_2-depleted field remains close to the electrode tip, the response time of the electrode can be tens of milliseconds (Schneiderman and Goldstick 1976), which we have achieved with the platinum-based O_2 sensors shown at the bottom of Table 4.1.

The platinum-based sensors are made by etching 25 μm diameter, platinum wire to a tip of about 1–3 μm diameter, inserting the etched wire into a micropipette similar to those used with the ISEs, immobilizing the platinum wire in the micropipette with a UV or heat curing epoxy, and then etching a second time to recess the electrolytic platinum surface (Jung et al. 2000a,b). Coated tips can help reduce the external O_2 depleted field and provide some added selectivity. Buerk (2004) provides an excellent overview of oxygen microelectrodes, their design and function.

Carbon fiber microelectrodes are made in a similar manner as the platinum wire electrodes. A fine carbon fiber 5–8 μm diameter is positioned near the tip of a finely pulled pipette tip and cemented into place with a UV or heat

curing epoxy. The carbon fiber electrode is then beveled to expose a cross-sectional surface of the fiber. Coatings are used to help impart selectivity (Friedemann et al. 1996).

4.2.4.5 Amperometric: selectivity

A constant polarization potential is applied to amperometric sensors to oxidize or reduce the analyte. The current generated is proportional to the concentration of the analyte. However the potential can oxidize or reduce other compounds in solution that are electrolyzed at or below the electrode holding potential. For example, nitric oxide (NO) oxidation at a carbon fiber begins to plateau between +0.8 to +0.9 V (Zhang et al. 2002). Neurotransmitters, ascorbic acid, nitrite and H_2O_2 can also be oxidized at this high voltage. A charged coating on the carbon fiber surface can eliminate passage of charged compounds (Friedemann et al. 1996; Zhang et al. 2002). However, H_2O_2, an uncharged molecule, will be oxidized as it can pass through the coatings. Addition of a layer of catalase to the charged coating layers, similar to the enzyme layers used by Csöregi et al. (1994), can eliminate H_2O_2 before it has chance to reach the electrolytic surface. Multiple coatings on a microelectrode will decrease sensitivity by reducing electrolytic surface area and slow response time by impeding diffusion of the analyte.

Another common problem with amperometric sensors is that they are strongly dependent on pH. One only has to look at a standard reduction potential table to see that H^+ consumption is involved with most every reaction. Take, for instance, O_2 reduction: $2O_2+4H^++4e^-\rightleftharpoons 2H_2O$. The rate of this reaction at a bare micro Pt disk electrode will be dependent on the limiting factor which should be diffusion of O_2 to the electrolytic surface. In practice this is not the case and the O_2 sensor can very quickly become a good H^+ sensor. Certainly the recessed tip, coated, Wood's metal electrodes purchased from Diamond General Co. can sense pH gradients (Messerli and Robinson, unpublished observations).

4.2.4.6 Amperometric: positional artifacts

In amperometric applications, the analyte is actually being consumed on the electrode surface. Therefore, an analyte depletion zone can form. An ideal electrode is built such that the analyte-depleted region is located primarily within the electrode itself. However, it can quickly be envisioned that even a small depletion of the analyte in the bulk can give rise to a measurement artifact. In the extreme case, placing the electrode up against an insulator will prevent any analyte from reaching the surface of the electrode resulting in no change in current for a change in analyte. Backing the electrode away from the insulator such that analyte can now diffuse, albeit in a restricted manner, will still give rise to a value below the real level. Moving back further, such

that diffusion of analyte is not impeded, will result in maximal current for a change in analyte concentration.

A second possible source of artifact is that reaction products can accumulate at the electrode surface when diffusion is restricted by the target. A good example of this comes from the study of Jung et al. (2001) during the development of the self-referencing glucose probe. This design incorporates glucose oxidase and measures glucose concentration indirectly though the production of H_2O_2. As long as glucose is present the glucose oxidase at the tip of the electrode will produce H_2O_2. The H_2O_2 that diffuses toward the electrolytic surface will be measured but the H_2O_2 that diffuses out into the bulk medium will be lost. However, in this case when the electrode came into close proximity to a HIT cell cluster (hamster insulinoma tumor) it appeared as if the cell was releasing glucose. Although this would have been an exciting result, the better hypothesis was the presence of an artifact, probably the accumulation of the H_2O_2 when the sensor was close to the source. A similar response, glucose production by a solid glass bead, confirmed H_2O_2 accumulation as the source of the artifact. In the biological application, the addition of catalase to remove sensor generated H_2O_2, converted apparent glucose efflux to the expected glucose influx.

Therefore, in practice the investigator is wise to assess the extent of these depletion and restrictive diffusion zones.

4.3 Self-referencing

4.3.1 Introduction

Self-referencing, with electrochemical sensors, is a modulation technique used to measure the concentration of an analyte at two positions within a chemical gradient of the analyte. The term self-referencing refers to the fact that the concentration measurements, collected by the single sensor, are compared to each other in order to determine the concentration difference between the two points. Each sensor has its own bath reference electrode. Commonly, the gradients that are measured with this technique exist along a path orthogonal to the cell/ tissue surface so the electrochemical sensor is oscillated repeatedly between two points, one closer to the cell (near pole) and one a set distance away (far pole), usually 10 μm. Figure 4.3 shows a potentiometric, ISE in both the far pole (top) and near pole (bottom) of translation near a growing lily pollen tube tip. Both potentiometric, ISEs and amperometric sensors have been used in this manner. The electrodes are translated between the two poles at a frequency of about 0.3 Hz, collecting an analyte concentration measurement at each pole. The difference in analyte concentration between the two poles can be used to calculate the flux of the analyte. While this sort of measurement could be achieved with two similar, stationary sensors, positioned at

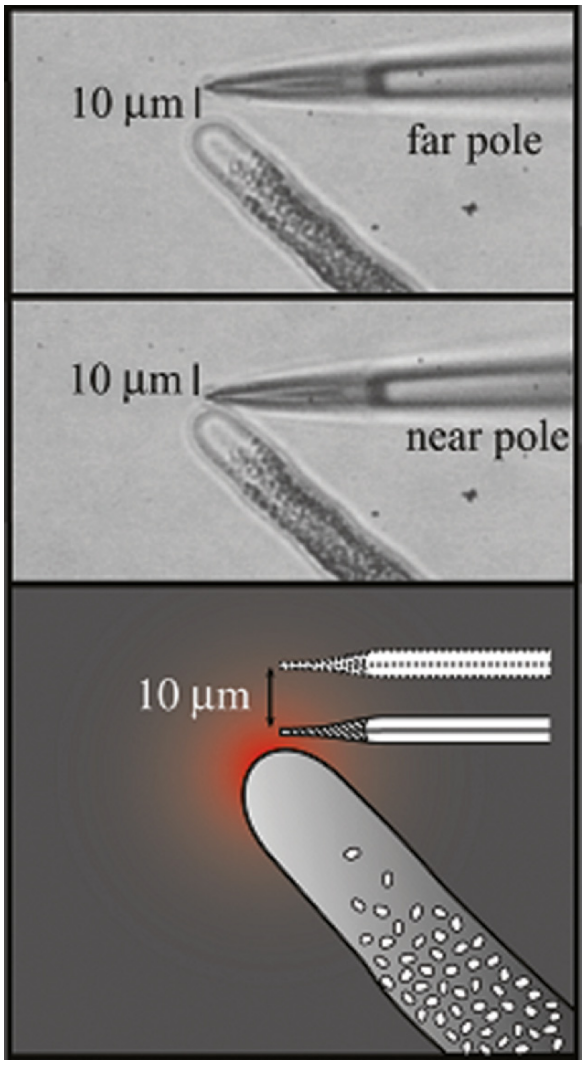

Fig. 4.3. Images of an ion-selective electrode during self-referencing measurements acquired at the tip of a growing pollen tube. The top image was acquired when the electrode was at the far pole of excursion while the middle image was acquired when the electrode moved to the near pole of excursion. The bottom image shows a conceptual representation of the electrode measuring at two points within the concentration gradient of the primary ion

known distances from the source, the system would suffer from the signal drift and noise inherent to two separate measuring systems. In a single electrode system, the effects of drift and noise can be minimized over time by regularly comparing the measurements between the two poles of excursion. Here lies one of the single most powerful reasons for using self-referencing, the

minimization of system drift and noise on analyte detection. We will first address the modulation of potentiometric sensors and then make direct comparison with modulation of amperometric sensors.

4.3.2 Self-referencing of ion-selective electrodes

Minimizing drift and noise for a potentiometric sensor can best be explained by introducing a formulation of the Nernst equation during self-referencing. The voltage difference at the two poles of excursion within the ionic gradient is related to the concentrations at the two poles by the following equation.

$$\begin{aligned} E_1 - E_2 &= (E_0 + S\log\ C_i)_1 - (E_0 + S\log\ C_i)_2 \\ \Delta E &= (S\log\ C_i)_1 - (S\log\ C_i)_2 \\ \Delta E &= \log\ C_{i\,(1)}^{s_1} - \log\ C_{i\,(2)}^{s_2} \\ \Delta E &= \log\left(\frac{C_{i\,(1)}^{s_1}}{C_{i\,(2)}^{s_2}}\right) \end{aligned} \tag{3}$$

E_1,$C_{i(1)}$, S_1 are the measured voltage, primary ion concentration and slope of the voltage-log(C_i) graph for the near pole of excursion. The subscript 2 has been used to label the same parameters for the far pole of excursion. By calculating the difference in potentials over short periods of time, the slower drifts, due to the constant potential differences throughout the system, are reduced. This places the emphasis of the potential difference measurement on the concentration difference of the ion. An important point should be raised here regarding the sensitivity of detection with regard to the background ion concentration during measurements. $C_{i(1)}$ is the sum of the background ion concentration and the concentration change generated by the source while $C_{i(2)}$, in most cases, is close to the background ion concentration. For a given change in ion concentration due to cellular activity, it is easier to generate a larger ΔE when the background concentration of the measured ion is lower. This has led to the lowering of the background ion concentration in order to generate ΔE with greater signal to noise. Care must be taken to ensure that changing the background concentration does not interfere with normal cellular activity or generate positional artifacts as discussed above.

Equation 3 can be simplified to a general form to determine the relationship between the ionic concentrations at the two points of excursion.

$$C_{i\,(1)} = C_{i\,(2)}^{S_2/S_1} \cdot 10^{\Delta E/S_1} \tag{4}$$

We have purposely allowed the slopes at two points of the calibration curve to remain, in order to address measurement of the primary ion under three different circumstances, 1) differential concentration of the primary ion in the absence of an interfering ion 2) differential concentration of the primary ion

in a constant concentration of an interfering ion and 3) differential concentration of a primary ion coexisting with a gradient of an interfering ion.

For an ideal electrode used in the absence of interfering ions, the slope is constant over a wide range of the primary ion concentration, usually described by the manufacturer, and close to the Nernstian slope discussed above in Fig. 4.2, i.e. $S_1=S_2=S$. Therefore, eq. 4 can be simplified to:

$$C_{i\,(1)} = C_{i\,(2)} \cdot 10^{\Delta E/S} \tag{5}$$

Under many circumstances the average concentration of the ion at the far pole, position 2, is not too different from the average concentration of that ion in the bulk solution. Therefore the difference in ion concentration between the two points of excursion can be described as follows.

$$\Delta C = C_{i\,(1)} - C_{i\,(2)} = C_{bath}\,10^{\Delta E/S} - C_{bath} \tag{6}$$

A primary assumption here is that the concentration difference measured between the two excursion points is linear. This is only true if the excursion distance is small compared to the extent that the gradient extends out into the bulk solution. For small cells an excursion of 10 µm will most likely sample over a distance in the gradient in which the concentration difference is not linear and therefore will lead the investigator to underestimate the true flux. Incorrect estimation of the true flux could also occur during a two-point measurement in a more intense, extended gradient, where the concentration of the ion in the far pole is substantially different from the background concentration of the ion. In both of these cases a three-point measurement can be performed in order to 1) more carefully map the concentration gradient with a third point to either ensure a linear relationship or determine a more accurate non-linear relationship and 2) to determine the concentrations in the gradient relative to the background concentration of the ion in the bath. For slow drift conditions the probe can simply be moved from position 3 (outside of the gradient) to position 2 (slightly into the gradient) to position 1 (deeper into the gradient). However, a more precise method is to regularly move between position 3 and positions 2 and 1, so a collection scheme goes from position 3 to 2 to 3 to 1 to 3 and so on.

Measurement of a concentration difference for a primary ion in the presence of a constant concentration of an interfering ion is a more difficult situation. Two variables in eq. 4 need to be determined, specifically the concentration of the ion in the near pole $C_{i(1)}$ and the new slope of the calibration curve in the near pole, S_1. Revisiting Fig. 4.2 gives insight into the problem. With a small $K_{ij} \cdot C_j$ compared to C_i the slope is close to Nernstian and eqs 5 and 6 can be used as discussed above. With a large $K_{ij} \cdot C_j$ compared with C_i the electrode is very insensitive to changes in the primary ion concentration. When the $(K_{ij} \cdot C_j)/C_i$ ratio is 10, the original Nernstian potential is only 10% of its original value and the measurement should probably not be attempted. The use of the electrode under these circumstances will depend on the signal to noise ratio of the system and therefore lies at the discretion of

the investigator. For the region in between these two zones the electrode is responsive to the concentration change in the primary ion concentration but the slope of the line changes with a change in concentration. Therefore, a relationship between the change in voltage and the change in slope needs to be established in order to measure two points in a concentration gradient of a primary ion in the presence of a constant concentration of an interfering ion. In Fig. 4.2 it can be seen that the slope and voltage are closely related in a predictable manner if the selectivity coefficient, K_{ij}, and the background concentration of the interfering ion, C_j, are known, i.e. a single voltage measurement can be used to determine both the slope and the concentration of the primary ion in the near position. We will address the presence of a single interfering ion below.

Rearranging the modified Nicolsky–Eisenman equation to get primary ion concentration in terms of voltage and finding $\frac{d}{dE}$ we can determine the relationship of the slope at any point along the curve in terms of voltage.

$$
\begin{aligned}
E &= S_N \cdot \log\left(C_i + K_{ij} \cdot C_j^{z_i/z_j}\right) \\
C_i &= 10^{E/S_N} - K_{ij} \cdot C_j^{z_i/z_j} \\
\log(C_i) &= \log\left(10^{E/S_N} - K_{ij} \cdot C_j^{z_i/z_j}\right) \\
\frac{1}{S} &= \frac{d\log(C_i)}{dE} = \frac{10^{E/S_N}}{S_N\left(10^{E/S_N} - K_{ij} \cdot C_j^{z_i/z_j}\right)}
\end{aligned}
\tag{7}
$$

'S_N' is $\frac{2.3RT}{z_i F}$ and S is the slope along the curve. In order to achieve this sort of measurement we need to know the starting position (voltage point) along the theoretical curve. We can calculate the starting voltage point on the theoretical graph by determining the slope in the bath empirically and solving for E in Eq. 7.

$$
E = S_N \log\left(\frac{S_N \cdot K_{ij} \cdot C_j^{z_i/z_j}}{S_N - S}\right) \tag{8}
$$

From this point on the theoretical curve, a small change in measured voltage, ΔE, either up or down the curve can be used to determine both the new slope at the near pole, eq. 7, and the concentration in the near pole, eq. 4. If the concentration of the ion in the far position is sufficiently different from the background concentration then a three-point measurement will have to be made, as discussed above. This method of calculation works for the three-point measurement as well.

The final case to consider is measurement of a gradient of a primary ion coexisting with a gradient of an interfering ion. Two variables from eq. 4 need to be determined, specifically the concentration of the primary ion and the

slope of the curve for the primary ion in the near pole. However, now these two variables are not easily predicted as above because the concentration of the interfering ion will influence both variables and the concentration of the interfering ion in the near pole is unknown. Figure 4.2 shows how the concentration of the interfering ion alters the voltage—concentration relationship and changes the slope of the curve. This means that a second ISE for the interfering ion must be used at the same time as the ISE for the primary ion. This will enable measurement of the interfering ion at the near pole and allow prediction of the concentration and slope of the curve for the primary ion in the near pole. If a relatively ideal ISE can be used to measure the interfering ion then the situation discussed above with eq. 7 can be used to solve for the primary ion flux. However, if the ISE used to measure the interfering ion can also sense the primary ion then no simple method to determine the flux of either ion exists.

4.3.3 Self-referencing of amperometric electrodes

Amperometric electrodes have also been used in self-referencing mode incorporating many of the advantages discussed above for the potentiometric electrodes. To date, all of the amperometric sensors have been used in constant potential mode, where the sensor is clamped at a specific holding voltage to oxidize or reduce the analyte. Electrodes are built so that measurement of the analyte is limited by diffusion of the analyte itself, attempting to ensure a current that is dependent on the analyte concentration and not the concentration of a secondary factor or byproduct. The current generated by this redox reaction is therefore proportional to the concentration of the analyte. In the special case of enzyme-based sensors, for instance using glucose oxidase to measure a concentration difference of glucose, a by-product of the enzyme-substrate reaction, H_2O_2, is measured (Jung et al. 2001). Many other forms of amperometric detection exist and are currently under investigation in order to increase the range of analytes than can be measured with self-referencing.

For an ideal electrode under constant holding potential, the measured current is proportional to the concentration of analyte. During self-referencing the differential current can be used to give a measurement of the differential analyte concentration.

$$\begin{aligned} I_1 - I_2 &= \left(I_O + S \cdot C\right)_1 - \left(I_O + S \cdot C\right)_2 \\ I_1 - I_2 &= S\left(C_1 - C_2\right) \\ \Delta C &= \frac{\Delta I}{S} \end{aligned} \tag{9}$$

I_1 and C_1 are the current and concentration of the analyte in the near pole of excursion. The subscript 2 has been used to identify the same parameters in the far pole of excursion. S is the slope of the calibration curve. Unlike ISEs, knowing the background concentration of the analyte is not necessary to determine the differential concentration due to the linearity of the current-concentration relationship of the electrodes and analytes used todate.

4.3.4 Calculation of flux

To quantify the analyte flux, the differential concentration measurement is converted to flux. This provides a direct means to count the number of molecules passing through a unit area during a unit time. Not only does flux give a value proportional to transport activity but it also can be used to calculate the total amount of analyte uptake or release by integrating the flux over space and time. Flux takes into account the diffusion coefficient of the analyte being measured, the distance over which the differential concentration measurement was acquired, the surface geometry of the source and the distance from the source. For cases where the measuring electrode is relatively close to a large source of the analyte gradient and the differential concentration is measured over a small distance Δx within the gradient, the source can be modeled as a planar source so the flux (J) is

$$J = -D\frac{\Delta C}{\Delta x} \tag{10}$$

where D is the diffusion coefficient of the measured analyte. By this model, the flux measured very far from the source is the same as the flux at the surface of the source. What constitutes a planar source? Kochian et al. (1992) found that the planar flux calculation was adequate for H^+ fluxes determine between a 30 μm distance, within 100 μm of a 1 mm diameter root. However, for smaller cells or tissues the geometry of the source must be taken into account (Henriksen et al. 1992; Messerli et al. 1999, 2004). In order to determine flux at the cell surface for known surface geometries it is useful to calculate analyte flow, i.e. the quantity of substance (Q) moving per unit time (Henriksen et al. 1992). Flow is the same for all concentric regions from the source surface. Flux at the source surface is the flow divided by the surface area of the source. Therefore, radially emanating flow from a cylindrical surface is:

$$Flow = \frac{Q}{t} = \frac{2\pi D}{\ln(b/a)}(\Delta C) \tag{11}$$

where D is the diffusion coefficient of the analyte and a and b are the radial distances between the center of the cylinder and the electrode tip at the near and far poles, respectively. These equations have been adapted from Crank (1967). Analyte flux at the surface of the cylinder is then determined by dividing by its surface area $2\pi rl$. A caveat of this approach is the assumption that the flow is equal at all points around the cylinder and along the shaft of the cylinder. An alternative is to calculate flux per unit length by dividing by $2\pi r$ (Henriksen et al. 1992). The flow from a spherical source is

$$Flow = \frac{Q}{t} = 4\pi D\frac{ab}{b-a}(\Delta C) \tag{12}$$

Flux at the cell surface can then be determined by dividing by the sphere surface area $4\pi r^2$. Many researchers have chosen to forgo flux calculations, as they are only interested in changes of the differential concentration measurement for cells and tissues under different conditions. Given that the cells

being used have relatively similar surface geometry and that the electrodes are positioned at a similar position with respect to the cell surface, this simple method is adequate.

4.3.5 Correction for analyte buffering

There are a number of circumstances that cause the calculated flux to be smaller than measured. In the first example discussed here extracellular buffers can collapse gradients of free analytes. This has been addressed for the collapsing of H^+ gradients by H^+ buffers (Arif et al. 1995; Demarest and Morgan 1995). The analyte can diffuse from the surface of the cell in either its free state or bound to the buffer. ISEs only measure the free concentration of the analyte. The actual H^+ flux from a source is the sum of the measured free H^+ flux and the unmeasured H^+ flux moving as H^+ bound to buffer.

$$J_{Htotal} = J_{Hmeasured} + J_{HB}$$

Knowing the conditions under which the H^+ flux was measured, i.e. $[H^+]$ of medium, Ka of the buffers and concentration of buffers present, a simple relationship can be derived to determine the ratio of H^+ diffusing as bound to buffer compared to the freely diffusing H^+. Arif et al. (1995) and Demarest and Morgan (1995) have derived two separate sets of equations that can be simplified to the same equation given below.

$$x_i = \frac{D_B}{D_{H^+}} \cdot [B] \cdot \frac{Ka}{\left(Ka + \left[H^+\right]\right)^2} \tag{13}$$

The correction factor, x_i, is the ratio of the H^+ bound buffer flux to the free H^+ flux. Therefore

$$J_{Htotal} = J_{Hmeasured} \left(1 + x_i + \ldots + x_n\right) \tag{14}$$

where a number of different H^+ buffers ($x_i + \ldots + x_n$) could be carrying H^+ away from the source. The correction factor is based on 3 criteria, the ratio of the diffusion coefficients of the protonated buffer to the proton, the buffer concentration and the Ka of the buffer compared to the $[H^+]$ of the medium. Under most conditions the first term will be relatively constant because buffer sizes and diffusion coefficients do not differ very much. The smaller bicarbonate ion, for example, (M_r 61 $D=1.2\times10^{-5}$ cm/s) will only produce a first term of 0.13. while PIPES (M_r 302 $D=0.52–10^{-5}$ cm/s) one of the largest Good buffers, will produce a first term of 0.056, a change of only 2.3 fold. The second term shows that correction factor is directly proportional to the buffer concentration. The last term, the relationship of the K_a of the buffer to the $[H^+]$, could have the most significant impact on the correction factor.

In the absence of intentionally added H^+ buffers, water and dissolved carbonates can have a significant buffering effect at neutral to alkaline pH (Arif et al. 1995). Water, at a concentration of about 56 M with a Ka of 10^{-16} begins

to impact the correction factor above pH 6. The correction factor due to water acting as a H^+ buffer contributes to the total flux by less than 1% when the pH is 6. Bicarbonate in solution, due to atmospheric CO_2, will also have more significant impact at neutral to alkaline pH. Bicarbonate will increase in concentration at more alkaline pH, and can add to the H^+ flux by about 2 and 21% at pH 7 and 8 respectively.

In order to minimize the effect of buffer on H^+ efflux a buffer with a K_a below the $[H^+]$ should be chosen such that most of the buffer will be in its protonated form reducing the effective buffering capacity. As in the former example investigators can choose buffers to suit their needs, either to remove a very large H^+ flux that is interfering with measurement of other analytes or to correct for the amount of H^+ passing through the plasma membrane in order to accurately quantitate such a flux. See Arif et al. (1995) for a mathematical solution to multiple buffers. This correction method is theoretically applicable to other forms of analyte buffering such as for Ca^{2+} or transition metals.

4.3.6 Other considerations for corrections

In addition to the correction factors discussed above there are other sources of errors that should be addressed. For instance, many plants drive transcellular currents through them, a result of ion transport across single cells or tissues. In low conductivity medium these currents generate substantial voltage gradients next to the cells, coexisting with the chemical gradients of the analytes that we have been discussing. The potentiometric electrodes may sense these small voltage gradients. Therefore the voltage difference measured by the potentiometric electrode will be the sum of the voltage differences due to the analyte concentration difference and the voltage difference based on the current density and medium conductivity. This artifact must be addressed on a sample-to-sample basis. For example, a peak voltage difference during oscillating current influx of about 9 μV would occur over a 10 μm distance immediately in front of a lily pollen tube where current density peaks around 0.4 $\mu A/cm^2$ at a distance of about 20 μm from the cell surface with a medium conductance of about 5000 ohm cm (Messerli and Robinson 1998). This voltage difference is just above the background noise of the system used at that time, ±5 μV for H^+ and Ca^{2+}, ±10 μV for K^+ ISEs (Messerli et al. 1999). The voltage signals due to chemical differences peaked about 6, 10 and 65 times larger for Ca^{2+}, K^+ and H^+ concentration differences, respectively, indicating that the voltage difference could have contributed to the differential analyte concentration by up to 15%, 10% and 1.5% for the Ca^{2+}, K^+ and H^+ measurements, respectively.

In a second example, the electric field determined near the surface of barley roots was considered to be negligible compared to the concentration dependent voltage (Henriksen et al. 1992). While it is important to be aware of such an artifact, in the two cases listed the differential voltage gradient did

little to influence the measured concentration differences. Also medium conductivity can be changed in order to collapse the voltage field without dramatically changing the background concentration of inorganic ions.

The mode of data acquisition itself could lead to underestimates of the true analyte concentration difference. Also, if the response time of the electrodes is slow compared to the acquisition of the differential concentration measurements, the electrode will not be at its steady state value by the time the data has been collected leading to an under measurement of the true concentration difference. As these two corrections are very dependent upon the system electronics and the scheme used for data selection, we will go into more detail about these factors as used with our systems.

4.3.7 Theoretical considerations for signal detection and increased signal to noise

Self-referencing of electrochemical sensors involves the extraction of small electrical signals, μV or fA differences on top of relatively large offset signals, ±100s mV or ±10–100s pA. The offset signals are usually large enough that only low-level gain can be used in order to keep the signal within the dynamic range of the amplifier. In order to supply sufficient gain to resolve the small electrical differences either 1) a nearly equal and opposite electrical offset must be supplied before amplification (sample hold mode) or 2) a running average of the low gain measurement can be subtracted from the real-time input before amplification (RC subtract mode). Sample hold mode either applies an offset selected by the user, or collects a voltage at a set point in time from the electrode output. It then applies the same magnitude offset of opposite sign to nullify the offset potential before applying 10^3 times gain. The primary disadvantage for this mode is that drift can take the system back out of the dynamic range of the amplifier so that a new potential must be applied regularly. The advantage is that it does not need an additional correction factor to compensate for the signal lost due to the filtering that occurs in RC subtract mode. In RC subtract mode a high-pass filter is used to collect a running average potential that is subtracted from the potentials collected in the near and far pole. The signals are then amplified 10^3 times before digitizing. We use a high-pass filter that has a time constant of 10 s. Figure 4.4 shows a 200-μV peak to peak square wave input, passed through the BioCurrents Research Center amplifier using Sample Hold and RC subtract mode acquisition. With sample hold mode, the acquired signal is a square wave. The RC subtract mode however, has been distorted due to the filter. RC subtract allows amplification for systems with large drift but involves a correction factor to offset the high-pass filter. The correction factor will be dependent on the time constant of the high-pass filter and the period of data acquisition. For our normal conditions a period of 3.3 s (0.3 Hz translation frequency), 40 μm/s translation speed, 10 s time constant of filter along with data selection of the

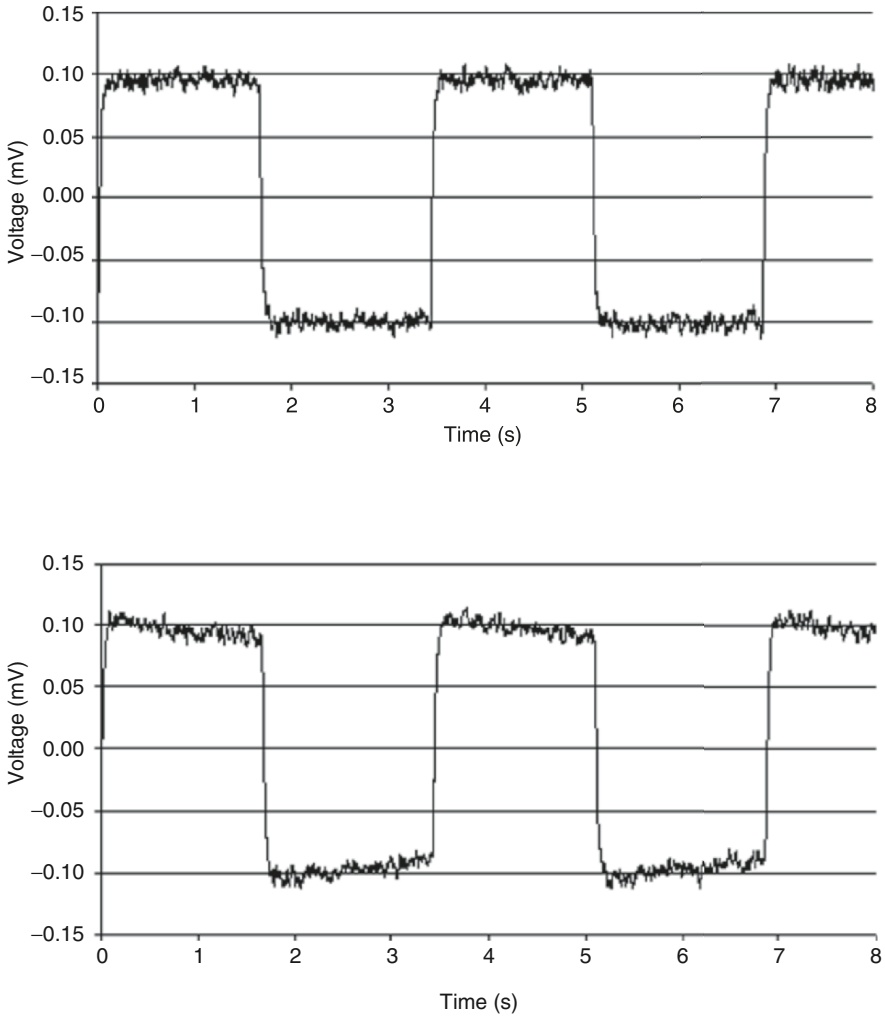

Fig. 4.4. Comparison of the waveform distortion that occurs between "sample hold" (upper) and "RC subtract" (lower) mode. No distortion occurs for a square wave input during sample hold acquisition mode. The highpass filter used during RC subtract mode does cause waveform distortion that needs to be accounted for when determining the differential concentration

last 70% of the half cycle (more below) we calculate that the signal is 7% smaller than a square wave with similar rise time.

The primary reason for the added level of amplification is to make use of poor resolution digital systems. A dynamic range of ±10 V provides only 4.9 mV/bit resolution for a 12-bit system, and 0.3 mV/bit for a 16-bit system. Therefore, amplification is necessary before digitization to provide adequate bit resolution at or below 1 μV. Now that 24-bit A/D cards exist, signal resolution of 1.2 μV can be attained over a dynamic range of ±10 V.

4.3.8 Data collection

In order to accurately measure the analyte concentration at two points in a gradient with an electrochemical sensor in self-referencing mode, gradient disruption by the electrode must be minimal and the movement time and response time of the electrode must be significantly faster than the excursion period. Gradient disruption will be minimal if a sufficient amount of time is allowed to pass for the gradient to be reestablished after sensor movement, as movement of the sensor may disturb the gradient. The slow movement of the probe, usually, 40 μm/s, does not cause turbulence that can be detected visually. Also, the Reynolds numbers calculated for the speed of movement of either the small tip, 1–4 μm diameter, or even up the shaft where the diameter reaches 50 μm are in the range of 10^{-4} – 10^{-3}, respectively, indicating that only laminar flow occurs around the tip of the sensor. However, if some disturbance does occur, how much time must pass to allow the gradient to be rebuilt? Considering the reestablishment of a K^+ gradient over the excursion distance of the probe, 10 μm, we find that it will only take about 8.3 ms, for K^+ to diffuse this short distance. This indicates that an ionic gradient would be rebuilt in a few tens of milliseconds. As long as turbulent flow does not occur, most small analyte gradients will be rebuilt very quickly.

A second issue to consider is that the sensor must be allowed to remain at each pole of excursion for a period of time long enough for it to acquire a steady state signal. This will inevitably depend on the response times of the sensors. As discussed above most sensors can reach 95% of their final value within 40–250 ms in physiological solutions. However, contaminants of ISEs can slow the electrode response and cause underestimation of concentration differences. Figure 4.5 shows the voltage response of a H^+-selective electrode, self-referencing near a H^+ sink, in low Ca^{2+} Dickinson's Medium, a culture medium used for growing pollen tubes (Messerli and Robinson 1997). A batch of these electrodes was characterized with the perfusion system and shown to possess an average response time of 223 ± 37 ms with an average Nernstian response of 27.8 ± 0.5 mV between pH 5.5 and 6.0 for a tip size of 1–2 μm listed in Table 4.1. The positional information has been added to the bottom of each graph to show the position and movement of the probe during translation. Figure 4.5 shows that the sensor reaches equilibrium at each

Fig. 4.5. Voltage response of a H^+-selective electrode collected continuously during translation between two position near a H^+ sink. The measurements were acquired in low Ca^{2+} Dickinson's medium. The three graphs correspond to the period of translation listed in the upper right of each trace. The voltage response of the H^+-selective electrode is shown at the top of each graph. The electrode equilibrated quickly with the new position, similar to the response time of the sensor collected in the flow streams listed in Table 4.1. The waveform at the bottom of each graph corresponds to the position of the electrode in the gradient as it changes with time. Translation of the electrode between the two poles is not instantaneous and must be taken into consideration when collecting a differential concentration measurement

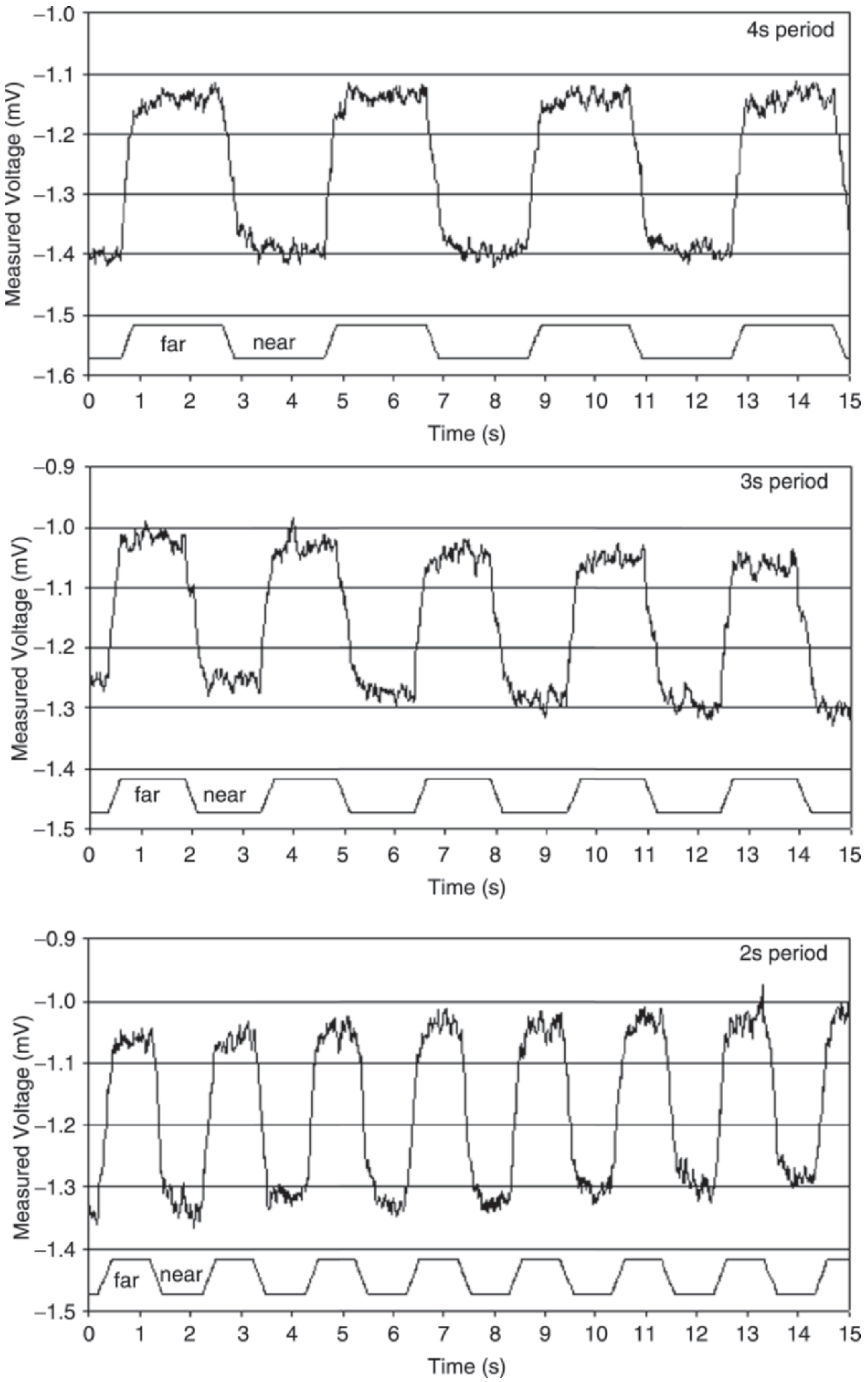
4s period
3s period
2s period
Measured Voltage (mV)
Time (s)
far
near

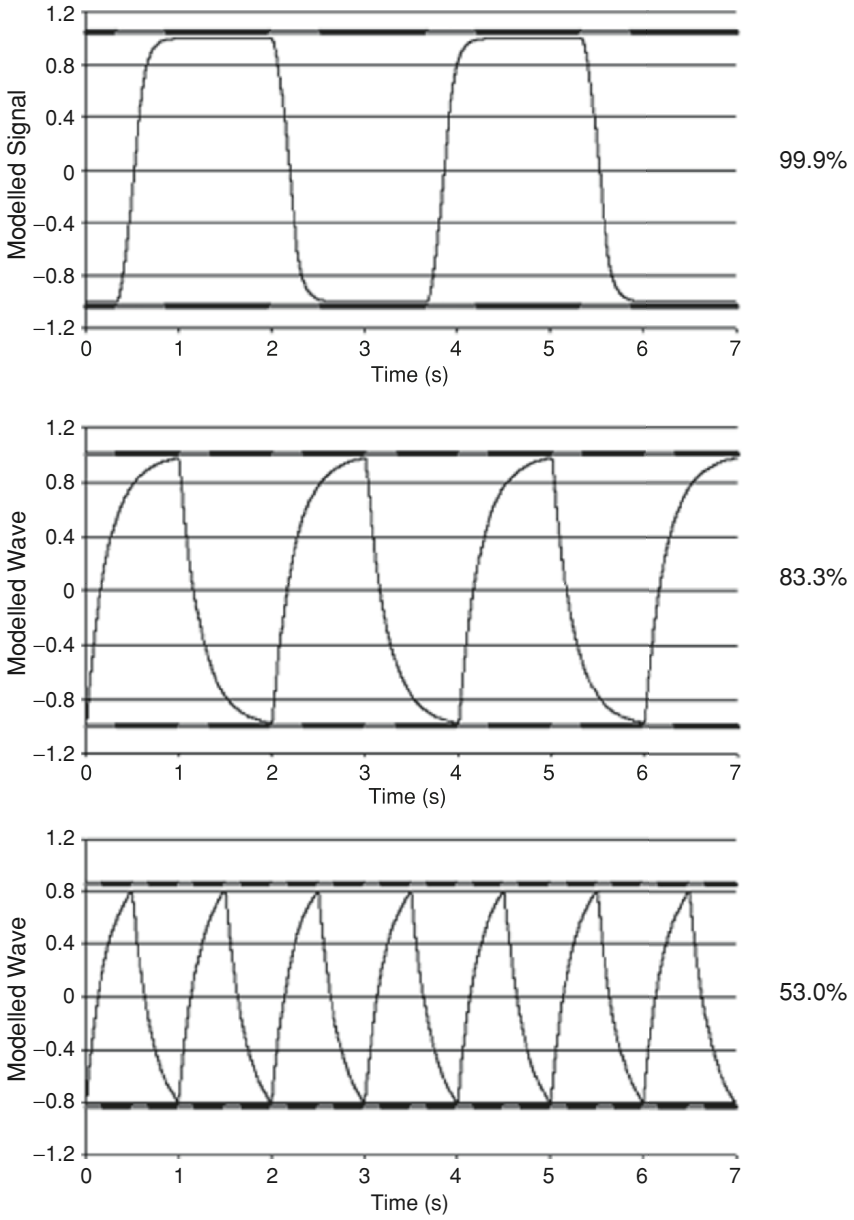

Fig. 4.6. Models of the voltage response for H^+-selective electrodes with different response times and collection periods. The *bars* at the top and bottom of each graph correspond to the 30% of the half cycle that is ignored as it accounts for translation and equilibration (*gray*) while the average of the remaining 70% (*black*) is used to determine a concentration measurement. The *top graph* was generated based on a sensor response time of 223 ms with an excursion time of 250 ms (translation speed 40 μm/s), similar to conditions used by Messerli et al. (1999). The response time is sufficiently fast and these collection parameters allow nearly 100% collection

pole with translation periods of 4, 3 and even 2 seconds because it can reach steady state very quickly. For our typical operating period, 3.3 s, we allow 30% of each half cycle, 0.5 s, for translation and electrode equilibration and then collect the average of the remaining 70%, 1.16 s, to use to determine the concentration. Figure 4.6A shows a model used to calculate the collection efficiency of an acquisition scheme using 250 ms movement time, 223 ms electrode response time and an excursion period of 3.3 s (0.3 Hz) similar to our normal operating parameters. For these parameters the system possesses 99.9% efficiency in collecting the concentration at either pole because the electrode has nearly reached equilibrium before the data has been collected. However, if an electrode was used with a slower response time and/ or a shorter oscillation period, with a similar data collection scheme, a significant underestimation of the concentration difference could result.

A recent example of this may have occurred leading, in part, to a 100–1000 fold discrepancy in H^+ influx at the tips growing pollen tubes (Feijó et al. 1999; Messerli et al. 1999). It must be considered that the cells generate different H^+ fluxes under the different extracellular pH used. However, we also find that there is a technical basis for some of the discrepancy. The parameters for the H^+ selective electrode used by Messerli et al. (1999), are listed above and modeled in Fig. 4.6A. However, with similar diameter electrodes we found that the electrode setup used by Feijó et al. (1999), using their same backfill and pollen tube growth medium along with a 10–15 μm length H^+-selective solvent possess a response time of 572–738 ms for different 0.5 pH steps between pH 5.5–6.5, see Table 4.1. For these studies Feijó et al. (1999) used an oscillation frequency of 0.5–1 Hz and a similar 30:70%, movement and equilibration: data collection scheme. Figure 4.6B and C show models of the output response based on the average response time 675 ms over the 5.5–6.5 pH range, during 0.5 Hz and 1 Hz oscillating frequency, respectively. The collection efficiency for the slower response time H^+ electrode at 0.5 Hz is 83.3% of maximum and is only 53.0% of maximum for 1 Hz. For this model, instantaneous translation has been used as no translation speed was listed. Of course the probes are not moved instantaneously and therefore the calculated efficiencies will be significantly lower. The voltage response to a pH change of 5.5–6.5 is only 37.3 ± 0.5 (n=4) indicating that the conditions used by (Feijó et al. 1999) most likely contained an interferent. The slow response times we measured also indicates the presence of an interferent. The conditions used by Feijó et al. (1999) created a subNernstian H^+ electrode with a slower response time giving rise to possible underestimation of the H^+

Fig. 4.6. (*Continued*) efficiency of concentration. The *middle* and *lower graph* correspond to the average response time of the H^+-selective electrode determined in the culture medium used by Feijó et al. (1999) (675 ms) along with the shorter collection periods that they used 2 s (*middle graph*), 1 s (*bottom graph*). The medium causes the electrode to respond more slowly such that it does not reach equilibrium before data collection occurs. This leads to only 83% and 53% efficiency, using the same 30%:70% collection scheme

concentration difference. This case study exemplifies the need to determine the response time and voltage response of the electrode in the medium used and to adjust the collection frequency of the system to accommodate slower sensors. We also encourage investigators to report the voltage/current response and response times of their sensors in order to provide a more solid foundation for independent verification of published results.

4.4 Self-referencing as applied to plants

Among the goals of the plant cell physiologist are the mapping of the movement of ions, metabolites and signaling molecules through the plasma membrane and the determination of the distribution of those ions and molecules within the cell. This section will examine and contrast various physiological techniques with an emphasis on self-referencing microelectrodes for accomplishing these goals, as applied to plant cells, and will evaluate those techniques in terms of sensitivity as well as spatial and temporal resolution.

4.4.1 Ca^{2+} fluxes in an alga: comparison of radiotracers and a self-referencing Ca^{2+} electrode

Perhaps the most direct comparison to information obtained with self-referencing measurements is that obtained by the use of tracers, particularly radioactive tracers. Pertinent to the present issue is the use of radioisotopes of small ions to monitor the movement of the ions into or out of cells. Useful tracers exist for Na^+, K^+, Ca^{2+}, Cl^-, SO_4^{2-}, and Mg^{2+}. Often, a radioisotope of Rb^+ has been used as a surrogate for K^+, as it is longer lived and does not emit gamma rays as ^{42}K does. If the flux of an ion into cells is to be measured, the cells are bathed in the tracer at a known specific activity and the amount of the ion that accumulates in the cells in a short time is measured. The length of time of the pulse is constrained on one side by the requirement that the intracellular pool not be significantly labeled so that loss of tracer through backflux will not occur, and on the other side by the need to accumulate a measurable amount of tracer in the cells. It is also possible to load cells with the tracer and then measure the efflux of the labeled ion from the cells. While flux measurements on single cells can be done in the case of certain giant cells, many cells usually must be used to get sufficient accumulation of radioactivity for measurement. Another caveat is the binding of ions to the cell wall; this is especially a problem for divalent cations.

The comparison of fluxes measured with tracers and self-referencing probes can best be illustrated by the case of the Ca^{2+} fluxes in the recently-fertilized eggs of the brown alga, *Silvetia compressa*. Both techniques have been applied to these cells in an effort to understand the role of Ca^{2+} in the establishment of developmental polarity in response to unilateral light. Using ^{45}Ca, it was shown

that the flux of Ca^{2+} into the cells was about 0.15 pmol cm^{-2} s^{-1}, and changed little during the light-induced polarization process (Robinson and Jaffe 1973). By inserting 25,000 cells in a nickel screen, the two hemispheres of the cells could be isolated and flux measurements at the two poles could be measured. It was found that in response to unilateral light, the Ca^{2+} influx became strongly asymmetric, with Ca^{2+} entering the shaded, future growth pole, and differentially left the future thallus end (Robinson and Jaffe 1975). These measurements led directly to the prediction that the formation of intracellular Ca^{2+} gradients is an early, essential step in development of polarity.

Recently, the self-referencing Ca^{2+} electrode has been employed to measure net Ca^{2+} fluxes in polarizing *Silvetia* zygotes, affording a direct comparison with the tracer flux data (Pu and Robinson 2003). As noted above, the sensitivity of the self-referencing ion probes declines as the background concentration of the sensed ion increases. In the case of the marine algae, the normal concentration of Ca^{2+} in the sea water is about 10 mM. That proved too high for flux measurements, so it was necessary to culture the cells in 1 mM Ca^{2+}. The cells polarized and germinated normally in the reduced Ca^{2+} medium. The electrode measurements showed that a highly localized region of net Ca^{2+} influx arose during the photopolarization process and was a highly accurate predictor of the locus of the future growth pole. In an individual cell, net influx was measured for a period of one to two hours and had a peak of about 15 pmol cm^{-2} s^{-1}. Net efflux could not be measured anywhere on the cell.

These experiments illustrate both strengths and weaknesses of self-referencing measurements. The locus of net Ca^{2+} influx and its timing could be identified with far more precision using the electrodes, compared to the tracer flux measurements, which required averaging over thousands of cells. However, alterations in the normal medium had to be made in order to carry out the electrode measurements. The electrodes did not detect the predicted asymmetry in efflux, presumably because it is not highly localized like the asymmetric influx. It should be mentioned that a marine cell poses the greatest challenge for self-referencing ion measurements as the background concentration of ions (except protons) is high.

The self-referencing measurement of ion fluxes is vastly more versatile than tracer fluxes. The ability to generate localized flux information using tracers depended on the unique qualities of the fucoid eggs, and the development of specialized techniques with little applicability to other biological systems. The tracer flux measurements also required 15 min to complete while the electrodes have a time resolution of a few seconds.

4.4.2 Evaluation of self-referencing of ion-selective electrodes on pollen tube ion dynamics

Perhaps no other plant system has been the subject of the application of so many different physiological techniques as the pollen tube. The techniques

include radiotracers, autoradiography, self-referencing current and ion flux measurements, voltage and patch clamp measurements and imaging. Thus, the literature on pollen tubes offers a rich array of possibilities for comparing the strengths and limitations of the self-referencing technique to other approaches as well as its ability to complement other approaches. The popularity of the pollen tube as model system stems both from its intrinsic importance in sexual reproduction and the fact that it represents an extreme case of morphological polarity. Pollen tubes can grow as fast as 5 $\mu m\ s^{-1}$ and they achieve this by adding new membrane and cell wall material in a precisely choreographed pattern at the growing tip. There is a strong temporal component, in addition to the spatial one, as growth is oscillatory.

A central role for ions in tip growth was indicated when it was found that Ca^{2+} is an essential component of any medium in which pollen tubes could germinate from the grain and grow (Brewbaker and Kwack 1963). In another early use of the self-referencing voltage probe, it was found that net current of about 0.5 $\mu A\ cm^{-2}$ entered the growing tip of lily pollen tubes (Weisenseel et al. 1975; Weisenseel and Jaffe 1976). Evidence that Ca^{2+} played a controlling role in this current led to the efforts to detect local Ca^{2+} entry using 1 min pulses of ^{45}Ca followed by low temperature (–60 °C) autoradiography of intact pollen tubes (Jaffe et al. 1975). All of the tubes showed accumulation of labeled Ca^{2+} at the tip, and in some cases, intense accumulation was seen.

There has been a resurgence of research on the physiology of pollen tube growth in which self-referencing techniques have played a key role. Ratiometric imaging revealed that there is an obligatory gradient of cytoplasmic Ca^{2+} in growing pollen tubes (Rathore et al. 1991; Miller et al. 1992), with elevated Ca^{2+} at the growing tip. Self-referencing Ca^{2+} electrode measurements showed that there is net Ca^{2+} influx at the growing tip of 1–10 $pmol\ cm^{-2}\ s^{-1}$, and that net influx ceased when growth and Ca^{2+} gradients were disrupted (Kühtreiber and Jaffe 1990; Pierson et al. 1994).

The subsequent finding that growth of pollen tubes is oscillatory (Pierson et al. 1995, 1996) added a temporal dimension to the measurements and it was shown that the Ca^{2+} concentration at the tip also oscillated with the same frequency as growth and nearly the same phase (Holdaway-Clarke et al. 1997; Messerli and Robinson 1997). However, a major discrepancy between the imaging data and the self-referencing Ca^{2+} influx data was evident. The oscillations in electrode-measured influx lagged the oscillations in intracellular Ca^{2+} by about 11 s out of a period of about 40 s (Holdaway-Clarke et al. 1997), a finding that was independently confirmed (Messerli et al. 1999). This discrepancy points out one drawback of the self-referencing electrodes as applied to plants: they cannot distinguish between ions moving into some extracellular sink, such as the cell wall, and true transmembrane flux. Thus, it has not yet been possible to elucidate the connection between the electrode-measured fluxes of Ca^{2+} and the oscillatory changes in cytoplasmic Ca^{2+} in the growing pollen tube.

The fluxes of two other ions have been measured in growing pollen tubes using the self-referencing technique, K^+ and H^+. Messerli et al. (1999) detected large inward oscillations of K^+ at the growing tip. The peaks of these pulses averaged nearly 700 pmol cm^{-2} s^{-1} and lagged the growth peaks by 100°. Clearly, this influx of K^+ is sufficient to have osmotic consequences and may provide a major source of solute for maintaining turgor pressure during rapid volume expansion.

The situation regarding H^+ fluxes is controversial. Messerli et al. (1999) detected large oscillatory proton influx at the tip (peak influx about 500 pmol cm^{-2} s^{-1} for tubes growing at pH 5.5) with smaller influx at least 50 μm behind the growing tip. On the other hand, Feijó et al. (1999) reported much smaller proton fluxes at the tip (about 0.1–1 pmol cm^{-2} s^{-1}) and a very different pattern that included proton efflux in a zone 20–40 μm behind the tip, at least at a medium pH of 6.5. Part of the difference in the magnitudes of the H^+ influx is attributable to the use of a correction factor for the presence of proton buffer in the medium used by Messerli et al. (1999), but that cannot entirely explain the difference. More recently, additional factors have been brought to light that have been discussed above. Specifically, the H^+-selective solvent under the conditions used by Feijó et al. (1999), responded in a subNernstian manner to changes in pH. Additionally the self-referencing frequency was faster and the response time was slower, leading to further possible signal loss. This will have caused Feijó et al. (1999) to greatly underestimate the proton fluxes. It also points to the importance of rigorous electrode calibration in the use of self-referencing electrodes.

Finally, there is a report of large Cl^- efflux from tobacco and lily pollen tubes (Zonia et al. 2002). A critical re-evaluation of that report shows that poor selectivity of the ion-selective solvent (Sigma-Aldrich/Fluka 24899) for the anionic form of the MES buffer that was used, as well as the lack of any Cl^- requirement for growth of lily pollen tubes undermines that claim (Messerli et al. 2004). The sensitivity of the Cl^--selective solvent for the anionic form of MES makes the electrodes indirectly sensitive to the steep pH gradients that exist near the pollen tube tip. These findings underscore the need for careful characterization of electrodes. Much of the published data and manufactures' claims are valid for the media in which animal cells are maintained, but plant cell culture media are quite different and the electrodes require careful evaluation of selectivity in the actual medium used.

The use of the patch clamp technique in various configurations allows the activity and properties of ion channels to be studied. The use of patch clamp requires the removal of the cell wall and necessarily the loss of turgor pressure. Most patch clamp measurements of pollen grains or tubes have utilized the whole-cell configuration with the loss of spatial information (e.g. Griessner and Obermeyer 2003), making direct comparison with extracellular self-referencing measurements difficult. Recently, a successful effort was made to preserve a degree of spatial information in single channel recordings

of patches pulled from defined locations on grain protoplasts or protoplasts from the pollen tube tip (Dutta and Robinson 2004). While three different channels were found on the grain, the only channel that was detected in the tip protoplasts was a stretch-activated (SA) Ca^{2+} channel with properties similar to the SA channel found in the grain. Two types of K^+ channels were found on the grain but no K^+ channels were ever observed on the tip protoplasts. Thus, there is a sharp discrepancy between the patch clamp results and the self-referencing K^+ measurements, which show net K^+ entry of 700 pmol cm^{-2} s^{-1}. Possible explanations are that the measured K^+ influx is not through a channel but a pump, perhaps a K^+/H^+ cotransporter, or the channel localization may be lost due to the disruption of its links to the cytoskeleton in the patch. Whatever the explanation, the self-referencing measurements must be regarded as definitive, net K^+ influx does occur, and its mechanism remains to be found. This illustrates the advantages of a non-invasive technique.

4.5 Conclusion

The development of methods for measuring analyte flux with high spatial and temporal resolving extracellular electrochemical sensors has added a vital new dimension to the study of plant physiology. This noninvasive approach has enabled the study of ion transport under normal growing conditions with turgor pressure and cell walls intact. While most of the work has involved monitoring uptake and release of H^+ and inorganic ions with potentiometric sensors, the advances in microscale amperometric detection have enabled the study of a whole new class of analytes, including O_2 and reactive oxygen species. This approach offers considerable promise for the future; for example, the detection of auxin fluxes with subcellular resolution in order to understand how polar auxin transport is organized. As with other physiological tools, continuous characterization of the strengths and weaknesses must occur to prevent misinterpretation of the results. The required characterization can be complex and often take the investigator in unexpected directions. In this review, we have attempted to highlight both the obvious and the more subtle problems with using electrochemical sensors particularly in a time-dependent modulation approach. However, when used properly with good speed and selectivity, the self-referencing approach has opened and will continue to open new avenues in plant research.

References

Ammann D (1986) Ion-selective micro-electrodes, principles, design and application. Springer, Berlin Heidelberg New York

Arif I, Newman IA (1993) Proton efflux from oat coleoptile cells and exchange with wall calcium after IAA or fusicoccin treatment. Planta 189:377–383

Arif I, Newman IA, Keenlyside N (1995) Proton flux measurement from tissues in buffered solution. Plant Cell Environ 18:1319–1324
Baikie ID, Smith PJS, Porterfield DM, Estrup PJ (1999) Multi-tip scanning Bio-Kelvin probe. Rev Sci Instr 70:1842–1850
Bakker E, Bühlmann P, Pretsch E (1997) Carrier-based ion-selective electrodes and bulk optodes. 1. General characteristics. Chem Rev 97:3083–3132
Blüh O, Scott BIH (1950) Vibrating probe electrometer for the measurement of bioelectric potentials. Rev Sci Inst 21:867–868
Bogorff DJ, Messerli MA, Malchow RP, Smith PJ (2003) Development and characterization of a self-referencing glutamate-selective micro biosensor. Biol Bull 205:207–208
Brewbaker JL, Kwack BH (1963) The essential role of calcium ion in pollen germination and pollen tube growth. Am J Bot 50:859–865
Buerk DG (2004) Measuring tissue PO_2 with microelectrodes. Method Enzymol 381:665–690
Crank J (1967) The mathematics of diffusion. Oxford University Press, London
Csöregi E, Quinn CP, Schmidtke DW, Lindquist S-E, Pishko MV, Ye L, Katakis I, Hubbell JA, Heller A (1994) Design, characterization, and one-point in vivo calibration of a subcutaneously implanted glucose electrode. Anal Chem 66:3131–3138
Davies PW (1966) Membrane potential and resistance of perfused skeletal muscle fibers with control of membrane current. Fed Proc 25:332
Demarest JR, Morgan JLM (1995) Effect of pH buffers on proton secretion from gastric oxyntic cells measured with vibrating ion-selective microelectrodes. Biol Bull 189:219–220
Doughty JM, Langton PD (2001) Measurement of chloride flux associated with the myogenic response in rat cerebral arteries. J Physiol 534(3):753–761
Dutta R, Robinson KR (2004) Identification and characterization of stretch-activated ion channels in pollen protoplasts. Plant Physiol 135:1398–1406
Feijó JA, Sainhas J, Hackett GR, Kunkel JG, Hepler PK (1999) Growing pollen tubes possess a constitutive alkaline band in the clear zone and a growth-dependent acidic tip. J Cell Biol 144:483–496
Fleet B, Ryan TH, Brand MJD (1974) Investigations of the factors affecting the response time of a calcium selective liquid membrane electrode. Anal Chem 46:12–15
Friedemann MN, Robinson SW, Gerhardt GA (1996) *O*-Phenylendediamine-modified carbon fiber electrodes for the detection of nitric oxide. Anal Chem 1023:421–425
Garber SS, Messerli MA, Hubert M, Lewis R, Hammar K, Indyk E, Smith PJS (2005) Monitoring Cl^- movement in single cells exposed to hypotonic solution. J Memb Biol 203:101–110
Gow NAR, Kropf DL, Harold FM (1984) Growing hyphae of *Achlya bisexualis* generate a longitudinal pH gradient in the surrounding medium. J Gen Microbiol 130:2967–2974
Grahm L (1964) Measurements of geoelectric and auxin-induced potentials in coleoptiles with a refined vibrating electrode technique. Physiol Plantarum 17:231–261
Grahm L, Hertz CH (1962) Measurement of the geoelectric effect in coleoptiles by a new technique. Physiol Plantarum 15:96–114
Grahm L, Hertz CH (1964) Measurement of the geoelectric effect in coleoptiles. Physiol Plantarum 17:186–201
Griessner M, Obermeyer G (2003) Characterization of whole-cell K^+ currents across the plasma membrane of pollen grain and tube protoplasts of *Lilium longiflorum*. J Membr Biol 193:99–108
Henriksen GH, Raman DR, Walker LP, Spanswick RM (1992) Measurement of net fluxes of ammonium and nitrate at the surface of barley roots using ion-selective microelectrodes. Plant Physiol 99:734–747
Holdaway-Clarke TL, Feijó JA, Hackett GR, Kunkel JG, Hepler PK (1997) Pollen tube growth and the intracellular cytosolic calcium gradient oscillate in phase while extracellular calcium influx is delayed. Plant Cell 9:1999–2010
Jaffe LA, Weisenseel MH, Jaffe LF (1975) Calcium accumulations within the growing tips of pollen tubes. J Cell Biol 67:488–492
Jaffe LF, Levy S (1987) Calcium gradients measured with a vibrating calcium-selective electrode. Proc IEEE/EMBS Conf 9:779–781

Jaffe LF, Nuccitelli R (1974) An ultrasensitive vibrating probe for measuring steady extracellular currents. J Cell Biol 63:614–628

Jung S-K, Hammar K, Smith PJS (2000a) Development of self-referencing oxygen microsensor and its application to single HIT cells. Biol Bull 199:197–198

Jung S-K, Kauri LM, Qian WJ, Kennedy RT (2000b) Correlated oscillations in glucose consumption, oxygen consumption, and intracellular free Ca^{2+} in single islets of Langerhans. J Biol Chem 275:6642–6650

Jung S-K, Trimarchi JR, Sanger RH, Smith PJS (2001) Development and application of a self-referencing glucose microsensor for the measurement of glucose consumption by pancreatic β-cells. Anal Chem 73:3759–3767

Kochian LV, Shaff JE, Kühtreiber WM, Jaffe LF, Lucas WJ (1992) Use of an extracellular, ion-selective, vibrating microelectrode system for the quantification of K^+, H^+, and Ca^{2+} fluxes in maize roots and maize suspension cells. Planta 188:601–610

Kühtreiber WM, Jaffe LF (1990). Detection of extracellular calcium gradients with a calcium-specific vibrating electrode. J Cell Biol 110:1565–1573

Kumar SM, Porterfield DM, Muller KJ, Smith PJ, Sahley CL (2001) Nerve injury induces a rapid efflux of nitric oxide (NO) detected with a novel NO microsensor. J Neurosci 21:215–220

Land SC, Porterfield DM, Sanger RH, Smith PJS (1999) The self-referencing oxygen-selective microelectrode: detection of transmembrane oxygen flux from single cells. J Exp Biol 202:211–218

Lindner E, Gyurcsányi RE, Buck RP (1999) Tailored transport through ion-selective membranes for improved detection limits and selectivity coefficients. Electroanalysis 11:695–702

Mancuso S, Paeschi G, Marras AM (2000) A polarographic, oxygen-selective, vibrating-microelectrode system for the spatial and temporal characterization of transmembrane oxygen fluxes in plants. Planta 211:384–389

Mathison S, Bakker E (1998) Effect of transmembrane electrolyte diffusion on the detection limit of carrier-based potentiometric ion sensors. Anal Chem 70:303–309

Messerli M, Robinson KR (1997) Tip localized Ca^{2+} pulses are coincident with peak pulsatile growth rates in pollen tubes of *Lilium longiflorum*. J Cell Sci 110:1269–1278

Messerli MA, Robinson KR (1998) Cytoplasmic acidification and current influx follow growth pulses of *Lilium longiflorum* pollen tubes. Plant J 16:87–91

Messerli MA, Danuser G, Robinson KR (1999) Pulsatile fluxes of H^+, K^+, and Ca^{2+} lag growth pulses of *Lilium longiflorum* pollen tubes. J Cell Sci 112:1497–1509

Messerli MA, Smith PJS, Lewis RC, Robinson KR (2004) Chloride fluxes in lily pollen tubes: a critical reevaluation. Plant J 40:799–812

Miller DD, Callaham DA, Gross DJ, Hepler PK (1992) Free Ca^{2+} gradient in growing pollen tubes of Lilium. J Cell Sci 101:7–12

Nuccitelli R (1991) Vibrating probe technique for studies of ion transport. In: Foskett JK, Grinstein S (eds) Noninvasive techniques in cell biology. Wiley-Liss, New York, pp 273–310

Pepperell JR, Porterfield DM, Keefe DL, Behrman HR, Smith PJS (2003) Control of ascorbic acid efflux in rat luteal cells: role of intracellular calcium and oxygen radicals. Am J Physiol 285:C642–C651

Pergel E, Gyurcsanyi RE, Toth K, Lindner E (2001) Picomolar detection limits with current-polarized Pb^{2+} ion-selective membranes. Anal Chem 73: 4249–4253

Phillips PEM, Wightman RM (2003) Critical guidelines for validation of the selectivity of in-vivo chemical microsensors. Trends Anal Chem 22:509–514

Pierson ES, Miller DD, Callaham DA, Shipley NM, Rivers BA, Hepler PK (1994) Pollen tube growth is coupled to the extracellular calcium ion flux and the intracellular calcium gradient: effect of BAPTA-type buffers and hypertonic medium. Plant Cell 6:1815–1828

Pierson ES, Li YQ, Zhang GQ, Willemse MTM, Liskens HF, Cresti M (1995) Pulsatory growth of pollen tubes: investigation of a possible relationship with the periodic distribution of cell wall components. Acta Bot Neerl 44:121–128

Pierson ES, Miller DD, Callaham DA, van Aken J, Hackett G, Hepler PK (1996) Tip-localized calcium entry fluctuates during pollen tube growth. Dev Biol 174:160–173

Pineros MA, Shaff JE, Kochian LV (1998) Development, characterization and application of a cadmium-selective microelectrode for the measurement of cadmium fluxes in roots of *Thlaspi* species and wheat. Plant Physiol 116:1393–1401

Porterfield DM, Laskin JD, Jung S-K, Malchow RP, Billack B, Smith PJS, Heck DE (2001) Proteins and lipids define the diffusional field of nitric oxide. Measurement of nitric oxide fluxes from macrophages using a self-referencing electrode. Am J Physiol 281:L904–L912

Pu RS, Robinson KR (2003) The involvement of Ca^{2+} gradients, Ca^{2+} fluxes, and CaM kinase II in polarization and germination of *Silvetia compressa* zygotes. Planta 217:407–416

Rathore KS, Cork RJ, Robinson KR (1991) A cytoplasmic gradient of Ca^{2+} is correlated with the growth of lily pollen tubes. Dev Biol 148:612–619

Robinson KR, Jaffe LF (1973) Ion movements in a developing fucoid egg. Dev Biol 35:349–361

Robinson KR, Jaffe LF (1975) Polarizing fucoid eggs drive a calcium current through themselves. Science 187:70–72

Sanger R, Karplus E, Jaffe LF (1990) An aerial vibrating probe. Biol Bull 179:225

Schneiderman G, Goldstick TK (1976) Oxygen fields induced by recessed and needle oxygen microelectrodes in homogenous media. Adv Exp Med Biol 75:9–16

Schneiderman G, Goldstick TK (1978) Oxygen electrode design criteria and performance characteristics: recessed cathode. J Appl Physiol 45:145–154

Shabala S, Newman I (1998) Light-induced changes in hydrogen, calcium, potassium, and chloride ion fluxes and concentrations from the mesophyll and epidermal tissues of bean leaves. Understanding the ionic basis of light-induced bioelectrogenesis. Plant Physiol 119:1115–1124

Shabala S, Babourina O, Newman I (2000) Ion-specific mechanisms of osmoregulation in bean mesophyll cells. J Exp Bot 51:1243–1253

Smith PJS, Hammar K, Porterfield DM, Sanger RH, Trimarchi JR (1999) Self-referencing, non-invasive, ion selective electrode for single cell detection of trans-plasma membrane calcium flux. Microsc Res Techniq 46:398–417

Twig G, Jung S-K, Messerli M, Smith PJS, Shirihai O (2001) Real-time detection of reactive oxygen intermediates from single microglial cells. Biol Bull 201:261–262

Twig G, Graf SA, Messerli MA, Smith PJS, Yoo SH, Shirihai OS (2005) Synergistic amplification of beta-amyloid- and interferon-gamma-induced microglial neurotoxic response by the senile plaque component chromogranin A. Am J Physiol 288:C169–C175

Weisenseel MH, Jaffe LF (1976) The major growth current through lily pollen tubes enters as K^+ and leaves as H^+. Planta 133:1–7

Weisenseel MH, Nuccitelli R, Jaffe LF (1975) Large electrical currents traverse growing pollen tubes. J Cell Biol 66:556–567

Whalen WJ, Riley J, Nair P (1967) A microelectrode for measuring intracellular PO_2. J Appl Physiol 23:798–801

Zhang X, Kislyak Y, Lin J, Dickson A, Coradosa L, Broderick M, Fein H (2002) Nanometer size electrode for nitric oxide and S-nitrosothiols measurement. Electrochem Commun 4:11–16

Zonia L, Cordeiro S, Tupy J, Feijó JA (2002) Oscillatory chloride efflux at the pollen tube apex has a role in growth and cell volume regulation and is targeted by inositol 3,4,5,6-tetrakisphosphate. Plant Cell 14:2233–2249

5 Use of Non-Invasive Ion-Selective Microelectrode Techniques for the Study of Plant Development

Joseph G. Kunkel,[1] Sofia Cordeiro,[2] Yu (Jeff) Xu,[1] Alan M. Shipley,[3] José A. Feijó[2]

5.1 Ion dynamics in plant development

Ion fluxes across membranes are known to have important biological roles. They exert their effect by two means: generating electrical fields and changing the local ion concentrations, thus affecting physiological processes that are dependent upon them.

Electrical fields exert force on charged particles, from molecules to organelles, and this has been proposed to lead to the movement of membrane proteins or cytoplasmic vesicles by field orientation, electrophoresis or electro-osmosis. On the other hand, cells react to the ions that carry these currents, many of which act via signal transduction pathways. If these ions have a catalytic or regulatory function, the biochemical consequences of any change in their concentration can be enough to trigger a response (Harold and Caldwell 1990; Feijó et al. 2004). Furthermore, accumulating evidence has shown that polarity, morphogenesis and many developmental steps in plant cells are defined by an intricate network of processes that often include ion distribution and concentration as major correlates. These phenomena are available for experimental manipulation and measurement during which one can seek evidence for causal relationships.

5.2 Molecular basis of ion fluxes in plants

Ionic equilibrium in plant cells is achieved, on the one hand, by the maintenance of an electrochemical gradient by proton ATPases on the plasma membrane (P-ATPases) and, on the other hand, by the flux of other ions, namely potassium, calcium and chloride through ion channels and transporters.

Turgor and volume regulation, two crucial parameters in plant physiology and development, are good examples of processes that are strictly dependent

[1] Department of Biology, University of Massachusetts Amherst, MA 01003-5810, USA

[2] Centro de Biologia do Desenvolvimento, Instituto Gulbenkian de Ciência, PT-2780-156 Oeiras, Portugal (e-mail: jfeijo@fc.ul.pt)

[3] Applicable Electronics Inc., Forestdale, MA 02644, USA

Plant Electrophysiology – Theory & Methods (ed. by Volkov)

upon ion regulation. Intracellular pressure in plant cells is achieved and maintained by the intracellular accumulation of ions and solutes, and their partition and sequestration in different osmotic biochemical forms in the vacuole (e.g. formation of salts or polymers). The turgor pressure thus created is required for cell expansion, elongation, gas exchange, transport of ions and solutes, etc.

Pivotal in the regulation is also the activity of the vacuolar proton ATPases (V-ATPases), much different from their plasma membrane counterparts both in structure and mechanism. Vacuolar pyrophosphatases (PPases) are a third active transport party in the system. The coordinated action of these three pump systems maintains the cytosol at a fairly constant and neutral pH, while keeping both vacuole and external apoplast acidic.

These pumps are the active source of energy for a number of channels and transporters (e.g. Sanders and Bethke 2000; Taiz and Zeiger 2002; Blatt 2004), many now well characterized as expressed in a number of tissues, evidenced by transcriptomics (e.g. Pina et al. 2005).

The particular ionic environment created by these conditions is cause and consequence of the ion fluxes across the cell's membranes, requiring tight regulatory mechanisms that keep calcium concentration low, potassium high and a pH neutral, among other homeostatic regulations (reviewed by Feijó et al. 1995; Holdaway-Clarke and Hepler 2003).

The study of plant ion dynamics is therefore of the utmost importance, and several laboratories have taken advantage of non-invasive microelectrode techniques, in particular scanning ion-selective probes, to approach it.

5.3 Scanning probe: technical advantages and disadvantages

In the past, we have reviewed the application of both voltage sensitive and ion-selective probes for the scanning of membrane domains underlying the development of plants, with special emphasis on a very specialized cell, the pollen tube (Shipley and Feijó 1999; Fig. 7C, D). To date, the pollen tube is probably the best-studied system in terms of ion fluxes, and the matter has been reviewed both for its occurrence and biological meaning (Feijó et al. 2001, 2004; Holdaway-Clarke and Hepler 2003). The reason for this specific cluster of applications lies in the absence of real alternatives to an extracellular scanning probe for use with plant cells. The analysis of ion fluxes in living cells has been accomplished through the use of invasive techniques such as impalement and patch clamp. These approaches usually allow one independent sample location per cell. Further sampling proceeds at the risk that prior sampling had an effect on the cell. Although results from these techniques have been remarkably important for the characterization of ion channel properties and activity in plant development, they are compromised by serious disadvantages. Since access to the plasma membrane is necessary for the

formation of a tight seal between the membrane and the patch pipette (giga-ohm seal), the plant cell wall has to be either enzymatically digested or mechanically removed, creating protoplasts. Both processes can alter plasma membrane properties, namely activity of membrane proteins, and more importantly induce a condition of stress that will likely hinder many underlying physiological processes. Moreover, the success rate of giga-ohm seal formation in plant protoplasts is generally low, which is probably caused by incomplete cell wall removal or immediate regeneration of a new cell wall. The use of extra-cellular vibrating or stepping probes, totally non-invasive methods, adds an important edge to the study of living cells.

Non-invasive scanning probes have gone through a series of transformations in use by diverse research groups.

One of the first vibrating calcium-selective electrode recording system was built, for the initial use of Jaffe and Levy (1987), as a direct coupled (DC) device by A.M. Shipley and C. Scheffey at the National Vibrating Probe Facility (MBL, Woods Hole).

The head stage used an AD515L chip with a 10 × gain fed to an AD524 amplifier set to 100 × gain with a DC offset control to cancel the Nernst potential on the ion-selective microelectrode. All measurements were referenced to an Ag-AgCl wire in a 3 M KCL salt bridge placed in the solution, millimeters away from the artificial calcium source. The microelectrode was vibrated at frequency of 0.5 Hz using a bench-top square-wave oscillator signal damped with an R/C network to smooth the vibratory movement of the microelectrode.

This original design was programmed in Pascal by Scheffey and it used a 60 Hz sampling routine to filter out line noise. This system measured the actual DC voltages (Nernst potential) across a ion selective liquid ion exchanger (LIX) column in the tip of a glass microelectrode positioned with a manual micromanipulator. Later a capacitively coupled (AC) device, introduced as described by Kühtreiber and Jaffe (1990), which "vibrated" between and paused at two extremes of a straight path. The system was controlled by a PC based Visual Basic computer program, DVIS written by W. Kuhtreiber. Vibration was via Burleigh piezopushers driven by an oscillator circuit. This AC design does not measure the actual voltage at the points of measurement and has efficiency properties based on both the LIX used and the circuit's capacitor that accumulates the voltage change. Using a capacitor, the efficiency of the system varies depending on the magnitude of voltage measured. This "self-referencing" AC system uses a continuous oscillation and the probe takes a few oscillations for overcoming hysteresis, a phenomenon whereby a circuit's current properties depend upon its past history, and become stable. Then the software accumulates a rolling average of the cyclical measurements. When a capacitor starts out it is uncharged; as it is oscillated in a field then its first oscillation starts with no charge and a few cycles of oscillation (discharge in one direction and recharge in the opposite direction) must occur before the charge on the capacitor has a symmetrical history comparing opposite polls of oscillation. Thus, at least the first hemi-oscillation must be dropped as not

equivalent to the next hemi-oscillations. In addition the early approach of using a rolling average creates statistical and instrumental strategy problems. Notably, the first available stable datum from this approach comes on the *k+1* oscillation, where *k* is the rolling average base number. This error-laden protocol contributed to several important papers on tip growing systems (Kühtreiber and Jaffe 1990; Schiefelbein et al. 1992). At this point, a division in measurement philosophy occurred with part of the groups returning to the DC device because of its potential as a more comprehensive approach and reliable measurement efficiency. Table 5.1 lists the dynamic efficiencies estimated for the DC coupled electrodes listed which were achieved by using the continuous stepping approach, SIET. These efficiencies were improvements over those achieved with the AC devices and were listed elsewhere (www.bio.umass.edu/biology/kunkel/nvp_cali.html). Unfortunately, this table of efficiencies was assumed to apply to all oscillating ion-selective probes and often AC device results were published without benefit of accurate efficiency estimates. This is a major problem for the AC devices, since there is no adequate approach to establishing the AC system's dynamic efficiencies. In the few measurements of the dynamic efficiency of the calcium LIX using the AC devices driven at identical Hz at the National Vibrating Probe Facility, the dynamic efficiency was substantially lower than with the DC amplifier. Using the DC device and software improvements to the DVIS software, it was possible to eliminate rolling averages that created correlations between adjacent measurements, making it a bad experimental design. Rolling averages were replaced with statistics on independent unit measurements and this approach was used in further tip growth studies (Holdaway-Clarke et al. 1997; Feijó et al. 1999; Cardenas et al. 2000). Since the idea is to detect specific ion concentration as a function of DC voltage change on a LIX microelectrode, it is crucial to accurately detect the microelectrode's DC voltage at each extreme of the movement excursion. Fundamentally, these systems are concentration meters that derive ion flux or movement as a function of the local ion concentration difference measured between two positions close to a membrane. To accomplish this, the SIET (scanning ion-electrode technology) system was developed (Shipley and Feijó 1999). A major change in measurement protocols with this DC device allows for faster, multidimensional- and multi-probe measurements. ASET (automated scanning electrode techniques) software, developed by E. Karplus, (Science Wares, E. Falmouth, Mass., USA) established the sampling-rule approach to measurement. The sampling rule defines a set of unit measurements that can be as simple as a stationary measurement at one point with one probe, or as complicated as three-dimensional flux measurements involving stepping in the micrometer range of differential distances to measure differential concentrations with multiple probes, whether voltametric, amperimetric or both. Statistics on sampling is accomplished by replicating sampling rule unit measurements using standard experimental designs and controlling the pattern of unit measurements via interactive software-defined patterns of sampling sites. Complications of hysteresis are avoided in the DC sampling rules because the symmetry of oscillatory

Table 5.1. Dynamic calibration of ion selective micro-electrodes. All dynamic efficiencies were determined using DC methods. Dynamic efficiencies while continuously oscillating (*Step eff%*) were determined using the older 3DVIS software initially written by WielKuhtreiber and modified for 3D measurements by J.G. Kunkel. Dynamic efficiencies based on sampling rules (*Rule eff%*) were determined using the newer ASET software from ScienceWares. For convenience to the reader, we list the technical parameters of each ion listed (diffusion coefficient at infinite dilution, D_o; valence, i and Nernst slope) as well as the LIX used and its 90% response time. The Hz quoted refers to the stepping frequency used in the older 3DVIS software. The bicarbonate diffusion coefficient is listed for the carbonate LIX because at physiological pHs the carbonate travels mainly in the bicarbonate form

Ion	Do	i	Nernst slope	LIX	t90	Hz	Step eff%	Rule eff%
K^+	19.6	1	58	Fl:K IB	<1 s.	0.3	70%	85%
H^+	93.7	1	58	Fl:H IIA	~0.6 s	0.3	80%	100%
Ca^{+2}	7.9	2	29	Fl:Ca IIA	<5 s	0.3	50%	80%
Mg^{+2}	7.1	2	29	Fl:Mg IV	<30 s	0.25	30%	na
Cl^-	20.3	−1	−58	IE:170	na	0.5	85%	100%
CO_3^{-2}	13.9	−2	−29	IE:310	na	na	na	40%

(differential) data does not intrude on the collection process. As a result, a substantial improvement of the dynamic efficiency is achieved for the DC sampling rule approach for all LIXes tested, as indicated in Table 5.1. It must be emphasized that establishment of the dynamic efficiency of the electrodes must be determined case-by-case within the context of a given sampling rule (cf. Table 5.2). Dynamic efficiency will vary with the length of waiting time for

Table 5.2. A sampling rule for a dual probe system. *Point name*: probe position names as shown in Fig. 5.1, e.g. "$H^+_{(1)}$" refers to H^+ probe in location 1; dX, dY, dZ: displacements (µm) in X,Y,Z dimensions respectively to get to their corresponding point name; *WaitSec* defines a waiting time in seconds at the point name; *AvgSec* seconds averaging at 1000 measurements per second. The probe tips were placed 40 µm apart in the Y dimension. The movement to each new location is accomplished in less than 0.1 s and is included in the WaitSec parameter so that the entire time for the dual probe 3-D unit sample to be taken is the sum of WaitSec and Avgsec=9.2 s

Point name	dX	dY	dZ	WaitSec	AvgSec
$H^+_{(1)}$	0	−20	0	0.8	0.5
$O_{2(1)}$	0	20	0	0.5	0.5
$H^+_{(2)}$	10	−20	0	0.8	0.5
$O_{2(2)}$	10	20	0	0.5	0.5
$H^+_{(3)}$	0	10	0	0.8	0.5
$O_{2(3)}$	0	30	0	0.5	0.5
$H^+_{(4)}$	0	−20	10	0.8	0.5
$O_{2(4)}$	0	20	10	0.5	0.5

LIX wobble to subside, length of probe integration of the signal, the properties of the LIX used and other factors. For instance, the strength of the buffer can dramatically influence the apparent flux of protons (Faszewski and Kunkel 2001). The 100% dynamic efficiency achieved with the DC sampling rule approach (Table 5.1) applies only to low- or un-buffered samples. With low buffer levels secretion of enough protons to clear the local culture media of effective buffer must occur, otherwise the buffer extinguishes protons as they are secreted and the probe has effectively no difference in concentration to measure (Kunkel et al. 2001). Use of traditional bicarbonate buffered culture media such as Holtfretter's solution will result in a substantial loss of efficiency (efficiency=63%) in measuring protons. Doubling the bicarbonate buffer in the Holtfreter's, results in a reduction in efficiency to 43% (Faszewski and Kunkel 2001). This example points clearly to the need of examining probe manuscripts with respect to their reliable dynamic calibrations for the specific conditions used.

The SIET approach is especially suited to development involving growth or morphogenesis of a cell or tissue. This is because the microelectrode can be non-invasively moved around the extracellular medium surrounding a specimen, thus allowing large spatial coverage, as well as tracking a modulating or growing point.

These non-invasive extracellular methods provide complimentary information to add to intracellular methods using fluorescent reporting molecules (e.g. Holdaway-Clarke et al. 1997). In their most ambitious applications with adequate calibration, non-invasive ion probes can be used to integrate the relatively steady ionic fluxes emanating from a region or unit surface area of a cell or cellular membrane (Cardenas et al. 1999, Fig. 8F). Often a probe has been used in a semi-quantitative way to observe relative ion flux spatial patterns focusing on temporal oscillatory patterns without calculating flux at other than the probe position in one dimension or extrapolating the flux to the cell surface (Holdaway-Clarke et al. 1997; Cardenas et al. 1999; Feijó et al. 1999; Zonia et al. 2001, 2002; Fig. 5.8E). Ion-selective probe calibration is essential to quantitative applications in which the properties of a particular region of a cell are of interest (Cardenas et al. 1999, Fig. 5.8F), or where the measurements are of importance in relating components of a model to one another (Feijó et al. 2001). The calibrations include simple calibration of the probe according to the Nernst equation [1]:

$$V = V_0 - (RT/zF) \cdot \ln(H/HA) \quad (1)$$

as well as determining the efficiency of the dynamic process of measuring the voltage difference between two points. In the later efficiency determination, there is a trade-off between allowing any probe wobble to come to rest after a move to a new location, the speed of the LIX to respond to the new location, the length of data collection, repetition of the measurement and how many other points one wants to measure in an experiment. Patterns of measurements that

include long movements between their starting positions require longer wait states to allow LIX wobble to subside. LIX wobble does not cause a decrease in efficiency; rather, it creates random noise resulting in outlier data. For that reason, more weight must be given to wobble suppression (via longer wait states) versus longer integration time. It is always possible to trade lower efficiency for faster measurements. The DC approach has an advantage over the AC approach in this respect. The AC approach has a symmetrical but additive loss of efficiency at both ends of the measurement cycle. As detailed earlier (Kunkel et al. 2001), the DC approach reduces the loss of dynamic efficiency by starting at an origin at which there is little or no loss of efficiency, cutting the loss of dynamic efficiency at least in half at each measurement site. DC measurement devices and protocols are a faster and more accurate measurement system than the AC approach. The DC approach also provides the user with a high gain device that can be used in a stationary way to measure flux oscillations in real time, which the AC system cannot do because of its limited frequency mode of measurement.

Stationary ion-selective microelectrodes can also be used to infer cellular activity but it is only applicable when large enough signals are being recorded, usually on large enough organs to generate sufficient detectable currents (e.g. roots). Vibrating or rather, as described above, stepping a microelectrode between two positions and measuring the DC voltage difference between the positions of the microelectrode greatly increases sensitivity and corrects for microelectrode drift as long as the stepping is much faster than the drift. This is particularly important when studying single or isolated cells that generate smaller currents than whole tissues or organs.

Unfortunately, the extracellular microelectrode used can only measure the ion concentration at points outside the cell wall of plants. However, the use of specific inhibitors for ion channels or transporters that putatively convey membrane fluxes provides clarification of the relative contribution of fluxes across the plasma membrane.

In a number of situations, intracellular ion concentration and its modulation by fluxes across the plasma membrane are potentially one of the earliest diagnoses of any changes that a cell displays. Therefore, the SIET has become a useful tool for the study of biological phenomena in which spatial and temporal resolution are an issue.

For reasons outside the scope of the present manuscript, the very same principle we describe here, with different instrumental interpretations, is used associated with various acronyms, namely MIFE (see Chapter 3), SERIS (see Chapter 6), and SIET here. In essence they all use the same basic relationship, the Nernst equation [1], which relates electrical potential to ionized compound concentrations. However, the DC and AC approaches diverge in technical design that sets limits or advantages for each. Self-referencing AC systems such as SERIS are based on the measurement of ion-selective microelectrode voltage differences (Nernst potentials) through a capacitor at opposite extremes of an

oscillation. The SERIS system does not directly measure the voltage on the microelectrode at each point but rather records the results in a software averaging algorithm accumulating the difference (delta V) between the two points. Though SERIS can measure the presence of a flux of an ion, it is unable to accurately measure the actual strength of the flux. The SERIS approach calibrates the electrode at low gain (DC × 10) mV sensitivity, but makes the delta microvolt measurement (gain × 1000) via a capacitor. Since efficiency of the LIX electrode is not measured at microvolt levels, it is unable to measure the flux accurately. In the AC SERIS protocol the local concentration of an ion is assumed to be close to the background media's composition (Kühtreiber and Jaffe 1990), which is a logical first guess but may not be accurate in situations where the cell is actively pumping the ion of interest. This is particularly true when dealing with H^+ secretion, where the local buffer concentration must be low enough for the cellular pumping to overcome it (Kunkel et al. 2001). SIET also allows sampling rules to be created for 1-, 2-, or 3-D measurements using one ion-selective microelectrode or sequential or interleaved measurements (Table 5.2) of multiple ion-selective microelectrodes in one or more dimensions (Faszewski and Kunkel 2001). SIET probes can also be interleaved with polarographic (amperimetric) microelectrodes by a sampling rule (Table 5.2) that extends the molecules measured beyond the current review's scope to non-ionic small molecules such as oxygen and nitric oxide (for an example of application see Prado et al. 2004).

This capability of measuring multiple ions is also critical to accurate estimation of certain ion fluxes. For instance, the LIX nominally used for measuring bicarbonate is primarily sensitive to carbonate which at physiological pH is a minority of ions present in the carbonate/bicarbonate equilibrium. In order to accurately measure the total carbonate/bicarbonate concentration one must also simultaneously measure local pH that is involved intimately in the equilibrium. In addition, many tip growth studies have common factors that allow correlation of the relative timing of internal and external ion movements (Holdaway-Clarke et al. 1997; Feijó et al. 1999; Roy et al. 1999). The sampling-rule approach is highly compatible with correlating the measurement of ion-selective probe data with interleaved cellular and intra-cellular data obtained from image analysis (Holdaway-Clarke et al. 1997; Feijó et al. 1999; Antoine et al. 2000, 2001, see below).

5.4 Capabilities of scanning microelectrode technology

In order to establish the capabilities of particular scanning microelectrode setups and analyze the data collected, we routinely use artificial ion sources or well defined model systems such as the growing pollen tube whose cylindrical shaft and hemispherical growing tip is easy to define geometrically. In that way, we can objectively test the limits of a new protocol or measurement system.

5.4.1 Artificial point source device

Measuring artificial sources or sinks similar to the types of currents measured in living material is a recommended first step when using this technology. Artificial ion point sources or sinks can be made using a glass capillary pulled in multiple stages to have a bee-stinger shape (Kühtreiber and Jaffe 1990). This will produce an infinite source or sink solution nearby the tip that represents the point source. This should have a tip diameter of 5–10 μm and be filled with low percentage agarose (around 0.5%) to stabilize the filling solution of the ion or molecule of interest, which should be 3 orders of magnitude higher or lower in concentration than the bathing media, thus producing a passive diffusion gradient. The agarose does not hinder the diffusion of the molecule through the tip but will stop bulk flow of the filling solution. An electrogenic flux can be simulated by a DC circuit through this source, provided that the source components are simple enough to allow the ion of interest to be a predictable component of the current. The predicted pattern of diffusing oxygen into a recessed platinum electrode surface can be seen in Fig. 5.1A, which illustrates a sagittal section through the artificial source tip and sphere of predictable oxygen concentration, according to the equations of Schneiderman and Goldstick (1978). The results of measuring the flux emanating in the three directions, x, y and z, from a point source in a grid of points in a YZ plane tangent to the sphere of molecules diffusing from a point source tip such as in Fig. 5.1A is plotted in various ways in Fig. 5.1B, E, F. Planar contour plotting functions of grid data (Fig. 5.1E) are available in many computational software packages such as MathCad, Matlab, or R. The characteristic reversals of flux components, as the probe passes high and low in the Z dimension, emanating from the source tip can also be seen in linear plots, Fig. 5.1E, of the J_y data from Fig. 5.1D. A more intuitive stereo view of total flux vectors, Fig. 5.1B, C, requires use of software packages such as Mage, able to represent points in space and provide stereo pairs. It is important to be aware of the total flux vectors involved at each point measured when plotting one or two-dimensional representations (e.g. Fig. 5.8A–C) of those vectors. In some cases a vector can represent a small local 1-D component of a larger 3-D flux associated with an adjacent localized point source or sink. Familiarity with the measurement phenomena, solid geometry and distance, inherent in Fig. 5.1 is critical to understanding fluxes measured from natural sources.

For testing multiple-probe arrays, one can devise gradients of each molecule of interest emanating from a single point source. For instance, to create a joint point source for protons and carbonate and point sink for oxygen, one can craft a small capillary with gaseous CO_2 forced to the tip presenting a small gaseous interface that releases CO_2 which associates with the water to form a point source of bicarbonate, carbonate and protons. In addition, the pure CO_2 bubble provides an infinite sink for dissolved oxygen. This artificial source has been used for testing multi-probe pairs such as HCO_3^- and protons (Faszewski and Kunkel 2001) or protons and O_2.

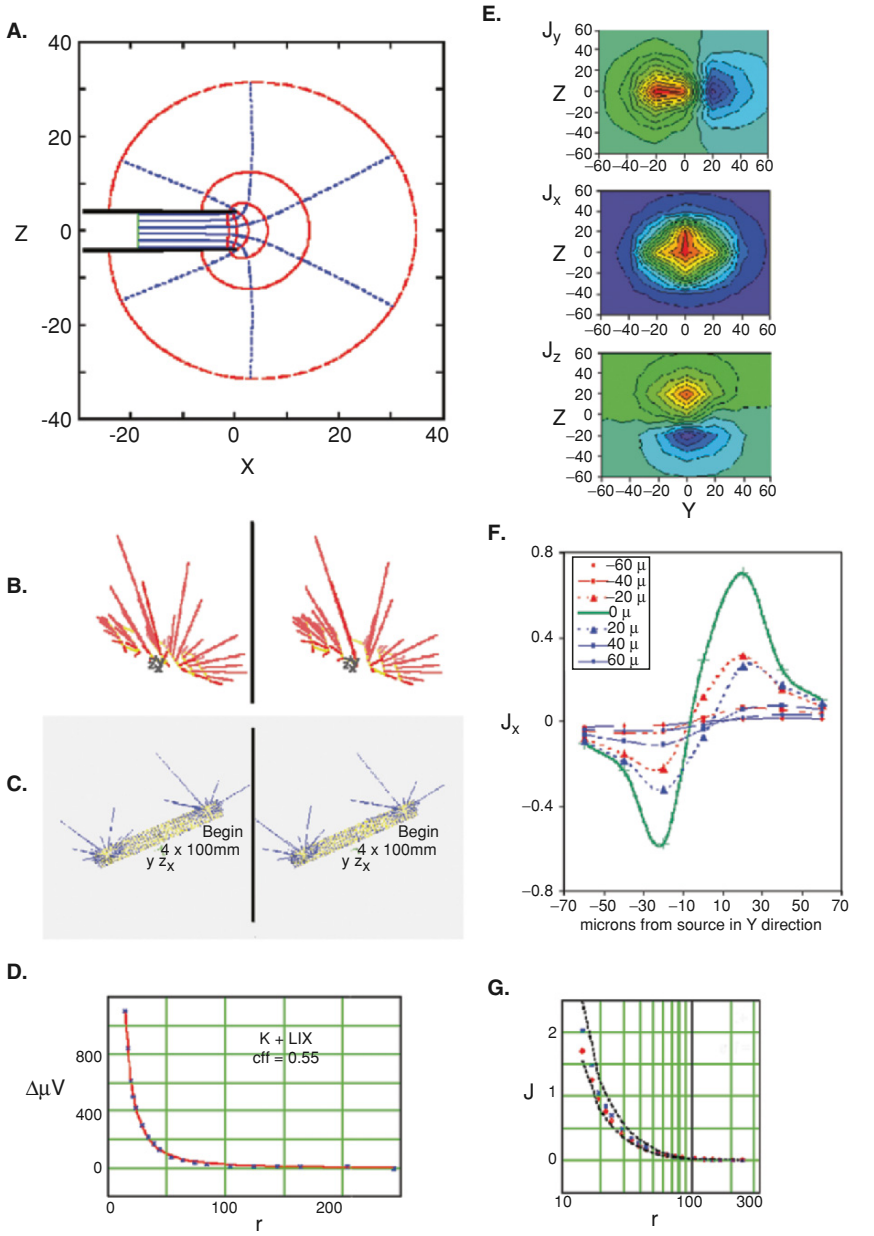

Fig. 5.1. Point source in theory and practice. **A** The computed pattern of oxygen diffusing into a capillary tube with a recessed platinum surface which serves as an oxygen sink. **B** Stereo image pair of calcium flux vectors emanating from a point source. **C** Stereo image pair of proton flux vectors emanating from a pair of point sources 1.5 mm separated. **D** Dynamically measured microvolt differences (ΔμV) measured at graded radial distances from a point source. The expected ΔμV was computed by extrapolation between known linear voltage versus 1/r points and multiplied by an estimate of the dynamic efficiency to attempt to fit a red line of expected

5.5 Calibrations of probes using particular sampling rules

Each LIX microelectrode has an efficiency of flux measurement dependant upon the time it takes to settle to a new voltage level at a new ion concentration. Calibration of a DC system in solutions of known concentration is a meaningful measurement of LIX responsiveness, and relates directly to how the electrode will be used in measuring gradients. When presented with a steady state ion flux from a point diffusion source (Fig. 5.1A), optimization requires waiting long enough at a given sample position with sufficient gain to record an accurate ion concentration measurement, and then moving to another position and re-measuring. The flux between the two points can be calculated from the values of *dC* and *dx* of equation [6] as explained below. Steady state sources are rare in live matrials, arguing for short waiting periods at each measurement point. The SIET system can record LIX microelectrode noise and drift, allowing the design of protocols to minimize them.

The two types of calibrations that must be made on each probe type before they can be used are both based on the Nernst equation: [1] one is the static calibration similar to calibrating a pH meter (Fig. 5.2A), estimating the slope, A, of the voltage versus log [H^+] plot using two standard solutions, a and b, [2, 3] (the same equations are valid for any other ion).

$$pH_a - pH_b = \log\left[H^+\right]_a - \log\left[H^+\right]_b = \left(mV_a - mV_b\right)/A, \tag{2}$$

$$A = \Delta mV/\Delta pH, \tag{3}$$

or a multipoint calibration by estimating the slope of the linear regression [4],

$$V = B + A \cdot \log\left[H^+\right]/eff_s \approx B + A \cdot \log\left[H^+\right], \tag{4}$$

using three or more of the standard solutions as seen in Fig. 5.2A.

The slope, A, and intercept, B, determined for the probe based on the set of standard solutions can be used to estimate future concentrations (cf. [5]) measured by that electrode within the range of the standards used:

$$\left[H^+\right] = 10^{\left(A - V * eff\right)/B} \approx 10^{(A - V)/B} \tag{5}$$

Experience shows that future replacement electrodes made with the same LIX and electrolyte backfill can be checked for an appropriate voltage with a single point calibration, namely the bathing solution in use. Thus the estimation of the

---

Fig. 5.1. (*Continued*) ΔμV to the observed-ΔμV (*blue x*). The guessed efficiency was adjusted to give a best fit (*red line*). **E** Contour plot of the dX, dY and dZ components of fluxes of protons eminating from a point source measured at an YZ plane about 10 microns from the tip source. **F** Linear plots of the dY data from **E** plotted against the Y location. **G** Observed flux (*blue x*) computed from the dynamic efficiency and observed ΔμV from **D**. Upper and lower 95% confidence intervals (*black dashed lines*) on the expected J (*red diamonds*) are computed from the variance of the observed about the expected ΔμV from **D**

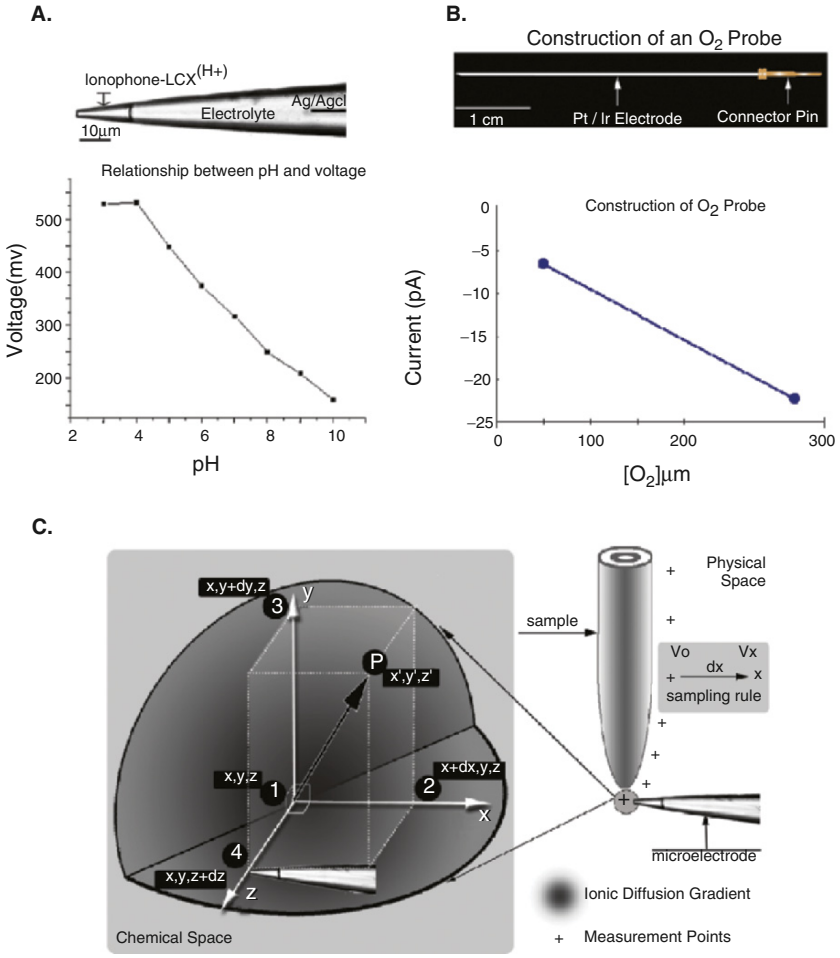

Fig. 5.2. H^+ and O_2 probes calibrations and sampling rules. **A** Construction and static calibration of a H^+ probe. Media composition for calibration was the same as pollen culture media except the pH was adjust to various values by adding either KOH or HCl. **B** Construction and calibration of an oxygen probe. The same media was bubbled with N_2 for over 30 min to achieve 0 µM oxygen concentration, while bubbled with air (18% O_2) for 30 min assumed to be 100% saturated (268 µM). **C** Sampling rules that control the movements of both H^+ and O_2 probes. At each measurement point in "physical space", both probes will make measurements from (1) ⇒ (2) ⇒ (3) ⇒ (4) ⇒ (1) in "chemical space"

concentration at the origin of a unit measurement, *Co*, is made using a static calibration curve similar to [5], for which there is close to 100% efficiency as there is with a pH meter. The other more critical calibration, in that it is less likely to be close to 100% efficient, is a dynamic calibration necessary for adequately estimating *Cx,* the concentration measured after the quick move to

position x. It depends on the LIX used and imposed sampling parameters such as the length of the LIX column, the wait before measuring and the length of the measurement phase, which jointly give rise to the probe dynamic efficiency (Fig. 5.1D). When divided into the observed microvolt difference, it allows prediction of the true microvolt difference critical to calculate the accurate flux (Fig. 5.1G).

$$J = D \cdot dC/dx = D \cdot (Cx - Co)/dx \quad (6)$$

Thus the loss due to dynamic inefficiency would show itself in the estimation of the C_x component of dC. The probe is allowed to sit at the measurement point for a wait-state long enough for the probe to reach close to its optimum voltage (i.e. ~100% efficient) where C_o is calculated using equation [5]. Then the probe is moved dx units to its position for measuring, C_x, where it is often necessary to take the voltage reading, V_x, (Fig. 5.2C) before the probe has come to equilibrium resulting in a loss of efficient measurement of V_x, underestimating the voltage. This inefficiency systematically underestimates the flux. One wants to take the V_x measurement at dx quickly in order to avoid any drift in the probe's voltage, and also quick to allow more measurements so to better represent the true dynamics of a living source. With a stable point source, the voltage at each point, r, away from the source can be measured with the probe in static, 100% efficient, positions. Then, V versus $1/r$ is plotted, a curve is fit to it and the expected voltage difference for the small extra move is calculated by interpolation between the measured points. In the same time frame as the static measurements are made, the voltage difference for a rapid dx move can be directly measured dynamically in real time. The difference between the measured and calculated voltage difference provides an estimate of the dynamic inefficiency of that sampling rule. This artificial source dynamic efficiency estimate provides the efficiency to use in correcting future experimental measurements of voltage differences. For a rapidly responding LIX such as the proton LIX there is almost no dynamic loss in efficiency in the measurements of the secondary voltages at dx, dy or dz and thus a 100% efficient estimate of a 3-D flux can be assumed (Table 5.1). This high dynamic efficiency is not true for the older continuous AC vibrating or SERIS methods, in which efficiency is lost at each end of the microelectrode oscillation, leading to further losses of efficiency for the proton electrode (Kunkel et al. 2001).

The concentration of ions diffusing from a point source such as displayed in Fig. 5.1, depend on diffusion alone and can be modeled as a hyperbola:

$$C_r = C_b + K/r, \quad (7)$$

where C_r is the concentration at radius r and K is a proportionality constant which includes the diffusion coefficient; C_b is the background concentration. Unfortunately, r is not the distance to the point source, but rather a hypothetical point up inside of the point-source-shaft that corresponds to the infinite source end of the hyperbola at which r is zero. This point can be esti-

mated, providing a straight-line theoretical curve of expected concentrations or microvolt differences at given diffusion radii. It is in such a context of expected μV differences that one can estimate the dynamic efficiency, eff_d. This dynamic efficiency is used in an equation [8] for estimating *dC*:

$$dC = C_r - C_{r+dx} = C_r - 10^{\left(mVr + \mu Vdiff/1000 * effd\right) - A)/B)}, \quad (8)$$

which can then be used to compute the flux using equation [6].

Despite the apparent mathematical sophistication, most of these equations have been introduced in simple worksheets of intuitive and simple usage and can be implemented by any inexperienced user in a matter of few hours.

5.6 Point sources used to test the resolution of microelectrodes

To establish the resolution of a measurement protocol and distinguish between point sources multiple sources can be created at fixed distances measured with a grid pattern (Fig. 5.1C; see also Somieski and Nagel 2001).

Measuring two molecular type sources (e.g. protons and oxygen) simultaneously presents a similar problem of resolution. The standard polarographic oxygen electrode (Fig. 5.2B) applies a steady voltage to its exposed platinum tip in order to make its measurement. The applied voltage of the oxygen electrode can interfere with an adjacent H^+-specific electrode (Figs 5.3, 5.4A). We quantified this interaction by measuring the oxygen electrode current and the H^+ electrode voltage with the two microelectrodes at different distances. While the oxygen electrode current (Fig. 5.5) is independent of the proton electrode, the proton electrode is affected by being less than 40 μm from the oxygen electrode tip.

Using a specific SIET sampling rule (Table 5.2) we were able to maintain a 40 μm distance between the two microelectrodes and sample an artificial source of protons and sink of oxygen to obtain a simultaneous measure of proton and oxygen flux (Fig. 5.4B–D). In that demonstration (Fig. 5.4B) the two contour plots of the data appear offset from one another due to the fixed distance between the two microelectrodes. By using a compensating adjustments via the sampling rules which sequentially steps the two microelectrodes to a common location while maintaining their physical distance (>35 μm apart) we are able to measure the oxygen and proton flux around the artificial source (Fig. 5.4) and the pattern of currents can be shown to be coincident. We subsequently applied this pairing of microelectrodes and sampling rule to a growing pollen tube tip (Fig. 5.6), and demonstrate the similar distribution of proton secretion and oxygen utilization in the region posterior to the growing tip known to be rich in mitochondria. This highlights the importance of studying model sources whenever multiple probes are used.

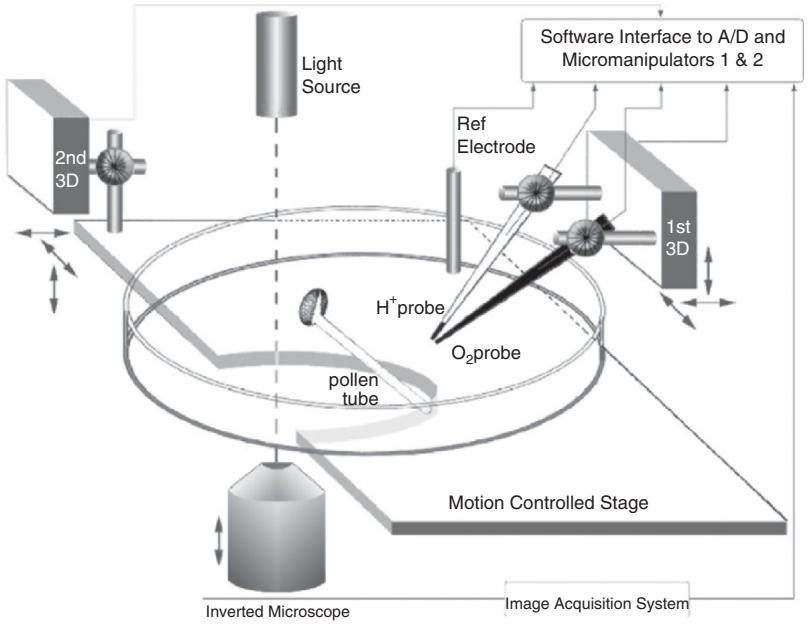

Fig. 5.3. Schematic diagram of multiprobe setup. H^+ and O_2 selective probes are plugged into pre-amplifiers (one a SIET and one polarographic). Both probes are mounted on a common 3D micromanipulator (*1st 3D*), by a motion controller. The pollen tube in its culture dish are held on a motion controlled stage held by a second 3D micro-manipulator (*2nd 3D*) controlled by a second motion controller which allows the rapidly growing tip to be maintained in the center of the stage. The probe amplifiers, two motion controllers and the camera are adjusted and controlled by the computer program ASET. A small drop of concentrated germinating pollen was spread evenly on the bottom of the Petri dish, which was coated with 10% poly-lysine. The 3 ml of liquid culture medium is added or changed in the Petri dish by gravity addition and maintained at a constant level by a suction skimmer

5.7 Different plant systems investigated

The SIET has been extensively used in a number of systems, from brown algae to higher plants, multi or unicellular systems but its use in single or isolated plant cells is of particular importance, since the currents generated are generally smaller in magnitude and therefore impossible to detect with stationary electrodes. This technique has allowed considerable advances in understanding some of these systems and therefore, we will focus on results obtained in single or isolated cells like pollen tubes (Fig. 5.7C–E; Fig. 5.8A), root hairs (Fig. 5.8D–F) and higher plant fertilization, studied through an in-vitro fusion system in maize (Fig. 5.9).

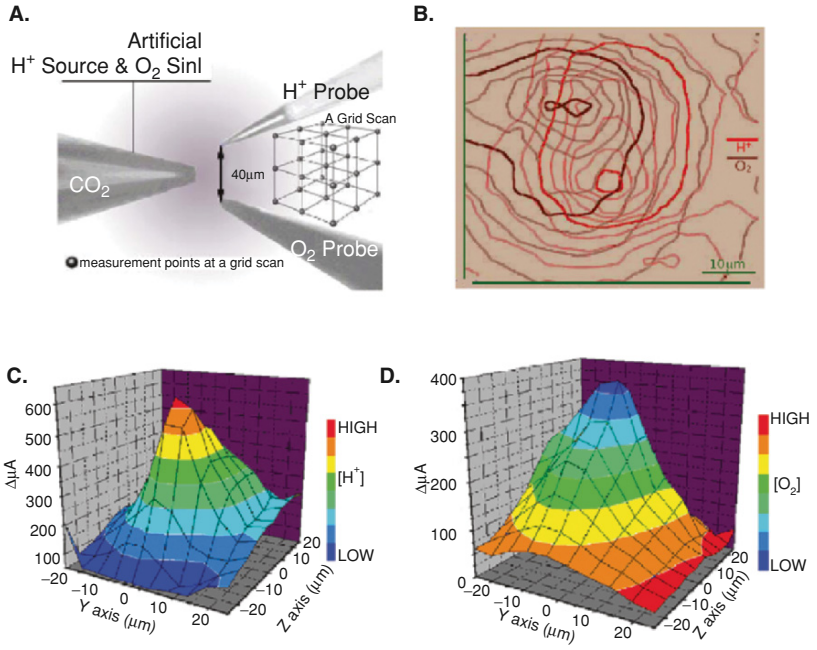

Fig. 5.4. No interference between H^+/O_2 probes using sampling rule with probes 40 µm apart. **A** Artificial dual source. A micropipette filled with CO_2 acts simultaneously as an H^+ source and O_2 sink. **B** Contour plot of micro-volt differences and pico-amp differences obtained from H^+ and O_2 probe readings respectively. **C** total μV-*difference* = $(\Delta\mu V_x^2 + \Delta\mu V_y^2 + \Delta\mu V_z^2)^{1/2}$ obtained from H^+ probe. **D** total μA-*difference* = $(\Delta\mu A_x^2 + \Delta\mu A_y^2 + \Delta\mu A_z^2)^{1/2}$ obtained from the O_2 probe. In both **C** and **D**, the total μV-*difference or* μA-*difference* was plotted onto the coordinate space of the probes reference position correcting for the 40 µm separation. In **B**, the contours are drawn with respect to the probes physical positions showing the 40 µm separation

5.8 Pollen tubes

The largest body of data acquired with extracellular, non-invasive techniques in single cells of higher plants was obtained on pollen tubes. These cells represent one of the most remarkable examples of polarized growth in nature. Since the early developments of the vibrating probe, they have been thoroughly used as a model and illustrate beautifully the potential of the technique.

Pollen tubes were first used by the group of L. Jaffe (Weisenseel et al. 1975) to demonstrate the use of the vibrating voltage probe, using germination media of ionic simplicity and low salt concentration, which yielded a high signal-to-noise ratio, and were able to demonstrate the existence of large electrical currents traversing pollen tubes, with the grain acting as the source of current and the tube as the sink. In parallel, Jaffe's group showed a common pattern in fucoid eggs undergoing tip growth, which were already known to drive electrical currents through themselves (Jaffe 1966, 1968). This similarity, albeit with huge physiological and genetic differences, suggested a causal

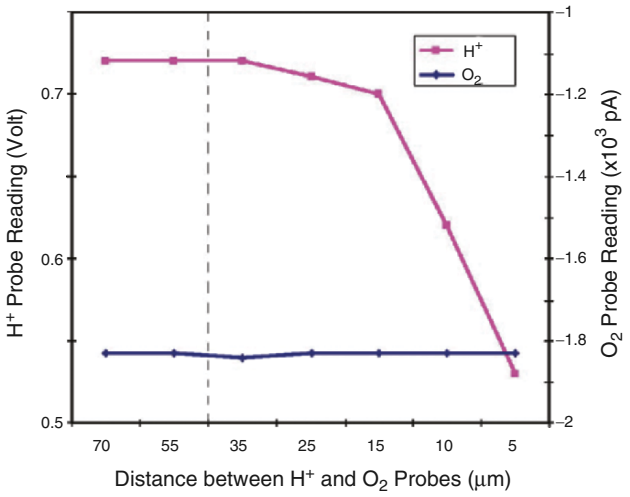

Fig. 5.5. Interferences between H^+ and O_2 probes. The two probes were manually adjusted to be separated by different distances while readings from both probes were collected. The media was the same as lily pollen culture media at pH 5.5, 100% air saturated. *Dotted line* indicates the recomended distance to avoid interference

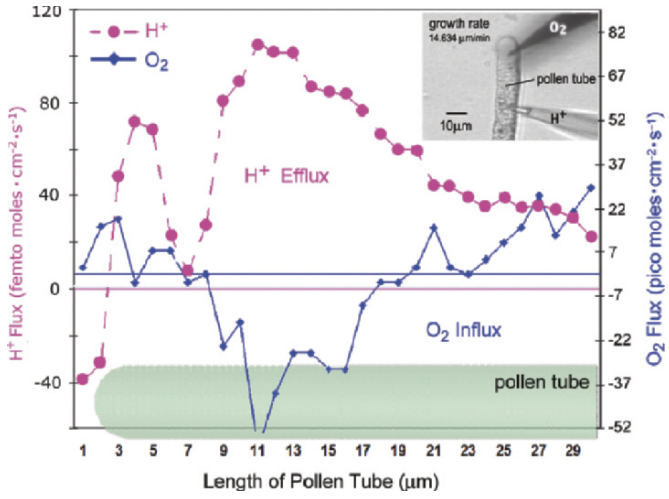

Fig. 5.6. H^+ efflux and O_2 influx in Z-axis plane over alkaline band region. Pollen tubes 800–2500 µm in length were selected for measurements. H^+/O_2 fluxes, as $\Delta\mu V_z$ and $\Delta\mu A_z$, at the surface of a pollen tube were measured by moving the electrode to within 2 µm from the tube surface. Background references were taken at least 500 µm away from any pollen grains or tubes and the value was subtracted from the surface measurements. The inset image is a screen shot showing the H^+/O_2 probes and a growing pollen tube with growth rate of 14.634 µm per min. This figure is a typical plot of five independent experiments

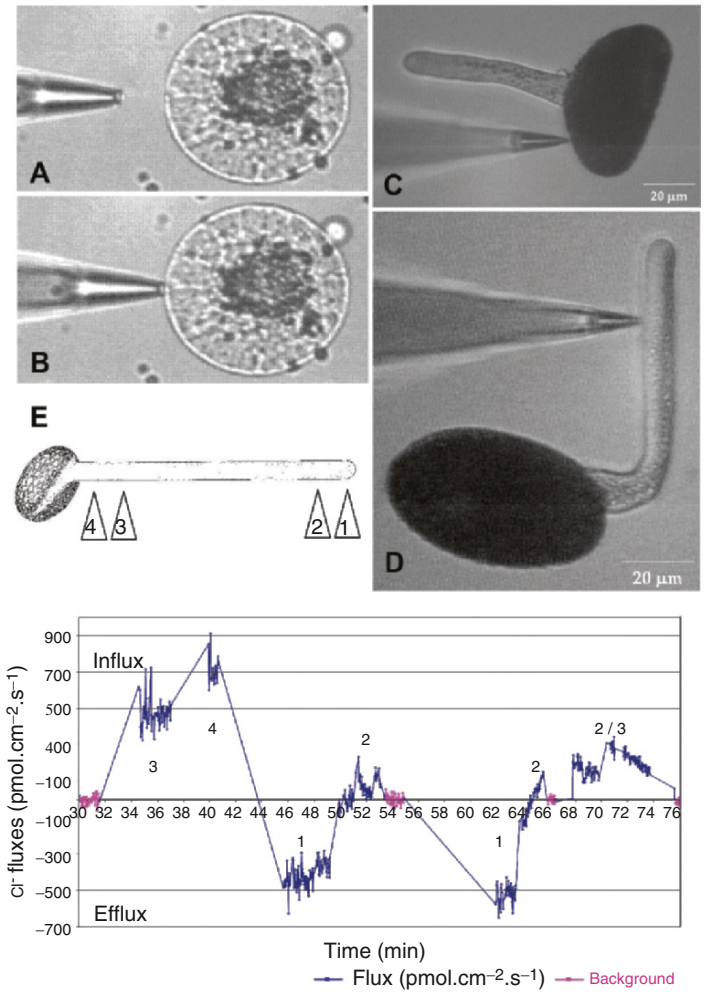

Fig. 5.7. **A, B** Ion-selective vibrating microelectrode recording of fluxes at the surface of an egg cell of maize before fusion (male gamete at the top right side). The microelectrode moves ("vibrates") between two positions, one away from the cell (**A**) and one close to the cell (**B**) repetitively and the delta V values are recorded. All microelectrode measurements are referred to an AgAGCl type reference electrode in the bath located far away (tens of millimetres) from the specimen. **C, D** Vibrating ion-selective microelectrode recording fluxes at the germinated pollen grain (**C**) and at the sub-apical flank of a growing pollen tube (**D**) of *Lilium longiflorum*. The ion-selective microelectrode positioning and repetitive movement is accomplished by a computer-controlled three-dimensional micro-stepping motor translation assembly providing sub-micrometer spatial resolution. **E** Chloride flux profile along a growing pollen tube of *Lilium longiflorum* between 200 and 400 µm long. The *arrows* in the scheme indicate the location of the measurements at the cell surface and correspond to the plot below. Positions *1* and *2* correspond to the apical domain and clear zone and *3* and *4* to the tube flank closer to the pollen grain

Fig. 5.8. **A** Extracellular proton flux profile on a growing pollen tube. The efflux region roughly corresponds to the domain occupied by the clear zone. A close correlation is observable between the cytosolic alkaline band (data not shown) and the patterns of proton efflux, suggesting that the elevation of pHc in the clear zone may correspond (at least partly) to an active proton efflux in the same area. (Adapted from Feijó et al. 1999, with permission from The Rockefeller University press.)

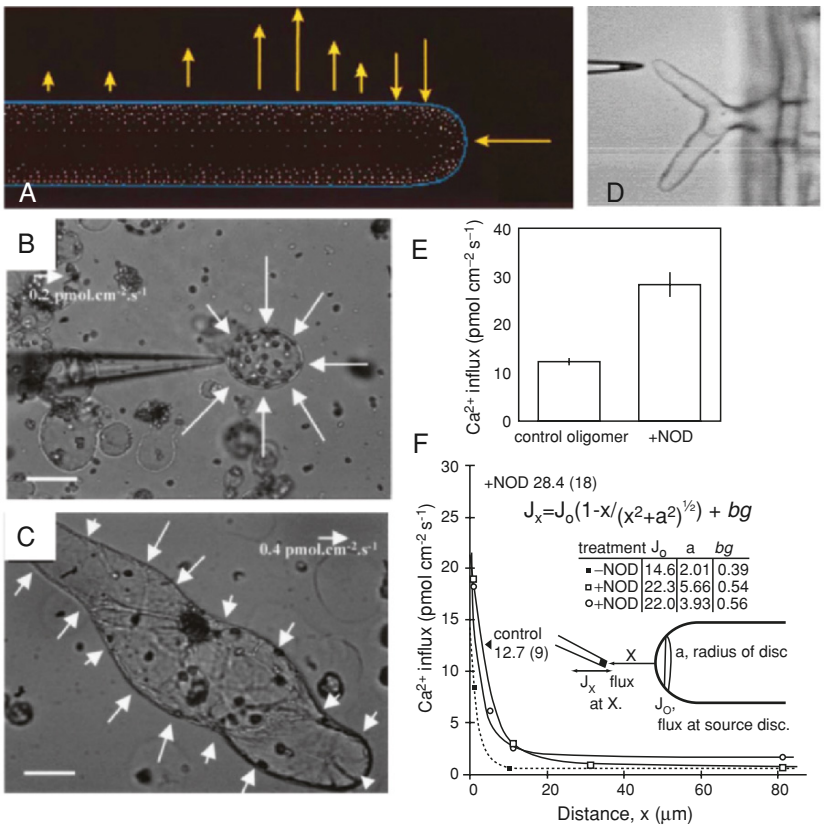

Fig. 5.8. (*Continued*) **B, C** Measurement of H^+-fluxes around elongating tobacco cells. **B** Young cell at the start of elongation, together with its pattern of proton fluxes, where the length of the arrows (scaled as indicated on the figure) is representative of the magnitude of the flux. **C** Older, well-elongated cell together with its pattern of proton fluxes. Bar=50 µm. (Adapted from Vissenberg et al. 2001, with permission from the Society for Experimental Biology.) **D** Measurement of ion fluxes in root hairs of *Arabidopsis* (in this case a *tip-1* mutant plant). **E, F** Extracellular Ca^{2+} fluxes in *P. vulgaris* root hairs responding to Nod factors. **E** Bar graph of nearest approach measurements at approximately 1 µm from the root hair apical surface. Control root hair cells exposed to chitin-oligomers (structurally similar to Nod factors but biologically inactive) for 5 min had an average Ca^{2+} influx at 1 µm from the tip of approximately 13 pmol cm^{-2} s^{-1} (n=9). Hairs exposed to Nod factors for 5 min on average had a higher Ca^{2+} influx of approximately 28 pmol cm^{-2} s^{-1} 1 µm from the tip (n=18). Error bars are SEM. **F** Estimation of the Ca^{2+} sink area at the tip of *P. vulgaris* root hairs responding to Nod factors. The graph shows step away measurements of Ca^{2+} influx in the X direction, J_x (in pmol cm^{-2} s^{-1}) at distances x, from the root hair tip in a control hair exposed to the inactive chitin-oligomer (*filled squares*) and two hairs treated with Nod factors (*hollow squares* and *circles*). *Lines* are theoretical plots obtained with the values shown in tabular form of parameters corresponding to (a), the radius (m) of the Ca^{2+} sink at the tip and *Jo*, the flux of Ca^{2+} at the tip surface (i.e. when x=0). The best fit was obtained by iteration; minimizing a chi-square statistic while changing the influx, Jo (pmol cm^2 s^1), and radius (a) parameters individually. In the control root hair (measured in the presence of the chitin-oligomer), the best fit was obtained with a radius of 2.01 m (*dotted line*), while in the two examples responding to the Nod factors, the best fit corresponded to a sink radius of 3.93 and 5.66 m, respectively. We made measurements at five step-away positions for each root hair. *Filled arrowheads* indicate average influx values 1 µm from the tip of root hairs treated with either inactive chitin-oligomers or Nod fractors, as shown in (a), number of cells measured shown in parentheses. (Adapted from Cárdenas et al. 1999, with permission from Blackwell Science Ltd.)

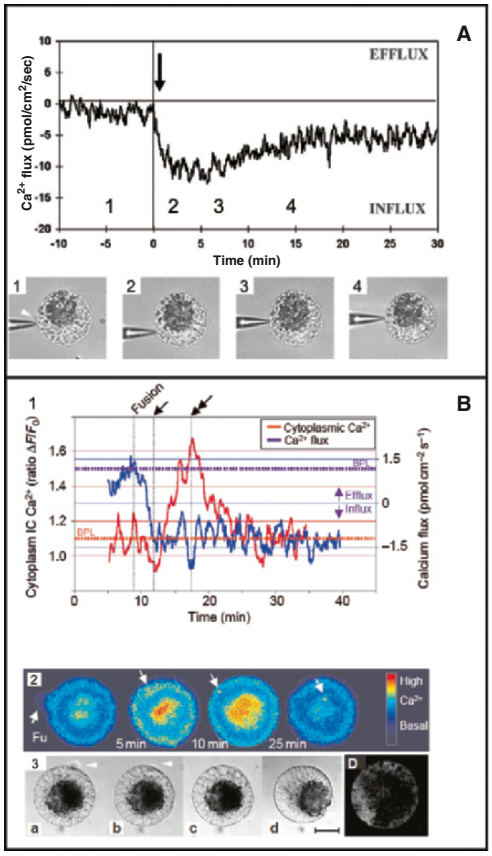

Fig. 5.9. **A** Ca^{2+} flux measurements during maize IVF. A typical recording is shown (n=61) illustrating the onset of a Ca^{2+} influx after fusion. Time 0 is chosen arbitrarily as the time of gametic fusion, as asserted by direct microscopic observation. The *arrow* shows the detectable onset of a Ca^{2+} influx after fusion. A clear Ca^{2+} influx was always detected in the egg membrane, with a delay to fusion dependence on the relative position of the probe and fusion site (*black arrow* in the plot). *1*, *2*, *3* and *4* refer to the time when the pictures (bottom) were taken. The following events are depicted: (1) egg cell before fusion (male gamete position is shown by a *white arrow*); (2) egg cell after fusion, just when contraction has started; (3) strong egg cell contraction; and (4) egg cell reshaping (adapted from Antoine et al. 2000, with permission from the National Academy of Sciences). **B** Simultaneous measurement of Ca^{2+} flux and $[Ca^{2+}]_{Cyt}$ during maize IVF. (1) typical experiment (n=7). Time zero is set at the time when gametes have adhered (*vertical line*). Fusion is followed by the onset of a Ca^{2+} influx (*blue line*; average Ca^{2+} influx of −1.19±0.01 pmol cm^{-2} s^{-1}) and by a transient increase in $[Ca^{2+}]_{Cyt}$ (*red line*). In this particular experiment, the onset of the rise in $[Ca^{2+}]_{Cyt}$ occurs when the influx stabilizes close to the maximum (*arrow*), and the peak $[Ca^{2+}]_{Cyt}$ is coincident with the peak of influx (*double arrow*). Nevertheless, this is not the rule for all the experiments; usually these two features behave without any visible correlation. *BPL* basal pre-fertilization level. (2) Sequence of typical raw images from which the line in 1 was computed. The first image shows sperm–egg cell adhesion (*arrowhead*). The sperm becomes visible after fusion because of Fluo-3 diffusion into it (*arrowheads*). Traces in (1) were computed by averaging the total egg—cell or zygote fluorescence as shown in **B** (ΔF/F0=(Ft-F0)/F0). (3) Different cytological events during maize IVF in standard conditions (n>100)

and general role for electrical currents in initiating and maintaining tip growth.

Their observations might have been tainted by the fact that the microelectrode vibration can affect the gradients that it is recording. The vibration frequency of the vibrating voltage microelectrode (200 cycles per second or more) was one of the major problems affecting this study. To obviate the movement that the cells would undergo due to stirring created by microelectrode vibration, these initial recordings were done using a cellophane membrane to immobilize the cells, which would otherwise be freely floating in the liquid germination media and impossible to track. This membrane does not create an electrical barrier and the recording is therefore not affected by it. However, the added distance due to the thickness of the cellophane does not match the geometry of the actual cell, creating a deformation in the electrical field as measured over the membrane.

Despite the possible artifacts, the observation that the steady currents formed a dipole in growing pollen tubes and that this was common to other cell types sharing a tip growth mechanism, was a conceptually important step. The determination of a current source and sink lead to the idea that in the developmental process of pollen tubes, membranes tends to form domains, one of which is an ion-leaky state in the sink region and the other is an ion-pumping domain in the source region. Also, it was speculated that an electrical current would therefore traverse pollen tubes, creating a loop. In turn, this could generate a movement of isolated cellular constituents that could be pulled forward by the current, since it was assumed that most are small and free enough to move through the cytoskeleton. This concept of membrane domain formation, together with the hypothesis of electrophoretic movement, was proposed as a way in which electrical currents could have important physiological consequences. The molecules in the cytosol are, however, buffered by such substantial Brownian motion energy that the actual induction of their translational movement in free solution by the ion current potentials is unlikely. A more likely hypothesis is that ion potentials could provide the orientation that provides the direction for actin or tubulin based cytoplasmic motility engines used for navigation. Another conceptually important aspect of this pioneering study was the presence of electrical currents predicting the tube germination site. This implied that electrical currents could be the basis of a morphogenetic process such as the onset of tip growth. At those early times, the currents were weak and likely

---

Fig. 5.9. (*Continued*) Gametes were isolated from the inbred line A188. *a* Gamete adhesion (*arrowhead* shows the sperm). *b* Fusion; the sperm can be seen penetrating the egg cell (*arrowhead*). *c* Mild contraction of the egg cell. *d* Reshaping of the cell; the organellar mass has taken a peripheral position, polarizing the zygote. **D** Two-photon microscopy section of the vacuolar zone in a typically Fluo3-AM loaded egg, showing that the vacuole and large organelles are not significantly sequestering the probe. Scale bar in bd, 20 m.) (Adapted from Antoine et al. 2001, with permission from Nature Publishing Group.)

mark the spot where an important process is to happen but are less likely to be the motive force (the quest for causal roles of currents, or ions as they move, remains at the centre of ion flux studies!).

The vibrating voltage probe did not, however, provide any information about the ionic nature of the currents. If at all, this could be inferred by changes in the composition of the medium used which can by themselves affect the physiology of the cells. Weisenseel et al. (1975), based on the dependence of current on the ionic composition of the medium, suggested that most of the inward current consisted of potassium (K^+) ions entering the whole pollen tube uniformly. At the growing tip, they speculated that calcium (Ca^{2+}) could be part of the current loop. To further examine the ionic nature of the currents, Weisenseel and Jaffe (1976) performed more media ion-substitution experiments. They implicated protons (H^+) as an important part of the outward current at the grain and K^+ as the major component of the inward current at the tube. But the development of the vibrating Ca^{2+} specific ion-selective probe (Kühtreiber and Jaffe 1990) uncovered an apparent contradiction with these conclusions since a Ca^{2+} influx was measured at the tip which could, by itself, account for most of the inward current. The accuracy of the results obtained with the ion-selective vibrating probe precluded previous vibrating voltage probe data from being quantitatively correct. The authors analyzed fucoid eggs, pollen, *Dyctiostelium discoideum*, amoebae, *Sarcophaga* follicles and fertilized ascidian eggs. In all of these systems, they detected Ca^{2+} currents with possible roles in development.

An important constraint of the vibrating ion-selective probe technique is that the Ca^{2+} specific LIX microelectrode performs better under low media calcium while not all biological material (e.g. marine) will behave normally under these conditions. Pierson et al. (1994) later confirmed Ca^{2+} influx at the growing tip of pollen tubes and related the extracellular Ca^{2+} influx to a tip-focused intracellular Ca^{2+} gradient through the activity of putative membrane channels.

Due to the importance attributed to Ca^{2+} in signaling, the first few years after the development of vibrating ion-selective microelectrodes were devoted to Ca^{2+} flux studies.

An important feature of the growth of pollen tubes of most species studied lies in the fact that tip growth is at some point oscillatory. Following Weisenseel et al.'s (1975) observation that total currents at the tip of growing pollen tubes were pulsatile after a certain tube length, Holdaway-Clarke et al. (1997) showed that Ca^{2+} was a part of this pulsatile component. Ca^{2+} influx oscillates and this correlates with the growth oscillations. Yet Ca^{2+} influx is delayed by 13 s relative to the growth pulse and seems to be secondary to growth oscillation. The reasoning that allows this inference is based on the strength of the cross-correlation when the phase of the oscillating components is shifted relative to one another (Holdaway-Clarke et al. 1997). Reasons for this delay have been proposed to reside on buffering capacity of the cell wall (Holdaway-Clarke et al. 1997) or a mechanism involving turgor

pressure (Messerli et al. 2000). Messerli and Robinson (2003) further tried to test these two models, by changing the growth medium's ionic composition and recording changes as a function of ion fluxes. They concluded that none is sufficiently robust to account for the experimental data.

When measuring ion fluxes and assessing the space and time correlation to growth, it is important to correlate these with the cytosol concentrations of the ion being studied. We have studied the contribution of protons to the tip growth process (Feijó et al. 1999), and demonstrated a tight correlation between the intracellular distribution pattern and the fluxes across the membrane. The pattern involves an influx of protons at the growing tip corresponding to an acidic domain in the cytosol and an efflux in the region that corresponds to the clear zone and to an intracellular constitutive alkaline zone (Fig. 5.8A). Whether the two are mechanistically related remains a matter of debate.

Messerli et al. (1999) reported oscillations in H^+, K^+ and Ca^{2+} fluxes at the growing tip, all lagging the growth pulses but failed to detect the efflux region of protons on the clear zone. However, the use of substantial amounts of buffer concentration in the medium by these authors (5 mM MES buffer, compared to 0.05 mM MES) is known to affect the measurement of H^+ gradients in a sufficient manner to mask these effluxes beyond detection (Kunkel et al. 2001). H^+ effluxes on the sub-apical area of pollen tubes had been previously measured in pollen tubes (Feijó et al. 1999), and correlated with the distribution of proton-pumping ATPases (Certal et al., unpublished data).

This later example argues that careful medium design for recording with particular microelectrodes is needed whenever applying ion-selective microelectrode measurement systems. Media should be ionically as simple as possible, especially with regard to the ion being measured, in order to increase the signal-to-noise ratio to record small signals. This technique records a specific concentration at each point of the measurement algorithm in the extracellular medium. A change in concentration implies a flux. When dealing with H^+, it is essential to think about the buffer used and its concentration and to test how this affects the measurement. Ideally, buffer concentrations should be kept as low as possible, so as not to interfere, since buffers will absorb protons and therefore, deflate the extension of concentration gradients (Kunkel et al. 2001).

Messerli et al. (1999) acknowledge that buffering has an effect on the measurement and they correct the flux values obtained according to previously determined correction factors (Arif et al. 1995; Demarest and Morgan 1995), however, do not account for the possibility that this not only affects the magnitude of H^+ fluxes but it might also alter the extracellular gradients such that some fluxes are no longer measurable. Kunkel et al. (2001) showed that several complications result from using pH buffers in the medium where proton-specific LIX microelectrodes are used. Facilitated diffusion enhances the measured H^+ flux due to proton equilibration with the buffer. The buffer absorbs local H^+, allowing them to escape the source more rapidly than by

simple diffusion, enhancing proton fluxes. The major conclusion from this study is to keep the culture media as simple as possible and reduce any buffer components to as low titer as possible.

Zonia et al. (2001, 2002) subsequently showed, for the first time, that chloride (Cl^-)efflux cycles at the growing tip, coupled- to and in-phase with cycles of growth, indicating that Cl^- dynamics is an important component in the network of events that regulate pollen tube homeostasis and growth. The rest of the tube exhibits Cl^- influx (Fig. 5.7E). Pharmacological studies revealed a correlation between Cl^- efflux at the growing tip and growth, and that Cl^- appeared intimately associated with the control of water flow. Care was taken to avoid affects by the chemicals used in this study on the Cl^--selective microelectrodes. Among the Cl^- channel inhibitors that have an effect on pollen tube growth, only DIDS was used since it was found not to interfere with sensitivity or selectivity of Cl^--selective micro-electrodes. Moreover, the authors, upon realization of this unexpected result, performed the necessary controls to ensure the validity of the Cl^- flux calculations. Tests were conducted in which the dynamic responses of Cl^--selective microelectrodes measuring an artificial Cl^- flux source were calculated to be 3 orders of magnitude higher than the other anions tested. Knowing that other anions can interfere with the measurement of Cl^- anions, they calculated Cl^- concentration in an alternative manner using a colorimetric assay. The results were consistent with those obtained with the Cl^--selective microelectrodes.

Messerli et al. (2004) argue that the fluxes measured were in fact changes in the concentration of the anionic form of the pH buffer (MES) and not changes in Cl^- concentration. In this study, the authors characterized the ionophore cocktails previously used by Zonia et al. (2002) and claim that the selectivity and possibly interference from other anions and chemicals used for chloride channel blocking would preclude the results previously obtained. However, using the buffer concentration that Zonia et al. (2002) use, Messerli et al. (2004) shows only a 3.38% reduction in potential responses to chloride concentration for a background concentration of chloride between 0.1 and 1.0 mM and 9.98% for a background concentration between 1 and 10.0 mM. Furthermore, on discussing their quantitative conclusions, these authors frequently confuse the results obtained by Zonia et al. (2002) from tobacco with the results from Lily.

This later controversy shows that when dealing with indirect evidence (such as extra-cellular concentration recordings to infer membrane fluxes), care needs be taken to ensure the validity and accuracy of the measurements. In this case, technical controls by Messerli et al. (2004) actually confirm the applicability of the technique under the conditions used by Zonia et al. (2002). Nevertheless, the controls performed show that each ionophore cocktail (LIX) used to produce an ion-selective microelectrode can not be applied universally and this example provides a model for the sorts of cautions that must be observed when testing a new ionophore cocktail or when a medium composition change or pharmacology is designed.

While it is generally agreed that healthy pollen tube growth is linked to coordinated entry of Ca^{2+} and other ions at the growing tip, the coordination of entry or exit in other regions is less documented. Best understood is perhaps the H^+ secretion in the region of the alkaline band, which may be associated with the mitochondrial rich zone and functionally related to secretion of H^+ accumulated in the cytosol from active mitochondrial respiration (Feijó et al. 1999). In addition, inactivation of pollen growth by incompatibility reactions has been linked to Ca^{2+} entry along the pollen tube shaft (Franklin-Tong et al. 2002).

5.9 Root hairs

Root hairs are highly specialized tip growing cells (Fig. 5.8D). Ca^{2+} dynamics was studied using the Ca^{2+}-selective vibrating probe by Schiefelbein et al. (1992), who detected a Ca^{2+} influx at the tip of growing root hair cells, but no fluxes at the sides or at the tip of non-growing root hair cells. Nifedipine, a Ca^{2+} channel blocker, confirmed the link between growth and the Ca^{2+} flux since its application inhibits both. Later, Felle and Hepler (1997) confirmed this Ca^{2+} influx by imaging cytosolic Ca^{2+} concentration. H^+ secretion by root tips has also been demonstrated by imaging external pH indicators (Jaillard et al. 1996) and this technology promises to allow flux calculations and applicability for studies of more localized cellular phenomenon (Tang et al. 2004).

Nod factors, which are lipochitin-oligosaccharides produced by bacteria in response to flavonoids present around roots, induce many processes associated with root nodule morphogenesis on host plants. Root hairs respond rapidly to these molecules and among the most rapid responses described are those involving changes in membrane potential and ions such as Ca^{2+}, Cl^- and H^+ (reviewed by Cardenas et al. 2000). Allen et al. (1994) first detected changes in the extracellular Ca^{2+} flux outside the root hairs after exposure to Nod factors using a Ca^{2+}-selective vibrating probe. Cardenas et al. (1999) further determined that these changes occur within the first 5–10 min of Nod factor application (Fig. 5.8E,F). A sharp increase in the Ca^{2+} influx level (from 12.7±0.7 to 28.4±2.8 $pmol.cm^{-2}.s^{-1}$) at the tip of root hair cells occurs concomitantly with an increase of the membrane area over which the influx occurs and with an increase in the concentration of the intracellular free ion. Technically, this study clearly showed the importance of using a protocol that estimates both the intensity and the area of current production, since the NOD induced increase of total Ca^{2+} flux at the root hair tip (Fig. 5.8F) is composed of both an increase in intensity as well as the area over which the flux occurs. This objective can be accomplished by either a scan of the source area close to the cell or doing a step-away measurement of the declining signal with distance (Fig. 5.8F).

As for H^+, although fluxes have been implicated in root hair growth and Nod factor response, only stationary ion-selective microelectrodes have been

used and the results were apparently contradictory. The pH around the root hair remains acidic, but becomes less so in response to Nod factors. Since intracellular pH increases, this alkalinization could be expected to correspond to an acidification of the extra-cellular medium so it is not clear why the intra- and extracellular changes occur in the same direction. Felle et al. (1998) justifies this by considering different buffering capabilities of the intra and extra-cellular compartments. Cardenas et al. (2000) also argue that, based on data from stationary ion-selective microelectrodes and scanning H^+-selective microelectrodes along the whole root, the complexity of H^+ regulation is likely to be the result of a system more elaborate than just two compartments with different buffering properties.

5.10 Fertilization in higher plants

More recently, the SIET contributed to a major breakthrough in plant development, when a study by Antoine et al. (2000) made a direct measurement of an influx of extracellular Ca^{2+} induced by gamete fusion in maize (Fig. 5.9). The extracellular fluxes measured at the surface of isolated egg cells, with or without adhesion of a male sperm cell were close to zero and stable over time. However, after gamete fusion, a Ca^{2+} influx was triggered close to the site of sperm entry with a delay of 1.8 ± 0.6 s (Fig. 5.9A). This influx spread throughout the whole cell, progressing at a rate of 1.13 $\mu m.s^{-1}$. After this wave front propagation, the Ca^{2+} influx intensity remained sustained, monotonic and homogeneous over the whole egg cell (average influx of 14.92 $pmol.cm^{-2}.s^{-1}$ lasting an average of 24.4 min). This characteristic influx, and the necessary channel opening, was shown to be the first embryonic event following and triggered by gamete membrane fusion. The cytological modifications observed after fertilization correlate well with the spread of the Ca^{2+} influx and the latter changes in cytosolic Ca^{2+} concentration may work as a trigger and possibly a space and time coordinator of many aspects of egg activation. It was shown that the Ca^{2+} influx has a determinant contribution, since application of a Ca^{2+} ionophore mimics some aspects of egg activation. Furthermore, the nature of the channels involved was assessed with the use of gadolinium (Gd^{3+}), which inhibited the influx, possibly implicating mechano-sensitive channels. In all species studied, gamete fusion triggers an increase in cytosolic Ca^{2+} concentration. This is accepted as part of the initial steps to egg activation, but the source and regulation of this Ca^{2+} signal and the way it is transduced inside the zygote are controversial. It was already known that after gamete fusion there was a rise in cytosolic Ca^{2+} (Digonnet et al. 1997), sufficient for egg activation, but the relationship between this and the wave front spread of Ca^{2+} influx from the fusion site was unknown. Antoine et al. (2001) addressed this question by simultaneously recording Ca^{2+} fluxes and cytosolic Ca^{2+} concentration, using a setup that combines the SIET and

ion-ratiometric widefield imaging. Under these conditions, it was possible to discriminate between the contribution of the cytoplasmic Ca^{2+} and Ca^{2+} influx. This unique technical combination allowed for the conclusion that the Ca^{2+} influx precedes the cytoplasmic Ca^{2+} elevation by 40–120 s, thus implicating the existence of separate mechanisms for both of these Ca^{2+} signals (Fig. 5.9B). Further pharmacology and buffer suppression of the cytoplasmic Ca^{2+} showed that its elevation is essential for egg activation, as measured by the initiation of cell wall deposition. However, the extracellular influx does not seem to be a necessary condition for egg activation. The inhibition of this influx does, however, prevent the sperm incorporation and consequent karyogamy, showing that both mechanisms should be combined to achieve eventual fertilization. Furthermore, it was shown that a Gd^{3+}-independent calcium influx is always present in the sperm plasma membrane after fusion, which might implicate a second type of calcium channel involved in the early activation steps of zygote formation.

5.11 Conclusions

It is clear that the scanning ion selective technique, SIET, is a powerful tool for cell biological research that has been effectively applied to various plant systems. Application of this technique requires a logical and methodical development of confidence in the tool by using model steady state sources on which to test out and calibrate the probes, after which the application to living systems can provide a rich data structure that can lead to breakthroughs in the understanding of cell growth and development if and when they have an ionic basis.

Acknowledgements. J.A.F.'s laboratory is supported by FCT grants POCTI/BCI/41725/2001, POCTI/BCI/46453/2002, POCTI/BIA-BCM/60046/2004 and POCTI/BIA-BCM/61270/2004. J.G.K.'s laboratory is partially supported by Applicable Electronics Inc.

References

Allen NS, Bennett MN, Cox DN, Shipley A, Ehrhardt DW, Long SR (1994) Effects of Nod factors on alfalfa root hair Ca^{++} and H^{+} currents and on cytoskeletal behavior. *In:* Daniels MJ, Downie JA, Osbourn AE (eds) Advances in molecular genetics of plant–microbe interactions, vol 3. Kluwer Academic, Netherlands

Antoine AF, Faure JE, Cordeiro S, Dumas C, Rougier M, Feijo JA (2000) A calcium influx is triggered and propagates in the zygote as a wavefront during in vitro fertilization of flowering plants. Proc Natl Acad Sci USA 97:10643–10648

Antoine AF, Faure JE, Dumas C, Feijo JA (2001) Differential contribution of cytoplasmic Ca^{2+} and Ca^{2+} influx to gamete fusion and egg activation in maize. Nature Cell Biol 3:1120–1123

Arif I, Newman IA, Keenlyside N (1995) Proton flux measurements from tissues in buffered solution. Plant Cell Environ 18:1319–1324

Blatt M (ed) (2004) Membrane transport in plants. Ann Plant Rev, vol 15. Blackwell, London
Cardenas L, Feijo JA, Kunkel JG, Sanchez F, Holdaway-Clarke T, Hepler PK, Quinto C (1999) Rhizobium nod factors induce increases in intracellular free calcium and extracellular calcium influxes in bean root hairs. Plant J 19:347–352
Cardenas L, Holdaway-Clarke TL, Sanchez F, Quinto C, Feijo JA, Kunkel JG, Hepler PK (2000) Ion changes in legume root hairs responding to Nod factors. Plant Physiol 123:443–452
Demarest JR, Morgan JLM (1995) Effect of pH buffers on proton secretion from gastric oxyntic cells measured with vibrating ion-selective microelectrodes. Biol Bull 189:219–220
Digonnet C, Aldon D, Ledue N, Dumas C, Rougier M (1997) First evidence of a calcium transient in flowering plants at fertilization. Development 124:2867–2874
Faszewski EE, Kunkel JG (2001) Covariance of ion flux measurements allows new interpretation of *Xenopus laevis* oocyte physiology. J Exp Zool 290:652–661
Feijó JA, Malhó RM, Obermeyer G (1995) Ion dynamics and its possible role during in vitro pollen germination and tube growth. *Protoplasma* 187:155–167
Feijó JA, Sainhas J, Hackett GR, Kunkel JG, Hepler PK (1999) Growing pollen tubes possess a constitutive alkaline band in the clear zone and a growth-dependent acidic tip. J Cell Biol 144:483–496
Feijó JA, Sainhas J, Holdaway-Clarke T, Cordeiro MS, Kunkel JG, Hepler PK (2001) Cellular oscillations and the regulation of growth: the pollen tube paradigm. Bioessays 23:86–94
Feijó JA, Costa SS, Prado AM, Becker JD, Certal AC (2004) Signalling by tips. Curr Opin Plant Biol 7:589–598
Felle HH, Hepler PK (1997) The cytosolic Ca^{2+} concentration gradient of *Sinapis alba* root hairs as revealed by Ca^{2+}-selective microelectrode tests and fura-dextran ratio imaging. Plant Physiol 114:39–45
Felle HH, Kondorosi E, Kondorosi Á, Schultze M (1998) The role of ion fluxes in Nod factor signalling in *Medicago sativa*. Plant Journal 13:455–463
Franklin-Tong VE, Holdaway-Clarke TL, Straatman KR, Kunkel JG, Hepler PK (2002) Involvement of extracellular calcium influx in the self-incompatibility response of *Papaver rhoeas*. Plant J 29:333–345
Harold FM, Caldwell JH (1990) Tips and currents: electrobiology of apical growth. In: Heath IB (ed) Tip growth in plant and fungal cells. Academic Press, New York
Holdaway-Clarke TL, Hepler PK (2003) Control of pollen tube growth: role of ion gradients and fluxes. New Phytologist 159:539–563
Holdaway-Clarke TL, Feijo JA, Hackett GR, Kunkel JG, Hepler PK (1997) Pollen tube growth and the intracellular cytosolic calcium gradient oscillate in phase while extracellular calcium influx is delayed. Plant Cell 9:1999–2010
Holdaway-Clarke TL, Weddle NM, Kim S, Robi A, Parris C, Kunkel JG, Hepler PK (2003) Effect of extracellular calcium, pH and borate on growth oscillations in *Lilium formosanum* pollen tubes. J Exp Bot 54:65–72
Jaffe LF (1966) Electrical currents through the developing fucus egg. PNAS 56:1102–1109
Jaffe LF (1968) Localization in the developing Fucus egg and the general role of localizing currents. Adv Morphog 7:295–328
Jaffe LF, Levy S (1987) Calcium gradients measured with a vibrating calcium-selective electrode. Proc IEEE/EMBS Conf 9:779–781
Jaillard B, Ruiz L, Arvieu JC (1996) pH mapping in transparent gel using color indicator videodensitometry. Plant Soil 183:1–11
Kühtreiber WM, Jaffe LF (1990) Detection of extra-cellular calcium gradients with a calcium-specific vibrating electrode. J Cell Biol 110:1565–1573
Kunkel JG, Lin L-Y, Xu Y, Prado AMM, Feijó JA, Hwang PP, Hepler PK (2001) The strategic use of Good buffers to measure proton gradients about growing pollen tubes. In: Geitman A (ed) Cell biology of plant and fungal tip growth. IOS Press, Amsterdam, 14 pp
Messerli MA, Robinson KR (2003) Ionic and osmotic disruptions of the lily pollen tube oscillator: testing proposed models. Planta 217:147–157

Messerli MA, Danuser G, Robinson KR (1999) Pulsatile influxes of H^+, K^+ and Ca^{2+} lag growth pulses of *Lilium longiflorum* pollen tubes. J Cell Sci 112:1497–1509

Messerli MA, Creton R, Jaffe LF, Robinson KR (2000) Periodic increases in elongation rate precede increases in cytosolic Ca^{2+} during pollen tube growth. Dev Biol 222:84–98

Messerli MA, Smith PJ, Lewis RC, Robinson KR (2004) Chloride fluxes in lily pollen tubes: a critical reevaluation. Plant J 40:799–812

Pierson ES, Miller DD, Callaham DA, Shipley AM, Rivers BA, Cresti M, Hepler PK (1994) Pollen tube growth is coupled to the extracellular calcium ion flux and the intracellular calcium gradient: effect of BAPTA-type buffers and hypertonic media. Plant Cell 6:1815–1828.

Pina C, Pinto F, Feijó JA, Becker JD (2005) Gene family analysis of the *Arabidopsis* pollen transcriptome reveals novel biological implications for cell growth and division control and gene expression regulation. Plant Physiol 138:744–756

Prado AM, Porterfield DM, Feijo JA (2004) Nitric oxide is involved in growth regulation and re-orientation of pollen tubes. Development 131:2707–2714

Roy SJ, Holdaway-Clarke TL, Hackett GR, Kunkel JG, Lord EM, Hepler PK (1999) Uncoupling secretion and tip growth in lily pollen tubes: evidence for the role of calcium in exocytosis. Plant J 19:379–386

Sanders D, Bethke P (2000) Membrane transport. In: Buchanan B, Gruissem W, Jones R (eds) Biochemistry and molecular biology of plants. ASPB, Rockville, Maryland, p 128

Schiefelbein JW, Shipley AM, Rowse P (1992) Calcium influx at the tip of growing root-hair cells of *Arabidopsis thaliana*. Planta 187:455–459

Schneiderman G, Goldstick TK (1978) Oxygen electrode design criteria and performance characteristics: recessed cathode. J Appl Physiol 45:145–154

Shipley AM, Feijó JA (1999) The use of the vibrating probe technique to study steady extracellular currents during pollen germination and tube growth. In: Cresti M, Cai G, Moscatelli S (eds) Fertilization in higher plants: molecular and cytological aspects. Springer, Berlin Heidelberg New York, pp 235–252

Somieski P, Nagel W (2001) Measurement of pH gradients using an ion-sensitive vibrating probe technique (IP). Pflugers Arch 442:142–149

Taiz L, Zeiger E (2002) Plant physiology. Sinauer, Sunderland, Mass., USA, pp 87–108

Tang C, Drevon JJ, Jaillard B, Souche G, Hinsinger P (2004) Proton release of two genotypes of bean (*Phaseolus vulgaris* L.) as affected by N nutrition and P deficiency. Plant Soil 260:59–68

Vissenberg K, Feijo JA, Weisenseel MH, Verbelen JP (2001) Ion fluxes, auxin and the induction of elongation growth in *Nicotiana tabacum* cells. J Exp Bot 52:2161–2167

Weisenseel MH, Jaffe LF (1976) The major growth current through lily pollen tubes enters as K^+ and leaves as H^+. Planta 133:1–7

Weisenseel MH, Nucitelli R, Jaffe LF (1975) Large electrical currents traverse growing pollen tubes. J Cell Biol 66:556–567

Zonia L, Cordeiro S, Feijó JA (2001) Ion dynamics and the control of hydrodynamics in the regulation of pollen tube growth. Sexual Plant Reprod 14(1–2):111–116

Zonia L, Cordeiro S, Tupy J, Feijo JA (2002) Oscillatory chloride efflux at the pollen tube apex has a role in growth and cell volume regulation and is targeted by inositol 3,4,5,6-tetrakisphosphate. Plant Cell 14:2233–2249

6 Use of Double Barrel Micropipettes to Voltage-Clamp Plant and Fungal Cells

ROGER R. LEW

6.1 Intracellular measurements in intact, turgid cell compared with protoplasts

In a paper published in 1977, Racusen et al. documented a startling property of higher plant cells: The membrane potential of a higher plant cell responds to the extracellular osmolarity, depolarizing under hyper-osmotic treatment, up to and including the point of plasmolysis. The effect was reversed by removing the extracellular osmoticum. Isolated protoplasts exhibited very depolarized potentials compared with intact turgid cells. Osmotic effects on the electrical properties extend beyond changes in the membrane potential. The conductance, a measure of the voltage dependence of ionic current flow across the plasma membrane, also changes in response to either hyper- or hypo-osmotic treatment (Lew 1996). Indeed, at least in *Arabidopsis thaliana* the electrical changes coincide with changes in the net ionic fluxes that contribute to turgor recovery after hyperosmotic treatment (Shabala and Lew 2002). These electrical changes are an important part of the cell's response to osmotic stresses, but their significance is even greater, because of the implications for the use of patch clamp to measure ionic properties of plant and fungal cells.

6.1.1 Protoplasts are required for patch clamp

Patch clamp (Hamill et al. 1981) revolutionized the study of ion transport in cells, including animal, fungal, algal and higher plant cells. The two major discoverers, Erwin Neher and Bert Sakmann, were awarded the Nobel Prize in 1991. The power of the patch clamp technique was 2-fold. First, it allowed individual ion channels to be measured in situ, in their natural states in the membrane. Second, with the whole cell mode, it enabled the experimenter to extend the range of possible measurements: to examine the voltage and time dependence of ionic currents and use this information to identify the specific ions contributing to the current. With patch clamp, a wealth of information has been uncovered about the molecular foundations of ionic transport in

York University, Department of Biology, Toronto, Ontario M3J 1P3, Canada

Plant Electrophysiology – Theory & Methods (ed. by Volkov)

cells. However, when the patch clamp technique is applied to walled cells, the wall must first be removed to expose the plasma membrane to the patch pipette. To avoid lysis, the cell must be held in a solution of osmolarity high enough to induce plasmolysis. This is necessary whether the wall is removed by enzymatic digestion or some other technique, such as laser ablation. This means that the advantage of patch clamp, to examine the voltage and time dependence of ion transport across the plasma membrane, is offset by the non-physiological condition of the cell, plasmolyzed and probably attempting turgor recovery. Certainly not growing, certainly in an abnormal physiological state, the plasmolyzed state of the cell is a technical problem that obscures the relevance of patch clamp measurements. The ideal way to overcome this is to perform measurements of the voltage and time dependence of ionic currents in intact, turgid, possibly even growing cells. But how can this be done in an intact cell?

6.2 Voltage clamping intact turgid cells

Voltage clamp is the technique of choice to measure the voltage and time dependence of ionic currents across the plasma membrane. In essence, the electronics are designed to inject a current sufficient to maintain the voltage of the plasma membrane at a specified level. Data for a number of different clamped voltages are compiled to create a current versus voltage relation, or current is monitored at a single voltage over time to measure time dependence, or both may be combined. It is useful to measure the cell membrane potential concurrent with current injection into the cell to confirm the fidelity of voltage clamping. There are three ways to voltage clamp intact turgid cells: discontinuous voltage clamp, dual impalements, and double barrel micropipettes. In all instances, the intent is to measure the voltage and time dependence of the plasma membrane ionic currents separate from any contribution of the micropipette itself. The micropipette resistance is a significant problem, because the resistance at the tip of the micropipette is often similar in magnitude to the resistance of the plasma membrane. This can cause an inability to separate the voltage and time dependence of ionic currents through the micropipette tip from the ionic currents through the plasma membrane.

6.2.1 Discontinuous voltage clamp: a single barrel used for both current injection and voltage monitoring

Finkel and Redman (1984) described the discontinuous single microelectrode voltage clamp technique. The technique has been used successfully in intact higher plant cells. The basic idea is that the time dependence of electrical currents at the microelectrode tip is very different from those of the plasma membrane because the capacitance of the micropipette tip is much lower

than the capacitance of the cell membrane. This will cause a much faster time response, τ, defined as resistance (R) $\times$ capacitance (C): $\tau = R \times C$. By rapidly switching between current injection and voltage measurements, it is possible to separate *temporally* the contribution of the micropipette from the contribution of the plasma membrane, as long as $\tau_{electrode} < \tau_{cell}$. A set of papers using the discontinuous single electrode voltage clamp technique illustrates the technique and problems. Forestier et al. (1998) explored the use of the technique to identify slow anion currents in guard cells. The advantage of the technique was that measurements could be done in intact cells. Since guard cells are turgor-active, that is, change their turgor in response to different stimuli to control stomata aperture in the epidermis of the leaf, intact cells offer much greater insight into ion transport required for turgor changes compared to the turgor-less protoplasts necessary for patch clamp. In the discontinuous single electrode voltage clamp technique, it is necessary to compensate electronically for the capacitance of the electrode. Roelfsema et al. (2001) raised doubts about the applicability of the discontinuous single-electrode voltage clamp technique in small cells, such as guard cells, because the low capacitance of small cells would be similar to the capacitance of the electrode ($\tau_{electrode} \sim \tau_{cell}$); thus, a clear separation of the contribution of the electrode and cell would be difficult. Raschke et al. (2003) confirmed the results of Forestier et al. (1998), noting that it is crucial to use micropipettes which possess a linear current-voltage relation to assure that their capacitance can be compensated electronically. That is, the resistance must be voltage independent to assure $R \times C$ is constant for all clamped voltages. Although others have used this technique, the three papers cited above give a flavor of the doubts associated with the method. There are two issues: whether it is electronically possible to compensate for the electrode capacitance (or more accurately, time response, $R \times C$) consistently, and whether the properties of the microelectrode tip are the same before and during insertion into the cell. In fact, Etherton et al. (1977) explored the latter question by directly comparing membrane resistance measurements obtained using two electrodes impaled separately into the same cell with single electrode impalements. They expressed the concern that the properties of the single electrode change upon impalement, rendering the technique questionable. Guard cells do not lend themselves to multiple impalements, so the discontinuous voltage clamp technique remains a useful technique to avoid the protoplasting required to patch clamp the cell, with caveats regarding the quality of the data. Supporting evidence, such as inhibitor effects (Forestier et al. 1998; Bouteau et al. 1999), bolsters interpretation of the data.

6.2.2 Dual impalements

Etherton et al. (1977) assumed that dual impalements with a voltage monitoring electrode and a current-injecting electrode were the "standard by which the accuracy" of single electrode techniques "could be judged". Since

the two processes, voltage monitoring and current injection, are separate, this is a likely assumption. One concern exists, that multiple impalements may affect the resistance of the plasma membrane due to membrane damage caused by the impalements, but Lew (2000) presented evidence discounting this possibility, at least in root hairs, by showing that multiple impalements do not cause a decrease in the potential, expected if the impalement site is the site of significant ionic leakage. Multiple impalements are technically difficult. The cells must be accessible, and good imaging is very helpful, to ensure the micropipettes are impaled into the same cellular compartment. Indeed, the "standard" to identify where the tips are located is fluorescent dye injection (Holdaway-Clarke et al. 1996). Because only a single impalement into the cell is required, double barrel micropipettes offer technical advantages, while retaining separation of the voltage and current-injecting microelectrodes.

6.2.3 Double barrel micropipettes

A number of researchers have used double barrel micropipettes over the years. Michael Blatt and others used them to perform voltage clamping of the filamentous fungus *Neurospora crassa* (Blatt and Slayman 1983, 1987). Blatt subsequently used the technique in guard cells (Blatt 1987), and wrote a primer on double barrel micropipettes and other electrophysiological techniques (Blatt 1991) which I recommend highly for new and experienced electrophysiologists.

6.3 Double barrel micropipette fabrication

The fabrication of double barrel micropipettes involves a sequential set of steps that are best performed by fabricating a batch of micropipettes at the same time. Borosilicate capillaries with internal filaments are first cut to an appropriate length (about 7 cm). We use 1 mm OD, 0.58 mm ID tubing. The two capillaries are inserted into a micropipette puller in which one of the two clamps on either side of the heating filament can be rotated (Fig. 6.1). When the heating filament has softened the glass, the capillaries are rotated by 360° to create a twist in the glass. Then standard pulling protocols are used to pull the micropipette. Once pulled, a small amount of fast-setting epoxy is applied just above the twist to strengthen the fused joint between the two capillaries. Finally, one of the barrels is heated and pulled away to form a Y-shape. This eases insertion of one of the barrels of the micropipette into a holder, and insertion of a chlorided silver wire into the other barrel. Photographs of some of the fabrication steps are shown in Fig. 6.2.

Typically, we fabricate eight to ten of the double barrel micropipettes at the same time, First, all are pulled. Then epoxy is applied. When hardened,

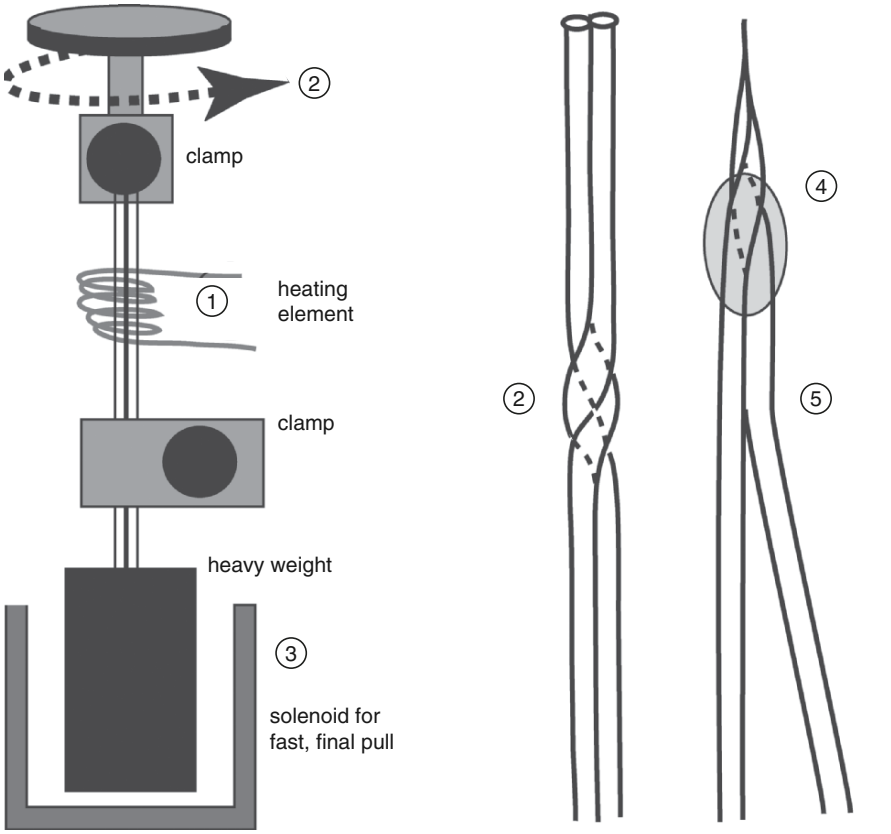

Fig. 6.1. Construction of a double barrel micropipette. Step 1: heat two capillaries held together in clamps above and below a heating element which heats the two capillaries in a localized region. Step 2: when the glass has softened, the two capillaries are twisted by rotating one of the clamps 360°. Step 3: the two capillaries are pulled to form the sharp tip, and removed from the pipette puller. Step 4: a drop of fast-setting epoxy is applied to the joint between the two barrels at the fused twist to strengthen the joint. Step 5: one of the capillaries is softened by localized heating and pulled away to produce a Y-shape

one barrel is pulled away to form a Y. Then they are stored in a covered dish until used. Fabrication takes about 1–2 h.

One problem that can arise is crack formation in one of the glass barrels, probably during the twisting if the glass has not softened enough during heating. The cracks are not visible (except as a stress crack under magnification), but reveal themselves when the micropipettes are being tested for tip resistance and crosstalk just prior to impalements. At this time, the crack causes an extremely low resistance in one of the barrels, far less than the 20 MΩ norm.

Filling of the micropipette barrels with electrolyte is done as with a single barrel electrode. Usually, a small amount of electrolyte is injected into the

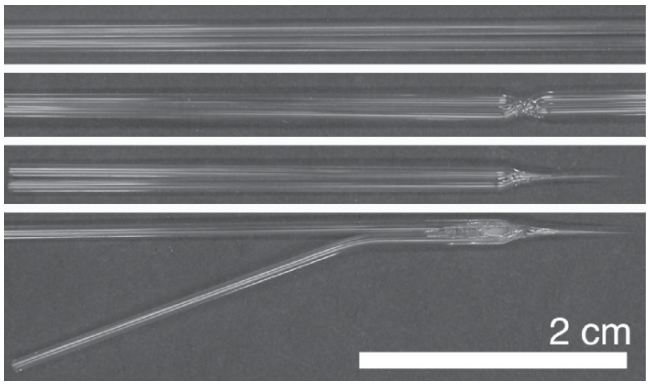

Fig. 6.2. Stages in the construction of a double barrel micropipette. The *upper panel* shows the two capillaries, twisted together in the *second panel*, pulled in the *third panel*, and after final fabrication in the *fourth panel*. Bar=2 cm

blunt end of capillaries; 10 min later, the tip will have filled due to capillary action because of the internal filament. Even the glass twist will have filled. Backfilling of the bent barrel requires a fine gauge needle, so that it can be easily inserted past the bend right up to the twist.

6.3.1 Limitations

There are limitations to the use of double barrel micropipettes due to crosstalk and the localized nature of the current injection and voltage monitoring

6.3.1.1 Crosstalk between barrels

In a double barrel micropipette, the glass wall separating the two barrels is twice the thickness of the outer glass walls (Fig. 6.3). However, it is possible that some current will "leak" across the wall. The response of both barrels to a current injected through one barrel is shown in Fig. 6.4. There are voltage deflections in the second barrel. Initially, there is a capacitance spike due to capacitative coupling between the two barrels, followed by a steady state deflection of very small magnitude. The deflection, expressed as percent coupling $[100 \times (\Delta E_2/\Delta E_1)]$, is about 1–2%.

6.3.1.2 Maximal current injection

As a consequence of the crosstalk between the two barrels, double barrel micropipettes are not suitable for measurements requiring large current injections. A 2 nA current causes a very small voltage deflection in the second

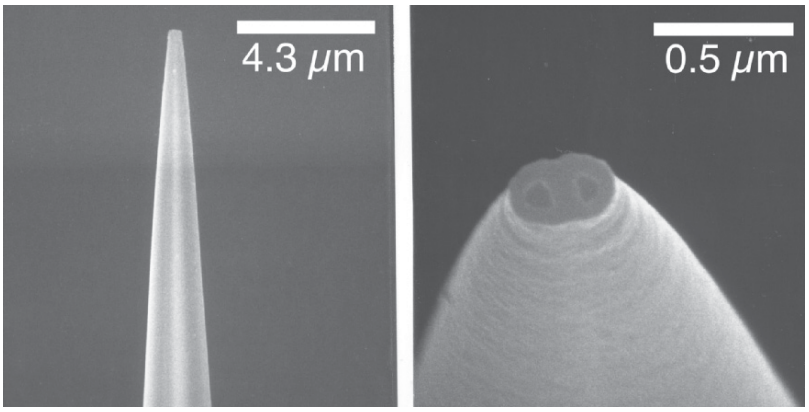

Fig. 6.3. Scanning electron microscopy of double barrel micropipette tip. The *left panel* shows the tip shape. The *right panel* shows the tip apertures. Note the double thickness of glass between the two apertures. Bars 4.3 and 0.5 μm, as shown

barrel, but a μA current will cause a deflection large enough to affect measurements in walled cells, whose membrane potentials range from –50 to –200 mV. Thus, double-barrel micropipettes are not suitable for measurements where μA currents are required, such as the green algae *Chara* and *Nitella*, although larger micropipette apertures may be a solution.

6.3.1.3 Space clamping

Another problem associated with large cells is the incomplete "spread" of voltage throughout the cell. When voltage clamping, the cell may not attain the specified voltage, this is incomplete space clamping. It is a problem for double barrel microelectrodes, because current injection and voltage monitoring occur in the same region within the cell. Incomplete space clamping should not be a problem for small, electrically isolated cells (such as guard cells). However, with large cells, or when there is electrical coupling between cells, the problem is pervasive. Under these conditions, quantitation requires multiple impalements, and correction depends upon assumptions about current spread and cell geometry. There is no simple authoritative solution. Examples of space clamping problems are shown for different cell types later in the chapter.

6.4 Use: electronics and computer control

There are many resources describing electronics and computer control of experiments. Purves (1981) is a classic, still timely today. Ogden (1994) includes very useful contributions on microelectrodes, voltage clamping

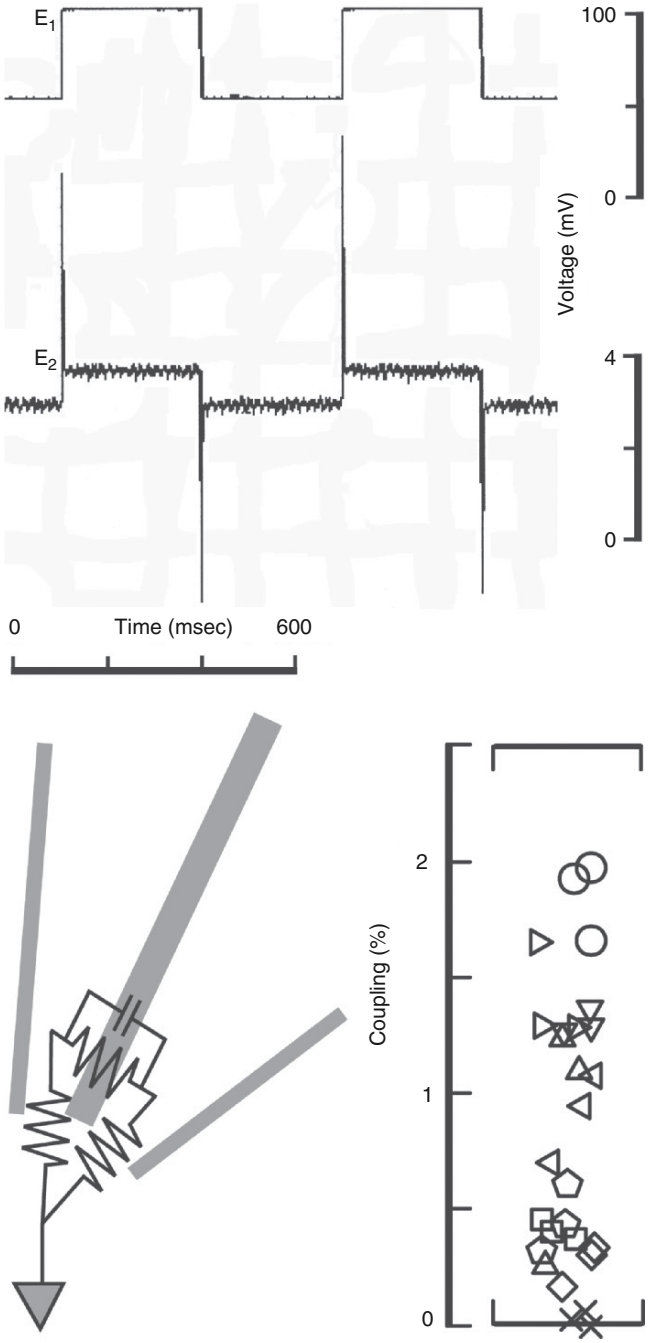

Fig. 6.4. Electrical properties of the double barrel micropipette. The upper panel shows the voltage response of the two barrels (E_1 and E_2) to a 2 nA peak to peak current injected into the first barrel (E_1). The large voltage deflection in the first barrel causes a large voltage deflection

techniques and computer control. For versatility, digital oscilloscopes are used to monitor experiments and print a copy of recordings. For computer control, we use analog/digital converters for measuring voltage and clamping currents, digital/analog converters for controlling the clamped voltage, digital input/output to switch voltage clamping on, and timers to control the duration of the voltage clamp; all are supplied by a Labmaster board from Scientific Solutions (Solon, Ohio, USA). The required software is written in C, compiled and run on a DOS computer. While this may seem anachronistic, the advantage for us is complete control of the experimental environment, including the CPU cycles of the computer. The technical specifications for hardware control have not changed, so newer systems offer little advantage. For new or experienced electrophysiologists, writing the software programs may be too daunting. If this is so, turnkey systems are available from many vendors at a significant cost. The latest development is the inclusion of a DSP (digital signal processor) chip in a stand alone system for performing measurements and voltage clamp.

6.4.1 Electrometers and voltage clamp circuit

Any electrometer with a sufficiently high input impedance ($>10^{11}$ Ω) will work. It is important to assure that the time responses of the voltage and current injecting headstages are the same, thus the input impedances should be matched. A voltage clamp circuit is connected to the electrometers. A schematic of the electronic circuit is shown in Fig. 6.5.

6.5 Examples of measurements

Examples of measurements in walled cells can include any situation where current injection and voltage measurements must be kept separate. It is important to emphasize that like any technique, double barrel micropipettes

---

Fig. 6.4. (*Continued*) due to the resistance of the micropipette tip, 25 MΩ in this example. Some of the current "leaks" across the glass barrier between the two barrels, causing a much smaller voltage deflection in the second barrel (E_2, about 1 mV). Note that there is a spike at each step transition in the current injection, caused by the capacitance of the glass barrier between the two barrels. The measurements were performed with 3 M KCl filling the barrels, and 150 mM KCl in the external solution to mimic the ionic conductivity of the cytoplasm. Grounding was performed using a chlorided silver wire (no agar salt bridge was used to minimize stray resistance that would cause a larger voltage deflection in E_2). The resistive network is shown in the lower left panel. By measuring the resistance of each barrel, and the amount of 'coupling' between the barrels ($100 \times (\Delta E_2/\Delta E_1)$) (shown in the *lower right panel*, data are jittered for clarity), it was possible to estimate the value of the resistance of the glass barrier between the two barrels. The value ranged from 500 MΩ to 100 GΩ, the median value was 3 GΩ. This is consistent with the known resistivity of borosilicate glass, about 10^{15} Ω × cm. With an estimated barrier thickness of 100 nm, the calculated resistance would be 10 GΩ

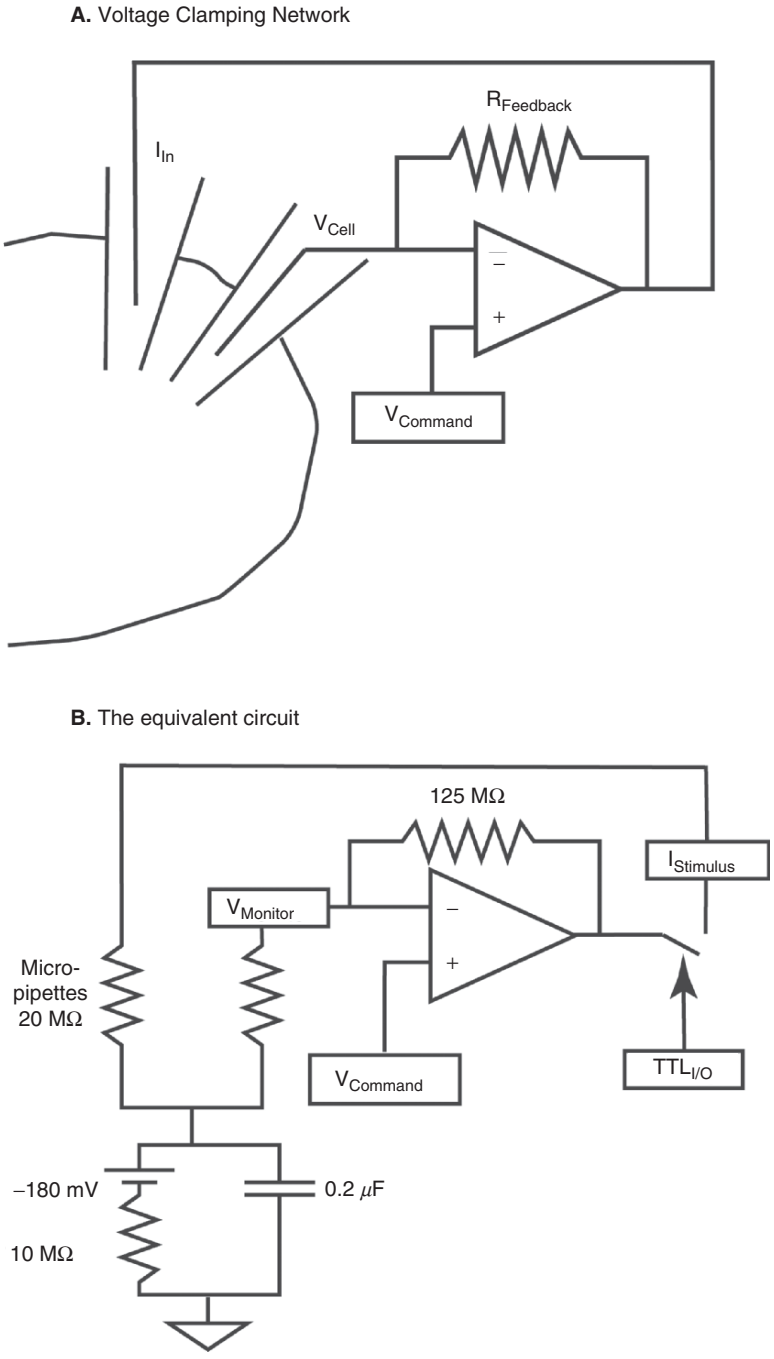

Fig. 6.5. Voltage clamping schematic. **A** If we specify $V_{Command}$, the operational amplifier will drive whatever current is necessary into the feedback system (the cell and feedback resistor $R_{Feedback}$) to maintain V_{Cell} at $V_{Command}$. **B** A more detailed equivalent circuit. The $TTL_{I/O}$ is a switch relay

may not be sufficient to resolve the electrical properties of a cell. Some of these issues are outlined in the following examples.

6.5.1 Input resistance

By injecting a known current through one barrel, the magnitude of the voltage deflection in the other barrel can be used to calculate the resistance of the cell. If the geometry of the cell is known, than the specific resistance can be calculated. An example of a measurement is shown in Fig. 6.6. The example is from

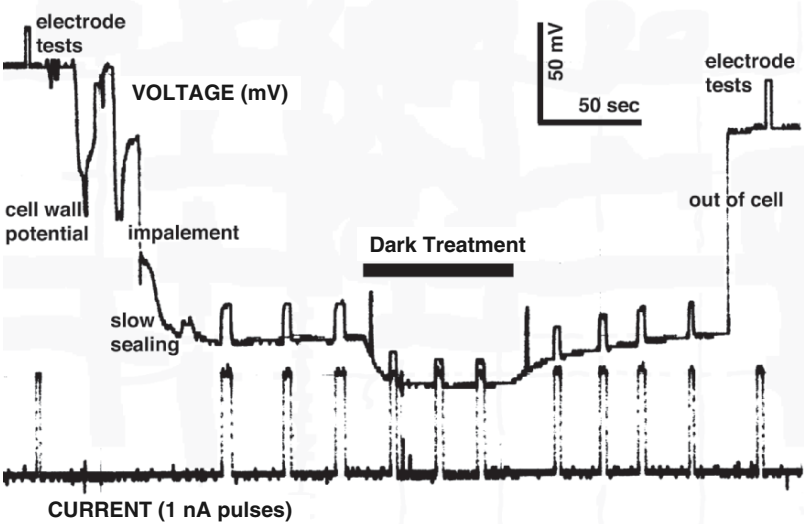

Fig. 6.6. Example of input resistance measurements from a mesophyll cell of *Ceratopteris richardii*. Both voltage (*top trace*) monitored with one barrel of the double barrel micropipette and current (*lower trace*) injected through the other barrel are shown. Prior to and after the experiment, electrode tests were conducted to assure there was no electrical crosstalk between the voltage monitoring and current injecting electrodes. Current injection through the voltage-monitoring electrode causes a voltage deflection as expected, but current injection through the current-injecting electrode caused no visible deflection in the voltage-monitoring electrode. Immediately following impalement, confirmed visually, a transient negative spike is followed by a slow sealing event that is characterized by a gradual hyperpolarization to a stable potential. After impalement, current injection through one barrel of the double barrel micropipette causes a voltage deflection in the other barrel due to the resistance of the plasma membrane. This confirmed that the impalement was successful. The response of the cell to changes in photosynthesis are documented in this experiment. Removal of the pipette from the cell results in a rapid depolarization to a value similar to what was observed before the cell was impaled

Fig. 6.5. (*Continued*) controlled by the computer to turn on the voltage clamping circuit. The V_{Cell} is measured at the electrometer ($V_{Monitor}$). The current is injected via the $I_{Stimulus}$ input of another electrometer. The feedback resistor in this example is very high (125 MΩ) and assures a fast response by the operational amplifier so that V_{Cell} is rapidly clamped with high fidelity

a mesophyll cell of a *Ceratopteris richardii* gametophyte. In these cells, dye injected into the cell was distributed throughout the cytoplasm and did not migrate into adjacent cells, indicating that the impalement was cytoplasmic, and that cell-to-cell coupling was minimal. Having measured the mesophyll cell dimensions, the specific resistance could be calculated: about 1.5 $k\Omega \times cm^2$.

6.5.2 Current–voltage relations

An example of a current-voltage measurement using voltage clamping is shown in Fig. 6.7, using trunk hyphae of the fungus *Neurospora crassa*. The measurement illustrates not only the voltage clamp technique, but also the issue of space clamping. A hyphal compartment was impaled with a double barrel micropipette, and an adjacent compartment (separated from the first by a septal pore) was impaled with a single barrel micropipette. Although voltage fidelity was observed for the voltage clamp in the first compartment, current leakage through the plasma membrane causes an attenuated voltage clamp in the second compartment. As a result, the clamping current overestimates the "real" clamping current in the first compartment. Cable theory can be used to correct for current attenuation in fungal hyphae (Gradmann et al. 1978).

6.5.3 Cell-to-cell coupling

An example of the use of double barrel micropipettes to measure electrical coupling through plasmodesmata is shown in Fig. 6.8. The example is adjacent root hairs on an *Arabidopsis thaliana* root. Analogous to fungal hyphae, electrical connections between cells results in significant current passage into adjacent cells, resulting in an overestimate of the clamping current in voltage clamp measurements.

6.6 Summary

Electrophysiological analyses of ion transport in walled cells are essential to our understanding of the life of the cell. Ion transport plays crucial roles in regulating the intracellular milieu of the cell, in signal transduction, osmotic regulation and cellular growth. A detailed characterization of the electrical properties of the cells relies upon multiple techniques, among them, voltage clamping is very useful. Voltage clamping with double barrel micropipettes is especially important given the "physiology problem" associated with patch clamp measurements on plasmolyzed protoplasts. Technical constraints and accessibility of the cell make voltage clamping a challenging endeavor, but

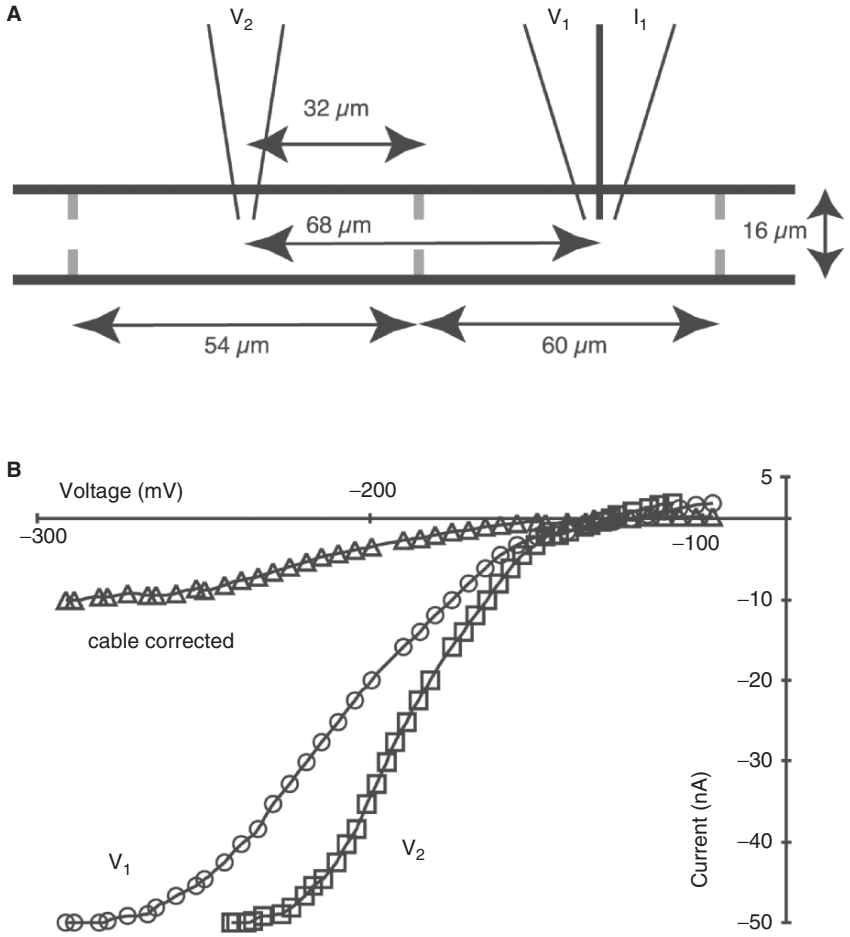

Fig. 6.7. Current–voltage measurement. The example is for a hyphal trunk of the fungus *Neurospora crassa*. A schematic of the two impalements, and hyphal geometry are shown in **A**. Note the presence of septal pores, which allow for the free movement of cytoplasm between each hyphal "cell" unit. Voltage clamping using the V_1 and I_1 microelectrodes was for the range –300 to –100 mV. The clamp duration was 50 ms, the voltage at V_1 and V_2, and the clamping current (I_1) were obtained by averaging the last five data samples before the end of the clamp. Note that the *real* voltages, rather than the computer specified clamped voltage were measured. Because of current attenuation as it passes along the hypha, the voltage at V_2 was less than the voltage at V_1. Thus space clamping was incomplete. To correct for current attenuation, the equation $I_m = I \times ln(\Delta V_1/\Delta V_2)$ was used (Rall 1977), where I is the total current, I_m is the cable corrected current, ΔV_1 is the clamped voltage minus the resting potential at V_1, and ΔV_2 is the clamped voltage minus the resting potential at V_2. The current density, A cm^{-1} can be calculated from $I_m/(2 \times \Delta x)$, where Δx is the distance between the two electrodes (68 μm in this example), and yields values in the range –0.74 to 0.021 μA cm^{-1}

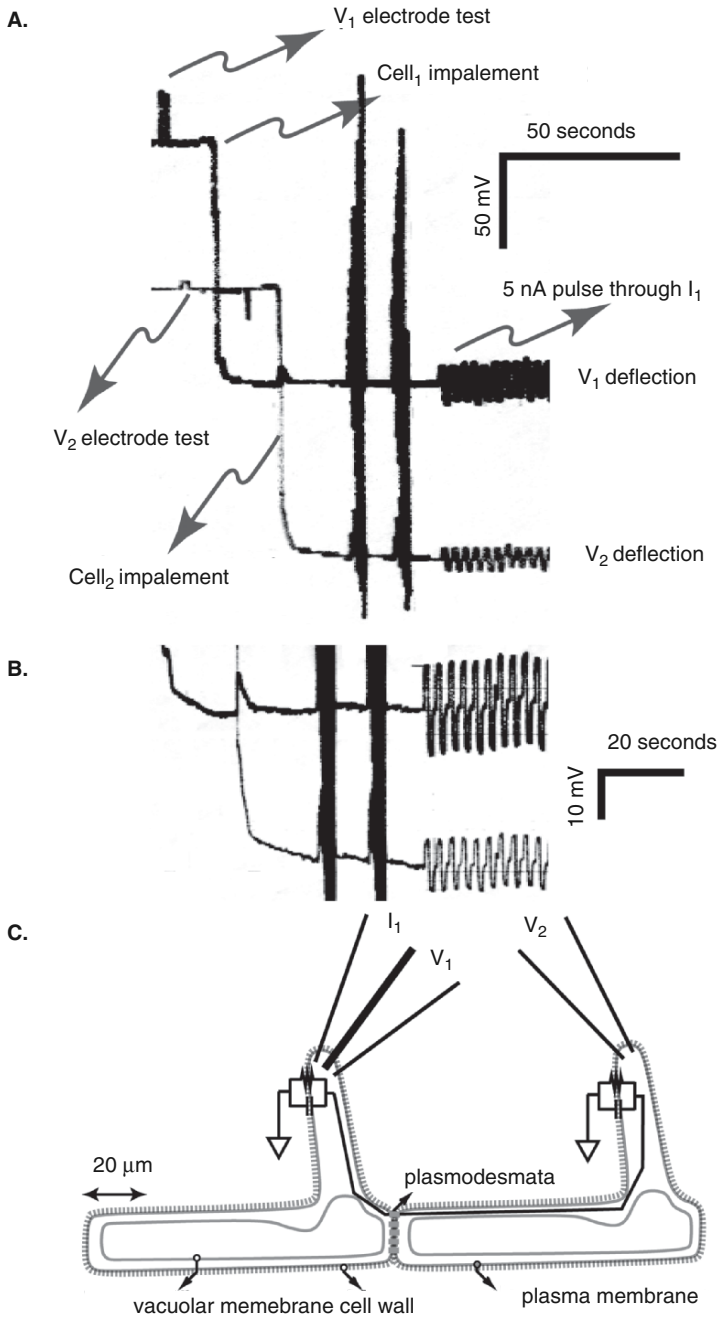

Fig. 6.8. Example of cell-to-cell coupling measurement. This example is for two root hairs adjacent to each other on a longitudinal file of an *Arabidopsis thaliana* root. **A** As marked, $cell_1$ is impaled with a double-barrel electrode, followed by a separate impalement into $cell_2$. A 5 nA

pulse through the current-injecting electrode in $cell_1$ results in a voltage deflection in both $cell_1$ and in $cell_2$, due to coupling through plasmodesmata. **B** A higher magnification segment of the traces shown in **A. C** A diagrammatic representation of cell-to-cell coupling through plasmodesmata. Regulation of cell-to-cell coupling between root hairs was described by Lew (1994)

double barrel micropipettes offer increased technical ease, simplifying the challenges faced by the researcher when working with intact cells. However, it should be clear from the examples presented in this chapter that double barrel micropipettes are not an absolute solution, but instead another step in our efforts to discover the roles of ion transport in cellular functions.

References

Blatt MR (1987) Electrical characteristics of stomatal guard cells: the ionic basis of the membrane potential and the consequence of potassium chloride leakage from microelectrodes. Planta 170:272–287

Blatt MR (1991) A primer in plant electrophysiological methods. In: Hostettmann K (ed) Methods in plant biochemistry, vol 6. Assays for bioactivity. Academic Press, London (xi and 360 pp), pp 281–321 (ISBN: 0124610161)

Blatt MR, Slayman CL (1983) KCl leakage from microelectrodes and its impact on the membrane parameters of a nonexcitable cell. J Membr Biol 72:223–234

Blatt MR, Slayman CL (1987) Role of "active" potassium transport in the regulation of cytoplasmic pH by nonanimal cells. Proc Natl Acad Sci USA 84:2737–2741

Bouteau F, Pennarun A-M, Kurkdjian A, Convert M, Cornel D, Monestiez M, Rona J-P, Bousquest U (1999) Ion channels of intact young root hairs from *Medicago sativa*. Plant Physiol Biochem 37:889–898

Etherton B, Keifer DW, Spanswick RM (1977) Comparison of three methods for measuring electrical resistances of plant cell membranes. Plant Physiol 60:684–688

Finkel AS, Redman S (1984) Theory and operation of a single microelectrode voltage clamp. J Neurosci Meth 11:101–127

Forestier C, Bouteau F, Leonhardt N, Vavasseur A (1998) Pharmacological properties of slow anion currents in intact guard cells of *Arabidopsis*. Application of the discontinuous single-electrode voltage-clamp to different species. Pflugers Arch 436:920–927

Gradmann D, Hansen U-P, Long WS, Slayman CL, Warncke J (1978) Current–voltage relationships for the plasma membrane and its principal electrogenic pump in *Neurospora crassa*: steady-state conditions. J Membr Biol 39:333–367

Hamill OP, Marty A, Neher E, Sakmann B, Sigworth FJ (1981) Improved patch-clamp techniques for high-resolution current recording from cells and cell-free membrane patches. Pflugers Arch 391:85–100

Holdaway-Clarke TL, Walker NA, Overall RL (1996) Measurement of the electrical resistance of plasmodesmata and membranes of corn suspension-culture cells. Planta 199:537–544

Lew RR (1994) Regulation of electrical coupling between *Arabidopsis* root hairs. Planta 193:67–73

Lew RR (1996) Pressure regulation of the electrical properties of growing *Arabidopsis thaliana* L. roothairs. Plant Physiol 112:1089–1100

Lew RR (2000) Electrobiology of root hairs. In: Ridge RW, Emons AMC (eds) Root hairs. Cell and molecular biology. Springer, Berlin Heidelberg New York, pp 115–139

Ogden D (ed) (1994) Microelectrode techniques. The Plymouth workshop handbook. The Company of Biologists, Cambridge, x + 448 pp

Purves RD (1981) Microelectrode methods for intracellular recording and ionophoresis. Academic Press, London, x + 146 pp

Racusen RH, Kinnersley AM, Galston AW (1977) Osmotically induced changes in electrical properties of plant protoplast membranes. Science 198:405–407

Rall W (1977) Core conductor theory and cable properties of neurons. In: Kandel ER (ed) Handbook of physiology, vol 1 (Cellular biology of neurons, part 1). American Physiological Society, Bethesda, pp 39–97

Raschke, K, Shabahang M, Wolf R (2003) The slow and the quick anion conductance in whole guard cells: their voltage-dependent alternation, and the modulation of their activities by abscisic acid and CO_2. Planta 217:639–650

Roelfsema, MRG, Steinmeyer R, Hedrich R (2001) Discontinuous single electrode voltage-clamp measurements: assessment of clamp accuracy in *Vicia faba* guard cells. J Exp Bot 52:1933–1939

Shabala S, Lew RR (2002) Turgor regulation in osmotically stressed *Arabidopsis thaliana* epidermal root cells: Direct support for the role of inorganic ion uptake as revealed by concurrent flux and cell turgor measurements. Plant Physiol 129:290–299

7 New Solid State Microsensors in Plant Physiology

Stefano Mancuso,[1] Anna Maria Marras[2]

7.1 Introduction

Solid state microelectrodes are being increasingly used in many areas of plant physiology, ranging from classical electrophysiology studies to new applications such as scanning tunneling microscopy or atomic force microscopy. When the size of the sensors is decreased from the millimeter to the micrometer scale, many changes occur in their behavior and use. These changes lead to dramatic improvements in the quality of physiological data and make achievable experiments previously impossible. The major areas of improvement include increased temporal resolution, increased sensitivity and the ability to make spatial resolved measurements.

Electrochemical methods have significant advantages over the other techniques to monitor local concentrations of a chemical compound near plant tissues. In fact, microelectrodes (amperometric or voltammetric) can be positioned close to the cells and provide a means to estimate the local concentration. Electrochemical sensors for use in plants should display high selectivity and sensitivity, long-term calibration stability, and possess a small size. In addition, if assessing concentrations at different distances from a tissue, as in the case of the self-referencing technique (see chapters by Smith et al.; Fejio; Shabala in this book for exhaustive details on the self-referencing technique), it is essential that the tips of the microelectrodes have a planar geometry so that precise concentrations at precise distances away from the source/sink, can be determined with good spatial resolution. Another factor of crucial importance in the use of the microelectrode as a vibrating probe is a fast response time. Indeed, the sensor remains in the two measurement positions for times not longer than few seconds (usually, less than 5 s, often 2–3 s). Ideally, the electrode response time should permits measurements to be made on a subsecond time scale.

In the following pages, four different new solid state microsensors to be used in plants research will be discussed:

[1] Laboratorio di Neurobiologia delle piante, Department of Horticulture, Polo Scientifico, University of Florence, Viale delle Idee 30, 50019 Sesto Fiorentino (FI), Italy (e-mail: stefano.mancuso@unifi.it)

[2] Department of Pharmaceutical Science, Polo Scientifico, Università di Firenze, via Ugo Schiff 6, 50019 Sesto Fiorentino (FI), Italy

Plant Electrophysiology – Theory & Methods (ed. by Volkov)

1. The IAA-selective microelectrode
2. The O_2-selective microelectrode
3. The NO-selective microelectrode
4. The Cu^{2+}-selective microelectrode

7.2 The IAA-selective microelectrode

Auxin (indole-3-acetic acid) has its name derived from the Greek word auxein, meaning "to increase". Indole-3-acetic acid (IAA) is a well-known regulator of plant growth and development, which is active in submicromolar amounts and is associated with a variety of physiological processes, including apical dominance, tropisms, shoot elongation, induction of cambial cell division, and lateral root initiation. The IAA content of plant tissues is believed to be regulated by several processes. Currently, the most popular view is that auxin is a hormone-like substance. However, there are several auxin features and actions that can be much better explained if one considers auxin to be a morphogen-like agent (Bhalerao and Bennett 2003) and even a neurotransmitter-like substance (Baluška et al. 2003a,b, 2004). IAA is well known also to be transported from cell to cell in a complex process based on vesicular traffickings (Baluška et al. 2003a; Geldner et al. 2003). The direction of polar auxin transport is essential for both spatially controlled cell expansion as well as for orientation of planes of division in meristematic cells. No other plant molecule is as important for driving pattern formation and shaping of the whole plant.

Researchers studying IAA both in roots and other plant organs need to measure dynamic IAA concentrations locally, directly and continuously. However, the detection and determination of IAA in plant tissue are notoriously difficult, due to its presence in minute amounts, its inherent tendency to be decomposed by heat, light and oxygen, as well as to the presence of a wide variety of molecules which modify IAA biochemically.

Because the traditional methods commonly used to measure IAA levels, such as GC (Hunter 1986; Hedden 1993; Sanchez et al. 1996) enzyme-linked immunosorbent assay (ELISA) and radioimmunoassay (RIA) (Weiler 1984), are either discontinuous or have other drawbacks, it is impossible to determine local in vivo concentrations of IAA in a real time. In fact, these approaches integrate IAA measurement over the entire tissue surface and provide an averaged measurement over a period of time.

Recently, our laboratory has developed a carbon nanotube-modified amperometric microelectrode that serves as very reliable sensor of IAA (Mancuso et al. 2005). To produce this sensor, we used a platinum microelectrode as a substrate electrode immobilizing carbon nanotubes (CNTs).

Carbon nanotubes are cylindrical carbon molecules with a structure similar to the fullerene, but where the fullerene molecule's symmetry is spherical,

that of a nanotube is cylindrical, with one end typically being capped with half a fullerene molecule. CNTs are molecular scale wires with high electrical conductivity, high chemical stability, and extremely high mechanical strength. They exhibit unusual strength and unique electrical properties, and are efficient conductors of heat (Liu et al. 1998; Baughman et al. 1999). There are two main types of nanotube: single-walled nanotubes (SWNT) and multi-walled nanotubes (MWNT). The exceptional properties of CNTs make them useful in a high number of applications ranging from nanoelectronic to biotechnology. Lately, there has been a growing interest in using CNTs in the realization of chemical sensors owing to their ability to promote electron transfer reactions.

7.2.1 Preparation of the IAA-selective microsensor

To prepare the IAA-selective microelectrode, we started preparing a platinum microsensor as for the fabrication of an oxygen selective microelectrode. The detailed procedure is reported in Mancuso et al. (2000). Next, a platinum wire 10 mm long and 0.2 mm in diameter was soldered to a silver connecting wire of the same diameter. This assembly was then mounted in a glass capillary (2 mm o.d., 1.12 i.d.; World Precision Instruments, Sarasota, Fla., USA) such that approximately 3 mm of the platinum wire protruded from the capillary tip. The microwire was secured in position by melting the glass tip of the capillary around the wire. Etching of the protruding wire to form a sharp tip was accomplished galvanically submerging the wire for 5 s in a mixture composed of KNO_3 + 5% $KHCO_3$ melted at 600 °C. A current flow of 1.3 A was applied between the microwire and a platinum laminar anode of about 1 cm^2. With this system, with a little practice, we easily obtained tips with a diameter of around 7–10 µm. Microwire insulation was achieved using an anodic electrodeposition paint (Glassophor ZQ 84–3225, BASF, Germany). The probe was completed with a platinum wire 10 mm long and 0.5 mm in diameter acting as auxiliary electrode and with a reference half-cell Ag/AgCl/KNO_3 0.1 M + NaCl 0.08 M. The cell was arranged in a three-electrode polarographic configuration which maintained the working microelectrode at a polarizing voltage of 0.7 V, ensuring a condition of diffusion limiting current for IAA oxidation. MWNTs were purified by refluxing them in a 2 M nitric acid solution for 10 h, then washed in twice distilled water and dried at room temperature. The MWNT suspension was prepared by dispersing the MWNTs in 2 ml of DMF (N,N-dimethyl formamide). The solution was then sonicated for 30 min to aid the dissolution. The bare platinum electrode was immersed in a 0.03 M MPS (3-mercaptopropyl) trimethoxysilane solution for 6 h, then taken out and washed carefully with twice distilled water to remove physically adsorbed MPS. The modified electrode was prepared by dropping 5 µl of MWNTs suspension on the surface of the MPS/Pt microelectrode and left to dry.

7.2.2 Calculation of the diffusion coefficient for IAA

The IAA-selective microelectrode was used in a self-referencing mode. IAA fluxes on this way can be calculated using Fick's first law of diffusion:

$$J = \frac{D(C_1 - C_2)}{\Delta x}$$

where J is the flux rate (mol cm^{-2} s^{-1}), D is the diffusion coefficient for IAA (0.677×10^{-5} cm^2 s^{-1} at 25 °C), C_1 and C_2 are the concentrations at the two measurement positions and Δx is the distance of measurement (cm).

The diffusion coefficient of many chemicals is tabulated in the usual handbooks of chemistry. However, not all the diffusion coefficients, as in the case of IAA, are available.

To overcome the difficulties arising from the lack of a tabulated diffusion coefficient the same procedure we used for the calculation of the diffusion coefficient of IAA can be followed. The diffusion coefficient D of IAA in dilute aqueous solution was estimated using the empirical relationship:

$$D = k \times M^{-1/2}$$

wherein k is a temperature-dependent constant and M is the molecular mass which should be smaller than 1000 and corrected, if applicable, for the mass of the solvation shell (Fisher Weiss 1996). To estimate k, a calibration curve was constructed using the experimentally determined (at 25 °C) diffusion constants compiled by Longsworth (1957) for a set of compounds (n=47) including amino acids, oligopeptides, mono- and oligosaccharides (Fig. 7.1). Linear regression (r=0.967; standard deviation with respect to regression=0.037×10^{-5}), afforded k=$(8.97 \pm 0.07) \times 10^{-5}$. Using these parameters, the diffusion coefficient of IAA (M=175.19) was calculated as $(0.677 \pm 0.006) \times 10^{-5}$ cm^2 s^{-1}.

7.2.3 Example of use of the IAA-selective microelectrode

Carbon-nanotube-modified and self-referencing IAA-selective microelectrode allow non-invasive recordings of IAA fluxes at intact root apex revealing that cells differ dramatically in their abilities to transport IAA. In the root apex, the most dramatic IAA influx was recorded at the distance of about 1–2 mm from the root cap junction (Fig. 7.2). These unique root cells terminate their mitotic activity and traverse a so-called transition zone which is critical for several sensory properties of root apices counting monitoring of gravity and light (Baluška et al. 2004, 2005). In the same figure, it is possible to see the effect of aluminum on the IAA influx profile, in a conditions of IAA saturation transport (external concentration 15 µM IAA). The treatment with 90 µmol of Al strongly suppressed IAA influx in the transition zone already after 10 min, supporting the fact that it is the transition zone the primary site of the aluminum action in the root apex (Sivaguru et al. 1999).

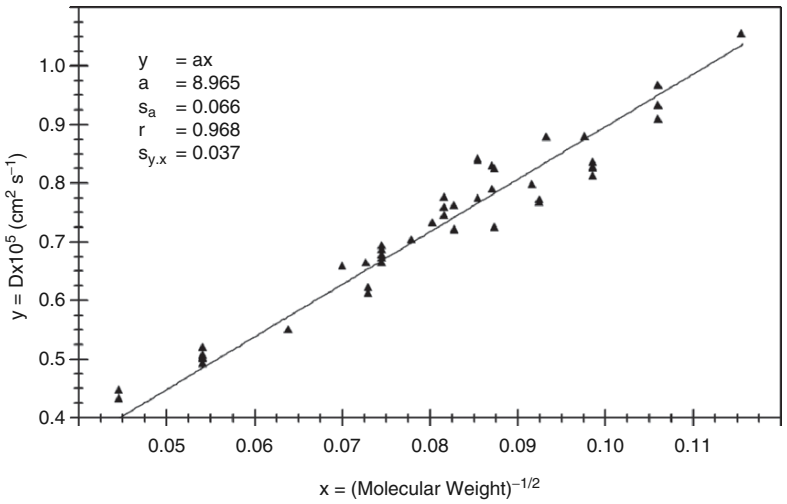

Fig. 7.1. Linear regression representing the dependence of the diffusion coefficient ($y_i=D_i\times 10^5$) on the inverse square root of the molecular weight [x_i=(mol. wt)$^{-1/2}$] for a set of 47 compounds used to compute the diffusion coefficient of IAA

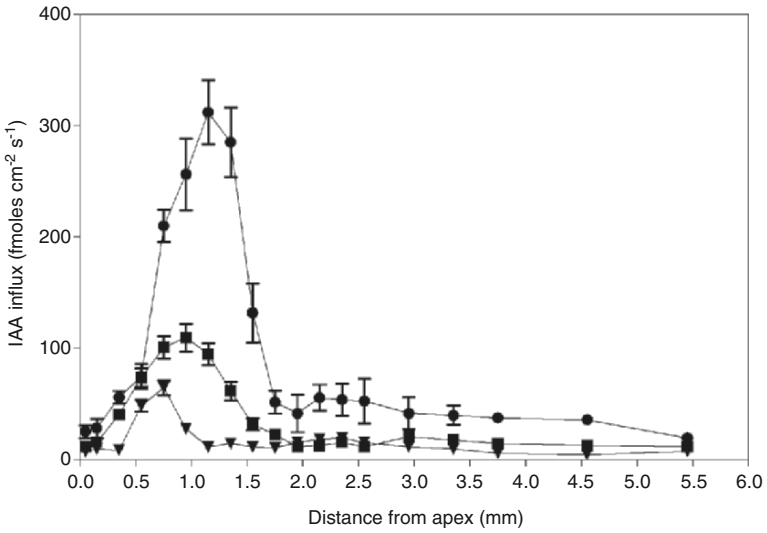

Fig. 7.2. Diagram illustrating the IAA influx profile along a single root of maize (Cv. Gritz) and the effect of aluminum in a conditions of IAA saturation transport (external concentration 15 µM IAA). Al 90 µM was supplied in a solution containing KCl and $CaCl_2$ at 200 µM each for 10 (■) and 30 (▼) min. ●, control (–Al). Differential current from an IAA-selective microelectrode placed 2 µm from the root surface and used in a self-referencing mode. The sensor was vibrated between two positions 10 µm distant at a rate of 0.1 Hz. Positive fluxes represent a net IAA influx. Data shown are means of 10 replicates. Error bars represent SE

In conclusion, the ability to perform non-invasive and real-time recordings of IAA fluxes over intact plant root apices provide us with critical tool for deepening our understanding how IAA drives gravity- and light-navigated growth of plant organs such as roots. In the first experiment we analyzed robust root apices of maize. Recently, we were able to refine the technique so that it was possible to measure IAA fluxes also around the tiny roots of *Arabidopsis* (Santelia et al. 2005). Roots of *Arabidopsis* with their diameter only around 100 µm are extremely suitable for in vivo confocal microscopy, allowing visualization of structures throughout their tissues. Moreover, powerful genetics and impressive amount of mutant collections will give us excellent prospects to decipher in details how IAA regulates gravity- and light-sensitive growth of plant organs and whole plants. Last but not least, this technique might also prove to be useful for the just emerging application of IAA in the cancer therapy.

7.3 The O_2-selective microelectrode

The experimental measurement of cellular O_2 level in the plants is fundamental when discriminating normal physiological function from abnormal or stressed states. Small differences (decreases or increases) in the physiological partial pressure of oxygen (pO_2) can induce stress and/or the formation of reactive species with deleterious effects. In studies on oxidative stress, there is more and more recognition that there is a need for systems that can detect very subtle variations of pO_2 in tissues, especially in vivo, in order to study the relevance of physiological situations. Several commercially available O_2 macro-sensors can be used to obtain estimates and to characterize oxygen fluxes in higher plant cells. However, these all integrate fluxes over the entire surface of the tissue, and provide a flux representing an average value over the period of measurement. Consequently, these techniques have a spatial and temporal resolution not adequate for studying the oxygen metabolism at the single-cell level. Microelectrodes also have been used for many years, invasively, for direct measurements of tissue oxygenation in animal and plant studies (Armstrong 1994; Ober and Sharp 1996). However, it is essential to demonstrate that the variations of pO_2 measured are related to physiological processes, and are not related to disturbances coming from the presence of the oxygen sensor inside the tissue. Thus, although the measurement of oxygen is a key factor in plant cell biology, there is a lack of methodologies able to report continuously, non-invasively, and accurately the pO_2 in tissues.

7.3.1 Preparation of the O_2-selective microsensor

In recent years, the manufacture and use of electrodes with characteristic dimensions in the micrometer to nanometer range is becoming more widespread

and common (Penner et al. 1990). There are a variety of techniques which now allow the production of very tiny electrodes. Many of these procedures arise from the development of tips used for scanning tunneling microscopy (STM) or scanning electrochemical microscopy (SECM) in solution (Bard et al. 1989; Frateur et al. 1999) and are interesting to us because they are typically constructed from platinum or platinum-iridium microwires, the same material used for the manufacture of oxygen cathode. The wires are usually electrochemically etched to a sharp point, and then coated with an insulating material, except at the very apex of the tip, thus providing a very small exposed electrode area.

Recently, Land et al. (1999) succeeded in measuring oxygen fluxes in an isolated neuron and in the filamentous alga *Spirogyra greveilina* taking advantage of the vibrating-electrode technology combined with the use of a membrane-tipped, polarographic oxygen microelectrode of the type developed by Whalen and co-workers (1967).

Recently we described a simple, inexpensive and highly successful procedure for the construction of platinum electrodes with dimension in the range of micrometers (see the paragraph about the preparation of IAA-selective microsensors for further details on the preparation of platinum microelectrodes) to be used as O_2-selective electrodes (Mancuso et al. 2000).

An important step in the production of platinum microelectrodes in the range of the few microns is the verification of the tip dimension. However, the use of appropriate microscopy for this task can be time- and money-consuming. In the absence of direct observations, the mass-transport-controlled limiting current i_{lim}, measured from the plateau region of the sigmoidal steady-state polarogram, can be related to the effective electrochemical radius of exposed metal using the following equation (Pendley and Abruña 1990):

$$i_{lim} = 4nFDC^{*}r$$

where F is the Faraday's constant, n is the number of electrons transferred per redox event, D is the diffusion coefficient of the reactant ($cm^2\ s^{-1}$), C^* is the bulk concentration of the reactant (mol cm^{-3}) and r is the radius of the section of the tip. A tacit assumption implied in the use of this equation is that the electrode has a disk geometry. The assumption of other exposed metal geometries (such as a hemisphere or a cone) would yield electrode radii that would be 20–30% smaller than those obtained.

7.3.2 Example of use of the O_2-selective microelectrode

The use of these microelectrodes coupled with the vibrating-probe technique gave us the means to monitor oxygen dynamics associated with single cells located at the surface of plant tissues, allowing the study of spatial and temporal differences and/or relationships which can not be detected by standard O_2 measurement systems (Mancuso et al. 2000; Mancuso and Boselli 2002; Mancuso and Marras 2003).

One of the most interesting feature of the use of an oxygen-selective microelectrode with the vibrating probe system is the possibility to obtain "topographical" images of the O_2 fluxes coming in and out from the tissues. For example in Fig. 7.3 it is possible to see the evolution of oxygen produced by a region of 120×120 µm of an illuminated leaf. The two peaks in the image correspond to the oxygen photosynthetically generated diffusing through two different stomata. The efflux values associated to these peaks are at least 3 times greater than the averaged background value.

Topographical images of the oxygen uptake by the different regions of the roots can be also of interest in root physiology studies. Figure 7.4 shows the influx of oxygen in a root apex of maize. Interestingly, in spite of some differences in the quantitative characteristics, all plants showed the same spatial organization in net O_2 influxes, with the transition zone of the root apex representing the largest sink for O_2 in root.

With an oxygen-selective microsensor used with the vibrating probe technology, a combination of topographic and electrochemical information at

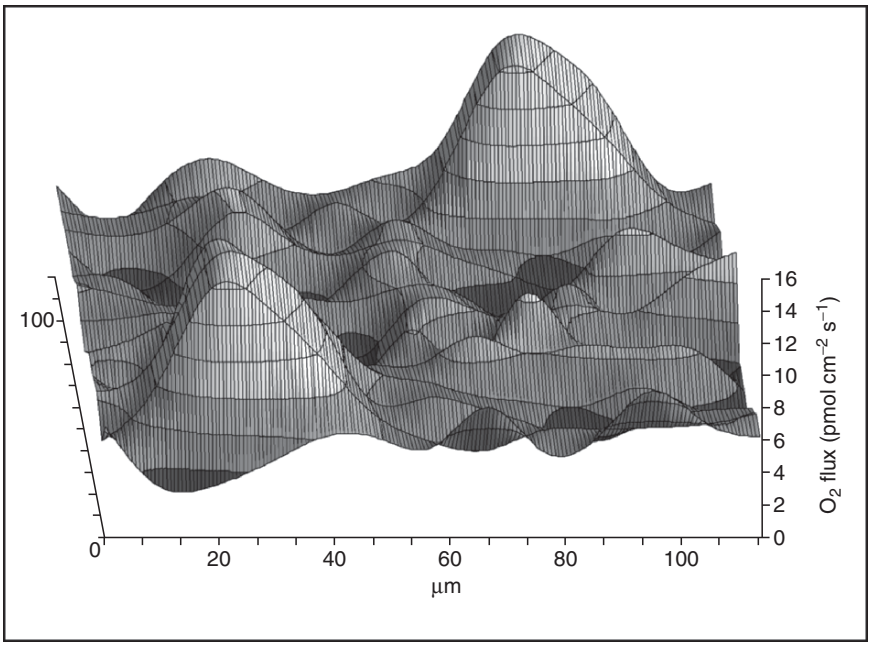

Fig. 7.3. 3D map showing oxygen evolution from two different stomata of an illuminated leaf of *Olea europaea*. The data was recorded oscillating the electrode as a square wave at 0.1 Hz between two points, 10 µm apart. The electrode was moved in the *x* direction collecting data every 2 µm. After finishing one pass, the microelectrode was moved 5 µm in the *y* direction and then returned in the opposite *x* direction

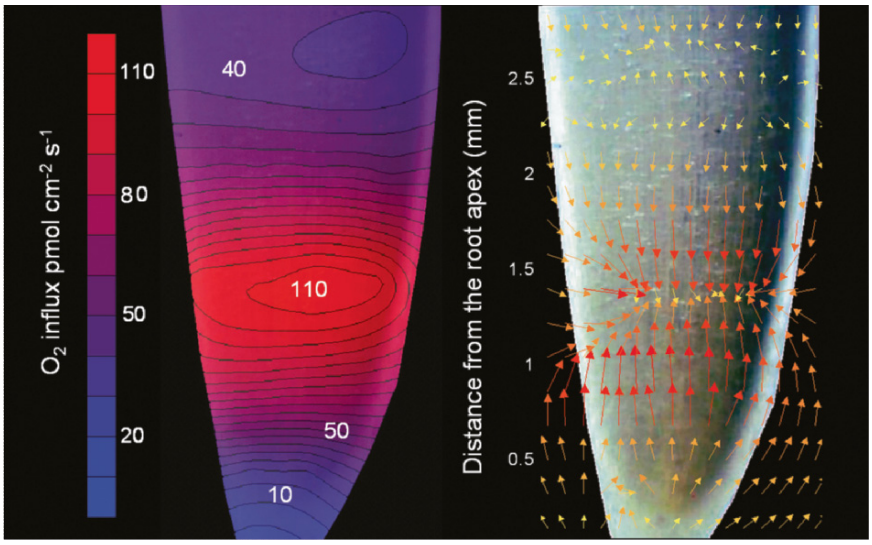

Fig. 7.4. Contour map (*left*) and vector map (*right*) showing oxygen influxes in a root apex of maize. The data were recorded oscillating the electrode as a square wave at 0.05 Hz between two points, 10 µm apart. The electrode was moved in the *x* direction collecting data every 100 µm. After finishing one pass, the microelectrode was moved 50 µm in the *y* direction and then returned in the opposite *x* direction. Both maps were constructed using the position data of the microsensor that were recorded by the data acquisition system together with the current output. Scattered X,Y,Z data were interpolated by using the software Surfer (Golden software, Golden, Colorado, USA)

micrometer scale is then available. This makes the system an efficient tool to study biological phenomenon involving oxygen diffusion. Among these the mechanism behind stomatal movements, i.e. the regulation of guard cell turgor by calcium, the response of stomata to CO_2 and the heterogeneity of the stomatal aperture over the leaf surface, together with the study of the hypoxia stress are among the most obvious possibilities.

7.4 The NO-selective microelectrode

Research on NO in plants has gained considerable attention in recent years as an increasing evidence of the role of this molecule in plant growth and development (Gouvea et al. 1997; Leshem 1996) as well as a plant defense signal against pathogen infection (Delledonne et al. 1998; Durner et al. 1998) was demonstrated.

Numerous good reviews on the biological function of nitric oxide as a signaling molecule and on its role during plant defence against pathogen attack have been published in recent years (Beligni and Lamattina 2001; Delledone et al. 2001; Wendehenne et al. 2001; Neill et al. 2002; Lamattina et al. 2003; Romero-Puertas and Delledonne 2003; Delledonne 2005).

Thus, NO is currently considered a vital bioregulatory molecule, and researchers studying NO need to measure its concentration locally, directly, and continuously to investigate NO production in vivo and in vitro. The difficulties in the detection and monitoring of NO are due to its short half-life (less than 30 s), which permits diffusion only over a short distance in a limited area and in a limited time period.

The methods commonly used to measure NO, such as the chemiluminescence method (Braman and Hendrix 1989), electron paramagnetic resonance spectrometry (Wennmalm et al. 1990) and the Griess method (Green et al. 1982), are discontinuous, indirect or have other disadvantages such as the impossibility of determining the local concentration of NO in real time. The use of microelectrodes might be the answer to these problems, being a direct and continuous NO measurement method with high spatial and temporal resolution. Indeed, amperometric detection of NO is currently the only sensitive technique available that is able to satisfy the real-time and in vivo measurement requirement of many NO related studies.

Several types of electrochemical NO electrodes have been reported in the literature (Shibuki 1990; Malinski and Taha 1992; Friedemann et al. 1996; Haruyama et al. 1998; Mitchell and Michaelis 1998; Jin et al. 1999; Mao et al. 2000; Kato et al. 2005). NO is oxidized anodically at bare and modified solid electrodes, the formation of the nitrosonium ion (NO^+) in the first step and NO^3 as a final product being well characterized in the literature (Dutta and Landolt 1972; Malinski and Taha 1992). In an attempt to increase the selectivity and sensitivity of the determinations, several approaches have been reported on the modification of the electrode surface with electropolymerized films of nickel porphyrin (Malinski et al. 1993), by the deposition of o-phenylenediamine layers (Friedemann et al. 1996) and the electrodeposition of palladium and iridium oxides (Xian et al. 1999).

The sensitivity of the nitric oxide sensors depends largely on the reactive surface area of the microelectrode. An electrode with a small surface area will show less sensitivity if compared with one with a larger surface area. In addiction, the detection limit of an electrode is at least as much important as the sensitivity. Noise problems, for example, may not be a problem in relatively high NO concentrations, whereas in low NO concentrations measurements can be hindered by too much noise. Fortunately, recent commercial NO microsensors can detect NO at levels of 1 nM or less, and are consequently appropriate for many experimental tasks.

In addition, the selectivity problem have been well addressed in the last years. An NO sensor is of no practical importance unless immune from the interferences of other species present in the measurement solution. Many

species present in normal nutrition solutions are oxidized at the same voltage used to detect NO (normally, in the range between 0.4–0.8 V). To enhance the selectivity and to prevent response from other species, including ascorbate, nitrite etc., the working surface of the electrode need to be modified with some organized layers. Indeed, a variety of membranes (e.g. cellulose acetate, Naflon, chloroprene, polycarbazole) have been used to modify the surface of such working microelectrode via electropolymerization of appropriate monomers or classical dip coating procedures. To further improve the selectivity multilayers of different membrane materials have also been applied (Malinsky and Taha 1992; Trevin et al. 1996). NO sensors coated with these multilayer membranes exhibited increased selectivity and sensitivity for NO, and, in addition, were shown to be immune from interference caused by a wide range of potentially interfering species (Zhang et al. 2000).

Microsensors have been used to examine NO production in plants (Leshem and Haramaty 1996; Yamasaki and Sakihama 2000). These papers demonstrate that such microelectrode sensors can be used to give valid measures of NO. However, the major justification for measuring NO signaling directly by microsensors arises from the necessity for accurate spatial and temporal resolution.

Figure 7.5 shows a schematic drawing for a NO microelectrode we recently used for the recording of NO fluxes in specific regions of the root apex. The dimensions, selectivity, and the response time (< 0.5 s) allowed us to use this

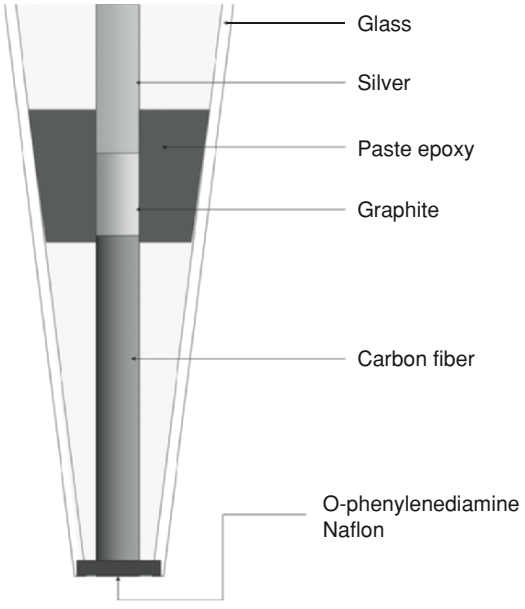

Fig. 7.5. Schematic drawing (not to scale) of a carbon fiber microelectrode NO-sensitive, showing the surface modification of the exposed carbon surface by O-phenylenediamine and Naflon

electrode in a self-referencing mode on root of maize. With this probe, we detected NO fluxes as small as 50 fmol cm^{-2} s^{-1} in different region of the root apex. In addition, in Fig. 7.6 it is possible to see that immediately after the onset of hypoxia, NO left the transition zone of the root apex with a mean peak efflux of 925±102 fmol NO cm^{-2} s^{-1} (Mancuso et al., unpublished).

In conclusion, electrochemical NO sensors provides an elegant and convenient way to detect NO in real time in plant samples. In addiction, currently they provide the only system to measure nitric oxide continuously, accurately and directly within tissues. The increasing approval of such microsensors will help to further understand the role of this interesting and ubiquitous molecule in plant physiology.

7.5 The Cu^{2+}-selective microelectrode

Several techniques have been used to obtain estimates and to characterize fluxes of macro- and micronutrient ions in higher plant cells. Intact tissue techniques have often relied on bulk-solution methods, such as radioisotope-flux techniques or solution-depletion measurements (Cataldo et al. 1983; Mullins and Sommers 1986). These techniques, however, are disadvantageous in terms of spatial and temporal resolution and are, usually, used to study ion uptake on

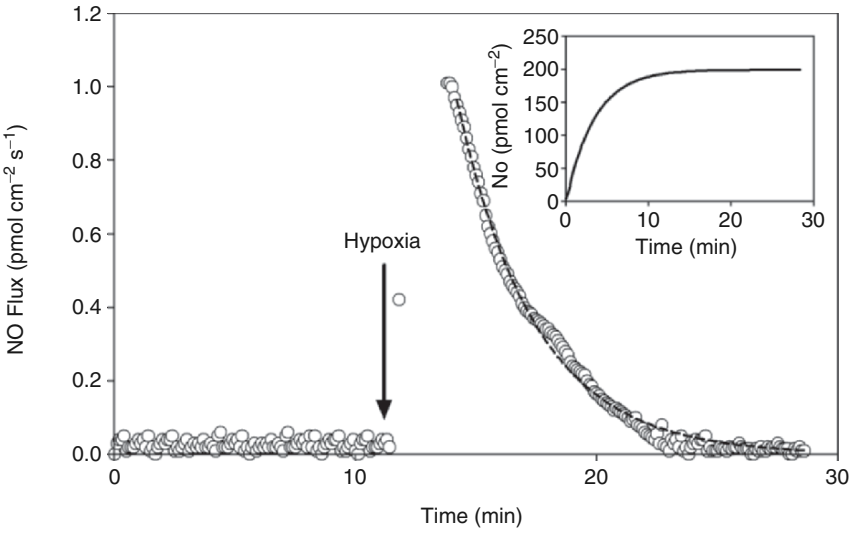

Fig. 7.6. NO emission from the transition zone of the root apex of *Vitis vinifera* after hypoxia treatment. The NO flux was measured by using an NO-selective microsensor in a self-referencing mode, by vibrating the probe as a square wave at 0.05 Hz between two points at 2 and 12 µm from the root surface

entire roots or root systems over quite long periods. The use of solid state microsensors associated with the vibrating probe technique, also enables the detection of some less studied micronutrients as copper.

Some years ago, we developed a Cu/CuSe microelectrode with the aim of using it to measure net fluxes of copper(II) ions in *Olea europaea* roots by the vibrating probe method (Papeschi et al. 2000). For the fabrication of the microelectrode a copper wire 75 μm in diameter insulated with a thin layer of lacquer was utilized. It was soldered at one connector and mounted in a glass capillary (2 mm o.d., 1.12 mm i.d.) used just as support. The tip of the wire was cut perpendicularly with a sharp surgical knife at a distance of about 3 mm from the capillary and the resulting copper disk was coated with a film of CuSe by cathodic deposition from a 0.1 M sodium selenite solution adjusted to about pH 6.0 with sulfuric acid. The reactions occurring on the copper disk were thought to be:

$$2H^+ + 2e^- = H2\,(ads)$$
$$2H_2(ads) + HSeO_3^- + H^+ = Se + 3H_2O$$
$$Se + Cu = CuSe$$

The pH value had significant influence on cathodic deposition: under pH 4.5, the formation of H_2 bubbles prevented selenium from reacting with the copper surface, taking it away from the metal in a powder form. In the range of pH 6.5–8.0, red flakes of selenium, that were unable to interact with the metal disk, were observed. Over pH 8, only gas development was recorded. The optimal pH for the coating was concluded to be between 5.0 and 6.0

The performance characteristics of the Cu/CuSe disk microelectrode in terms of its selectivity towards cupric ions, Nerstian response, limit of detection and response time were studied before its application in detecting temporal and spatial localization of copper (II) fluxes along *Olea europaea* roots. First the calibration of the microelectrode was performed using unbuffered copper solutions made by serial dilution from a 0.1 M stock solution of $Cu(NO_3)_2$ in water with a background of 50 μM $Ca(NO_3)_2$; subsequently, the response time was evaluated recording on chart the electrode potential changes occurred after small and appropriate aliquots of copper ion had been added to the well stirred 50 μM $Ca(NO_3)_2$ solution containing the electrode. Results showed response time to be shorter than 0.5 s. It was a crucial point for the use of the microelectrode with the vibrating probe technique.

Finally, the selectivity of the Cu/CuSe microelectrode with respect to five cations (Na^+, K^+, NH_4^+, Ca^{2+}, Mg^{2+}), usually contained in nutritive solutions used in plant physiology, was verified by the mixed solution method, which is based on the sequential additions of the primary ion to a fixed aliquot of interferent ion. The selectivity of Cu/CuSe microelectrode in the presence of the primary (Cu^{2+}) and the interfering ions was described by the selectivity coefficient according to the Nicolskii–Eisenman equation:

$$E = E_i^o + \left(2.303\, RT/z_i F\right) log\left[\left(a_i\right) + K_{iw}\left(a_w\right)^{zil zw}\right]$$

where: E is the membrane potential, $Ei0$ is the standard potential of primary ion, a_i, a_w is the activity of primary and interfering ions, respectively; z_i, z_w is the charge of primary and interfering ions, respectively; K_{iw} is the selectivity coefficient; R is the ideal gas constant; T, the absolute temperature and F, the Faraday's constant.

The results obtained by using this microelectrode in a self-referencing mode, allowed us to detect copper(II) fluxes with a great spatial and time resolution. In Fig. 7.7 is shown the profile of the Cu^{2+} fluxes in a root apex of olive. A maximum uptake at around 1.5 mm from the root apex is evident. In addiction, when monitoring the fluxes for periods as long as 2 h, we were able to demonstrate a clear rhythmic pattern in the flux of copper(II) in the region of maximum uptake.

7.6 Future prospects

The use of electrodes with dimensions of a few microns has many advantages in plant physiology research. The acceptance and diffusion of such electrodes is increasing inside the plant cell biology community and it is predictable that in the next few years, techniques based on micro- or nano-size selective electrodes will become standard in many laboratories. When new techniques become more widely applied, many new potential applications emerge, some of which reveal deficiency of the existing technology and thus, are powerful drive for further innovations. We see several areas of interest: new sensors,

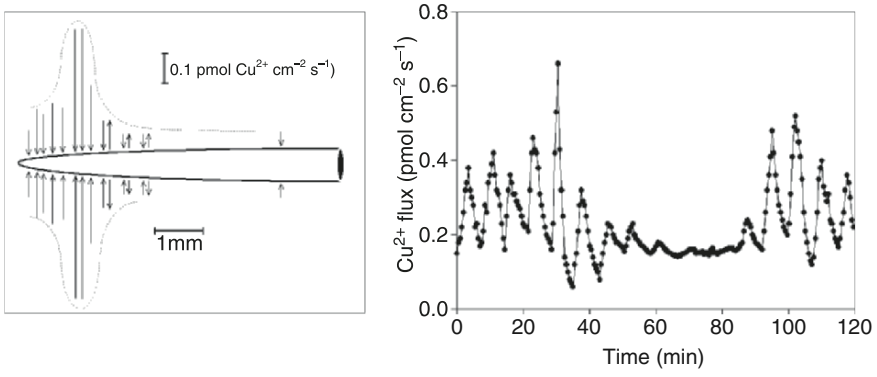

Fig. 7.7. Cu^{2+} fluxes in root of *Olea europaea*. *Left*: copper(II) flux profile along the root apex. The position and magnitude of the fluxes are indicated by *arrows*: arrows directed toward the root indicate influx and arrows directed away from the root denote efflux. *Right*: oscillatory behavior of Cu^{2+} flux around the region 2 mm from root apex (from Papeschi et al. 2000)

smaller and faster in the response; sensor arrays for detecting several compounds, or the same analyte in different positions, at the same time; novel sensors for new chemical of interest. These new advances will give unparalleled spatial and temporal resolution around single cells or structures that will be of invaluable help in supporting new and emerging fields of the plant physiology, namely the plant neurobiology.

References

Armstrong W (1994) Polarographic oxygen electrodes and their use in plant aeration studies. Proc R Soc Edinb 102B:511–527

Baluška F, Šamaj J, Menzel D (2003a) Polar transport of auxin: carrier-mediated flux across the plasma membrane or neurotransmitter-like secretion? Trends Cell Biol 13:282–285

Baluška F, Wojtaszek P, Volkmann D, Barlow PW (2003b) The architecture of polarized cell growth: the unique status of elongating plant cells. BioEssays 25:569–576

Baluška F, Mancuso S, Volkmann D, Barlow PW (2004) Root apices as plant command centres: the unique "brain-like" status of the root apex transition zone. Biologia 59:7–19

Baluška F, Hlavacka A, Mancuso S, Volkmann D, Barlow PW (2005) Neurobiological view of plants and their body plan. In: Baluška F, Mancuso S, Volkmann D (eds) Communication in plants: neuronal aspects of plant life. Springer, Berlin Heidelberg New York (in press)

Bard AJ, Fan FRF, Kwak J, Lev O (1989) Scanning electrochemical microscopy: introduction and principles. Anal Chem 61:132–138

Baughman RH, Cui C, Zakhidov AA, Iqbal Z, Barisci JN, Spinks GM, Wallace GG, Mazzoldi A, de Rossi D, Rinzler AG, Jaschinski O, Roth S, Kertesz M (1999) Carbon nanotube actuators. Science 284:1340–1344

Beligni MV, Lamattina L (2001) Nitric oxide in plants: the history is just beginning. Plant Cell Environ 24:267–278

Bhalerao RP, Bennett MJ (2003) The case for morphogens in plants. Nat Cell Biol 5:939–943

Braman RS, Hendrix SA (1989) Nanogram nitrite and nitrate determination in environmental and biological materials by Vanadium(III) reduction with chemiluminescence detection. Anal Chem 61:2715–2718

Cataldo DA, Garland TR, Wildung RE (1983) Cadmium uptake kinetics in intact soybean plants. Plant Physiol 73:844–848

Delledonne M (2005) NO news is good news for plants. Curr Opin Plant Biol 8:390–396

Delledonne M, Xia YJ, Dixon RA, Lamb C (1998) Nitric oxide functions as a signal in plant disease resistance. Nature 394:585–588

Delledone M, Zeier J, Marocco A, Lamb C (2001) Signal interactions between nitric oxide and reactive oxygen intermediates in the plant hypersensitive disease-resistance response. Proc Nat Acad Sci USA 98:13454–13459

Durner J, Wendehenne D, Klessig DF (1998) Defense gene induction in tobacco by nitric oxide, cyclic GMP, and cyclic ADP-ribose. Proc Nat Acad Sci USA 95:10328–10333

Dutta D, Landolt D (1972) Electrochemical behavior of nitric oxide in 4 M H_2SO_4 on platinum. J Electrochem Soc 119:1320–1325

Fischer Weiss T (1996) Cellular Biophysics, Vol. 1, MIT Press, Cambridge, Massachusetts

Frateur I, Bayet E, Keddam M, Tribollet B (1999) Local redox potential measurement. Electrochem Commun 1:336–340

Friedemann MN, Robinson SW, Gerhardt GA (1996) o-Phenylenediamine-modified carbon fiber electrodes for the detection of nitric oxide. Anal Chem 68:2621–2628

Geldner N, Anders N, Wolters H, Keicher J, Kornberger W, Muller P, Delbarre A, Ueda T, Nakano A, Jurgens G (2003) The *Arabidopsis* GNOM ARF-GEF mediates endosomal recycling, auxin transport, and auxin-dependent plant growth. Cell 112:219–230

Gouvea CMCP, Souza JF, Magalhaes MIS (1997) NO-releasing substances that induce growth elongation in maize root segments. Plant Growth Reg 21:183–187

Green LC, Wagner DA, Glagowski J (1982) Analysis of nitrate, nitrite and [^{15}N] nitrate in biological fluids. Anal Biochem 126:131–138

Haruyama T, Shiino S, Yanagida Y, Kobatake E, Aizawa M (1998) Two types of electrochemical nitric oxide (NO) sensing systems with heat-denatured Cyt C and radical scavenger PTIO. Biosens Bioelectron 13:763–769

Hedden P (1993) Modern methods for the quantitative analysis of plant hormones. Annu Rev Plant Physiol 44:107–129

Hunter WJ (1986) High-performance gas chromatography method for the estimation of the indole-3-acetic acid content of plant materials. J Chromatogr A 362:430–435

Jin JT, Mao ML, Tu H, Jin L (1999) Determination of nitric oxide with ultramicrosensors based on electropolymerized films of metal tetraaminophthalocyanines. Talanta 48:1005–1011

Kato D, Kunitake M, Nishizawa M, Matsue T, Mizutani F (2005) Amperometric nitric oxide microsensor using two-dimensional cross-linked Langmuir–Blodgett films of polysiloxane copolymer. Sensors Actuators B 108:384–388

Lamattina L, García-Mata C, Graziano M, Pagnussat G (2003) Nitric oxide: the versatility of an extensive signal molecule. Annu Rev Plant Biol 54:109–136

Land SC, Porterfield DM, Sanger RH, Smith PJS (1999) The self-referencing oxygen-selective microelectrode: detection of transmembrane oxygen flux from single cells. J Exp Biol 202:211–218

Leshem YY (1996) Nitric oxide in biological systems. Plant Growth Regul 18:155–159

Leshem YY, Haramaty E (1996) The characterization and contrasting effects of the nitric oxide free radical in vegetative stress and senescence of *Pisum sativum* Linn. foliage. J Plant Physiol 148:258–263

Liu J, Rinzler AG, Dai H, Hafner JH, Bradley RK, Boul PJ, Lu A, Iverson T, Shelimov K, HuVman CB, Rodriguez-Macias F, Shon YS, Lee TR, Colbert DT, Smalley RE (1998) Fullerene pipes. Science 280:1253–1256

Longsworth LG (1957) Diffusion in Liquids. In: Gray DE (ed) *American Institute of Physics Handbook*. McGraw-Hill, New York

Malinski T, Taha Z (1992) Nitric oxide release from a single cell measured in situ by a porphyrinic-based microsensor. Nature 358:676–678

Malinski T, Taha Z, Grunfeld S, Burewicz A, Tomboulian P, Kiechle F (1993) Measurements of nitric oxide in biological materials using a porphyrinic microsensor. Anal Chim Acta 279:135–140

Mancuso S, Boselli M (2002) Characterisation of the oxygen fluxes in the division, elongation and mature zone of *Vitis* roots: influence of oxygen availability. Planta 214:767–774

Mancuso S, Marras AM (2003) Different pathways of the oxygen supply in the sapwood of young *Olea europaea* trees. Planta 216:1028–1033

Mancuso S, Papeschi G, Marras AM (2000) A polarographic, oxygen-selective, vibrating-microelectrode system for the spatial and temporal characterisation of transmembrane oxygen fluxes in plants. Planta 21:384–389

Mancuso S, Marras AM, Volker M, Baluska F (2005) Non-invasive and continuous recordings of auxin fluxes in intact root apex with a carbon-nanotube-modified and self-referencing microelectrode. Anal Biochem 341:344–351

Mao L, Yamamoto K, Zhou W, Jin L (2000) Electrochemical nitric oxide sensors based on electropolymerized film of M(salen) with central ions of Fe, Co, Cu, and Mn. Electroanalysis 12:72–77

Mitchell KM, Michaelis EK (1998) Multimembrane carbon fiber electrodes for physiological measurements of nitric oxide. Electroanalysis 10:81–88

Mullins GL, Sommers LE (1986) Cadmium and zinc influx characteristics by intact corn (*Zea mays* L.) seedlings. Plant Soil 96:153-164

Neill SJ, Desikan R, Clarke A, Hancock JT (2002) Nitric oxide is a novel component of abscisic acid signalling in stomatal guard cells. Plant Physiol 128:13–16

Ober ES, Sharp RE (1996) A microsensor for direct measurements of O2 partial pressure within plant tissue. J Exp Bot 296:447–454
Papeschi G, Mancuso S, Marras AM (2000) Electrochemical behaviour of Cu/CuSe microelectrode and its application in detecting temporal and spatial localisation of copper(II) fluxes along *Olea europaea* roots. J Solid Stat Electrochem 4:325–329
Pendley BD, Abruña HD (1990) Construction of submicrometer voltammetric electrodes. Anal Chem 62:782–784
Penner RM, Heben MJ, Longin TL, Lewis NS (1990) Fabrication and use of nanometer-sized electrodes in electrochemistry. Science 250:1118–1121
Romero-Puertas MC, Delledonne M (2003) Nitric oxide signalling in plant-pathogen interactions. IUBMB Life 55:579–583
Sanchez FG, Diaz AN, Pareja AJ (1996) Micellar liquid chromatography of plant growth regulators detected by derivative fluorometry. J Chromatogr A 723:227–233
Santelia D, Vincenzetti V, Azzarello E, Bovet L, Fukao Y, Düchtig P, Mancuso S, Martinoia E, Geisler M (2005) MDR-like ABC transporter AtPGP4 is involved in auxin-mediated lateral root and root hair development. FEBS Lett 579:5399–5406
Shibuki K (1990) An electrochemical microprobe for detecting nitric oxide release in brain tissue. Neurosci Res 9:69–76
Sivaguru M, Baluska F, Volkmann D, Felle HH, Horst WJ 1999 Impacts of aluminum on the cytoskeleton of the maize root apex. Short-term effects on the distal part of the transition zone. Plant Physiol 119:1073–1082
Trevin S, Bedioui F, Devynck J (1996) New electropolymerized nickel porphyrin films in aqueous solution. Application to the detection of nitric oxide. J Electroanal Chem 408:261–265
Weiler EW (1984) Immunoassay of plant growth regulators. Annu Rev Plant Physiol 35:85–95
Wendehenne D, Pugin A, Klessig DF, Durner J (2001) Nitric oxide: comparative synthesis and signalling in animal and plant cells. Trends Plant Sci 6:177–183
Wennmalm A, Lanne B, Petersson AS (1990) Detection of endothelial-derived relaxing factor in human plasma in the basal state and following ischemia using electron paramagnetic resonance spectrometry. Anal Biochem 187:359–63
Whalen WJ, Riley J, Nair P (1967) A microelectrode for measuring intracellular pO_2. J Appl Physiol 23:798–801
Xian Y, Sun W, Xue J, Luo M, Jin L (1999) Iridium oxide and palladium modified nitric oxide microsensor. Anal Chim Acta 381:191–196
Yamasaki H, Sakihama Y (2000) Simultaneous production of nitric oxide and peroxynitrite by plant nitrate reductase: in vitro evidence for the NR-dependent formation. FEBS Lett 468:89–92
Zhang XL, Cardoso L, Broderick M, Fein F, Lin J (2000) Novel integrated nitric oxide sensor based on carbon fiber electrode coated with NO-selective membranes. Electroanalysis 12:1113–1117

8 Electrophysiological Characterization of Plant Cation Channels

VADIM DEMIDCHIK,[1] ANATOLY SOKOLIK,[2] VLADIMIR YURIN[3]

8.1 Introduction

Cation channels are macromolecular protein pores in bio-membranes that catalyze passive cation influx and efflux (MacKinnon 2004). They do not use ATP energy to transport cations as opposed to active transporters such as pumps and carriers. Since cation channels are not limited by the rate of metabolic interactions, they saturate at much higher concentrations than active transporters and demonstrate low Q_{10} coefficients (<2.0). Cation channels consist of several transmembrane alpha helices that are also called transmembrane spans or transmembrane domains. These transmembrane domains form a pore region with a selectivity filter that selects cations over anions. Rearrangement of transmembrane domains causes pore opening (activation) or closing (deactivation). Different cation channels have different activators and inhibitors, including membrane voltage (V_m), H^+, divalent cations, G-proteins, ATP, cyclic nucleotides, hormones, ROS, amino acids, stretching and gravity. Specific chemical sites in the channel macromolecule are responsible for interactions with activating and inhibiting factors. Some cation channels have fixed anion surface charges outside and/or inside of the channel entry. These charges increase a local cation concentration and modify voltage-dependence, gating and selectivity of the channel (Green and Anderson 1991; Miedema 2002). Protons and divalent cations effectively screen surface charges and cause significant changes in the channel function. Cation channels are sensitive to a range of specific and non-specific blockers. Experiments with blockers, or so-called pharmacological analysis, are necessary for the selection between several groups of channels. For example, tetraethylammonium (TEA^+) is a specific blocker of K^+ channels that does not affect other cation channels (reviewed by Demidchik et al. 2002a). Blockers can be of "natural" origin, such as Ca^{2+}, Mg^{2+}, Zn^{2+} or H^+, or xenobiotics, for example Ba^{2+}, TEA^+, Cs^+, lanthanides, dihypropiridines, phenylalkylamines

[1] Department of Plant Sciences, University of Cambridge, Downing Street, Cambridge CB23EA, UK

[2] Laboratory of Plant Cell Physiology, Biological Faculty, Belarusian State University, 4 Skaryna Avenue, 220050, Minsk, Belarus

[3] Department of Physiology and Biochemistry of Plants, Biological Faculty, Belarusian State University, 4 Skaryna Avenue, 220050, Minsk, Belarus

Plant Electrophysiology – Theory & Methods (ed. by Volkov)

among others. Analysis of blockage provides important information about molecular determinants of the channel (Hille 1994).

Cation channels play multiple physiological roles in plants. They catalyze nutritional uptake of N (taken up as NH_4^+), macronutrient and micronutrient cations such as K^+, Ca^{2+}, Na^+, Fe^{2+}, Cu^{2+}, Ni^{2+}, Co^{2+}, Zn^{2+} and Mn^{2+}. Cation channels are responsible for the generation of negative resting V_m and action potentials. This is necessary for maintaining structural and functional integrity of the membrane, signaling processes and polarity. Cation channels are directly involved in osmotic balance and regulation of the turgor. This property of cation channels underlies stomata opening and closing. Calcium-permeable cation channels trigger Ca^{2+} signaling in plants that is involved in tissue and organ coordinated growth, development and stress responses. ROS, amino acids, purines, elicitors, hormones, gravity, different stresses and stretching act through activation of cationic channels. Having multiple physiological roles in plants, cation channels have been a subject of extensive study. Different physiological and molecular techniques have been employed for examination of physiology and structure of cation channels. Unfortunately, the crystal structure of plant cation channels remains unknown.

Significant progress has been achieved in our understanding of the molecular nature of cation channels in the last decade (reviewed by Davenport 2002; Demidchik et al. 2002a; White et al. 2002; Véry and Sentenac 2003). Many genes encoding plant cation channels have been identified and characterized molecularly. Analyses of knock-out plants and plants over-expressing K^+ channels showed for the first time physiological consequences of the lack or abundance of the particular channel. Nevertheless, molecular studies do not provide information regarding physiological characteristics of cation channels in intact cells. Electrophysiological techniques should be employed to establish channel properties in in vivo conditions. Here, we briefly review some of the most important electrophysiological techniques and provide examples of their use for studies of cation channels in plants.

8.2 Overview of electrophysiological techniques

The main question of the physiology of cation channels is how cations are transported through the channel and how this transport is regulated by internal and external factors. To investigate this, electrical currents or net fluxes mediated by cation movement through the channel should be measured.

There are two main types of electrophysiological recordings in plant cells: extracellular and intracellular recordings. Techniques for extracellular electrophysiological recordings include extracellular electrodes and "microelectrode ion flux estimation" (MIFE®). Intracellular recordings can be performed by impaling a cell with one or more fine-tipped electrodes (so-called "impalement techniques"), or by sticking a cell to the glass micropipette (so-called

patch-clamp technique). Intracellular recordings allow measuring V_m and/or membrane current (I_m). All these techniques have played significant roles in the characterization of plant cation channels. They have many advantages and disadvantages that are discussed below. Plant cation channels can also be characterized electrophysiologically by incorporation of purified channels into the planar lipid bilayers that mimic the cell membrane. This technique is not discussed here because it is reviewed elsewhere (Tester 1990; White 1998).

8.2.1 Extracellular recordings

In recording with extracellular electrodes, an electrode is placed in the extracellular medium and field-potentials contributed by the action potentials of many small cells or one giant alga cell are measured (Zawadzki 1980). This technique is useful for examination of generalized electrical responses of higher plant tissue or large cells, for example giant alga internodes. Despite their frequent use in early works, extracellular electrodes have not found much application in recent studies. For example, Favre et al. (2001) have applied extracellular electrodes for studying action potentials induced in *Arabidopsis thaliana* leaves by wounding and externally applied high concentration of KCl.

Another extracellular technique, namely MIFE®, has revolutionized the field of non-invasive plant membrane biology during the last decade (Shabala et al. 1997; Shabala 2000; Newman 2001; Babourina et al. 2002; Demidchik et al. 2002b, 2003; Hush et al. 1992; reviewed in this issue by Shabala). In this technique extracellular ion-selective microelectrodes "vibrate" (move forward/backward) with a period of few seconds near the surface of plant tissue or protoplast, with the simultaneous recording activities of several ions. Measuring ionic activity at two points at given distances (usually at about 50 and 100 μM from the tissue surface) provides a difference in ionic activity near the cell surface. Using the magnitude of this difference and taking into account the geometry of the surface, a special software calculates net ionic flux across the membrane surface. In contrast to extracellular electrodes MIFE® provides information about the ion selectivity of fluxes and numeric data on these fluxes. MIFE® can be applied to different types of tissues (including different root and leaf tissues), protoplasts (Shabala et al. 1998), root hairs (Babourina et al. 2001) and pollen tube (Tegg et al. 2005).

Apart from its many advantages, MIFE® also has limitations. Firstly, MIFE® does not allow recording ion activities higher than 0.2–1 mM. For example, this limitation renders impossible measurement of the toxic Na^+ influx under salinity conditions when [Na^+] is too high. Secondly, MIFE® recordings require a pause of about 2 min after addition of test substances to the assay chamber for mixing of solutions. This limitation is crucial when fluxes show fast kinetics of activation. Demidchik and Shabala (unpublished) have recently tried to decrease this pause and have developed a new MIFE®-based

approach to study fast changes in plant cation fluxes. They have minimized the volume of the assay chamber, changed the system for addition of solutions and decreased the time of mixing. This reduced the pause after mixing by several times. Thirdly, some dyes for MIFE® electrodes are not very selective between cations. For example, Na^+-selective dye also senses K^+. Therefore, corrections should be made if several cations are present in the assay solution. Fourthly, using MIFE® is strictly limited by surfaces that are directly exposed to the bathing medium. This technique does not allow measurements of fluxes in internal tissues that are covered by several layers of cells.

A pioneering combination of MIFE® with patch-clamp technique has been recently developed in Australia (Tyerman et al. 2001). This novel approach allows simultaneous measurements of cationic conductance and corresponded fluxes that makes it possible an accurate identification of ion-specificity of the conductance. Work on coupling MIFE with other electrophysiological (two-electrode voltage-clamp) and cellular (confocal imaging) techniques is now in progress in our laboratories and in the laboratory of Dr. Sergey Shabala. Successful combinations of these techniques will open new horizons in non-invasive technologies for the membrane biology of plants. Combination of MIFE®, two-electrode voltage-clamp and confocal microscopy will be particularly important for studying membrane systems that lack activities in patch-clamp configurations, for example plant neurotransmitter-activated receptors (Demidchik et al. 2004).

8.2.2 Intracellular recordings

8.2.2.1 Measurement of membrane potential by impaling with single electrode

Ideas of selective permeability to cations of the plant plasma membrane were developed in the beginning of the twentieth century by Osterhout in Harvard University (Osterhout 1908). This was followed by the first measurements of the plasma membrane potential in sea green alga *Valonia macrophysa* using impalements with sharp glass microelectrodes (Osterhout et al. 1927). In the next 30–40 years, membrane potentials were examined in *Valonia, Halicystis*, *Nitella, Chara,* and *Nitellopsis* (reviewed by Osterhout 1958; Hope and Walker 1975). In these experiments, giant plant cells were impaled with one electrode and V_m was measured between this electrode and indifferent electrode in the bathing solution. Studies of V_m in different conditions played significant roles in the plant physiology, particularly for understanding membrane selective permeability, electrogenic processes and action potentials. These studies predicted existence of cation channels in plant cell membranes. These days, measurement of V_m remains a useful tool in plant electrophysiology. For

example, using this technique, Ehrhardt et al. (1992) discovered Nod-factor-induced depolarization of the plasma membrane of plant root cells that later on was shown to be an effect of activation of inwardly rectifying K^+ channels (Kurkdjian et al. 2000; Ivashikina et al. 2001). Measuring V_m response to purines, Lew and Dearnaley (2000) have found depolarizing effect of these substances on the root plasma membrane. In 2003, Demidchik et al. showed that purine-activated cation channels that are similar to animal purinoceptors probably catalyze this depolarization effect. Dennison and Spalding (2000) found that glutamate depolarizes the plasma membrane of *Arabidopsis* root cells. This finding has led to the discovery of plant glutamate-activated cation channels (Demidchik et al. 2004). Impalement with sharp microelectrodes was a basis for development of intracellular ion-selective electrodes—a powerful experimental tool allowing measurements of activities of different cations in the cytosol and other cellular compartments (reviewed by Miller et al. 2001).

8.2.2.2 Two-electrode voltage-clamp technique

Measurement of V_m changes can indirectly show that cation channels exist in the cell membrane, but it does not inform on properties of cationic currents flowing through these channels. The nature of plant cationic conductances remained unclear until the first application on plants of two-electrode voltage-clamp technique by Findley (1961) and Hope (1961). This technique was previously successfully used in animal physiology by Hodgkin and Huxley (1952) for creation of "ion channel theory". Two-electrode voltage-clamp technique "clamps" or maintains V_m at a value the experimenter specifies. Voltage control is established using feedback through an operational amplifier circuit (see details in Halliwell et al. 1994). The main value of the voltage-clamp technique is that it allows one to measure the amount of ionic current crossing a membrane at any given voltage at a given time. Using two-electrode voltage-clamp, Belarusian and Russian physiologists characterized for the first time plant K^+ channels (Sokolik and Yurin 1981, 1986), Ca^{2+} channels (Plaks et al. 1979, 1980; Lunevsky et al. 1983) and non-selective cation channels (NSCC) (Yurin et al. 1991). Results that were obtained in experiments with giant alga cells have been summarized and reviewed by Tester in 1990.

A particular success in characterization of cation channels in alga was achieved due to the development of a very efficient voltage-clamp method that required only one electrode impalement (Sokolik and Yurin 1981, 1986; see Demidchik et al. 1997 for details). Impaling with one electrode decreased the damage of cells and significantly increased a percentage of successful preparations. In this method a second electrode was placed in extracellular space in 100 mM KCl solution (as in the cytosol) near nodes, which were isolated electrically from the middle of the cell by white petroleum jelly. The plasma membrane in

nodes has very low resistance. Therefore, extracellular electrodes are in contact with the cytosol, providing high quality voltage-clamping. An exciting development of this electrophysiological method was combined voltage-clamp and "turgescent" perfusion of the alga cell (Plaks et al. 1979, 1980) that allowed the study of tonoplast cation channels in vivo (without damaging cytoplasm). In this method, the perfusion of vacuole sap was carried out without rupture of the plasma membrane and cytoplasm. This was achieved by impaling glass microneedles into the vacuole through both nodes. Solution flow between two microneedles allowed changing the vacuole solution.

Two-electrode voltage-clamp technique is much less invasive than patch-clamp technique because it does not damage cell wall, membranes and the cytosol. However, this technique has not been extensively used for characterization of cation channels in higher plants. The main reasons of this include: inconvenience of using small cells, preparation problems in highly organized and specialized multi-cellular tissues and organs, impossibility to manipulate the intracellular solution and electrolyte leakage from the electrode to the cytosol that was significant in cells smaller than giant alga. Experimental conditions allowed using two-electrode voltage-clamp for studying cation channels only in a few higher plants. For example, this technique was used for the characterization of K^+ channels in guard cells (Blatt 1988; Langer et al. 2004) and root hairs (Lew 1991). In experiments on large cells of higher plants, for example root hairs, another significant limitation is current dissipation along the length of the cells (Meharg et al. 1994). This result in distortions of the current–voltage (I–V) curve, including consistent underestimation of the membrane current, linearization of the I–V and masking of conductance changes in the presence of transported substrates.

Current recording by two-electrode voltage-clamp technique has been recently coupled with the measurements of cytosolic Ca^{2+} activity in application on guard cells (Levchenko et al. 2005). Three-barreled electrodes were used: two barrels clamped voltage and third barrel loaded fluorescent dye FURA into the cytoplasm. Recordings were carried out on intact leaves that were not excised from the plant. This novel technique has a great potential for studying plant cation channels, particularly Ca^{2+} channels. This technique has already shown that data on ABA regulation of Ca^{2+} channels in protoplasts derived from guard cell should be revised (Levchenko et al. 2005).

Two-electrode voltage-clamp is also extensively used for characterization of plant cation channels heterologously expressed in *Xenopus laevis* oocytes (reviewed by Dreyer et al. 1999; Miller and Zhou 2000). Probably the most successful functional expression in *Xenopus* oocytes was carried out in the case of *Arabidopsis* K^+ channels (reviewed by Véry and Sentenac 2002).

In the late 1980s, two-electrode voltage-clamp was replaced by patch-clamp technique that brought electrophysiological measurements to a new quality by allowing the testing of protoplasts derived form small cells and different plant tissues.

8.2.2.3 Patch-clamp technique

Patch-clamp technique was developed in the 1970s by Erwin Neher and Bert Sakmann, who received the Nobel Prize in 1991. With this technique a glass micropipette with large diameter at the tip (> 1 μm) forms a high resistance contact (so-called gigaohm seal) with a protoplast derived from plant cells. Only one electrode measures voltage and injects current to clamp the voltage at constant level. Types of patch-clamp modes are shown in Fig. 8.1. They include: cell attached, whole cell, inside-out and outside-out modes that have advantages and disadvantages as shown in Fig. 8.1. Inside-out and outside-out modes are also called excised patches. Whole-cell and outside-out modes are the most frequently used patch-clamp configurations for studies plant cation channels. Patch-clamp can also be used in combination with imaging techniques (Taylor et al. 1997; Pei et al. 2000) and MIFE® (see above).

The first experiments with patch-clamp technique on plant cells were carried out in parallel by German and Israeli laboratories in middle eighties

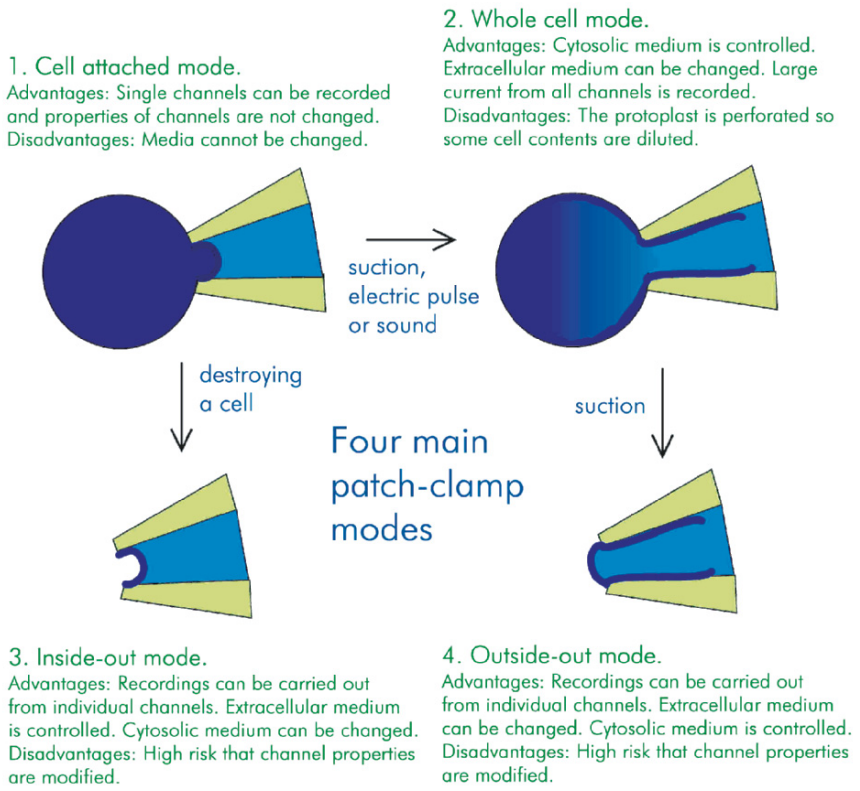

Fig. 8.1. Patch-clamp modes

(Moran et al. 1984; Schroeder et al. 1984). Two types of cation channels were characterized in these early studies. After these pioneering works, many laboratories worldwide employed patch-clamping for studying cation channels. Our modern knowledge about cation channels in higher plants is based on patch-clamp studies that were carried out in the last 20 years (reviewed by Hedrich and Schroeder 1989; Tester 1990; Tyerman and Schachtman 1992; Barkla and Pantoja 1996; Tanner and Caspari 1996; White 1998; Tyerman and Skerrett 1999; Zimmermann et al. 1999; Demidchik et al. 2002b; Véry and Sentenac 2002, 2003; White and Broadley 2003; Scholz-Starke et al. 2005).

Data accumulated in patch-clamp studies led to the functional classification of plant cation channels. They can be divided into three main groups. The first identified group is K^+ channels that includes two large classes of outwardly and inwardly rectifying K^+ channels, or so-called KOR and KIR, respectively. These channels are selective for K^+ and NH_4^+ over other cations and catalyze passive influx and redistribution of these cations. There is also physiological-molecular evidence that K^+ channels regulate stomata function (Hosy et al. 2003). Calcium channels are the second group of plant cation channels. This group include two main types including depolarization- (Thion et al. 1996, 1998) and hyperpolarization-activated Ca^{2+} channels (Gelli and Blumwald 1997; Hamilton et al. 2000, 2001; Kiegle et al. 2000; Véry and Davies 2000; Demidchik et al. 2002b; Stoelzle et al. 2003) (DACC and HACC, respectively). Calcium channels catalyze hormone-, elicitor-, and cyclic nucleotide-induced Ca^{2+} influx, and elevated Ca^{2+} uptake by growing cells. There is strong experimental evidence that these channels are crucial for plant signaling, stress responses, growth, development, mineral nutrition and other physiological functions (White 1998; White and Broadley 2003). It is still unclear whether plant Ca^{2+} channels are highly selective for Ca^{2+} over all other cations (like animal Ca^{2+} channel) or not. Genes encoding classic voltage-gated Ca^{2+} channels that are similar to animal counterparts have not been identified in plants (White et al. 2002; White and Broadley 2003). Therefore, many plant Ca^{2+}-permeable channels probably belong to non-selective cation channels (NSCC). NSCC are the third group of plant cation channels. They have about equal permeability for K^+ and Na^+ ($P_K/P_{Na} < 3$) and higher Ca^{2+} permeability ($P_{Ca}/P_K > 0.1–0.2$) (Demidchik et al. 2002a). Plant NSCC exist in the plasma membrane and in the tonoplast. Tonoplast NSCC are well studied at the physiological level in many species. There are two main classes of tonoplast NSCC: "slow-activating vacuolar channels" (SV channels) and "fast-activating vacuolar channels" (FV channels). SV channels show slow kinetics and activation at $[Ca^{2+}]_{cyt.} > 0.5–5$ μM. FV channels rapidly activate and function at physiological $[Ca^{2+}]_{cyt.}$ ($< 0.3–1$ μM). The laboratory of Professor Dale Sanders (University of York) has recently characterized, for the first time, tonoplast NSCC at the molecular level (Peiter et al. 2005). They have shown that TPC1 homologue is a part of SV channel in the tonoplast of *Arabidopsis* leaf cells and that this channel is involved in the regulation of stomata closing at high extracellular Ca^{2+} concentrations. Plasma membrane NSCC embrace

four main classes: (1) constitutive NSCC; (2) reactive oxygen specie-activated (ROS-activated) NSCC; (3) ligand-activated NSCC; and (4) mechanosensitive NSCC. Constitutive NSCC are active in the plasma membrane without activating factors. For opening ligand-activated NSCC interact with a chemical ligand. ROS-activated NSCC require H_2O_2 or $OH^{\bullet}$ for the activation. Mechanosensitive NSCC require plasma membrane stretching for activation. All these channels vary in their voltage-dependence, pharmacology and characteristics of unitary conductances (see review by Demidchik et al. 2002a).

Apart from its many advantages, the patch-clamp technique also has some problems. On of the main problems is that treatment of plant cells by cellulytic enzymes damages native channels and their regulation. For example, the treatment by cellulases during protoplast isolation induces a oxidative burst in plant cells and activations of hydrolytic enzymes (Brudern and Thiel 1999; Kennedy and de Filippis 2004). This can lead to degradation of membrane and cytosolic proteins and to changes of cation channel properties or even disappearance of some cation channels (Demidchik, unpublished data). Treatment of plants with SH-reducing agents is a possible way to avoid undesirable artifacts from the oxidative damage. However, it is not a "panacea" because in natural conditions SH-groups are not maintained as permanently reduced, so SH-reducing agents may cause artifacts too.

Another major problem of patch-clamp technique is the replacement of the cytosolic native solution by artificial solution in whole cell mode. This provides the control of intracellular medium but, on the other hand, it also damages cytosolic regulation of the channels. This problem underlies the lack of successful patch-clamp characterization of plant ionotropic receptors (Demidchik et al. 2004). Experiments with plant purine-activated conductances have recently shown that purines cause reliable Ca^{2+} influx (as measured by aequorin luminometry and MIFE®) in all root cells and root-derived protoplasts; however, they are 5 times less effective in patch-clamped protoplasts (Demidchik et al., unpublished).

The quality of voltage-clamping in patch-clamp experiments is good if protoplast membrane resistance is higher than resistance of the patch pipette. The technical problem arises when the ratio between the resistance of patch pipette and protoplast membrane increases. If the resistance of the patch pipette is higher than the resistance of the patched membrane, the voltage is manly clamped on the tip of the pipette but not on the membrane. This particularly affects I-V curve rectification and currents recorded under maximally depolarized or hyperpolarized voltages. The study of vacuolar cation channels are particularly in danger of artifacts due to very low resistance of isolated vacuoles. For example, this phenomenon explains the absence of rectification in many early recordings made on tonoplast cationic conductances. Smaller patches, diluted solutions and lower resistance of the pipette help to avoid artifacts.

Another obvious problem of patch-clamp technique is that not all plant cells and tissues give protoplasts suitable for patching. It is also difficult to

select between protoplasts that are derived from different tissues. Specific GFP labeling of plant tissues was successfully used for the selection of tissue-specific protoplasts in *Arabidopsis* (Kiegle et al. 2000; Demidchik et al. 2003). Using laser ablation in combination with plasmolysis/deplasmolysis step is another approach to isolate protoplasts from specific tissues (Taylor et al. 1997; Véry and Davies 2000; Foreman et al. 2003). Using this method protoplasts were isolated from *Fucus* pollen tube and *Arabidopsis* root hairs that allowed characterization of Ca^{2+} channels in these species.

8.3 Conclusions and perspectives

Electrophysiological characterization of cationic conductances and cation channels in plants has been progressing during almost 80 years. It adapted many methods from animal physiology but also developed plant-specific approaches, for example MIFE® and cell wall laser microsurgery for protoplast isolation. Application of voltage-clamp techniques resulted in the characterization of cation channels in many plant species and in different tissues and functional classification of plant cation channels. Electrophysiological techniques should be used with care and experimenters must take into account possible artifacts and problems. The future of plant electrophysiology is in developing new non-invasive techniques and approaches that cause less damage to the cell and channels than patch-clamping. Combining different physiological methods with electrophysiological techniques also have good perspectives.

References

Babourina O, Hawkins B, Lew RR, Newman I, Shabala S (2001) K^+ transport by *Arabidopsis* root hairs at low pH. Aust J Plant Physiol 28:635–641

Babourina O, Newman I, Shabala S (2002) Blue light-induced kinetics of H^+ and Ca^{2+} fluxes in etiolated wild-type and phototropin-mutant *Arabidopsis* seedlings. Proc Natl Acad Sci USA 99:2433–2438

Barkla BJ, Pantoja O (1996) Physiology of ion transport across the tonoplast of higher plants. Annu Rev Plant Physiol Plant Mol Biol 47:159–184

Blatt (1988) Potassium-dependent, bipolar gating of K^+ channels in guard cells. J Membr Biol 102:235–246

Brudern A, Thiel G (1999) Effect of cell-wall-digesting enzymes on physiological state and competence of maize coleoptile cells. Protoplasma 209:246–255

Davenport R (2002) Glutamate receptors in plants. Ann Bot 90:549–557

Demidchik V, Sokolik A, Yurin V (1997) The effect of Cu^{2+} on ion transport systems of the plant cell plasmalemma. Plant Physiol 114:1313–1325

Demidchik V, Davenport RJ, Tester MA (2002a) Nonselective cation channels in plants. Annu Rev Plant Biol 53:67–107

Demidchik V, Bowen HC, Maathuis FJM, Shabala SN, Tester MA, White PJ, Davies JM (2002b) *Arabidopsis thaliana* root non-selective cation channels mediate calcium uptake and are involved in growth. Plant J 32:799–808

Demidchik V, Shabala SN, Coutts KB, Tester MA, Davies JM (2003) Free oxygen radicals regulate plasma membrane Ca^{2+} and K^+-permeable channels in plant root cells. J Cell Sci 116:81–88

Demidchik V, Adobea P, Tester MA (2004) Glutamate activates sodium and calcium currents in the plasma membrane of *Arabidopsis* root cells. Planta 219:167–175

Dennison KL, Spalding EP (2000) Glutamate-gated calcium fluxes in *Arabidopsis*. Plant Physiol 124:1511–1514

Dreyer I, Horeau C, Lemaillet G, Zimmermann S, Bush DR, Rodriguez-Navarro A, Schachtman DP, Spalding EP, Sentenac H, Gaber RF (1999) Identification and characterization of plant transporters using heterologous expression systems. J Exp Bot 50:1073–1087

Ehrhardt DW, Atkinson EM, Long SR (1992) Depolarization of Alfaalfa root hair membrane potential by *Rhizobium mellitoti* Nod factors. Science 256:998–1000

Favre P, Greppin H, Agosti RD (2001) Repetitive action potentials induced in *Arabidopsis thaliana* leaves by wounding and potassium chloride application. Plant Physiol Biochem 39:961–969

Findley GP (1961) Voltage-clamp experiments with *Nitella*. Nature 191:812–814

Foreman J, Demidchik V, Bothwell JHF, Mylona P, Miedema H, Torres MA, Linstead P, Costa S, Brownlee C, Jones JDG, Davies JM, Dolan L (2003) Reactive oxygen species produced by NADPH oxidase regulate plant cell growth. Nature 422:442–446

Gelli A, Blumwald E (1997) Hyperpolarization-activated Ca^{2+}-permeable channels in the plasma membrane of tomato cells. J Membr Biol 155:35–45

Green WN, Anderson OS (1991) Surface charges and ion channel function. Annu Rev Physiol 53:341–359

Halliwell JV, Plant TD, Robbins J, Standen NB (1994) Voltage clamp techniques. In: Ogden DC (ed) Microelectrode techniques. The Plymouth workshop handbook, 2nd edn. Company of Biologists, Cambridge, UK

Hamilton DWA, Hills A, Kohler B, Blatt MR (2000) Ca^{2+} channels at the plasma membrane of stomatal guard cells are activated by hyperpolarization and abscisic acid. Proc Natl Acad Sci USA 97: 4967–4972

Hamilton DWA, Hills A, Kohler B, Blatt MR (2001) Extracellular Ba^{2+} and voltage interact to gate Ca^{2+} channels at the plasma membrane of stomatal guard cells. FEBS Lett 491: 99–103

Hedrich R, Schroeder JI (1989) The physiology of ion channels and electrogenic pumps in higher plants. Annu Rev Plant Physiol Plant Mol Biol 40:539–569

Hille B (1994) Ionic channels of excitable membranes. Sinauer, Sunderland, Mass.

Hodgkin AL, Huxley AF (1952) A Quantitative description of membrane current and its application to conduction and excitation in nerve. J Physiol 117:500–544

Hope AB (1961) Ionic relation of cells of *Chara australis*. V. The action potential. Aust J Biol Sci 15:69–82

Hope AB, Walker NA (1975) The physiology of giant algal cells. Cambridge University Press, Cambridge

Hosy E, Vavasseur A, Mouline K, Dreyer I, Gaymard F, Poree F, Boucherez J, Lebaudy A, Bouchez D, Very AA, Simonneau T, Thibaud JB, Sentenac H (2003) The *Arabidopsis* outward K^+ channel GORK is involved in regulation of stomatal movements and plant transpiration. Proc Natl Acad Sci USA 100:5549–5554

Hush JM, Newman IA, Overall RL (1992) Utilization of the vibrating probe and ion-selective microelectrode techniques to investigate electrophysiological responses to wounding in pea roots. J Exp Bot 43:1251–1257

Ivashikina N, Becker D, Ache P, Meyerhoff O, Felle HH, Hedrich R (2001) K^+ channel profile and electrical properties of *Arabidopsis* root hairs. FEBS Lett 508:463–469

Kennedy BF, de Filippis LF (2004) Tissue degradation and enzymatic activity observed during protoplast isolation in two ornamental *Grevillea* species. In Vitro Cell Dev Biol Plant 40:119–125

Kiegle E, Gilliham M, Haseloff J, Tester M (2000) Hyperpolarisation-activated calcium currents found only in cells from the elongation zone of *Arabidopsis thaliana* roots. Plant J 21:225–229

Kurkdjian A, Bouteau F, Pennarun AM, Convert M, Cornel D, Rona JP, Bousquet U (2000) Ion currents involved in early Nod factor response in *Medicago sativa* root hairs: a discontinuous single-electrode voltage-clamp study. Plant J 22:9–17

Langer K, Levchenko V, Fromm J, Geiger D, Steinmeyer R, Lautner S, Ache P, Hedrich R (2004) The poplar K^+ channel KPT1 is associated with K^+ uptake during stomatal opening and bud development. Plant J 37:828–838

Levchenko V, Konrad KR, Dietrich P, Roelfsema MRG, Hedrich R (2005) Cytosolic abscisic acid activates guard cell anion channels without preceding Ca^{2+} signals. Proc Natl Acad Sci USA 102:4203–4208

Lew RR (1991) Electrogenic transport properties of growing *Arabidopsis* root hairs—the plasma membrane proton pump and potassium channels. Plant Physiol 97:1527–1534

Lew RR, Dearnaley JDW (2000) Extracellular nucleotide effects on the electrical properties of growing *Arabidopsis thaliana* root hairs. Plant Sci 153:1–6

Miller AJ, Zhou JJ (2000) *Xenopus* oocytes as an expression system for plant transporters. Biochim Biophys Acta Biomembr 1465:343–358

Lunevsky VZ, Zherelova OM, Vostrikov IY, Berestobsky GN (1983) Excitation of characeae cell membranes as a result of activation of calcium and chloride channels. J Membr Biol 72:43–58

MacKinnon R (2004) Potassium channels and the atomic basis of selective ion conduction (Nobel lecture). Angew Chem Int Edit 43:4265–4277

Meharg AA, Maurosset L, Blatt MR (1994) Cable correction of membrane currents from root hairs of *Arabidopsis thaliana* L. J Exp Bot 45:1–6

Miedema H (2002) Surface potentials and the calculated selectivity of ion channels. Biophys J 82:156–159

Miller AJ, Zhou JJ (2000) *Xenopus* oocytes as an expression system for plant transporters. Biochim Biophys Acta Biomembr 1465:343–358

Miller AJ, Cookson SJ, Smith SJ, Wells DM (2001) The use of microelectrodes to investigate compartmentation and the transport of metabolized inorganic ions in plants. J Exp Bot 52:541–549

Moran N, Ehrenshtein G, Iwasa K, Bare C, Mischke C (1984) Ion channels in plasmalemma of wheat protoplasts. Science 226:835–838

Newman IA (2001) Ion transport in roots: measurement of fluxes using ion-selective microelectrodes to characterize transporter function. Plant Cell Environ 24:1–14

Osterhout WJV (1908) The organization of the cell with respect to permeability. Science 38:408–409

Osterhout WJV (1958) The use of aquatic plants in the study of some fundamental problems. Annu Rev Plant Physiol 8:1–11

Osterhout WJV, Damon EB, Jacques AG (1927) Dissimilarity of inner and outer protoplasmic surfaces in *Valonia*. J Gen Physiol 11:193–205

Pei ZM, Murata Y, Benning G, Thomine S, Klusener B, Allen GJ, Grill E, Schroeder JI (2000) Calcium channels activated by hydrogen peroxide mediate abscisic acid signalling in guard cells. Nature 406:731–734

Peiter E, Maathuis FJM, Mills LN, Knight H, Pelloux M, Hetherington AM, Sanders D (2005) The vacuolar Ca^{2+}-activated channel TPC1 regulates germination and stomatal movement. Nature 434:404–408

Plaks AV, Sokolik AI, Yurin VM, Goncharik MN (1979) Chloride channel activation and excitation of *Nitella* cell tonoplast. Rep Acad Sci Belarus 23:947–949

Plaks AV, Sokolik AI, Yurin VM (1980) Excitable calcium channels of *Nitella* cell tonoplast. Izvestiya of the Academy of Sciences of BSSR, Biology section 1:121–124

Schroeder JI, Hedrich R, Fernandez JM (1984) Potassium-selective single channels in guard cell protoplasts of *Vicia faba*. Nature 312:361–362

Scholz-Starke J, Gambale F, Carpaneto A (2005) Modulation of plant ion channels by oxidizing and reducing agents. Arch Biochem Biophys 434:43–50

Shabala S (2000) Ionic and osmotic components of salt stress specifically modulate net ion fluxes from bean leaf mesophyll. Plant Cell Environ 23:825–837

Shabala SN, Newman IA, Morris J (1997) Oscillations in H^+ and Ca^{2+} ion fluxes around the elongation region of corn roots and effects of external pH. Plant Physiol 113:111–118
Shabala SN, Newman IA, Whittington J, Juswono UP (1998) Protoplast ion fluxes: their measurements and variation with time, position and osmoticum. Planta 204:146–152
Sokolik AI, Yurin VM (1981) Transport activity of potassium channels in the plasmalemma of *Nitella* cells at rest. Soviet Plant Physiol 28:294–301
Sokolik AI, Yurin VM (1986) Potassium channels in plasmalemma of *Nitella* cells at rest. J Membr Biol 89:9–22
Stoelzle S, Kagawa T, Wada M, Hedrich R, Dietrich P (2003) Blue light activates calcium-permeable channels in *Arabidopsis* mesophyll cells via the phototropin signaling pathway. Proc Natl Acad Sci USA 100:1456–1461
Tanner W, Caspari T (1996) Membrane transport carriers. Annu Rev Plant Physiol Plant Mol Biol 47:595–626
Taylor A, Manison N, Brownlee C (1997) Regulation of channel activity underlying cell volume and polarity signals in Fucus. J Exp Bot 48:579–588
Tegg RS, Melian L, Wilson CR, Shabala S (2005) Plant cell growth and ion flux responses to the streptomycete phytotoxin thaxtomin A: calcium and hydrogen flux patterns revealed by the non-invasive MIFE technique. Plant Cell Physiol 46:638–648
Tester M (1990) Plant ion channels: whole-cell and single channel studies. New Phytol 114:305–40
Thion L, Mazars C, Thuleau P, Graziana A, Rossignol M, Moreau M, Ranjeva R (1996) Activation of plasma membrane voltage-dependent calcium-permeable channels by disruption of microtubules in carrot cells. FEBS Lett 393:13–18
Thion L, Mazars C, Nacry P, Bouchez D, Moreau M, Ranjeva R, Thuleau P (1998) Plasma membrane depolarization-activated calcium channels, stimulated by microtubule-depolymerizing drugs in wild-type *Arabidopsis thaliana* protoplasts, display constitutively large activities and a longer half-life in ton 2 mutant cells affected in the organization of cortical microtubules. Plant J 13:603–610
Tyerman SD, Schachtman DP (1992) The role of ion channels in plant nutrition and prospects for their genetic manipulation. Plant Soil 146:137–144
Tyerman SD, Skerrett IM (1999) Root ion channels and salinity. Sci Hortic 78:175–235
Tyerman SD, Beilby M, Whittington J, Juswono U, Newman I, Shabala S (2001) Oscillations in proton transport revealed from simultaneous measurements of net current and net proton fluxes from isolated root protoplasts: MIFE meets patch-clamp. Austr J Plant Physiol 28:591–604
Véry AA, Davies JM (2000) Hyperpolarization-activated calcium channels at the tip of *Arabidopsis* root hairs. Proc Natl Acad Sci USA 97:9801–9806
Véry A-A, Sentenac H (2002) Cation channels in the *Arabidopsis* plasma membrane. Trends Plant Sci 7:168–175
Véry A-A, Sentenac H (2003) Molecular mechanisms and regulation of K^+ transport in higher plants. Annu Rev Plant Biol 54:575–603
White PJ (1998) Calcium channels in the plasma membrane of root cells. Ann Bot 81:173–183
White PJ, Broadley MR (2003) Calcium in plants. Ann Bot 92:487–511
White PJ, Bowen HC, Demidchik V, Nichols C, Davies JM (2002) Genes for calcium-permeable channels in the plasma membrane of plant root cells. Biochim Biophys Acta Rev Biomembr 1564:299–309
Yurin VM, Sokolik AI, Kudryashov AP (1991) Regulation of ion transport through plant cell membranes. Science and Engineering, Minsk
Zawadzki T (1980) Action potentials in *Lupinus angustifolius* L. shoots. 5. Spread of excitation in the stem, leaves, and root. J Exp Bot 31:1371–1377
Zimmermann S, Ehrhardt T, Plesch G, Muller-Rober B (1999) Ion channels in plant signalling. Cell Mol Life Sci 55:183–203

9 Magnetic Measurements in Plant Electrophysiology

Zvonko Trontelj,[1] Gerhard Thiel,[2] Vojko Jazbinsek[1]

9.1 Introduction

Plants show a huge range of dynamic electrical phenomena, including triggered (Umrath 1929) and autonomous action potentials (AP) (Gradmann et al. 1993), or stimulus-evoked slow transient depolarizations (Roblin and Bonnemain 1985). This electrical activity can comprise singular events (Umrath 1929), trains of periodic activity (Williams and Pickard 1972) or even long lasting periodic oscillations of the membrane voltage (Gradmann et al. 1993). Electrical activity can occur in single cells (Gradmann 1976; Bauer et al. 1997) as well as in complex plant tissues (Bentrup 1979). Many of these electrical phenomena resemble electrical activity in animal cells, and by pure analogy it has been proposed that plant cells may function like nerves, and that plants may even have the equivalent of a nervous system (Baluska et al. 2005). Irrational views like these are only possible on the background of a serious ignorance of the physics and molecular basis of electrical activity in plants. Currently we neither really understand the elementary mechanisms underlying electrical activity in plants on the same level as for example the action potential in animal cells, nor do we have clear-cut ideas on their physiological roles. In most cases also, the cellular connections and pathways that propagate electrical activity are not yet certain. Consequently, the mechanistic basis for propagation of electrical activity is also not resolved; it is still a matter of debate whether the signal is really propagated electrically like in nerves or the result of a traveling chemical wave.

The application of new experimental methods such as patch clamp technology (Okihara et al. 1991; Homann and Thiel 1994) has in the past 2 decades brought some deeper insight into the molecular basis of membrane excitation in plants. Combination of classical electrophysiology with fluorescent markers (Rhodes et al. 1996) or molecular sensors (Pena-Cortes et al. 1995) is now also paving the way to address fundamental questions on long distance propagation. A new promising method to address many of these open questions is provided by the magnetic measurements of electrical

[1] Physics Department, IMFM, University of Ljubljana, 1000-Ljubljana, Slovenia (e-mail: zvonko.trontelj@fmf.uni-lj.si)

[2] Institute for Botany, Plant Biophysics, Darmstadt University of Technology, D-64287, Darmstadt, Germany

Plant Electrophysiology – Theory & Methods (ed. by Volkov)

activity in plants. This non-invasive method presents a tool for both high-resolution recordings on the cellular level and time resolved imaging of electrical activity over a whole plant. The present review guides through the theoretical background of the method and shows its application in a few case studies.

9.2 On SQUID sensors

A suitable method to obtain electric current is by measuring the magnetic field and calculating the current by applying Ampère's law or Biot-Savart's law. This method has in addition the advantage of being non-disturbing—what is more than non-invasive—it does not even touch the current source. The frequency of measured current is also an important parameter. High frequency currents can be easily detected even if they are very weak. On the other side, weak quasi-dc or even dc currents are not easily detected magnetically.

The promising magnetic detector of weak quasi-dc currents became operational with the development of superconducting quantum interference devices, known by the acronym SQUID. These most sensitive sensors for low frequency magnetic fields are available since early the 1970s (Zimmerman et al. 1970). Today, they have improved to the extent that we can also measure the very weak human brain signals and practically all other electrophysiological signals in living organisms.

What is the SQUID (See for instance Tinkham 1996) and how does it work? The quick answer is: SQUID is a very sensitive magnetic flux-to-voltage converter for low frequency magnetic fields. In order to get a view into the functioning of SQUID, we have to apply the rules for describing physics of the micro-world: the quantum mechanics. We need to look at three important facts in physics: superconductivity, quantum tunneling and magnetic flux quantization.

The phenomenon of superconductivity was discovered in 1911 by the Dutch physicist Heike Kamerlingh Onnes (1911). He noticed that mercury shows no electrical resistance when cooled to the temperature of liquid helium (4.2 K). Later on, several other metals and alloys were found to experience the same effect when cooled to very low temperatures. The explanation of this low temperature superconductivity [in opposition to the high temperature conductivity discovered by Karl Alex Mueller and Johannes Georg Bednorz in 1986 (Bednorz and Mueller 1986) and not yet sufficiently explained] came rather late: In 1957, John Bardeen, Leon N. Cooper and J. Robert Schrieffer published the theory (Bardeen et al. 1957) now known as the BCS theory of superconductivity. They have explained superconductivity as a result of the existence of pairs of electrons, now called Cooper pairs, each of which is formed of two electrons of opposite spin and momentum. Hence, the Cooper pair has a zero net spin and zero net momentum. Pairing of electrons is caused

by the attractive force. Behind is an interaction between the negative charge of electrons and the positive charge of the ion cores in the material that is in the superconducting phase. The binding energy of the Cooper pair is very low (in the range of meV), but high enough to prevent each pair from moving apart by scattering. Consequently, pairs of electrons can move through the superconducting material without being affected by opposing forces and superconductive material shows no macroscopic electric resistance. On the other side, single electrons in normal conductors experience several obstacles: lattice vibrations, impurities, defects in crystal lattice. This scattering of electron is macroscopically demonstrated by the electric resistance.

Quantum mechanical description of superconducting current formed by the Cooper pairs requires the knowledge of a wave function. This useful mathematical tool to describe the micro-world of quantum systems is characterized by the amplitude and the phase, similarly as in all forms of waves in physics. Superconductors here also are something special: They need only one wave function to describe all Cooper pairs. If no current flows, all the pairs also have the same phase (they are phase coherent).

After the BCS theory appeared, several calculations followed and in 1962 Brian D. Josephson (Josephson 1962) predicted an effect, now called the Josephson effect. He considered two superconductors separated by a thin layer of an insulating material, which acts as a barrier for the current flow. What will happen with the superconducting current if the current circuit is established (Fig. 9.1)? It is reasonable to expect that the wave function enters the barrier region from both sides of the superconductors, since there are Cooper pairs on both sides of the barrier. If the barrier is thin enough, the wave functions from both sides will overlap. And if the overlap is sufficient over the barrier space, the phases of both wave functions are locked together. Consequently, the Cooper pairs can experience what is called in quantum mechanics tunneling. That means they can penetrate the barrier without breaking up. This kind of Cooper pair tunneling is the Josephson tunneling. The Josephson junction of the two superconductors separated by the insulation barrier acts as some sort of weak superconductor. The maximal supercurrent that flows through this weak superconductor is determined by barrier geometry, material and temperature. Quantitatively, the current through the junction is given

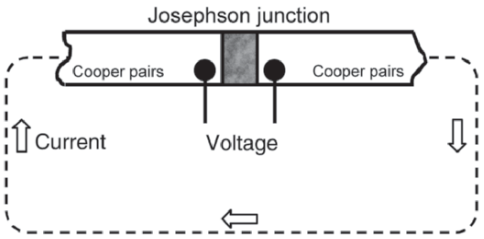

Fig. 9.1. Josephson junction in superconducting circuit

by the first Josephson equation. This effect is called the direct-current (dc) Josephson effect, to distinguish it from the also existing alternating-current (ac) Josephson effect, described by the second Josephson equation.

Josephson junctions have several applications in the superconducting electronics, however their most spread application until now is in SQUIDs.

Before describing SQUID in detail, we have to mention the last fundamental stone: the magnetic flux quantization. This is an example of quantization which is observable in macroscopic dimension. Considering a superconducting ring or a hole in a superconductor, F. London has shown that the fluxoid ϕ', defined as

$$\phi' = \phi + \frac{m^*}{n_s^* e^{*2}} \oint \mathbf{j}_s \cdot d\mathbf{s}, \tag{1}$$

takes only values of integral multiples of the flux quantum $\phi_0 = h/2e = 2.07 \cdot 10^{-15}$ Vs. ϕ is here the outer magnetic flux through the surface encircled by the integration path, $\mathbf{j}_s$ is the supercurrent density, m^*, n_s^*, e^* refer to the mass, density and charge of a Cooper pair. Taking the integration path deeper inside the superconducting ring, we see that there is $\mathbf{j}_s = 0$ and consequently $\phi' = \phi = n\phi_0$, i.e. the flux itself is quantized in such a case. The flux quantization was experimentally demonstrated in 1961 (Deaver and Fairbank 1961).

Today, we use SQUID mainly in the so-called dc-SQUID configuration. Basically, it consists of a superconducting ring interrupted by two Josephson junctions (Fig. 9.2a). To get out of this geometrical configuration sensor, which could be described as a flux-to-voltage converter, we have a) to cool the dc-SQUID to the superconducting state (usually we work with classical superconductors and we cool the dc-SQUID to 4.2 K, to the temperature of liquid helium) and b) we have to send current (mainly of Cooper pairs of electrons) symmetrically through it (Fig. 9.2b). According to that mentioned earlier, the Cooper pairs will tunnel trough both Josephson junctions (weak

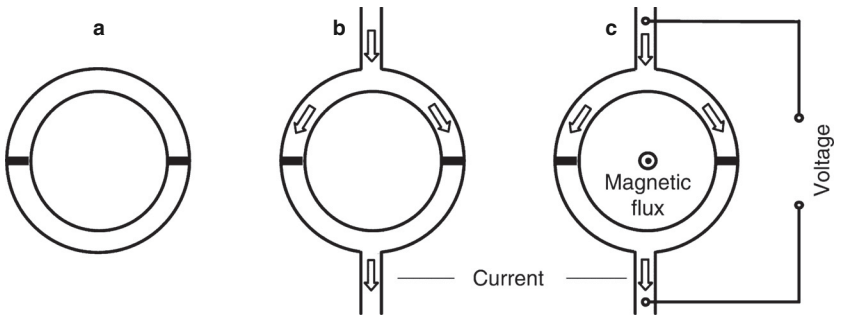

Fig. 9.2. dc-SQUID configuration: **a** superconducting ring with two Josephson junctions, **b** the same with bias current, **c** with magnetic flux threading the ring

links) and afterwards proceed the flow on (Fig. 9.2b). Let us now apply a slowly increasing magnetic field to the dc-SQUID with biased current so that some magnetic flux will thread the ring. This magnetic field will alter the current. Primarily, the quantum mechanical phase difference across each of the two junctions will be changed and consequently the critical current of the SQUID: We will observe that the current will oscillate between the maximal and minimal value as the magnetic flux will increase trough the ring. (The same alteration in current happens if the magnetic flux through the ring decreases.) The current maximum occurs always when the flux trough the ring equals to the integer number of flux quanta ϕ_0. The minimum of current corresponds to the half integer values of ϕ_0. What we measure is not the current, but rather the voltage across the SQUID (Fig. 9.2c). Voltage, which also oscillates between the maximal and minimal values, is more practical for further detection with the commonly used procedure in electronic devices, including the lock-in-amplification and the negative feedback loop technique, so that we finally have a zero balance detector, which enables us to measure 10^{-5} ϕ_0 or better on the linear part of the slope between N and $N+1/2$ ϕ_0. In Fig. 9.3a one can see schematically the current versus voltage dependence for both extreme values of magnetic flux and voltage versus magnetic flux dependence. The pattern in V versus ϕ/ϕ_0 curve (Fig. 9.3b) reminds us to the interference phenomena in waves, as for instance in optics. Therefore the name quantum interference effect. Here we observe the interference of two wave functions describing the events in both Josephson junctions of a dc-SQUID.

Knowing the energy associated with magnetic flux $\left(\frac{1}{2}LI^2\right)$ we can obtain for the SQUIDs of today's production a sensitivity in the order of about 10^{-32} J. That is not far from the limit following from the Heisenberg's uncertainty principle. Obviously, we have to "bring" the measured magnetic field to the SQUID, which is cooled with the liquid He in the cryostat and is also well protected with the superconducting shield (the Meissner effect is exploited). We do that by inductive coupling of the measured magnetic field with the dc-SQUID via the so called flux transformer (Fig. 9.4). We see from Fig. 9.4 that the flux transformer can be in a form of magnetometer or gradiometer of different order. All these input circuits, as they are often called,

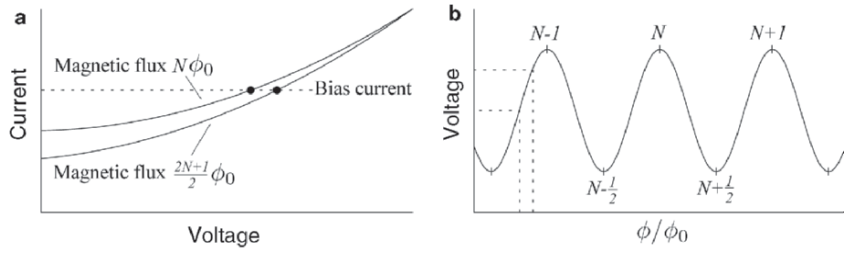

Fig. 9.3. **a** Current vs voltage, **b** voltage vs ϕ/ϕ_0 for dc-SQUID

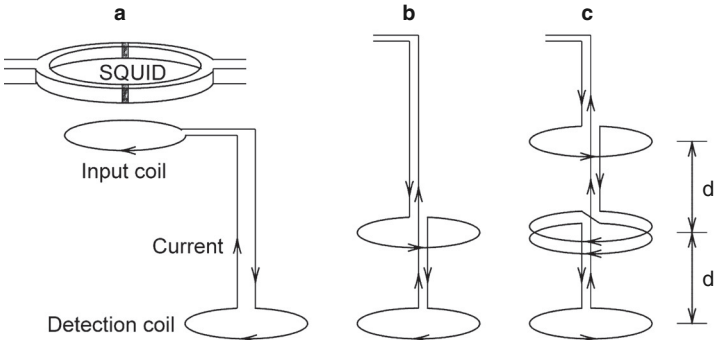

Fig. 9.4. **a** Schematic presentation of flux transformer, which consists of a detection coil (magnetometer) connected with the SQUID's input coil. In noisy environment, the detection coil can be arranged in **b** 1st order gradiometer or **c** 2nd order gradiometer configuration

are built of superconducting material and inductively coupled to the dc-SQUID. Hence, they experience the appearance (or change) of supercurrent if an external magnetic field is present or if it alters. This current causes a flux in the dc-SQUID and we read it as an output signal in terms of a voltage change in SQUID electronics. Because the magnetometer's detection coil is often larger then the dc-SQUID ring, we reach higher final sensitivity. The resolution of a good system is close to 1 fT (1femtotesla=10^{-15} T). The magnetometer input coil is practically applicable only in the extremely well magnetically shielded measuring room (Erné et al. 1981). With the gradiometer configuration, we can further eliminate disturbances and noise if their source is far enough from the two in opposite direction wound coils. Such an extensively disturbing source can be considered as uniform at the point of the two gradiometer coils and its contribution cancels out. The gradiometer of the 2nd order cancels out the homogeneous contribution and the 1st gradient. In practice, we go up to 3rd order gradiometer.

So far, we have described the single dc-SQUID with the proper input circuit and magnetic shielding. Historically, the first SQUID measuring systems were using the radiofrequency field as the biasing source (Zimmerman et al. 1970). This type of SQUD is called the rf-SQUID, and consists of a single Josephson junction in a superconducting ring. The ring is inductively coupled with the coil of an rf oscillator, which forms a resonant circuit. The driving current is the rf current. The voltage across the resonant circuit oscillates when the outer magnetic flux alters. Very few rf-SQUIDs are still in operation. They are less sensitive then the dc-SQUIDs. The production of dc-SQUID is based on the multilayer thin film technology known from microelectronics and it can be done in a high number of samples on a silicon substrate.

During the 40 years (Jaklevic et al. 1964) of SQUIDs history we have seen considerable progress. Until the early 1980s, we were using single channel measuring systems and performing scanning over the area where the magnetic field distribution was later re-constructed offline. In the mid and late 1980s the multichannel devices came in use and they were consisting of more and more SQUIDs built in the system (4, 7, . . . 37) (Koch et al. 1991). The new combinations included the electronic design of gradiometers in different parallel planes (Drung 1995) and also spatial 3D orientation of some magnetometers. This provides real 3D information by using all three components of the measured magnetic field vector (Kotani et al. 1997).

One sector of SQUID development in the recent years went towards construction of SQUID systems (usually one channel) with the highest spatial resolution. Sometimes the expression SQUID-microscope (Baudenbacher et al. 2002) is used for these devices. While large multichannel SQUID measuring system covers with their detection coils an area of several 10 cm^2, a high spatial resolution SQUID system covers a surface of 1/4 mm^2 or less. In order to best exploit this small area of detecting coil, it has to be brought as close as possible (maybe a few 100 μm) to the plane of measurement. This is a severe technical problem, since the detection coil is in the superconducting state.

The high temperature superconductors are also the "raw" materials for the high T_c SQUIDs. Soon after the discovery of the high temperature superconducting material $YBa_2Cu_3O_{7-\delta}$, also called YBCO (yttrium barium copper oxide), with $\delta \sim 0.15$ and with the transition temperature close to 90 K, it was possible to manufacture good SQUIDs. This ceramic material is suitable to be deposited in form of a thin film using the laser deposition technique. The YBCO thin film is epitaxially grown on a substrate.

YBCO SQUIDs were constructed in different geometrics and they need a suitable flux transformer for better sensitivity. They reach a white noise level of some 20–30 f $T/Hz^{1/2}$. They operate at liquid nitrogen (77 K) and this is an advantage when liquid helium is difficult to purchase for some reason. However, the high temperature SQUIDs will never reach the resolution of their low temperature predecessors due to different kT (k is the Boltzmann constant, T is the absolute temperature of cooling medium 77 K and 4 K). They will be used in applications where the highest sensitivity and resolution is not essential.

9.3 Basic steps in analysis and modeling of sources of electric activity connected to electric and magnetic measurements

There are different approaches to model bioelectric phenomena. They range from single cell events to complex macroscopic electric and/or magnetic measurements on, for instance, parts of the human body or electric events in

particular electrically active organ. We will briefly mention the principles and later, apply some of them to measurements on plant cells and to parts of a plant.

9.3.1 Direct and inverse problem

Knowing the bioelectric current source(s) and the electrical properties of the tissue around an electrically active organ, we can calculate the electric potential on some surface encircling (embodying) this organ at some distance. This type of calculation is known as a direct problem (Plonsey 1969). The direct problem has always a unique solution, i.e. a given distribution of currents in an electrically active organ leads to one and only one surface distribution of electric potential. The calculation is based on the second Green's theorem (Stratton 1941) and requires in three-dimensional geometry numerical integration and implication of standard methods like the boundary element method (Brebbia et al. 1984) and the finite element method (Burnett 1987). As an illustration we may mention the probably most known direct problem—the human heart and the electric potential on the torso (Barr et al. 1977). The potential on the human torso is connected to the potential distribution on the surface of the heart (epicardium)

$$\Phi_T = \mathbf{Z}_{TE}\Phi_E. \tag{2}$$

Here is $\Phi_T = \left(\Phi_T^1, \Phi_T^2, \ldots \Phi_T^{N_T}\right)$ a vector formed by discrete values of potential in N_T points, $\Phi_E = \left(\Phi_E^1, \Phi_E^2, \ldots \Phi_E^{N_E}\right)$ is a vector formed with the potentials values in N_E points on the epicardial surface and $\mathbf{Z}_{TE}$ is a matrix of geometric coefficients with the $(N_T \times N_E)$ dimension.

Eq. (2) enables us to calculate the potential on the torso surface from the known distribution of potentials over the epicardium, provided that we know the matrix $\mathbf{Z}_{TE}$. This is the case in studies of animal subjects where we measure the potential on the epicardium (Ramsey et al. 1977). In human subjects we measure the potential distribution in points (up to 200) on the torso surface and we calculate the potential distribution over the epicardium. That means that we have to solve the inverse problem. We can represent it in a similar way as the direct problem

$$\Phi_E = \mathbf{Z}_{ET}\Phi_T. \tag{3}$$

Here is $\mathbf{Z}_{ET}$ matrix of geometric coefficients with the $(N_E \times N_T)$ dimension. The $\mathbf{Z}_{ET}$ matrix determines the relation between $\mathbf{\Phi}_E$ and $\mathbf{\Phi}_T$. It has to be noticed that the inverse problem is an ill-posed problem. The number of linear independent solutions is smaller in comparison to the number of unknowns. Special care must be taken to assure that we chose a proper solution of the inverse problem (Hansen 1992).

9.3.2 Single cylindrically shaped cell [core (volume) conductor model]

The research of a long single cell is to a good approximation a one-dimensional case. As a consequence, several analytical solutions are possible. Historically, first a mathematical evaluation for the core conductor model (Clark and Plonsey 1966) was obtained. Later the extension towards the calculation of magnetic field for a single axon (Woosley et al. 1985) was completed. Similar calculations for the internodal cell of *Chara corallina* were done (Slibar et al. 2000). In all three mentioned works, the calculation starts with the evaluation of the electric potential from the Laplace's equation

$$\Delta\Phi = 0 \tag{4}$$

with the boundary conditions: the transmembrane potential Φ_m is equal to the difference of intracellular Φ_i and extracellular potential Φ_e: $\Phi_m(z) = \Phi_i(a,z) - \Phi_e(a,z)$, and the normal component of current density at the membrane surface is continuous: $\mathbf{n}\cdot\mathbf{J}_i(a,z) = \mathbf{n}\cdot\mathbf{J}_e(a,z)$. Here $\mathbf{n}$ is normal to the membrane surface; $\mathbf{J}_i$ and $\mathbf{J}_e$ are intracellular and extracellular current densities, respectively. The meaning of all quantities is evident from Figs. 9.5 and 9.10 For Φ_i and Φ_e the following expressions were obtained (Clark and Plonsey 1966)

$$\Phi_i(\rho,z) = \frac{1}{2\pi}\int_{-\infty}^{\infty} \frac{I_0(|k|\rho)}{\beta(|k|a)\,I_0(|k|a)}\,\varphi_m(k)e^{-ikz}dk, \tag{5}$$

$$\Phi_e(\rho,z) = \frac{1}{2\pi}\int_{-\infty}^{\infty} \frac{K_0(|k|\rho)}{\alpha(|k|a)\,K_0(|k|a)}\,\varphi_m(k)e^{-ikz}dk. \tag{6}$$

Here are $\alpha(|k|a) = -\left[1+\gamma(|k|a)\right]$, $\beta(|k|a) = 1+\dfrac{1}{\gamma(|k|a)}$,

$\gamma(|k|a) = \dfrac{\sigma_e K_1(|k|a)\,I_0(|k|a)}{\sigma_i K_0(|k|a)\,I_1(|k|a)}$. I_0, I_1, K_1 and K_1 are the modified Bessel functions, and $\varphi_m(k)$ is the spatial Fourier transform of the transmembrane potential

$$\varphi_m(k) = \int_{-\infty}^{\infty}\Phi_m(z)e^{ikz}dz. \tag{7}$$

Combining Eqs. 5–7, the following connections were obtained (Woosley et al. 1985)

$$\varphi_i(\rho,k) = \frac{I_0(|k|\rho)}{\beta(|k|a)\,I_0(|k|a)}\,\varphi_m(k), \tag{8}$$

$$\varphi_e(\rho,k) = \frac{K_0(|k|\rho)}{\alpha(|k|a)\,K_0(|k|a)}\,\varphi_m(k). \tag{9}$$

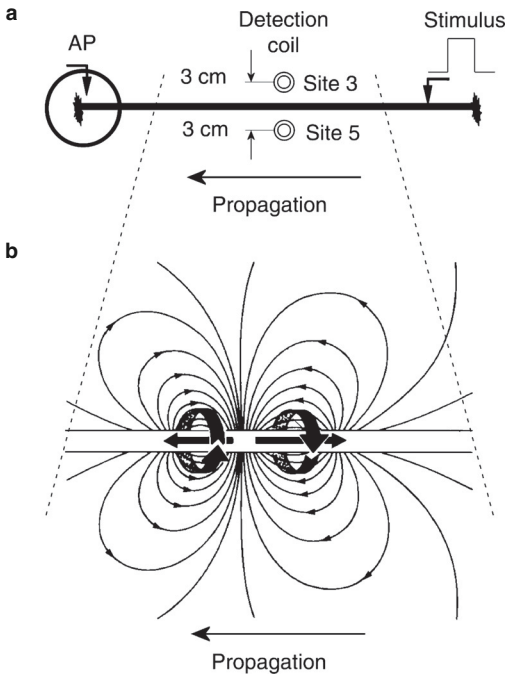

Fig. 9.5. **a** Schematic of *Chara corallina* internodal cell (*top view*) indicating the location of the stimulus, the AP and the magnetic field measurement sites. **b** Schematic distribution of intracellular current (two current dipoles within the internodal cell) and extracellular current (thin lines) for a propagating AP along the *Chara corallina* internodal cell. The contribution of the extracellular current to the measured magnetic field is negligible in an extended bath. The magnetic field due to the intracellular current in the vicinity of the internodal cell is represented as a ring around the cell. The depolarized part of the cell is shown on the left side, the repolarised on the right side

They also calculated the magnetic field B_i due to the intracellular current density by applying the law of Biot-Savart or Ampère

$$B_i(\rho,z) = \int_{-\infty}^{\infty} G(\rho,a,z-z')J_i^z(a,z')dz. \tag{10}$$

Here J_i^z is the intracellular current density component along the cell and G is the Green function of a ring around the membrane at z′

$$G(\rho,a,z-z') = \frac{\mu_0}{4\pi}\int_{-\pi}^{\pi} \frac{a}{\sqrt{\rho^2+a^2-2a\rho\cos\vartheta+(z-z')^2}}\,d\vartheta, \tag{11}$$

In the k-space, the connection with the $\varphi_m(k)$ was obtained

$$b_i(\rho,k) = i\mu_0 a\sigma_i k \frac{I_1(|k|a)K_1(|k|\rho)}{\beta(|k|a)}\varphi_m(k). \tag{12}$$

They added results for $B_e(\rho,z)$ and $b_e(\rho,k)$ due to the extracellular current density. The total magnetic field was obtained by summing $b_i(\rho,k)+b_e(\rho,k) = b(\rho,k)$. With the Fourier transformation we obtain magnetic field $B(\rho,k)$. The path of calculations can be presented as

$$\Phi_m(z) \underset{F^{-1}}{\overset{F}{\rightleftarrows}} \varphi_m(k) \rightleftarrows b(\rho,k) \underset{F}{\overset{F^{-1}}{\rightleftarrows}} B(\rho,z), \tag{13}$$

where F and F^{-1} denote the Fourier and inverse Fourier transformations, respectively. Applications of these calculations to the internodal cell of *Chara corallina* will be shown in section 9.4.

9.3.3 Covariance method—dc fields

The covariance method turned out to be suitable in extracting the dc component of the modulated magnetic field data. This is important in studies of electric response to injury (Curio et al. 1993; Wübbeler et al. 1998). The covariance of the discrete measured magnetic signal (B^k) and the modulation signal (m) during n periods of modulation signal is by the definition

$$\operatorname{cov}\left(B^k, m\right) = \frac{1}{N}\sum_{i=1}^{N}\left(B_i^k - \overline{B}^k\right)\left(m_i - \overline{m}\right) = \frac{1}{2}A\left(B^k\right)M. \tag{14}$$

Here $N=nf_s/f_m$ is the number of measured points in the given time interval, f_s is a sampling frequency and f_m is a modulation frequency. $\overline{B}^k$ and $\overline{m}$ are the mean values of B^k and m. The modulation amplitude is

$$M = \sqrt{2\operatorname{cov}(m,m)} \tag{15}$$

The response of the measured subject follows from eqs (14) and (15) as

$$A\left(B^k\right) = \sqrt{\frac{2}{N}}\frac{\sum_{i=1}^{N}\left(B_i^k - \overline{B}^k\right)\left(m_i - \overline{m}\right)}{\sum_{i=1}^{N}\left(m_i - \overline{m}\right)^2}. \tag{16}$$

9.3.4 Current distribution with the minimum norm estimation

This is a method that can also be used in solving the inverse problem. This means that we can limit the space where to reconstruct the current sources and then search for the suitable current distribution based on the estimation of the minimal norm in the distribution of primary currents (Parker 1977; Sarvas 1987).

Magnetic field (B_i) at the position ($\mathbf{r}$) of the i-th detector ($\mathbf{e}_i$-unit vector corresponded to the direction of the measured magnetic field) and the current caused by a primary current source ($\mathbf{j}_p$) in an infinite homogeneous medium, may be obtained from the Biot-Savart law as

$$B_i = \mathbf{B}(\mathbf{r}) \cdot \mathbf{e}_i = \frac{\mu_0}{4\pi} \int_V \frac{\mathbf{j}_p \times (\mathbf{r} - \mathbf{r}') \cdot \mathbf{e}_i}{|\mathbf{r} - \mathbf{r}'|^3} \, dV'. \tag{17}$$

This field can be rewritten in the form

$$B_i = \int_V \mathbf{L}_i(\mathbf{r}') \cdot \mathbf{j}_p(\mathbf{r}') \, dV' = \langle \mathbf{L}_i, \mathbf{j}_p \rangle, \tag{18}$$

where $\langle \mathrm{L}_i, \mathrm{j}_p \rangle$ denotes a dot product in a linear functional space ***J*** of all primary current sources and $\mathbf{L}_i$ is the so-called lead function of the i-th detector

$$\mathbf{L}_\mathrm{i}(\mathbf{r}') = \frac{\mu_0}{4\pi} \frac{(\mathbf{r} - \mathbf{r}') \times \mathbf{e}_\mathrm{i}}{|\mathbf{r} - \mathbf{r}'|^3}. \tag{19}$$

Lead function $\mathbf{L}_i$ represents transfer between the unit current dipole in **r'** and the measured magnetic field B_i in **r**. The current source $\mathbf{j}^*$ in ***J***, which can explain the measured magnetic field, is obtained as linear combination of lead functions

$$\mathbf{j}^*(\mathbf{r}') = \sum_{k=1}^{N} w_k \mathbf{L}_k(\mathbf{r}'), \tag{20}$$

where *N* is number of magnetic field detectors. Eqs (18) and (20) lead to a system of linear equations

$$B_i = \sum_{k=1}^{N} w_k \langle \mathbf{L}_i, \mathbf{L}_k \rangle = \sum_{k=1}^{N} \Gamma_{ik} w_k \,, \; i = 1, 2, \ldots N. \tag{21}$$

If we suppose that the inverse of the lead matrix Γ exists, then the solution of Eq. (21) is

$$\mathbf{W} = \left(w_1, w_1, \ldots w_N\right)^T = \Gamma^{-1}\left(B_1, B_2, \ldots B_N\right)^T = \Gamma^{-1}\mathbf{B}. \tag{22}$$

The solution $\mathbf{j}^*$ in Eq. (22) is an orthogonal projection of the primary currents in subspace in ***J***, determined by the lead functions. It has consequently the minimum norm out of all possible current distributions ($\mathbf{j}' \in \boldsymbol{J}$), which solve Eq. (20); this gave the name to the present method (Sarvas 1987). The conditions for the existence of a solution in Eq. (22) can be further proven. However, it has to be mentioned here that all difficulties inherent to the inverse problem appear also in this method. One has to know, for instance from the physiological information, where/when the current distribution is relevant, in order to exclude non-relevant current distributions (Hämäläinen and Ilmoniemi 1994).

9.4 Case studies

Methods and models mentioned in sections 9.2 and 9.3 were also applied to the world of plants. In the following we present, to some extent historically, a few magneto- and electrophysiologic experiments in plants.

To illustrate magnetic studies on electrophysiology in plants it is suitable to start in analogy to the research on signal transmission in simple excitable systems like the giant squid axon (Wikswo et al. 1980) and the peripheral nerve (Trahms et al. 1989). The ideal candidate for this is obviously the internodal cell of the green algae *Chara corallina*.

Electrophysiologic research on electrical phenomena on internodal cells of the giant green algae the *Characeae* started already in 1929 (Umrath 1929) and was extensively followed by others (Hope and Findlay 1964; Hope and Walker 1975) until now. Experimental work was certainly favored by the dimensions of the *Characeae* internodal cells; they can be as long as 10 cm with a diameter of about 1 mm. Any manipulation and microsurgery of such cells was successful (e.g. Beilby 1990; Shimmen et al. 1994). Because of its simple geometry, its electrical excitability and because of the huge body of work done on these cells it is justified to say that the species *Chara corallina* is the plant equivalent to the squid axon when studying ion transport in plants.

Already in the late 1970s, Frank Blatt from the University of Michigan had started the first measurements on magnetic field changes related to electrical activity in *Chara*. However, this had to wait some more years and improvement of SQUID sensors to successfully record magnetic equivalent signals to electric measurements in *Chara* (Trontelj et al. 1994). In the following, we shall mainly stay with SQUID measurements of magnetic field caused by ionic currents in electrically excited internodal cell of *Chara corallina*. Magnetic measurements will almost always be shown in parallel with electric measurements; the latter were conducted with a technique that does not disturb the SQUID sensor(s). Multichannel SQUID measurements and high spatial resolution SQUID measurements will be used.

9.4.1 Measurements of action current (AC)—magnetic analogy to action potential (AP) in *Chara corallina* using the multichannel SQUID measuring system

It seems to be a very obvious idea to measure the magnetic field or a component of it in the vicinity of a cell; in this way it is possible to obtain the value of the intracellular ionic current in the internodal cell of *Chara corallina* from measurements of AP (see chapter 2 in this book). Ampère's law gives easy first magnetic field estimation, assuming that we are so close to the cell that the excited length of the internodal cell is much longer than the distance from the cell to the sensor. Taking for the intracellular axial current I=1 μA we obtain for d=1 mm away from the cell surface $B=\mu_0 I/2\pi r$ 10^{-10} T=100 pT. This is a measurable magnetic field but only if the SQUID input coil is not more than a 1 mm away from the *Chara corallina* internodal cell. Such a close positioning can be achieved only with the high spatial resolution set-up (SQUID microscope). In the multichannel SQUID system within the Dewar vessel of about 30 cm diameter, a distance from the SQUID detection coil to the cell is at least 3–5 cm. With this arrangement the signal is reduced due to

(i) the increased distance and (ii) due to the fact that in this case the current source in form of a current dipole has to be considered. The total estimated reduction is 2 orders of magnitude, i.e. we have at the detection coil only 1 pT. Figure 9.5 shows the geometry (schematically) of a *Chara corallina* cell and the positions of two out of 37 detection coils. The drawing also illustrates the position for the AP measurement, and the site of stimulation. Finally the drawing shows the positions of the current dipole, which cause the depolarizing and repolarizing AC with the corresponding volume currents and indication of the corresponding magnetic field. Such a measuring condition requires a very good magnetic shielding and carefully prepared measurement, since we cannot count on averaging to improve the signal/noise ratio. Successful measurement were done (Trontelj et al. 1994) in the Berlin magnetically shielded room (Erné et al. 1981) and here are some experimental details: A single *Chara corallina* internodal cell was isolated from the adjacent cells and placed in artificial pond water (APW) for 1 or 2 days before being used in experiments. One end of the internodal cell was mounted into a Plexiglas support (Fig. 9.6), which allowed electrical isolation of this end by means of a groove containing grease; note the junction between the APW and KCl compartment in Fig. 9.6. The internodal cell was inserted in a horizontal Plexiglas tube with large holes in the wall. The size off each hole was ~20 mm × 5 mm and all together constituted more than 50% of the Plexiglas tube surface. Such large holes are necessary to provide undisturbed circulation of the return (volume) current. The Plexiglas support together with the *Chara* corallina internodal cell was then submerged in a Petri dish of 220 mm inner diameter. Recording of the action potential was similar to that described previously (Moriyasu et al. 1984; Clint and MacRobbie 1987). Briefly, the

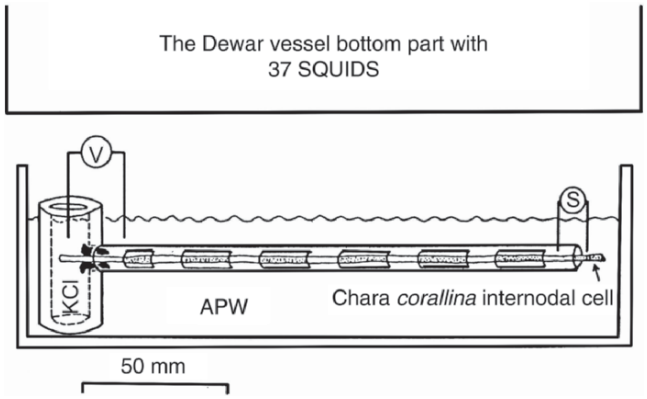

Fig. 9.6. Schematic representation of recording configuration. Magnetic recording of the action potential was carried out by 37 dc-SQUID magnetometers mounted in a cryostat filled with liquid helium and positioned above the *Chara corallina* internodal cell. The distance between the plane containing SQUID magnetometers and the cell was 50 mm

Plexiglas support compartment was filled with 100 mM KCl. This compartment served as the reference point for electrical measurements by a voltage follower. Suprathreshold stimulation was obtained by a pulse generator. The measurement set-up for electric potential measurements has a bandwidth dc –50 Hz. Ag/AgCl electrodes were used and resting potential was determined as the potential difference between the APW and KCl compartment. Internodal cells of 140–210 mm length and about 1 mm diameter were selected. With a 120-s stimulation period, some cells were responsive to several tens of stimulations.

The magnetic field was measured simultaneously at 37 points on a horizontal plane 50 mm above the *Chara corallin*a internodal cell with a multichannel magnetometer system consisting of 37 dc-SQUID magnetometers. Each of them had a 50 mm^2 pick-up coil area and 0.016–250 Hz band width (Fig. 9.6) (Koch et al. 1991).

Figure 9.7a,b show the time evolution of two characteristic magnetic signals (vertical components from channels 3 and 5) out of 37 signals. The detection coils nos. 3 and 5 are positioned on different sides of the *Chara corallina* internodal cell (see numbers in Fig. 9.7c). Hence an inverse polarity of both signals has to be expected. Also there is no signal detected in all detection coils (for instance, coils 0, 1, 4) just above the internodal cell. In this case the magnetic field lines are parallel to the plane of the detection coil and contribute zero to magnetic flux through the detection coil. With this

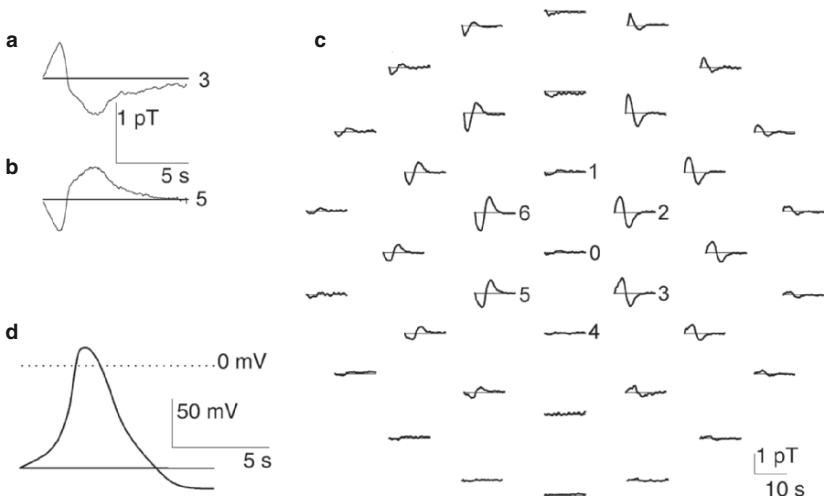

Fig. 9.7. **a** The time evolution of magnetic field measured with the detection coil no. 3 and **b** the same, only the detection coil no. 5 is on the opposite site of the cell. **c** The time evolution of magnetic field (vertical component) in 37 points in a plane 50 mm above Chara corallina internodal cell. The signal amplitude just above the cell, place in the middle of the figure extending top to bottom, is practically 0, as is expected for the current dipole travelling along the cell. **d** The time evolution of action potential. The first 10 s are shown

information in mind, the picture of all 37 magnetic channels simultaneously measured (Fig. 9.7c) becomes understandable. The time evolution of the corresponding electrically measured AP is shown on Fig. 9.7d. With the information presented in Fig. 9.7c we can also obtain after an interpolation procedure the isofield representation for a particular time. Results for three consecutive time points are presented in Fig. 9.8. They indicate a vertical component of the magnetic field values. The time between two representations is 300 ms. The dipolar distribution of the magnetic field suggests that the current generator behaves similar to that of animal cells, and the spatial co-ordinates of the central part of the intracellular current distribution can be estimated. Close inspection of Fig. 9.8 also indicates the motion of excitation along the cell. The projection of the stimulus location corresponds to the point in the central upper part of each image in Fig. 9.8. The excitation is spreading from top to bottom in each picture. The time increases from left to right. By comparing the position of the magnetic field extrema, indicated by the + and − signs, this propagation can be followed as a shift in position of both extrema in time. By evaluating the movement of the extrema per unit time, we obtained a speed for excitation propagation of 3–5 cm/s. This value is in agreement with values for excitation propagation in *Chara* obtained by different groups (Findlay and Hoppe 1976; Tester 1990).

Another choice of time intervals after the cell's excitation and between isofield representations enables us to demonstrate the depolarization and the repolarization phase in the same sequence of pictures. This is demonstrated in the first row of Fig. 9.9a–c. The second and the third rows in Fig. 9.9a–c show the calculated equivalent current dipoles (central row) and the current distribution (bottom row) along the *Chara corallina* internodal cell. The calculation was based on the estimation of minimal norm (see Section 9.3.4) in the distribution of equivalent intracellular currents according to Eqs 17–22 in section 9.3.4.

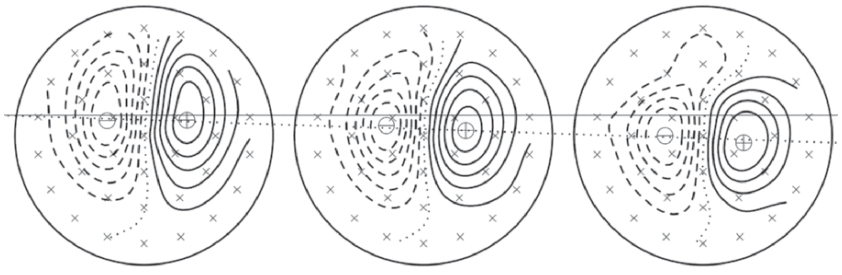

Fig. 9.8. The isofield line representation at three particular times, from left to right at 1300 ms, 1600 ms and 1900 ms after the stimulus. The solid line (a reference) and the *dotted line* lead the eyes to follow the displaced extrema as it explained in the text. The *crosses* indicate the points where magnetic field was measured. They are arranged in three concentric circles with radii of 3.5, 7, and 10.5 cm. The two neighboring isofield lines are 150 f T apart

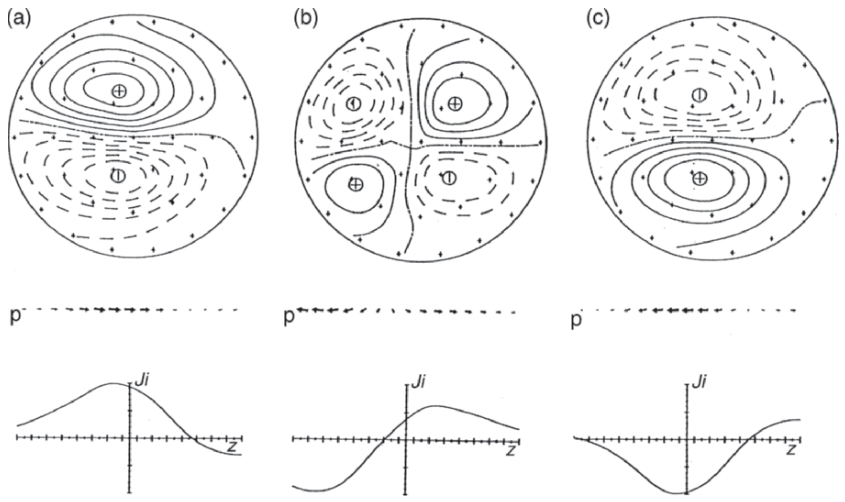

Fig. 9.9. The isofield representation (*first row*), and the model calculation of current dipoles (**p**, *second row*) and current density (J_i, *third row*) along the cell for: (a) the depolarization, (b) depolarization+repolarization, and (c) repolarization at times 1.4, 2.5 and 3.6 s after stimulus

The *Chara corallina* internodal cell offers a convenient model system to test calculations (Clark and Plonsey 1966; Woosley et al. 1985; Slibar et al. 2000) of relations between intracellular current, magnetic field and electric potential. The respective calculations are briefly mentioned in section 9.3.2 (Eqs. 5–13). Considering the cylindrical symmetry of *Chara corallina* internodal cells we represent this cell geometrically according to Fig. 9.10. Transformations from measured the AP→the calculated AC (magnetic field)

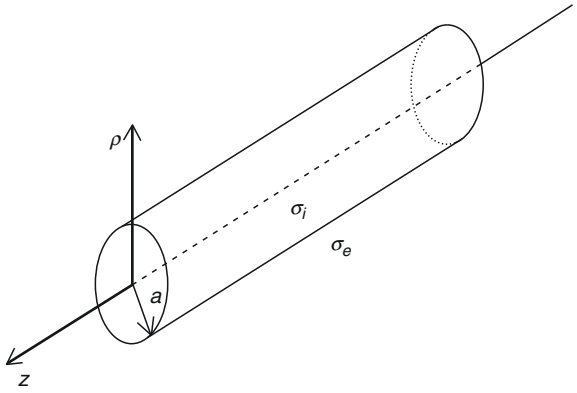

Fig. 9.10. The cell model. σ =1.2 $\Omega^{-1}m^{-1}$, σ_e=0.025 $\Omega^{-1}m^{-1}$, and 2a=1 mm

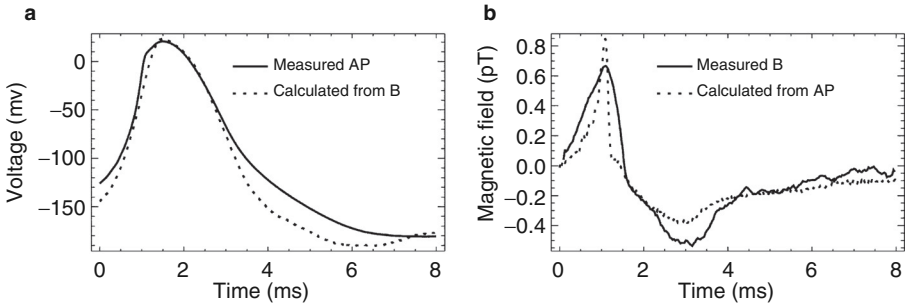

Fig. 9.11. **a** The first 8 s of measured AP (*solid line*) in the *Chara corallina* internodal cell and calculated AP (*dashed line*) from the measured magnetic field. **b** Measured magnetic field 6 cm away from the *Chara corallina* internodal cell (*solid line*) and calculated magnetic field (*dashed line*) from the measured AP

and the inverse process from the measured AC (magnetic field)→the calculated AP are presented in Fig. 9.11. Comparisons of all calculations (Clark and Plonsey 1966; Woosley et al. 1985; Slibar et al. 2000) with experimental data show that the peak forward AC (magnetic field) occurs approximately simultaneously with the maximum time derivative of the AP. The maximum backward AC coincides with the most rapid change of the AP during the repolarization. The time of the peak AP corresponds to the zero-crossing between the forward and backward phases of the AC. Here adjustments in time scale have to be considered if the AP and AC were not measured at the same position. On the other hand, there are also differences in the shape of the signals. The internodal cell of *Chara corallina* was submersed up to 10 mm into APW. We did not like to have it deeper, since the distance between the cell and the detection coil should be as short as possible in order to have better signal/noise ratios. Hence within the cell and 5 mm around the cell we have completely fulfilled the condition for the assumed cylindrical symmetry. On the upper part of the internodal cell it may be that the volume currents partly modify the integral magnetic field, i.e. the field that we measure. At the same time there is no such effect to be expected when measuring AP.

9.4.2 The chemical nature of the AP in *Chara corallina* as it can be seen from the non-invasive observation (by SQUID microscope) of the intracellular current under the influence of light

Though we still do not understand in all details the process of electrical stimulation of the AP in *Chara corallina* there is no doubt that a rise in cytoplasmic Ca^{2+} plays a dominant role (Williamson and Ashley 1982; Kikuyama and Tazawa 1983; Wacke and Thiel 2001). This rise in Ca^{2+} is believed to activate Ca^{2+}-sensitive Cl^- channels (Okihara et al. 1991; Homann and Thiel 1994) and

with that generate the depolarization. The activation of K^+ channels supports the repolarization (Thiel et al. 1997).

According to some authors Ca^{2+} enters the cytoplasm via voltage-dependent channels (Tazawa and Kikuyama 2003; Berestovsky and Kataev 2005). On the other hand, investigations have revealed that the threshold for excitation is posed by a quasi all-or-none type liberation of Ca^{2+} from internal stores (Wacke and Thiel 2001; Wacke et al. 2003). In this sense, the AP in *Chara* occurs not to function like a classical Hodgkin Huxley (HH) type AP. This means that the AP is not entirely based on the time and voltage dependent activation properties of plasma membrane ion channels but on a complex signal transduction cascade (Wacke et al. 2003). Similar mechanisms of membrane excitation, which are based on Ca^{2+} release from internal stores, are also well known from animal cells where they are found in muscles (Nelson et al. 1995) and even some neurons (Chavis et al. 1996).

The latter type of a "chemical" action potential was in the past well described by models, which include a non linear dynamic interplay of cytosolic Ca^{2+} ($[Ca^{2+}]_c$) and second messenger stimulated release of Ca^{2+} from internal stores (Othmer 1997). The same modeling approach was also suitable to simulate a large spectrum of phenomena related to membrane excitation in *Chara* (Wacke et al. 2003). One parameter in this model, which is predicted to effect the kinetics of Ca^{2+} mobilization and hence the kinetics, is the cytoplasmic concentration of Ca^{2+} prior to stimulation.

To further test the validity of the model, we examined the kinetics of the AP under conditions in which $[Ca^{2+}]_c$ is altered. This was done by transferring the plants from the dark into the light, because it is known that $[Ca^{2+}]_c$ is in these cells reduced under the influence of light (Miller and Sanders 1987; Plieth et al. 1998). The high spatial resolution SQUID measuring system (SQUID microscope) was used for non-invasive magnetic measurements of AC. Measurements were done in the laboratory of John P. Wikswo at the Department of Physics and Astronomy, Vanderbilt University, Nashville, Tenn., USA (Baudenbacher et al. 2005).

9.4.2.1 Experimental

The internodal cell was held in a horizontal Plexiglas half-tube, similar to that described in section 9.4.1; it is schematically shown in Fig. 9.12. The leveling stage allowed the bath to be moved up and down to adjust the distance between the cell and the tail of the SQUID microscope Dewar vessel. A 10 µm thick Mylar film prevented contact between the cell and the SQUID microscope sapphire window and stabilized the position of the internodal *Chara corallina* cell during scanning. One end of the internodal cell was mounted in a small Plexiglas compartment in order to electrically isolate this end of the cell (the left end in Fig. 9.12) from the bath with a petroleum jelly seal (Fig. 9.12), similarly as in the experiment in section 9.4.1. *Chara corallina*

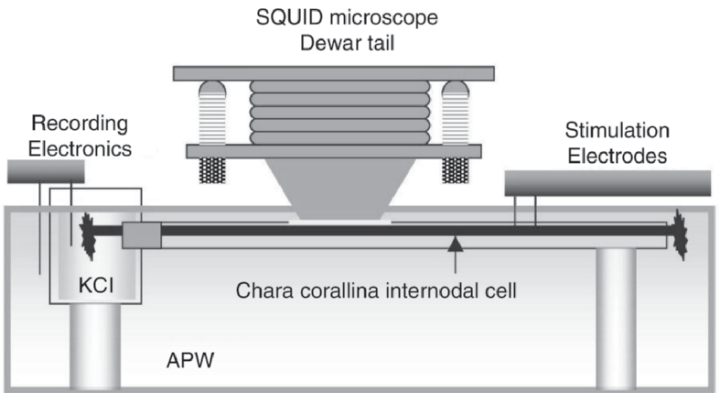

Fig. 9.12. Schematic experimental setup (*side view*) used for electric and magnetic measurements on *Chara corallina* internodal cell. The Plexiglas holder supporting the cell is terminated on the left side in a sealed compartment to record the transmembrane potential

internodal cells were at least 8 cm long to allow simultaneous measurement of the electric potential differences (AP) and the associated magnetic field due to action currents (AC). For the measurements reported here, selected internodal cells were up to 15 cm long with diameters between 0.8 and 1.1 mm.

The bath temperature was carefully monitored during each experiment and was maintained at 20 °C. All measurements were performed in an air-conditioned, magnetically shielded room (Vacuumschmelze, Hanau, Germany). During an average two-hour measuring session, the temperature varied by only 0.20 °C.

The cell illumination was provided by a light source with a spectrum similar to daylight with 5–10 Wm^{-2} delivered to the cell by a fibre-optic bundle that passed through an opening into the magnetically shielded room to eliminate power supply noise of the light source.

By measuring magnetic fields in the vicinity of a *Chara corallina* internodal cell after the AP was electrically elicited, we basically measure the contribution of total ionic current, associated with the propagating action potential (AP). The measured *Chara corallina* internodal cell is in APW bath solution and extracellular ionic currents, caused by the AP propagation along the cell, are spread through the whole APW volume. Their density is very small and their contribution to the measured magnetic field is negligible. In practice, only the magnetic field due to axial intracellular current, the so-called action current (AC), will be measured. To measure it a single SQUID magnetometer was chosen. Its small detection coil can be positioned extremely close to the measured object—SQUID microscope (Baudenbacher et al. 2002). With this configuration, it was possible to obtain a high signal-to-noise ratio (small distance from detection coil to the cell) and high spatial resolution (due to small diameter of detection coil).

In this SQUID microscope design, a hand wound niobium detection coil is coupled to a commercially available low temperature SQUID sensor. The SQUID sensor and the detection coil are in the vacuum space of the cryostat separated typically by approximately 100 µm from the room-temperature sample by a thin sapphire window. A computerized non-magnetic scanning stage with sub-micron resolution in combination with a tripod leveling system allows samples to be scanned at levels of 10 µm below the sapphire window. For a 20 turn, 500 fm diameter detection coil a field sensitivity of 350 $fT/Hz^{1/2}$ was achieved. For a large 40 turn 1 mm diameter coil 50 $fT/Hz^{1/2}$ for frequencies above 1 Hz for the vertical component of the magnetic field was obtained. The voltage output of the SQUID electronics corresponding to the vertical magnetic field component generated by propagating AC was recorded at a bandwidth of DC-500 Hz for a period of 30 s at a position along the cell where the magnetic signal was maximal.

There are some understandable differences in recorded results obtained with the multichannel SQUID magnetometer (Fig. 9.7a–c) and the SQUID microscope (Fig. 9.13a, b). These differences are the result of different distances between the detection coil and the *Chara corallina* internodal cell

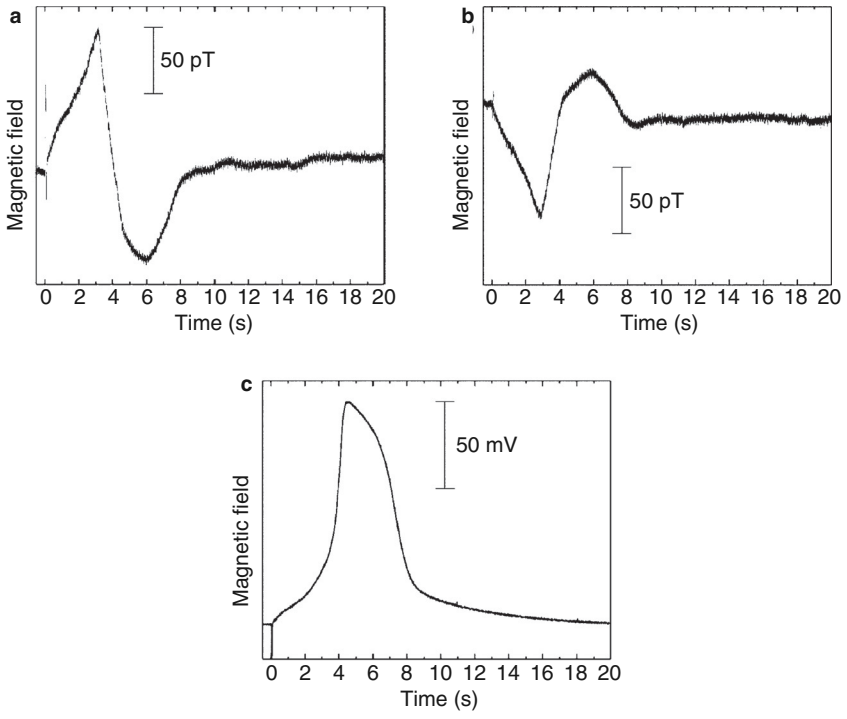

Fig. 9.13. **a** Magnetic field measured at the right side of *Chara corallina* internodal cell and **b** the same at the left side; **c** AP recorded by the K^+ anaesthesia technique

(5 cm for the multichannel SQUID magnetometer and about 200 μm for the SQUID microscope). The amplitude of the vertical component of the measured magnetic field is about 100 times bigger for the single channel SQUID microscope. Since the 500 μm diameter detection coil is so close to the cell, we can say that we are practically observing the linear intracellular ionic current with no influence of a few cm long current dipole. Small differences in peak amplitudes between Fig. 9.13 a and b reflect scattering between two measuring sessions; possibly also small deviation from symmetrically located measuring points contribute to these differences.

The AP was measured simultaneously at a point along the cell 50 mm away from the detection coil position and is shown in Fig. 9.13c. The spatial separation of magnetic and electric measuring points leads to a time shift of 1.1–1.2 s. From these values, the AP propagation velocity can be calculated to be about 4 cm/s, which is in good agreement with the previously mentioned results (section 9.4.1). Before and during these measurements, the *Chara corallina* internodal cell was kept in darkness for at least one hour. The detection coil was placed 2 mm right (Fig. 9.13a) and 2 mm left (Fig. 9.13b) lateral to the internodal cell surface. The vertical distance from the detection coil to the cell surface was 200 μm. The measurements shown in Fig. 9.13 are single shot measurement with no averaging of the data.

Under constant illumination and temperature, the transmembrane potential and the magnetic field generated by AC revealed only small variations either when different cells or when one *Chara corallina* internodal cell was measured repetitively.

Figure 9.14 left panel, traces a–i show the time dependence of the vertical component of the magnetic field measured at y=2 mm lateral to the cell's geometrical axis under different illumination conditions. In this series of experiments, the internodal cell was in darkness for 60 min prior to the first measurement of AP propagation. Figure 9.14, left panel, trace a shows the magnetic field generated by AC just before the light was turned on. Subsequent recordings were done under constant illumination after particular time intervals as shown in Fig. 9.14, left panel, traces b–e. It can be seen that, as a response to illumination, the temporal evolution of the magnetic field changes over a period of less than 1 hour before reaching a new steady state. Most pronounced is the time shift of the positive peak of the magnetic signal associated with the depolarization. The negative peak associated with the repolarization is less expressed.

The temporal characteristic of the magnetic field is reversible. Upon transferring the cell back from light into darkness, the temporal field changes became progressively closer to the initially measured magnetic field as shown in the sequence of Fig. 9.14, left panel (traces f–i).

Parallel electrical measurements (Fig. 9.14 right panel, traces b–e and traces f–i) demonstrate a similar dependence of the AP time evolution on light/darkness. A transition of a cell from darkness to light prolonged the duration of the membrane depolarization for about 2 s after a transitional

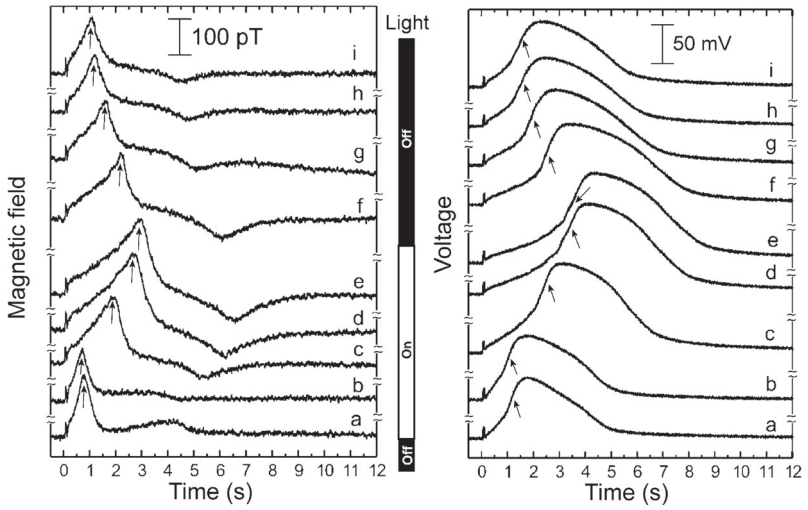

Fig. 9.14. Recordings of the time dependent vertical component of the magnetic field (*left panel*) generated by a propagating AC and simultaneous AP recordings (*right panel*) measured as a function of illumination starting after one hour dark accommodation. Trace *a*, light off, trace *b*, 10 min light on, trace *c*. 20 min light on, trace *d*, 30 min light on, trace *e*, 40 min light on (here we waited for an additional 20 min to complete 1 h in the light accommodation), trace *f*, 10 min light off, trace *g*, 20 min light off, trace *h*, 30 min light off, trace *i*, 40 min light off. *Small arrows* indicate where the temporal shift was observed

period of about 20–30 min on average. The depolarization time prolongation was accompanied by an increase in the depolarization peak of about 10–15%. This can be attributed to the hyperpolarization of the resting potential under illumination (Mimura and Tazawa 1986).

Several tens of internodal cells were measured. They all demonstrate the same behavior under the mentioned sequences of illumination and dark phase. The reversible effect of light/dark transitions on the kinetics of membrane excitation suggests a coupling between photosynthesis and membrane excitation. To examine this hypothesis, the influence of a common photosynthesis inhibitor, DCMU (3,-(3,4-dichlorophenyl)-1,1-dimethylurea) at a concentration of 10 μM on the kinetics of excitation was measured. In this case, a *Chara corallina* cell was exposed to light for a period of 60 min in the presence of DCMU in the bath solution. The light/dark dependent shift in the magnetic signals disappeared, as expected. Two cells were tested with both showing the same behavior.

9.4.2.2 Modeling

The here described light/dark experiments are suitable to demonstrate that the AP in *Chara corallina* shows a similarity to APs in those animal cells (heart,

brain) in which a "biochemical AP" is known. Also in these cases excitation can not be explained by the straight forward Hodgkin–Huxley (HH) (Hodgkin and Huxley 1952) model. Previous work has shown that $[Ca^{2+}]_c$ is altered under the influence of light/dark transitions (Miller and Sanders 1987). The simple HH type mode, which is solely based on the kinetics of plasma membrane channels and electrical properties of the membranes cannot take the changes in $[Ca^{2+}]_c$ into account. In the work of Baudenbacher and co workers (Baudenbacher et al. 2005), an adaptation of the model by Othmer to *Chara* (Wacke et al. 2003) was applied. This model describes the dynamics of $[Ca^{2+}]_c$ in the context of a second messenger system. Using this approach the AP in *Chara* is successfully described by an electrically stimulated release of Ca^{2+} from internal stores. The resulting changes in membrane conductance are the direct consequence of this dynamic change in $[Ca^{2+}]_c$. In this extended model, the threshold-like dependence of Ca^{2+} mobilization on electrical stimulation can be simulated by combining the following two processes:

i. The voltage dependent synthesis/breakdown of the second messenger inositol 1,4,5-trisphosphate (IP_3).
ii. The concerted action of IP_3 and Ca^{2+} on the gating of the receptor channels, which conduct Ca^{2+} release from internal stores.

The model can simulate several experimental results connected to AP in *Chara*. This leads to the conclusion that the all-or-none type activation of the action potential is only the consequence of the preceding all-or-none type mobilization of Ca^{2+} from internal stores. The dependency of the gating of the receptor channel on $[Ca^{2+}]_c$ suggests that the Ca^{2+} concentration prior to stimulation of the AP has an influence on the following excitation kinetics.

To examine the effect of variable $[Ca^{2+}]_c$ on the kinetics of the electrically stimulated changes in Ca^{2+}, we modified the model as follows: cells move excess Ca^{2+} from the cytoplasm back into internal stores by an endogenous Ca^{2+} pump system (e.g. Reddy 2001). In the model, i.e. in the rate equation for Ca^{2+} concentration change with time, this process is accounted for by a Hill function

$$\overline{g}(C) = \frac{\overline{p_1} C^4}{C^4 + \overline{p_2}^4}. \tag{23}$$

In this equation, $\overline{p_1}$ and $\overline{p_2}$ are the Hill coefficients, C is the cytosolic Ca^{2+} concentration. For more details, see Othmer (1997). To achieve different $[Ca^{2+}]_c$ under resting conditions which are known to occur during light/dark transitions (Miller and Sanders 1987; Plieth et al. 1998), the Hill factor $\overline{p_2}$ in Eq. (23) was varied. This procedure is only an indirect approach, since the chloroplasts from which the Ca^{2+} originates during light/dark transitions (Miller and Sanders 1987) are not considered as extra Ca^{2+} pool in the model for $[Ca^{2+}]_c$ dynamics. Nonetheless, this simple manipulation of the model should be sufficient to provide basic insight into the dependency of Ca^{2+} mobilization on $[Ca^{2+}]_c$.

Figure 9.15 illustrates the results of this simulation. As a consequence of a reduced Ca^{2+} pump activity, the resting $[Ca^{2+}]_c$ increases over the physiological range from about 20 nM to 200 nM. This roughly covers the changes in $[Ca^{2+}]_c$ of 50–250 nM found in response to light/dark transitions in *Chara* (Miller and Sanders 1987; Plieth et al. 1998). The simulation further shows that an elevation of $[Ca^{2+}]_c$ prior to the stimulation results in a progressive shortening of the delay time between stimulation and the rapid phase of $[Ca^{2+}]_c$ rise. The dependence of this delay time on the resting $[Ca^{2+}]_c$ concentration is plotted in the inset of Fig. 9.15.

On the assumption that the change in membrane voltage during the AP is only the consequence of an activation of $[Ca^{2+}]_c$ sensitive Cl^-channels (Thiel et al. 1997; Biskup et al. 1999), the model simulation compares well with the light/dark SQUID microscope experimental data. The assumed progressive decrease in $[Ca^{2+}]_c$ of about 150 nM following the transition from dark to light results in an increasing delay time between the electrical stimulus and the rapid phase of $[Ca^{2+}]_c$ rise, or the activation of the Cl^- channels, respectively.

These observed changes in the kinetics of the *Chara* AP could in principle also be modeled by a classical HH approach by adding a variable delay factor. However, there is no mechanistic motivation for such a delay factor and it is difficult to envisage how a first order voltage dependent process such as the voltage dependent activation of plasma membrane channels could produce such a long and variable delay.

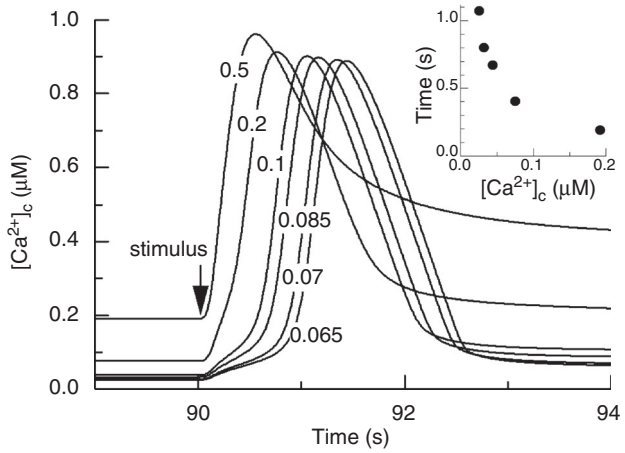

Fig. 9.15. Simulated $[Ca^{2+}]_c$ transients in response to a single electrical stimulation (100 ms/5 µA). Data were calculated with model parameters reported in Wacke et al. (2003). Different curves are obtained by changing the Hill coefficients p_2 in the model term, which describes the buffering of $[Ca^{2+}]_c$. An increase in p_2 over a range of 0.065–0.5 µM results in reduced Ca^{2+} buffering and a consequent increase in the resting $[Ca^{2+}]_c$. In the simulation pulses were started after 90 s in which the system was allowed to equilibrate. Inset: delay time between stimulus and maximal slope of $[Ca^{2+}]_c$ increase as a function of resting $[Ca^{2+}]_c$ before stimulation

Assuming that the activation of the Cl^- channels, which cause the depolarization, is the direct consequence of the change in $[Ca^{2+}]_c$, the measured data nicely match the model prediction, even on a quantitative basis. The model further predicts that a modulation of the resting $[Ca^{2+}]_c$ has no big effect on the kinetics of the bulk changes of $[Ca^{2+}]_c$. Again, this prediction is met by the present data because the features in the temporal evolution of the AC/AP were basically unchanged.

9.4.2.3 Other studies on Chara corallina

Chara corallina is a suitable model system for further investigations using the SQUID magnetometer in different configurations. The authors are aware of (i) research regarding the transnodal conductivity (Belsak 2005) and (ii) preliminary studies of the well known bending phenomenon in *Chara* (Z. Trontelj 2001, private communication).

9.4.3 Magnetic detection of injury induced ionic currents

Magnetic detection of ionic currents was performed also in higher plants. Injury induced quasi-dc ionic currents were detected by the PTB Berlin 49 channel magnetometer (Drung 1995) combined with a suitable modulation on *Vicia faba* plants (Jazbinsek et al. 2000). The temporal and spatial evolution of magnetic field accompanying stimulation by burning and/or cutting of *Vicia faba* plants were measured. Various kinds of local woundings in plants trigger long distance signaling processes. In response to signaling the synthesis of proteins used in defense against insect predators are initiated (Bowles 1990). These proteins which comprise among others protease inhibitors are synthesized not only at the site of wounding but also in distant parts of the plant (Chessin and Zipf 1990; Ryan 1992). This supports the view that at the site of wounding a signal is initiated which is rapidly propagated systemically throughout the plant with the consequence that shortly after the wounding protein synthesis is induced even in parts of the plant distant from the site of wounding (Ryan 1992). Currently, three hypotheses are being discussed for long distant signaling: i) the transmission of a chemical compound in the vessels, ii) propagation of changes in electrical voltage or iii) trauma-evoked hydraulic pressure changes.

Studies using extracellular and intracellular electrodes have revealed that wounding of tissue causes in a variety of plants changes in the electrical membrane voltage (e.g. Roblin 1985; Roblin and Bonnemain 1985; Wildon et al. 1992; Herde et al. 1998). Typically, the electrical response consists of a rapid action potential like depolarization followed by a slower long-lasting depolarization usually termed the variation potential. Wounding induced voltage changes are transmitted from the site of wounding along the plant with a velocity of less than 1 cm/s (Wildon et al. 1992; Roblin and Bonnemein 1995)

and reach the remote tissue before the systemic molecular responses are initiated in this tissue (Stankovic and Davies 1998). From the perspective of magnetic measurements it is important to note that any electric potential difference (voltage) in conducting living tissue is connected with ionic currents. Based on Biot-Savart's law these currents can also be detected magnetically.

To further elucidate the mechanism of electrically based signaling biomagnetic measurements of electrical activity in bean plants have been conducted over the entire plant. This approach takes advantage of the fact that the multichannel SQUID device is able to image electrical activity basically over the whole plant.

For recording the biomagnetic field the currents causing this field should be closed within a large volume. This can be achieved by immersing the whole plant in a suitable ionic solution. This non-invasive and non-touchable method has been used in the past to monitor electrical activity in animal cells, which also respond to injury with electrical activity (Trontelj et al. 1989; Curio et al. 1993). Equivalent to experiments in wounding of animals the measurements with bean plants were aiming to provide information on electrical propagation, injury induced currents and the source of currents in wound stimulated tissue.

One example for a measurement with a cutting injury is shown in Fig. 9.16. In panel (a) of this figure the time evolution of a plant response before introducing a large wound is shown in all 49 channels. Under these conditions, small activity in the area above the plant's leaves can be noticed (dashed lines show the distribution of leaves). Figure 9.16d shows the characteristic isofield map corresponding to the resting situation. There is no indication of symmetry between positive and negative isofield pattern, which is typical for a dipolar isofield pattern. In contrary, there is a dramatic change in the field distribution after cutting the stem and removing the apical part of the plant. A clear symmetric dipolar-like isofield pattern indicates an active localizable current source (Fig. 9.16e). From the time evolution (Fig. 9.16b,c) of the signal $A(B^k)$, defined by Eq. (16), an exponential decay of electrical activity is clearly noticeable. The characteristic decay time was about 10 min.

This biomagnetic measurements on *Vicia faba* plants provide complementary information to electric potential difference measurements on beans (Roblin 1985; Roblin and Bonnemain 1985) and other plant species in responds to local wounding (e.g. Wildon et al. 1992; Herde et al. 1998). This additional information is obtained non-invasively and without touching the plant. In some cases where the isofield maps were obtained in the form close to the dipolar field distribution, an equivalent current dipole (ECD) was used to model the magnetic field distribution over the *Vicia faba* plant. Though it is difficult to find an electrophysiologic explanation for this type of current source in most cases, it seems to be a reasonable description of a current source in the case of a big wound (Fig. 9.16e). In this case, a strong localizable flow of ions takes place at the wound. The estimated ECD strength p and

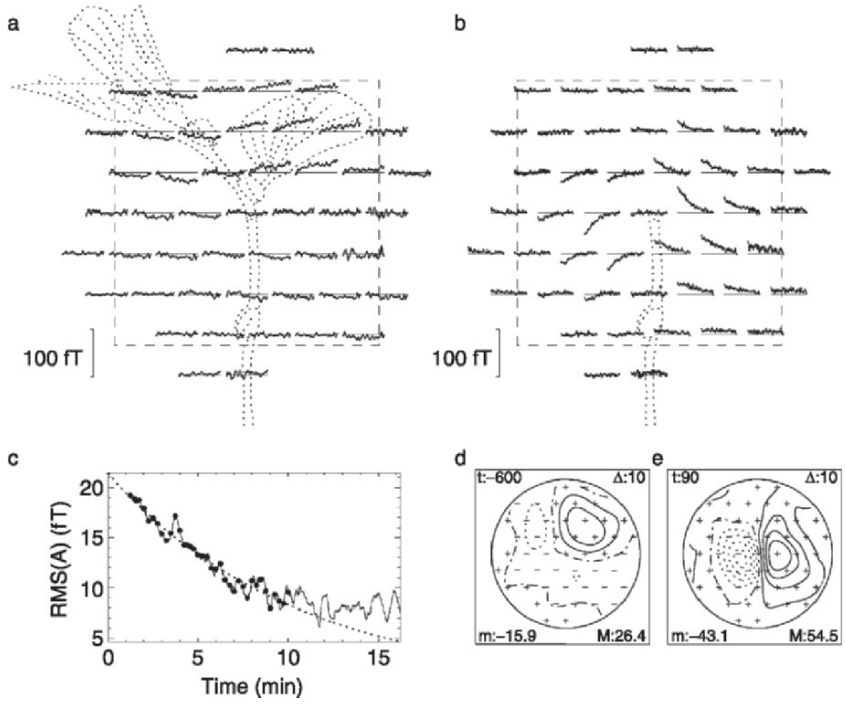

Fig. 9.16. Time evolution of magnetic field in all channels: **a** 25-10 min before cutting the plant and **b** 1–16 min after cutting. Sketch of plant is shown with *dotted lines* and inner side of the chamber is indicated by *dashed line*. **c** *Solid line* represents time evolution of injury related RMS magnetic field from **b**, bullets shows RMS values of magnetic field each 15 s in the first 10 min after the injury. These values were fitted with exponential decay function shown by dotted line. **d** and **e** isofield maps 10 min before and 1.5 min after the injury, respectively. Here t denotes time from the injury in *s*, m and M are minimal and maximal field values in *fT*, and Δ step between two isofield lines in *fT*. Solid, dash-dot-dash and dot line styles represent positive, zero and negative isofield lines, respectively. Positions of magnetic sensors are shown by + and − in accordance with the measured field sign

current J associated with the ionic transport obtained 1.5 min after the cutting injury were 6.6 nAm and 0.14 μA, respectively. The maximal currents obtained in plants with burning stimulation were between 0.1 and 0.24 μA. These values were estimated from the ECD strength p and the source length $2a$ ($J=p/2a$). From this current one can estimate the average order of magnitude for the current density of 0.01 μA/mm^2, where it is assumed that the bean stem cross-section is approximately 20 mm^2. The localization of maximal electrical activity—the position of equivalent current source—overlaps with the stem location with accuracy of better than 1 cm.

All investigated plants responded to stimulation by burning or cutting and the phenomenon was magnetically detected. Magnetic measurements could

not confirm a long distance spreading of electric activity. Correspondingly, it is not yet possible to favor one of the three possible hypotheses on long distance signaling in wounded plants.

Acknowledgement We thank to the colleagues from the Physikalisch-Technische Bundesanstalt, Institut Berlin, where the first biomagnetic measurements on the internodal cell of Chara corallina were performed, as well as to the colleagues from the Living state group of the Department of Physics and Astronomy of the Vanderbilt University, Nashville, TN, where the first SQUID microscopy measurements on Chara corallina cells were done. We also thank to the Biophysical Journal for the permission of reprinting Figs. 9.5, 9.6, 9.7, 9.8, 9.12, 9.13 and 9.15, as well as to the European Biophysics Journal for the permission of reprinting Fig. 9.16.

References

Baluska F, Volkmann D, Menzel D (2005) Plant synapses: actin-based domains for cell-to-cell communication. Trends Plant Sci 10:106–111

Barr RC, Ramsey M, Spach MS (1977) Relating epicardial to body-surface potential distributions by means of transfer-coefficients based on geometry measurements. IEEE T Biomed Eng 24:1–11

Bardeen J, Cooper LN, Schrieffer JR (1957) Theory of superconductivity. Phys Rev 5:1175–1204

Baudenbacher F, Peters NT, Wikswo JP (2002) High resolution low-temperature superconductivity superconducting quantum interference device microscope for imaging magnetic fields of samples at room temperatures. Rev Sci Instrum 73:1247–1254

Baudenbacher F, Fong LE, Thiel G, Wacke M, Jazbinsek V, Holzer JR, Stampfl A, Trontelj Z (2005) Intracellular axial current in *Chara corallina* reflects the altered kinetics of ions in cytoplasm under the influence of light. Biophys J 88:690–697

Bauer CS, Plieth C, Hansen UP, Sattelmacher B, Simonis W, Schonknecht G (1997) Repetitive Ca^{2+} spikes in a unicellular green alga. FEBS Lett 405:390–393

Bentrup FW (1979) Reception and transduction of electrical and mechanical stimuli. In: Haupt W, Feinleib ME (eds) Physiology of movement. Encyclopedia of plant physiology, new series. Springer, Berlin Heidelberg New York

Bednorz JG, Mueller KA (1986) Possible high Tc superconductivity in the barium-lanthanum-copper-oxygen system. Z Phys B 64:189–193

Beilby MJ (1990) Current-voltage curves for plant membrane studies: a critical analysis of the method. J Exp Bot 41:165–182

Belsak M (2005) Diploma thesis, Faculty of Mathematics and Physics, University of Ljubljana

Berestovsky GN, Kataev AA (2002) Voltage-gated calcium and Ca^{2+}-activated chloride channels and Ca^{2+} transients: voltage-clamp studies of perfused and intact cells of Chara. Eur Biophys J (published online)

Berestovsky GN, Kataev AA (2005) Voltage-gated calcium and Ca^{2+}-activated chloride channels and Ca^{2+} transients: voltage-clamp studies of perfused and intact cells of Chara. Eur Bio J 34:973–986

Biskup B, Gradmann D, Thiel G (1999) Calcium release from $InsP_3$-sensitive internal stores initiates action potential in chara. FEBS Lett 453:72–76

Bowles DJ (1990) Defence-related proteins in higher plants. Annu Rev Biochem 59:873–907

Brebbia CA, Telles JCF, Wrobel LC (1984) Boundary element techniques: theory and applications in engineering. Springer, Berlin Heidelberg New York

Burnett DS (1987) Finite element analysis. Addison-Wesley, Reading, MA

Chavis P, Fagni L, Lansman JB, Bockaert J (1996) Functional coupling between ryanodine receptors and L-type calcium channels in neurons. Nature 382:719–722

Chessin M, Zipf AE (1990) Alarm systems in higher plants. Bot Rev 56:193–235

Clark J, Plonsey R (1966) A mathematical evaluation of the core conductor model. Biophys J 6:95–112

Clint GM, MacRobbie EAC (1987) Sodium efflux from perfused giant algal cells. Planta 171:247–253

Curio G, Erné SN, Burghoff M, Wolff H-D, Pilz A (1993) Non-invasive neuromagnetic monitoring of nerve and muscle injury currents. Electroenceph Clin Neurophys 89:154–160

Deaver BS, Fairbank WM (1961) Experimental evidence for quantized flux in superconducting cylinders. Phys Rev Lett 7:43–46

Drung D (1995) The PTB 83-SQUID system for biomagnetic applications in a clinic. IEEE T Appl Supercon 5:2112–2117

Erné SN, Hahlbohm D, Scheer H, Trontelj Z (1981) Berlin magnetically shielded room (BMSR). In: Erné SN, Hahlbohm D, Lübbig H (eds) Biomagnetism, Proceedings of the Third International Workshop on Biomagnetism, Berlin, May 1980. Walter de Gruyter, Berlin, pp 79–89

Findlay GP, Hoppe AB (1976) Electrical properties of plants. In: Luttge U, Pitman MG (eds) Transport in plants II. Springer, Berlin Heidelberg New York, pp 79–92

Gradmann D (1976) "Metabolic" action potentials in *Acetabularia*. J Membr Biol 29:23–45

Gradmann D, Blatt MR, Thiel G (1993) Electrocoupling of ion transporters in plants. J Membr Biol 136:327–332

Hämäläinen MS, Ilmoniemi RJ (1994) Interpreting magnetic fields of the brain: minimum-norm estimates. Med Biol Eng Comput 32:35–42

Hansen PC (1992) Numerical tools for analysis and solution of Fredholm integral-equations of the 1st kind. Inverse Problems 8:849–872

Herde O, Pena-Cortes H, Willmitzer L, Fisahn J (1998) Remote stimulation by heat induces characteristic membrane-potential responses in the vein of wild-type and abscisic acid-deficient tomato plants. Planta 206:146–153

Hodgkin AL, Huxley AF (1952) A quantitative description of membrane current and its application to conductance and excitation in nerve. J Physiol Lond 117:500–544

Homann U, Thiel G (1994) Cl^- and K^+ channel currents during the action potential in chara; simultaneous recording of membrane voltage and patch currents. J Membrane Biol 141:297–309

Hope AB, Findlay GP (1964) The action potential in chara. Plant Cell Physiol 5:377–379

Hope AB, Walker NA (1975) Physiology of giant algal cells. Cambridge University Press, London

Jaklevic RC, Lambe J, Silver AH, Mercereau JE (1964) Quantum interference effects in Josephson tunneling. Phys Rev Lett 12:159–160

Jazbinsek V, Thiel G, Wübbeler G, Müller W, Trontelj Z (2000) Magnetic detection of injury-induced ionic currents in bean plants. Eur Biophys J 29:515–522

Josephson BD (1962) Possible new effects in superconductive tunnelling. Phys Lett 1:251–253

Kikuyama M, Tazawa M (1983) Transient increase of intracellular Ca^{2+} during excitation of tonoplast-free chara cells. Protoplasma 117:62–67

Koch H, Cantor R, Erné SN, Matthies KP, Peters M, Ryhänen T, Scheer HJ, Hahlbohm HD (1991) A 37 channel dc-SQUID magnetometer system. IEEE Trans Magn 27:2793–2796

Kotani M, Uchikawa Y, Kawakatsu M, Tsukada K, Kandori A, Sasabuti H, Suzuki H, Kondo S, Matsuda N, Shinada K, Yamada Y (1997) A whole-head SQUID system for detecting vector components. Appl Supercon 5:399–403

Miller AJ, Sanders D (1987) Depletion of cytosolic free calcium induced by photosynthesis. Nature 326:397–400

Mimura T, Tazawa M (1986) Light-induced membrane hyperpolarization and adenin nucleotide levels in perfused characean cells. Plant Cell Physiol 27:319–330

Moriyasu Y, Shimmen T, Tazawa M (1984) Electric characteristics of the vacuolar membrane of Chara in relation to pHv regulation. Cell Struct Funct 9:235–246

Nelson MT, Cheng H, Rubart M, Santana LF, Bonev AD, Knot HJ, Lederer WJ (1995) Relaxation of arterial smooth muscle by calcium sparks. Science 270:633–637

Okihara K, Ohkawa T, Tsutsui I, Kasai M (1991) A calcium dependent and voltage-dependent chloride-sensitive anion channel in the chara plasmalemma. A patch clamp study. Plant Cell Physiol 32:593–602

Onnes HK (1911) The superconductivity of mercury. Comm Phys Lab 12:120
Othmer HG (1997) Signal transduction and second messenger systems. In: Othmer HG, Adler FR, Lewis MA, Dallon J (eds) Case studies in mathematical modeling—ecology, physiology and cell biology. Prentice Hall, Upper Saddle River, New Jersey, pp 99–126
Pena-Cortes H, Fisahn J, Willmitzer L. (1995) Signals involved in wound-induced proteinase inhibitor II gene expression in tomato and potato plants. Proc Natl Acad Sci USA. 92:4106–4113
Parker RL (1977) Understanding inverse theory. Annu Rev Earth Planet Sci 5:35–64
Plieth C, Sattelmacher B, Hansen UP (1998) Light-induced cytosolic calcium transients in green plant cells. I. Methodological aspects of chlorotetracycline usage in algae and higher-plant cells. Planta 207:42–51
Plonsey R (1969) Bioelectric phenomena. McGraw-Hill, New York
Ramsey M, Barr RC, Spach MS (1977) Comparison of measured torso potentials with those simulated from epicardial potentials for ventricular depolarization and repolarization in intact dog. Circ Res 41:660–667
Reddy ASN (2001) Calcium: silver bullet in signalling. Plant Sci 160:381–404
Rhodes JD, Thain JF, Wildon DC (1996) The pathway for systemic electrical signal conduction in the wounded tomato plant. Planta 200:50–57
Roblin G (1985) Analysis of the variation potential induced by wounding in plants. Plant Cell Physiol 26:455–461
Roblin G, Bonnemain J-L (1985) Propagation in *Vicia faba* stem of a potential variation induced by wounding. Plant Cell Physiol 26:1273–1283
Ryan CA (1992) The search for the proteinase-inhibitor inducing factor PIIF. Plant Mol Biol 19:123–133
Sarvas J (1987) Basic mathematical and electromagnetic concepts of the biomagnetic inverse problem. Phys Med Biol 32:11–22
Shimmen T, Mimura T, Kikuyama M, Tazawa M (1994) Characean cells as a tool for studying electrophysiological characteristics of plant cells. Cell Struct Funct 19:263–278
Slibar M, Trontelj Z, Jazbinsek V, Thiel G, Mueller W (2000) Magnetic field and electric potential of excited plant cell *Chara corallina*: calculation and comparison with experiment. In: Aine CJ, Okada Y, Stroink G, Swithenby SJ, Wood CC (eds) Biomag 96: proceedings of the 10th international conference on biomagnetism. Springer, Berlin Heidelberg New York, pp 679–682
Stankovic B, Davies E (1998) The wound response in tomato involves rapid growth and electrical responses, systemically up-regulated transcription of proteinase inhibitors and calmodulin and down regulated translation. Plant Cell Physiol 39:268–274
Stratton JA (1941) Electromagnetic theory. McGraw-Hill, New York
Tazawa M, Kikuyama M (2003) Is Ca^{2+} release from internal stores involved in membrane excitation in characean cells? Plant Cell Physiol 44:518–526
Tester M (1990) Plant ion channels: whole-cell and single channel studies. New Phytol 114:305–340
Thiel G, Homann U, Plieth C (1997) Ion channel activity during the action potential in chara: new insights with new techniques. J Exp Bot 48:609–622
Tinkham M (1996) Introduction to superconductivity, second edition. McGraw-Hill, Inc., New york.
Trahms L, Erné SN, Trontelj Z, Curio G, Aust P (1989) Biomagnetic functional localization of a peripheral-nerve in man. Biophys J 55:1145–1153
Trontelj Z, Pirnat J, Luznik J, Jazbinsek V, Valencic V, Krizaj D, Vodovnik L, Jercinovic A (1989) Measurement of magnetic field near an acute surgical Injury on the rabbit's thigh. In: Williamson SJ, Hoke M, Stroink G, Kotani M (eds) Advances in biomagnetism. Plenum Press, New York, pp 517–520
Trontelj Z, Zorec R, Jazbinsek V, Erné SN (1994) Magnetic detection of a single action potential in *Chara corallina* internodal cells. Biophys J 66:1694–1696
Umrath K (1929) Über Erregungsleitung bei höheren Pflanzen. Planta 7:174–207

Wacke M, Thiel G (2001) Electrically triggered all-or-none Ca^{2+} liberation during action potential in the giant alga chara. J Gen Physiol 118:11–21

Wacke M, Thiel G, Hütt MT (2003) Ca^{2+} dynamics during membrane excitation of green alga chara: model simulations and experimental data. J Membr Biol 191:179–192

Wikswo JP, Barach JP, Freeman JA (1980) Magnetic-field of a nerve impulse—1st measurements. Science 208:53–55

Wildon DC, Thain JF, Minchin PEH, Gubb IR, Reilly AJ, Skipper YD, Doherty HM, O'Donnell PJ, Bowles DJ (1992) Electrical signalling and systemic proteinase inhibitor induction in the wounded plant. Nature 360:62–65

Williamson RE, Ashley CC (1982) Free Ca^{2+} and cytoplasmic streaming in the alga chara. Nature 296:647–651

Williams SE, Pickard B (1972) Receptor potentials and action potentials in Drosera tentacles. Planta 103:193–221

Woosley JK, Roth BJ, Wikswo JP (1985) The magnetic field of a single axon: a volume conductor model. Math Biosci 76:1–36

Wübbeler G, Mackert J, Armbrust F, Burghoff M, Mackert B, Wolff K-D, Ramsbacher J, Curio G, Trahms L (1998) SQUID measurements of human nerve and muscle near-DC injury-currents using a mechanical modulation of the source position. Appl Supercond 6:559–565

Zimmerman JE, Thiene P, Harding JT (1970) Design and operation of stable RF-biased superconducting point-contact quantum devices, and a note on properties of perfectly clean metal contacts. J Appl Phys 41:1572–1580

PART II PLANT ELECTROPHYSIOLOGY

10 Electrogenic Pumps

ROGER M. SPANSWICK

10.1 Introduction

The electrical properties of plant cell membranes are quite diverse, reflecting the wide range of environmental conditions to which plant cells are exposed. However, it appears that electrogenic pumps almost always make important contributions to the magnitude of the membrane potential and, in some cases, the membrane conductance (Higinbotham 1973; Spanswick 1981).

Early studies of membrane potentials using intracellular electrodes were summarized by Blinks (1949). Due to technical limitations, the early work involved the use of large freshwater or marine algal cells such as *Valonia*, and it was not until the development of modern microelectrode techniques and electronics that the methods became more reliable, beginning in the late 1950s. Initial approaches to the problem of accounting for the magnitudes of the membrane potential and conductance and their response to changes in external ion concentrations were influenced strongly by the success of animal physiologists in making the simplifying assumption that the gradients of ion concentrations across the plasma membrane were established by neutral ion pumps, i.e. pumps that would not generate a current. It was also assumed that the electrical properties of the membrane were determined entirely by passive diffusion of the ions across the membrane down the gradient for each ion that resulted from its concentration gradient and the common electrical potential gradient, summed as the electrochemical potential gradient. The assumption of a constant electric potential gradient (electric field) within the membrane, together with a constant partition coefficient for an ion at both surfaces of the membrane, makes it possible to integrate the diffusion equations across the membrane and yields an equation for the net passive flux, J. The flux, J_K, for potassium, as an example, is:

$$J_K = -P_K\left(\frac{FE}{RT}\right)\frac{\left\{\left[K_o^+\right]-\left[K_i^+\right]\exp\left(FE/RT\right)\right\}}{\left\{1-\exp\left(FE/RT\right)\right\}} \tag{10.1}$$

where P_K is the permeability coefficient, E is the difference in electrical potential across the membrane (the membrane potential), $[K_o^+]$ and $[K_i^+]$ are the

Department of Biological and Environmental Engineering, Riley-Robb Hall, Cornell University, Ithaca NY 14853-5701, USA (e-mail: rms6@cornell.edu)

Plant Electrophysiology – Theory & Methods (ed. by Volkov)

external and internal potassium concentrations, respectively, F is the faraday and R and T have their usual meanings. The further assumption of a steady state, or specifically that there is no net charge accumulation in the cell, means that the net currents carried by the individual ions must sum to zero. It leads to the equation, usually referred to as the Goldman–Hodgkin–Katz (or GHK) equation (Goldman 1943; Hodgkin and Katz 1949), which, assuming that sodium, potassium and chloride are the only ions transported, has the form:

$$E = \left(\frac{RT}{F}\right) \ln \frac{P_K\left[K_o^+\right] + P_{Na}\left[Na_o^+\right] + P_{Cl}\left[Cl_i^-\right]}{P_K\left[K_i^+\right] + P_{Na}\left[Na_i^+\right] + P_{Cl}\left[Cl_o^-\right]} \tag{10.2}$$

[See Nobel (2005) for a detailed derivation of this equation.]

It is also possible to find an expression for the conductance in terms of the concentrations and permeability coefficients by first applying the condition:

$$\Sigma z_j F J_j = I, \tag{10.3}$$

where I is the applied current, z_j is the valence of the ion j, and $\Sigma z_j F J_j$ is the sum of the currents due to the fluxes of the individual ions. Differentiating, to obtain dI/dE, gives the conductance:

$$G_m = \left[\frac{F^3 E}{(RT)^2}\right]\left[\frac{wy}{w-y}\right] \tag{10.4}$$

in the limit $I \rightarrow 0$, where G_m ($S.m^{-2}$) is the specific conductance of the membrane, $w = P_K[K_o^+] + P_{Na}[Na_o^+] + P_{Cl}[Cl_i^-]$ and $y = P_K[K_i^+] + P_{Na}[Na_i^+] + P_{Cl}[Cl_o^-]$. This expression was also derived by Hodgkin and Katz (1949).

Equations 10.1, 10.2 and 10.4 provide the basis for determining whether the electrical properties of the membrane can be accounted for simply by passive diffusion of the ions. The permeability coefficients are defined by Eq. (10.1), or partial equations for the unidirectional fluxes derived from it. Since the membrane potential appears in all the equations, they are not independent. However, if the assumption of passive ion diffusion is valid, the equations should give consistent results. They can, of course, be extended to include other ions that have significant fluxes across the membrane.

The results of early attempts to apply this approach to plant cells were presented clearly by Dainty (1962). Even at that stage, problems were becoming evident. However, the approach does provide a sound quantitative theoretical basis on which to proceed. Thus, permeability coefficients could be calculated from the passive components of the major ion fluxes and used with concentration data to make predictions about the magnitude of the membrane potential and conductance or the response to changes in external ion concentrations.

10.2 Problems with the neutral ion pump assumption

Freshwater characean internodal cells provided the most useful experimental material for early experiments on plant cell electrophysiology because their large size permits, with relative ease, the measurement of the separate electrical potentials across the plasma membrane and tonoplast as well as the concentrations in the cytoplasm and the vacuole (Spanswick and Williams 1964).

10.2.1 Effects of external ion concentrations

As Nobel (2005) points out, Eq. (10.2) can be used to predict the membrane potential of *Nitella translucens* in artificial pond water (APW; unbuffered 0.1 mM KCl + 1 mM NaCl + 0.1 mM $CaCl_2$) from the permeability coefficients determined by MacRobbie (1962) in combination with the ion concentrations measured by Spanswick and Williams (1964). The predicted value (−138 mV) is very close to the measured value (−140 mV; Spanswick and Williams 1964). However, the equation fails, except under special conditions, to account for the changes in membrane potential produced by changes in the external ion concentrations. Kishimoto (1959) demonstrated the lack of response of the membrane potential of *Chara corallina* to external potassium concentrations up to 1 mM, and only a relatively small response up to 10 mM. Hope and Walker (1961) were able to describe the response of the membrane potential of *Chara australis* to external potassium using Eq. (10.2) with terms for only sodium and potassium. However, it required pretreatment of the cells in 5 mM NaCl for several hours followed by the use of experimental solutions containing no calcium. A more detailed investigation (Spanswick et al. 1967), based on the data available for *Nitella translucens*, showed that the effect of a change in potassium concentration in APW from 0.1 mM to 1.0 mM produced a change in potential of 9 mV when calcium was present, far less than the 32 mV predicted by Eq. (10.2). Thus, in this concentration range, there is a discrepancy between the diffusion hypothesis and observation.

10.2.2 Membrane conductance

A similar problem arises when the measured conductance of the membrane is compared to the value predicted on the basis of the permeability coefficients. Williams et al. (1964) made careful conductance measurements on *Nitella translucens*, taking into account the cable properties of the cells, and obtained a mean value of 0.47 S m^{-2}. On the basis of permeability coefficients calculated from the passive fluxes of sodium and potassium (MacRobbie 1962), they calculated that the conductance due to the passive diffusion of these ions would be 0.033 S m^{-2}. Taking into account the passive flux of chloride (Hope et al. 1966), the calculated conductance increases to about 0.050 S m^{-2}. Even then,

there is a discrepancy of an order of magnitude between the observed conductance and the conductance calculated from the passive fluxes of the major ions. Discrepancies of 3- to 4-fold in animal cells have been accounted for as underestimates of the passive fluxes due to filing of the labeled ions in pores (Hodgkin and Keynes 1955). However, in this case it would take an occupancy of about ten ions per pore to explain the discrepancy, and that appears to be unrealistic.

10.3 Alternatives to the neutral pump assumption

Since there were problems in applying a theory based on the assumption that the electrical properties of the plasma membrane are controlled only by passive ion diffusion, it appeared that there was a factor or factors that had been overlooked. Possibilities included the presence of an electrogenic pump and/or a significant current due to the passage of one of the minor ions across the membrane.

10.3.1 Criteria for electrogenic ion pumps

One of the more rigorous proofs for the existence of an electrogenic pump was the classic "frog skin" experiment of Ussing (Ussing and Zerahn 1951) in which the epithelium was inserted between two chambers containing identical solutions. Passage of an electric current was required to bring the electric potential difference across the epithelium to zero. Since there was a virtual equilibrium across the epithelium under these conditions, passive currents did not contribute to the current, which could be attributed to an electrogenic pump. On the basis of flux measurements, the ion involved was identified as sodium.

It is not possible to apply this "short-circuit" technique to individual cells, so an alternative approach is required. One approach involves inactivating the pump and observing the effect on the membrane potential. If the ion is pumped into the cell, it is a straightforward matter to stop the pump by removing the ion from the solution flowing past the cell. This works well in identifying the electrogenic chloride pump in marine algae (see below). However, the electrogenic pump in freshwater algae and higher plants does not appear to be an inwardly directed anion pump. Rapid depletion of the concentration of an ion in the cytoplasm is not feasible, so an alternative approach is needed.

Another way to halt the pump is the use of inhibitors that affect the pump directly or deplete the energy supply. An early example of this approach was the application of the uncoupler DNP to oat coleoptile cells (Etherton and Higinbotham 1960). There was a depolarization of the membrane potential that could be interpreted as inhibition of an electrogenic pump. However, in

using inhibitors there is always the possibility that the inhibitor is directly affecting the membrane potential via an effect on the permeability coefficients in Eq. (10.2). It was later demonstrated that this was not the case (Higinbotham et al. 1970). However, the number of flux measurements required to do this is very demanding.

Avoidance of the use of inhibitors, except as a secondary confirmation of the presence of an electrogenic pump or as an aid in identifying the energy source for the pump, can be achieved either by choosing plant cells with large negative membrane potentials or by manipulating the environmental conditions to achieve potentials beyond the limit of the diffusion potential given by Eq. (10.2). Examination of the equation will show that the diffusion potential has a range of possible values dependent on the relative values of the permeability coefficients. The extreme values are set by the ions with the most positive and most negative Nernst potentials, since in the GHK equation the potential tends towards the Nernst potential for a particular ion when the permeability coefficient for that ion increases to values at which the other terms in the equation are negligible compared to the products of the permeability coefficient times the concentration for that ion. For example, potassium is the major ion with the most negative Nernst potential (−178 mV) for the plasma membrane of a cell of *Nitella translucens* in APW (Spanswick and Williams 1964). The observed membrane potential (−138 mV) is within the range of theoretically possible diffusion potentials and does not provide evidence for the existence of an electrogenic pump without further manipulation of the system.

There are, however, systems that do meet the criterion without any special experimental conditions. Slayman (1965a) showed that the membrane potential in the fungus *Neurospora crassa* is about −200 mV, while E_K is around −70 mV. The potential was very sensitive to inhibitors, and Slayman (1965b) suggested tentatively that *Neurospora* might have an electrogenic H^+ pump. *Elodea* is an example of a plant that has a membrane potential as large as −300 mV (Spanswick 1972a). It would require something like 9 M K^+ in the cell for it to be a K^+ diffusion potential. Even if there were K^+ salts soluble at that concentration, such high concentrations could clearly be ruled out on osmotic grounds.

10.4 Electrophysiological evidence for electrogenic pumps at the plasma membrane

The growing realization that electrogenic ion pumps were important in plants made it important to be able to demonstrate that they existed in plant cells that did not exhibit unusually large membrane potentials. It was also necessary to identify the ion being transported by the pump.

10.4.1 Electrophysiology of characean cells

Kishimoto (1959) found an effect of the pH of unbuffered solutions on the membrane potential of *Chara corallina*, the most negative values being at around neutral pH, but did not interpret the result in terms of H^+ transport. Hope (1965) observed a large hyperpolarization of the membrane potential (50–70 mV) of *Chara* upon substituting bicarbonate for Cl^- in APW. Since the bicarbonate ions also caused an increase in external pH from 5.5 to 7.8, Hope suggested that the effect could have been due (a) to diffusion of H^+ if P_H, the permeability coefficient for H^+, is high, or (b) to an electrogenic bicarbonate pump. He rejected (a) because the internal (cytosolic) pH would have had to be in the range 3–4 to explain the large observed values of the membrane potential, and came down tentatively in favor of (b). However, it was later shown that, in *Nitella translucens*, buffered solutions with a pH equal to that of solutions containing bicarbonate produced a partly transient hyperpolarization of the membrane potential but subsequent application of bicarbonate at constant pH had little effect (Spanswick 1970). This appeared to rule out the possibility of a primary electrogenic bicarbonate pump.

Kitasato (1968), meanwhile, made a detailed investigation of the effects of pH on the electrophysiology of *Nitella clavata* using solutions buffered with 0.2 mM tris (hydroxymethyl) aminomethane. The membrane potential exhibited a Nernstian slope with respect to pH in the range 4–6. The potential reached its most negative value at pH 7 and then depolarized slightly at pH 8. As in other work, the membrane potential was insensitive to changes in external K^+ in the range 0.1–1.0 mM in the presence of calcium. Kitasato was able to rule out the possibility that the effect of pH was exerted via an effect on the permeability coefficients of potassium or chloride by making measurements of the (passive) effluxes of these ions in the range pH 6-8. In this species too, the sum of the calculated conductances due to the individual major ions was much less than the observed membrane conductance.

The hypothesis proposed by Kitasato (1968) to explain his observations was, at first sight, both revolutionary and ingenious in that it could account for both the control of the membrane potential and the discrepancy between observed and calculated membrane conductances in terms of the role of hydrogen ions (referred to here, interchangeably, as protons). He suggested that the response of the membrane potential to changes in pH did indeed imply that the plasma membrane has a high permeability to H^+, and estimated that the passive influx was about 400 nmol m^{-2} s^{-1} at an external pH of 5.0. The high value for the permeability coefficient, P_H, associated with this influx would require inclusion of a term $P_H[H^+_o]$ in the numerator of Eq. (10.2) that would give a value for the diffusion potential much more positive than the observed value. However, since an active efflux mechanism would be needed to balance the influx and avoid acidification of the cytoplasm, Kitasato (1968) suggested that if the efflux were via an electrogenic proton pump it could hyperpolarize the membrane to match the observed values of

the membrane potential. He initially described this using the equation for a "constant current" electrogenic pump often used in animal physiology:

$$E = \left(E_m\right)_o + \frac{FJ_j}{g_m} \tag{10.5}$$

where $(E_m)_o$ is the diffusion potential given by Eq. (10.2), in this case including terms for protons, J_j is the flux through the pump and g_m is the "membrane conductance", assumed to include only the conductances due to passive ion movements.

The difficulty of testing this hypothesis is compounded by the fact that protons exchange with water, making it impossible to use tritium as a tracer to measure unidirectional fluxes. However, a detailed examination of the applicability of this hypothesis to *Nitella translucens* (Spanswick 1972b) revealed difficulties, some of which were present in the original work. For example, at an external pH of 8.0, the membrane potential levels off as a function of pH and, according to Eq. (10.2) with terms for protons, the term $P_K[K_o^+]$ should become dominant in the numerator so that the membrane potential is affected primarily by the external potassium concentration. However, Kitasato himself showed that a change in potassium concentration from 0.1 to 1.0 mM depolarized the membrane potential by only 5 mV at pH 8 (Table I in Kitasato 1968).

There is also a problem in accounting for the membrane conductance as primarily due to passive proton currents. At high external pH (8 or 9) the membrane conductance should decrease due to the decrease in external $[H^+]$ and also, most likely (Smith 1984), a decrease in internal $[H^+]$. In fact an increase in conductance was observed in *Nitella translucens* (Spanswick 1972b) and in *Nitella axilliformis* (Saito and Senda 1974).

A further inconsistency occurred in a voltage-clamp experiment (Fig. 11 in Kitasato 1968) in which the membrane potential was clamped at −110 mV in APW containing 1 mM K^+. Decreases in pH from 8 to 6, 5 and then 4 led to an apparent increase in inward current, interpreted by Kitasato (1968) as due to the passive influx of H^+. However, the resting potential of these cells in this solution was reported as −109 mV (Table 1, Kitasato 1968). Thus the clamp current at pH 5 should have been close to zero, and the change in current between pH 8 and pH 5 could be reinterpreted as a decrease in an outward current.

Thus there appear to be problems in interpreting the electrophysiological properties of the membrane as being due primarily to the passive diffusion of H^+. An alternative hypothesis (Spanswick 1972b, 1981) was presented in which the passive permeability of the membrane to protons was assumed to be low and an electrogenic proton pump was postulated to account for the high membrane conductance as well as the large effect of pH on the membrane potential. First, however, it was necessary to demonstrate unambiguously the presence of an electrogenic pump in *Nitella translucens* which, in unbuffered APW, had a membrane potential within the range of possible

diffusion potentials (Spanswick and Williams 1964). This was made possible by adjusting the environmental factors (Spanswick 1972b). First, the pH was buffered with 1 mM zwitterionic buffer at pH 6 (APW6), which makes the membrane potential more negative than the value in unbuffered APW (pH about 5.5 following exposure to atmospheric CO_2). Second, the potassium concentration in the solution was raised from 0.1 mM to 0.5 mM, a value that has little effect on the membrane potential but makes the negative limit of the diffusion potential more positive by about 40 mV. Third, it was found that the use of CO_2-free solutions stabilized the membrane potential at more negative values in the light. In this species, also, raising the potassium concentration in the solution to 10 mM depolarized the membrane to a potential close to the calculated value of E_K, the Nernst potential for K^+. The change in potential was usually achieved following a spontaneous action potential, and a large increase in membrane conductance indicated that it was due to an increase in P_K. This permitted the value of E_K for an individual cell to be calculated for any other value of external potassium concentration. Since E_K sets the negative limit of the diffusion potential at 0.5 mM K^+, this limit could be determined for individual cells by measuring the membrane potential in 10 mM K^+ at the end of an experimental run. In the dark, the membrane potential in this species was close to E_K. However, exposure to light produced a small transient depolarization followed by a hyperpolarization of 50 mV to a stable membrane potential about 44 mV more negative than E_K. Since the potential under these conditions is clearly beyond the negative limit of the diffusion potential, this experimental condition provides unambiguous evidence for the presence of an electrogenic ion pump that is activated in the light. This was supported by the greater response of the membrane potential to changes in temperature in the light.

The response of the membrane potential to inhibitors is also consistent with the presence of an electrogenic pump. Kitasato (1968) showed that 1 mM DNP, an uncoupling agent, depolarized the cell to a value close to E_K in a solution containing 1 mM K^+ at pH 6, and to more positive values at pH 5. However, the action of DNP has since been shown to be strongly dependent on the pH of the external solution, and can cause irreversible damage at low pH (Homblé 1987). More detailed investigations with a range of inhibitors on both *Nitella translucens* (Spanswick 1974) and *Chara corallina* (Keifer and Spanswick 1979) have shown that conditions that reduce the cellular ATP level produce depolarization of the membrane potential, the exception being darkness, which does not affect the ATP level (Penth and Weigl 1971; Spanswick and Miller 1977b; Keifer and Spanswick 1979). The dependence on ATP is consistent with the demonstration that internally perfused *Chara* cells demonstrate a hyperpolarization dependent on the presence of ATP (Shimmen and Tazawa 1977). However, the membrane potential in the inhibited state tended to be close to the diffusion potential for potassium, not the more positive potential given by the GHK equation modified to take into account a large permeability coefficient for H^+.

Another problem for the Kitasato hypothesis of a constant current pump was that inactivation of the pump in *Nitella translucens*, by darkness, inhibitors or CO_2, was accompanied by a decrease in membrane conductance (Spanswick 1974). The transition from light to dark was accompanied by a 6-fold decrease in conductance; decreases in conductance were also produced by 1 μM CCCP or 50 μM DCCD. Similar observations were made in *Chara corallina* (Keifer and Spanswick 1979). Since the I-V (current-voltage) curve in the light was linear over the range of potentials encompassing the activated and inhibited pump, the change in conductance was not due simply to the shift of the resting potential to a different position on the I–V curve.

The association between pump activity and high membrane conductance appeared to be difficult to account for on the basis of a constant current pump and a high passive proton flux because it would require an assumption, for which there was no obvious justification, that all the conditions that led to inhibition of the pump would also reduce the permeability of the membrane to protons. As an alternative, it was suggested (Spanswick 1972b, 1981) that an electrogenic pump with conductance might account for both the high membrane conductance and the response of the membrane potential to external pH.

A simple equivalent circuit for a membrane with a conducting pump, having a conductance g_P in parallel with a lumped conductance, g_D, representing the passive ion pathways is shown in Fig. 10.1. Slayman (1965b) had previously

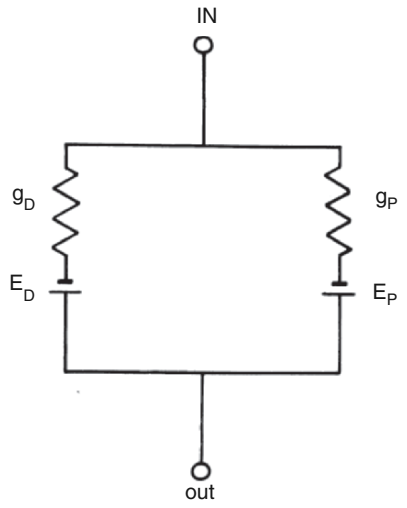

Fig. 10.1. An equivalent circuit for a membrane with an electrogenic pump (*P*) in parallel with the lumped conductances for the passive diffusion pathways (*D*). The pump has been assigned a conductance, g_P, in series with an EMF, E_P. The conductances for the passive pathways are lumped together as a single conductance g_D, which is in series with the diffusion potential E_D. (From Spanswick 1981, with permission)

considered this model, first put forward by Finkelstein (1964), in his work on *Neurospora crassa* but, on the basis of analysis of the current–voltage curves before and after treatment with CN^-, concluded that the pump conductance did not contribute more than 5–10% of the total membrane conductance. In a more detailed assessment, this estimate was raised to 15–20% of the conductance at the resting potential (Gradmann et al. 1978).

At this stage, the identity of the ion being pumped was not established. However, removal of Cl^- from APW did not produce an immediate depolarization of the membrane potential (Spanswick 1972b), thus eliminating the active chloride influx from consideration. Ouabain, a putative inhibitor of the active Na^+ efflux (MacRobbie 1970), had no effect on the membrane potential or conductance (Spanswick 1974). Since the pump operated in the absence of external bicarbonate, and bicarbonate had no effect on the potential at constant pH, bicarbonate could also be eliminated. A significant electrogenic Ca^{2+} efflux seemed a remote possibility. In fact, the major ions could be ruled out by considering the current required to reduce the membrane potential to the negative limit of the diffusion potential (Spanswick 1972b). This provides a minimum estimate of the current through the pump under these conditions since reduction of the membrane potential to the diffusion potential, defined as the potential at which the net current through the passive pathways is zero, would be slightly more positive than E_K due to the effect of other ions on the diffusion potential (Eq. 10.2). The measured current of 0.22 mA m^{-2} was equivalent to a flux (220 nmol m^{-2} s^{-1} for a monovalent ion) at least an order of magnitude larger than the fluxes of the major ions that had been measured in *Nitella translucens*, including Ca^{2+} (Spanswick and Williams 1965), thus appearing to leave H^+ as the remaining candidate. It was several years later that this was confirmed directly using isolated plasma membrane vesicles from higher plants (see below). It should be emphasized that, for a conducting pump, the large flux estimated above at the voltage equal to the diffusion potential is not equal to the flux at the resting potential; the current flowing through the pump will be reduced at the more negative resting potential, presumably bringing it into balance with the net current through the other transport systems in the membrane.

It is easy to show (e.g. Spanswick 1980) for the equivalent circuit in Fig. 10.1 that:

$$E_m = \frac{\left(g_D E_D + g_P E_P\right)}{\left(g_D + g_P\right)} \tag{10.6}$$

and that E_m will be closer to E_D, the diffusion potential, or E_p, the EMF of the electrogenic pump, depending on whether g_D, the sum of the conductances of the passive channels, or g_p, the conductance of the electrogenic pump, is greater.

It is then necessary to consider how one can describe E_p. By definition, the EMF is the potential across the membrane at which no current flows through the pump.

A theory put forward by Rapoport (1970), originally in the context of the electrogenic Na^+, K^+-ATPase, was very useful in looking at this problem (Spanswick 1972b) and in deriving an expression for E_p. However, a simpler way to derive this relationship is simply to consider the EMF as the potential at which the pump will stop, i.e. when $\Delta\overline{\mu}_H = \Delta\mu p/n_j$, where $\Delta\overline{\mu}_H$ is the difference in electrochemical potential across the membrane for H^+, $\Delta\mu_p$ represents the chemical potential of the driving reaction and n_j is the stoichiometric coefficient of the pump. E_p is also known as the "reversal potential" for the pump, since making the potential even larger causes the pump to run in the opposite direction if it is kinetically feasible. Expanding the term for $\Delta\overline{\mu}_H$:

$$\begin{aligned}\Delta\mu_p &= n_j\Delta\overline{\mu}_H \\ &= n_j\left\{RT\ln\left(\left[H_i^+\right]/\left[H_o^+\right]\right) + zFE\right\}\end{aligned}$$

This simplifies to give:

$$E = \left(\Delta\mu_p/zFn_j\right) + (RT/zF)\,\mathrm{In}\left(\left[H_o^+\right]/\left[H_i^+\right]\right) = E_p \qquad (10.7)$$

Note that the dependence of the EMF on $\ln[H_o^+]$ means that, if H^+ is the ion being pumped, we can explain the effect of external pH on the membrane potential as an effect of pH on the pump EMF rather than as an effect on the diffusion potential. It would also require that $g_P > g_D$ and this, in turn, would provide a possible explanation for the discrepancy between the measured conductance (equal to $g_P + g_D$) and that calculated from the passive fluxes of the major ions (equal to g_D only). In other words, the missing conductance could be attributed to the pump, not the passive flux of an ion such as H^+.

When the pump is working slowly, e.g. in the dark or in the presence of certain inhibitors, the membrane conductance is relatively low. If the change in observed membrane conductance, which would be equal to the total membrane conductance $g_D + g_P$ (Fig. 10.1), were not due to a reduction in g_P, one would have to assume arbitrarily that light and inhibitors affect g_D via an effect on P_H. However, the use of Eq. (10.6) to explain the effects of inhibitors on the membrane potential has been limited. Presumably, this is because it involves both the thermodynamic factors that determine E_p and also the kinetic factors that affect g_P, and hence value of g_P relative to g_D.

Recent reviews by Kitasato (2003) and Tazawa (2003) reach conclusions that appear to be compatible with this interpretation of a pump with conductance and a membrane with limited H^+ permeability. Tazawa (2003) discusses the mechanism that may be involved in activation of the pump by light.

The initial effect on the membrane potential of a change in pH from acid (pH 5) to more alkaline values can be ascribed to the dependence of E_p on external pH (Eq. 10.7). This short-term change in potential is generally greater in the light than in the dark (Spanswick 1972b; Saito and Senda 1973a) and is decreased greatly at low temperature (Saito and Senda 1973b). The

subsequent decline in the membrane potential at pH 7 and above might be ascribed to an increase in cytoplasmic pH. However, the limited dependence of cytoplasmic pH on external pH (Smith 1984) is not sufficient to account for the change via the effect on E_P (Eq. 10.7). An alternative explanation would involve the effect of cytoplasmic pH on the kinetics of the pump. Fujii et al. (1979) varied the internal pH of tonoplast-free, perfused cells of *Chara australis* and showed that the membrane potential in the presence of ATP demonstrates a maximally hyperpolarized value in the range pH 6–7. A similar result was obtained with *Nitellopsis* (Mimura and Tazawa 1984). This corresponds to the pH maxima of pH 6.5 for both ATPase activity and proton pumping by the higher plant plasma membrane H^+-ATPase (O'Neill and Spanswick 1984; De Michelis and Spanswick 1986). Since the pH of the cytosol in Characean cells is in the range 7.5-7.8 when the external pH is 6.0–6.3 (Walker and Smith 1975; Spanswick and Miller 1977a; Mimura and Kirino 1984; Smith 1984), a similar pH-dependence of the electrogenic pump would result in a reduced rate for a slight increase in pH. One indication that this can occur is that the light-induced hyperpolarization at pH 6 in *Nitella translucens* may occasionally decay after some time but can be rapidly restored upon acid loading the cytoplasm by application of 5 mM DMO, a weak acid that is permeant in its neutral form (Spanswick and Miller 1977b). Similarly, prolonged treatment with Cl^--free solutions can also produce a depolarization (Spanswick 1974), perhaps due to the effect of interruption of the Cl^-/H^+ cotransport system on cytoplasmic pH (but see Smith and MacRobbie 1981); this can also be reversed with DMO (Spanswick 1980). Thus, while thermodynamic factors control the magnitude of E_P, it appears that kinetic factors, evidently involving activation of the ATPase rather than mass action by the substrate, may affect g_P and therefore the degree to which E_P controls the membrane potential. This approach was also useful in describing the relationship between the membrane potential and conductance during the course of inhibition by 1 mM CO_2/HCO_3^- in *Nitella translucens* (Spanswick 1980). Fitting the data for a typical experiment (Fig. 10.2) using Eq. (10.6), and attributing the decline in membrane conductance entirely to a change in g_P, yields reasonable values for E_D (−115 mV), E_P (−182 mV) and g_D (0.088 S m^{-2}).

The use of inhibitors to separate the contributions of the pump and passive diffusion to the electrical properties of the membrane is usually complicated by lack of specificity or the indirect nature of the inhibition. For example, inhibitors that act by reducing the ATP level also affect ATP-dependent channels responsible for excitation (Shimmen and Tazawa 1977). Nevertheless, inhibitors that reduce the ATP level to less than about 35% of the control value (5 μM CCCP, 0.1 mM DNP, 50 μM DCCD, and 40 μM DES) do produce a depolarization and also decrease the membrane conductance (Keifer and Spanswick 1979) in agreement with internal perfusion studies (Mimura et al. 1983; Tsutsui and Ohkawa 2001). Vanadate applied externally to *Nitella translucens* was reported to inhibit the electrogenic pump and

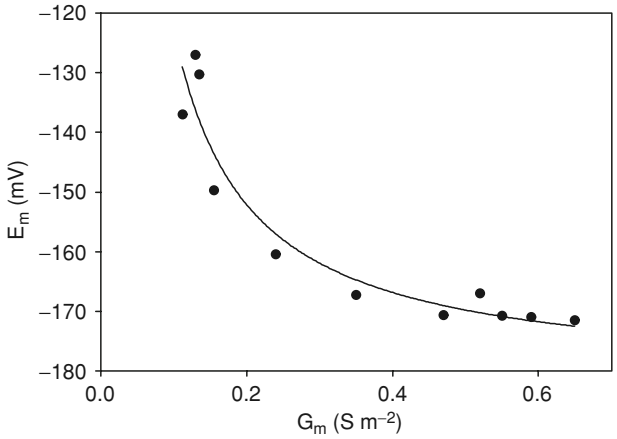

Fig. 10.2. The relationship between the membrane conductance (G_m) and the membrane potential (E_m) during the course of inhibition of the electrogenic pump in *Nitella translucens* by 1 mM CO_2/HCO_3^- at pH 6. The line connecting the points is fit to Eq. (10.6) with E_P= −182 mV, E_D= −115 mV and g_D=0.088 S m^{-2}. (Replotted data from Spanswick 1980.)

decrease the membrane conductivity (Cruz-Mireles and Ortega-Blake 1991). Unfortunately, the ability of Characean cells to take up vanadate appears to vary with the growth conditions, and the experiments are difficult to replicate (Spanswick, unpublished). Internal perfusion with vanadate also inhibits the pump (Shimmen and Tazawa 1982), but again there is variability and a time-dependent recovery that suggest modification of the vanadate by cellular components, possibly glutathione (Macara et al. 1980).

An interesting observation is that gluteraldehyde, although presumably unspecific in its effects, maintains the low permeability of the membranes of *Chara corallina* for up to 3.5 h (Shimmen 2004). The treatment produces a depolarization, a decrease in membrane conductance and also a decrease in the response to a pH change from 5 to 7, data compatible with the hypothesis that its primary effect is on a conducting electrogenic pump.

A detailed analysis of the inhibition of the electrogenic pump of *Chara corallina* by DCCD was carried out by Kishimoto's laboratory (Kishimoto et al. 1984, 1985; Takeuchi et al. 1985). By assuming that the current-voltage relationships after 100 min of inhibition by 50 μM DCCD represented the properties of the passive diffusion channels only, they were able to subtract this curve from those obtained earlier during the course of inhibition to obtain the current-voltage curves for the pump (Kishimoto et al. 1984). Analysis of the effect of pH over the range 6.5–7.5 showed only a minor effect on the current–voltage curve of the passive diffusion component, while the current–voltage curves for the pump were shifted parallel to the pump current axis by the change in pH. The results could be described kinetically by a 5-state or a reduced 2-state kinetic

model, the reversal potential for the pump being consistent with a stoichiometry of $2H^+$/ATP (Takeuchi et al. 1985). This is consistent with the value of E_P obtained by fitting the results of CO_2/HCO_3^- inhibition of the pump in *Nitella translucens* (Spanswick 1980; 10.2) or from the intersection of the current-voltage curves in the light and dark (Spanswick 1972b; Saito and Senda 1974). Note, however, that Beilby (1984) suggested a stoichiometry of 1.0, and more direct measurements based for the higher plant plasma membrane ATPase have also indicated a value of 1.0 (Briskin and Reynolds-Niesman 1991). Blatt (1986) and Blatt et al. (1990) have presented a more detailed discussion of the assumptions that may complicate the deduction of stoichiometry from electrophysiological experiments.

10.4.2 Electrophysiology of marine algae—the electrogenic Cl^- pump of *Acetabularia*

While attention in this chapter has been focused on the electrogenic proton pump that is of primary importance in freshwater algae and higher plants, there is strong evidence for an electrogenic Cl^- pump in the marine alga *Acetabularia* (Gradmann and Bentrup 1970; Saddler 1970). The evidence for an electrogenic Cl^- pump is relatively straightforward in that substitution of other anions for Cl^- in the medium results a large depolarization of the membrane potential from its normal value of −170 mV in the light. Inhibitor and low temperature experiments give results consistent with this hypothesis. Gradmann (1984) has reviewed the extensive work on this system, primarily from his laboratory. One unusual aspect is that a slow propagated electrical depolarization, which has all the properties of an action potential, results from a change in the activity of the electrogenic pump.

10.4.3 Electrophysiology of higher plant cells

As pointed out earlier (10.3.1), large negative membrane potentials, beyond the limit of the diffusion potential, provide a sound criterion for the presence of an electrogenic pump. In addition to *Elodea* (Jeschke 1970; Spanswick 1972b, 1973; Marrè et al. 1989), such potentials have been observed in leaf cells of *Lemna* (Young and Sims 1973; Novacky et al. 1978; Löppert 1979), red beet storage tissue (Mercier and Poole 1980), carrot root cells (Anderson et al. 1977), cells for which raising the external potassium concentration leaves the membrane potential at a value more negative than E_K the (Higinbotham and Anderson 1974), soybean root cells (Lew and Spanswick 1984a) and *Vallisneria* leaf cells (Prins et al. 1980; Harada et al. 2002).

One limitation in investigating the electrophysiology of cells in a higher plant tissue is that measurements of membrane conductance are complicated by the fact that an unknown proportion of the current injected into a cell will pass to neighboring cells via plasmodesmata (Spanswick 1972a),

thereby making it difficult to estimate the conductance accurately. However, *Arabidopsis* root hair cells provide a system in which this problem is minimized (Meharg et al. 1994) and in which it has been demonstrated that double-barreled microelectrodes can be used for voltage-clamp experiments (Lew 1991). *Arabidopsis* root hairs were also a system in which vanadate could be used to inhibit the electrogenic pump when applied externally. Current–voltage curves before and after inhibition by cyanide or vanadate suggested that the electrogenic pump was of the constant-current type (Lew 1991). However, Lew (1991) expressed some reservations concerning the validity of this interpretation given the uncertainty in this system regarding the uniformity of the membrane properties and the limitations presented by current injection and voltage measurement at the same site near the base of the cell (see also Meharg et al. 1994).

While the emphasis here is on the proton pumps deduced to operate in plants that grow under non-saline conditions, it should be pointed out that strong evidence for an electrogenic Cl^- pump in the salt glands of *Limonium vulgare* was provided by Hill (1970) using a short-circuit technique.

10.5 Plant plasma membrane H^+-ATPase

Direct measurement of the flux of H^+ through the postulated electrogenic proton pump encountered technical problems resulting from the chemistry of H^+. The exchange of protons with water, combined with the high values for water fluxes, makes it impossible to use a radioactive tracer to estimate the unidirectional fluxes of H^+ across cell membranes. The alternative is to measure the net flux (influx minus efflux) but this is also beset with technical problems, including the buffer capacity of cell walls, the pH changes outside the cells brought about by net transport of CO_2 as a result of photosynthesis and/or respiration, the unknown magnitude of the passive influx, and the existence of alternative routes of transport that became evident with the discovery of proton cotransport systems (Slayman and Slayman 1974; Poole 1978). In an effort to test the validity of the chemiosmotic hypothesis (Mitchell 1961) for energy transduction in mitochondria and chloroplasts, a variety of methods had been developed earlier to assay proton gradients and electrical potentials in membrane vesicles and reconstituted systems (liposomes). The adaptation of optical probe techniques for use with plant membrane vesicles (Bennett and Spanswick 1985) made it possible to determine both relative initial rates of H^+ transport (Bennett and Spanswick 1983) and measure membrane potentials. Several groups published investigations on proton transport in plant membrane vesicles at about the same time (see Sze 1985 for an account of the early work). With improvements in methods for separating vesicles derived from the plasma membrane and the tonoplast, it quickly became possible to characterize the systems responsible for net H^+

transport. From an experimental point of view, the advantage of this approach is that it eliminates the problems associated with the cell wall buffering capacity and with changes in CO_2 concentration. Careful design of assay buffers, based on knowledge of the diversity of proton cotransport systems, also reduces the likelihood that H^+ transport is via a pathway other than the one that is the object of study. Another advantage is that, given the correct membrane orientation, i.e. with the catalytic site on the exterior surface, the energy supply can be controlled at will.

10.5.1 Isolated plasma membrane vesicles

Initial studies of H^+ transport in isolated plant membrane vesicles revealed ATPase activity and H^+ transport that were both stimulated by chloride (Hager and Helmle 1981). Comparison with ATPase data on intact vacuoles (Admon et al. 1981; Walker and Leigh 1981) suggested that this activity was associated with tonoplast vesicles (DuPont et al. 1982a,b; Mettler et al. 1982). It was well established from earlier work (e.g. Hodges et al. 1972) and from external membrane labeling studies (Perlin and Spanswick 1980) that the ATPase activity associated with the plasma membrane was stimulated by K^+ and was affected very little by anions. It soon became evident (Churchill et al. 1983; De Michelis et al. 1983; Bennett et al. 1984; Hager and Biber 1984; Lew and Spanswick 1984b) that two ATP-dependent H^+ transport activities could be separated by density gradient centrifugation. The ATPase and H^+ transport associated with the low density fraction was anion-stimulated and inhibited by nitrate but not vanadate, as in earlier work, while the ATPase and H^+ transport in the high density fraction were not stimulated by anions or inhibited by nitrate but were inhibited by vanadate. While these activities have become de facto markers for the tonoplast and plasma membrane, respectively, other ATPase activities are associated with each membrane. These include the Ca^{2+}-ATPase (Sze et al. 2000) at the plasma membrane and ABC-type transporters at the tonoplast and potentially at the plasma membrane (Jasinski et al. 2003). However, there appears to be little quantitative information available on the contribution of these transport systems to the total ATPase activities.

Early work on potassium stimulation of the plasma membrane ATPase (Fisher et al. 1970) showed a correlation across cereal species between Rb^+ influx in roots and the stimulation of ATPase activity by the same ion. This was initially taken to indicate a direct link between ATPase activity and K^+ transport and, later, that H^+ and K^+ transport might both occur via the ATPase (Briskin 1986). However, the K^+:H^+ stoichiometric ratio would have to be less than 1:1 because the pump is electrogenic. Briskin and Gawienowski (1996) examined the question of K^+ transport by inserting the partially purified ATPase into planar lipid bilayer membranes and looking at the potential required to stall the ATPase. Difference curves (dI-V) were obtained from the I-V curves in the

presence and absence of vanadate. The point of intersection with the V axis, the potential at which the ATPase was stalled (the reversal potential), was unaffected by the potassium gradient across the membrane and was consistent with the transport of $1H^+$ per ATP, rather than with $1H^+$ and a fraction of a K^+ ion. This suggests that K^+ transport occurs via a separate system.

An indirect indication of the generation of a membrane potential by the ATPase came from the work of Vara and Serrano (1982). In the first study of H^+ transport by the partially purified and reconstituted plasma membrane ATPase from oats, the net transport of H^+ was dependent on the presence of an anion for transport across the membrane. Direct detection of membrane potential changes in suspensions of membrane vesicles can be made using the molecular probes oxonol V and oxonol VI (Scherman and Henry 1980; Bennett and Spanswick 1985). The membrane vesicle preparations for which it was first reported that the membrane potential changed upon addition of ATP (Rasi-Caldogno et al. 1981; Sze and Churchill 1981) were probably dominated by vesicles of tonoplast origin. However, later work confirmed that the transport in plasma membrane vesicles is electrogenic (Rasi-Caldogno et al. 1985; Galtier et al. 1988; Grouzis et al. 1997; Briskin and Gawienowski 1996). The aqueous polymer two-phase technique can be used to produce highly enriched preparations of plasma membrane vesicles from a microsomal preparation containing a mixture of membranes. The vesicles have a predominantly right-side-out orientation but a proportion, perhaps approaching 50%, can be reoriented by repetitive freeze/thaw treatments (Palmgren et al. 1990). Addition of ATP to a plasma membrane preparation from maize roots prepared in this manner produces a distinct quench of oxonol V fluorescence in the presence of 50 mM K_2SO_4 (Faraday and Spanswick 1995). Unlike maize root tonoplast vesicles (Bennett and Spanswick 1983), the quench is only slightly reversed by the addition of 50 mM KCl. However, the initial rate of proton transport was increased 14-fold while the ATPase activity was increased by less than 10%. This raises questions concerning the coupling between ATPase activity and proton transport that remain unresolved.

10.6 Tonoplast

10.6.1 Electrophysiology

As an internal membrane, the tonoplast has been somewhat inaccessible with regard to conventional electrophysiological techniques. Simultaneous measurement with two microelectrodes showed the potential of the cytoplasm with respect to the vacuole in *Nitella translucens* was −18 mV (Spanswick and Williams 1964). Similar values have been recorded in a number of plant cells (Dunlop 1976), indicating that in vivo the plasma membrane has a much larger membrane potential than the tonoplast.

The patch-clamp technique, used in the "whole-vacuole" mode, can be used to demonstrate a potential of similar magnitude produced by addition of ATP to a single isolated vacuole (Bentrup et al. 1985; Hedrich and Schroeder 1989). This technique can also be used to show the additive effects on the clamp current of ATP, the substrate for what has become known as the V-type ATPase, and PP_i, the substrate for the other H^+ transporting system at the tonoplast, the pyrophosphatase (Hedrich et al. 1989). Use of patch-clamp in the whole-vacuole mode to investigate the current-voltage relationship for the tonoplast is complicated by the existence of the series resistance of the patch pipet and a parallel resistance due to the "leak" at the junction of the pipet and the membrane. Sometimes these do not appear to have been compensated for. However, the series resistance is often insignificant. The current through the leak resistance, if unchanged by the inhibitor, cancels in experiments in which the I-V characteristic of the pump is determined by subtraction of the I-V curve in the presence of a specific inhibitor of the transporter from the control I-V curve in the absence of the inhibitor. An investigation of this type on isolated red beet vacuoles, using bafilomycin A_1 as a specific inhibitor of the ATPase, yielded the result that the value of the coupling ratio (a term used to describe a variable stoichiometry) ranged from 1.75 to 3.28 H^+/ATP depending on the pH values on either side of the membrane (Davies et al. 1994). Similar experiments were performed on yeast vacuoles (Kettner et al. 2003), but with the condition that ATP was omitted from the mix of ATP, ADP and P_i to stop the pump. Kettner et al. (2003) plotted the coupling ratios for both sets of results against ΔpH and showed that the coupling ratio varied from a value > 4 H^+/ATP for a ΔpH of 1.0 to a value < 2.0 H^+/ATP for a ΔpH of 5.0. They discuss an explanation which involves a form of "slip" in which a conducting path exists for flow of H^+ in the reverse direction through the ATPase.

10.6.2 Isolated tonoplast vesicles

As mentioned above (10.5.1), the tonoplast was the source of membrane vesicles for the first plant studies on ATP-dependent H^+ transport in isolated vesicles. Although anions (typically as 50 mM Cl^-) do stimulate the activity of the ATPase by about 40–50%, the effect on the initial H^+ flux (about 10-fold) is too large to be accounted for simply as a direct stimulation of the ATPase by Cl^- (Bennett and Spanswick 1983). The idea arose that the stimulation was due to the action of the anion as a "permeant anion" in that it would cross the membrane passively and, in so doing, reduce the membrane potential and accelerate the transport process. Using oxonol VI, Bennett and Spanswick (1983) demonstrated that ATP-dependent H^+ transport resulted in the formation of a positive membrane potential in the interior of the vesicles. Furthermore, as a function of increasing KCl concentration, there was an inverse relationship between the initial rate of H^+ transport and the membrane potential (Fig. 10.3; Bennett and Spanswick 1983), consistent with the idea that Cl^- acted as a permeant anion. Ward and Sze (1992) showed a much smaller

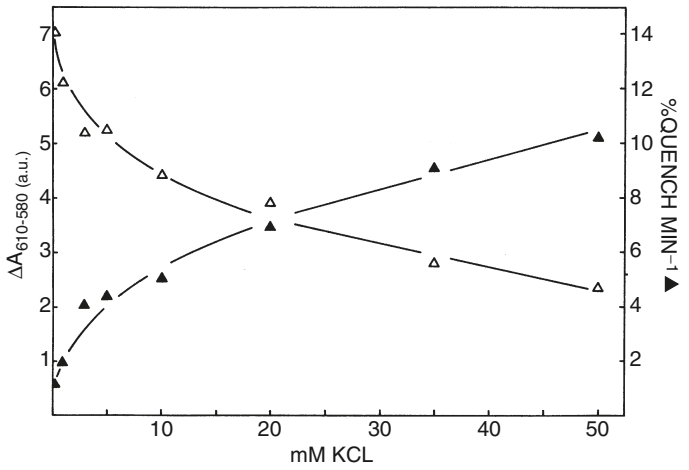

Fig. 10.3. Effect of KCl on the ATP-dependent initial rates of H^+ transport, proportional to the initial rate of quench of 9-aminoacridine fluorescence (▲), and the membrane potential, expressed as absorbance changes of Oxonol VI (Δ), in microsomal vesicles from maize roots. (From Bennett and Spanswick 1983, with permission)

effect of Cl^- on the initial rate of proton transport in the purified and reconstituted tonoplast ATPase from oat roots. Indeed, for the sample trace showing the effect of 5 mM Cl^- on amino acridine orange fluorescence (Fig. 5B in Ward and Sze 1992) there is no discernable effect on the initial rate of quench, only an effect on the extent of quench. The small effect of Cl^- on H^+ transport in these experiments may reflect the fact that they were carried out in the presence of valinomycin, which would fix the membrane potential according to the potassium gradient across the membrane.

A series of papers (Müller et al. 1996, 1997, 1999) on the vacuolar H+-ATPase from lemon fruits supports the idea of a variable coupling ratio. Lemon fruit sacs represent an extreme case in which the vacuolar pH declines to 2.2 during maturation, suggesting that the pump can support a gradient of ~5 pH units, requiring an ATPase with a coupling ratio less than 2 (Müller et al. 1996). A further complication (Müller and Taiz 2002) is that there is not only a V-ATPase with a variable coupling ratio but present also in the fruit vacuolar membranes is a nitrate-insensitive V-ATPase with a coupling ratio of 1.

10.7 Conclusions

The early work on electrogenic proton pumps overlapped with the demonstration that Cl^- transport was dependent on the pH gradient across the plasma membrane (Spear et al. 1969; Smith 1970). Influenced by the chemiosmotic hypothesis (Mitchell 1961, 1970), these facts soon became incorporated

in a "chemiosmotic scheme" for ion transport in plants (Raven and Smith 1973; Poole 1978; Smith and Raven 1979; Spanswick 1989) that has been a major paradigm guiding research in this area for the past 30 years. In this context, the idea of membranes having high permeability to H^+ would be a difficulty in that large passive fluxes of H^+ would short-circuit the proton cotransport systems now thought to be responsible for the transport of Na^+, anions, sugars and amino acids. This is not to imply that passive fluxes of H^+ do not exist but rather that they are likely to be limited in magnitude. In this context, it is interesting that sterols appear to play a role in reducing the passive permeability of natural membranes (Haines 2001) and that this has been demonstrated to be important in reconstitution of plant ATPases (Yamanishi and Kasamo 1994).

The revival of the acid growth theory for auxin-mediated cell wall extension (Rayle and Cleland 1970; Hager et al. 1971) also occurred at about the same time as the development of ideas about proton pumps, and remains a viable theory (Rayle and Cleland 1992; Hager 2003). Since the proton pump at the plasma membrane was postulated to provide the acidification of the cell wall that led to wall loosening, the acid growth theory boosted interest in proton pumps.

One technical advance that would be useful in resolving questions regarding some of the uncertainties as to the fluxes supported by the plasma membrane proton pump in vivo is an improved method for estimating the passive H^+ influx in intact cells. Passive fluxes can be estimated in membrane vesicles (Paula et al. 1996) and in bacterial cells (Maloney 1979; Bond and Russell 2000). However, there appear to be a significant problem in measuring net influx in plant cells, including the high buffer capacity of plant cell walls, even in the absence of proton cotransport system activity. Given the experimental difficulties (Kiyosawa 1990), it may be necessary to approach the problem indirectly by attempting to account for all the component fluxes due to the primary and secondary systems transporting H^+, together with any biochemical consumption or production of H^+, and then consider the passive flux necessary to achieve homeostasis. A beginning has been made in examining the interactions between transporters in the membrane (Gradmann et al. 1993; Gradmann and Hoffstadt 1998), but further progress is necessary.

Despite the technical difficulties, particularly those inherent in investigating the transport of H^+, the importance of electrogenic ion pumps in plants is now firmly established.

References

Admon AB, Jacoby B, Goldsmith EE (1981) Some characteristics of the Mg-ATPase of isolated red beet vacuoles. Plant Sci Lett 22:89–96

Anderson WP, Robertson RN, Wright BJ (1977) Membrane potentials in carrot root cells. Austr J Plant Physiol 4:241–252

Beilby MJ (1984) Current–voltage characteristics of the proton pump at *Chara* plasmalemma: I. pH dependence. J Membr Biol 81:113–125

Bennett AB, O'Neill SD, Spanswick RM (1984) H^+-ATPase activity from storage tissue of *Beta vulgaris*. I. Identification and characterization of an anion-sensitive H^+-ATPase. Plant Physiol 74:538–544

Bennett AB, Spanswick RM (1983) Optical measurements of ΔpH and $\Delta E\Psi$ in corn root membrane vesicles: kinetic analysis of Cl^- effects on a proton-translocating ATPase. J Membr Biol 71:95–107

Bennett AB, Spanswick RM (1985) The use of optical probes to measure pH gradients and membrane potential in tonoplast membrane vesicles. In: Marin BP (ed) Biochemistry and function of vacuolar ATPase in fungi and plants. Springer, Berlin Heidelberg New York, pp 119–128

Bentrup F-W, Hoffmann B, Gogarten-Boekels M, Gogarten JP, Baumann C (1985) A patch clamp study of tonoplast electrical properties in isolated vacuoles from *Chenopodium rubrum* suspension cells. Z Naturforsch 40c:886–890

Blatt MR (1986) Interpretation of steady-state current-voltage curves: consequences and implications of current subtraction in transport studies. J Membr Biol 92:91–110

Blatt MR, Beilby MJ, Tester M (1990) Voltage dependence of the *Chara* proton pump revealed by current–voltage measurement during rapid metabolic blockade with cyanide. J Membr Biol 114:205–223

Blinks LR (1949) The source of the bioelectric potentials in large plant cells. Proc Natl Acad Sci USA 35:566–575

Bond DR, Russell JB (2000) Proton motive force regulates the membrane conductance of *Streptococcus bovis* in a non-ohmic fashion. Microbiol 146:687–694

Briskin DP (1986) Plasma membrane H^+-transporting ATPase: role in potassium ion transport? Physiol Plant 68:159–163

Briskin DP, Gawienowski MC (1996) Role of the plasma membrane H^+-ATPase in K^+ transport? Plant Physiol 111:1199–1207

Briskin DP, Reynolds-Niesman I (1991) Determination of H^+/ATP stoichiometry for the plasma membrane H^+-ATPase from red beet (*Beta vulgaris* L.) storage tissue. Plant Physiol 95:242–250

Churchill KA, Holoway B, Sze H (1983) Separation of two types of electrogenic H^+-pumping ATPases from oat roots. Plant Physiol 73:921–928

Cruz-Mireles RM, Ortega-Blake I (1991) Effect of Na_3VO_4 on the P state of *Nitella translucens*. Plant Physiol 96:91–97

Dainty J (1962) Ion transport and electrical potentials in plant cells. Annu Rev Plant Physiol 13:379–402

Davies JM, Hunt I, Sanders D (1994) Vacuolar H^+-pumping ATPase variable coupling ratio controlled by pH. Proc Natl Acad Sci USA 91:8547–8551

De Michelis MI, Spanswick RM (1986) H^+-pumping driven by the vanadate-sensitive ATPase in membrane vesicles from corn roots. Plant Physiol 81:542–547

De Michelis MI, Pugliarello MC, Rasi-Caldogno F (1983) Two distinct proton translocating ATPases are present in membrane vesicles from radish seedlings. FEBS Lett 162:85–90

Dunlop J (1976) The electrical potential difference across the tonoplast of root cells. J Exp Bot 27: 908–915

DuPont FM, Bennett AB, Spanswick RM (1982a) Localization of a proton-translocating ATPase on sucrose gradients. Plant Physiol 70:1115–1119

DuPont FM, Giorgi DL, Spanswick RM (1982b) Characterization of a proton-translocating ATPase in microsomal vesicles from corn roots. Plant Physiol 70:1694–1699

Etherton B, Higinbotham N (1960) Transmembrane potential measurements of cells of higher plants as related to salt uptake. Science 131:409–410

Faraday CD, Spanswick RM (1995) Differential stimulation by Cl^- of H^+ transport and ATPase activity in purified plasma membrane vesicles from maize (*Zea mays* L.) roots. J Exp Bot 46:1169–1176

Finkelstein A (1964) Carrier model for active transport of ions across a mosaic membrane. Biophys J 4:421–440
Fisher JD, Hansen D, Hodges TK (1970) Correlation between ion fluxes and ion-stimulated adenosine triphosphatase activity of plant roots. Plant Physiol 46:812–814
Fujii S, Shimmen T, Tazawa M (1979) Effect of intracellular pH on the light-induced potential change and electrogenic activity in tonoplast-free cells of *Chara australis*. Plant Cell Physiol 20:1315–1328
Galtier N, Belver A, Gibrat R, Grouzis J-P, Rigaud J, Grignon C (1988) Preparation of corn root plasmalemma with low Mg-ATPase latency and high electrogenic H^+ pumping activity after phase partitioning. Plant Physiol 87:491–497
Goldman DE (1943) Potential, impedance, and rectification in membranes. J Gen Physiol 27:37–60
Gradmann D (1984) Electrogenic Cl^- pump in the marine alga *Acetabularia*. In: Gerencer GA (ed) Chloride transport coupling in biological membranes and epithelia. Elsevier Science, Amsterdam, pp 13–61
Gradmann D, Bentrup F-W (1970) Light-induced membrane potential changes and rectification in *Acetabularia*. Naturwissenschaften 57:46–47
Gradmann D, Hoffstadt J (1998) Electrocoupling of ion transporters in plants: interaction with internal ion concentrations. J Membr Biol 166:51–59
Gradmann D, Hansen U-P, Long WS, Slayman CL, Warncke J (1978) Current–voltage relationships for the plasma membrane and its principal electrogenic pump in *Neurospora crassa*. I. Steady-state conditions. J Membr Biol 39:333–367
Gradmann D, Blatt MR, Thiel G (1993) Electrocoupling of ion transporters in plants. J Membr Biol 136:327–332
Grouzis J-P, Pouliquin P, Riguad J, Grignon C, Gibrat R (1997) In vitro study of passive nitrate transport by native and reconstituted plasma membrane vesicles from corn root cells. Biochim Biophys Acta 1325:329–342
Hager A (2003) Role of the plasma membrane H^+-ATPase in auxin-induced elongation growth: historical and new aspects. J Plant Res 116:483–505
Hager A, Biber W (1984) Functional and regulatory properties of H^+ pumps at the tonoplast and plasma membranes of *Zea mays* coleoptiles. Z Naturforsch 39c:927–937
Hager A, Helmle M (1981) Properties of an ATP-fueled, Cl-dependent proton pump localized in membranes of microsomal vesicles from maize coleoptiles. Z Naturforsch 36c:997–1008
Hager A, Menzel H, Krauss A (1971) Versuche und Hypothese zur Primarwirkung des Auxins beim Streckungswachstum. Planta 100:47–75
Haines TH (2001) Do sterols reduce proton and sodium leaks through lipid bilayers? Prog Lipid Res 40:299–324
Harada A, Okazaki Y, Takagi S (2002) Photosynthetic control of the plasma membrane H^+-ATPase in *Vallisneria* leaves. I. Regulation of activity during light-induced membrane hyperpolarization. Planta 214:863–869
Hedrich R, Schroeder JI (1989) The physiology of ion channels and electrogenic pumps in higher plants. Annu Rev Plant Physiol 40:539–569
Hedrich R, Kurkdjian A, Guern J, Flügge UI (1989) Comparative studies on the electrical properties of the H^+ translocating ATPase and pyrophosphatase of the vacuolar-lysosomal compartment. EMBO J 8:2835–2841
Higinbotham N (1973) Electropotentials of plant cells. Annu Rev Plant Physiol 24:25–46
Higinbotham N, Anderson WP (1974) Electrogenic pumps in higher plant cells. Can J Bot 52:1011–1021
Higinbotham N, Graves JS, Davis RF (1970) Evidence for an electrogenic ion transport pump in cells of higher plants. J Membr Biol 3:210–222
Hill AE (1970) Ion and water transport in *Limonium*. II. Short-circuit analysis. Biochim Biophys Acta 135:461–465
Hodges TK, Leonard RT, Bracker CE, Keenan TW (1972) Purification of an ion-stimulated ATPase from plant roots: association with plasma membranes. Proc Natl Acad Sci USA 69:3307–3311

Hodgkin AL, Katz B (1949) The effect of sodium ions on the electrical activity of the giant axon of the squid. J Physiol 108:37–77
Hodgkin AL, Keynes RD (1955) The potassium permeability of a giant nerve fibre. J Physiol 128:61–88
Homblé F (1987) Effect of dinitrophenol on membrane potential, membrane resistance and chlorophyll fluorescence of *Chara corallina* internodal cells at various pH values. Bioelec Bioenerg 17:165–174
Hope AB (1965) Ionic relations of cells of *Chara australis*. X. Effects of bicarbonate ions on electrical properties. Austr J Biol Sci 18:789–801
Hope AB, Walker NA (1961) Ionic relations of *Chara australis* R.Br. IV. Membrane potential differences and resistances. Austr J Biol Sci 14:26–44
Hope AB, Simpson A, Walker NA (1966) The efflux of chloride from cells of *Nitella* and *Chara*. Austr J Biol Sci 19:355–362
Jasinski M, Ducos E, Martinoia E, Boutry M (2003) The ATP-binding cassette transporters: structure, function, and gene family comparison between rice and *Arabidopsis*. Plant Physiol 131:1169–1177
Jeschke WD (1970) Lichtabhängige Veränderungen der Membranpotentials bei Blattzellen von *Elodea densa*. Z Pflanzenphysiol 62:158–172
Keifer DW, Spanswick RM (1979) Correlation of ATP levels in *Chara corallina* with the activity of the electrogenic pump. Plant Physiol 64:165–168
Kettner C, Bertl A, Obermeyer G, Slayman C, Bihler H (2003) Electrophysiological analysis of the yeast V-type proton pump: variable coupling ratio and proton shunt. Biophys J 85:3730–3738
Kishimoto U (1959) Electrical characteristics of *Chara corallina*. Annu Rep Sci Works, Fac Sci Osaka University 7:115–146
Kishimoto U, Kami-ike N, Takeuchi Y, Ohkawa T (1984) A kinetic analysis of the electrogenic pump of *Chara corallina*: I. Inhibition of the pump by DCCD. J Membr Biol 80:175–183
Kishimoto U, Takeuchi Y, Ohkawa TA, Kami-ike N (1985) A kinetic analysis of the electrogenic pump of *Chara corallina*: III. Pump activity during the action potential. J Membr Biol 86:27–36
Kitasato H (1968) The influence of H^+ on the membrane potential and ion fluxes of *Nitella*. J Genl Physiol 52:60–87
Kitasato H (2003) Membrane potential genesis in *Nitella* cells, mitochondria and thylakoids. J Plant Res 116:401–418
Kiyosawa K (1990) H^+ tolerance of *Chara* internodal cells and apparent net influx of H^+ in weakly acidic solutions: implication of the net flux of H^+ as a minor component among the total net flux of ions across the intact cell membrane of *Chara*. Plant Cell Physiol 31:347–355
Lew RR (1991) Electrogenic transport properties of growing *Arabidopsis* root hairs. The plasma membrane proton pump and potassium channels. Plant Physiol 97:1527–1534
Lew RR, Spanswick RM (1984a) Characterization of the electrogenicity of soybean (*Glycine max* L.) roots. Plant Physiol 75:1–6
Lew RR, Spanswick RM (1984b) Proton-pumping activities of soybean (*Glycine max* L.) root microsomes: localization and sensitivity to nitrate and vanadate. Plant Sci Lett 36:187–193
Löppert H (1979) Evidence for electrogenic proton extrusion by subepidermal cells of *Lemna paucicostata* 6746. Planta 144:311–315
Macara IG, Kustin K, Cantley LC Jr (1980) Glutathione reduces cytoplasmic vanadate. Mechanism and physiological implications. Biochim Biophys Acta 629:95–106
MacRobbie EAC (1962) Ionic relations of *Nitella translucens*. J Gen Physiol 45:861–878
MacRobbie EAC (1970) The active transport of ions in plant cells. Quart Rev Biophys 3:251–294
Maloney PC (1979) Membrane H^+ conductance of *Streptococcus lactis*. J Bacteriol 140:197–205
Marrè MT, Albergoni FG, Moroni A, Pugliarello MC (1989) Evidence that H^+ extrusion in *Elodea densa* leaves is mediated by an ATP-driven H^+ pump. Plant Sci 62:21–28
Meharg AA, Maurousset L, Blatt MR (1994) Cable correction of membrane currents recorded from root hairs of *Arabidopsis thaliana* L. J Exp Bot 45:1–6

Mercier JA, Poole RJ (1980) Electrogenic pump activity in red beet: its relation to ATP levels and to cation influx. J Membr Biol 55:165–174
Mettler IJ, Mandala S, Taiz L (1982) Characterization of in vitro proton pumping by microsomal vesicles isolated from corn coleoptiles. Plant Physiol 70:1738–1742
Mimura T, Kirino Y (1984) Changes in cytoplasmic pH measured by ^{31}P-NMR in cells of *Nitellopsis obtusa*. Plant Cell Physiol 25:813–820
Mimura T, Tazawa M (1984) Membrane potential and resistance in relation to cytoplasmic pH in *Nitellopsis*. Plant Cell Physiol 25:1009–1016
Mimura T, Shimmen T, Tazawa M (1983) Dependence of the membrane potential on intracellular ATP concentration in tonoplast-free cells of *Nitellopsis obtusa*. Planta 157:97–104
Mitchell P (1961) Coupling of phosphorylation to electron and hydrogen transfer by a chemiosmotic type of mechanism. Nature 191:144–148
Mitchell P (1970) Reversible coupling between transport and chemical reactions. In: Bittar EW (ed) Membranes and ion transport. Wiley, New York, pp 192–256
Müller ML, Taiz L (2002) Regulation of the lemon-fruit V-ATPase by variable stoichiometry and organic acids. J Membr Biol 185:209–220
Müller ML, Irkens-Kiesecker U, Rubinstein B, Taiz L (1996) On the mechanism of hyperacidification in lemon. Comparison of the vacuolar H^+-ATPase activities of fruits and epicotyls. J Biol Chem 271:1916–1924
Müller ML, Irkens-Kiesecker U, Kramer D, Taiz L (1997) Purification and reconstitution of the vacuolar H^+-ATPases from lemon and epicotyls. J Biol Chem 272:12762–12770
Müller ML, Jensen M, Taiz L (1999) The vacuolar H^+-ATPase of lemon fruits is regulated by variable H^+/ATP coupling and slip. J Biol Chem 274:10706–10716
Nobel PS (2005) Physicochemical and environmental plant physiology, 3rd edn. Elsevier, Boston
Novacky A, Ullrich-Eberius CI, Lüttge U (1978) Membrane potential changes during transport of hexoses in *Lemna gibba* G1. Planta 138:262–270
O'Neill SD, Spanswick RM (1984) Characterization of native and reconstituted plasma membrane H^+-ATPase from the plasma membrane of *Beta vulgaris*. J Membr Biol 79:245–256
Palmgren MG, Askerlund P, Fredrikson K, Widell S, Sommarin M, Larsson C (1990) Sealed inside-out and right-side-put plasma membrane vesicles. Optimal conditions for formation and separation. Plant Physiol 92:871–880
Paula S, Volkov AG, Van Hoek AN, Haines TH, Deamer DW (1996) Permeation of protons, potassium ions, and small polar molecules through lipid bilayers as a function of membrane thickness. Biophys J 170:339–348
Penth B, Weigl J (1971) Anionen-Influx, ATP-Spiegel und CO_2-Fixierung in *Limnophila gratioloides* und *Chara foetida*. Planta 96:212–223
Perlin DS, Spanswick RM (1980) Labeling and isolation of plasma membranes from corn leaf protoplasts. Plant Physiol 65:1053–1057
Poole RJ (1978) Energy coupling for membrane transport. Annu Rev Plant Physiol 29:437–460
Prins HBA, Harper JR, Higinbotham N (1980) Membrane potentials of *Valisneria* leaf cells and their relation to photosynthesis. Plant Physiol 65:1–5
Rapoport SI (1970) The sodium-potassium exchange pump: relation of metabolism to electrical properties of the cell. I. Theory. Biophys J 10:246–259
Rasi-Caldogno F, De Michelis MI, Pugliarello MC (1981) Evidence for an electrogenic ATPase in microsomal vesicles from pea internodes. Biochim Biophys Acta 642:37–45
Rasi-Caldogno F, Pugliarello MC, De Michelis MI (1985) Electrogenic transport of protons driven by the plasma membrane ATPase in membrane vesicles from radish. Plant Physiol 77:200–205
Raven JA, Smith FA (1973) The regulation of intracellular pH as a fundamental biological process. In: Anderson WP (ed) Ion transport in plants. Academic Press, London, pp 271–278
Rayle DL, Cleland R (1970) Enhancement of wall loosening and elongation by acid solutions. Plant Physiol 46:250–253

Rayle DL, Cleland R (1992) The acid growth theory of auxin-induced cell elongation is alive and well. Plant Physiol 99:1271–1274
Saddler HDW (1970) The membrane potential of *Acetabularia mediterranea*. J Gen Physiol 55:802–821
Saito K, Senda M (1973a) The light-dependent effect of external pH on the membrane potential of *Nitella*. Plant Cell Physiol 14:147–156
Saito K, Senda M (1973b) The effect of external pH on the membrane potential of *Nitella* and its linkage to metabolism. Plant Cell Physiol 14:1045–1052
Saito K, Senda M (1974) The electrogenic ion pump revealed by the external pH effect on the membrane potential of *Nitella*. Influences of external ions and electric current on the pH effect. Plant Cell Physiol 15:1007–1016
Scherman D, Henry JP (1980) Oxonol-V as a probe of chromaffin granule membrane potentials. Biochim Biophys Acta 599:150–166
Shimmen T (2004) Studies on semipermeability and electrical characteristics in membranes of *Chara* cells fixed with glutaraldehyde. J Plant Res 117:291–295
Shimmen T, Tazawa M (1977) Control of membrane potential and excitability of *Chara* cells with ATP and Mg^{2+}. J Membr Biol 37:167–192
Shimmen T, Tazawa M (1982) Effects of intracellular vanadate on electrogenesis, excitability and cytoplasmic streaming in *Nitellopsis obtusa*. Plant Cell Physiol 23:669–677
Slayman CL (1965a) Electrical properties of *Neurospora crassa*. Effects of external cations on the electrical potential. J Gen Physiol 49:69–72
Slayman CL (1965b) Electrical properties of *Neurospora crassa*. Respiration and the intracellular potential. J Gen Physiol 49:93–116
Slayman CL, Slayman CW (1974) Depolarization of the plasma membrane of *Neurospora* during active transport of glucose: evidence for a proton-dependent cotransport system. Proc Natl Acad Sci USA 71:1935–1939
Smith FA (1970) The mechanism of chloride transport in characean cells. New Phytol 69:903–917
Smith FA (1984) Regulation of the cytoplasmic pH of *Chara corallina*: response to changes in external pH. J Exp Bot 35:43–50
Smith FA, MacRobbie EAC (1981) Comparison of cytoplasmic pH and Cl^- influx in cells of *Chara corallina* following "Cl^- starvation". J Exp Bot 32:827–835
Smith FA, Raven JA (1979) Intracellular pH and its regulation. Annu Rev Plant Physiol 30:289–311
Spanswick RM (1970) The effects of bicarbonate ions and external pH on the membrane potential and resistance of *Nitella translucens*. J Membr Biol 2:59–70
Spanswick RM (1972a) Electrical coupling between the cells of higher plants: a direct demonstration of intercellular transport. Planta 102:215–227
Spanswick RM (1972b) Evidence for an electrogenic pump in *Nitella translucens*. I. The effects of pH, K^+, Na^+, light and temperature on the membrane potential and resistance. Biochim Biophys Acta 288:73–89
Spanswick RM (1973) Electrogenesis in photosynthetic tissues. In: Anderson WP (ed) Workshop on ion transport in plants. Academic Press, London, pp 113–128
Spanswick RM (1974) Evidence for an electrogenic pump in *Nitella translucens*. II. Control of the light-stimulated component of the membrane potential. Biochim Biophys Acta 332:387–398
Spanswick RM (1980) Biophysical control of electrogenic pumps in the Characeae. In: Spanswick RM, Lucas WJ, Dainty J (eds) Plant membrane transport: current conceptual issues. Elsevier/North Holland Biomedical Press, Amsterdam, pp 305–313
Spanswick RM (1981) Electrogenic ion pumps. Annu Rev Plant Physiol 32:267–289
Spanswick RM (1989) Vacuolar and cell membrane H^+-ATPases of plant cells. Ann NY Acad Sci 574:180–188
Spanswick RM, Miller AG (1977a) Measurement of the cytoplasmic pH in *Nitella translucens*: comparison of the values obtained by the microelectrode and weak acid methods. Plant Physiol 59:664–666

Spanswick RM, Miller AG (1977b) The effect of CO_2 on the Cl^- influx and electrogenic pump in *Nitella translucens*. Transmembrane ionic exchanges in plants. CNRS, Paris, pp 239–240
Spanswick RM, Williams EJ (1964) Electrical potentials and Na, K, and Cl concentrations in the vacuole and cytoplasm of *Nitella translucens*. J Exp Bot 15:193–200
Spanswick RM, Williams EJ (1965) Ca fluxes and membrane potentials in *Nitella translucens*. J Exp Bot 16:463–473
Spanswick RM, Stolarek J, Williams EJ (1967) The membrane potential of *Nitella translucens*. J Exp Bot 18:1–16
Spear DG, Barr JK, Barr CE (1969) Localization of hydrogen ion fluxes in *Nitella*. J Gen Physiol 54:397–414
Sze H (1985) H^+-translocating ATPases: advances using membrane vesicles. Annu Rev Plant Physiol 36:175–208
Sze H, Churchill KA (1981) Mg^{2+}/KCl-ATPase of plant plasma membranes is an electrogenic pump. Proc Natl Acad Sci USA 78:5578–5582
Sze H, Liang F, Hwang I, Curran AC, Harper JF (2000) Diversity and regulation of plant Ca^{2+} pumps: insights from expression in yeast. Annu Rev Plant Physiol Plant Mol Biol 51:433–462
Takeuchi Y, Kishimoto U, Ohkawa T, Kmi-ike N (1985) A kinetic analysis of the electrogenic pump of *Chara corallina*. II. Dependence of the pump activity on external pH. J Membr Biol 86:17–26
Tazawa M (2003) Cell physiological aspects of the plasma membrane H^+ pump. J Plant Res 116:419–442
Tsutsui I, Ohkawa T (2001) Regulation of the H^+ pump activity in the plasma membrane of internally perfused *Chara corallina*. Plant Cell Physiol 42:531–537
Ussing HH, Zerahn K (1951) Active transport of sodium as the source of electric current in the short-circuited isolated frog skin. Acta Physiol Scand 23:110–127
Vara F, Serrano R (1982) Partial purification and properties of the proton-translocating ATPase of plant plasma membranes. J Biol Chem 257:12826–12830
Walker NA, Smith FA (1975) Intracellular pH in *Chara corallina* measured by DMO distribution. Plant Sci Lett 4:125–132
Walker RR, Leigh RA (1981) Characterisation of a salt-stimulated ATPase activity associated with vacuoles isolated from storage roots of red beet (*Beta vulgaris* L.). Planta 153:140–149
Ward JM, Sze H (1992) Proton transport activity of the purified vacuolar H^+-ATPase from oats. Direct stimulation by Cl^-. Plant Physiol 99:925–931
Williams EJ, Johnston RJ, Dainty J (1964) The electrical resistance and capacitance of the membranes of *Nitella translucens*. J Exp Bot 15:1–14
Yamanishi H, Kasamo K (1994) Effects of cerebroside and cholesterol on the reconstitution of tonoplast H^+-ATPase purified from mung bean (*Vigna radiata* L.) hypocotyls in liposomes. Plant Cell Physiol 35:655–663
Young M, Sims AP (1973) The potassium relations of *Lemna minor* L. II. The mechanism of potassium uptake. J Exp Bot 24:317

11 Effects of Electrical and Electromagnetic Fields on Plants and Related Topics

ANDREW GOLDSWORTHY

Anyone reading this book cannot fail to realize the importance of self-generated electric fields and currents in the energetics and control of metabolism in plants. We should therefore not be too surprised to find that externally applied fields also have effects. In this chapter, I will describe a few of the more significant findings from over a century of research and try to explain and sometimes reinterpret them in the light of more modern knowledge. The work is divided into three sections. Section 1 is on the non-polar effects of DC fields, where the effects are not related to the direction of the field. It ranges from responses to massive electric fields, such as those found in thunderstorms, to the effects of much weaker ones on the growth and differentiation of tissue cultures. Section 2 is on the polar effects of DC fields, where the direction of the response is related to the direction of the field and includes effects on polar growth and tropisms. Section 3 is on the effects of time-varying and alternating electromagnetic fields, where I will present evidence that a simple change in membrane stability can account for virtually all of the hitherto mysterious biological effects of weak electromagnetic radiation.

11.1 Non-polar effects of DC electric fields

11.1.1 High voltage natural fields and the rise and fall of electroculture

11.1.1.1 Phenomenology

Work on the effects of electrical fields on plants goes back several centuries, but the first person to carry out large scale experiments was Karl Lemström, who was a Professor of Physics at Helsinki. He had paid several visits to the Arctic, and was surprised how green and healthy the vegetation looked, despite the low light and temperature. He wondered whether this might be due to the weak electric currents carried through the atmosphere by air ions from the aurora borealis. His suspicions were confirmed when he looked at

6 Sandall Road, London W5 1JD, UK

Plant Electrophysiology – Theory & Methods (ed. by Volkov)

the annual growth rings of fir trees in the region, which showed a periodicity, with best growth during the peaks of sunspot cycles when the aurora would have been most active. To test his theory, he exposed a range of different crops in several European countries to high voltage gradients from wires suspended above them. The voltages were produced by an electrostatic generator and, from the length of the sparks it could produce, we can estimate that the gradients applied to the plants were approximately 10 kV/m. He found that the treated plants were greener, sturdier and often showed dramatic increases in yield, compared with the controls. Although the technique didn't always work, on average there was a yield stimulation of around 45% (Lemström 1904). This led to a flurry of activity by agricultural scientists hoping to exploit this effect, which had now been given the name *electroculture*. Amongst these were Blackman and his co-workers of Imperial College London, who used higher voltage gradients (20–40 kV/m) in both field and pot experiments. They found that it did not matter whether the overhead wires were positive or negative, but the amount of current flowing was important. A current of 10^{-11}–10^{-8} amps per plant normally stimulated growth but higher values were injurious (Blackman 1924; Blackman and Legg 1924). But the stimulations did not occur all the time. Out of 18 field trials with wheat, barley and oats performed by Blackman (1924), only 14 gave significant increases in dry weight, Murr (1963) only found a greening effect, and Briggs et al. (1926) found no significant response in a whole series of experiments in the USA. There were many claims and counter-claims about the beneficial effects of electroculture and the matter was highly controversial. However, most of the agriculturally oriented work was discontinued in the 1930s, largely because the cost, electrical hazards, and the uncertainty of getting positive results, made it uneconomic.

11.1.1.2 Ecological significance of natural electric fields

The conflicting results of these early workers now make sense. Plants seem to be using the very strong electrostatic fields associated with thunderstorms as a signal to let them make the best use of the rain (Goldsworthy 1996). If a plant in otherwise dry conditions is to use the rain to best advantage, it must respond quickly before the water drains away. But the synthesis of new proteins, chlorophyll etc. takes several hours, so it will be of selective advantage to start before the water trickles through the soil and can be sensed by the roots. The electric fields from thunderclouds are an excellent signal for this. Schonland (1928) measured voltage gradients of up to 16 kV/m under thunderclouds, which is the sort of gradient that was effective in the electroculture experiments. The first clue that plants may actually be *using* natural electric fields to stimulate growth came from Lemström (1904), who reported that electroculture was often *inhibitory* in dry weather, presumably because the anticipated rain never came and the plants' resources were being wasted. The

next clue came from Blackman et al. (1923) who found that exposing cereal seedlings to an electric field for just one hour was enough to stimulate growth, and the growth-rate continued to increase for at least four hours after the current was turned off. This suggests that the field had activated growth-promoting genes, which then remained active for some time. This phenomenon may explain the common perception that vegetation often looks unusually green after a thunderstorm. The requirement for subsequent rain may also explain the negative results for electroculture obtained by Briggs et al. (1926), since their work was conducted in one of the drier regions of the United States and, in order to avoid arcing, they switched off the current whenever rain was expected!

11.1.2 Low voltage fields and plant tissue cultures

Effects similar to high voltage electroculture can occur when weak DC currents are applied to plant tissue cultures. Currents of one or two microamps, of either polarity, applied between an electrode in tobacco callus and another in the culture medium gave several-fold increases in plantlet regeneration (Rathore and Goldsworthy 1985; Rathore et al. 1988). Even isolated protoplasts can be affected. Dijak et al. (1986) found that 20 mV applied for 4 h between a central silver anode and a circular silver cathode 25 mm apart in the culture medium caused a massive production of somatic embryos by *Medicago* protoplasts, whereas none appeared in the controls.

11.1.3 Mechanism of the non-polar effects of DC fields

The fact that stimulation of growth and regeneration by direct currents can occur in undifferentiated tissue cultures and isolated protoplasts suggests that the main effect is at the cellular level. In the light of modern knowledge, electrically induced calcium ingress into their cytosols seems the most likely cause. Most of the applied voltage will appear across the cell membranes because of the relatively low resistance of the cell contents. This will add to the membrane potential on one side of the cells and subtract from it on the other. Where it subtracts, it may open voltage-gated calcium channels and where it adds, there could be a non-specific increase in permeability due to transient pore formation in the hyperpolarized membrane (see Melikov et al. 2001). Either way, there will be an increase in membrane permeability to calcium ions. Because of the huge electrochemical gradient for calcium across the plasma membrane (about 4 orders of magnitude), even a very small increase in permeability to calcium will have a large impact on its cytosolic concentration. This can increase the rate of metabolism because calcium ions often form an integral part of the enzyme cascades that control many intracellular signaling processes. These cascades are enzyme-based amplifiers, where one enzyme molecule activates a large number of molecules of another

enzyme, which in turn activates a third enzyme and so on (Alberts et al. 2002). They normally allow very small stimuli such as a few hormone molecules to control often massive biological responses. By taking part in these cascades, calcium ions act as master gain controls that regulate many aspects of metabolism, and could affect chlorophyll synthesis, and the growth and regeneration in whole plants and tissue cultures.

11.2 Polar effects of DC electric fields

11.2.1 Direct current effects on single cells

Weak artificially applied electric currents can initiate the development of electrical polarity in single cells such as zygotes and so affect their direction of growth. This is probably because the asymmetric calcium ingress on the positive and negative sides of the cells results in metabolic gradients that determine which end of the cell grows first. A link between artificially applied electric currents and polar growth was first shown by Lund (1923) in zygotes of the seaweed *Fucus*, which becomes polar when it germinates. Although their direction of growth is normally controlled by the direction of light, Lund found that a weak electric current applied in the dark made them grow with their rhizoids (the first visible sign of germination) in line with the current. He speculated that the zygotes' polarities were normally controlled by electric currents generated by the cells themselves; but we had to wait until the 1960s for the work of Lionel Jaffe and his co-workers using *Fucus* and its close relative *Pelvetia* for these currents to be confirmed and measured. They used a vibrating probe to measure the current densities and radioactive tracers to determine their ionic composition (see Jaffe et al. 1974; Jaffe and Nuccitelli 1977). They found that following unilateral illumination, a weak electric current entered at a point that predicted the emergence of the rhizoid and left over the remainder of the cell surface. Similar currents predict the primary region of growth in many polarizing cells, including, moss spores, pollen grains and animal zygotes (Jaffe and Nuccitelli 1977). Artificially applied voltages seem to initiate polar growth, by triggering the development of the natural currents.

An interesting observation is that the direction of electrically-induced growth doesn't always correspond to the sign of the applied voltage. Peng and Jaffe (1976) showed that zygote growth usually begins towards the cathode, but it could also be towards the anode depending on the batch of cells used. This effect could also be voltage-dependent, since some batches of cells grew towards the cathode at low voltages but towards the anode at higher voltages. There is a similar voltage-dependence in the galvanotactic migration of animal cells (Mycielska and Djamgoz 2004), but the mechanism of this reversal is not yet understood. It does, however, indicate that the cells' voltage sensing

mechanisms may be more complex than once thought, and are programmable to give responses in either direction.

Novák and Bentrup (1973) discovered that the electrical effects on the germination of the *Fucus* zygote were voltage rather than current dependent when they found that they also occurred in pure electrostatic fields. This suggests that voltage-gated ion channels may be the sensors. The first ion to show polar uptake in the fucoid zygote is calcium (Jaffe et al. 1974), which suggests that voltage-gated calcium channels may be the main ones involved. It is argued that the localized calcium uptake stimulates metabolism around its point of entry and initiates rhizoid development. It also increases the translocation of other ions to give a much larger inflow of current, which is tightly focused at the point of calcium entry. The main function of this "amplified" trans-cellular current is probably to drive the electrophoresis of proteins with different charge densities to different regions along the electrical axis of the cell in the fluid mosaic of its membranes (Jaffe et al. 1974). These proteins could be enzymes or anchorage points for specific elements of the cytoskeleton, but the main effect is to establish a physiological polarity that controls the direction of growth and other polar metabolic functions. This mechanism is of fundamental importance to living cells since it provides a means for DNA, by determining the overall charge on proteins, not only to define their nature, but also to direct them precisely to different regions along a cell's axis using an electrical frame of reference. However, as far as the experimental scientist is concerned, the trans-cellular currents responsible for this are excellent indicators of cellular polarity that can be readily measured with a vibrating probe.

11.2.2 Direct current effects on multicellular structures

11.2.2.1 Effects on plant tissue cultures

The electrical control of cell polarity also occurs in the cells and tissues of higher plants, where it may help coordinate the polarities of neighboring cells. Although cellular polarity is normally quite stable, it does have to change occasionally, such as when a stem or a root initiates a branch or when there is a tropic curvature. Evidence for the mechanisms by which cellular polarities are regulated comes from vibrating probe studies on tobacco tissue cultures, where they seem to be controlled by both polar auxin transport and by electrical gradients.

Goldsworthy and Mina (1991) found evidence that polar auxin transport was important when they looked at the growth and electrical patterns of tobacco cells cultured with different auxins. When they were cultured in media containing the natural auxin indole-3-acetic acid (which can undergo polar transport) they tended to grow as filaments of elongated cells that were electrically polarized longitudinally; mostly in the same direction. However,

in a medium containing the synthetic auxin 2,4-dichlorophenoxy acetic acid (2,4-D) (which does not show polar transport), the cells were more commonly isodiametric and grew as random clusters with unstable and randomly oriented trans-cellular currents. This suggests that the polar transport of auxin is a prerequisite for clearly defined trans-cellular currents and orderly polar growth. This is consistent with recent work by Friml et al. (2003), with auxin transport mutants of *Arabidopsis*, from which they concluded that auxin gradients are important in establishing the apical–basal axis of the embryo. In particular, the polar efflux of auxin from donor cells appeared to determine the polarity and growth of its daughter cells so that they grew in orderly columns.

Higher plant cell polarities are also under electrical control. Mina and Goldsworthy (1991) applied a transverse positive electric current of either 3 or 100 $\mu A/cm^2$ originating from a point source to individual cells of tobacco cell filaments and mapped their own currents after the applied current was switched off. They found the cells had electrically re-polarized in line with the applied current, with their new negative ends next to the positive electrode. This effect would stabilize the polarities of the cells in a filament since the negative end of one cell is normally adjacent to the positive end of its neighbor. Closer examination revealed that the electrical patterns of the repolarized cell resembled those of a polarizing fucoid zygote. Current was entering at the point that had been nearest the electrode, but was leaving more uniformly over the rest of the cell; so could the mechanism be similar? Since calcium is important in controlling the polarization of the fucoid zygote, the tobacco experiment was repeated with no calcium in the external medium. Although the natural currents were not significantly smaller without calcium, the cells were unable to repolarize. The same happened even in the presence of calcium if cobalt ions were added. Since cobalt blocks calcium channels, it suggests that the cells responded to weak electric currents by opening voltage-gated calcium channels, which then reprogrammed their polarities in a way similar to that of germinating zygotes (Mina and Goldsworthy 1992).

The exact relationship between the control of polarity by auxin and electric currents is still unclear, but a simple explanation is that the day-to-day physiological polarities of cells are still controlled by the electrophoresis of membrane proteins driven by their trans-cellular currents as proposed by Jaffe et al. (1974), and it is this that makes them vulnerable to externally applied currents. The function of auxin is to focus the electrical patterns of the cells more precisely to accentuate cellular polarity. The mechanism by which this might occur is surprisingly simple. The point of current entry into the cell is already tightly focused at the apical end as described above for the fucoid zygote, but current egress (mostly via H^+ATPases) is more uniformly spread over the rest of the cell surface, to give only a crude electrical polarity. Polar auxin transport should sharpen this by generating a positive feedback loop that limits current efflux to a relatively small region near the basal end of the cell as follows. If, as might be expected from the proposals of Jaffe et al. (1974), the auxin efflux system is

targeted electrophoretically[1] away from the cell apex, it would still be relatively broadly distributed and give only a weakly polar auxin output towards the base. However, the released auxin should stimulate the activity of the local plasma membrane H^+ATPases (Taiz and Zeiger 2002), to give a corresponding pattern of proton efflux, also with maximum near the base. This will concentrate trans-cellular current-flow to this region and attract still more of the auxin efflux system. The process continues until most of the auxin efflux and proton efflux becomes focused in small area so as to amplify and stabilize cellular polarity. Cells then divide transversely to the direction of current and auxin flow, with the daughter cells sharing the same polarity to give the ordered polar filaments seen by Goldsworthy and Mina (1991). Therefore, both polar auxin transport and polar current-flow seem essential for the development of normal cell polarity in nature. Given the simplicity of the mechanism just proposed for auxin focusing trans-cellular currents and the fundamental importance of this for organized growth, we may be looking at one of the first functions for auxin ever to have evolved, perhaps preceding all others.

11.2.2.2 Tropic curvatures

The interaction between auxin and trans-cellular currents proposed above can also account for the transverse electrical potentials that occur in plant organs prior to tropic curvatures. For example, many workers have reported that the lower surfaces of organs (such as cereal coleoptiles) showing negative gravitropism become electrically positive when placed horizontally, and this is associated with an excess of auxin in the lower region. Also, adding auxin asymmetrically to the apex of the vertical organ gives a similar electrical effect and curvature.

We can now explain this by saying that the transverse auxin imbalance partially reorients the electrical polarities of the organ's cells by stimulating proton efflux from the parts of their plasma membranes exposed to the highest auxin concentration. The result is the development of the observed transverse electrical potentials and also the transverse pH gradients reported by Mulkey et al. (1981) in tropically stimulated organs. What it means is that the cells' normally longitudinal electrical polarities are now partially redirected sideways, which gives a tropic curvature as their direction of growth attempts to follow their new electrical polarities.

The reader will recognize the above as being a modification of the original Cholodny–Went hypothesis described in most textbooks (e.g. Taiz and Zeiger 2002). It still needs an apical transverse redistribution of auxin in response to the stimulus, and also a basipetal transmission of this imbalance, but the main

[1]The auxin efflux system is transported in vesicles via the cytoskeleton to its destination (see Muday et al. 2003 for a brief review) but the plasma membrane proteins that act as the targets for this transport are probably still put in position electrophoretically.

driving force for curvature is now a change in the direction of the polar growth of individual cells rather than a differential growth rate on either side of the organ. This overcomes one of the major objections to the original Cholodny–Went hypothesis; that being that the measured 2:1 ratio of auxin on either side of the organ is not enough to cause the observed difference in growth-rate. Because the relationship between auxin concentration and growth-rate is logarithmic, a difference in auxin concentration of orders of magnitude would be required if a growth-rate differential were to be the main driving force.

11.3 Effects of weak time-varying electromagnetic fields

11.3.1 Phenomenology

The effects of weak time-varying electromagnetic fields on living organisms are many and varied, and they have spawned a vast literature, largely in response to their alleged links to the promotion of cancer in animals (Wilson et al. 1990). Experiments have often proved difficult to reproduce in different laboratories for reasons to be described later, but there is little doubt that many of the effects are real.

Both the electrical and the magnetic components of the electromagnetic fields are effective. Biological effects have been reported with electric fields in the region of 10–10,000 mV/m (Adey 1990) and magnetic flux densities of the order of microtesla. It is difficult to be precise about the magnetic flux densities needed since the effect probably depends on their ability to induce electric currents in the tissue, and this depends on a number of other factors such as waveform. For example, pulses and square waves are more effective than sine-waves, at least partly because their rapid rise and fall times generate larger current spikes. It has been calculated that time-varying fields must induce tissue current densities greater than about 1 mA/m^2 if they are to produce biological effects (Tenforde 1990).

Effects of weak electromagnetic fields on growth and metabolism have been reported at all levels of evolution throughout the eukaryotes, with plants being no exception. They include changes in the motility of diatoms (McLeod et al. 1987), changes in the germination and seedling growth of radish (Smith et al. 1993), stimulation of root growth in maize (Muraji et al. 1998) and cress (Stenz et al. 1998) and cytological changes with faster resin production and senescence in mature pine trees (Selaga and Selaga 1996). Effects are most apparent at low frequencies (below a few thousand Hz) and much of the research work has concentrated on the extremely low frequency range, especially around 60 Hz, which is the frequency of domestic electricity supplies in the USA. Radio frequencies are mostly ineffective unless they are amplitude modulated at a low frequency, in which case they have a similar biological effect to the low frequency modulation envelope.

The fact that responses to electromagnetic field are so widespread and that they also occur in unicells suggests that they have a common mechanism based at the cellular level, but until now there has been no convincing explanation. Any explanation must account for each of the following generally accepted facts:

1. The observed biological effects of weak electromagnetic fields differ in different organisms and tissues, and their expression may also depend on their previous history.
2. The fields involved are usually too weak to cause significant heating.
3. The fields concerned usually contain both electrical and magnetic components but either can be effective on its own.
4. Pulses are often more effective than sine waves.
5. Weak fields may be more effective than strong ones and there may be one or more "amplitude windows" where they give maximal effects.
6. Only low frequencies work and some specific frequencies such as 16 Hz may be especially effective to give so called "frequency windows".
7. Radio frequencies can have biological effects, provided that they are amplitude modulated with a biologically active low frequency.

Despite the seeming complexity of the above phenomena, they can all be explained by a new and very simple hypothesis based on electromagnetically induced changes in the permeability of the phospholipid fraction of cell membranes.

11.3.2 Hypothesis

1. Weak time-varying electromagnetic fields are detected by living organisms because they generate eddy currents in and around their cells.
2. Low frequency eddy currents selectively remove calcium ions that normally stabilize cell membranes and replace them by less effective monovalent ions (mainly potassium), which increases their permeability.
3. This process is enhanced at the ion cyclotron resonant frequency for potassium because it increases the kinetic energy of potassium ions in the diffuse ion layer around the membrane and therefore their ability to replace calcium.
4. Voltage-gated calcium ion channels are involved indirectly by amplifying the effects initiated by the change in phospholipid permeability.
5. Radio waves that are amplitude modulated at the resonant frequencies for biologically active ions give responses because the asymmetrical motion of ions adjacent to the membrane demodulate the signal and promote their resonance.
6. The electromagnetically induced increase in membrane permeability weakens cellular compartmentation and lets in more free calcium ions into the cytosol to interfere with cell signaling.

   I will now discuss each item of the hypothesis in turn.

11.3.3 Why are eddy currents necessary?

A major problem in explaining the biological effects of weak electromagnetic fields is fact that they do not have enough energy to give chemical effects on individual molecules. The energy available to a molecule from biologically active signals may be many orders of magnitude below the thermal energy of that molecule (kT) and should therefore be negligible. However, in an electrically conducting medium such as a living cell or its aqueous surroundings, the electromagnetic forces can be summed by countless ions to generate eddy currents in synchrony with the incoming electromagnetic signal and so collect enough energy to give significant effects. A non-biological example of this is the antenna of a radio picking up weak signals from a distant transmitter. They may be orders of magnitude below the thermal energy of the atoms of the antenna but can still be detected by the currents they generate, which are then amplified by its transistors. Living cells can behave in a way analogous to transistors. Weak eddy currents flowing in and around them can selectively remove calcium ions bound to the phospholipid fraction of their membranes to make them more permeable (equivalent to the base of the transistor). This permits the entry of many more free calcium ions down a huge electrochemical gradient into the cytosol (equivalent to the collector current of the transistor), which reduces the membrane potential and interferes with calcium-based cell signaling.

11.3.4 How do low frequency eddy currents affect membrane permeability?

It is now widely accepted that biological membranes are stabilized by divalent cations (Baureus Koch et al. 2003). Evidence for this is that erythrocyte ghosts (red blood cells that have lost their contents) are protected from breaking up into vesicles by divalent cations (Steck et al. 1970; Lew et al. 1988). Also washed carrot discs leak intracellular potassium ions into distilled water but not into 1 mM calcium chloride solution (Goldsworthy, unpublished). The latter is probably due to the transient formation of pores in the phospholipid fraction of cell membranes, which gives a relatively non-specific increase in permeability. The generation and re-sealing of such pores has been demonstrated in artificial planar phospholipid membranes as spontaneous transient changes in their conductance (Melikov et al. 2001). Ha (2001) made a theoretical study of the role of divalent ions such as calcium in stabilizing membranes against pore formation. He concluded that their double positive charge is more effective at screening the natural repulsive forces between the negative phospholipids and, by being divalent, they can cross-link neighboring phospholipid molecules. Monovalent ions such as potassium are much less able to do either of these, so an electromagnetically induced loss of calcium from cell membranes and their replacement by

monovalent ions should increase their tendency to pore-formation and increase their permeability.

The first evidence that electromagnetic fields can remove membrane-bound calcium came from Bawin et al. (1975) and Bawin and Adey (1976). They exposed chick and cat brain slices to $^{45}Ca^{2+}$ and examined the effects of electromagnetic exposure on its subsequent release. They found that its release was stimulated when the tissue was exposed to VHF signals, amplitude modulated at what we now know to be the resonant frequency for potassium ions. This effect was insensitive to cyanide and they concluded that a purely physical process was releasing ions bound to the cell membranes. However, when the experiment was repeated with the low frequency component of the signal on its own, the effect was reversed. There was now a *minimum* for calcium release at the potassium frequency. This suggests that some of the dislodged calcium was now being absorbed into the tissue down its natural electrochemical gradient. The cause of this "mirror image" effect was unknown at the time, but can now be explained by the hypothesis. The explanation is that the tissue can extract the biologically active low frequency component from the signal (see section 3.7) but only at a low level. It may have been strong enough to release some of the membrane-bound calcium, but not enough to trigger the large-scale inward leakage of free calcium seen with the pure low frequency signal.

We can postulate two mechanisms by which weak electromagnetic signals remove membrane-bound calcium. One is amplitude-dependent and the other is frequency-dependent. Although they will interact with one another, it is convenient to consider them separately to begin with. In this section, I will concentrate on the amplitude dependent mechanism. The frequency dependent mechanism will be explained in section 3.5.

11.3.4.1 Amplitude dependent mechanism

Cell membranes are usually negatively charged and bind mineral cations reversibly (Ha 2001). Applying an alternating electric field tends to drive these ions off and on the membrane with each half-cycle. However, they will only dislodge if the combined effects of thermal agitation and the electrical forces trying to remove them exceed the forces binding them to the membrane. The threshold at which this occurs will depend on the charge/mass ratio of the ion concerned, the natural affinity of the membrane for it, and the availability of ions with a lower charge/mass ratio, with which it might exchange. In general, ions with high charge/mass ratios should be affected more and be dislodged at a lower voltage. The exact effect will depend on strength of the field. If it is below the threshold for any ion to dislodge, nothing much will happen. If the threshold voltage for all ions is exceeded, they will all have an equal tendency to dislodge but will return in the same proportions when the field reverses. Again, there will be no observable effect.

Between these extremes, there will be a range when the thresholds for only some ions will be exceeded and these will be preferentially dislodged. They may return when the field reverses, but if they have diffused too far, they may be replaced by other ions in proportion to their *local activities*. This will change the relative concentrations of the different ions bound to the membrane since specific ions with a high charge/mass ratio are being removed, but they are being replaced by a less specific mixture. The process will be repeated with every cycle to give a selective and progressive loss of ions with high charge/mass ratios.

Many ions may contribute to this effect by competing for sites on the membrane, but the most important for membrane stability are calcium and potassium. Calcium has a high affinity for the membrane and stabilizes it against temporary pore-formation (Ha 2001). Potassium has a lower affinity for the membrane but this is compensated by its high intracellular concentration. Potassium is easily the most abundant cation in living cells. A typical plant cell has a potassium concentration of 100 mM or more, which is about 5 orders of magnitude greater than cytosolic calcium. It is therefore a serious competitor with calcium for sites on the membrane. Since it has a charge/mass ratio only half that of calcium, it will also be harder to dislodge electrically and will be the most likely ion to replace any lost calcium.

Since the selective release of calcium described above can occur only over a narrow range of voltages, this gives us an "amplitude window" for changes in membrane permeability and their biological effects. Such windows have been reported by many workers (Bawin and Adey 1976; Blackman et al. 1982; Blackman 1990; Liboff et al. 1990), where biological effects were maximal within distinct but varied ranges of signal amplitude. Often, there were two or more windows. Multiple windows may be explained because eukaryotic cells have several membrane systems, each with differing surface properties, ionic environments and exposures to the electrical component of the applied field. All of these factors will affect the ease with which bound calcium might be replaced by other ions and therefore the optimum strength of electromagnetic signal needed. Each membrane system could therefore have its own window for maximum permeability and, since they often surround calcium-rich organelles, there could be several amplitude windows for biological activity, even in a single cell.

The proposed hypothesis also explains why the effects of weak electromagnetic fields only occur at low frequencies. This is because there must be time for the released calcium ions to diffuse well away from the membrane if they are to be replaced by monovalent ions before the field reverses. Also explained is the observation that pulses and square waves are more effective than sine waves of the same amplitude. This is because the rapid rise and fall times of the magnetic component of these fields give voltage spikes that catapult the calcium ions quickly away from the membrane, followed by a relatively long period for the lost ions to be replaced by less affected species such as potassium before the field reverses.

11.3.5 Why are some frequencies more effective than others?

The ability of different ions to replace dislodged calcium will depend on their relative chemical activities in the surrounding medium rather than their concentrations. These activities also include other components that may affect their ability to react, such as an increase in kinetic activity due to ion cyclotron resonance. The response will therefore hit an extreme value at the resonant frequency for the ion concerned.

11.3.5.1 What is ion cyclotron resonance?

Ion cyclotron resonance can occur when ions move through a steady magnetic field. Lorentz forces drive them into orbit around the lines of force of the steady field at a characteristic "resonant" frequency that depends on their charge/mass ratio and the strength of the steady field. If these ions are simultaneously exposed to either an electrical or a magnetic field that oscillates at this frequency, they absorb its energy and gradually increase the size of their orbits. This increases their kinetic energy, which increases their chemical activity and ability to react. The resonant frequency for any ion can be determined from the formula:

$$\text{Frequency (Hz)} = \frac{\text{Ion Charge (Coulombs)} \times \text{Steady Field Strength (Tesla)}}{\text{Ion Mass (Kg)} \times 2\pi}$$

11.3.5.2 What are the biological effects of resonance?

The two most important frequencies for biological effects are those for potassium and calcium. The resonant frequency for potassium in the Earth's magnetic field is around 16 Hz and that for calcium is about 32 Hz (the exact values depend on local field strength). The frequencies for these ions are important since they give extreme but opposite biological effects (Smith et al. 1993; Mehedintu and Berg 1997). Extreme responses at the potassium frequency have been reported so many times that their reality is beyond dispute (Tenforde 1990). Evidence that it is due ion cyclotron resonance was obtained by adjusting the steady magnetic field to different values, when the peak response occurred at the predicted new resonant frequencies (Smith et al. 1993). But until now, there has been no satisfactory explanation. An early proposal by Liboff (1985) that the helical movement of resonating ions lets them corkscrew their way through ion channels was criticized by several workers (Halle 1988; Tenforde 1990) because it needs an exact alignment of the channels with the magnetic field, their transit time in the channels is too short for even one orbit, and their high frequency of collision with other molecules in the solution and with the stationary sides of the channel may not permit their resonance anyway.

The present hypothesis avoids these difficulties. There is no time limit for resonance to build up, and the ions do not have to move in any particular direction. All they need do is to increase their kinetic energy and so enhance their chemical activity compared with competing ions. Collisions are also less problematical, since most of the ions near the negatively-charged cell membrane will be positively charged and will all tend to vibrate in synchrony with the electromagnetic field. This will occur regardless of whether they are actually resonating. They may also transfer some of this energy to adjacent uncharged molecules so that the whole region next to the membrane will have a component of its molecular motion that is synchronous with the applied field. Consequently, collisions of a resonating ion with any of these molecules will tend to reinforce rather than detract from its resonance.

Evidence that resonance can increase chemical activity, even in purely physical systems, comes from the work of Zhadin et al. (1998), who showed that the electrolysis of glutamate was enhanced by an electromagnetic field at its resonant frequency. The frequency corresponded to that of the unhydrated ion, which suggests that it is an effect at the electrode surface, since ions in the bulk solution are normally hydrated and would have a different frequency. I suggest that the most likely interpretation of these results is that the electromagnetic exposure of the glutamate ion to its resonant frequency increased its kinetic energy and chemical activity, which assisted its discharge at the electrode. It therefore seems probable that a similar electromagnetically induced increase in the chemical activity of potassium ions will enhance their ability to deposit on cell membranes to replace bound calcium and increase permeability.

Further evidence supporting the hypothesis comes from the observations that electromagnetic exposure near the resonant frequency for calcium gives opposite biological effects to the potassium frequency. Mehedintu and Berg (1997) found a significant stimulation of yeast multiplication at the potassium frequency but an inhibition at the calcium frequency. Smith et al. (1993) found that the potassium frequency stimulated the germination of radish seeds but the calcium frequency inhibited it. This is what we would expect, since the potassium frequency would enhance ambient potassium activity, help it replace membrane-bound calcium and *increase* permeability. The calcium frequency would increase the activity of ambient *calcium* ions so that they compete more effectively with potassium and *decrease* permeability. The two frequencies should therefore affect cell signaling and their metabolic consequences in opposite directions. This effect may prove useful in mitigating some of the claimed ill effects of electromagnetic exposure at 16 Hz and possibly other frequencies.

The hypothesis also explains some of the other more curious "frequency windows" phenomena. For example, Liboff et al. (1990) quote a maximum for diatom motility not only at the potassium resonant frequency but also at its even harmonics. However, the odd harmonics were inhibitory. Blackman (1990) quotes similar results for calcium release from brain tissue. We would

expect potassium resonance also to be supported by its harmonics and stimulate calcium release and diatom motility, but why were the odd harmonics inhibitory? This too can be explained by the hypothesis since the charge/mass ratio for the calcium ion is almost exactly double that for potassium. This means that the fundamental frequency for calcium corresponds to the first harmonic for potassium; thereafter every odd potassium harmonic corresponds to a calcium harmonic. Simultaneous calcium resonance where the harmonics share a frequency (the odd potassium harmonics) should therefore reverse the extra calcium release and consequent increase in permeability that might have occurred from potassium resonance. But not all frequency windows can be explained in terms of calcium and potassium harmonics. Blackman (1990) also reports some extrema for calcium release that didn't correspond to this relationship. We might be tempted to think that they could correspond to the resonant frequencies (or their harmonics) of other ions to allow them also to compete more effectively for the calcium sites on the membrane, but this needs further investigation.

11.3.6 How are ion channels involved?

Much research has been done on the possible roles of ion channels in bioelectromagnetic responses, but there is no convincing evidence that they are the *primary* receptors of the stimulus. By contrast, as we have just seen, there is considerable evidence that the phospholipid fraction of the cell membrane may be responsible. But if this is so, we must explain the observation by Barbier et al. (1996) that blocking calcium channels partially inhibited the electromagnetically-induced uptake of calcium in cultured cells, which suggests that ion channels must also play a role. This could be true, since even a non-specific increase in the permeability of the lipid fraction would partially short-circuit the membrane potential, reduce its voltage and open voltage-gated calcium channels. This would then amplify the effect, and make the whole response partially (but not completely) sensitive to the channel blocker. This interpretation is supported by Obo et al. (2002), who found no effect of electromagnetic treatment on calcium channel currents in animal cells when they were patch-clamped at a constant voltage. However, Baureus Koch et al. (2003) were able to show an increase in the passive leakage of $^{45}Ca^{2+}$ from inside-out spinach plasma membrane vesicles at the calcium frequency, presumably via voltage gated calcium channels, since these would be fully open in the absence of an actively maintained membrane potential. This is not inconsistent with our hypothesis since an electromagnetically-induced increase in calcium activity would also promote its *passive diffusion* through the ion channels. However, this still does not explain what happens under natural conditions, when these calcium channels would normally be held closed by the membrane potential. They also found no effect on calcium efflux at the potassium resonant frequency corresponding to that found by

Bawin et al. (1975), so it is probable that the two phenomena are not related and the hypothesis that it is the phospholipid fraction of the cell membrane that normally perceives the electromagnetic stimulus remains intact. However, we cannot deny that voltage gated calcium channels play a part in the biological responses to electromagnetic fields, but they seem only to amplify the response after the membrane potential has been reduced by the change in phospholipid permeability.

11.3.7 How do modulated radio waves give their effects?

Although much work has been done on the effects of radio waves on animals, relatively little has been done on their effects on plants. However, significant abnormalities have been detected in plants as diverse as pine trees (Selaga and Selaga 1996) and duckweed (Magone 1996) following exposure to pulsed radiation from radar installations, and there is no reason to believe that the mechanism by which they are perceived is significantly different from that in animals. It is widely accepted that continuous unmodulated radio waves are of too high a frequency to give biological effects but they do become effective when pulsed or amplitude modulated at a low frequency. It was once thought that non-linearities in the electrical properties of cell membranes rectify and demodulate the signal to regenerate the biologically-active low frequency. But these non-linearities disappear with carrier waves above a few MHz and the biological effects of modulated signals extend well beyond this. Also, even if the membranes could rectify these signals, it still does not explain how any extracted low-frequency component might work.

However, the present hypothesis explains how amplitude modulated radio signals, even at very high frequencies, can affect calcium release, membrane permeability and cell signaling; all without rectification. Let us draw an analogy with a child continuously bouncing a ball. The harder he hits it, the higher it bounces and the greater is its mean height. A coherent radio signal will do the same for the diffuse layer of unhydrated cations layer next to the negative surface of a membrane. Because the motion of the ions is limited in one direction by the membrane, the mean electrical centre of the layer will rise and fall in synchrony with the amplitude of the low-frequency envelope. These excursions are limited by the amplitude of the carrier wave and may be too small to give a direct biological response, particularly with high carrier frequencies. But if the modulating frequency corresponds to the resonant frequencies of any ambient ions, they will absorb energy from the slowly oscillating electrical centre of the cation layer and increase their chemical activity. This would explain the findings of Bawin et al. (1975) when they treated [potassium rich] brain slices with amplitude modulated VHF signals. The signals released calcium from the tissue, but only when the modulating frequency corresponded to the resonant frequency for potassium.

11.3.8 How does membrane permeability affect metabolism?

It has long been suspected that the multitude of different effects of weak electromagnetic radiation in different tissues is due to its promoting the entry of calcium into the cytosol, where it interferes with their characteristic cell signaling patterns. Liburdy et al. (1993) found evidence for this when they showed that the transcription of genes in cultured rat cells was enhanced by electromagnetic treatment and that this was associated with a calcium influx. They proposed that the extra calcium interfered with intracellular signaling cascades to affect gene transcription. Calcium ions often take part in these cascades, where they help to activate many aspects of metabolism. The huge variety of biological responses to electromagnetic fields can therefore be explained by the cells of different tissues or species having different cascades available for activation. These proposals also explain the poor reproducibility of many bioelectromagnetic experiments, since similar cells with different histories may have different cascades available. Also any factors that impair the cells ability to expel surplus calcium, such a starvation or stress, will affect the final response. Last but not least, a large increase in cell permeability to calcium may itself give stress responses, since cells are also programmed to use high levels of internal calcium as an indication of serious membrane damage. Responses to high calcium include the closure of gap junctions (Alberts et al. 2002) and possibly plasmodesmata, which could inhibit the transmission of an electrical signal through a tissue and affect our experiments. It may also be why electromagnetic exposure can also promote the transcription of stress-related genes such as that for the heat-shock protein hsp70 (Goodman et al. 1994). It therefore probable that an over-large increase in electromagnetic exposure could convert what might have been a stimulatory response into an inhibitory one.

Many attempts have been made to verify Liburdy's hypothesis by measuring cytosolic calcium with fluorescent probes such as fura-2. Although some significant effects of electromagnetic treatment have been reported, many of the results have been inconclusive. This is partly because it only measures transient free cytosolic calcium and not that which has been bound to organic molecules or homeostatically expelled from the cytosol. There are also technical problems, for example Ihrig et al. (1997) found that increasing the dose of UV to excite the probe gave an unexplained increase in the response to electromagnetic treatment. Perhaps the UV was damaging the ATP-driven calcium extrusion system to make electromagnetically induced calcium uptake more visible, which is consistent with Liburdy's proposals. Another extremely important finding by Ihrig et al. (1997) was that cells showing a significant increase in cytosolic calcium in response to electromagnetic treatment also showed a greater leakage of the fura-2. This suggests that the electromagnetically induced increase in membrane permeability *is not specific for calcium*. This is consistent with the present hypothesis and implies

that at least some of the metabolic effects of electromagnetic exposure may also be due to a more general breakdown of membrane containment and intracellular compartmentation.

11.3.9 Summary of the hypothesis

Time-varying electromagnetic fields induce eddy currents in and around living cells that remove some of the calcium ions that help to stabilize their membranes. These calcium ions are replaced by ions with a lower charge/mass ratio (mainly potassium) less able to stabilize the membrane. This increases the formation of transient pores to increase membrane permeability and affect metabolism.

Only low frequency signals are effective because a slow diffusion process must occur within each half-cycle for the membrane-bound calcium to be replaced by other ions. The *selective* removal of calcium from membranes can only occur at voltages close to the threshold for its release and results in "amplitude windows" for the biological response. Multiple amplitude windows occur because eukaryotic cells have several membrane systems, each with their own characteristics for calcium release.

Electromagnetic fields at specific frequencies are particularly effective and give rise to "frequency windows" for biological responses. These often correspond to the ion cyclotron resonance frequencies (and their harmonics) for biologically important ions; notably those for potassium and calcium. When an ion is exposed to its resonant frequency, it increases its kinetic energy and ability to compete for binding sites on cell membranes. Exposure at the potassium frequency (16 Hz) increases the kinetic energy of potassium ions, which enables it to replace calcium more easily in the cell membrane to *increase* permeability. Exposure at 32 Hz (the calcium frequency) increases the activity of calcium and makes it compete more effectively with potassium, to *reduce* membrane permeability. They therefore give opposite biological effects. The ability of the calcium frequency to reverse the effects of the potassium frequency (and possibly of those of other frequencies) is important, since it may provide a way to mitigate some of the claimed ill effects of exposure to weak time-varying electromagnetic fields.

Radio waves can also give biological effects, but only if they are pulsed or amplitude modulated at biologically active low frequencies. This is because the modulated wave makes the layer of cations next to the membrane swell and shrink in time with the low frequency envelope. The consequent rise and fall of its electrical centre feeds the resonance of ions tuned to the modulating frequency and allow them to accumulate enough energy, even from weak signals, to give biological effects.

The electromagnetically induced changes in membrane permeability affect metabolism principally by allowing calcium to enter the cytosol down a very large electrochemical gradient, where they give a variety of effects by

interfering with cell signaling. However, because the change in membrane permeability is not specific, there could also be other effects not necessarily attributable to calcium ingress.

References

Adey WR (1990) Electromagnetic fields, cell membrane amplification, and cancer promotion. In: Wilson BW, Stevens RG, Anderson LE (eds) Extremely low frequency electromagnetic fields: the question of cancer. Battelle Press, Columbus, Ohio, pp 211–249

Alberts B, Bray D, Lewis J et al. (2002) Molecular biology of the cell. Garland Science, New York

Barbier E, Veyret B, Dufy B (1996) Stimulation of Ca^{2+} influx in rat pituitary cells under exposure to a 50 Hz magnetic field. Bioelectromagnetics 17:303–311

Baureus Koch CLM, Sommarin M, Persson BRR, Salford LG, Eberhardt JL (2003) Interaction between weak low frequency magnetic fields and cell membranes. Bioelectromagnetics 24:395–402

Bawin SM, Adey WR (1976) Sensitivity of calcium binding in cerebral tissue to weak environmental electric fields oscillating at low frequency. Proc Natl Acad Sci USA 73:1999–2003

Bawin SM, Kaczmarek KL, Adey WR (1975) Effects of modulated VHF fields on the central nervous system. Ann N Y Acad Sci 247:74–81

Blackman CF (1990) ELF effects on calcium homeostasis. In: Wilson BW, Stevens RG, Anderson LE (eds) Extremely low frequency electromagnetic fields: the question of cancer. Battelle Press, Columbus, Ohio, pp 189–208

Blackman CF, Benane SG, Kinney LS, House DE, Joines WT (1982) Effects of ELF fields on calcium-ion efflux from brain tissue in vitro. Radiat Res 92:510–520

Blackman VH (1924) Field experiments in electroculture. J Agricult Sci 14:240–267

Blackman VH, Legg AT (1924) Pot culture experiments with an electric discharge. J Agricult Sci 14:268–273

Blackman VH, Legg AT, Gregory FG (1923) The effect of direct current of very low intensity on the rate of growth of the coleoptile of barley. Proc R Soc Lond B 95:214–228

Briggs LJ, Campbell AB, Heald RH, Flint LH (1926) Electroculture. US Dept Agriculture, Bulletin 1379

Dijak M, Smith DL, Wilson TJ, Brown DCW (1986) Stimulation of direct embryogenesis from mesophyll protoplasts of *Medicago sativa*. Plant Cell Rep 5:468–470

Friml J, Vieten A, Sauer M, Weijers D, Schwarz H, Hanann T, Offringa R, Jurgens G (2003) Efflux-dependent auxin gradients establish the apical-basal axis of *Arabidopsis*. Nature 246:147–153

Goldsworthy A (1996) Electrostimulation of cells by weak electric currents. In: Lynch PT, Davey NR (eds) Electrical manipulation of cells. Chapman and Hall, New York, pp 249–272

Goldsworthy A, Mina MG (1991) Electrical patterns of tobacco cells in media containing indole-3-acetic acid or 2,4-dichlorophenoxyacetic acid. Planta 183:368–373

Goodman R, Blank M, Lin H, Dai R, Khorkova O, Soo L, Weisbrot D, Henderson A (1994) Increased levels of hsp70 transcripts induced when cells are exposed to low frequency electromagnetic fields. Bioelectrochem Bioenerg 33:115–120

Ha B-Y (2001) Stabilization and destabilization of cell membranes by multivalent ions. Phys Rev E 64:051902 (5 pages)

Halle B (1988) On the cyclotron resonance mechanism for magnetic field effects on transmembrane ion conductivity. Bioelectromagnetics 9:381–385

Ihrig I, Heese C, Glaser R (1997) Alterations in intracellular calcium concentration in mice neuroblastoma cells by electrical field and UVA. Bioelectromagnetics 18:595–597

Jaffe LF, Nuccitelli R (1977) Electrical controls of development. Annu Rev Biophys Bioeng 6:445–476

Jaffe LF, Robinson KR, Nuccitelli R (1974) Local cation entry and self-electrophoresis as an intracellular localisation mechanism. Ann N Y Acad Sci 238:372–389
Lemström K (1904) Electricity in agriculture and horticulture. Electrician Publications, London
Lew VL, Hockaday A, Freeman CJ, Bookchin RM (1988) Mechanism of spontaneous inside-out vesiculation of red cell membranes. J Cell Biol 106:1893–1901
Liburdy RP, Callahan DE, Harland J, Dunham E, Sloma TR, Yaswen P (1993) Experimental evidence for 60 Hz magnetic fields operation through the signal transduction cascade. FEBS 334:301–308
Liboff AR (1985) Geomagnetic cyclotron resonance in living cells. J Biol Phys 13:39–51
Liboff AR, McLeod BR, Smith SD (1990) Ion cyclotron resonance effects of ELF fields in biological systems. In: Wilson BW, Stevens RG, Anderson LE (eds) Extremely low frequency electromagnetic fields: the question of cancer. Battelle Press, Columbus, Ohio, pp 251–289
Lund EJ (1923) Electrical control of organic polarity in the egg of *Fucus*. Bot Gaz 76:288–301
Magone I (1996) The effect of electromagnetic radiation from the Skrunda Radio Location Station on *Spirodela polyrhiza* (L) Schleiden cultures. Sci Total Environ 180:75–80
McLeod BR, Smith SD, Liboff AR (1987) Potassium and calcium cyclotron resonance curves and harmonics in diatoms (*A. coffeaeformis*). J Bioelectr 6:153–168
Mehedintu M, Berg H (1997) Proliferation response of yeast *Saccharomyces cerevisiae* on electromagnetic field parameters. Bioelectrochem Bioenerg 43:67–70
Melikov KC, Frolov VA, Shcherbakov A, Samsonov AV, Chizmadzhev YA, Chernomordik LV (2001) Voltage-induced nonconductive pre-pores and metastable single pores in unmodified planar lipid bilayer. Biophys J 80:1829–1836
Mina MG, Goldsworthy A (1991) Changes in the electrical polarity of tobacco cells following the application of weak external currents. Planta 186:104–108
Mina MG, Goldsworthy A (1992) Electrical polarization of tobacco cells by Ca^{2+} ion channels. J Exp Bot 43:449–454
Muday GK, Peer WA, Murphy AS (2003) Vesicular cycling mechanisms that control auxin transport polarity. Trends Plant Sci 8:301–304
Mulkey TI, Kuzmanoff KM, Evans MI (1981) Correlations between proton efflux and growth patterns during geotropism and phototropism in maize and sunflower. Planta 152:239–241
Muraji M, Asai T, Wataru T (1998) Primary root growth rate of *Zea mays* seedlings grown in an alternating magnetic field of different frequencies. Bioelectrochem Bioenerg 44:271–273
Murr LE (1963) Plant growth responses in a stimulated electric field environment. Nature 200:490–491
Mycielska ME, Djamgoz MBA (2004) Cellular mechanisms of direct-current electric fields effects: galvanotaxis and metastatic disease. J Cell Sci 117:1631–1639
Novák B, Bentrup FW (1973) Orientation of *Fucus* egg polarity by electric ac and dc fields. Biophysik 9:253–260
Obo M, Konishi S, Otaka Y, Kitamura S (2002) Effect of magnetic field exposure on calcium channel currents using patch clamp technique. Bioelectromagnetics 23:306–314
Peng HB, Jaffe LF (1976) Polarization of fucoid eggs by steady electrical fields. Dev Biol 53:277–284
Rathore KS, Goldsworthy A (1985) Electrical control of shoot regeneration in plant tissue cultures. Bio/Technol 3:1107–1109
Rathore KS, Hodges TK, Robinson KR (1988) A refined technique to apply electrical currents to callus cultures. Plant Physiol 88:515–517
Schonland BFJ (1928) The interchange of electricity between thunderclouds and the earth. Proc R Soc Lond A 118:242–262
Selaga T, Selaga M (1996) Response of *Pinus sylvestris* L needles to electromagnetic fields. Cytological and ultrastructural aspects. Sci Total Environ 180:65–73
Smith SD. McLeod BR, Liboff AR (1993) Effects of SR tuning 60 Hz magnetic fields on sprouting and early growth of *Raphanus sativus*. Bioelectrochem Bioenerg 32:67–76
Steck TL, Weinstein RS, Straus, JH, Wallach DFH (1970) Inside-out red cell membrane vesicles: preparation and purification. Science 168:255–257

Stenz H-G, Wohlwend B, Weisenseel MH (1998) Weak AC electric fields promote root growth and ER abundance of root cap cells. Bioelectrochem Bioenerg 44:261–269

Taiz L, Zeiger E (2002) Plant Physiology. Sinauer, Sunderland, Mass.

Tenforde TS (1990) Biological interactions and human health effects of extremely low frequency magnetic fields. In: Wilson BW, Stevens RG, Anderson LE (eds) Extremely low frequency electromagnetic fields: the question of cancer. Battelle Press, Columbus, Ohio, pp 291–315

Wilson BW, Stevens RG, Anderson LE (eds) (1990) Extremely low frequency electromagnetic fields: the question of cancer. Battelle Press, Columbus, Ohio

Zhadin MN, Novikov VV, Barnes FS, Pergola NF (1998) Combined action of static and alternating magnetic fields on ionic current in aqueous glutamic acid solution. Bioelectromagnetics 19:41–45

12 Long-Distance Electrical Signaling and Physiological Functions in Higher Plants

JÖRG FROMM

12.1 Introduction

Plants possess most of the chemistry of the neuromotoric system in animals, i.e. neurotransmitter such as acetylcholine, cellular messengers like calmodulin, cellular motors, e.g. actin and myosin, voltage-gated ion channels and sensors for touch, light, gravity and temperature. Although this nerve-like cellular equipment has not reached the same great complexity as is the case in nerves, a simple neural network has been formed within the phloem, enabling it to communicate successfully over long distances. The reason why plants have developed pathways for electrical signal transmission most probably lies in the necessity to respond rapidly to environmental stress factors. Different environmental stimuli evoke specific responses in living cells which have the capacity to transmit a signal to the responding region. In contrast to chemical signals such as hormones, electrical signals are able to rapidly transmit information over long distances. Most of the plant action potentials studied so far have a velocity in the range of 0.01–0.2 m s^{-1}. However, in soybean, action potentials reached conduction rates of up to 30 m s^{-1}, similar to the speed of action potentials in nerves (Volkov et al. 2000).

As regards the origin of the neuronal system in plants, it appears unlikely that it was adopted from animals. In our search for the common evolutionary roots of action potentials in plants and animals, we need to look at unicellular ancestors which do not need to transmit signals over long distances. The function of electrical transmission has most probably evolved at a later evolutionary stage. The assumption is that in the course of evolution the development of plants and animals branched off into different directions. Since cellular excitability was found to exist in primitive organisms, it is obvious that both plants and animals inherited their basic neuronal capabilities from their bacterial ancestors (Simons 1992). Szmelcman and Adler (1976) observed changes in membrane potential during bacterial chemotaxis. Even the sensitivity to mechanical touch is known to be an early evolutionary achievement. Martinac et al. (1987) detected pressure-sensitive ion channels

Fachgebiet Holzbiologie, TU München, Winzererstrasse 45, 80797 München, Germany (e-mail: fromm@wzw.tum.de)

Plant Electrophysiology – Theory & Methods (ed. by Volkov)

in *Escherichia coli*, suggesting that these channels have an osmotic function. For the early evolution of action potentials, an osmotic function can also be assumed in unicellular alga such as *Acetabularia* (Mummert and Gradmann 1976). A mechanosensitive ion channel was also found in the yeast plasma membrane (Gustin et al. 1988), providing convincing evidence that plants inherited mechanical sensitivity from bacterial ancestors in the course of millions of years of evolution. The characean algae, which include *Chara* and *Nitella*, are also known to be the ancestors of higher plants. Action potentials were observed in the internodal cells of *Nitella* in 1898 by Hörmann, who used extracellular electrodes long before they were observed in isolated nerve cells by Adrian and Bronk (1928). Characean internodal cells respond to electrical stimulation in a manner similar to the contraction response displayed by skeletal muscles following electrical stimulation by nerve cells. In characean cells, electrical stimulation causes the cessation of protoplasmic streaming which is incited by the same interactions between actin and myosin that cause contraction in muscles (Hörmann 1898). In the course of evolution, once plants had gained and settled on dry land, their excitability and neuronal capability were used to develop numerous survival tactics. For instance, one important step was the development of fast-moving stomatal guard cells in response to environmental changes, while another was the electrical communication system which uses the phloem to transmit information over long distances within the plant body (Fromm and Lautner 2005).

12.2 Perception of electrical signals

Electrical signals can be generated at any site of the symplastic continuum by environmental stimuli such as changes in temperature, touch or wounding. Recently, it was found that acid rain also induces action potentials (Shvetsova et al. 2002), as well as irradiation at various wavelengths which induces action potentials in soybean with duration times and amplitudes of approximately 0.3 ms and 60 mV, respectively (Volkov et al. 2004). Upon perception, electrical signals can be propagated via plasmodesmata to other cells of the symplast (van Bel and Ehlers 2005). As a first step, the plasma membrane is being depolarized, a process known as formation of the receptor potential, e.g. by mechanical stimulation as observed in *Chara* (Kishimoto 1968). The receptor potential is an electrical replica of the stimulus lasting for the period of time that the stimulus is present. An action potential is evoked when the stimulus is great enough to depolarize the membrane to below a certain threshold. Subsequently, the action potential characterized by a large transient depolarization allows the rapid transmission of information via plasmodesmata (Fig. 12.1). An action potential usually has an all-or-nothing and self-amplifying character, and it travels with constant velocity and magnitude (Zawadzki et al. 1991). Electrical coupling via plasmodesmata was demonstrated in a variety of species such as *Nitella*

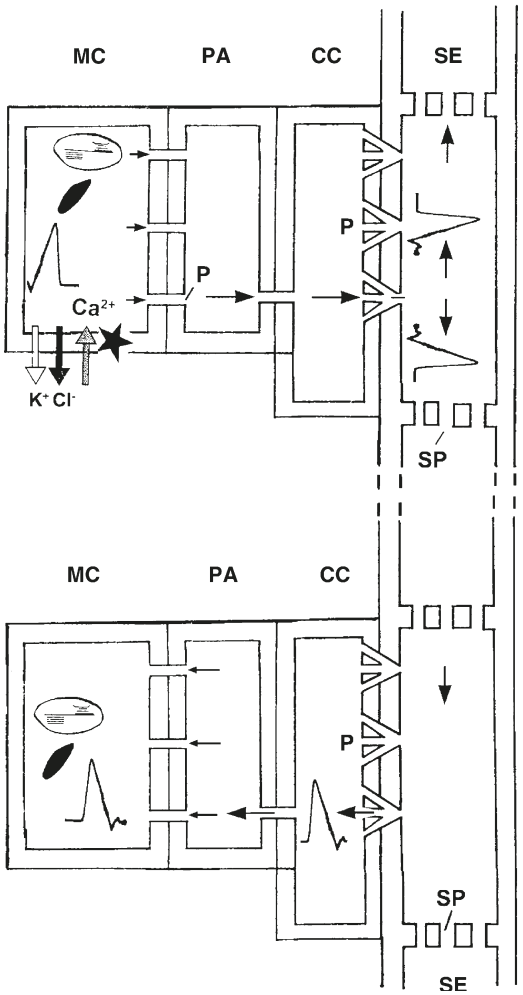

Fig. 12.1. Electrical signaling in higher plants. Stimulation by cold-shock or touch (*star*) induces calcium influx into a living cell, e.g. a mesophyll cell (*MC*, *above*). After the membrane potential is depolarized below a certain threshold level, an action potential is elicited by chloride and potassium efflux. The signal is propagated over short distances through plasmodesmal (*P*) networks and, after it passed the few plasmodesmata between sieve element/companion cells (*SE/CCs*) and phloem parenchyma cells (*PA*), will enter the SE/CC-complex to be transmitted over long distances. Sieve pores (*SP*) with their large diameters present low-resistance corridors for a rapid propagation of electrical signals along the SE plasma membrane. Such signals can leave the phloem at any site via plasmodesmata (*below*) to affect certain physiological processes in the neighbouring tissue

(Spanswick and Costerton 1967), *Elodea* and *Avena* (Spanswick 1972) and *Lupinus* (van Bel and van Rijen 1994), indicating that plasmodesmata are relays in the signaling network between cells. However, long distances between

different organs can be bridged rapidly only via low resistance connections, which extend continuously throughout the whole plant. The sieve tube system seems to fulfill these conditions, because the structure of the sieve tube members is unique and appears to be suitable for the transmission of electrical signals due to the relatively large, unoccluded sieve plate pores, continuity of the plasma membrane and ER (Evert et al. 1973), as well as lack of vacuoles. Moreover, the low degree of electrical coupling in lateral direction caused by only few plasmodesmata at the interface between companion cells and phloem parenchyma cells (Kempers et al. 1998) facilitates long distance signaling. However, the plasmodesmata may open up, making it possible for lateral electrical signaling from neighboring cells to be transmitted to the sieve elements/companion cells (SE/CC, Fig. 12.1). In summary, signal transmission within the plant depends on the electrical conductance of plasmodesmata in lateral direction as well as on the high degree of electrical coupling via the sieve pores in longitudinal direction.

12.3 Aphid technique as a tool for measuring electrical signals in the phloem

Since the phloem is located inside the plant body several cell layers distant from the plant surface, experiments on electrical signaling via the phloem of intact plants are difficult to perform. Microelectrode measurements in combination with dye solutions injected into the cell to be measured after obtaining electrophysiological results is a time-consuming technique because the measured cell type can only be roughly estimated at the beginning and very often the microelectrode tip was not properly inserted in the phloem as revealed by microscopic checks after the experiment. Microelectrodes brought into contact with sieve tube exudates that appear at the cut end of an aphid stylet (Wright and Fisher 1981; Fromm and Eschrich 1988b), enabled us to monitor the membrane potential of sieve tubes and its changes after plant stimulation (Fig. 12.2A, B). The successful use of aphid stylets to measure electrical signals within the sieve tubes depends on their functioning as an effective salt bridge between the sieve tube cytoplasm and the microelectrode. Sieve tube exudates typically contain high K^+ concentrations; measurements on barley leaves gave values ranging from 50 to 110 mM (Fromm and Eschrich 1989). The stylet's food canal dimensions can be used to roughly calculate its electrical resistance. Using an average area of 6 μm^2 and assuming the canal to be filled with 100 mM KCl, its resistance would be about 2.6×10^9 Ω (Wright and Fisher 1981). Although this value is about 3 times greater than the typical resistance of a glass microelectrode, it is still within the measuring capacities of the electrometer used (input impedance $>10^{12}$ Ω). The stylets are embedded in hardened saliva, which insulates electrically. For

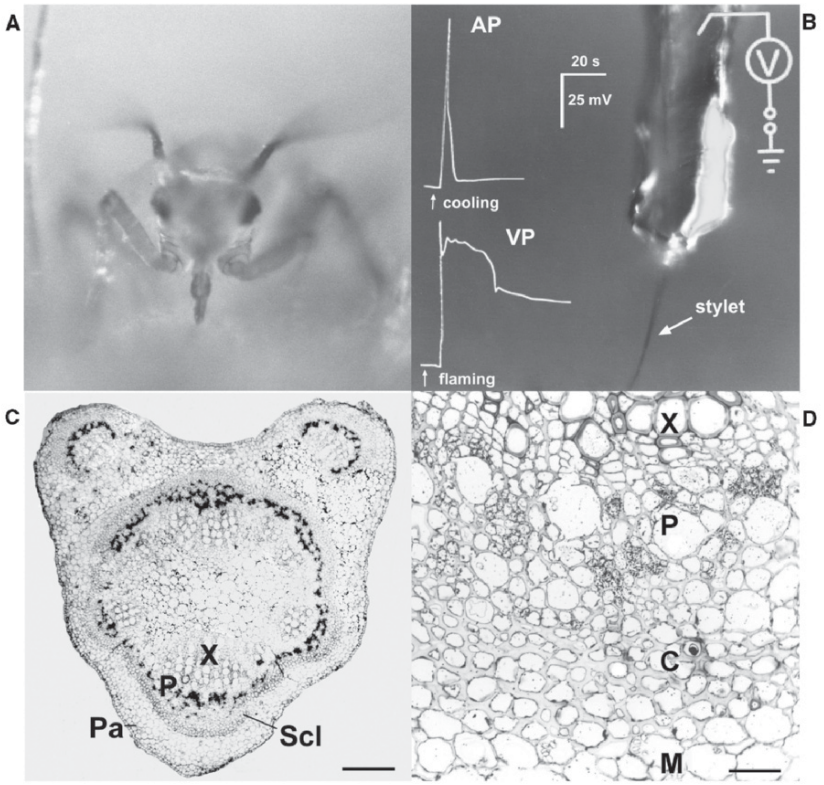

Fig. 12.2. Transmission of action potentials (*AP*) and variation potentials (*VP*) in sieve tubes of *Mimosa*. **A** Front-view of *Rhopalosiphum padi* sucking at the base of a petiolus with its stylet inserted into a sieve element (×32). **B** After the aphid separated from its stylet by a laser pulse, the stylet stump exuded sieve tube sap to which the tip of a microelectrode was attached (×400). Cooling the apical end of the petilous evoked an action potential (*AP*) while flaming triggered a variation potential (*VP*) transmitted basipetally within the sieve tubes. **C** Microautoradiography of the petiolus. ^{14}C-labeled photoassimilates from the leaves accumulated in the phloem (P) which is surrounded by a sclerenchyma sheath (*Scl*) in order to restrict electrical signaling to the phloem. *Bar*, 150 µm. **D** Microautoradiograph of a cross section of the primary pulvinus at the base of the petiolus. Labeled photoassimilates are restricted to the phloem strands (*P*). Since sclerenchyma tissue is absent, electrical signals can be transmitted laterally from the phloem via living collenchyma cells (*C*) to the motor cells (*M*) which cause the leaf movements by either losing or gaining turgor. *X* xylem; *Pa* parenchyma. *Bar*, 30 µm

instance in *Mimosa pudica*, a classic example for the conductance of rapid excitation in higher plants, the microelectrode tip was brought into contact with the stylet stump at the petiolus with its cut end sealed into saline solution to which the Ag/AgCl reference electrode was connected. After successful connection of stylet and mirocelectrode tip a resting potential of −160 mV

was established, well in line with values found in other species and by other methods (Eschrich et al. 1988; van Bel and van Rijen 1994). Cooling the apical end of the petiolus evoked a rapidly moving action potential transmitted basipetally within the sieve tubes at the rate of up to 3–5 cm s^{-1} (AP, Fig. 12.2B). By contrast, wounding by flaming induced a more slowly moving signal, also called variation potential, with irregular form and of long duration (VP, Fig. 12.2B). The variation potential varies with the degree of stimulus, is non-self-perpetuating and appears to be a local change to either a hydraulic surge or chemicals transmitted in the dead xylem (Davies 2004). In *Mimosa*, both action and variation potentials become immediately evident as the bending pulvini cause impressive movements of the paired leaflets. Microautoradiography of the petiolus showed the localization of the phloem by ^{14}C-labeled photoassimilates from the leaves exposed to $^{14}CO_2$ (Fig. 12.2C). The vascular bundles are surrounded by a sclerenchyma sheath in order to restrict electrical signaling to the phloem. When a phloem-transmitted action potential reaches the pulvinus which has no sclerenchyma (Fig. 12.2D; Fromm and Eschrich 1988a), it is transmitted laterally via plasmodesmata into the cells of the motor cortex. The latter possess voltage-gated ion channels which respond to the signal, causing ion efflux associated with water efflux, which leads to leaf movements (Fromm and Eschrich 1988c).

12.4 Electrical properties of the phloem and characteristics of phloem-transmitted signals

The phloem presents a network for assimilate allocation as well as chemical and electrical communication within the plant. Concerning assimilate transport, osmolytes like sucrose generate the hydrostatic pressure which drives nutrient and water flow between the source and the sink phloem. Proton-coupled sucrose symporters, such as ZmSUT1, localized to the sieve tube and companion cell plasma membrane are capable of mediating both, the sucrose uptake into the phloem in mature leaves and the desorption of sugar from the phloem into sink tissues. The use of patch-clamp techniques revealed that the ZmSUT1-mediated sucrose-coupled proton current depended on the direction of the sucrose and pH gradient as well as on the membrane potential across the transporter (Carpaneto et al. 2005). Concerning the membrane potential, it has been shown that a sink-source-regulated and sugar-inducible K^+ channel (VFK1) dominates the electrical properties of the sieve tube plasma membrane (Ache et al. 2001). The source site of phloem cells is characterized by K^+ concentrations of about 100 mM within the cytoplasm and 10 mM in the apoplast (Mühling and Sattelmacher 1997), resulting in an equilibrium potential for potassium ions (E_K) of around –60 mV. Since the membrane potential of the SE/CC is between –130 and –200 mV (van Bel 1993; Ache et al. 2001) and thus more negative than E_K, VFK1 loads K^+ into the phloem. Furthermore,

K^+ channels of the AKT2/3 family have been identified as photosynthate-induced phloem channels. From studies of an AKT2/3 loss-of-function mutant, it was shown that this mutant exhibited reduced K^+ dependence of the phloem potential and that AKT2/3 regulates sucrose/H^+ symporters via the membrane potential (Deeken et al. 2002). Furthermore, there is an electrogenic component of the sieve tube membrane potential, the magnitude of which is substantially greater than that predicted for E_K (Wright and Fisher 1981). With regard to calcium, (DHP)-type Ca^{2+} channels were localized in the phloem of leaf veins from *Nicotiana* and *Pistia* by immunolabeling techniques (Volk and Franceschi 2000), indicating that Ca^{2+} channels are also abundant in sieve elements. Most likely, these channels are involved in the generation of electrical signals, making them the subject of further studies.

The ion transport processes which create the conditions necessary for the generation of an action potential were investigated intensively in members of the green algal family Characaea (Tazawa et al. 1987). One of the ion transport mechanisms responsible for depolarization is based on chloride the efflux of which increases upon membrane stimulation (Gaffey and Mullins 1958; Oda 1976). Another ion involved in plasma membrane excitation is calcium where studies showed that both the peak of the action potential (Hope 1961) and the inward current (Findlay 1961, 1962) are dependent on the calcium concentration outside the cell. Some workers suggest that both chloride and calcium are involved in the formation of an individual action potential (Beilby and Coster 1979; Lunevsky et al. 1983). In addition to these ions, it was found that potassium efflux from the cell increases upon stimulation of the membrane (Spyropoulos et al. 1961; Oda 1976).

These ion shifts during an action potential were confirmed in trees by a method which uses inhibitors of ionic channels as well as energy-dispersive X-ray microanalysis (Fromm and Spanswick 1993). Results indicate that calcium influx as well as potassium and chloride efflux are involved in the generation of action potentials. When action potentials were induced by electrical stimulation in willow, it became clear that the required stimulus depends on both, its intensity and duration (Fromm and Spanswick 1993). An increase in stimulus strength does not produce any change in the amplitude nor in the form of the action potential once it has been induced, showing that it conforms to the all-or-nothing law. Concerning refractory periods, they were found to be much longer in plants than in animal systems, with durations between 50 s (Fromm and Bauer 1994) up to 5 h (Zawadzki et al. 1991).

12.5 Electrical signaling via the phloem and its effect on phloem transport

Strong evidence has accumulated that electrical transmission in sieve elements also occurs in species that do not perform rapid leaf movements as, e.g. in Mimosa. In zucchini plants, electrical signal transmission via sieve

tubes between a growing fruit and the petiole of a mature leaf reached maximum velocities of 10 cm s^{-1} (Eschrich et al. 1988). This is in the same velocity range as the movement of the action potential in sieve tubes of *Mimosa pudica* (Fromm and Eschrich 1988b). It is obvious that no chemical substance is capable of moving so fast in the assimilate flow. By contrast, hydraulic signals might transmit stimulations, but they would not be able to carry encoded plus- or minus-signals for hyperpolarization or depolarization, respectively, as shown in poplar sieve tubes (Lautner et al. 2005). It has not yet been shown whether hydraulic signals occur in the turgescent sieve tube system. In the wounded tomato plant, the pathway for systemic electrical signal transmission is also associated with the phloem (Rhodes et al. 1996), indicating that it regulates the induction of proteinase inhibitor activity in parts of the shoot distant from the wound (Wildon et al. 1992). As regards the function of the phloem, it has been shown that action potentials propagating in sieve tubes of *Mimosa* trigger phloem unloading in the pulvini (Fromm and Eschrich 1990; Fromm 1991).

In maize leaves, both electrical stimulation as well as cold-stimulation induce action potentials with amplitudes higher than 50 mV that are propagated basipetally in sieve tubes at speeds of 3–5 cm s^{-1} (Fromm and Bauer 1994). Stimulation with ice water has been reported to induce action potentials in a number of plant species, including *Biophytum* (Sibaoka 1973) as well as pumpkin and tomato (van Sambeek and Pickard 1976). The fact that Woodley et al. (1976) observed that localized chilling temporarily stops or reduces translocation of ^{14}C in sunflowers for 10–15 min and that this reduction in translocation corresponds closely to electrical changes measured along the stem gave rise to the idea of a possible relationship between action potentials and the cold-shock-induced inhibition of phloem transport. In addition, Minchin and Thorpe (1983) showed that rapid temperature drops of only 2.5 °C caused a brief abeyance of phloem transport in *Ipomea purpurea*, *Phaseolus vulgaris* and *Nymphoides geminata*, a phenomenon not observed when the temperature was reduced at a slower rate. In maize leaves, rapid cold-shock treatments cause sieve elements to trigger action potentials while phloem transport in distant leaf parts is strongly reduced, as shown by autoradiography at a distance of over 15 cm from the site of cold-stimulation (Fromm and Bauer 1994). When a maize leaf was stimulated electrically (10 V) via surface electrodes action potentials were induced and phloem transport was interrupted at the site of stimulation. Evidence of a link between electrical signaling and the reduction of phloem transport was found based on the decrease in symplastic K^+ and Cl^- concentration. In *Luffa cylindrica* action potentials affected elongation growth of the stem, most likely by K^+ and Cl^- efflux which reduced cell turgor and caused growth retardation (Shiina and Tazawa 1986). Since the concentrations of either ion are also reduced in the sieve element cytoplasm after stimulation (Fromm and Bauer 1994), decreased cell turgor may have

caused the reduction in phloem translocation since the latter requires the intracellular movement of water as a transport medium. However, the reduction in phloem translocation may have also been caused by a closure of sieve pores or a reduction of phloem loading because the latter depends on the membrane potential as well as on the K^+ concentration in sieve tubes, both of which changed during stimulation. To obtain a better insight into the electrical controlling points in the phloem transport system, further work is required.

12.6 Role of electrical signals in root-to-shoot communication of water-stressed plants

Non-hydraulic signaling between roots and shoots of plants growing in drying soil has evoked considerable interest in recent years. Since plants growing in drying soil showed stomatal closure and leaf growth inhibition before the reductions in leaf turgor were measured, non-hydraulic signals from roots may serve as a sensitive link between soil water changes and shoot responses (Davies and Zhang 1991). Therefore, stomata appear to be able to receive information on the soil water status independent of the leaf water potential. Evidence that the nature of this information is chemical was obtained by analyzing the xylem sap from unwatered plants, indicating the involvement of ion content, pH, amino acids and hormones (Schurr and Gollan 1990). Since the velocity of a chemical substance in the phloem is relatively slow and typically proved to be 50–100 cm h^{-1} (Canny 1975), the open question was how is the leaf capable of responding rapidly to the changing water status of the soil. Evidence of electrical root-to-shoot signaling was obtained by both, extra- and intracellular potential measurements on 80 cm tall maize plants. They were subjected to a drying cycle of 5 days showing a decrease in CO_2 uptake and transpiration rate while the electrical potential difference between two surface points showed a daily rhythm which seemed to be correlated with the soil water status (Fromm and Fei 1998). After soil drying the plants were watered and increases in CO_2 and H_2O exchange were demonstrated to follow the arrival of an action potential in the leaves. Experiments with dye solution showed that the increase in gas exchange could not be triggered by water ascent. In addition, the use of aphid stylets as "bioelectrodes" showed that sieve tubes served as a pathway for electrical signaling. The membrane potential of the sieve tubes responded rapidly upon watering the dried plants as well as after inducing spontaneous water stress to the roots by polyethylene glycol (Fromm and Fei 1998). Results therefore suggest that electrical root to shoot communication plays an essential role in the co-ordination of processes between roots and leaves, especially via long pathways.

12.7 Role of electrical signaling during fertilization

Strong evidence also exists that electrical signals evoke specific responses of the ovary during the processes of pollination and fertilization. As regards pollination, two different kinds of electric potential changes were measured in the style of flowers. First, Sinyukhin and Britikov (1967) recorded an action potential in the style of *Lilium martagon* and *Incarvillea grandiflora* a few minutes after placing pollen on the stigma lobes. Furthermore, an action potential was detected after mere mechanical irritation of the *Incarvillea* lobe, causing closure of the stigma lobes without further transmission. In both species the pollen-induced action potentials propagated towards the ovary to stimulate the oxygen consumption by 5–11%, 60–90 s after arrival of the action potential. At this moment, most likely post-pollination effects begin, such as the induction of ovary enlargement and wilting of the corolla, which occur long before fertilization. Second, electrical potential changes were measured in the style of *Lilium longiflorum* flowers 5–6 h after pollination (Spanjers 1981). No signals were detectable when applying killed pollen or pollen of other species. In *Hibiscus rosa-sinensis*, different stimuli applied to the stigma of flowers evoke specific electrical signals that propagate toward the ovary at speeds of 1.3–3.5 cm s^{-1} (Fromm et al. 1995). To investigate the first reactions of the ovarian metabolism, various metabolites were analysed 10 min after stimulating the stigma by pollen, wounding or cold-shock. Self- as well as cross-pollination hyperpolarized the resting potential of style cells 50–100 s later, followed by a series of 10–15 action potentials. At 3–5 min after pollination, the ovarian respiration rate increased transiently by 12%, with the levels of ATP, ADP and starch rising significantly (Fromm et al. 1995). By contrast, cold-shock of the stigma caused a single action potential, whereas wounding generated a strong depolarization of the membrane potential with an irregular form and at a lower transmission rate. Either treatment caused a spontaneous decrease in the ovarian respiration rate, as well as reduced metabolite concentrations in the ovary. Since there was no evidence that a chemical substance had been transported within 10 min over a distance of 8–10 cm from the stigma to the ovary, the metabolism must have responded to the electrical signals (Fromm et al. 1995). In the light of these results, the question arises how does an electrical signal cause the biochemical response. Most likely the latter may be achieved through subcellular changes of K^+, Cl^-, and Ca^{2+} ions which are responsible for the generation of action potentials. According to Davies (1987) local changes in ion concentration can lead to modified activities of enzymes in the cell wall, the plasmalemma, and the cytoplasm. This kind of mechanism may also be involved in the fluctuation of the starch level of the ovary after stigma stimulation. The biochemical regulation of starch synthesis is centered almost exclusively on ADP-Glc-pyrophosphorylase (Preiss et al. 1985). The characteristics of this enzyme in ovaries will therefore be analyzed in future to gain

a better understanding of the biochemical role of electrical signaling during fertilization.

12.8 Long-distance electrical signaling in woody plants

In trees in particular, communication over long distances may be achieved through phloem-transmitted electrical signals. Bridging long distances between different organs, these rapid signals possess the ability to coordinate physiological activities. Due to environmental changes, different electrical signals can be evoked in the symplast and transmitted to distant organs, with concomitant specific effects on various physiological processes.

12.8.1 Membrane potential, electrical signals and growth of willow roots

Since willow roots were shown to respond to hormones with propagating action potentials (Fromm and Eschrich 1993), it was an important challenge to measure the magnitude of the current that flows during action potentials. With the use of the vibrating probe technique it was possible to quantify the current, the sensitivity of the probe being in the range of $\mu A\ cm^{-2}$, i.e. sufficiently sensitive to measure ion fluxes of $pmol\ cm^{-2}\ s^{-1}$ (Fromm et al. 1997). Therefore, microelectrode recordings and vibrating probe measurements were used in tandem to correlate changes in membrane potential with changes in endogenous current. Transient depolarizations were elicited in root cortex cells by spermine, while abscisic acid caused a transient hyperpolarization. For the latter we assume that K^+ leaves the cortex cells, similar to the K^+ efflux measured in guard cells (Mansfield et al. 1990). All changes in membrane potential were accompanied by transient responses of the endogenous current. These responses suggested that first anions and then cations leave the root during spermine-induced depolarizations. From the changes in the endogenous current an apparent efflux of anions (presumably Cl^-) and cations (presumably K^+) of 200–700 $pmol\ cm^{-2}$ per signal was calculated (Fromm et al. 1997). Furthermore, it was possible to demonstrate the effect of the growth regulators spermine and abscisic acid on root growth. The mean growth rate of roots increased by up to 30% after application of spermine, while it almost came to a standstill after treatment with abscisic acid.

12.8.2 Electrical properties of wood-producing cells

In the course of the evolutionary process, plants found it necessary to develop wood in order to increase their mechanical strength so as to be able to reach tree heights of 100 m and more. Extensive literature exists that addresses wood anatomy, chemistry and physical properties. However, we have only

just begun to form an understanding of the molecular and electrophysiological mechanisms of cambial activity and wood formation, a field now considered a main research area in tree physiology. One of the main model tree species for basic wood research is poplar. Because of its suitability for genetic transformation and its ease of vegetative propagation, poplar has become the commonly used model tree species in Europe and the United States. To give a description of the electrophysiological processes in wood formation biophysical and molecular techniques have been used to analyze K^+ transporters of poplar. K^+ transporters homologous to those of known function in *Arabidopsis* phloem and xylem physiology were isolated from a poplar wood EST library and the expression profile of three distinct K^+ channel types was analysed by quantitative RT-PCR (Langer et al. 2002). Thus, it was found that the *P. tremula* outward rectifying K^+ channel (PTORK) and the *P. tremula* K^+ channel 2 (PTK2) correlated with the seasonal wood production. Both K^+ channel genes are expressed in young poplar twigs, and while PTK2 was predominantly found in the phloem fraction, PTORK was detected in both phloem and xylem fractions. Following the heterologous expression in *Xenopus* oocytes the biophysical properties of the different channels were determined. PTORK, upon membrane depolarization mediates potassium release, while PTK2 is almost voltage-independent, carrying inward K^+ flux at hyperpolarized potential and K^+ release upon depolarization (Langer et al. 2002). In addition, in-vivo patch-clamp studies were performed on isolated protoplasts from PTORK and PTK2 expressing suspension cultures. Poplar branches were therefore induced to build callus and the resulting meristematic tissues were used to generate suspension cultures. Protoplasts were isolated and the plasma membrane potassium conductances were compared with the electrical properties of *Xenopus* oocytes expressing PTORK and PTK2 individually. Concerning PTORK, it was shown that the properties of this channel are similar in both experimental systems and also to other plant depolarization-activated K^+ release channels (Gaymard et al. 1998; Ache et al. 2000; Langer et al. 2002). In coincidence with the activity of the K^+ channels a plasma membrane H^+-ATPase, generating the necessary H^+ gradient (protonmotive force) for the uptake of K^+ into xylem cells, was localized in the poplar stem using specific antibodies (Arend et al. 2002, 2004). Since potassium is the most abundant cation in plants, playing a central role in many aspects of plant physiology, we conclude that K^+ channels are involved in the regulation of K^+-dependent wood formation. Since seasonal changes in cambial potassium content correlate strongly with the osmotic potential of the cambial zone (Wind et al. 2004), potassium may well play a key role in the regulation of wood formation due to its strong impact on osmoregulation in expanding cambial cells. On the other hand, since PTORK appears in the plasma membrane of sieve elements of the phloem as well as in xylem rays, this channel may play a role in the generation of electrical signals within the poplar phloem and xylem. However, the potential role of xylem ray cells in radial

transmission of electrical signals within the tree stem will have to be proved in the future.

12.8.3 Role of electrical signaling in the regulation of photosynthesis

Most of the work on functions for electrical signals in plants focused on responses evoked by heating and evidence exists of their role in transcription, translation and respiration (Stankovic and Davies 1997; Davies 2004). Recently, evidence was found of a link between electrical signaling and photosynthetic response in *Mimosa* (Koziolek et al. 2004). Flaming of a leaf pinna evoked a variation potential that travels at a speed of 4–8 mm s^{-1} into the neighboring pinna of the leaf to transiently reduce the net CO_2 uptake rate. Simultaneously, the PSII quantum yield of electron transport is reduced. Two-dimensional imaging analysis of the chlorophyll fluorescence signal showed that the yield reduction spreads acropetally through the pinna and via the veins through the leaflets. The results provide evidence of the role of electrical signals in the regulation of photosynthesis because the high speed of the signals rules out the involvement of a slow-moving chemical signal. In addition to the photosynthetic response, it was shown that wounding causes lateral chloroplast movement within 10 min after wounding in *Elodea canadensis* (Gamalei et al. 1994). The time course of chloroplast movement coincides with rapid changes in the membrane potential with low amplitudes (humming, 4–7 mV), recorded by microelectrodes impaled into the midrib of the attached leaf.

With regard to trees, hormone-induced action potentials in the roots were shown to propagate throughout willow plants at velocities of 2–5 cm s^{-1} in order to affect the gas exchange of the leaves (Fromm and Eschrich 1993). To gain a deeper understanding of the role of electrical signaling in the photosynthesis of trees, poplar shoots were stimulated by flaming. In this species, depolarizing signals travel over long distances across the stem from heat-wounded leaves to adjacent leaves where the net CO_2 uptake rate is temporarily depressed towards compensation (Lautner et al. 2005). Surprisingly, signals induced by cold-shock did not affect photosynthesis. In coincidence with the results on *Mimosa,* electrical signaling also significantly reduced the quantum yield of electron transport through PSII in poplar. Cold-blocking of the stem proved that the electrical signal transmission via the phloem becomes disrupted, causing the leaf gas exchange to remain unaffected. Furthermore, calcium-deficient trees showed a marked contrast inasmuch as the amplitude of the electrical signal was distinctly reduced, concomitant with the absence of a significant response in leaf gas exchange upon flame-wounding (Lautner et al. 2005). Further research has to be done on the responsiveness of the various types of molecules that are involved in electron transport as well as on enzymes involved in the uptake of CO_2 during electrical signaling.

12.9 Conclusions

So far, we have seen glimpses of a complex electrical long-distance signaling system in plants and obtained evidence of the role played by electrical signals in the daily processes of plant life. Obviously, plants have developed a simple neural network which responds to a variety of environmental stimuli which may be both, abiotic as well as biotic. Due to the impulses generated by environmental changes action and variation potentials serve as information carriers. The primary step in signal perception may be the opening of plasmalemmal calcium or chloride channels, leading to ion fluxes which generate action or variation potentials. Astounding similarities exist between action potentials in plants and animals. The generation of action potentials in plants follows the all-or-nothing law too (Shiina and Tazawa 1986; Fromm and Spanswick 1993), and plant action potentials also show refractory periods. Furthermore, the use of new methods provides opportunities for detection of fast action potentials which reach speeds up to 40 m s^{-1} (Volkov and Mwesigwa 2000), i.e. similar to the velocities of action potentials in nerves. In higher plants, electrical signals are transmitted from cell to cell via plasmodesmata over short distances, while propagation over long-distances along the plasma membrane of sieve tubes occurs through the successive opening and closure of ion channels (Fig. 12.1). Calcium, chloride and potassium channels are involved in the generation of action potentials and several ion channels postulated to be involved in electrical transmission were identified in the phloem and xylem (Ache et al. 2001; Langer et al. 2002).

Concerning the physiological functions of electrical signals, numerous examples exist. Apart from the role of action and variation potentials in carnivorous plants and *Mimosa*, a concrete relationship between electrical stimulation and the increased production of proteinase inhibitors was found to exist in tomato (Stankovic and Davies 1997). Other work showed that action potentials regulate respiration (Dziubinska et al. 1989), phloem transport (Fromm and Bauer 1994), fertilization (Sinyukhin and Britikov 1967; Fromm et al. 1995) and photosynthesis (Koziolek et al. 2004; Lautner et al. 2005). It is to be expected that future improvements in investigation methods will reveal more aspects of the signaling complexity and its physiological responses that are as yet not fully understood.

References

Ache P, Becker D, Ivashikina N, Dietrich P, Roelfsema MRG, Hedrich R (2000) GORK, a delayed outward rectifier expressed in guard cells of *Arabidopsis thaliana*, is a K^+ selective, K^+ sensing ion channel. FEBS Lett 486:93–98

Ache P, Becker D, Deeken R, Dreyer I, Weber H, Fromm J, Hedrich R (2001) VFK1, a *Vicia faba* K^+ channel involved in phloem unloading. Plant J 27:571–580

Adrian ED, Bronk DW (1928) The discharge of impulses in motor nerve fibres. I. Impulses in single fibres of the phrenic nerve. J Physiol 66:81–101
Arend M, Weisenseel MH, Brummer M, Osswald W, Fromm J (2002) Seasonal changes of plasma membrane H^+-ATPase and endogenous ion current during growth in poplar plants. Plant Physiol 129:1651–1663
Arend M, Monshausen G, Wind C, Weisenseel MH, Fromm J (2004) Effect of potassium deficiency on the plasma membrane H^+-ATPase of the wood ray parenchyma in poplar. Plant Cell Environ 27:1288–1296
Beilby MJ, Coster HGL (1979) The action potential in *Chara corallina*. II. Two activation-inactivation transients in voltage clamps of plasmalemma. Aust J Plant Physiol 6:329–335
Canny MJP (1975) Mass transfer. In: Zimmermann HM, Milburn JA (eds) Encyclopedia of plant physiology. Springer, Berlin Heidelberg New York, pp 139–153
Carpaneto A, Geiger D, Bamberg E, Sauer N, Fromm J, Hedrich R (2005) Phloem-localized, proton-coupled sucrose carrier ZmSUT1 mediates sucrose efflux under control of sucrose gradient and pmf. J Biol Chem 280:21437–21443
Davies E (1987) Action potentials as multifunctional signals in plants: a unifying hypothesis to explain apparently disparate wound responses. Plant Cell Environ 10:623–631
Davies E (2004) New functions for electrical signals in plants. New Phytol 161:607–610
Davies WJ, Zhang J (1991) Root signals and the regulation of growth and development of plants in drying soil. Annu Rev Plant Physiol Plant Mol Biol 42:55–76
Deeken R, Geiger D, Fromm J, Koroleva O, Ache P, Langenfeld-Heyser R, Sauer N, May ST, Hedrich R (2002) Loss of the AKT2/3 potassium channel affects sugar loading into the phloem of *Arabidopsis*. Planta 216:334–344
Dziubinska H, Trebacz K, Zawadzki T (1989) The effect of excitation on the rate of respiration in the liverwort *Conocephalum conicum*. Physiol Plant 75:417–423
Eschrich W, Fromm J, Evert RF (1988) Transmission of electric signals in sieve tubes of zucchini plants. Bot Acta 101:327–331
Evert RF, Eschrich W, Eichhorn SE (1973) P-protein distribution in mature sieve elements of *Cucurbita maxima*. Planta 109:193–210
Findlay GP (1961) Voltage-clamp experiments with *Nitella*. Nature 191:812–814
Findlay GP (1962) Calcium ions and the action potential in *Nitella*. Aust J Biol Sci 15:69–82
Fromm J (1991) Control of phloem unloading by action potentials in *Mimosa*. Physiol Plant 83:529–533
Fromm J, Bauer T (1994) Action potentials in maize sieve tubes change phloem translocation. J Exp Bot 45:463–469
Fromm J, Eschrich W (1988a) Transport processes in stimulated and non-stimulated leaves of *Mimosa pudica*. I. The movement of ^{14}C-labelled photoassimilates. Trees 2:7–17
Fromm J, Eschrich W (1988b) Transport processes in stimulated and non-stimulated leaves of *Mimosa pudica*. II. Energesis and transmission of seismic stimulations. Trees 2:18–24
Fromm J, Eschrich W (1988c) Transport processes in stimulated and non-stimulated leaves of *Mimosa pudica*. III. Displacement of ions during seismonastic leaf movements. Trees 2:65–72
Fromm J, Eschrich W (1989) Correlation of ionic movements with phloem unloading and loading in barley leaves. Plant Physiol Biochem 27:577–585
Fromm J, Eschrich W (1990) Seismonastic movements in *Mimosa*. In: Satter RL, Gorton HL, Vogelmann TC (eds) The pulvinus: motor organ for leaf movement. Am Soc Plant Physiol, Rockville, pp 25–43
Fromm J, Eschrich W (1993) Electric signals released from roots of willow (*Salix viminalis* L.) change transpiration and photosynthesis. J Plant Physiol 141:673–680
Fromm J, Fei H (1998) Electrical signaling and gas exchange in maize plants of drying soil. Plant Sci 132:203–213
Fromm J, Lautner S (2005) Characteristics and functions of phloem-transmitted electrical signals in higher plants. In: Baluska F, Mancuso S, Volkmann D (eds) Communication in plants—neuronal aspects of plant life. Springer, Berlin Heidelberg New York

Fromm J, Spanswick R (1993) Characteristics of action potentials in willow (*Salix viminalis* L.). J Exp Bot 44:1119–1125

Fromm J, Hajirezaei M, Wilke I (1995) The biochemical response of electrical signaling in the reproductive system of *Hibiscus* plants. Plant Physiol 109:375–384

Fromm J, Meyer AJ, Weisenseel MH (1997) Growth, membrane potential and endogenous ion currents of willow (*Salix viminalis*) roots are all affected by abscisic acid and spermine. Physiol Plant 99:529–537

Gaffey CT, Mullins LJ (1958) Ion fluxes during the action potential in *Chara*. J Physiol 144:505–524

Gamalei YV, Fromm J, Krabel D, Eschrich W (1994) Chloroplast movement as response to wounding in *Elodea canadensis*. J Plant Physiol 144:518–524

Gaymard F, Pilot G, Lacombe B, Bouchez D, Bruneau D, Boucherez J, Michaux-Ferriere N, Thibaud JB, Sentenac H (1998) Identification and disruption of a plant shaker-like outward channel involved in K^+ release into the xylem sap. Cell 94:647–655

Gustin MC, Zhou XL, Martinac B, Kung C (1988) A mechanosensitive ion channel in the yeast plasma membrane. Science 242:762–765

Hörmann G (1898) Studien über die Protoplasmaströmung bei den Characaean. Fischer, Jena

Hope AB (1961) Ionic relations of cells of *Chara corallina*. V. The action potential. Aust J Biol Sci 14:312–322

Kempers R, Ammerlaan A, van Bel AJE (1998) Symplasmic constriction and ultrastructural features of the sieve element/companion cell complex in the transport phloem of apoplasmically and symplasmically phloem-loading species. Plant Physiol 116:271–278

Kishimoto U (1968) Response of *Chara* internodes to mechanical stimulation. Ann Rep Biol Works, Fac Sci, Osaka Univ 16:61–66

Koziolek C, Grams TEE, Schreiber U, Matyssek R, Fromm J (2004) Transient knockout of photosynthesis mediated by electrical signals. New Phytol 161:715–722

Langer K, Ache P, Geiger D, Stinzing A, Arend M, Wind C, Regan S, Fromm J, Hedrich R (2002) Poplar potassium transporters capable of controlling K^+ homeostasis and K^+ dependent xylogenesis. Plant J 32:997–1009

Lautner S, Grams TE, Matyssek R, Fromm J (2005) Characteristics of electrical signals in poplar and responses in photosynthesis. Plant Physiol 138:2200–2209

Lunevsky VZ, Zherelova OM, Vostrikov IY, Berestovsky GN (1983) Excitation of Characeae cell membranes as a result of activation of calcium and chloride channels. J Membrane Biol 72:43–58

Mansfield TA, Hetherington AM, Atkinson CJ (1990) Some current aspects of stomatal physiology. Annu Rev Plant Physiol Plant Mol Biol 41:55–75

Martinac B, Buechner M, Delcour AH, Adler J, Kung C (1987) Pressure-sensitive ion channel in *Escherichia coli*. Proc Natl Acad Sci USA 84:2297–2301

Minchin PEH, Thorpe MR (1983) A rate of cooling response in phloem translocation. J Exp Bot 34:529–536

Mühling KH, Sattelmacher B (1997) Determination of apoplastic K^+ in intact leaves by ratio imaging of PBFI fluorescence. J Exp Bot 48:1609–1614

Mummert E, Gradmann D (1976) Voltage dependent potassium fluxes and the significance of action potentials in *Acetabularia*. Biochim Biophys Acta 443:443–450

Oda K (1976) Simultaneous recording of potassium and chloride effluxes during an action potential in *Chara corallina*. Plant Cell Physiol 17:1085–1088

Preiss J, Robinson N, Spilatro S, McNamara K (1985) Starch synthesis and its regulation. In: Heath R, Preiss J (eds) Regulation of carbon partitioning in photosynthetic tissue. Am Soc Plant Physiol, Rockville, pp 1–26

Rhodes J, Thain JF, Wildon DC (1996) The pathway for systemic electrical signal transduction in the wounded tomato plant. Planta 200:50–57

Schurr U, Gollan T (1990) Composition of xylem sap of plants experiencing root water stress: a descriptive study. In: Davies WJ, Jeffcoat B (eds) Importance of root to shoot communication in the response to environmental stress. Br Soc Plant Growth Regul, Bristol, pp 201–214

Shiina T, Tazawa M (1986) Action potential in *Luffa cylindrica* and its effects on elongation growth. Plant Cell Physiol 27:1081–1089
Shvetsova T, Mwesigwa J, Labady A, Kelly S, Thomas D, Lewis K, Volkov AG (2002) Soybean electrophysiology: effects of acid rain. Plant Sci 162:723–731
Sibaoka T (1973) Transmission of action potentials in *Biophytum*. Bot Mag 86:51–61
Simons P (1992) The action plant. Movement and nervous behaviour in plants. Blackwell, Oxford
Sinyukhin AM, Britikov EA (1967) Action potentials in the reproductive system of plants. Nature 215:1278–1280
Spanjers AW (1981) Bioelectric potential changes in the style of *Lilium longiflorum* Thunb. after self- and cross-pollination of the stigma. Planta 153:1–5
Spanswick RM (1972) Electrical coupling between cells of higher plants: a direct demonstration of intercellular communication. Planta 102:215–227
Spanswick RM, Costerton JWF (1967) Plasmodesmata in *Nitella translucens*: structure and electrical resistance. J Cell Sci 2:451–464
Spyropoulos CS, Tasaki I, Hayward G (1961) Fractination of tracer effluxes during action potential. Science 133:2064–2065
Stankovic B, Davies E (1997) Intercellular communication in plants: electrical stimulation of proteinase inhibitor gene expression in tomato. Planta 202:402–406
Szmelcman S, Adler J (1976) Change in membrane potential during bacterial chemotaxis. Proc Natl Acad Sci USA 73:4387–4391
Tazawa M, Shimmen T, Mimura T (1987) Membrane control in the Characeae. Annu Rev Plant Physiol 38:95–117
Van Bel AJE (1993) The transport phloem. Specifics of its functioning. Prog Bot 54:134–150
Van Bel AJE, Ehlers K (2005) Electrical signalling via plasmodesmata. In: Oparka KJ (ed) Plasmodesmata. Blackwell, Oxford
Van Bel AJE, van Rijen HVM (1994) Microelectrode-recorded development of symplasmic autonomy of the sieve element/companion cell complex in the stem phloem of *Lupinus luteus*. Planta 192:165–175
Van Sambeek JW, Pickard BG (1976) Mediation of rapid electrical, metabolic, transpirational and photosynthetic changes by factors released from wounds. I. Variation potentials and putative action potentials in intact plants. Can J Bot 54:2642–2650
Volk G, Franceschi VR (2000) Localization of a calcium-channel-like protein in the sieve element plasma membrane. Aust J Plant Physiol 27:779–786
Volkov AG, Mwesigwa J (2000) Interfacial electrical phenomena in green plants: action potentials. In: Volkov AG (ed) Liquid interfaces in chemical, biological, and pharmaceutical applications. Dekker, New York, pp 649–681
Volkov AG, Collins DJ, Mwesigwa J (2000) Plant electrophysiology: pentachlorophenol induces fast action potentials in soybean. Plant Sci 153:185–190
Volkov AG, Dunkley TC, Morgan SA, Ruff D II, Boyce YL, Labady AJ (2004) Bioelectrochemical signaling in green plants induced by photosensory systems. Bioelectrochem 63:91–94
Wildon DC, Thain JF, Minchin PEH, Gubb IR, Reilly AJ, Skipper YD, Doherty HM, Odonnell PJ, Bowles DJ (1992) Electrical signaling and systemic proteinase-inhibitor induction in the wounded plant. Nature 360:62–65
Wind C, Arend M, Fromm J (2004) Potassium-dependent cambial growth in poplar. Plant Biol 6:30–37
Woodley SJ, Fensom DS, Thompson RG (1976) Biopotentials along the stem of *Helianthus* in association with short-term translocation of ^{14}C and chilling. Can J Bot 54:1246–1256
Wright JP, Fisher DB (1981) Measurement of the sieve tube membrane potential. Plant Physiol 67:845–848
Zawadzki T, Davies E, Dziubinska H, Trebacz K (1991) Characteristics of action potentials in *Helianthus annuus*. Physiol Plant 83:601–604

13 Potassium Homeostasis in Salinized Plant Tissues

Tracey A. Cuin, Sergey Shabala

13.1 Introduction

Potassium is an essential cation, comprising ~6% of a plant's dry weight and is involved in numerous functions such as osmo- and turgor regulation, charge balance, and control of stomata and organ movement. K^+ activates over 50 enzymes critical for numerous metabolic processes, including photosynthesis, oxidative metabolism and protein synthesis (Marschner 1995). Within the cytosol, K^+ neutralizes the soluble and insoluble macromolecular anions and stabilizes the pH at the level optimal for most enzymatic reactions (pH ~7.2). Thus, cytosolic K^+ homeostasis is crucial to optimal cell metabolism.

In contrast to K^+, Na^+ is not essential for plants (Marschner 1995). For the majority of crop species, Na^+ is toxic at mM concentrations in the cytosol. With cytosolic K^+ concentrations being around 150 mM (Leigh and Wyn Jones 1984; Leigh 2001) and cytosolic Na^+ in a lower mM range (Carden et al. 2003), the cytosolic K^+/Na^+ ratio is high, enabling many K^+-dependent metabolic processes to proceed (Rubio et al. 1995; Maathuis and Amtmann 1999). Under saline conditions, cytosolic Na^+ levels increase dramatically, estimates varying from 10 to 30 mM, up to 200 mM (Koyro and Stelzer 1988; Flowers and Hajibagheri 2001; Carden et al. 2003). At the same time, cytosolic K^+ content decreases dramatically. An almost 2-fold decrease in cytosolic K^+ activity was measured in salinized roots of barley (Carden et al. 2003), and cytosolic K^+ activity as low as 15 mM in epidermal leaf cells has been reported (Cuin et al. 2003). Thus the cytosolic K^+/Na^+ ratio falls dramatically under saline conditions, severely impairing cell metabolism (Maathuis and Amtmann 1999; Flowers and Hajibagheri 2001; Munns 2002). Not surprising, the ability to maintain a high cytosolic K^+/Na^+ ratio has often been cited as a key feature in plant salt tolerance (Gorham et al. 1990; Maathuis and Amtmann 1999; Tester and Davenport 2003; Chen et al. 2005).

Within the vacuole, K^+ mediates osmoregulation, and within specialized cells, stomatal movements and tropisms. Here the K^+ concentration is much more flexible and can be more readily replaced by other cations, including

School of Agricultural Science, University of Tasmania, Private Bag 54, Hobart, Tas 7001, Australia (e-mail: Sergey.Shabala@utas.edu.au)

Plant Electrophysiology – Theory & Methods (ed. by Volkov)

Na^+ (Leigh et al. 1986). However, the vacuolar PP-ase is critically dependent on K^+ for both hydrolytic activity and H^+ pumping (White et al. 1990). Thus, even in this organelle, maintenance of a minimal level of K^+ is vitally important for optimal plant performance. How is this achieved?

Molecular and ionic mechanisms of K^+ transport have been the subject of a large number of comprehensive reviews in recent years (Maathuis and Amtmann 1999; Maathuis and Sanders 1999; Tyerman and Skerrett 1999; Schachtman 2000; Mäser et al. 2001; Véry and Sentenac 2002, 2003; Shabala 2003) so are only briefly revised in our review. Many important questions, however, remain to be answered. It is not clear how the levels and ratios of K^+ to Na^+ are maintained within the plant, and why these ratios are different in cells within various plant tissues. It is also remains to be answered how plants distinguish between K^+ and Na^+, both at the root and cellular levels. This latter problem is not trivial, due to the similarity in ionic radius and ion hydration energies for K^+ and Na^+ (Hille 1992), factors which determine both the ion transport mode and the competition for enzyme binding sites within the cytosol. Despite a recent plethora of research (Apse et al. 1999, 2003; Hasegawa et al. 2000; Zhu 2000, 2003; Zhang and Blumwald 2001), we are still lacking full knowledge of the signal-transduction pathways involved in K^+ homeostasis and maintenance of the critical K^+/Na^+ ratios under salt stressed conditions.

This review addresses some of the above issues and summarizes molecular and electrophysiological evidence regarding mechanisms regulating K^+ homeostasis in salinized plant tissues. The main emphasis is made on the integration of K^+ transport mechanisms at various levels of plant structural organization.

13.2 Potassium acquisition and distribution in plants

Potassium enters the root symplast via the cell plasma membrane (PM). From there, it can travel through the symplast to the vascular tissues, where it is unloaded from the xylem parenchyma into xylem vessels for long-distance transport to leaves. K^+ is reabsorbed from the xylem into leaf cells. Being a highly mobile element (Marschner 1995), it can be easily loaded into the phloem for translocation to actively growing sink tissues (e.g. shoot and root apices) where it can be unloaded by way of symplasmic or apoplastic pathways. K^+ can also cross the tonoplast membrane for storage in vacuoles of both root and shoot cells. The integration and regulation of K^+ transport systems at different sites along the long-distance pathway allows the plant to direct the partitioning and circulation of K^+. Such an integrated system plays a central role in plant growth and development and in the allocation of mineral nutrients in response to changes in nutrient availability. This section

very briefly summarizes uptake and compartmentation of K^+ within a plant, at a physiological level.

13.2.1 Uptake at the root level

Net K^+ uptake at the root PM is classically viewed as the result of the operation of both active and passive transporters with different affinities for K^+ (systems *I* and *II*; Epstein et al. 1963). While the high-affinity K^+ uptake system *I* is strongly selective for K^+ over other alkali cations and shows increased gene expression or transport activity under K^+ starvation conditions, the low-affinity K^+ transport system *II* is less selective for K^+ over Na^+ and less influenced by changes in the K^+ status of the plant (Marschner 1995). Patch-clamp studies suggest that system *I* is an active transport mechanism (Maathuis and Sanders 1993), most likely via a K^+/H^+ symporter (Maathuis and Sanders 1994). The inward-rectifying K^+-selective (KIR) channels mediate uptake within the concentration range of system *II* (above 1 mM). These channels have been found in root cells of various species (White and Tester 1992; Gassmann and Schroeder 1994; Maathuis and Sanders 1995; Roberts and Tester 1995) and can mediate long-term K^+ influx into the cell (Schroeder et al. 1994; Schachtman et al. 1992; Gaymard et al. 1996). KIR channels are also found in root hairs (Gassmann and Schroeder 1994), suggesting their important role in K^+ acquisition beyond the root depletion zone.

13.2.2 Xylem loading

Once inside the root, K^+ is transported to the vascular tissues where it is unloaded from xylem parenchyma into xylem vessels for long-distance transport to leaves. Patch-clamp studies have demonstrated the presence of both anion and cation channels likely to be responsible for loading of solutes into the xylem for transport to the shoot (Maathuis et al. 1998; Köhler and Raschke 2000). The PM of cortical cells is dominated by a K^+ channel that favors K^+ influx into the cells, and thus uptake into the root, whereas the stelar cells are dominated by a K^+ channel favoring K^+ efflux into the apoplast, resulting in xylem loading (Roberts and Tester 1995). However, such clear-cut differences in channel activities are not seen in *Arabidopsis* cortical and stellar tissues (Maathuis et al. 1998). Some authors have argued against the role of outward K^+ channels in xylem sap K^+ loading (de Boer 1999), suggesting instead that K^+ secretion into the xylem occurs against the K^+ electrochemical gradient in a process mediated by active transport systems (Kochian and Lucas 1988; Moshelion et al. 2002). More likely, both types of K^+ transporters are involved. Experiments on SKOR, the *Arabidopsis* outward-rectifying Shaker channel, estimated that its activity contribute to about 50% of K^+ translocated towards

the shoot (Gaymard et al. 1998; Lacombe et al. 2000). The remainder might be attributed to some active transport system.

13.2.3 Potassium compartmentation at the tissue and whole-plant levels

Under normal growth conditions, K^+ is the most abundant cation in both the cytosol and the vacuole. The concentration to which K^+ accumulates is, however, different in root and leaf cells. K^+ activities in the leaf cell vacuoles were approximately 230 mM (Cuin et al. 2003) compared with 120 mM in the root cell vacuoles (Walker et al. 1996), while the cytosolic K^+ activities in root and leaf cells were comparable (Walker et al. 1996; Cuin et al. 2003).

There is also a certain degree of heterogeneity between the vacuolar (but not cytosolic) K^+ content of different cell types in leaves under K^+-replete conditions (Cuin et al. 2003). Barley K^+ concentrations were only slightly lower in the mesophyll cells than the epidermal cells (Fricke et al. 1994; Cuin et al. 2003). Slight differences in vacuolar K^+ content between abaxial and adaxial epidermal cells were reported in *Lupinus* (Treeby and van Steveninck 1988) and *Sorghum* (Boursier and Läuchli 1989). However, the substantial heterogeneity in K^+ concentration between different cell types only became pronounced under K^+-limiting conditions, where concentrations were maintained in the mesophyll cells, but decreased in the epidermal cells (Fricke et al. 1994). Salinity is one such condition.

13.2.4 Intracellular K^+ compartmentation

The cytoplasmic K^+ level is strictly controlled (80–100 mM activity; Maathuis and Sanders 1994; Walker et al. 1996; Cuin et al. 2003), a homeostasis that is achieved by both the control of K^+ influx across the PM and by mobilizing K^+ from vacuolar reserves (Glass and Fernando 1992; Walker et al. 1996). Vacuolar K^+ content is not so strictly regulated and shows large fluctuations depending on K^+ supply (Leigh and Wyn Jones 1984; Walker et al. 1996). Under K^+-replete conditions, vacuolar K^+ is typically around 200–250 mM reaching 500 mM in open stomatal guard cells (MacRobbie 1998) but decreasing to 10 mM under K^+-deficient conditions (Walker et al. 1996). As the major role of K^+ in the vacuoles is in maintenance of cell turgor (required for cell extension and stomata opening), the osmotic functions of K^+ in the vacuole may replaceable to a varying degree by other cations (such as Na^+, Mg^{2+} and Ca^{2+}) or organic solutes (e.g. sugars). The concentration of K^+ in the apoplast is usually low (between 2 and 20 mM; Karley et al. 2000; Roelfsema and Hedrich 2002) with the exception of specialized cells or tissues such as stomata and pulvini, where it may transiently rise to 100 mM (Roelfsema and Hedrich 2002).

Potassium content is also high in chloroplasts, with 50–100 mM concentration range reported (Demmig and Gimmler 1983; Pier and Berkowitz 1987). In

addition to being an important stromal enzyme involved in leaf photochemistry, K^+ also plays a key role in charge balancing the massive light-driven transport of H^+ into the thylakoid lumen required for ATP synthesis (Pottosin and Schönknecht 1996). The extent to which intact chloroplasts are able to maintain a constant K^+ concentration, independently of changes in the external medium, is unknown. Also limited is our knowledge of K^+ transporters in this organelle. In addition to several types of cation-permeable channels (reviewed by Shabala 2003), there are also suggestions that various secondary active transport systems are present at the chloroplast envelope (Demming and Gimmler 1983; Wu and Berkowitz 1992). Recently, an apparently neutral $K^+(Na^+)/H^+$ antiporter has been characterized in the envelope membranes of *Arabidopsis* chloroplasts (Song et al. 2004). This exchanger was suggested to be located in the chloroplast envelope and is thought to function in the adjustment of pH in the cytosol thereby maintaining a high pH level in the chloroplast stroma. Much still remains to be described about K^+ homeostasis within this vitally important organelle.

13.2.5 Remobilization and recycling

After delivery to the leaf tissue, K^+ can be loaded into phloem cells for translocation to actively growing sink tissues (e.g. shoot and root apices), where it can be unloaded by way of symplasmic or apoplastic pathways.

Classical electrophysiological analysis shows that uptake by roots is tuned in response to shoot demand and K^+ recirculation via the phloem sap from shoots to roots is involved in this control. In this scheme, the rate of K^+ unloading from the root stele would act as a signal that would regulate, via as yet unidentified negative feedback mechanisms, K^+ uptake activity in root periphery cells (Kochian and Lucas 1988). This hypothesis has been supported by kinetic studies with rye (White 1997), and is likely to be significant in maintaining K^+ homeostasis, although the specific details on the underlying ionic mechanisms remain to be determined.

13.3 Ionic mechanisms of K^+ acquisition and transport in plants

13.3.1 General features of K^+ transporters in plants

Since the classical work of Epstein and coworkers (1963), many advanced electrophysiological and molecular techniques have become available, allowing considerable progress in the analysis of K^+ transport in plants at both the molecular and physiological level.

The recent completion of the *Arabidopsis* genome sequence has offered the opportunity to make an inventory of all the putative plant transporter

proteins (Ward 2001). A genome wide survey revealed seven major families of *Arabidopsis* cation transporters (75 genes in total) which mediate K^+ transport across plant membranes. These include (Mäser et al. 2001; Véry and Sentenac 2002, 2003; Shabala 2003): (i) Shaker-type K^+ channels (nine genes); (ii) two-pore K^+ channels (six genes); (iii) cyclic-nucleotide-gate channels (20 genes); (iv) putative K^+/H^+ antiporters (six genes); (v) KUP/HAK/KT transporters (13 genes); (vi) HKT transporters (one gene); (vii) glutamate receptors (20 genes). In addition, a low-affinity K^+-permeable transporter (LCT1) has been identified in wheat (Schachtman et al. 1997).

13.3.2 Basic features and control modes of potassium transporters

13.3.2.1 Shaker family of potassium channels

The Shaker family of K^+ channels comprises nine members in *Arabidopsis* (Mäser et al. 2001). They are related to animal K^+ channels initially cloned from *Drosophila* (thus, "Shakers"). Members of this family have also been identified in a number of other plant species (Véry and Sentenac 2003). Comparison of the functional properties of these channels in heterologous expression systems with channel activity recorded in planta suggests that they are active at the PM and mediate most K^+-selective voltage-gated currents that dominate the membrane K^+ conductance at hyper- and depolarized membrane potential (E_m) (Véry and Sentenac 2002). These channels are present in numerous cell types and operate at mM K^+ concentrations. They represent the best-characterized family of plant transporters at the molecular level.

Plant Shaker polypeptides typically display a short (about 60 amino acid) intracytoplasmic N-terminal domain, followed by a hydrophobic core composed of six transmembrane segments (S1–S6), the pore domain being inserted between S5 and S6, and a long intracytoplasmic region representing more than half the sequence (Véry and Sentenac 2003). The transmembrane segment 4 harbors positively charged amino acids and is expected to act as a voltage sensor. A highly conserved pore domain, carrying the hallmark GYGD/E motif of highly K^+ selective channels, is present between S5 and S6. The long C-terminal region harbors a putative cyclic nucleotide-binding domain and, in most Shaker channels, an ankyrin domain potentially involved in protein-protein interactions (Véry and Sentenac 2003).

Most plant Shaker-type K^+ channels identified so far have been successfully expressed and characterized in heterologous systems. Based on their voltage dependency, these channels can be grouped into three functional subfamilies: (i) inward, (ii) weakly-inward, and (iii) outward-rectifying (Véry and Sentenac 2003). Inward-rectifying channels are activated by membrane hyperpolarization from a threshold more negative than the K^+ equilibrium potential (E_k), and are mainly involved in K^+ uptake. Weak inward-rectifiers also are activated by membrane hyperpolarization, but

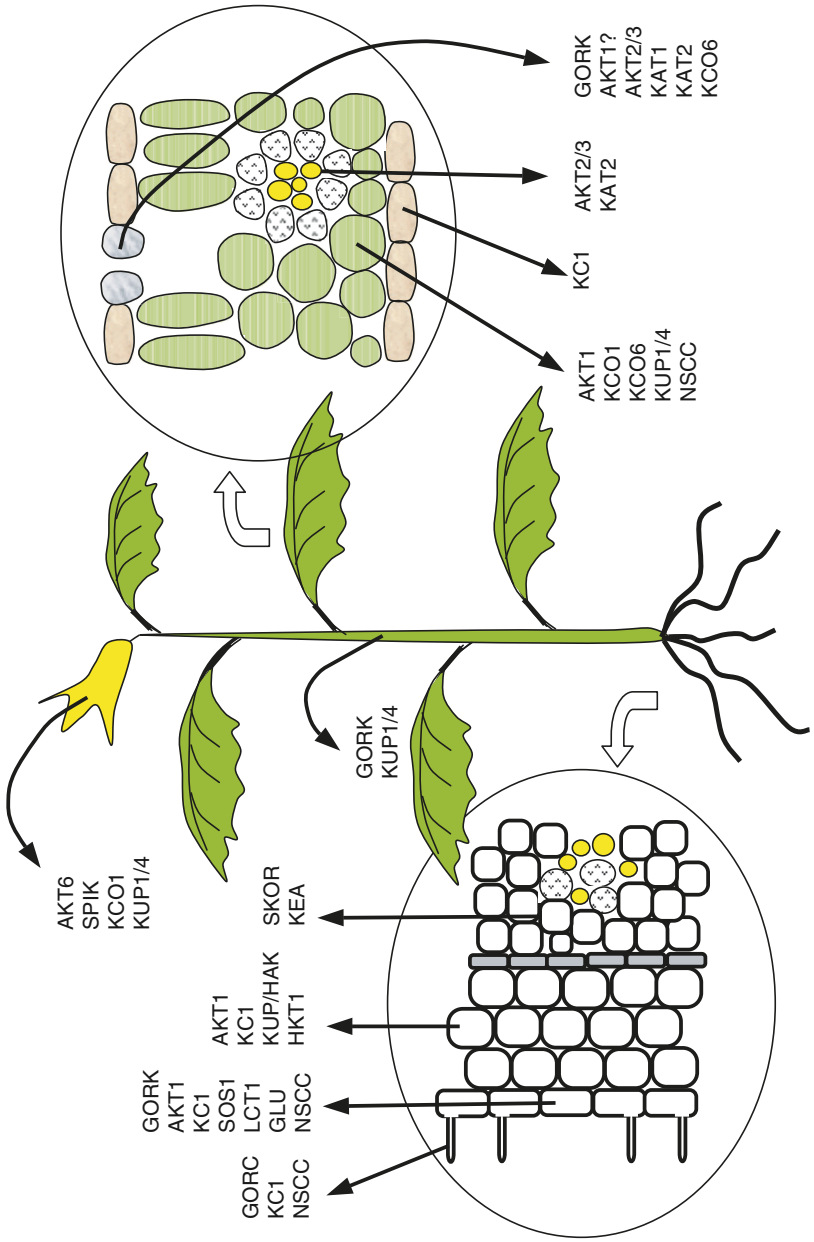

Fig. 13.1. Tissue-specific expression of K^+ transporters in plants. Most of the data comes from experiments with *Arabidopsis*, although results from other plant species are also included. With the exception of KCO channels, all other transporters shown are likely to be expressed at cell PM

never display null open probabilities within a physiological E_m range and are potentially able to mediate both K^+ uptake and release. Outward-rectifying channels activate at E_m more positive than E_k and are specialized in K^+ release (Véry and Sentenac 2003).

Physiological roles and functional expression of the channels from the Shaker family are diverse. AKT1 is a hyperpolarization-activated K^+ channel (Bertl et al. 1994) that is expressed in the roots (Lagarde et al. 1996) and plays a role in K^+ uptake, provided that the external K^+ concentration is in the mM range and the E_m is negative enough (Hirsch et al. 1998). SKOR is expressed in stelar tissue of the root and is thought to be involved in K^+ release into the xylem sap (Gaymard et al. 1998). KAT1 takes part in guard cell K^+ uptake, but is not essential for stomatal opening (Szyroki et al. 2001), probably because of inward-rectifier redundancy in guard cells (Pilot et al. 2001). SPIK is involved in K^+ uptake in pollen and is required for optimal pollen tube development and pollen competitive ability (Mouline et al. 2002). The roles of the other five Shakers are less well understood. Current data support the hypothesis that AKT2/3 is involved in long-distance K^+ transport via the phloem sap (Deeken et al. 2000; Lacombe et al. 2000). This channel has also been shown to be an important contributor, along with AKT1, to the mesophyll K^+ permeability (Dennison et al. 2001). Like KAT1, KAT2 is thought to play a role in K^+ influx into guard cells during stomatal opening (Pilot et al. 2001) and GORK to mediate K^+ release from these cells during stomatal closure (Ache et al. 2001; Hosy et al. 2003). GORK is also expressed in root hairs, where it could play a role in osmoregulation (Ivashikina et al. 2001). AtKC1 is expressed in root periphery cells (Ivashikina et al. 2001; Pilot et al. 2003) where it would be an integral component of functional K^+ uptake channels (Reintanz et al. 2002). Only localization data have been obtained for the remaining *Arabidopsis* Shaker channel, AKT6 (Lacombe et al. 2000), revealing expression in flowers.

13.3.2.2 "Two-pore" potassium channels

Two-pore K^+ channels display a hydrophobic core composed of either 4 TMS and 2 P domains (KCO-2P family) or 2 TMS and 1 P domain (KCO-1P family); none of the TMS acts as a voltage sensor. Their pore domains bear a high K^+ permeability hallmark motif. The channels have putative Ca^{2+}-binding sites in their cytosolic C-terminal region (Czempinski et al. 1999; Moshelion et al. 2002) and share some structural homologies with 4TMS-2P (leak-like) and 2TMS-1P (inward-rectifying) animal K^+ channels, respectively (Doupnik et al. 1995).

In *Arabidopsis*, the KCO-2P family has five members and the KCO-1P family, a single member (Czempinski et al. 2002). Only *KCO1* has been characterized, where it was shown to encode a K^+ selective outward-rectifying channel activated by cytosolic Ca^{2+} (Czempinski et al. 1999). KCO1 can also

be functionally distinguished from outward-rectifying Shaker channels by faster and non-sigmoidal kinetics of current activation and a higher single channel conductance. KCO1 is expressed throughout the plant (Czempinski et al. 2002). At the subcellular level, it has been localized at the tonoplast (Czempinski et al. 2002).

13.3.2.3 Cyclic nucleotide-gated (CNG) channels

Twenty members of CNG family were found in *Arabidopsis* (Köhler et al. 1999; Mäser et al. 2001), with CNG channel homologs identified in barley (Schuurink et al. 1998) and tobacco (Arazi et al. 1999). They share structural homologies with the animal cyclic nucleotide-gated channels (CNGCs) first identified in sensory cells. CNGCs are related to the Shaker family, but without the high K^+ selectivity hallmark motif in their P domains. As a result, they readily conduct both mono- and divalent cations (Véry and Sentenac 2002) and do not distinguish well between Na^+ and K^+ (Gamel and Torre 2000). Similar to their animal counterparts, CNG channels are gated by intracellular cGMP or cAMP (Maathuis and Sanders 2001), Ca^{2+} and calmodulin (Mäser et al. 2001; Véry and Sentenac 2002). Their physiological role is likely to be in cell signaling (Demidchik et al. 2002; Véry and Sentenac 2002).

13.3.2.4 K^+/H^+ antiporters

A family of cation/H^+ antiporters (CPA), comprising six putative K^+/H^+ antiporters, has been identified in *Arabidopsis* (Mäser et al. 2001). The latter systems (called KEA for *K*$^+$ *e*fflux *a*ntiporter) show substantial sequence similarities (up to 35% identity) with bacterial Ker (K^+ efflux) antiporters regulated by glutathione (Yao et al. 1997). Their tissue and subcellular localizations are unknown. Due to poor ion selectivity, other members of CPA family might also exchange H^+ for K^+, in addition to other ions. For instance, the AtNHX1 tonoplast located Na^+/H^+ exchanger (Apse et al. 1999) was shown to transport Na^+ and K^+ with equal affinity in reconstituted liposomes (Venema et al. 2002). Plant K^+/H^+ exchange activity is expected, at least at the tonoplast, to be an important mechanism in K^+ loading into the vacuole. AtNHX1 might be involved in osmoregulation and Na^+ detoxification of the cytoplasm, as well as in cytosolic pH regulation (Venema et al. 2002). It has also been suggested that K^+/H^+ exchangers might be at work at the PM, contributing to active K^+ secretion in the xylem sap (Kochian and Lucas 1988).

13.3.2.5 KUP/HAK/KT transporters

This is a class of transporters which are homologous to the H^+-K^+ symporters first identified in *E. coli* (Schleyer and Bakker 1993) and *S. occidentalis* (Bañuelos et al. 1995). The plant homologues, called KUP (Fu and Luan 1998;

Kim et al. 1998), HAK (Santa-María et al. 1997; Rubio et al. 2000), or KT (Quintero and Blatt 1997), form a large family, with 13 members in *Arabidopsis* (Mäser et al. 2002) and at least 17 members in rice (Bañuelos et al. 2002). Little is known about the structure of these transporters. Hydrophobicity profiles suggest that they might possess 12 TMS and a long cytosolic loop between the second and third TMS (Kim et al. 1998; Rubio et al. 2000; Bañuelos et al. 2002).

Four groups of plant KUP/HAK/KT transporters can be distinguished on a phylogenetic tree (Rubio et al. 2000; Bañuelos et al. 2002); two of these have been characterized at the functional level (Rodríguez-Navarro 2000). While some transporters in group *I* are classified as high-affinity K^+ transporters, all members from group *II* operate in the low-affinity (mM) range. These are active transport systems, with poor discrimination between K^+, Rb^+ and Cs^+ (Rubio et al. 2000; Bañuelos et al. 2002) but reduced permeability to Na^+ and NH_4^+ (Fu and Luan 1998; Santa-María et al. 2000; Bañuelos et al. 2002). Their activity is inhibited by elevated Na^+ levels (Quintero and Blatt 1997; Kim et al. 1998) and alkaline pH (Garciadeblás et al. 2002), suggesting H^+-K^+ stoichiometry. These systems can mediate both influx and efflux of K^+ (Bañuelos et al. 2002; Garciadeblás et al. 2002).

Although both high- and low-affinity KUP/HAK/KT transporters are expressed in various plant organs/tissues, their subcellular localization is largely unknown. At least one of 17 members of OsHAK family in rice was targeted to the tonoplast (Bañuelos et al. 2002), while others were more likely to be located at the PM. Most of these transporters are expressed in roots (Santa-María et al. 1997; Kim et al. 1998; Rubio et al. 2000; Rigas et al. 2001) and are believed to mediate high-affinity K^+ uptake through the PM.

13.3.2.6 HKT transporters

Plant HKT transporters are related to the fungal Trk transporters and prokaryote KtrB and TrkH K^+ transporter subunits (Rodríguez-Navarro 2000). Sequence analysis suggests that these transporters evolved from bacterial 2TMS K^+ channels. They display a core structure with eight TMS and four P-forming domains, four repeats of 1TMS-1P-1TMS, with the four P loops lining a central P, and C-terminal cytosolic region (Durell et al. 1999; Kato et al. 2001).

Although HKT homologues have been isolated or detected in many species, including *Arabidopsis*, eucalyptus, rice, ice plant (*Mesembryanthemum crystallinum*) and poplar (Fairbairn et al. 2000; Uozumi et al. 2000; Horie et al. 2001), they do not constitute multigene families. There is only one member of this group in *Arabidopsis* (AtHKT1; Uozumi et al. 2000) and in diploid wheat (HKT1; Schachtman and Schroeder 1994). Eucalyptus and rice each have two HKT paralogs (Fairbairn et al. 2000; Horie et al. 2001). The only exception is japonica rice in which the genome shows the presence of up to nine OsHKT genes (Garciadeblás et al. 2003). All HKT transporters identified so far are expressed predominantly in roots.

Available information suggests that HKT homologues may operate in two transport modes. One has only a limited ability to transport K^+, while in the other mode, HKT transporters transport K^+ as readily as Na^+. For example, K^+ uptake was not observed when the *Arabidopsis* homolog AtHKT1 was expressed in either yeast or *Xenopus* oocytes, although high Na^+ uptake activity was detected (Uozumi et al. 2000). Wheat, TaHKT1 operates as a high affinity Na^+-K^+ symporter in the presence of low K^+ and Na^+ concentrations, and as a low-affinity Na^+-Na^+ (co)-transporter when the Na^+/K^+ ratio in the external solution is high (Rubio et al. 1995; Gassmann et al. 1996). In eucalyptus, two HKT1 homologs (EcHKT1 and EcHKT2) both show K^+ and Na^+ currents when expressed in *Xenopus* oocytes (Fairbairn et al. 2000). Experiments on rice suggested that the OsHKT1 isoform operated as a Na^+ transporter, while OsHKT2 displayed K^+-Na^+ symport activity (Horie et al. 2001).

Wheat HKT1 is expressed in the root cortex (Schachtman and Schroeder 1994) where it functions as a low-affinity Na^+ transport under low K^+:Na^+ ratios. K^+ starvation induces HKT1 expression in wheat and barley (Wang et al. 1998) as well as inward Na^+ currents in wheat root cortical cells (Buschmann et al. 2000). HKT1 plays a role in net Na^+ accumulation (Uozumi et al. 2000; Laurie et al. 2002; Mäser et al. 2002) and its decreased expression under salt stress often correlates with plant salt tolerance (Golldack et al. 1997). Direct evidence for the involvement of AtHKT1 in Na^+ uptake and salt sensitivity in *Arabidopsis* has emerged from a screen for suppressor mutations of the *Arabidopsis sos3* mutant (Liu and Zhu 1998). Disruption of AtHKT1 suppressed the *sodium-overly-sensitive* (*sos*) phenotype (Rus et al. 2001) and *sos3/athkt1* double mutant seedlings took up less Na^+ than either *sos3* or wild type (WT) plants (Rus et al. 2001). Not surprisingly, HKT1 has been proposed to be a determinant of salt sensitivity in plants (Rubio et al. 1995).

13.3.2.7 LCT1

LCT1 is low-affinity transporter found only in wheat. It is capable of mediating uptake of a wide range of monovalent cations, including K^+ and Na^+ (Schachtman et al. 1997; Amtmann et al. 2001) and is expressed in both roots and leaves (Schachtman et al. 1997). Expression of LCT1 in yeast caused Na^+ hypersensitivity (Amtmann et al. 2001), and LCT1 mediated Na^+ transport was inhibited by Ca^{2+} (Schachtman et al. 1997; Amtmann et al. 2001). LCT1 has no counterpart in *Arabidopsis* and shares no sequence homology with any other gene. Nonselective cation conductances have been described in vivo in wheat roots. The hypothesis of a role for LCT1 in this activity would, however, be highly speculative because poorly selective cation conductances have also been described in many species, including *Arabidopsis* (Demidchik et al. 2002).

13.3.2.8 Glutamate receptors

A family of polypeptides related to animal ionotropic glutamate receptors has been found in plants (Lam et al. 1998), with 20 members in *Arabidopsis* (Lacombe et al. 2001). Although the P domains of plant and animal receptors are quite distant, plant glutamate receptors might, like their animal counterparts, form cation channels permeable to K^+, Na^+ and/or Ca^{2+} (Lam et al. 1998; Nakanishi et al. 1990). Plant glutamate receptors are usually expressed in roots (Chiu et al. 2002). Their physiological role in plants remains unknown.

13.3.2.9 Other transport systems

Non-selective cation channels. Non-selective cation channels (NSCC) are a large, heterogeneous group of channels. In addition to CNG channels and glutamate receptors, the group also includes a large number of other channels which show high selectivity for cations over anions, but low selectivity among monovalent cations under a wide range of ionic conditions (Demidchik et al. 2002) and usually have similar permeability to a wide range of monovalent cations. They show K^+:Na^+ selectivity ratios typically between 0.3 and 3, and make a key contribution to the uptake of Na^+ by plant cells (Tyerman et al. 1997; Demidchik et al. 2002; Tester and Davenport 2003). NSCC channels have been found at the PM, tonoplast and other endomembranes. Numerous methods of activation of these channels have been reported, and they are thought to function in low-affinity nutrient uptake (see Demidchik et al. 2002 for review). They are gated by diverse mechanisms including voltage, cyclic nucleotides, glutamate, reactive oxygen species and stretch.

CCC family. A few putative members of the cation chloride cotransporter family (CCC) have been found in plants (Véry and Sentenac 2003). In animal cells, the CCC family comprises K^+-Cl^-, Na^+-Cl^- and Na^+-K^+-$2Cl^-$ cotransporters (Gamba et al. 1993; Gillen et al. 1996; Isenring and Forbush 1997). Members of this family have important roles in cellular ionic and osmotic homeostasis in animal cells.

13.4 Specificity of salinity effect on K^+ homeostasis in plant tissues

13.4.1 K^+/Na^+ competition for uptake—channels and symporters

As Na^+ is not an essential element, it is no surprise that as yet, no specific Na^+-selective channels have been identified in higher plants. Due to their similar physicochemical structures, excessive Na^+ in the soil solution competes with binding sites in transport systems that mediate K^+ uptake resulting in K^+

deficiency (Niu et al. 1995; Hasegawa et al. 2000). The ionic mechanisms of pathways of Na^+ uptake into plant cells have been a subject of extensive electrophysiological studies (Maathuis and Sanders 1993, 1995; Gassmann and Schroeder 1994; Amtmann et al. 1997, 1999; Tyerman et al. 1997; Buschmann et al. 2000; Davenport and Tester 2000; Demidchik and Tester 2002). However, the task of attributing known ion currents to corresponding transporter genes appears to be particularly difficult for Na^+, since it is likely that several transporters contribute to Na^+.

Candidate genes for root Na^+ uptake are found in several K^+ transporter families. The high-affinity K^+ transporter (HKT1), low affinity cation transporter (LCT1) and nonselective cation channels (NSCCs) are the most likely specific transport systems that mediate Na^+ influx (Schachtman and Schroeder 1994; Schachtman et al. 1997; Amtmann and Sanders 1999; Davenport and Tester 2000; Amtmann et al. 2001). Genome wide analyses indicate that additional classes of Na^+ transporters are likely to exist and characterization of further complexities and interesting functions of Na^+ are on the horizon.

13.4.1.1 Inward-rectifying channels from the Shaker family

Under saline conditions, Na^+ would passively diffuse into the cell cytoplasm through Na^+-permeable PM channels. However, most inward-rectifying K^+ (KIR) channels from the Shaker family appear to be highly selective for K^+ over Na^+ (Amtmann and Sanders 1999) thus are unlikely to mediate significant net Na^+ influx into plant cells.

Despite this, there are reports in the literature of an adverse affect of Na^+ on the functioning of KIRs (e.g. AKT1). Sodium may have a direct effect on the AKT channel protein, an interaction that reduces the open probability or conductance of the channel (Qi and Spalding 2004). Alternatively, Na^+ impairs the activity of a positive regulator of AKT1 or interferes with the delivery of AKT1 channels to the membrane. Thus, KIRs functioning may be impaired by excessive Na^+, but it is not likely that these channels play any substantial role in Na^+ transport into the cell.

13.4.1.2 KUP/HAK/KT transporters

The KUP/HAK/KT family of K^+ transporters might mediate some low-affinity Na^+ influx at high Na^+ concentrations, although the full extent is not known. When expressed in yeast, HvHAK1 from barley mediated low-affinity Na^+ transport in addition to high-affinity K^+ uptake (Santa-María et al. 1997). Elevated Na^+ also inhibits K^+ transport through heterologously expressed AtKUP1 (Fu and Luan 1998) and AtHAK5 (Rubio et al. 2000). At the same time, the upregulation of *Mesembryanthemum crystallinum* McHAK1 and McHAK2 under both K^+ starvation and NaCl stress in roots and leaves has been reported (Su et al. 2002).

13.4.1.3 High affinity transporters—HKT1

Two different transport modes have been reported for HKT1: (i) a saturable high-affinity K^+-Na^+ symport and (ii) a low-affinity Na^+ transport, the latter operating at high external Na^+ concentrations when the transport of K^+ is blocked (Rubio et al. 1995; Gassmann et al. 1996).

The in planta function of AtHKT1 as an effector of Na^+ influx has been confirmed (Rus et al. 2001). T-DNA insertional and deletion mutants of AtHKT1 were identified in a screen for suppressors of NaCl sensitivity of the *sos3-1* mutant (Liu and Zhu 1997; Rus et al. 2001). Suppression of *sos3-1* NaCl sensitivity is related to reduced cellular accumulation of Na^+ and increased capacity to maintain internal K^+. Together, these results establish that AtHKT1 controls Na^+ influx into plants. It is likely that AtHKT1 is a Na^+ influx system but its function as a regulator of Na^+ and K^+ influx systems cannot be precluded. As the transcript is expressed predominantly in root cortical cells in wheat (Schachtman and Schroeder 1994), HKT1 most probably functions in the control of Na^+ loading into the xylem for export to the shoot (Uozumi et al. 2000; Rus et al. 2001). Through a combination of functional chimeric HKT analysis and sequence analyses, an amino acid was identified in HKT transporters that play an important role in determining the transport mode of HKT transporters (Mäser et al. 2002). This amino acid lies within the predicted "pore-loop" domain. The presence of a Gly residue resulted in K^+-Na^+ transport, whereas a Ser residue in this position caused more Na^+ selective transport (described above). Evidence is mounting that HKT1 systems are conserved in plant species and that these function in Na^+ transport (Rus et al. 2001; Golldack et al. 2002; Laurie et al. 2002; Garciadeblás et al. 2003).

Several reports have analyzed the physiological roles of HKT transporters in vivo. Laurie et al. (2002) found that transgenic wheat plants expressing an HKT1 antisense construct showed Na^+ tolerance under saline conditions with reduced Na^+ uptake activity and accumulation. However, Mäser et al. (2002) and Berthomieu et al. (2003) showed that loss-of-function mutations in the AtHKT1 gene lead to overaccumulation of Na^+ in shoots and rendered leaves Na^+ hypersensitive. Transgenic plants harboring an AtHKT1 promoter-GUS construct showed HKT1 expression in vascular tissues (Mäser et al. 2002; Berthomieu et al. 2003). Thus, a model was proposed in which AtHKT1 would facilitate recirculation of the Na^+ from the shoot to the root, thereby restricting its accumulation in the aerial part of the plant (Mäser et al. 2002; Berthomieu et al. 2003). These authors postulated that, in the shoot, HKT1 loads Na^+ into the phloem, which is then translocated to the root and removal of Na^+ from the root phloem occurs by efflux down the electrochemical gradient (Berthomieu et al. 2003). This model is support by Laurie et al. (2002), who showed that reduction of TaHKT1 expression in wheat resulted in a marked decrease in the root stele Na^+ content while poorly affecting the root epidermal and cortical contents.

13.4.1.4 LCT1

LCT1 is proposed to play a role in Na^+ uptake in wheat. When expressed in yeast, it functions as a non-selective cation permeable transporter, mediating both Na^+ and K^+ transport (Schachtman et al. 1997), and rendered yeast more salt sensitive (Amtmann et al. 2001). However, further analyses will be required to determine where LCT1 is targeted, as well as to quantify its contribution to the regulation of K^+ homeostasis in salinized plant tissues.

13.4.1.5 Non-selective cation channels

Physiological data implicate the involvement of non-selective cation channels (NSCCs) in Na^+ influx and these are considered to be the major route for Na^+ entry into plant cells (Tyerman et al. 1997; Amtmann and Sanders 1999; Tyerman and Skerrett 1999; Davenport and Tester 2000; Tyerman 2002). These channels have a similar permeability for K^+ and Na^+ (Amtmann and Sanders 1999). Na^+ influx currents through NSCC have been characterized electrophysiologically in root cortical cells of wheat (Tyerman et al. 1997; Davenport and Tester 2000), maize (Roberts and Tester 1997) and *Arabidopsis* (Demidchik and Tester 2002), as well as in barley suspension cells (Amtmann et al. 1997). The current amplitude of these channels was dependent on both the external Na^+ concentration and the external Ca^{2+} concentration. At a low Ca^{2+} concentration (40–100 μM), large increases were observed in the amplitude of the Na^+-dependent inward currents. At higher Ca^{2+} concentrations, Na^+ currents through NSCC were inhibited (Tyerman et al. 1997; Buschmann et al. 2000; Davenport and Tester 2000; Demidchik and Tester 2002), correlating with the reduction of Na^+ uptake by increased external Ca^{2+} concentration (LaHaye and Epstein 1969).

Calcium inhibition of NSCC conductance is not complete, so it is possible that these ion channels allow a substantial leak for Na^+ influx, particularly under high saline conditions (Davenport and Tester 2000; Demidchik and Tester 2002). This suggests that Ca^{2+}-insensitive Na^+ uptake pathways are probably also present and involved in Na^+ uptake. However, their full contribution to Na^+ uptake remains unknown.

13.4.2 Sodium/cation antiporters

Low cytosolic Na^+ concentration is attained by the operation of Na^+/H^+ antiporters located at both the PM (Shi et al. 2000) and the tonoplast (Apse et al. 1999). Electrochemical K^+ gradients generated by H^+-pumps at the PM (H^+-ATPase) and the tonoplast (H^+-ATPase, H^+-PPase) provide the energy used by the PM and tonoplast bound Na^+/H^+ antiporters to couple the passive movement of H^+ to the active movement of Na^+ out of the cell and into the

vacuole. The recent characterization of these systems has added considerably to our awareness of cytosolic Na^+ control. The identification and characterization of the yeast HAL1 gene which facilitates K^+/Na^+ selectivity and salt tolerance in yeast cells gives another dimension to our understanding of this issue. Consequently, our insight into Na^+ transport at both these membranes, and the control over K^+ and Na^+ homeostasis, has increased considerably, knowledge which is finally giving us the possibility of generating salt tolerant crops.

13.4.2.1 The SOS-signal transduction pathway

The SOS (for *S*alt-*O*verly-*S*ensitive) signal-transduction pathway is important in controlling ion homeostasis and salt tolerance in plants (Hasegawa et al. 2000; Sanders 2000; Zhu 2000, 2003). The current model for the SOS signal-transduction pathway is that high Na^+ induces a Ca^{2+} signal (Knight et al. 1997). A myristoylated Ca^{2+}-binding protein senses the salt-elicited Ca^{2+} signal and translates it to downstream responses (Liu and Zhu 1998; Ishitani et al. 2000). SOS3 interacts with, and activates SOS2, a serine/threonine protein kinase (Halfter et al. 2000; Liu et al. 2000). This SOS2/SOS3 complex regulates the expression level of SOS1, a salt effector gene encoding a PM Na^+/H^+ antiporter. The SOS1 Na^+/H^+ exchanger serves to extrude excess Na^+ from the cytosol and out of the cell, thereby maintaining a low cytosolic Na^+ concentration (Shi et al. 2000).

Activity of the SOS1 promoter has been found ubiquitously in virtually all tissues, but its greatest activity is found in root epidermal cells, particularly at the root tip and in cells bordering the vascular tissue (Shi et al. 2002). This suggests three major roles: (i) mediating Na^+ efflux from cytosol to the root medium, (ii) buying time for Na^+ storage in the vacuole by slowing down Na^+ accumulation in the cytoplasm, and (iii) controlling long-distance Na^+ transport between roots and shoots by loading Na^+ into and unloading Na^+ from the xylem and phloem (Zhu 2003). The role of SOS1 in long distance transport is important for coordination between transpirational Na^+ flow and the vacuolar sequestration of Na^+ in leaves. A higher concentration of Na^+ accumulates in shoots of *sos1* mutants than in WT, and transgenic plants overexpressing SOS1 showed improved salt tolerance and accumulated less Na^+ in the xylem transpiration stream as well as in the shoot (Shi et al. 2003).

Extrusion of excess Na^+ from the cell is a straightforward way to avoid Na^+ accumulation in the cytosol, so is widely employed by root epidermal cells, where SOS1 is preferentially expressed (Shi et al. 2002). This strategy would be problematic for most other types of cells, where extruded Na^+ will immediately become a problem for neighboring cells. This is especially important in leaves where, due to the small apoplasmic volume (~3%; Flowers and Yeo 1986), Na^+ extrusion via SOS1 would cause a rapid increase of apoplasmic Na^+ leading to cell dehydration, turgor loss and even death of leaf cells and tissues (Marschner 1995).

The problem may be overcome if SOS1 acts in concert with AtHKT1, which has been suggested to mediate Na^+ loading into the phloem in leaves and unloading in roots (Nublat et al. 2001; Berthomieu et al. 2003). These two mechanisms could remove Na^+ from the apoplast and symplast as long as their combined efficiency is greater than the rate of Na^+ delivery. According to this scenario, SOS1 Na^+/H^+ exchanger will remove Na^+ from the cell and AtHKT1 will load it into phloem for removal from the shoot. Earlier Rus et al. (2001) explained why the mutations in the AtHKT1 gene suppress the *sos3* mutant phenotype by this functional interaction between SOS1 and AtHKT1. The above model of functional interaction between AtHKT1 and AtNHX1 can also explain the otherwise puzzling result that transgenic plants overexpressing AtNHX1 accumulate about 30% more Na^+ in leaves than control plants (Apse et al. 1999). However, there are no reports of the functional expression or physiological characterization of the SOS-signaling pathway in leaves, and few on the functioning of the AtHKT1 gene and associated transporters. Therefore, the occurrence of this model in planta remains to be confirmed.

The SOS3-SOS2 kinase complex may also regulate Na^+ compartmentation by (i) activating NHX1 at the tonoplast, (ii) restricting Na^+ entry into the cytosol (by inhibiting the PM Na^+ transporter HKT1 activity; Zhu 2002), (iii) negatively controlling the expression of AtNHX family members (Yokoi et al. 2002), and (iv) controlling K^+ acquisition by the root (Wu et al. 1996). The latter is confirmed by the fact that under NaCl conditions, *sos1* mutant plants accumulate more Na^+ and less K^+ (Wu et al. 1996; Ding and Zhu 1997; Rus et al. 2001) and overexpression of SOS1 has been shown to result in increased Na^+ export from the cell and improved salt tolerance in transgenic *Arabidopsis* (Shi et al. 2002). Also, all *sos* mutants had a growth defect under K^+-limiting conditions (Zhu et al. 1998). Which specific K^+ transport system is targeted by SOS signaling pathway, remains a mystery. Patch-clamp experiments suggest that the extrusion of Na^+ from the cytoplasm by SOS1 protects the K^+ permeability of the membrane, and the AKT1 K^+ channel in particular, from inhibition by Na^+ (Qi and Spalding 2004). However, experiments in our laboratory showed no difference in NaCl-induced K^+ fluxes from roots of WT and *akt1 Arabidopsis* mutant (S. Shabala and L. Shabala, unpublished) questioning the AKT1 involvement. Also, NaCl-induced K^+ efflux from barley mesophyll was strongly inhibited by K^+ channel blocker TEA^+ (Shabala et al. 2005). The possible involvement of other K^+ transporters remains to be evaluated.

13.4.2.2 Tonoplast Na^+/H^+ antiporters

Compartmentation of Na^+ into the vacuole is important in the maintenance of lower cytosolic Na^+ concentrations, while maintaining a lower cellular osmotic potential. Significant progress has been made in deducing the genes and transporters responsible for Na^+ sequestration. Active transport across the tonoplast utilizes the electrochemical gradient generated by V-type H^+-ATPase and H^+-PPase. Vacuolar Na^+/H^+ antiporter activity was first measured in tonoplast

enriched membranes isolated from red beet storage tissue (Blumwald and Poole 1985), and has subsequently been measured in many plants (Apse et al. 1999; Blumwald et al. 2000 and references within). Salinity also upregulates the expression of a V-type H-ATPase (Golldack and Dietz 2001), and overexpression of the native vacuolar H^+-PPase gene (AVP1) increases salt tolerance in *Arabidopsis* (Gaxiola et al. 2001).

Cloning of AtNHX1 (Apse et al. 1999; Gaxiola et al. 1999) was followed by its functional complementation in yeast *nhx1* mutants (Gaxiola et al. 1999), measurement of its Na^+/H^+ exchange activity in vacuoles isolated from AtNHX1 overexpressing *Arabidopsis* (Apse et al. 1999) and in vacuolar vesicle membranes isolated from yeast expressing AtNHX1 (Darley et al. 2000). These studies clearly confirm the function of AtNHX1 as an Na^+/H^+ antiporter. Increased expression of AtNHX1 by transformation with AtNHX driven by a strong constitutive promoter, improves salinity tolerance in *Arabidopsis* (Apse et al. 1999), *Brassica napus* (Zhang et al. 2001) and tomato (Zhang and Blumwald 2001). These results show that an increased capacity for vacuolar Na^+ sequestration is important for salinity tolerance. Importantly, transgenic tomato and *Brassica* plants accumulated a high concentration of Na^+ in leaves, but not in fruit or seed, thus were highly tolerant of salt stress while at the same time maintaining the quality of fruit and oil (Zhang and Blumwald 2001; Zhang et al. 2001). This is the first real progress in the development of genetically modified salt tolerant crop species.

This increased capacity for Na^+ uptake by vacuoles by a NHX1 Na^+/H^+ antiport is found in many salt tolerant species, e.g. *Beta maritima*, *Atriplex gmelini* and *Mesembryanthemum crystallinum*. All show strong induction of both Na^+/H^+ antiporter expression and activity in response to NaCl treatment (Barkla et al. 1995; Hamada et al. 2001; Xia et al. 2002).

The AtNHX1 gene is also able to mediate K^+ transport in addition to Na^+/H^+ exchange (Zhang and Blumwald 2001; Venema et al. 2002; Apse et al. 2003). Similar K^+ transporter activity has been reported in rice, where overexpression of the tonoplast located OsNHX1 increased salt tolerance (Fukuda et al. 2004). A tomato tonoplast LeNHX2 antiporter maintained higher K^+ concentration in intracellular compartments under salt stress conditions (Venema et al. 2003) The AtCHX17 in *Arabidopsis* was reported to have a greater role in K^+ acquisition and homeostasis rather than in Na^+ transport (Cellier et al. 2004). This suggests that members of the NHX family may have different substrate specificities and play different roles in salt tolerance (Yokoi et al. 2002). Overall, the importance of NHX Na^+/H^+ antiporters at the tonoplast in the maintenance of K^+ and Na^+ homeostasis in plant cells is beyond doubt.

13.4.2.3 HAL genes

The yeast *HAL1* and *HAL3* genes are proposed to improve salt tolerance by increasing the cellular K^+/Na^+ ratio (Gaxiola et al. 1992; Serrano 1996; Rios et al. 1997). Transcription of HAL1 favors Na^+ extrusion and restricts K^+ efflux

through an unknown pathway (Bordas et al. 1997), effectively increasing the intracellular K^+/Na^+ ratio (Gaxiola et al. 1992).

In yeast, *HAL1* expression is induced by salt (Gaxiola et al. 1992) and its overexpression confers increased salt tolerance in transgenic *Saccharomyces cerevisiae* (Rios et al. 1997). Increased salt tolerance has also been reported in transgenic plants expressing the *HAL1* gene, including tomato (Gisbert et al. 2000; Rus et al. 2001) and melon (Bordas et al. 1997). Genes homologous to the yeast HAL genes could be present in higher plants and may be relevant to salt tolerance (Bordas et al. 1997). For example, Espinosa-Ruiz et al. (1999) isolated two *Arabidopsis* genes AtHAL3a and AtHAL3b which show homology with HAL3. Gain of AtHAL3a function *Arabidopsis* show increased growth rates and improved salt tolerance. Alterations in intracellular cation concentrations associated with changes in HAL3 expression indicated that HAL3 directly increased cytoplasmic K^+ concentration and decreased Na^+ concentrations (Espinosa-Ruiz et al. 1999).

13.4.3 Mitigating effect of calcium

An important determinant for plant salt tolerance that is particularly relevant to Na^+ and K^+ homeostasis is the sensitivity of many transport processes to Ca^{2+}. Increased Ca^{2+} supply has a protective effect on plants under salt stress (reviewed by Rengel 1992). Physiological effects of supplemental Ca^{2+} include (i) diminished membrane leakiness, (ii) improved PM structural integrity, (iii) improved K^+ status of the cell and (iv) reduced Na^+ accumulation in plants (Cramer et al. 1985, 1987; Rengel 1992; Bressan et al. 1998; Munns 2002).

At the transporter level, the traditional view is that elevated Ca^{2+} restricts Na^+ uptake via NSCC (Tyerman et al. 1997; Demidchik and Tester 2002; Tester and Davenport 2003). Other divalent cations may also control NSCC permeability for Na^+ (Elphick et al. 2001; Demidchik and Tester 2002). However, work in our laboratory suggested that NSCC blockage by elevated Ca^{2+} is not the only mechanism involved. MIFE experiments on root (Shabala et al. 2003) and leaf (Shabala 2000; Shabala et al. 2005) tissue of various species showed that both supplemental Ca^{2+} and other divalent cations (Mg^{2+}, Ba^{2+}, Zn^{2+}) reduce or prevent NaCl-induced K^+ efflux from the cell. Thus, our results suggest that, in addition to their known ability to block NSCC, divalent cations also control the activity or gating properties of PM K^+ transporters, assisting in maintaining an optimal K^+/Na^+ ratio. Results of pharmacological studies and patch-clamp experiments suggest that depolarization-activated outward-rectifying K^+ channels are involved (S. Shabala, V. Demidchik and J. Davies, unpublished data).

13.4.4 Ion compartmentation between roots and shoots

The regulation of Na^+ transport to the shoot is another feature that governs plant responses to salinity. The differences in the growth responses of salt

tolerant and salt sensitive species are often related to differences in the translocation of Na^+ to leaves (Marschner 1995). In salt tolerant species, increased salt supply leads to a large accumulation of Na^+ in the shoots where it is utilized in the vacuoles of leaf cells for osmotic adjustment (Flowers and Läuchli 1983), often replacing most of K^+ in the vacuole (Hawker et al. 1974). In more salt sensitive species, substitution of K^+ by Na^+ is much more limited. The higher salt tolerance of many species is often attributed to a more effective restriction on shoot directed transport of Na^+ (Tester and Davenport 2003). There is also some evidence of extensive recirculation of shoot Na^+ to the roots (Mäser et al. 2002; Berthomieu et al. 2003), although it has been suggested that Na^+ transport is largely unidirectional and results in progressive accumulation of Na^+ as the leaves age (Tester and Davenport 2003). As such, retranslocation of Na^+ from shoots to roots was found to contribute to low Na^+ contents in the shoots of beans (Matsushita and Matoh 1991) and clover (Winter 1982), but not barley (Munns et al. 1987).

The importance of Na^+ and K^+ compartmentation at the whole-plant level was highlighted in a recent study on two closely related species, contrasting in their salt tolerance. *Thellungiella halophila* (salt cress) is closely related to *Arabidopsis* (90–95% identity at the cDNA level; Bressan et al. 2001). Volkov et al. (2003) showed that under saline conditions *T. halophila* had a much better ability to retain or even increase shoot elemental K^+ content compared with *Arabidopsis*. The observed differences in K^+ accumulation were larger in roots than in shoots. At the same time, the differences in Na^+ accumulation (higher in *Arabidopsis*) were more pronounced in shoots than in roots. This suggests that control of Na^+ loading into xylem is particularly strong in *T. halophila* (Volkov et al. 2003).

The control of shoot Na^+ will undoubtedly affect the K^+/Na^+ ratio in leaf cells. For example, the *sas1* mutant of *Arabidopsis* shows a deficiency in the control of radial transport of Na^+ (Nublat et al. 2001). This led to a 5.5-fold higher concentration of Na^+ in the xylem and a severe overaccumulation of Na^+ in the shoot, corresponding with increased sensitivity to NaCl. Although Na^+ was accumulated preferentially over K^+ in a similar manner for *sas1* and WT, the greater amounts of Na^+ in the *sas1* mutants resulted in a much higher Na^+/K^+ ratio than in the WT. Overaccumulation of Na^+ was only in shoots, not in roots, which suggested that *sas1* mutation impaired Na^+ long-distance transport from roots to shoots. This emphasizes the importance of xylem loading in salinity tolerance. In wheat, a K^+/Na^+ discrimination factor limiting Na^+ translocation to the shoot for the benefit of K^+ loading operates at the xylem uptake step (Gorham et al. 1990). In soybean, Na^+ is removed from the xylem vessels and exchanged for K^+ at the xylem parenchyma (Läuchli 1976; Lacan and Durand 1996).

Another component regulating Na^+ xylem content is SOS1. In *sos1* mutants, the Na^+ concentration in the xylem sap is higher than in the WT, suggesting that SOS1 controls Na^+ loading into, and/or retrieval from the xylem (Zhu 2003). SOS1 is expressed around the vacuolar tissue, consistent with it function in xylem Na^+ concentration (Shi et al. 2002).

13.4.5 Compartmentation at the tissue level

Salt stress is known to have different effects on the K^+/Na^+ ratio in various plant tissues in both roots and leaves (Fricke 2004). In leaves, epidermal cells accumulate a greater amount of Na^+ than the mesophyll cells and the latter show a greater ability to maintain a high K^+ levels (Fricke et al. 1996; Cuin et al. 2003). Volkov et al. (2003) found different trends in the distribution between the epidermis and the bulk tissue of *T. halophila* and *Arabidopsis*. Salt stress decreased epidermal K^+ concentrations dramatically, but bulk K^+ increased in *T. halophila* while decreasing in both epidermal and bulk K^+ after salt treatment in *Arabidopsis* (Volkov et al. 2003). This is consistent with the important role of the tissue-specific compartmentation of Na^+ and K^+ for plant salt tolerance and suggests that some mechanisms are in place within the mesophyll, but not the epidermis, to ameliorate ionic changes and protect and maintain the photosynthetic activity of the mesophyll cells. This is consistent with recent studies in our laboratory showing that improving K^+/Na^+ ratios by externally applied divalent cations enables normal leaf photochemistry in plant grown even under high (100 mM) salinity conditions (Shabala et al. 2005).

The ionic mechanisms underlying the above difference in Na^+ and K^+ compartmentation between epidermis and mesophyll remain to be revealed. One explanation could be that differences in gene expression account for the differences in ion compartmentation under saline conditions. For example, in fully expanded leaves, under unsalinized conditions, the K^+ channel genes AtKC1 and AKT1 are expressed in hydrathodes and stipules (Lagarde et al. 1996; Pilot et al. 2003). However, upon the imposition of salt stress, the expression pattern of AtKC1 broadens out to the leaf epidermis (Pilot et al. 2003) where both AKT1 and AKT2 are also expressed (Dennison et al. 2001), indicating reprogramming of K^+ channel gene expression in leaves (Pilot et al. 2003). The strong increase in expression in leaves upon salt stress could underlie changes in the compartmentalization of Na^+ and K^+ ions between the different tissues. As described above, in barley, the leaf epidermis may act as a "storage compartment" for Na^+, thus protecting the mesophyll cells, at least for a period, from Na^+ toxicity, allowing it to maintain higher concentrations of K^+ (Dietz et al. 1992; Fricke et al. 1996). It might be speculated that the leaf epidermis in *Arabidopsis* could play a similar role, requiring high AtKC1 expression levels for as yet unidentified reasons.

However, Karley et al. (2000) reported similar types of ion-selective channels and membrane transporters catalyzing the transport of K^+ and Na^+ in epidermal and mesophyll cells from barley. They suggest that the presence or absence of ion transporters cannot explain cell type specific differences in K^+/Na^+ ratios. More likely, altered permeability or gating properties of these transporters may be the key to understanding salt tolerance. The difference in salt tolerance between *T. halophila* and *Arabidopsis* was attributed to much higher selectivity for K^+ over Na^+ of both inward- and outward-rectifying K^+ channels between these species (Volkov et al. 2003). This highlights the

importance of a plant's ability to retain K^+ as a key feature of salt tolerance and is consistent with our recent findings that the magnitude of NaCl-induced K^+ efflux from plant roots correlates with salt tolerance in barley (Chen et al. 2005).

13.5 Conclusions and future perspectives

Knowledge regarding K^+ transport and the effects of salinity on K^+ homeostasis has increased considerably in recent years. New awareness concerning Na^+ compartmentalization into the vacuole opens up exciting prospects for developing salt tolerant crops. The sequencing of the *Arabidopsis* genome has led to the identification of a plethora of K^+ transporters, some of which have already been characterized electrophysiologically. Microarray experiments are starting to indicate the genes induced by salt stress. The more recent sequencing of the rice genome, which is likely to be followed by other crops, will add to our knowledge of K^+ transporters and the effects of salinity on these, as these putative genes are characterized.

However, there is still a very long way to go to gain a full extent of knowledge about the mechanisms of salt tolerance in plants. Only a small numbers of genes responsible for K^+ or Na^+ transport are characterized physiologically. Moreover, the majority of these results are through experiments in heterologous systems. Thus, in planta studies on ionic mechanisms regulating K^+ homeostasis under saline conditions are needed. Also, we have just scratched the surface of the signaling mechanisms that mediate the salt stress regulation of the expression and activities of ion transporters. Other questions such as the involvement of compatible solutes in ion homeostasis and the interaction of salt stress with other abiotic stress such as drought, high temperatures, light intensity, pollution etc also remain a grey area.

Much research on salinity tolerance has recently focused on *Arabidopsis*. Being methodologically convenient, this species is rather "non-typical" from the point of view of plant physiologists. As a result, direct extrapolation of findings from *Arabidopsis* to other species is not always possible. Now that we appear to have most of the "basics" concerning *Arabidopsis* salt tolerance mechanisms, it is time that the salt tolerance mechanisms other species are tackled at the same level of scrutiny.

Another area that is severely lacking information and is of particular concern is the regulation of K^+ and Na^+ at the leaf level, most studies on K^+ transport under saline conditions have been attributed to root tissues. Being central to plant photosynthesis, leaf mesophyll cells are almost crying to be studied in this context!

Finally, with all the excitement of a magic of molecular techniques, we should not forget that plants are more than a combination of genes. Therefore, the whole-plant perspective should be also kept in mind when

doing in-depth studies on expression and control modes of some specific transporters mediating K^+ homeostasis in plants under saline conditions.

Acknowledgements. This work was supported by the ARC Discovery and DEST grants to S. Shabala.

References

Ache P, Becker D, Deeken R, Dreyer I, Weber H, Fromm J, Hedrich R (2001) VFK1, a *Vicia faba* K^+ channel involved in phloem unloading. Plant J 27:571-580

Amtmann A, Sanders D (1999) Mechanisms of Na^+ uptake by plant cells. Adv Bot Res 29:75-112

Amtmann A, Laurie S, Leigh R, Sanders D (1997) Multiple inward channels provide flexibility in Na^+/K^+ discrimination at the plasma membrane of barley suspension culture cells. J Exp Bot 48:481-497

Amtmann A, Jelitto TC, Sanders D (1999) K^+-selective inward-rectifying channels and apoplastic pH in barley roots. Plant Physiol 120:331-338

Amtmann A, Fischer M, Marsh EL, Stefanovic A, Sanders D, Schachtman DP (2001) The wheat cDNA LCT1 generates hypersensitivity to sodium in a salt sensitive yeast strain. Plant Physiol 126:1061-1071

Apse MP, Aharon GS, Snedden WA, Blumwald E (1999) Salt tolerance conferred by overexpression of a vacuolar Na^+/H^+ antiport in *Arabidopsis*. Science 285:1256-1258

Apse MP, Sottosanto JB, Blumwald E (2003) Vacuolar cation/H^+ exchange, ion homeostasis, and leaf development are altered in a T-DNA insertional mutant of AtNHX1, the *Arabidopsis* vacuolar Na^+/H^+ antiporter. Plant J 36:229-239

Arazi T, Sunkar R, Kaplan B, Fromm H (1999) A tobacco plasma membrane calmodulin-binding transporter confers Ni^{2+} tolerance and Pb^{2+} hypersensitivity in transgenic plants. Plant J 20:171-182

Bañuelos MA, Klein RD, Alexander-Bowman SJ, Rodríguez-Navarro A (1995) A potassium transporter of the yeast *Schwanniomyces occidentalis* homologous to the KUP system of *Escherichia coli* has a high concentrative capacity. EMBO J 14:3021-3027

Bañuelos MA, Garciadeblás B, Cubero B, Rodríguez-Navarro A (2002) Inventory and functional characterization of the HAK potassium transporters of rice. Plant Physiol 130:784-795

Barkla BJ, Zingarelli L, Blumwald E, Smith JAC (1995) Tonoplast Na^+/H^+ antiport activity and its energization by the vacuolar H^+-ATPase in the halophytic plant *Mesembryanthemum crystallinum* L. Plant Physiol 109:549-556

Berthomieu P, Conejero G, Nublat A, Brackenbury WJ, Lambert C, Savio C, Uozumi N, Oiki S, Yamada K, Cellier F, Gosti F, Simonneau T, Essah PA, Tester M, Very AA, Sentenac H, Casse F (2003) Functional analysis of AtHKT1 in *Arabidopsis* shows that Na^+ recirculation by the phloem is crucial for salt tolerance. EMBO J 22:2004-2014

Bertl A, Anderson JA, Slayman CL, Sentenac H, Gaber RF (1994) Inward and outward rectifying potassium currents in *Saccharomyces cerevisiae* mediated by endogenous and heterologously expressed ion channels. Folia Microbiol 39:507-509

Blumwald E, Poole RJ (1985) Na^+/H^+ antiport in isolated tonoplast vesicles from storage tissue of *Beta vulgaris*. Plant Physiol 78:163-167

Blumwald E, Aharon GS, Apse MP (2000) Sodium transport in plant cells. Biochim Biophys Acta 1465:140-151

Bordas M, Montesinos C, Dabauza M, Salvador A, Roig LA, Serrano R, Moreno V (1997) Transfer of the yeast salt tolerance gene HAL1 to *Cucumis melo* L cultivars and in vitro evaluation of salt tolerance. Transgenic Res 6:41-50

Boursier P. Läuchli A (1989) Mechanism of chloride partitioning in leaves of salt-stressed *Sorghum bicolor* L. Physiol Plant 77:537-544

Bressan RA, Hasegawa PM, Pardo JM (1998) Plants use calcium to resolve salt stress. Trend Plant Sci 3:411-412

Bressan W, Siqueira JO, Vasconcellos CA, Purcino AAC (2001) Myccorhizal fungi and phosphorus on growth, yield and nutrition of intercropped grain sorghum and soybean. Pesq Agropec Brasil 36:315-323

Buschmann PH, Vaidyanathan R, Gassmann W, Schroeder JI (2000) Enhancement of Na^+ uptake currents, time-dependent inward-rectifying K^+ channel currents, and K^+ channel transcripts by K^+ starvation in wheat root cells. Plant Physiol 122:1387-1397

Carden DE, Walker DJ, Flowers TJ, Miller AJ (2003) Single-cell measurements of the contributions of cytosolic Na^+ and K^+ to salt tolerance. Plant Physiol 131:676-683

Cellier F, Conejero G, Ricaud L, Luu DT, Lepetit M, Gosti F, Casse F (2004) Characterization of AtCHX17, a member of the cation/H^+ exchangers, CHX family, from *Arabidopsis thaliana* suggests a role in K^+ homeostasis. Plant J 39:834-846

Chen Z, Newman I, Zhou M, Mendham N, Zhang G, Shabala S (2005) Screening plants for salt tolerance by measuring K^+ flux: a case study for barley. Plant Cell Environ (in press)

Chiu JC, Brenner ED, DeSalle R, Nitabach MN, Holmes TC, Coruzzi GM (2002) Phylogenetic and expression analysis of the glutamate-receptor-like gene family in *Arabidopsis thaliana*. Mol Biol Evolut 19:1066-1082

Cramer GR, Läuchli A, Polito VS (1985) Displacement of Ca^{2+} by Na^+ from the plasmalemma of root cells—a primary response to salt stress. Plant Physiol 79:207-211

Cramer GR, Lynch J, Läuchli A, Epstein E (1987) Influx of Na^+, K^+, and Ca^{2+} into roots of salt-stressed cotton seedlings—effects of supplemental Ca^{2+}. Plant Physiol 83:510-516

Cuin TA, Miller AJ, Laurie SA, Leigh RA (2003) Potassium activities in cell compartments of salt-grown barley leaves. J Exp Bot 54:657-661

Czempinski K, Gaedeke N, Zimmermann S, Müller-Röber B (1999) Molecular mechanisms and regulation of plant ion channels. J Exp Bot 50:955-966

Czempinski K, Frachisse JM, Maurel C, Barbier-Brygoo H, Müller-Röber B (2002) Vacuolar membrane localization of the *Arabidopsis* "two-pore" K^+ channel KCO1. Plant J 29:809-820

Darley CP, van Wuytswinkel OCM, van der Woude K, Mager WH, de Boer AH (2000) *Arabidopsis thaliana* and *Saccharomyces cerevisiae* NHX1 genes encode amiloride sensitive electroneutral Na^+/H^+ exchangers. Biochem J 351:241-249

Davenport RJ, Tester M (2000) A weakly voltage-dependent, nonselective cation channel mediates toxic sodium influx in wheat. Plant Physiol 122:823-834

De Boer AH (1999) Potassium translocation into the root xylem. Plant Biol 1:36-45

Deeken R, Sanders C, Ache P, Hedrich R (2000) Developmental and light-dependent regulation of a phloem-localised K^+ channel of *Arabidopsis thaliana*. Plant J 23:285-290

Demidchik V, Tester M (2002) Sodium fluxes through nonselective cation channels in the plasma membrane of protoplasts from *Arabidopsis* roots. Plant Physiol 128:379-387

Demidchik V, Davenport RJ, Tester M (2002) Nonselective cation channels in plants. Annu Rev Plant Biol 53:67-107

Demmig B, Gimmler H (1983) Properties of the isolated intact chloroplast at cytoplasmic K^+ concentrations. I. Light-induced cation uptake into intact chloroplasts is driven by an electric potential difference. Plant Physiol 73:169-174

Dennison KL, Robertson WR, Lewis BD, Hirsch RE, Sussman MR, Spalding EP (2001) Functions of AKT1 and AKT2 potassium channels determined by studies of single and double mutants of *Arabidopsis*. Plant Physiol 127:1012-1019

Dietz KJ, Schramm M, Betz M, Busch H, Durr C, Martinoia E (1992) Characterization of the epidermis from barley primary leaves. 1. Isolation of epidermal protoplasts. Planta 187:425-430

Ding L, Zhu JK (1997) Reduced Na^+ uptake in the NaCl-hypersensitive *sos1* mutant of *Arabidopsis thaliana*. Plant Physiol 113:795-799

Doupnik CA, Davidson N, Lester HA (1995) The inward rectifier potassium channel family. Curr Opin Neurobiol 5:268-277

Durell SR, Hao YL, Nakamura T, Bakker EP, Guy HR (1999) Evolutionary relationship between K^+ channels and symporters. Biophys J 77:775-788

Elphick CH, Sanders D, Maathuis FJM (2001) Critical role of divalent cations and Na^+ efflux in *Arabidopsis thaliana* salt tolerance. Plant Cell Environ 24:733-740

Epstein E, Rains DW, Elzam OE (1963) Resolution of dual mechanisms of potassium absorption by barley roots. Proc Natl Acad Sci USA 49:684-692

Espinosa-Ruiz A, Bellés JM, Serrano R, Culiáñez-Macià FA (1999) *Arabidopsis thaliana* AtHAL3: a flavoprotein related to salt and osmotic tolerance and plant growth. Plant J 20:529-539

Fairbairn DJ, Liu WH, Schachtman DP, Gomez-Gallego S, Day SR, Teasdale RD (2000) Characterisation of two distinct HKT1-like potassium transporters from *Eucalyptus camaldulensis*. Plant Mol Biol 43:515-525

Flowers TJ, Hajibagheri MA (2001) Salinity tolerance in *Hordeum vulgare*: ion concentrations in root cells of cultivars differing in salt tolerance. Plant Soil 231:1-9

Flowers TJ, Läuchli A (1983) Sodium versus potassium: substitution and compartmentation. In: Läuchli A, Bieleski RL (eds) Encyclopedia of plant physiology, new series. Springer, Berlin Heidelberg New York, pp 651-681

Flowers TJ, Yeo AR (1986) Ion relations of plant under drought and salinity. Aust J Plant Physiol 13:75-91

Fricke W (2004) Rapid and tissue-specific accumulation of solutes in the growth zone of barley leaves in response to salinity. Planta 219:515-525

Fricke W, Pritchard E, Leigh RA, Tomes AD (1994) Cells of the upper and lower epidermis of barley (*Hordeum vulgare* L) leaves exhibit distinct patterns of vacuolar solutes. Plant Physiol 104:1201-1208

Fricke W, Leigh RA, Tomos AD (1996) The intercellular distribution of vacuolar solutes in the epidermis and mesophyll of barley leaves changes in response to NaCl. J Exp Bot 47:1413-1426

Fu HH, Luan S (1998) AtKUP1: a dual-affinity K^+ transporter from *Arabidopsis*. Plant Cell 10:63-73

Fukuda A, Nakamura A, Tagiri A, Tanaka H, Miyao A, Hirochika H, Tanaka Y (2004) Function, intracellular localization and the importance in salt tolerance of a vacuolar Na^+/H^+ antiporter from rice. Plant Cell Physiol 45:146-159

Gamba G, Saltzberg SN, Lombardi M, Miyanoshita A, Lytton J, Hediger MA, Brenner BM, Hebert SC (1993) Primary structure and functional expression of a cDNA-encoding the thiazide-sensitive, electroneutral sodium-chloride cotransporter. Proc Natl Acad Sci USA 90:2749-2753

Gamel K, Torre V (2000) The interaction of Na^+ and K^+ in the pore of cyclic nucleotide-gated channels. Biophys J 79:2475-2493

Garciadeblás B, Benito B, Rodríguez-Navarro A (2002) Molecular cloning and functional expression in bacteria of the potassium transporters CnHAK1 and CnHAK2 of the seagrass *Cymodocea nodosa*. Plant Mol Biol 50:623-633

Garciadeblás B, Senn ME, Bañuelos MA, Rodríguez-Navarro A (2003) Sodium transport and HKT transporters: the rice model. Plant J 34:788-801

Gassmann W, Schroeder JI (1994) Inward-rectifying K^+ channels in root hairs of wheat—a mechanism for aluminum-sensitive low-affinity K^+ uptake and membrane-potential control. Plant Physiol 105:1399-1408

Gassmann W, Rubio F, Schroeder JI (1996) Alkali cation selectivity of the wheat root high-affinity potassium transporter HKT1. Plant J 10:869-882

Gaxiola R, Delarrinoa IF, Villalba JM, Serrano R (1992) A novel and conserved salt-induced protein is an important determinant of salt tolerance in yeast. EMBO J 11:3157-3164

Gaxiola RA, Rao R, Sherman A, Grisafi P, Alper SL, Fink GR (1999) The *Arabidopsis thaliana* proton transporters, AtNhx1 and Avp1, can function in cation detoxification in yeast. Proc Natl Acad Sci USA 96:1480-1485

Gaxiola RA, Li JS, Undurraga S, Dang LM, Allen GJ, Alper SL, Fink GR (2001) Drought- and salt-tolerant plants result from overexpression of the AVP1 H^+-pump. Proc Natl Acad Sci USA 98:11444-11449

Gaymard F, Cerutti M, Horeau C, Lemaillet G, Urbach S, Ravallec M, Devauchelle G, Sentenac H, Thibaud JB (1996) The baculovirus/insect cell system as an alternative to *Xenopus*

oocytes—first characterization of the AKT1 K^+ channel from *Arabidopsis thaliana*. J Biol Chem 271:22863-22870

Gaymard F, Pilot G, Lacombe B, Bouchez D, Bruneau D, Boucherez J, Michaux-Ferriere N, Thibaud JB, Sentenac H (1998) Identification and disruption of a plant shaker-like outward channel involved in K^+ release into the xylem sap. Cell 94:647-655

Gillen CM, Stirewalt VL, Bryant DA, Forbush B (1996) Cloning, sequencing, and initial characterization of a putative ion cotransport protein from cyanobacterium *Synechococcus sp* PCC 7002. Biophys J 70:MP293-MP293

Gisbert C, Rus AM, Bolarin MC, Lopez-Coronado JM, Arrillaga I, Montesinos C, Caro M, Serrano R, Moreno V (2000) The yeast HAL1 gene improves salt tolerance of transgenic tomato. Plant Physiol 123:393-402

Glass ADM, Fernando M (1992) Homeostatic processes for the maintenance of the K^+ content of plant cells: a model. Israel J Bot 41:145-166

Golldack D, Dietz KJ (2001) Salt-induced expression of the vacuolar H^+-ATPase in the common ice plant is developmentally controlled and tissue specific. Plant Physiol 125:1643-1654

Golldack D, Kamasani UR, Quigley F, Bennett J, Bohnert HJ (1997) Salt stress-dependent expression of a HKT1-type high affinity potassium transporter in rice. Plant Physiol 114:529-529

Golldack D, Su H, Quigley F, Kamasani UR, Munoz-Garay C, Balderas E, Popova OV, Bennett J, Bohnert HJ, Pantoja O (2002) Characterization of a HKT-type transporter in rice as a general alkali cation transporter. Plant J 31:529-542

Gorham J, Bristol A, Young EM, Jones RGW, Kashour G (1990) Salt tolerance in the *Triticeae*—K/Na discrimination in barley. J Exp Bot 41:1095-1101

Halfter U, Ishitani M, Zhu JK (2000) The *Arabidopsis* SOS2 protein kinase physically interacts with and is activated by the calcium-binding protein SOS3. Proc Natl Acad Sci USA 97:3735-3740

Hamada A, Shono M, Xia T, Ohta M, Hayashi Y, Tanaka A, Hayakawa T (2001) Isolation and characterization of a Na^+/H^+ antiporter gene from the halophyte *Atriplex gmelini*. Plant Mol Biol 46:35-42

Hasegawa PM, Bressan RA, Zhu JK, Bohnert HJ (2000) Plant cellular and molecular responses to high salinity. Annu Rev Plant Physiol Plant Mol Biol 51:463-499

Hawker JS, Marschner H, Downton WJS (1974) Effects of sodium and potassium on starch synthesis in leaves. Aust J Plant Physiol 1:491-501

Hille B (2001) Ionic channels of excitable membranes, 3rd edn. Sinauer Association Inc., USA

Hirsch RE, Lewis BD, Spalding EP, Sussman MR (1998) A role for the AKT1 potassium channel in plant nutrition. Science 280:918-921

Horie T, Yoshida K, Nakayama H, Yamada K, Oiki S, Shinmyo A (2001) Two types of HKT transporters with different properties of Na+ and K+ transport in *Oryza sativa*. Plant J 27:129-138

Hosy E, Vavasseur A, Mouline K, Dreyer I, Gaymard F, Poree F, Boucherez J, Lebaudy A, Bouchez D, Very AA, Simonneau T, Thibaud JB, Sentenac H (2003) The *Arabidopsis* outward K^+ channel GORK is involved in regulation of stomatal movements and plant transpiration. Proc Natl Acad Sci USA 100:5549-5554

Isenring P, Forbush B (1997) Ion and bumetanide binding by the Na-K-Cl cotransporter—importance of transmembrane domains. J Biol Chem 272:24556-24562

Ishitani M, Liu JP, Halfter U, Kim CS, Shi WM, Zhu JK (2000) SOS3 function in plant salt tolerance requires N-myristoylation and calcium binding. Plant Cell 12:1667-1677

Ivashikina N, Becker D, Ache P, Meyerhoff O, Felle HH, Hedrich R (2001) K^+ channel profile and electrical properties of *Arabidopsis* root hairs. FEBS Let 508:463-469

Karley AJ, Leigh RA, Sanders D (2000) Differential ion accumulation and ion fluxes in the mesophyll and epidermis of barley. Plant Physiol 122:835-844

Kato Y, Sakaguchi M, Mori Y, Saito K, Nakamura T, Bakker EP, Sato Y, Goshima S, Uozumi N (2001) Evidence in support of a four transmembrane-pore-transmembrane topology model for the *Arabidopsis thaliana* Na^+/K^+ translocating AtHKT1 protein, a member of the superfamily of K^+ transporters. Proc Natl Acad Sci USA 98:6488-6493

Kim EJ, Kwak JM, Uozumi N, Schroeder JI (1998) AtKUP1: an *Arabidopsis* gene encoding high-affinity potassium transport activity. Plant Cell 10:51-62

Knight H, Trewavas AJ, Knight MR (1997) Calcium signalling in *Arabidopsis thaliana* responding to drought and salinity. Plant J 12:1067-1078

Kochian LV, Lucas WJ (1988) Potassium transport in roots. Adv Bot Res 15:93-178

Köhler C, Merkle T, Neuhaus G (1999) Characterisation of a novel gene family of putative cyclic nucleotide- and calmodulin-regulated ion channels in *Arabidopsis thaliana*. Plant J 18:97-104

Köhler B, Raschke K (2000) The delivery of salts to the xylem. Three types of anion conductance in the plasmalemma of the xylem parenchyma of roots of barley. Plant Physiol 122:243-254

Koyro HW, Stelzer R (1988) Ion concentrations in the cytoplasm and vacuoles of rhizodermis cells from NaCl treated *Sorghum*, *Spartina* and *Puccinellia* plants. J Plant Physiol 133:441-446

Lacan D, Durand M (1996) Na^+-K^+ exchange at the xylem/symplast boundary. Plant Physiol 110:705-711

Lacombe B, Pilot G, Michard E, Gaymard F, Sentenac H, Thibaud JB (2000) A shaker-like K^+ channel with weak rectification is expressed in both source and sink phloem tissues of *Arabidopsis*. Plant Cell 12:837-851

Lacombe B, Becker D, Hedrich R, DeSalle R, Hollmann M, Kwak JM, Schroeder JI, Le Novere N, Nam HG, Spalding EP, Tester M, Turano FJ, Chiu J, Coruzzi G (2001) The identity of plant glutamate receptors. Science 292:1486-1487

Lagarde D, Basset M, Lepetit M, Conejero G, Gaymard F, Astruc S, Grignon C (1996) Tissue-specific expression of *Arabidopsis* AKT1 gene is consistent with a role in K^+ nutrition. Plant J 9:195-203

LaHaye PA, Epstein E (1969) Salt tolerance in plants: enhancement with calcium. Science 166:395-396

Lam M, Bhat MB, Nunez G, Ma JJ, Distelhorst CW (1998) Regulation of Bcl-xl channel activity by calcium. J Biol Chem 273:17307-17310

Läuchli A (1976) Symplasmic transport and ion release to the xylem. In: Wardlaw IF (ed) Transport and transfer processes in plants. Academic Press, New York, pp 101-112

Laurie S, Feeney KA, Maathuis FJM, Heard PJ, Brown SJ, Leigh RA (2002) A role for HKT1 in sodium uptake by wheat roots. Plant J 32:139-149

Leigh RA (2001) Potassium homeostasis and membrane transport. J Plant Nutrit Soil Sci 164:193-198

Leigh RA, Wyn Jones RG (1984) A hypothesis relating critical potassium concentrations for growth to the distribution and functions of this ion in the plant cell. New Phytol 97:1-13

Leigh RA, Chater M, Storey R, Johnston AE (1986) Accumulation and subcellular distribution of cations in relation to the growth of potassium-deficient barley. Plant Cell Environ 9:595-604

Liu JP, Zhu JK (1997) An *Arabidopsis* mutant that requires increased calcium for potassium nutrition and salt tolerance. Proc Natl Acad Sci USA 94:14960-14964

Liu JP, Zhu JK (1998) A calcium sensor homolog required for plant salt tolerance. Science 280:1943-1945

Liu K, Fu HH, Bei QX, Luan S (2000) Inward potassium channel in guard cells as a target for polyamine regulation of stomatal movements. Plant Physiol 124:1315-1325

Maathuis FJM, Amtmann A (1999) K^+ nutrition and Na^+ toxicity: The basis of cellular K^+/Na^+ ratios. Ann Bot 84:123-133

Maathuis FJM, Sanders D (1993) Energization of potassium uptake in *Arabidopsis thaliana*. Planta 191:302-307

Maathuis FJM, Sanders D (1994) Mechanism of high-affinity potassium uptake in roots of *Arabidopsis thaliana*. Proc Natl Acad Sci USA 91:9272-9276

Maathuis FJM, Sanders D (1995) Contrasting roles in ion-transport of two K^+-channel types in root-cells of *Arabidopsis thaliana*. Planta 197:456-464

Maathuis FJM, May ST, Graham NS, Bowen HC, Jelitto TC, Trimmer P, Bennett MJ, Sanders D, White PJ (1998) Cell marking in *Arabidopsis thaliana* and its application to patch-clamp studies. Plant J 15:843-851

Maathuis FJM, Sanders D (1999) Plasma membrane transport in context—making sense out of complexity. Curr Opin Plant Biol 2:236-243

Maathuis FJM, Sanders D (2001) Sodium uptake in *Arabidopsis* roots is regulated by cyclic nucleotides. Plant Physiol 127:1617-1625

MacRobbie EAC (1998) Signal transduction and ion channels in guard cells. Philos Trans R Soc Lond Ser B 353:1475-1488

Marschner H (1995) The mineral nutrition of higher plants. Academic Press, London

Mäser P, Thomine S, Schroeder JI, Ward JM, Hirschi K, Sze H, Talke IN, Amtmann A, Maathuis FJM, Sanders D, Harper JF, Tchieu J, Gribskov M, Persans MW, Salt DE, Kim SA, Guerinot ML (2001) Phylogenetic relationships within cation transporter families of *Arabidopsis*. Plant Physiol 126:1646-1667

Mäser P, Gierth M, Schroeder JI (2002) Molecular mechanisms of potassium and sodium uptake in plants. Plant Soil 247:43-54

Matsushita N, Matoh T (1991) Characterization of Na^+ exclusion mechanisms of salt-tolerant reed plants in comparison with salt-sensitive rice plants. Physiol Plant 83:170-176

Moshelion M, Becker D, Czempinski K, Mueller-Roeber B, Attali B, Hedrich R, Moran N (2002) Diurnal and circadian regulation of putative potassium channels in a leaf moving organ. Plant Physiol 128:634-642

Mouline K, Very AA, Gaymard F, Boucherez J, Pilot G, Devic M, Bouchez D, Thibaud JB, Sentenac H (2002) Pollen tube development and competitive ability are impaired by disruption of a Shaker K^+ channel in *Arabidopsis*. Genes Dev 16:339-350

Munns R (2002) Comparative physiology of salt and water stress. Plant Cell Environ 25:239-250

Munns R, Fisher DB, Tonnet ML (1987) Na^+ and Cl^- transport in the phloem from leaves of NaCl-treated barley. Aust J Plant Physiol 13:757-766

Nakanishi N, Shneider NA, Axel R (1990) A family of glutamate receptor genes—evidence for the formation of heteromultimeric receptors with distinct channel properties. Neuron 5:569-581

Niu XM, Bressan RA, Hasegawa PM, Pardo JM (1995) Ion homeostasis in NaCl stress environments. Plant Physiol 109:735-742

Nublat A, Desplans J, Casse F, Berthomieu P (2001) sas1, an *Arabidopsis* mutant overaccumulating sodium in the shoot, shows deficiency in the control of the root radial transport of sodium. Plant Cell 13:125-137

Pier PA, Berkowitz GA (1987) Modulation of water-stress effects on photosynthesis by altered leaf K^+. Plant Physiol 85:655-661

Pilot G, Lacombe B, Gaymard F, Cherel I, Boucherez J, Thibaud JB, Sentenac H (2001) Guard cell inward K^+ channel activity in *Arabidopsis* involves expression of the twin channel subunits KAT1 and KAT2. J Biol Chem 276:3215-3221

Pilot G, Gaymard F, Mouline K, Cherel I, Sentenac H (2003) Regulated expression of *Arabidopsis* Shaker K^+ channel genes involved in K^+ uptake and distribution in the plant. Plant Mol Biol 51:773-787

Pottosin II, Schöonknecht G (1996) Ion channel permeable for divalent and monovalent cations in native spinach thylakoid membranes. J Membr Biol 152:223-233

Qi Z, Spalding EP (2004) Protection of plasma membrane K^+ transport by the *salt overly sensitive1* Na^+/H^+ antiporter during salinity stress. Plant Physiol 136:2548-2555

Quintero FJ, Blatt MR (1997) A new family of KC transporters from *Arabidopsis* that are conserved across phyla. FEBS Lett 415:206-211

Reintanz B, Szyroki A, Ivashikina N, Ache P, Godde M, Becker D, Palme K, Hedrich R (2002) AtKC1, a silent *Arabidopsis* potassium channel alpha-subunit modulates root hair K^+ influx. Proc Natl Acad Sci USA 99:4079-4084

Rengel Z (1992) The role of calcium in salt toxicity. Plant Cell Environ 15:625-632

Rigas S, Debrosses G, Haralampidis K, Vicente-Agullo F, Feldmann KA, Grabov A, Dolan L, Hatzopoulos P (2001) TRH1 encodes a potassium transporter required for tip growth in *Arabidopsis* root hairs. Plant Cell 13:139-151

Rios G, Ferrando A, Serrano R (1997) Mechanisms of salt tolerance conferred by overexpression of the HAL1 gene in *Saccharomyces cerevisiae*. Yeast 13:515-528

Roberts SK, Tester M (1995) Inward and outward K^+-selective currents in the plasma membrane of protoplasts from maize root cortex and stele. Plant J 8:811-825

Roberts SK, Tester M (1997) Permeation of Ca^{2+} and monovalent cations through an outwardly rectifying channel in maize root stelar cells. J Exp Bot 48:839-846

Rodríguez-Navarro A (2000) Potassium transport in fungi and plants. Biochim Biophys Acta 1469:1-30

Roelfsema MRG, Hedrich R (2002) Studying guard cells in the intact plant: modulation of stomatal movement by apoplastic factors. New Phytol 153:425-431

Rubio F, Gassmann W, Schroeder JI (1995) Sodium-driven potassium uptake by the plant potassium transporter HKT1 and mutations conferring salt tolerance. Science 270:1660-1663

Rubio F, Santa-María GE, Rodríguez-Navarro A (2000) Cloning of *Arabidopsis* and barley cDNAs encoding HAK potassium transporters in root and shoot cells. Physiol Plant 109:34-43

Rus A, Yokoi S, Sharkhuu A, Reddy M, Lee BH, Matsumoto TK, Koiwa H, Zhu JK, Bressan RA, Hasegawa PM (2001) AtHKT1 is a salt tolerance determinant that controls Na^+ entry into plant roots. Proc Natl Acad Sci USA 98:14150-14155

Sanders D (2000) Plant biology: the salty tale of *Arabidopsis*. Curr Biol 10:R486-R488

Santa-María GE, Rubio F, Dubcovsky J, Rodriguez-Navarro A (1997) The HAK1 gene of barley is a member of a large gene family and encodes a high-affinity potassium transporter. Plant Cell 9:2281-2289

Santa-María GE, Danna CH, Czibener C (2000) High-affinity potassium transport in barley roots. Ammonium-sensitive and -insensitive pathways. Plant Physiol 123:297-306

Schachtman DP (2000) Molecular insights into the structure and function of plant K^+ transport mechanisms. Biochim Biophys Acta 1465:127-139

Schachtman DP, Schroeder JI (1994) Structure and transport mechanism of a high-affinity potassium uptake transporter from higher plants. Nature 370:655-658

Schachtman DP, Schroeder JI, Lucas WJ, Anderson JA, Gaber RF (1992) Expression of an inward-rectifying potassium channel by the *Arabidopsis* KAT1 cDNA. Science 258:1654-1658

Schachtman DP, Kumar R, Schroeder JI, Marsh EL (1997) Molecular and functional characterization of a novel low-affinity cation transporter (LCT1) in higher plants. Proc Natl Acad Sci USA 94:11079-11084

Schleyer M, Bakker EP (1993) Nucleotide-sequence and 3'-end deletion studies indicate that the K^+-uptake protein KUP from *Escherichia coli* is composed of a hydrophobic core linked to a large and partially essential hydrophilic-C terminus. J Bacteriol 175:6925-6931

Schroeder JI, Ward JM, Gassmann W (1994) Perspectives on the physiology and structure of inward-rectifying K^+ channels in higher-plants—biophysical implications for K^+ uptake. Annu Rev Biophys Biomol Struct 23:441-471

Schuurink RC, Shartzer SF, Fath A, Jones RL (1998) Characterization of a calmodulin-binding transporter from the plasma membrane of barley aleurone. Proc Natl Acad Sci USA 95:1944-1949

Serrano R (1996) Salt tolerance in plants and microorganisms: toxicity targets and defense responses. Int Rev Cytol 165:1-52

Shabala S (2000) Ionic and osmotic components of salt stress specifically modulate net ion fluxes from bean leaf mesophyll. Plant Cell Environ 23:825-837

Shabala S (2003) Regulation of potassium transport in leaves: from molecular to tissue level. Ann Bot 92:627-634

Shabala S, Shabala L, van Volkenburgh E (2003) Effect of calcium on root development and root ion fluxes in salinised barley seedlings. Funct Plant Biol 30:507-514

Shabala S, Shabala L, van Volkenburgh E, Newman I (2005) Effect of divalent cations on ion fluxes and leaf photochemistry in salinised barley leaves. J Exp Bot 56:1369-1378

Shi HZ, Ishitani M, Kim CS, Zhu JK (2000) The *Arabidopsis thaliana* salt tolerance gene SOS1 encodes a putative Na^+/H^+ antiporter. Proc Natl Acad Sci USA 97:6896-6901

Shi HZ, Quintero FJ, Pardo JM, Zhu JK (2002) The putative plasma membrane Na^+/H^+ antiporter SOS1 controls long-distance Na^+ transport in plants. Plant Cell 14:465-477

Shi HZ, Lee BH, Wu SJ, Zhu JK (2003) Overexpression of a plasma membrane Na^+/H^+ antiporter gene improves salt tolerance in *Arabidopsis thaliana*. Nature Biotechnol 21:81-85

Song CP, Guo Y, Qiu QS, Lambert G, Galbraith DW, Jagendorf A, Zhu JK (2004) A probable $Na^+(K^+)/H^+$ exchanger on the chloroplast envelope functions in pH homeostasis and chloroplast development in *Arabidopsis thaliana*. Proc Natl Acad Sci USA 101:10211-10216

Su H, Golldack D, Zhao CS, Bohnert HJ (2002) The expression of HAK-type K^+ transporters is regulated in response to salinity stress in common ice plant. Plant Physiol 129:1482-1493

Szyroki A, Ivashikina N, Dietrich P, Roelfsema MRG, Ache P, Reintanz B, Deeken R, Godde M, Felle H, Steinmeyer R, Palme K, Hedrich R (2001) KAT1 is not essential for stomatal opening. Proc Natl Acad Sci USA 98:2917-2921

Tester M, Davenport R (2003) Na^+ tolerance and Na^+ transport in higher plants. Ann Bot 91:503-527

Treeby MT, van Steveninck RFM (1988) Effects of salinity and phosphate on ion distribution in lupin leaflets. Physiol Plant 73:317-322

Tyerman SD (2002) Nonselective cation channels. Multiple functions and commonalities. Plant Physiol 128:327-328

Tyerman SD, Skerrett IM (1999) Root ion channels and salinity. Sci Hort 78:175-235

Tyerman SD, Skerrett M, Garrill A, Findlay GP, Leigh RA (1997) Pathways for the permeation of Na^+ and Cl^- into protoplasts derived from the cortex of wheat roots. J Exp Bot 48:459-480

Uozumi N, Kim EJ, Rubio F, Yamaguchi T, Muto S, Tsuboi A, Bakker EP, Nakamura T, Schroeder JI (2000) The *Arabidopsis* HKT1 gene homolog mediates inward Na^+ currents in *Xenopus laevis* oocytes and Na^+ uptake in *Saccharomyces cerevisiae*. Plant Physiol 122:1249-1259

Venema K, Quintero FJ, Pardo JM, Donaire JP (2002) The Arabidopsis Na^+/H^+ exchanger AtNHX1 catalyzes low affinity Na^+ and K^+ transport in reconstituted liposomes. J Biol Chem 277:2413-2418

Venema K, Belver A, Marin-Manzano MC, Rodriguez-Rosales MP, Donaire JP (2003) A novel intracellular K^+/H^+ antiporter related to Na^+/H^+ antiporters is important for K^+ ion homeostasis in plants. J Biol Chem 278:22453-22459

Véry AA, Sentenac H (2002) Cation channels in the *Arabidopsis* plasma membrane. Trends Plant Sci 7:168-175

Véry AA, Sentenac H (2003) Molecular mechanisms and regulation of K^+ transport in higher plants. Annu Rev Plant Biol 54:575-603

Volkov V, Wang B, Dominy PJ, Fricke W, Amtmann A (2003) *Thellungiella halophila*, a salt-tolerant relative of *Arabidopsis thaliana*, possesses effective mechanisms to discriminate between potassium and sodium. Plant Cell Environ 27:1-14

Walker DJ, Leigh RA, Miller AJ (1996) Potassium homeostasis in vacuolate plant cells. Proc Natl Acad Sci USA 93:10510-10514

Wang TB, Gassmann W, Rubio F, Schroeder JI, Glass ADM (1998) Rapid up-regulation of HKT1, a high-affinity potassium transporter gene, in roots of barley and wheat following withdrawal of potassium. Plant Physiol 118:651-659

Ward JM (2001) Identification of novel families of membrane proteins from the model plant *Arabidopsis thaliana*. Bioinformatics 17:560-563

White PJ (1997) Cation channels in the plasma membrane of rye roots. J Exp Bot 48:499-514

White PJ, Tester MA (1992) Potassium channels from the plasma-membrane of rye roots characterized following incorporation into planar lipid bilayers. Planta 186:188-202

White PJ, Marshall J, Smith JAC (1990) Substrate kinetics of the tonoplast H^+-translocating inorganic pyrophosphatase and its activation by free Mg^{2+}. Plant Physiol 93:1063-1070

Winter E (1982) Salt tolerance of *Trifolium alexandrinum* L. III. Effects of salt on ultrastructure of phloem and xylem transfer cells in petioles and leaves. Aust J Plant Physiol 9:227-237

Wu WH, Berkowitz GA (1992) Stromal pH and photosynthesis are affected by electroneutral K^+ and H^+ exchange through chloroplast envelope ion channels. Plant Physiol 98:666-672

Wu SJ, Ding L, Zhu JK (1996) SOS1, a genetic locus essential for salt tolerance and potassium acquisition. Plant Cell 8:617-627

Xia T, Apse MP, Aharon GS, Blumwald E (2002) Identification and characterization of a NaCl-inducible vacuolar Na^+/H^+ antiporter in *Beta vulgaris*. Physiol Plant 116:206-212
Yao W, Hadjeb N, Berkowitz GA (1997) Molecular cloning and characterization of the first plant K(Na)/proton antiporter. Plant Physiol 114S:200
Yokoi S, Quintero FJ, Cubero B, Ruiz MT, Bressan RA, Hasegawa PM, Pardo JM (2002) Differential expression and function of *Arabidopsis thaliana* NHX Na^+/H^+ antiporters in the salt stress response. Plant J 30:529-539
Zhang HX, Blumwald E (2001) Transgenic salt-tolerant tomato plants accumulate salt in foliage but not in fruit. Nature Biotechnol 19:765-768
Zhang HX, Hodson JN, Williams JP, Blumwald E (2001) Engineering salt-tolerant *Brassica* plants: Characterization of yield and seed oil quality in transgenic plants with increased vacuolar sodium accumulation. Proc Natl Acad Sci USA 98:12832-12836
Zhu JK (2000) Genetic analysis of plant salt tolerance using *Arabidopsis*. Plant Physiol 124:941-948
Zhu JK (2002) Salt and drought stress signal transduction in plants. Annu Rev Plant Biol 53:247-273
Zhu JK (2003) Regulation of ion homeostasis under salt stress. Curr Opin Plant Biol 6:441-445
Zhu JK, Liu JP, Xiong LM (1998) Genetic analysis of salt tolerance in *Arabidopsis*: evidence for a critical role of potassium nutrition. Plant Cell 10:1181-1191

14 Electrophysiology in Mechanosensing and Wounding Response

TERUO SHIMMEN

14.1 Mechanosensing

14.1.1 Responses of plants to mechanical stimulus

Touch induces rapid leaf movement in "sensitive" plants such as *Mimosa pudica*. This characteristic response indicates the recognition of mechanical stimuli, and it is termed thigmonasty or seismonasty. On the other hand, "insensitive" plants move passively in response to touch. The passive movement is believed to indicate a lack of recognition. However, this is not the case. After daily touching, the plants become shorter and thicker. Increased thickness reinforces the physical strength of the plant, therefore reducing the impact of mechanical stress on the plants. According to Jaffe and Forbes (1993), this phenomenon is termed thigmomophogenesis. Aequorin-expressing, transgenic plants undergo increases in cytoplasmic free Ca^{2+}, a second messenger (Knight et al. 1992). Thus, it is clear that even insensitive plants can sense mechanical stimuli.

In the plasma membrane, ionic processes are believed to play important roles in stimulus-perception and signal processing. Electrophysiological techniques are useful when monitoring the rapid ionic processes in the mechanosensing of plants.

14.1.2 Receptor potential in higher plants

Since the perception of the stimuli can easily be visualized, action plants are frequently utilized in mechanosensing analysis. *M. pudica* is the most common plant used in this type of investigation (Fig. 14.1). The leaves are equipped with three types of motile structures: main pulvinus (primary pulvinus), sub-pulvinus (secondary pulvinus) and pulvinule (tertiary pulvinus). These structures are responsible for movement of the petiole, pinna, and leaflet, respectively. The mechanosensitive leaf movement of *M. pudica* has been extensively studied. In the first step of mechanoperception, mechanical

Department of Life Science, Graduate School of Life Science, Himeji Institute of Technology, Harima Science Park City, Hyogo, 678-1297 Japan

Plant Electrophysiology – Theory & Methods (ed. by Volkov)

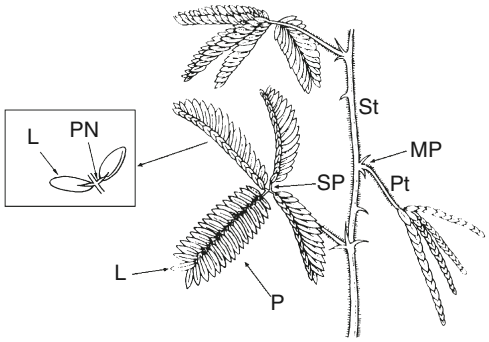

Fig. 14.1. Leaf movement of *Mimosa pudia*. Leaf is equipped with three kinds of motile structures, main pulvinus (*MP*), sub-pulvinus (*SP*) and pulvinule (*PN*), and responsible for movement of petiole (*Pt*), pinna (*P*) and leaflet (*L*), respectively. *St* stem. *Left leaves*: before stimulation. *Right leaf*: after stimulation. (Modified from Ishikawa 2003)

stimuli must be transformed into electrical signals or receptor potentials. Sibaoka (personal communication) suggested that pulvini are mechanosensitive organs. However, the sensory cell has not been identified in this material.

Receptor cells have been identified in action plants such as the terrestrial *Dionaea muscipula* and aquatic *Aldrovanda vesiculosa*. Although their habitats are different, both plants are carnivorous. The leaves are modified as traps for prey, and each trap is composed of paired lobes containing sensory hairs. The lobes are connected by the motile midrib (Fig. 14.2). When the sensory hairs are bent by the prey, the trap quickly closes to catch the prey.

In case of *A. vesiculosa*, each lobe has 20 sensory hairs. Individual hairs have four small sensory cells. Using sophisticated techniques, Iijima and Sibaoka analyzed the receptor potentials and action potentials (Sibaoka 1991) (Fig. 14.3). One microelectrode was inserted into a sensory cell and other into an epidermal cell of a lobe. When a stimulus was applied by bending the hair, the receptor cell showed depolarization. The amplitude of the depolarization increased as the bending force increased, indicating that the response is a receptor potential. When depolarization reaches its threshold level, an action potential is recorded in a cell of a lobe. This action potential is transmitted to the midrib of the trap, inducing closure. The receptor potentials and action potentials were generated upon mechanical stimulation. Voltage-sensitive and mechanosensitive ion channels should be involved, respectively.

14.1.3 Analysis of receptor potential in Characean cells

Internodal cells of Characeae have been useful materials for the study of plant electrophysiology for the following reasons: (1) due to the simple morphology, the electrical responses of a target cell can be easily measured, (2) since

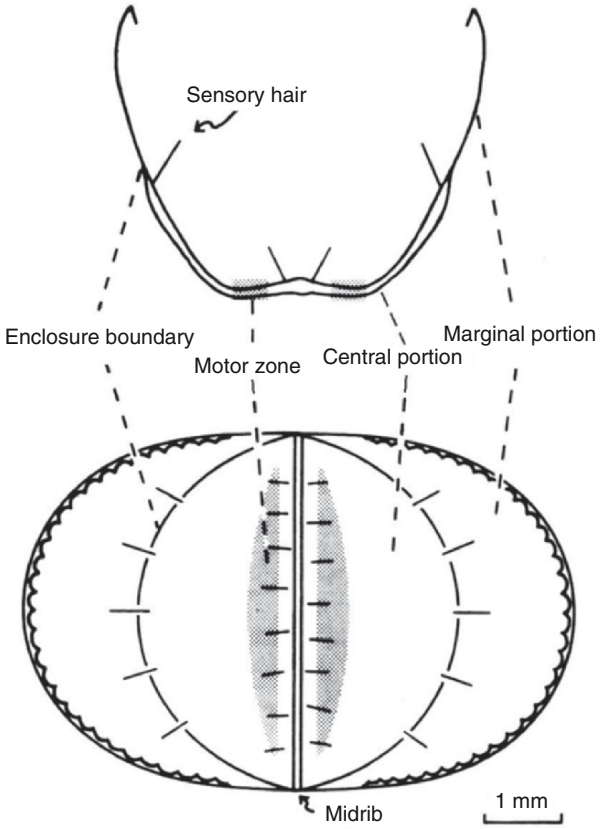

Fig. 14.2. Trap of *Aldrovanda vesiculosa*. Cross-section (*upper*) and upper view (*lower*). (Modified from IIjima and Sibaoka 1981)

internodal cells are large and cylindrical, various cell surgery techniques such as cutting, ligating and intracellular perfusion, can be applied, and (3) Since Characeae is an aquatic plant, electrical measurement can be carried out under their native external condition, aquatic solution. Three genera of Characeae are generally used: *Chara, Nitella* and *Nitellopsis*.

Kishimoto (1968) was the first to successfully record a receptor potential upon mechanical stimulation in Characeae. He stimulated one portion of an internodal cell using an electromagnet. Staves and Wayne (1993) stimulated an internodal cell of *Chara* using a micromanipulator analyzing action potentials but not receptor potentials. Shimmen (1996) developed a simple method to analyze receptor potentials and action potentials induced by mechanical stimulation (Fig. 14.4). A cell is separated into two halves, and the potential difference between pools A and B is measured. A small glass rod (stimulator) is placed on the cell. The cell is stimulated by dropping glass tubing onto the

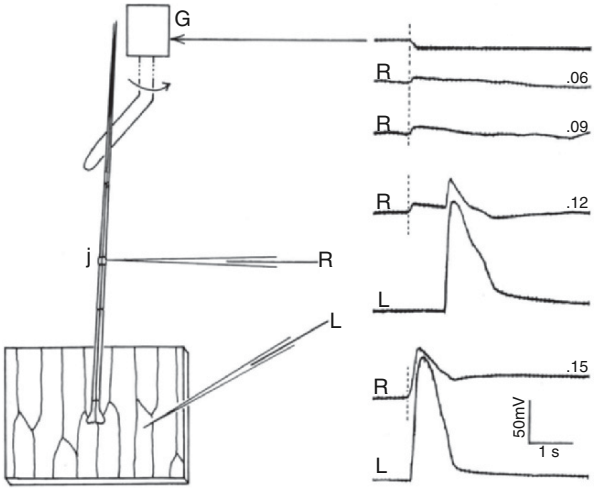

Fig. 14.3. Measurement of electrical responses in *Aldrovanda vesiculosa* on mechanical stimulation. **A** Microelectrodes were inserted into either a sensory cell at the joint (*j*) of a sensory hair (*R*) and into a epidermal cell of lobe (*L*). *G* Distal position of the hair is pushed with a fine glass rod connected to a pen-writing galvanometer. **B** Electrical responses in sensory cell (*R*) and lobe cell (*L*). (Modified from Sibaoka 1991)

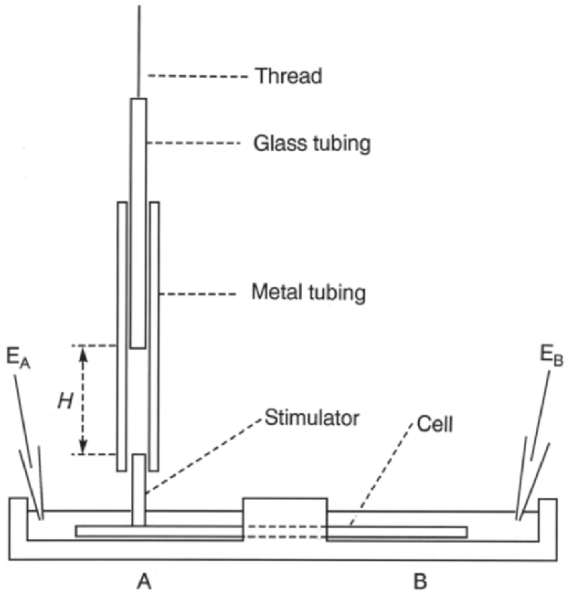

Fig. 14.4. Apparatus for measurement of receptor potential and action potential in internodal cell of *Characeae* upon mechanical stimulation. An internodal cell is separated into two halves (**A**, **B**) and the potential difference is measured using two electrodes (E_A and E_B). *H* height from which glass tubing is dropped. Fixed metal tubing is used as a guide to drop glass tubing onto Stimulator. (Cited from Shimmen 1996)

stimulator. The strength of the stimulation can be controlled by either changing the weight of the glass tubing or changing the height from which the glass tubing is dropped.

A typical measurement is shown in Fig. 14.5. The strength of stimulation was controlled by changing the height from which the glass tubing was dropped. With an increase in stimulation strength, the amplitude of the receptor potential also increased. When depolarization reached the threshold level, an action potential was induced in the cell part in pool A due to activation of a voltage-sensitive channel. It transmitted to the cell part in pool B.

To analyze the ionic mechanism for generation of receptor potentials, the membrane potential must be measured but not the change in membrane potential, since the relation between membrane potential and equilibrium potential for ions across the membrane must be compared. It is not recommended to use microelectrodes in studies where drastic mechanical stimulation is applied to the cell. In Characean cells, membrane potential can be measured without inserting microelectrodes (Shimmen et al. 1976). When the external K^+ concentration was increased up to 100 mM in pool B (Fig. 14.4),

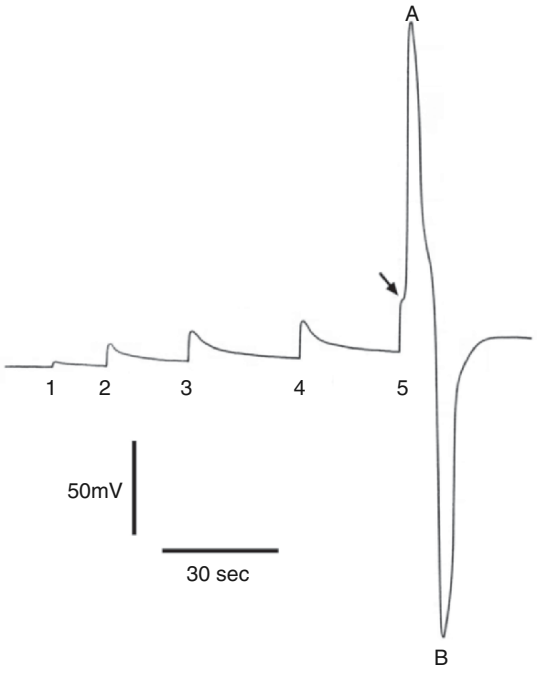

Fig. 14.5. Receptor potentials and action potentials induced by mechanical stimulation in *Chara* internodal cell. Cell was stimulated using a apparatus shown in Fig. 14.4. Numbers in the figure show height from which a glass tubing (1.3 g) was dropped. When depolarization of a receptor potential reached a threshold (*arrow*), action potential was induced first in the cell part in pool A (**A**) and then it was transmitted to the cell part in pool B (**B**). (Cited from Shimmen 1996)

membrane potential of the cell part B depolarizes to about 0 mV. Therefore, potential difference measured between pools A and B represents membrane potential of the cell part in the pool A. Sorbitol (180 mM) isotonic to 100 mM KCl must be added to pool B.

Membrane potentials of plant cell comprise two components: a passive diffusion component and an active component generated by electrogenic H^+-pump (Shimmen and Tazawa 1977). The resting membrane potential of *Chara* is more negative than −200 mV. Two possibilities are suggested for membrane depolarization upon mechanical stimulation: either inhibition of the electrogenic proton pump or change of ion channel permeability. When cells were treated with N, N′-cyclohexylcarbodiimide, an inhibitor of H^+-pump, the resting membrane potential depolarized to about −130 mV indicating that the pump was inhibited. However, the amplitude of receptor potential did not change after inhibition of the pump (Shimmen 1997a). In addition, it was found that electrical resistance decreased during generation of a receptor potential (Shimmen 1997c). These results indicate that a receptor potential is generated by activation of ion channel(s) but not by inhibition of the electrogenic H^+-pump.

Ca^{2+} and Cl^- channels are candidates for membrane depolarization in the generation of receptor potentials since the equilibrium potential of these ions across the plasma membrane are positive inside. Various inhibitors of these ion channels failed to inhibit receptor potentials (Shimmen 1997a). However, more recent experiments indicated that activation of the Cl^- channel is involved (Fig. 14.6). When 100 mM KCl was added to the external medium, membrane potential depolarized to 0 mV. The membrane potential changed

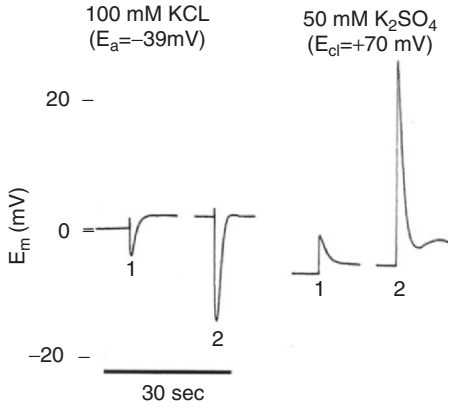

Fig. 14.6. Electric response induced by mechanical stimulation of *Chara* cell under K^+-induced depolarization. By applying 100 mM K^+ to the external medium, membrane potential depolarize to the level close to 0 mV. Upon mechanical stimulation, response to the negative direction is induced in the presence of 100 mM KCl and that to the positive direction in the presence of 50 mM K_2SO_4 (1.3 mM Cl^-). Numbers in the figure show the height from which glass tubing was dropped. Equilibrium potential for Cl^- across the plasma membrane (ECl^-) is shown. (Modified from Shimmen 1997b)

to the negative direction upon mechanical stimulation. When 50 mM K_2SO_4 (containing 1.3 mM Cl^-) was added to the external medium, the membrane potential changed to the positive direction upon mechanical stimulation. Assuming the Cl^- concentration of the cytopolasm to be 21 mM (Tazawa et al. 1974), equilibrium potential for Cl^- is calculated to be –39 mV in the presence of 100 mM Cl^- and +70 mV in the presence of 1.3 mM Cl^- in the external medium. Thus, the membrane potential changes to the direction of equilibrium potential for Cl^- upon mechanical stimulation, indicating activation of the Cl^- channel (Shimmen 1997b).

Kaneko et al. (2005) found an increase in cytoplasmic Ca^{2+} upon mechanical stimulation. They microinjected aequorin into the cytoplasm. Since an action potential was generated by activation of both Ca^{2+} and Cl^- channels (Shimmen et al. 1994), cytoplasmic Ca^{2+} also increased (Williamson and Ashley 1982). Therefore, experiments were carried out in the presence of a high K^+ concentration which inhibits generation of an action potential. Mechanical stimulation induced a significant increase in light emission from cytoplasmic aequorin, suggesting that Ca^{2+} channel was activated. One of the characteristics of the receptor potential is its graded increase to stimulus intensity. Since the extent of light emission was dependent on the amplitude of stimulation, it was suggested that the Ca^{2+} channel be dedicated to the generation of receptor potentials. To answer the question of which channel is mechanosensitive or if both channels are mechanosensitive, it has been reported that the characean plasma membrane is equipped with the Ca^{2+}-activatable Cl^- channel (Shiina and Tazawa 1988; Mimura and Shimmen 1994). Therefore, a possibility is suggested that Cl^- channel is activated by Ca^{2+} flowing into the cell through mechanosensitive Ca^{2+} channels. However, the possibility still remains that both channels are mechanosensitive.

14.1.4 Stretch-activated channel

Development of the patch-clamp method brought revolutionary change in electrophysiology. This made it possible to analyze close-open response in a single ion channel. This method also made it possible to identify stretch-activated ion channels (SA channel). SA channels are activated by the stretching of the membranes due to application of suction force to a measuring pipette. Such SA channels have been identified in epidermal cells of higher plants. Ding and Pickard (1993) found Ca^{2+}-selective SA channels. Falk et al. (1988) and Qi et al. (2004) found anion-selective SA channels. However, it cannot be concluded that these SA-channels are involved in mechanosensing.

14.1.5 Signal transmission by action potential

The occurrence of action potentials has been reported in various plant materials (Davies 1987). As seen in *D. muscipula* and *A. vesiculosa*, an action potential is initiated by a receptor potential and transmitted to the motile

cells of midrib to induce movement. Thus, an action potential is dedicated to the transmission of signals in plants as in the case of animal nerve cells. In both carnivorous plant species, the peak potential of action potentials changes to the positive direction when extracellular Ca^{2+} concentration was increased (Iijima and Sibaoka 1985; Hodick and Sievers 1986), suggesting that the Ca^{2+} channel is dedicated to the generation of action potentials.

14.1.6 Ionic mechanism of action potential analyzed in Characeae

Ionic mechanism of action potentials has been studied extensively in characean cells. Since the generation of action potential is dependent on both intracellular and extracellular chemical composition, modification of chemical composition at both sides of the plasma membrane is recommended. The development of an intracellular perfusion technique made it possible to control intracellular chemical composition in characean cells (Tazawa et al. 1976). After cutting both ends of an internodal cell, vacuolar space is perfused with an artificial medium. By this procedure, natural vacuolar sap is replaced with a perfusion medium (Fig. 14.7b). When a Ca^{2+}-chelator is contained in the perfusion medium, the tonoplast is disintegrated (tonoplast-free cell) (c). By the following perfusion, chemical composition inside the plasma membrane can be thoroughly controlled (d). Using this tonoplast-free cell, ATP-dependent generation of the membrane potential due to the activity of the electrogenic H^+ pump was unequivocally demonstrated (Shimmen and Tazawa 1977).

Since both equilibrium potentials for Ca^{2+} and Cl^- are inside positive, involvement of these ions in generation of action potentials has been suggested: influx of Ca^{2+} and efflux of Cl^-. When cytoplasmic Cl^- concentration was decreased to 0.01 mM in tonoplast-free cells, action potentials were still generated (Shimmen and Tazawa 1978). Since the Cl—hypothesis was prevalent at that time, this result was confusing. However, this suggested that the action potential was generated by activation of Ca^{2+} channel. Accordingly, increase in Ca^{2+} influx upon generation of action potentials was demonstrated (Hayama et al. 1979; Shiina and Tazawa 1987b).

Upon membrane excitation, increase in Cl^- efflux had also been reported (Oda 1976; Kikuyama 1986a; Shiina and Tazawa 1987a), indicating activation of Cl^- channel upon excitation. Analysis using tonoplast-free cells demonstrated the presence of Ca^{2+}-activated Cl^- channel in the plasma membrane. When intracellular Ca^{2+} was increased by the perfusion, Cl^- efflux increased significantly (Shiina and Tazawa 1988; Mimura and Shimmen 1994). Thus, it is believed that Ca^{2+} flow into the cell activates the Ca^{2+}-activated Cl^- channel of the plasma membrane. In tonoplast-free cells, Cl^- efflux during membrane excitation is not observed (Kikuyama et al. 1984). This is reasonable since Ca^{2+} should be bound by a Ca^{2+} chelator,

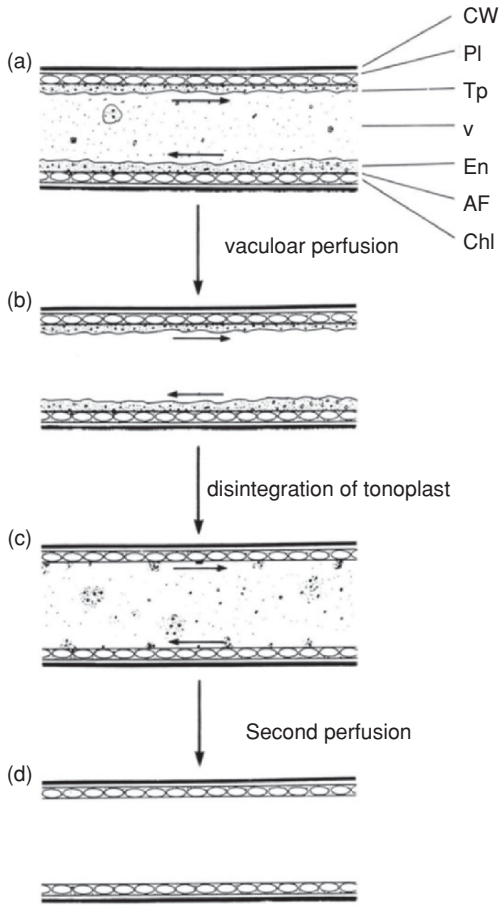

Fig. 14.7. Intracellular perfusion in internodal cells of Characeae. (a) Before treatment. (b) After butting both cell ends, the vacuolar sap was replaced with an artificial medium by intracellular perfusion. (c) Disintegration of tonoplast (tonoplast-free cell). Perfusion medium and cytoplasmic component is mixed. (d) By intracellular perfusion, chemical composition just inside the plasma membrane can be controlled. *CW* cell wall, *Pl* plasma membrane, *Tp* tonoplast (vacuolar membrane), *V* vacuole, *En* streaming sol endoplasm, *AF* bundles of actin filament responsible for cytoplasmic streaming, *Chl* chloroplast fixed to the gel layer. *Arrows* indicate direction of cytoplasmic streaming. (Cited from Shimmen 1988)

which had been introduced into the cell by the intracellular perfusion. It was found that significant increase in Cl^- efflux did not occur occasionally, even when an intact cell generated an action potential (Kikuyama et al. 1984). It is believed that activation of Cl^- channel was uncoupled because of unidentified mechanism. Thus, both Ca^{2+} and Cl^- channels are involved in generation of action potentials in Characeae.

14.1.7 Control by action potential

14.1.7.1 Turgor movement in M. pudica

Transmission of signals via action potentials in *D. muscipula* and *A. vesiculosa* is analogous to that of nerve cell. When an action potential of an axon reached the surface of the skeletal muscle, an action potential was generated at the plasma membrane of the muscle cell, triggering contraction. Thus, the action potential of the effector cell causes a specific response. A similar situation can be envisaged in *M. pudica*. When an action potential of the petiole reached a main pulvinus, an action potential is induced in cortex cells of the pulvinus, and downward movement of the petiole is induced (turgor movement). Samejima and Sibaoka (1980) inserted Cl—sensitive electrodes into the cortex of the main pulvinus. Since the tip of the electrode is located in the apoplast (cell wall outside of the cortex cell), an increase in Cl^- concentration indicates efflux of Cl^- from cortex cells. Action potentials are observed in both upper and lower sides of the pulvinus upon stimulation. However, significant efflux of Cl^- occurs only in cells of the lower side (Fig. 14.8). Kumon and Tsurumi (1984) found a significant increase in extracellular K^+ at the lower cortex of a main pulvinus in photo-stimulated movement. Thus, significant ion efflux occurs in the lower cortex but not in the upper cortex of the main pulvinus. The imbalance of turgor pressure between upper and lower parts causes quick downward movement of the petiole. Involvement of protein phosphorylation in this turgor movement was reported (Kameyama et al. 2000). The relation between protein phosphorylation and turgor movement remains to be solved.

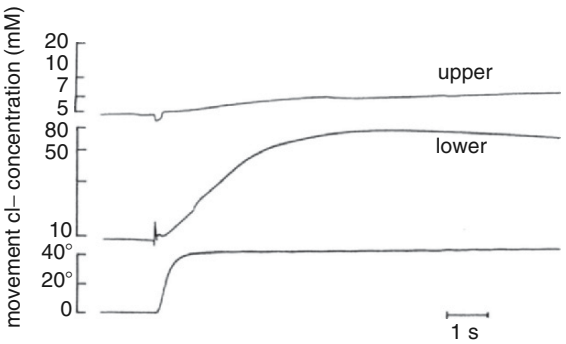

Fig. 14.8. Cl^- efflux from cortex cells of main pulvinus of *Mimosa pudica*. Cl^- electrodes had been inserted into the extracellular space of cortex. When cortex cells generated an action potential, Cl^- efflux (increase in extracellular Cl^- concentration) occurs in lower cortex but not in upper cortex. (Cited from Samejima and Sibaoka 1980)

14.1.7.2 Intracellular signal processing induced by action potential

In *M. pudica*, intracellular processes induced by action potential are not known. In Characeae, however, signal processing upon excitation of the plasma membrane has been studied extensively. It is believed that Ca^{2+} flows into the cell via voltage-sensitive Ca^{2+} channels during action potential. Increase in cytoplasmic free Ca^{2+} during membrane excitation has been demonstrated using aequorin emission (Williamson and Ashley 1982; Kikuyama and Tazawa 1983). Increased cytoplasmic Ca^{2+} works as a second messenger to induce physiological phenomena.

14.1.7.2.1 Tonoplast action potential

When an action potential was generated at the plasma membrane, a potential change at the tonoplast to the inside positive direction was induced (tonoplast action potential: references cited in Shimmen and Nishikawa 1988). In most characean species, it is difficult to distinguish between action potentials at the plasma membrane and the tonoplast. In *Nitella flexilis*, however, generation of these action potentials is temporally separated (Shimmen and Nishikawa 1988). In Fig. 14.9, an internodal cell of *N. flexilis* was mechanically stimulated. When the membrane potential reached its threshold upon generation of a receptor potential, quick action potential at the plasma membrane is induced (arrow) and then the slow action potential at the tonoplast is induced.

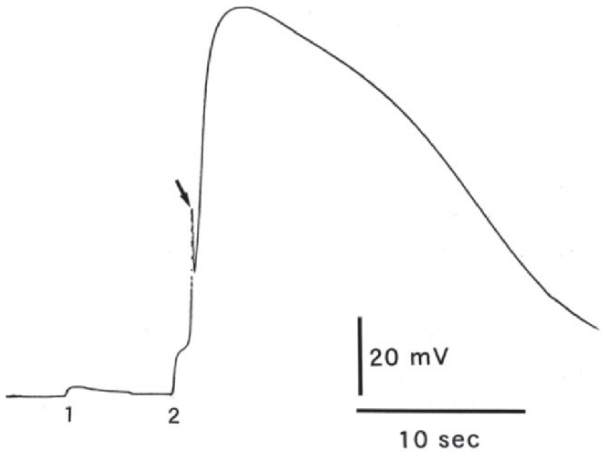

Fig. 14.9. Tonoplast action potential in *Nitella flexilis*. Internodal cell was mechanically stimulated as shown in Fig. 14.4. Numbers show height from which glass tubing was dropped. When glass tubing was dropped from the position of 2 cm high, large receptor potential was generated and then an action potential at plasma membrane was (*arrow*). With a slight delay, large action potential at the tonoplast was induced (original figure)

Tonoplast action potential is caused by activation of the Cl^- channel of the tonoplast (Kikuyama and Tazawa 1976; Shimmen and Nishikawa 1988). Permeabilization of the plasma membrane by plasmolysis method, developed for studying cytoplasmic streaming of characean cells, was also useful for the analysis of the tonoplast function (Shimmen and Tazawa 1983). Using a permeabilized cell, the presence of two proton pumps in the tonoplast was unequivocally demonstrated (Shimmen and MacRobbie 1987). Kikuyama (1988) found that application of Ca^{2+} to the external medium induced Cl^- efflux from the vacuole in permeabilized *Nitella* internodal cells. In addition, injection of Ca^{2+} into the cytoplasm of an intact *Nitella* cell induced a potential change at the tonoplast (Kikuyama 1986b). These facts indicate that the characean tonoplast is equipped with a Ca^{2+}-activated Cl^- channel.

14.1.7.2.2 Cytoplasmic streaming

Characeae has been also a suitable material for studies on cytoplasmic streaming (cf. Kamiya 1986). It has been established that the motive force is generated by the actin–myosin system (Shimmen and Yokota 2004). As early as in 1921, Lauterbach found that the cytoplasmic streaming of characean cell stops upon application of the mechanical stimuli (Kamiya 1959). It became evident that action potentials mediate mechanoperception and stoppage of cytoplasmic streaming. Involvement of Ca^{2+} as a second messenger was first suggested by an experiment of Barry (1968). *Nitella* cells generated action potentials in the medium containing $CaCl_2$, $MgCl_2$, $BaCl_2$ or $SrCl_2$, suggesting that the voltage-sensitive channel responsible for generation of an action potential is permeable to these divalent cations in the *Nitella* species. In the presence of either $MgCl_2$ or $BaCl_2$, uncoupling between excitation and stoppage of streaming is induced. However, increase in $CaCl_2$ concentration in these media containing either $MgCl_2$ or $BaCl_2$ relieved the cell from uncoupling, suggesting an essential role of Ca^{2+}. Increase in Ca^{2+} influx (Hayama et al. 1979; Shiina and Tazawa 1987b) and that in cytoplasmic free Ca^{2+} (Williamson and Ashley 1982; Kikuyama and Tazawa 1983) suggest that Ca^{2+} is involved in stoppage of cytoplasmic streaming. Using permeabilized cell, cytoplasmic streaming was found to be inhibited by Ca^{2+} of physiological concentrations, μM order (Tominaga et al. 1983). Although involvement of protein phosphorylation was suggested based on pharmacological analysis, the relation between the increase in Ca^{2+} and protein phosphorylation has not yet been found (Tominaga et al. 1987).

14.1.7.2.3 Signal processing in characean cell upon mechanical stimulation

Figure 14.10 depicts the possible signal processing induced by action potential in characean cells. Upon mechanical stimulation, a receptor potential is generated due to the activation of mechanosensitive Ca^{2+} and/or Cl^- channel (not shown). When the membrane potential reached a threshold level, action potentials are generated due to the activation of voltage-sensitive Ca^{2+}

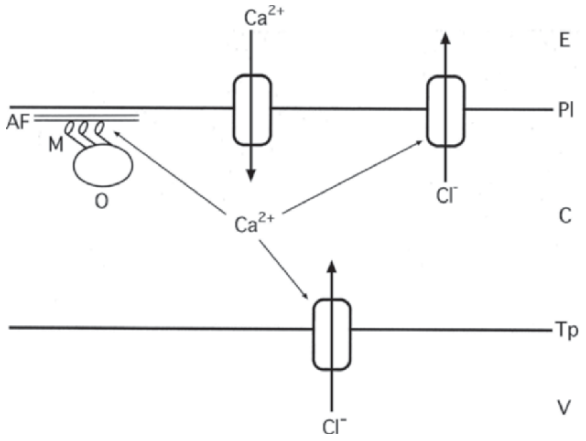

Fig. 14.10. Signal processing upon activation of voltage sensitive Ca^{2+} channel in characean cells. Ca^{2+} activates Cl^- channels of plasma membrane and that of tonoplast, and inhibits actin–myosin system. *Thick arrows* show flux of ions and *thin ones* show effect of Ca^{2+} *AF* bundle of actin filaments, *M* myosin, *O* organelle (original figure)

channel, resulting in the increase of cytoplasmic free Ca^{2+}. Ca^{2+} works as a second messenger and activates Cl^- channels of the plasma membrane and the tonoplast. It inhibits the actin–myosin system, causing stoppage of cytoplasmic streaming. It is not evident whether mechanosensitive and voltage-sensitive Ca^{2+} channels of the plasma membrane are the same or not. The possibility also remains that Ca^{2+} is mobilized not only from the cell exterior but also from intracellular organelles.

14.2 Wounding response

14.2.1 Electrical response in wounded plants

Plants show various responses to wounding and membrane depolarization is the earliest response shown. In some plants, electrical response is induced at the limited region near the wounding (Mertz and Hignbotham 1976; Stahlberg and Cosgrove 1994; Meyer and Weisenseel 1997). On the other hand, action potentials and/or variation potentials propagate systemically in many plants (Frachisse et al. 1985; Robin 1985; Robin and Bonnemain 1985; Julien et al. 1991; Julien and Frachisse 1992; Fromm and Eschrich 1993; Rhodes et al. 1996; Stankovic and Davies 1996). The shape and amplitude of variation potentials (or slow waves) are variable, showing a clear contrast with action potentials. Involvement of electrical signaling in systemic synthesis of proteinase inhibitor in wounded tomato plants clearly showed

the importance of membrane phenomena in the wounding response of plants (Wildon et al. 1992).

14.2.1.1 Leaf movement in Mimosa pudica

Signal transmission upon wounding had been extensively documented in *M. pudica*. Three types of signal has been suggested: m-wave (1.5–4 cm/s), s-wave (0.2–0.5 cm/s) and r-wave (6–12 cm/s). The entity of the m-wave is an action potential, and it cannot pass through the pulvinus. The s-wave is a variation potential associated with movement of unidentified substance. The s-wave can pass through a pulvinus. The entity of the r-wave has not been identified. Severe stimuli such as burning or cutting induce both the m-wave and the s-wave. Mild stimulation such as an electrical current or the application of cold water induces only the m-wave (Robin 1979; Sibaoka 1981).

When a severe stimulus was applied to one terminal leaflet of a pinna by heating, both the m-wave and the s-wave were generated [Fig. 14.11 (1)]. The action potential stimulated the pulvinule but could not pass through it. The s-wave entered the pinna-rachis, and an action potential was generated. This new action potential was transmitted basipetally and successively stimulated pulvinules to induce closure of the leaflets (2). The action potential stimulates the sub-pulvinus (1) to induce movement of the pinna. At this step, movement in the leaf was not observed for a while since the action potential could not pass the sub-pulvinus. During this quiet period, the s-wave moved basipetally in the pinna-rachis and entered the petiole. A new action potential was generated,

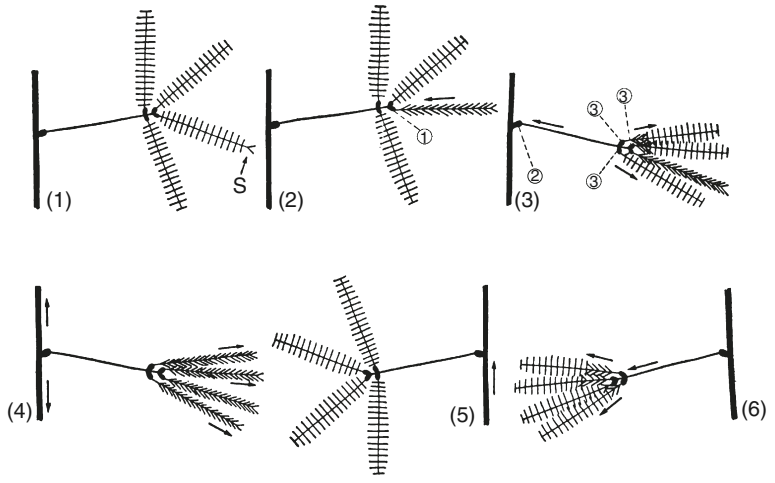

Fig. 14.11. Signal transmission upon wounding terminal leaflet as speculated from leaf movement. *s* Terminal leaflet was stimulating by heating. *Arrows* indicate the direction of signal transmission. For explanation, see text. (Cited from Sibaoka 1964)

and it stimulated three other sub-pulvini (3). It moved basipetally in the petiole and stimulated the main pulvinus (2).

The s-wave entered the pinna-rachis of the three other pinnas and generated new action potentials. These action potentials were transmitted acropetally and induced closure of leaflets in each pinna (3, 4) When the heat stimulus was strong enough, the s-wave entered the stem by passing through the main pulvinus and induced the movement in other upper and lower leaves (4–6). Thus, signal transmission can be observed without electrical instrument in *M. pudica*.

14.2.1.2 Propagation of action potential and variation potential

The generation of an electrical response in a leaf of *M. pudica* is shown in Fig. 14.12 (left). When an electric pulse was applied to the petiole, an action potential was transmitted basipetally. During the refractory period, burning of the terminal leaflet induced a variation potential, and it was transmitted to the petiole. The result in a tomato leaf is also shown in Fig. 14.12 (right). By burning of a leaflet blade, a variation potential was generated, and the petiole was transmitted basipetally. In both *Mimosa* and tomato, a spike was observed at the beginning of the variation potential. This nature has remained unsolved.

14.2.2 Analysis in Characean cells

When a plant suffered wounding, cells close to the dead cell were the first to perceive the "death signal". In higher plants, however, it is hard to pick up a

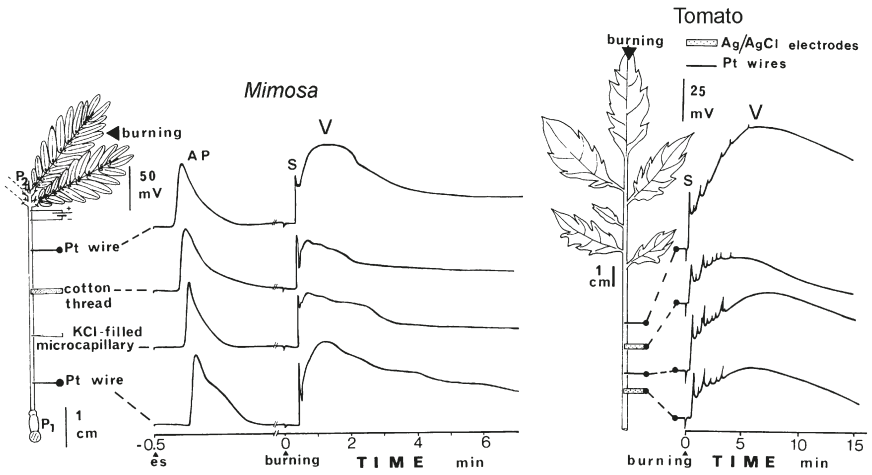

Fig. 14.12. Variation potential in *Mimosa* and tomato. *AP* action potential, *es* electrical stimulation, *s* spike, *V* variation potential. (Cited from Robin 1985)

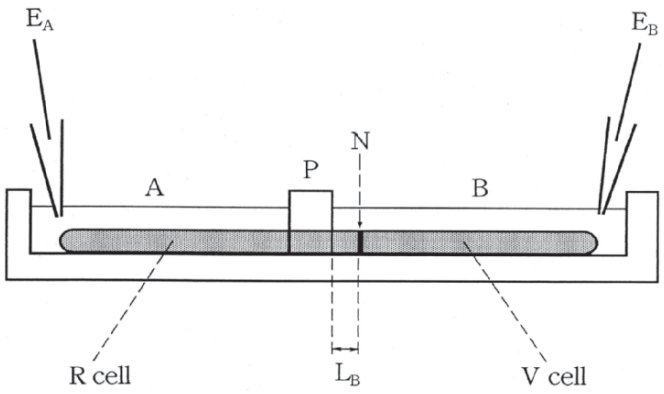

Fig. 14.13. Side view of experimental set up for analysis of wounding electrical response in Characeae. *R cell* receptor cell, *V cell* victim cell, *N* node, *A* and *B* pools, *P* partition between pools, L_B length of part of R cell in pool B (2 mm). E_A and E_B electrodes. (Cited from Shimmen 2002)

electrical signal from a target cell. Characeae can offer a suitable system for such analysis (Fig. 14.13). A specimen comprising two adjoining internodal cells is prepared. Two internodal cells are connected at the node. A specimen is mounted in the chamber so that one receptor cell (R cell) is situated in the 1 mm groove in the partition between two pools, A and B. The R cell is sealed into the groove at the partition with white Vaseline. The potential difference between the two pools is measured with electrodes (E_A and E_B). The length of the part of R cell in the pool B (L_B) is about 2 mm.

An example of measurement is shown in Fig. 14.14. When the victim cell (V cell) was cut, the membrane depolarized (a), and a long lasting component

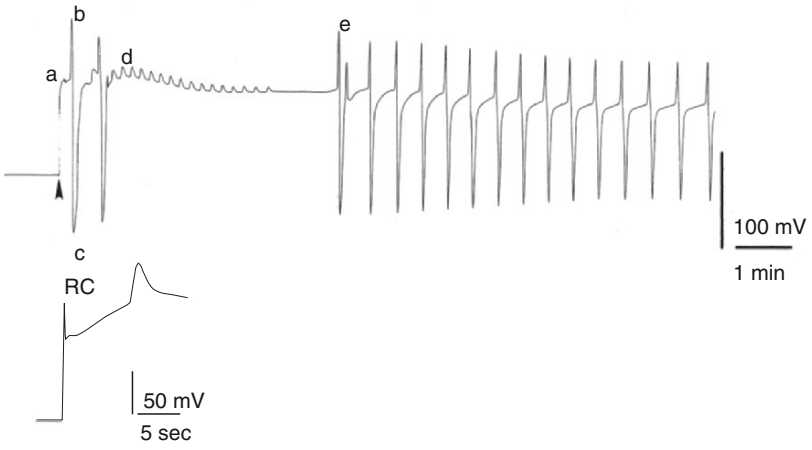

Fig. 14.14. Depolarization in wounding response of Characeae. At the time shown with an *arrow head*, V cell was cut (*upper record*). *Lower record* shows initial part of the response showing a rapid component (RC). For further explanation, see text. (Cited from Shimmen 2002)

continued for more than 30 min. During long-lasting depolarization, two components are superimposed. An action potential is generated in the cell part of R cell in the pool B (b), and it is transmitted to the cell part in the pool A (c). Then, small spikes are generated (d). Again, action potentials are generated (e). Just after cutting, a very rapid component is generated before the start of long-lasting component (Fig. 14.14 lower). When the amplitude of the long-lasting depolarization was large, this rapid component was masked (not shown). Systematic analyses showed that the long-lasting component and rapid components were generated at the end of the R cell in the pool B and that action potential is generated at the flank of the R cell. Rapid components and long-lasting depolarization are not transmitted. On the other hand, an action potential is transmitted in the longitudinal direction of an internodal cell. It is also transmitted to the neighboring internodal cell (Sibaoka and Tabata 1981). Thus, a long-lasting component is a type of receptor potential in wounding response, and this depolarization stimulates voltage-activated ion channels resulting in the action potential responsible for transmission of signals.

It is believed that K^+ released from the V cell is responsible for inducing the long-lasting depolarization (Shimmen, 2005, 2006). The amplitude of a long-lasting component decreases when the cell turgor pressure is decreased, indicating the stretching of the plasma membrane at the end of the R cell by the turgor pressure (Shimmen 2001). Thus, K^+-induced depolarization and membrane-stretching may be responsible for the generation of long-lasting component. When the electrogenic proton pump is inhibited by treatment with an inhibitor, the resting membrane potential is drastically depolarized. However, long-lasting component is generated, indicating that electrogenic proton pump does not play a central role (Shimmen 2001). The electrical resistance decreases during the depolarization (Shimmen 2005), indicating that the activation of ion channel(s) is involved. Pharmacological analysis failed to identify the ion channel involved. However, analysis under K^+-induced depolarization (c.f. Fig. 14.6) indicated the activation of Cl^- channel (Shimmen 2002). Thus, the electric phenomena in cells neighboring the dead cell can be analyzed by taking advantage of this material.

14.2.3 Transformation of pressure signal into electrical signal

In higher plants, it has been suggested that wound-induced hydraulic signals are the trigger for generation of variation potentials, i.e. transformation of pressure signal into electrical signal (Malone and Stankovic 1991; Malone 1992; Stankovic et al. 1997). The characean cell can be also a suitable material for the analysis of this phenomenon (Shimmen 2003). A specimen composed of a single internodal cell is prepared (Fig. 14.15, upper). One native end of the cell is removed by ligation and cutting. This cell now has a native nodal end and a ligated end. The cell is mounted so that the native node is located in pool B and the ligated end is located in pool A. The length of the

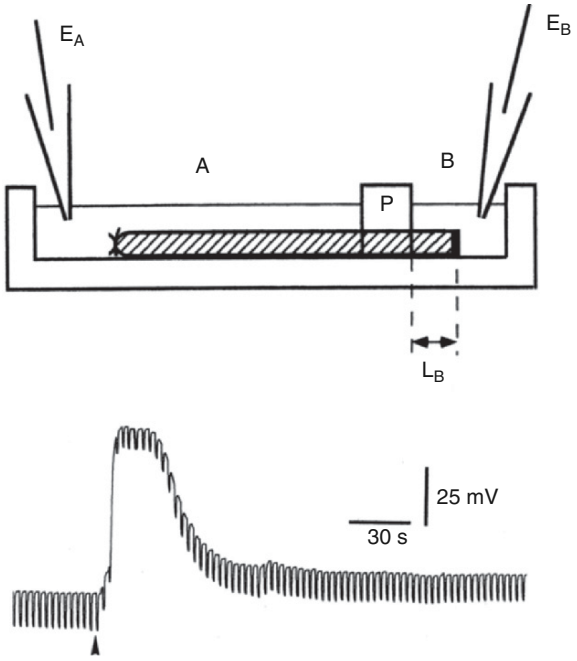

Fig. 14.15. Transformation of pressure signal into electrical signal in internodal cell of *Chara*. *Upper figure* shows apparatus and lower figure shows a record. Electric current pulses were applied between two pools during the measurement. *A* and *B* pools, *P* partition between pools, L_B length of cell part in pool B (about 2 mm), E_A and E_B electrodes. At the peak of depolarization, membrane resistance still seems high. However, most part of this resistance originates from resistance of intracellular fluid at the partition. (Cited from Shimmen 2003)

cell part in pool B is about 2 mm. When the osmolarity of pool B is increased, transient depolarization is generated (Fig. 14.15, lower). This response could also be induced when osmolarity of pool A was increased or if the osmolarity of both pools was increased. Thus, the decrease in cell turgor pressure is responsible and not the movement of water along osmotic pressure gradient. This response is generated at the distal end but not at the flank of the cell. Therefore, the response is not generated at the ligated end. In the measurement of Fig. 14.15 (lower), constant current pulses were applied, and the deviation of the membrane potential represents the change of the membrane resistance. Since it decreased during the depolarization, it is suggested that activation of ion channel is involved. The ion channel involved is remained to be identified. It is expected that this experimental set-up will open the way for the analysis of the transformation of a pressure signal to an electrical signal.

References

Barry WH (1968) Coupling of excitation and cessation of cyclosis in *Nitella*: role of divalent cations. J Cell Physiol 72:153–160

Davies E (1987) Action potentials as multifunctional signals in plants: a unifying hypothesis to explain apparently disparate wound responses. Plant Cell Environ 10:623–631

Ding JP, Pickard BG (1993) Mechanosensory calcium-selective cation channels in epidermal cells. Plant J 3:83–110

Falk LC, Edwards KL, Pickard BG, Misler S (1988) A stretch-activated anion channel in tobacco protoplast. FEBS Lett 237:141–144

Franchisse J-M, Desbiez O, Champagnat P, Thellier M (1985) Transmission of a traumatic signal via a wave of electric depolarization and induction of correlations between the cotyledonary buds in *Bidens pilosus*. Physiol Plant 64:48–52

Fromm J, Eschrich W (1993) Electric signals released from roots of willow (*Salix viminalis* L.) change transpiration and photosynthesis. J Plant Physiol 141:673–680

Hayama T, Shimmen T, Tazawa M (1979) Participation of Ca^{2+} in cessation of cytoplasmic streaming induced by membrane excitation in *Characeae* internodal cells. Protoplasma 99:305–321

Hodick D, Sievers A (1986) The influence of Ca^{2+} on the action potential in mesophyll cells of *Dionaea muscipula* Ellis. Protoplasma 133:83–84

Iijima T, Sibaoka T (1981) Action potential in the trap-lobes of *Aldrovanda vesiculosa*. Plant Cell Physiol 22:1595–1601

Iijima T, Sibaoka T (1985) Membrane potentials in excitable cells of *Aldrovanda vesiculosa* trap-lobes. Plant Cell Physiol 26:1–13

Jaffe MJ, Forbes S (1993) Thigmomorphogenesis: the effect of mechanical perturbation on plants. Plant Growth Regul 12:313–324

Julien JL, Frachisse JM (1992) Involvement of the proton pump and proton conductance change in the wave of depolarization induced by wounding in *Bidens pilosa*. Can J Bot 70:1451–1458

Julien JL, Desbiez MO, de Jaegher M, Frachisse JM (1991) Characteristics of the wave of depolarization induced by wounding in *Bidens pilosa* L. J Exp Bot 42:131–137

Kameyama K, Kishi Y, Yoshimura M, Kanzawa N, Sameshima M, Tsuchiya T (2000) Tyrosine phosphorylation in plant bending. Nature 407:37

Kamiya N (1959) Protoplasmic streaming. Protoplasmatologia VIII/3/a. Springer, Vienna

Kamiya N (1986) Cytoplasamic streaming in giant algal cells: a historical survey of experimental approaches. Bot Mag Tokyo 99:441–467

KanekoT, Saito C, ShimmenT, Kikuyama, M. (2005) Possible involvement of mechanosensitive Ca^{2+} channels of plasma membrane in mechanoperception in *Chara*. Plant Cell Physiol. 46: 130–135

Kikuyama M (1986a) Ion fluxes during excitation of Characeae. Plant Cell Physiol 27:1213–1216

Kikuyama M (1986b) Tonoplast action potential of Characeae. Plant Cell Physiol 27:1461–1468

Kikuyama M (1988) Ca^{2+}-increases the Cl^- efflux of the permeabilized *Chara*. Plant Cell Physiol 29:105–108

Kikuyama M, Tazawa M (1976) Tonoplast action potential in *Nitella* in relation to vacuolar chloride concentration. J Membr Biol 29:95–110

Kikuyama M, Tazawa M (1983) Transient increase of intracellular Ca^{2+} during excitation of tonoplast-fee *Chara* cells. Protoplasma 117:62–67

Kikuyama M, Oda K, Shimmen T, Hayama T, Tazawa M (1984) Potassium and chloride effluxes during excitation of Characeae cells. Plant Cell Physiol 25:965–974

Kishimoto U (1968) Response of *Chara* internodes to mechanical stimulation. Ann Rep Biol Works, Fac Sci, Osaka Univ 16:61–66

Knight MR, Smith SM, Trewavas AJ (1992) Wind-induced plant motion immediately increases cytosolic calcium. Proc Natl Acad Sci USA 89:4967–4971

Kumon K, Tsurumi S (1984) Ion efflux from pulvinar cells during slow downward movement of the petiole of *Mimosa pudica* L. induced by photostimulation. J Plant Physiol 115:439–443
Malone M (1992) Kinetics of wound-induced hydraulic signals and variation potentials in wheat seedlings. Planta 187:505–510
Malone M, Stankovic B (1991) Surface potentials and hydraulic signals in wheat leaves following localized wounding by heat. Plant Cell Environ 14:431–436
Mertz SM Jr, Higinbotham N (1976) Transmembrane electropotential in barley roots as related to cell type, cell location, and cutting and aging effects. Plant Physiol 57:123–128
Meyer AJ, Weisenseel MH (1997) Wound-induced changes of membrane voltage, endogenous currents, and ion fluxes in primary roots of maize. Plant Physiol 114:989–998
Mimura T, Shimmen T (1994) Characterization of the Ca^{2+}-dependent Cl^- efflux in perfused *Chara* cells. Plant Cell Physiol 35:793–800
Oda K (1976) Simultaneous recording of potassium and chloride effluxes during an action potential in *Chara corallina*. Plant Cell Physiol 17:525–528
Qi Z, Kishigami A, Nakagawa Y, Iida H, Sokabe M (2004) A mechanosensitive anion channels in *Arabidopsis thaliana* mesophyll cells. Plant Cell Physiol 45:1704–1708
Rhodes JD, Thain JF, Wildon DC (1996) The pathway for systemic electrical signal conduction in the wounded tomato plant. Planta 200:50–57
Robin G (1979) *Mimosa pudica*: a model for the study of the excitability in plants. Biol Rev 54:135–153
Robin G (1985) Analysis of the variation potential induced by wounding in plants. Plant Cell Physiol 26:455–461
Robin G, Bonnemain J-L (1985) Propagation in *Vicia faba* stem of a potential variation induced by wounding. Plant Cell Physiol 26:1273–1283
Samejima M, Sibaoka T (1980) Changes in the extracellular ion concentration in the main pulvinus of *Mimosa pudica* during rapid movement and recovery. Plant Cell Physiol 21:467–479
Shiina T, Tazawa M (1987a) Ca^{2+}-activated Cl^- channel in plasmalemma of *Nitellopsis obtusa*. J Membr Biol 99:137–146
Shiina T, Tazawa M (1987b) Demonstration and characterization of Ca^{2+} channel in tonoplast-free cells of *Nitellopsis obtusa*. J Membrane Biol 96:263–276
Shiina T, Tazawa M (1988) Ca^{2+}-dependent Cl^- efflux in tonolast-free cells of *Nitellopsis obtusa*. J Membr Biol 106:135–139
Shimmen T (1988) Characean actin bundles as a tool for studying actomyosin-based motility. Bot Mag Tokyo 101:533–544
Shimmen T (1996) Studies on mechanoperception in characean cells: development of a monitoring apparatus. Plant Cell Physiol 37:591–597
Shimmen T (1997a) Studies on mechanoperception in characean cells: pharmacological analysis. Plant Cell Physiol 38:139–148
Shimmen T (1997b) Studies on mechanoperception in Characeae: effect of external Ca^{2+} and Cl^-. Plant Cell Physiol 38:691–697
Shimmen T (1997c) Studies on mechanoperception in Characeae: decrease in electrical membrane resistance in receptor potentials. Plant Cell Physiol 38:1298–1301
Shimmen T (2001) Electrical perception of "death message" in *Chara*: involvement of turgor pressure. Plant Cell Physiol 42:366–373
Shimmen T (2002) Electrical perception of "death message" in *Chara*: analysis of rapid component and ionic process. Plant Cell Physiol 43:1575–1584
Shimmen T (2003) Studies on mechanoperception in the Characeae: transduction of pressure signals into electrical signals. Plant Cell Physiol 44:1215–1224
Shimmen T (2005) Electrical perception of "death message" in *Chara*: analysis of K^+-sensitive depolarization. Plant Cell Physiol. 46: 1839–1847
Shimmen T (2006) Electrical perception of "death message" in *Chara*: characterization of K^+-induced depolarization. Plant Cell Physiol. 47:559–562
Shimmen T, MacRobbie EAC (1987) Characterization of two proton transport systems in the tonoplast of plasmalemma-permeabilized *Nitella* cells. Plant Cell Physiol 28:1023–1031

Shimmen T, Nishikawa S (1988) Studies on the tonoplast action potential of *Nitella flexlilis*. J Membr Biol 101:133–140
Shimmen T, Tazawa M (1977) Control of membrane potential and excitability of *Chara* cells with ATP and Mg^{2+}. J Membr Biol 37:167–192
Shimmen T, Tazawa M (1978) Intracellular chloride and potassium in relation to excitability of *Chara* membrane. J Membr Biol 55:223–232
Shimmen T, Tazawa M (1983) Control of cytoplasmic streaming by ATP, Mg^{2+} and cytochalasin B in permeabilized Characeae cell. Protoplasma 115:18–24
Shimmen T, Yokota E (2004) Cytoplasmic streaming in plants. Curr Opin Cell Biol 16:68–72
Shimmen T, Kikuyama M, Tazawa M (1976) Demonstration of two stable potential states of plasmalemma of *Chara* without tonoplast. J Membr Biol 30:249–270
Shimmen T, Mimura T, Kikuyama M, Tazawa M (1994) Characean cells as a tool for studying electrophysiological charcteristics of pant cells. Cell Struct Funct 19:263–278
Sibaoka T (1964) Response of plants to stimuli. In: Ashida J, Kawakita A, Yoshikawa H, Miyachi D, Okada I, Sakaguchi K, Tamiya H, Yamada T (eds) Seibutsu-no-hannousei (in Japanese). Kyoritsu-Shuppan, Tokyo, pp 133–166
Sibaoka T (1981) Ugoku-Shokubutsu (action plants) (in Japanese). Tokyo Daigaku-Shuppankai, Tokyo
Sibaoka T (1991) Rapid plant movement triggered by action potentials. Bot Mag Tokyo 104:73–95
Sibaoka T, Tabata T (1981) Electrotonic coupling between adjacent internodal cells of *Chara braunii*: transmission of action potentials beyond the node. Plant Cell Physiol 22:397–411
Stahlberg R, Cosgrove DJ (1994) Comparison of electric and growth responses to excision in cucumber and pea seedlings. I. Short-distance effects are a result of wounding. Plant Cell Environ 17:1143–1151
Stankovic B, Davies E (1996) Both action potential and variation potential induce proteinase inhibitor gene expression in tomato. FEBS Lett 390:275–279
Stankovic B, Zawadzki T, Davies E (1997) Characterization of the variation potential in sunflower. Plant Physiol 115:1083–1088
Staves MP, Wayne R (1993) The touch-induced action potential in *Chara*: inquiry into the ionic bases and the mechanoreceptor. Aust J Plant Physiol 20:471–488
Tazawa M, Kishimoto U, Kikuyama M (1974) Potassium, sodium and chloride in the protoplasm of Characeae. Plant Cell Physiol 15:103–110
Tazawa M, Kikuyama M, Shimmen T (1976) Electric characteristics and cytoplasmic streaming of Characeae cell lacking tonoplast. Cell Struct Funct 1:165–176
Tominaga Y, Shimmen T, Tazawa M (1983) Control of cytoplasmic streaming by extracllular Ca^{2+} in permeabilized *Nitella* cells. Protoplasma 116:75–77
Tominaga Y, Wayne R, Tung HYL, Tazawa M (1987) Phosphorylation-dephosphorylation is involved in Ca^{2+}-controlled cytoplasmic streaming in characean cells. Protoplasma 136:161–169
Wildon DC, Thain JF, Minchin PEH, Bugg IR, Reilly AJ, Skipper YD, Doherty HM, O'Donnell J, Bowles DJ (1992) Electrical signalling and systemic proteinase inhibitor induction in the wounded plant. Nature 360:62–65
Williamson RE, Ashley CC (1982) Free Ca^{2+} and cytoplasmic streaming in the alga *Chara*. Nature 296:647–651

15 Electrochemical Potential around the Plant Root in Relation to Metabolism and Growth Acceleration

Tsutomu Takamura

15.1 Introduction

In order to keep our globe in a natural state, the protection of plants becomes more important in our future life. Practically, it is desired to provide suitable environmental conditions for plants to grow. In higher plants, the roots play an important role in their growth since the uptake of all the nutrition, including water, is done through the root (Bibikova and Gilroy 2003). This means that control of the chemistry of the environment around the roots is the key factor for plants to grow strongly.

Recently, electrochemical signal detection for the intact higher plants around the roots has been investigated. For example, Iwabuchi et al. (1989) observed the electric patterns around growing cress roots. They reported that a change in the electric patterns was brought about by the growth of the root in a given environment. Toko and coworkers reported on the occurrence of current flow around plant roots (Ezaki et al. 1988), the current flow picture outside the root being shown to be related to growth. Miwa and Kushihashi (1992) reported on the stereoscopic electric current density picture around the root. Their current flow picture was constructed on the basis of the measured spatial assumption of the presence of an active ionic flow. They expected H^+ accumulation in the region of the growing position of the root. However, neither the ionic concentration profile nor the time dependence of the potential profile appears to have been studied in detail for the root surface during growth. It is interesting to measure directly the ionic concentration profiled during the growth.

Electrochemistry can afford to control the electric field near the plant root as desired. If the electrochemical potential is applied to the root, the signal is supposed to be sensed near the interior of the root, which may possibly stimulate the growth of the plant. We found that growth was accelerated by the application of DC or square wave voltage to the root of a bean radicle planted in a culturing bath (Mizuguchi et al. 1994). It is worthwhile to study how the growing intact plant root is related to the presence of the substance which originates the potential distribution around the root surface. The ATP cycle

Department of Applied Chemistry, Harbin Institute of Technology, 92 West Dazhi Street, Harbin, China 150001 (e-mail: takamur@green.ocn.ne.jp)

Plant Electrophysiology – Theory & Methods (ed. by Volkov)

is suggested to take part in the growth rate change. This implies that the plant growth is influenced dynamically not only by the concentration of the chemical entities, but also by the profile of electrochemical potential distribution in connection with ATP cycles.

In this context, this article will introduce our work at first on the relation of the potential distribution and the ionic entities around the root, especially paying attention to the proton concentration, followed by showing proton concentration image around the root during the growth and how the proton concentration affects the growth, leading to the effective potential application to the root for accelerating the growth, and finally the investigation of the mechanism of the growth acceleration will be shown.

15.2 Potential distribution around root of seedling in culturing solution

15.2.1 Introduction

Investigation of the relationship between the plant metabolism and the electrochemical potential near the root surface is of great interest to an electrochemist. To allow for easier measurement, due to its large root size, we adopted a bean sprout which was laid down in the culturing solution as the specimen and the potential near the root of the sprout was measured by constructing a measuring device where position of the probe micro-electrode could be moved precisely around the root. The potential distribution map was constructed, which can be correlated to the ion concentration distribution map, based on the Henderson equation.

Takeuchi at al. (1994) found the presence of a large negative potential well in the growing tip region. In addition, the lateral root is an important organ for plant growth, since the growth rate of a plant is roughly proportional to the effective surface area of its roots (Bibikova and Gilroy 2003). It is important to observe the potential in the lateral roots emerging region. A striking feature of the lateral root is that it makes it possible to observe all the changes from the initial period of germination. The lateral root begins to grow from a lateral root primordial whose metabolic activity during segmentation is expected to extend out to the root surface as an electrochemical signal. The emerging of lateral roots plays an important role in plant growth, and the potential change during the emerging of a lateral root attracted our attention. The potential and ionic concentration distributions were measured precisely at the lateral root emerging point. Observation showed the appearance of a negative potential well preceded the initiation of an emerging lateral root (Watanabe et al. 1995).

In this section, the precise measurement of the potential distribution around the root surface will be shown in connection with the measured

concentration profile of ions, which were generated by the metabolism of the plant. All the potential data can be reasonably explained on the basis of the theoretical equation for liquid junction (diffusion) potential.

15.2.2 Experimental set-up

For the purpose of measuring potential distribution on a micrometer scale, a glass capillary microelectrode was prepared with the use of a micro-glass extruder. The capillary tip, as thin as less than one micrometer (Fig. 15.1), was filled with an electrolyte solution (0.1 mM KCl or K_2HPO_4). The electrochemical potential of the desired position was measured at 22˚C with a micro-pipette electrode connected to a normal Ag/AgCl reference electrode against the other same reference electrode placed in bulk solution.

The potassium ion sensing micro-capillary electrode was prepared by coating the pipette wall with silicone resin, followed by filling the pipette with liquid potassium ion exchanger (World Precision Instrument Inc., IEI90). The back face of the liquid was kept in contact with a KCl saturated aqueous

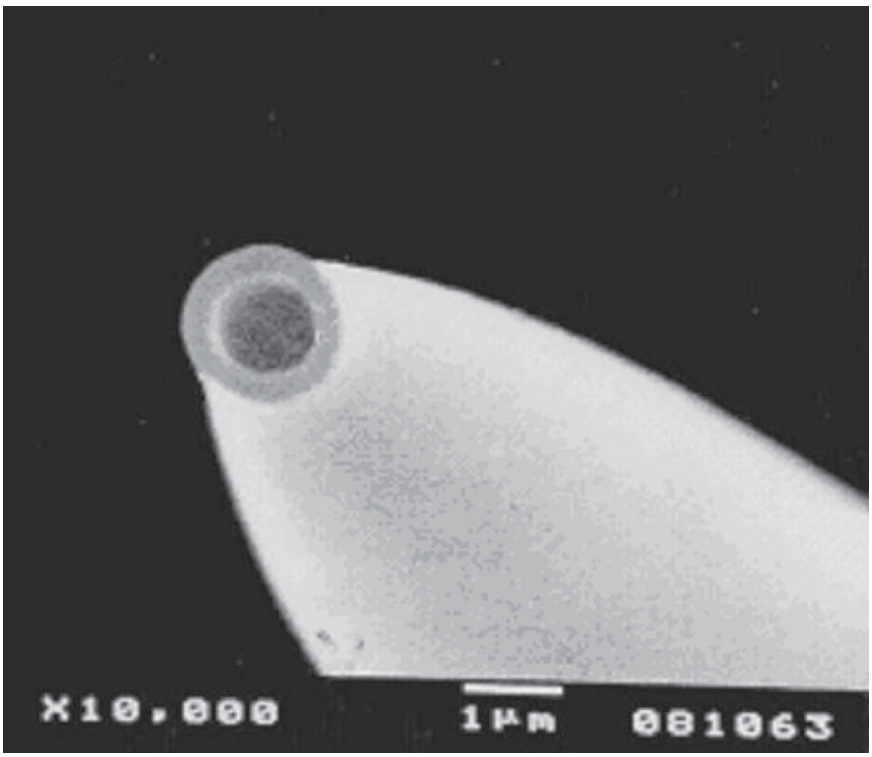

Fig. 15.1. SEM image of a glass capillary micropipette electrode

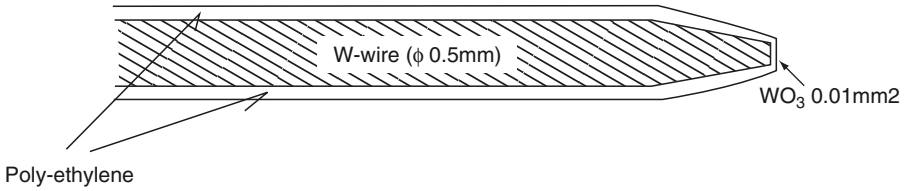

Fig. 15.2. A pH measuring micro electrode comprised of a thin tungsten wire inserted tightly in a polyethylene tube whose tip was sharpened and the exposing tungsten surface was oxidized anodically in sulfuric acid to form WO_3

solution where the needle of Ag/AgCl electrode was inserted. For measuring the concentration of a specified ion, the ion-sensing compound for the specified ion was filled in the capillary tip.

The proton concentration measurement was done by preparing a W/WO_3 micro electrode for pH measurement (Fig. 15.2). The linearity of the electrode potential versus Ag/AgCl electrode against the pH of the solution was excellent in the pH range of 3–7, but the slope was 36 mV/pH decade.

For measurement of the major constituent anion, viz. Cl^-, an Ag wire coated with AgCl by anodic polarization in KCl solution was used as Ag/AgCl sensing electrode.

The equipment system for the potential profile and ion concentration profile measurement around the sprout specimen is shown in Fig. 15.3. The

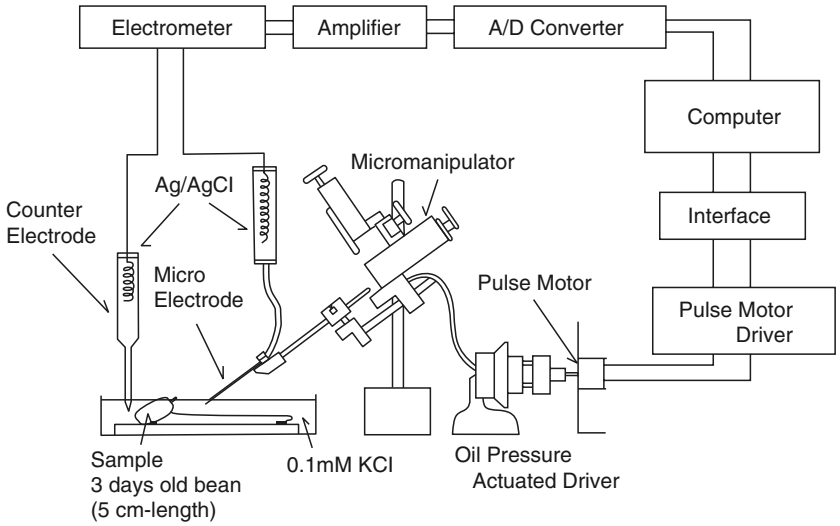

Fig. 15.3. Micromanipulator driven micro-capillary electrode system for measuring potential and ion concentration profile near the sprout root surface. The sprout specimen was fixed by laying down in a plastic Petri dish filled with culturing solution. The micromanipulator can be driven precisely by the pulse motor via oil pressure actuated driver (Watanabe et al. 1995)

microelectrode was connected to the Ag/AgCl reference electrode via KCl aqueous solution and mounted tightly on the micromanipulator, whose 3D movement was driven by a pulse motor, actuated by a pulse motor generator connected to a computer via interface. On the other hand, the potential and the concentration measurement could be determined by the use of an electrometer connected with an amplifier and an A/D converter whose output was fed to a computer.

As the measuring specimen we chose a bean seedling big enough to measure easily. Bean seeds (*Vigna mungo* (L.) Hepper) were sterilized with 70% ethanol and 1% NaClO, and stabilized for 24 h in an agar gel medium (0.35%). A seed grown to sprout having a root of 1–1.5 cm length was transferred to a shallow plastic Petri dish filled with sterilized water, the body being laid down and fixed at the bottom. After 24 h, the seedling was grown to be 5–8 cm in length and the water was replaced by 0.1 mM KCl solution. After 2 h, the specimen was ready to be examined.

15.2.3 Results and discussion

At first the electrochemical potential profile from the bulk solution side toward the root was obtained. The potential profile is shown in Fig. 15.4, where the potential near the root is notably negative against the bulk solution. The potential distribution along the root direction was measured as well. The values were scattered to some extent so that it was necessary to measure with repetition. The results are shown in Fig. 15.5. The potential at 40 μm from the root surface was varied along the root surface, giving rise to a potential well near the root tip.

The cause of the negative potential around the root is expected to be attributed to the concentration variation of the ionic species near the root, which was verified by the determination of the ion concentration by the use of ion sensing capillary electrode. All the concentrations of major constituting ion species were determined by the use of micro-ion sensitive electrodes. Examples of K^+ and H^+ are shown in Fig. 15.6.

If two intermingling solutions have different ionic species and their concentrations are in contact with each other, the contact potential between the two phases is given by the Henderson equation (1907) which is given by

$$\delta\Phi = \Phi^{\mathrm{I}} - \Phi^{\mathrm{II}} = \frac{\sum_i u_i / z_i \left(C_i^{\mathrm{I}} - C_i^{\mathrm{II}}\right)}{\sum_i u_i \left(C_i^{\mathrm{I}} - C_i^{\mathrm{II}}\right)} \frac{RT}{F} \ln \frac{\sum u_i C_i^{\mathrm{II}}}{\sum u_i C_i^{\mathrm{I}}}$$

where C_i is the concentration of i species; u_i the mobility; and z_i the charge of the ion. (Watanabe et al. 1995)

In the present case, phase I is the solution near the root surface and phase II is the bulk phase. Provided that all the concentrations are obtained by measurement, the potential difference can be evaluated between two phases.

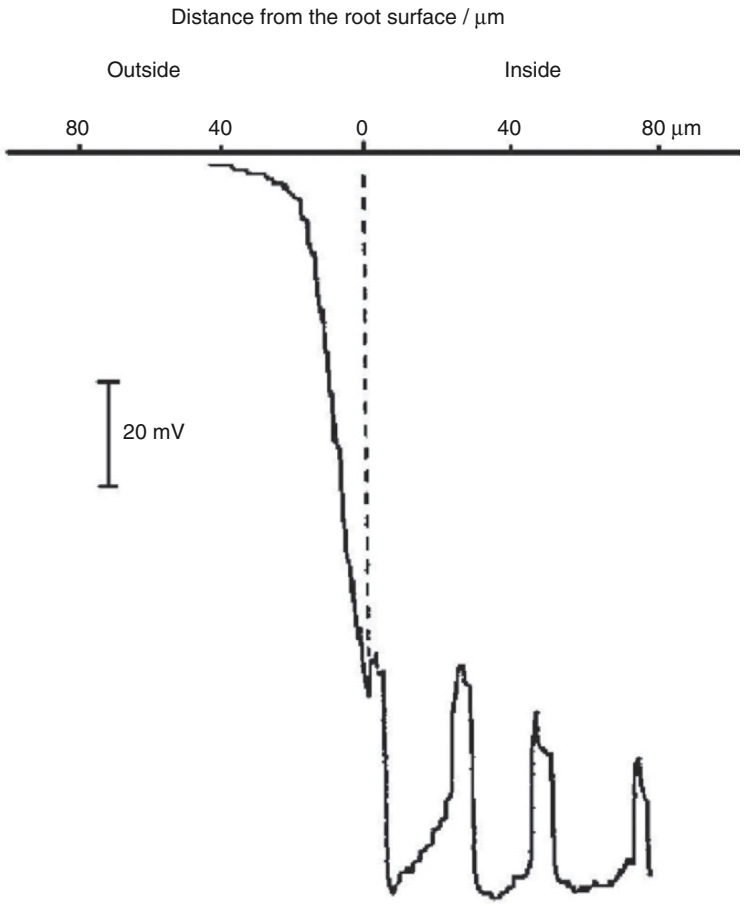

Fig. 15.4. Potential profile near the sprout root (*Vigna mungo* (L.) Hepper) in 0.1 mM KCl solution. The micro-pipette electrode was driven from the bulk toward the root surface and pierced into the sprout body. The up and down repetition of the potential is due to the passing over of the electrode from one cell to another neighboring cell. The horizontal position of the electrode was 5 mm from the root tip (Takeuchi et al. 1993)

The obtained values are shown in Fig. 15.7 as a function of the distance along the primary root from the root tip. The dots are measured values and the dashed line is the calculated line based on the Henderson equation, where the coincidence between them is satisfactory. This means that the existing potential can be attributed to the ionic diffusion potential, a potential indicative of the metabolism of a living plant.

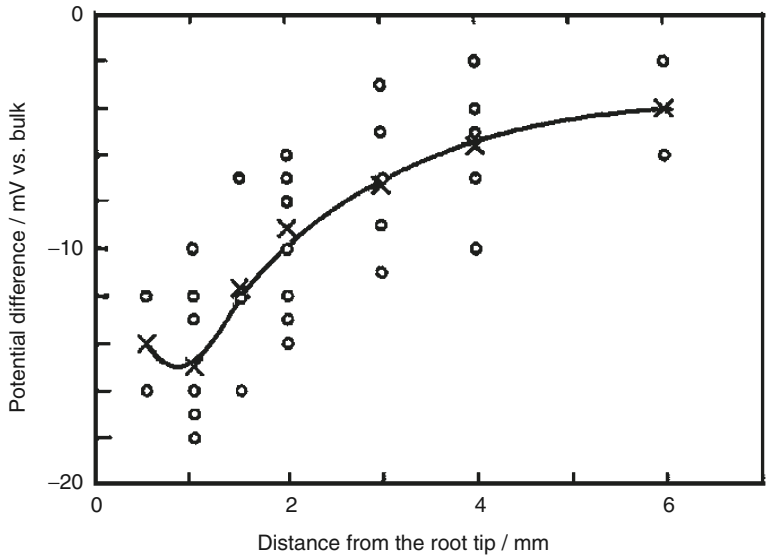

Fig. 15.5. Electrochemical potential distribution along the seedling of *Vigna mungo* root surface with a distance of 40 μm from the root surface in the culturing bath of 1 mM KCl. Due to the scattering of the measured values the average values from several measurement were obtained (× *marks*). The negative potential gave a well near the root tip (Takeuchi et al. 1993)

15.3 pH change around the root during growth of seedlings

15.3.1 Introduction

It is well known that the energy required to activate the metabolism of a plant is supplied as a result of the ATP/ADP cycle, where inorganic phosphoric acid is released by a proton pump during consumption of nutrition. This means that the proton concentration becomes increased around the root during the growth. In this section, increased proton concentration will be shown visually, not only for the dicotyledon plant but also for the monocotyledon plant. The affects of increased proton concentration on growth rate of the plant will also be shown.

15.3.2 Experimental

In order to show the change in H^+ concentration visually, a pH indicator reagent was utilized. It is necessary to prevent the convection effect in the culturing bath during culturing and to fix the position of the seedling specimen. Agar was used in preparing the solution, although agar by itself has a pH

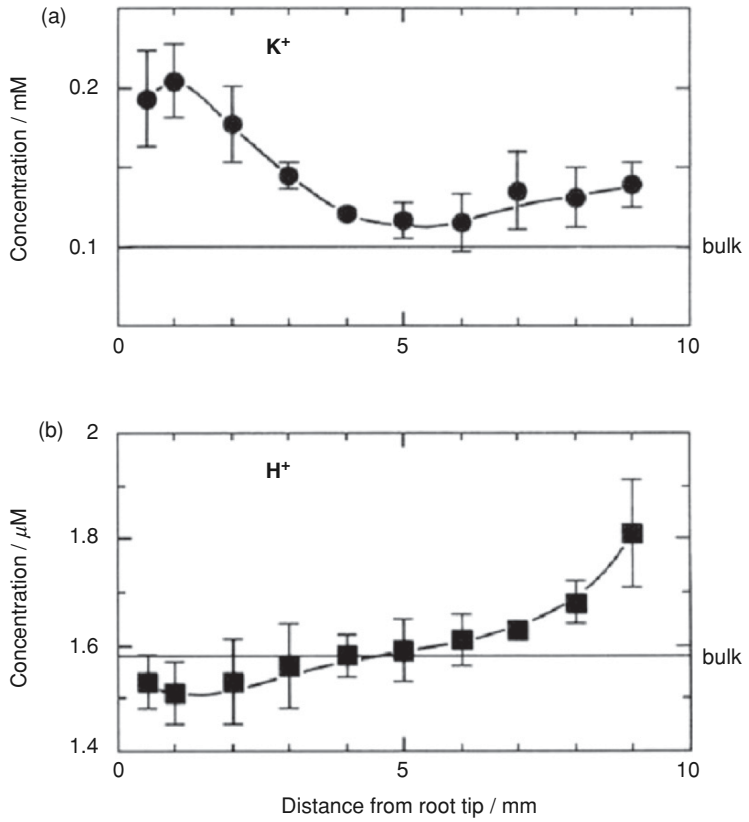

Fig. 15.6. K^+ (a) and H^+ (b) concentration distribution along the root of bean seedling from the tip to the base measured with the prepared sensor electrodes (Watanabe et al. 1995)

buffering effect, which was small enough to be ignored. The planting cell was prepared with two 10×10 cm square glass plates 2 mm thick. They were faced together, keeping a constant gap of 4 mm, using a U-shaped rubber spacer and fixed with clamps. The appropriate amount of bromocresol purple was dissolved in distilled water containing 0.1 mM K_2SO_4, warmed up and 3% of agar was dissolved in the solution. After standing for cooling, the seedling specimen was planted in the cell before solidifying of the agar solution. The cell was kept vertically standing in an incubation container.

For the purpose of measuring pH dependency of the released amount of H^+ from the seedling specimen, we prepared three different culturing solutions of pH 7.50, 6.01, and 4.86, respectively, by mixing appropriate amounts of sulfuric acid and potassium hydroxide. Ten specimens of 2-day-old *Vigna mungo* seedlings were planted in 20 ml of culturing solution in a glass cylindrical

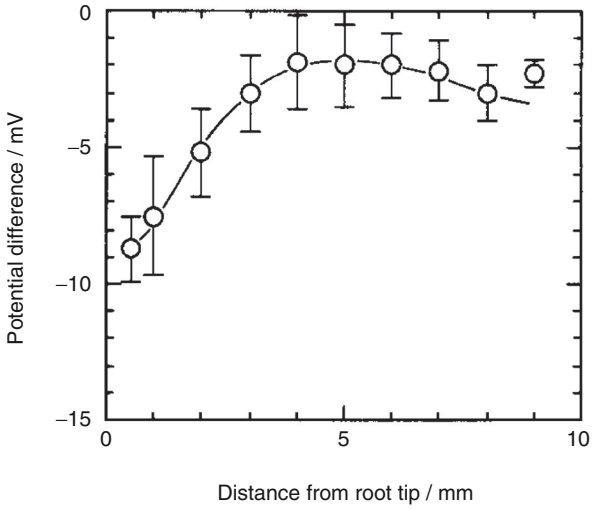

Fig. 15.7. Potential distribution around the bean root of *Vigna mungo* seedling. *Circle*: measured value; *dashed line*: calculated line by the use of Henderson equation where the all the observed ion concentrations were put in (Watanabe et al. 1995)

vessel where a W/WO_3 pH sensing electrode was inserted. The released amount of H^+ was calculated from the measured pH by taking the ionic concentration into consideration.

15.3.3 Results and discussion

Examples of the color change due to the release of H^+ are shown in shown in Figs 15.8, 15.9, and 15.10. Figure. 15.8 shows the color change caused one day after the planting of *Vigna mungo* seedling in the agar bath. The purple color of the bath changed to yellow around the root, indicating H^+ was released from the root as a result of the proton pump action due to the ATP/ADP cycle. Such a H^+ release action should be observed as long as the plant continues to live. Figure 15.9 was obtained 5 days after the specimen in Fig. 15.8. Figure 15.9 shows that H^+ was also released from the lateral root. We examined whether such a color change can be seen not only for the dicotyledonous plant but also for the monocotyledon plant. Figure 15.10 is for the case of *Oryza sativa* (L.). Release of H^+ can be seen on the entire surface of the root. Irrespective of the buffer action of agar, distinct color change was revealed implying the rate of the release is rather rapid. The presence of the root hair cannot be recognized from the figures, but precise observation made it possible to recognize that the release amount is correlated to the density of the root hair, indicating the root hair is taking part in the release.

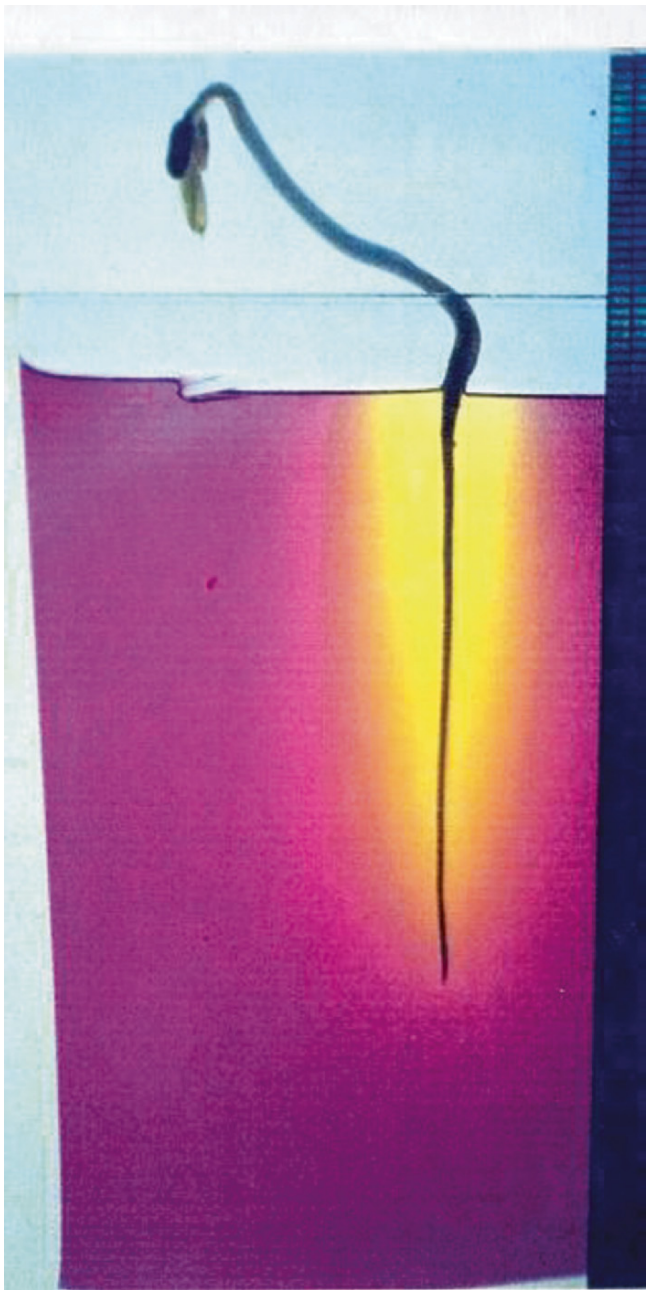

Fig. 15.8. Color change from purple to yellow due to the H^+ release from the root of *Vigna mungo* planted after 1 day in agar culture bath containing bromocresol purple (Watanabe et al. 1995)

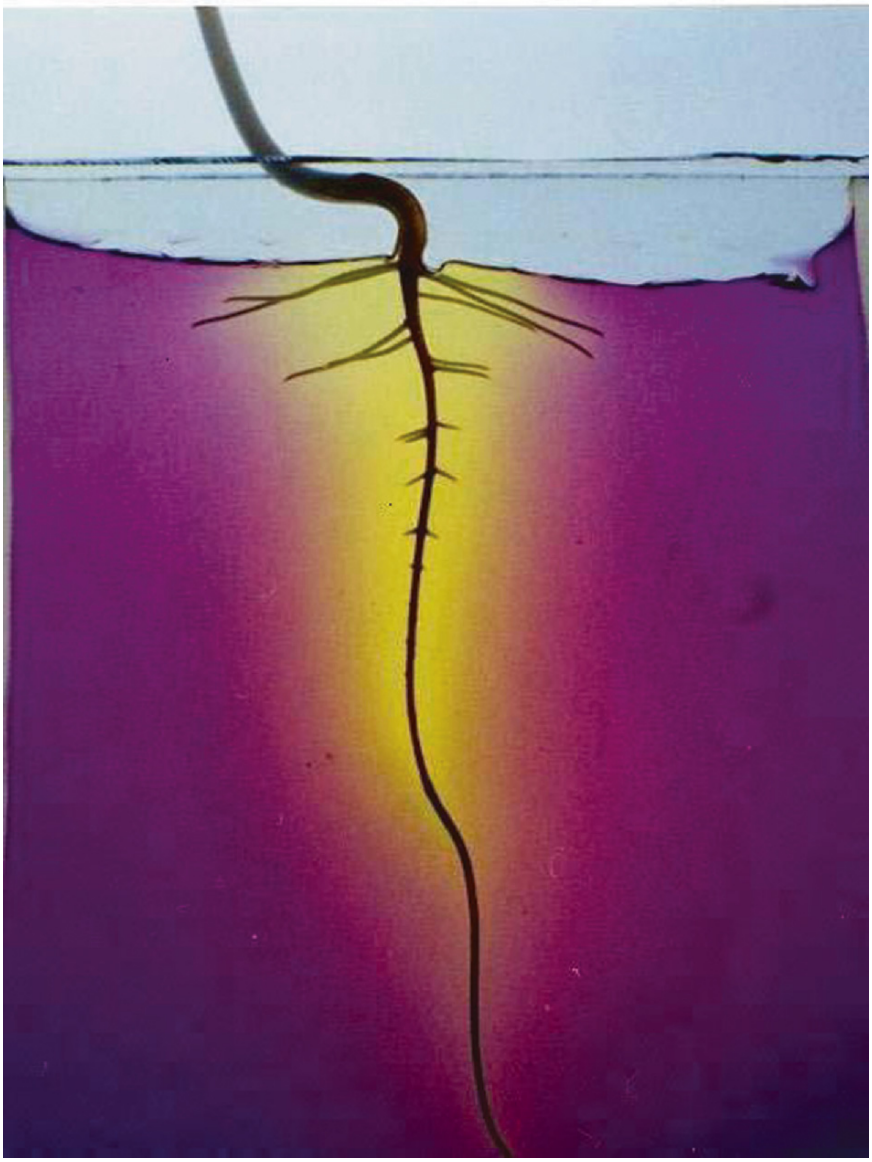

Fig. 15.9. The same as the case in Fig. 15.8 but photographed after 5 days. The magnification is different

The effect of the environmental acidity was examined in relation to the proton releasing action. The released amount of proton was determined by the use of a W/WO_3 microelectrode placed near the root during culturing. The amount was drastically dependent on the pH of the culturing solution as

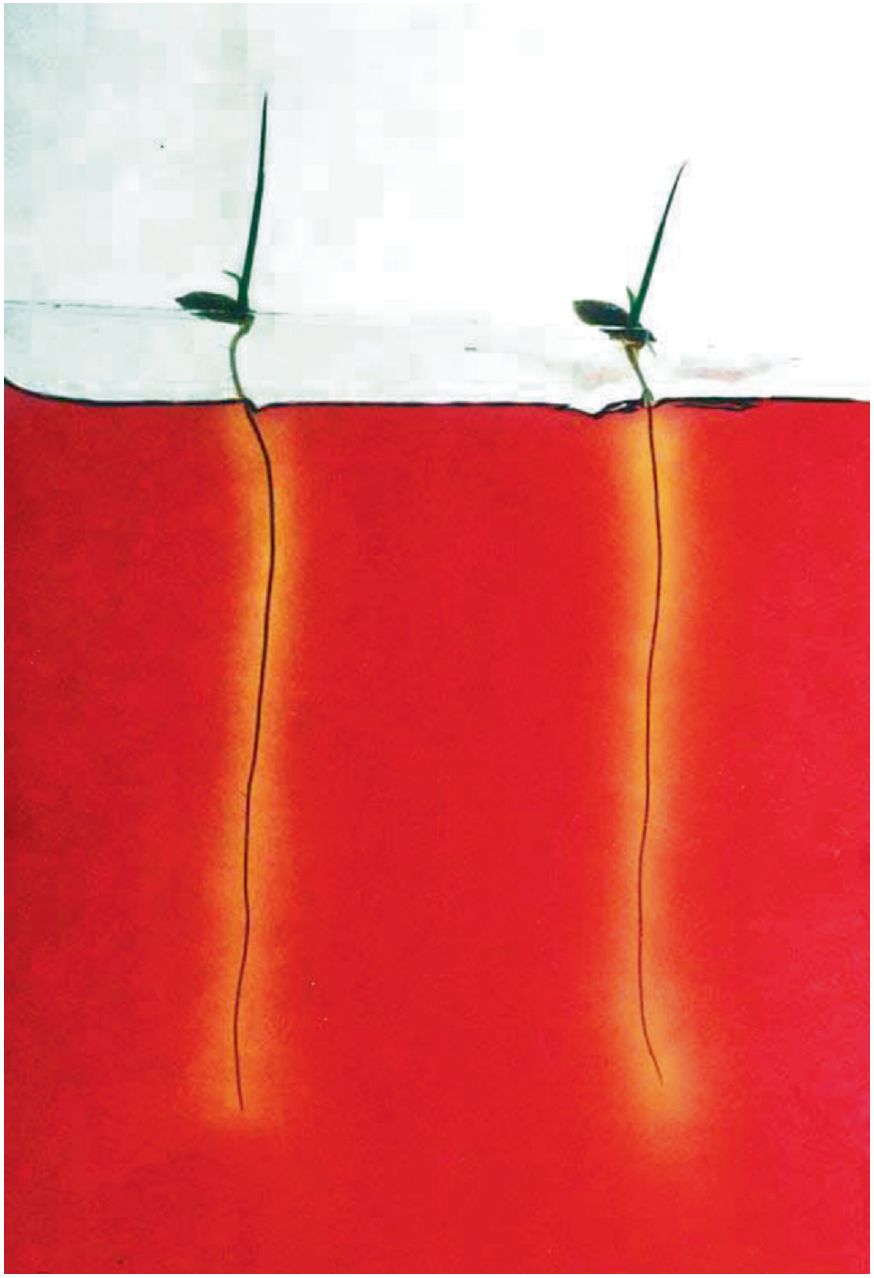

Fig. 15.10. Color change from red to yellow due to the H^+ release from the root of *Oryza sativa* (L.) planted after 1 day in agar culture bath containing bromocresol purple (Ashisada M 1995)

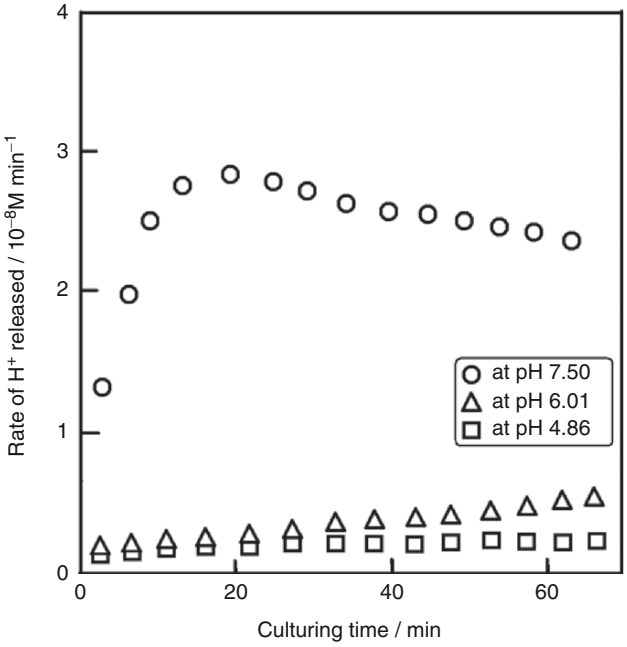

Fig. 15.11. Rate of proton release from the root of *Vigna mungo* seedling into the culturing solution whose initial pH was fixed at a selected value. The solutions having different pH were prepared for culturing. The rate was determined with a W/WO_3 micro sensor electrode set near the root surface

shown in Fig. 15.11. The releasing rate was very rapid in the pH 7.50 solution, while it was strongly suppressed at lower pH solution implying a strong suppression of metabolism in acidic environments. This clearly suggests that the acid effect causes disastrous effects to forests, as in the case of Schwarz Wald in Germany.

Attention was paid on the shooting of the lateral root in relation to the change in the potential near the root. The potential was found to change from time to time within a certain range of the root, also identified as the lateral root shooting range. During the early growing stage of the seedling, lateral roots began to shoot at specified parts in the grown region (see Fig. 15.12). In this region, the electrochemical potential was measured by repeatedly sweeping the capillary electrode.

A shallow potential well happened to appear on the smooth surface of the primary root [corresponding to (a) in Fig. 15.13]. The well grew deeper within 16 h as shown in Fig. 15.13. Finally, a lateral root began to appear in sight on the position just corresponding to that of the well. The structure change inside the root during the growing of potential well was intriguing.

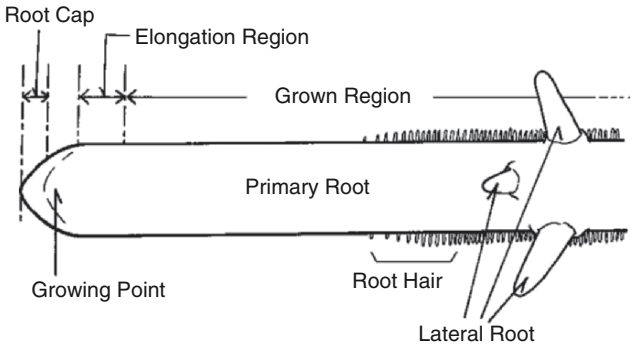

Fig. 15.12. Schematic illustration of the root of a bean seedling

Among many seedlings, a specimen giving the same potential well, as corresponding to (a) in Fig. 15.13, was picked up and the root was sliced at the position corresponding to the well. Such was done at different position corresponding to (b), etc.

The obtained microscopic photographs are shown in Fig. 15.14 where we see clearly the growing of primordia in the primary root. After about 20 h, the shooting of the lateral root at the position could be recognized leading to a preindication of the lateral root shooting before a full day. As mentioned already, the potential well is caused by the enhanced release and uptake of ions as a result of enhanced metabolism in the primordia growing position, shown recently by Dubrovsky et al. (2001).

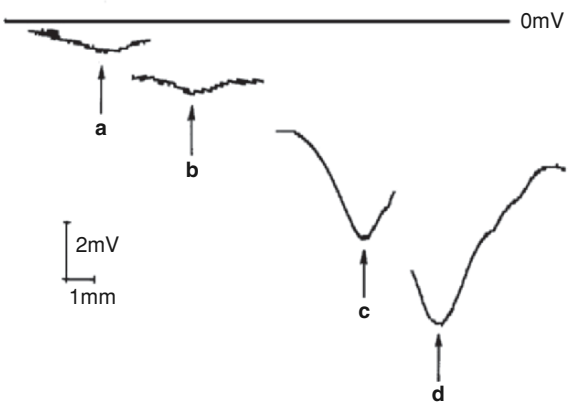

Fig. 15.13. Growing of a potential well detected on the smooth surface of a primary root. **a** Initial stage, **b** after 5 h, **c** after 12 h, **d** after 16 h (Watanabe et al. 1995)

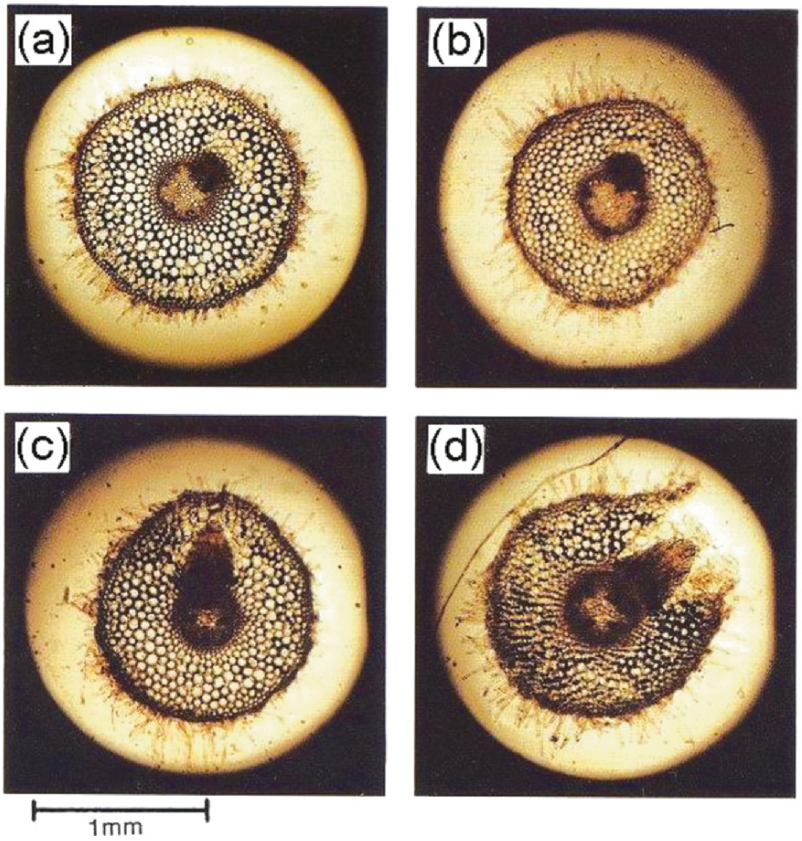

Fig. 15.14. Microscopic photographs of the primary root cross-section in the region of the lateral root primordia. Seedlings giving a similar size of potential well were cut to obtain the cross-section, where we see the primordia is growing in a parallel manner to the size of the potential well (Watanabe et al. 1995)

15.4 Effect of cotyledon on electrochemical potential near the root

15.4.1 Introduction

In the preceding section, presence of a potential well around the primary root of a bean seedling cultured in a culturing solution was demonstrated and explained on the basis of the uptake and release of ions through the ion pump as a result of metabolism. The potential well has been examined for the seedling specimen having cotyledon, a source of nutrients for the seedling to grow during the sprout stage. It is interesting to examine how the cotyledon affects the formation of the potential well. In this section, the magnitude of the potential well will be shown for the bean seedlings with and without cotyledon.

15.4.2 Experimental

A seedling of *Vigna mungo* (L.) Hepper about 5 cm in length was set in the measuring cell shown in Fig. 15.3. The potential around the root was stabilized within about 1 hour in 0.05 mM K_2HPO_4 solution, then measurements began. As the measuring specimen, two kinds of specimens were prepared, one with cotyledon as grown and the other whose cotyledons were fully removed before the setting. In the latter case, three different kinds of culturing solutions were examined: 1) 0.05 mM K_2HPO_4 solution; 2) 0.05 mM K_2HPO_4 + 0.2 mM $CaSO_4$; 3) 10 times diluted MS Culturing Solution, whose main consituents are 2.05 mM NH_4NO_3, 1.88 mM KNO_3, 0.30 mM $CaCl_2$, and 0.15 mM $MgSO_4$. On the other hand, microamount constituents such as H_3BO_3, $MnSO_4$, $ZnSO_4$, KI, Na_2MoO_4, $CuSO_4$, $CoCl_2$, Na_2EDTA, and $FeSO_4$ were also contained.

15.4.3 Results and discussion

The presence of a potential well near the root tip is clearly shown in Fig. 15.15 which was obtained with a proper seedling having cotyledon. The profile is

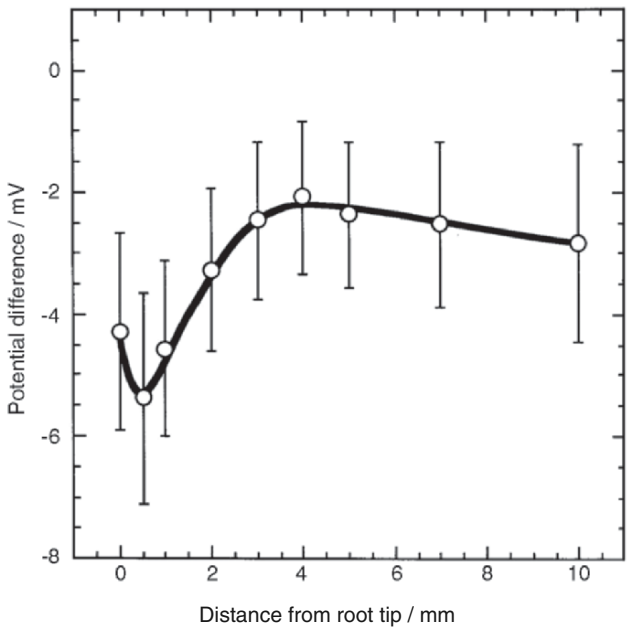

Fig. 15.15. Electrochemical potential measured near the root surface of a *Vigna mungo* seedling having cotyledon cultured in a 0.05 mM K_2HPO_4 solution. The potential was measured at the distance of 100 µm from the primary root surface with the same method shown in Fig. 15.3 (Tachizawa M 1995)

exactly the same as that calculated with the measured concentrations of such ions as H^+, K^+, Cl^-, etc. In contrast, the seedling whose cotyledons were removed revealed a very shallow potential well, as shown in Fig. 15.16, implying that the metabolism is very weak.

However, when the seedling without cotyledon was cultured in a solution containing 0.0 5 mM K_2HPO_4 + 0.2 mM $CaSO_4$, the potential well was emphasized again, as shown in Fig. 15.17, though the well depth is still shallow. The culturing solution containing full nutrients involving not only inorganic constituents but also organic nutrients (MS Culturing Solution) was then tried. The results are shown in Fig. 15.18, where we see the depth of the potential well is nearly fully recovered. From these results, one can conclude that the electrochemical potential well near the primary root surface indicates the metabolism in seedlings whose activity is the result of the uptake of nutrients, irrespective of the supply source albeit from cotylodon or its surroundings.

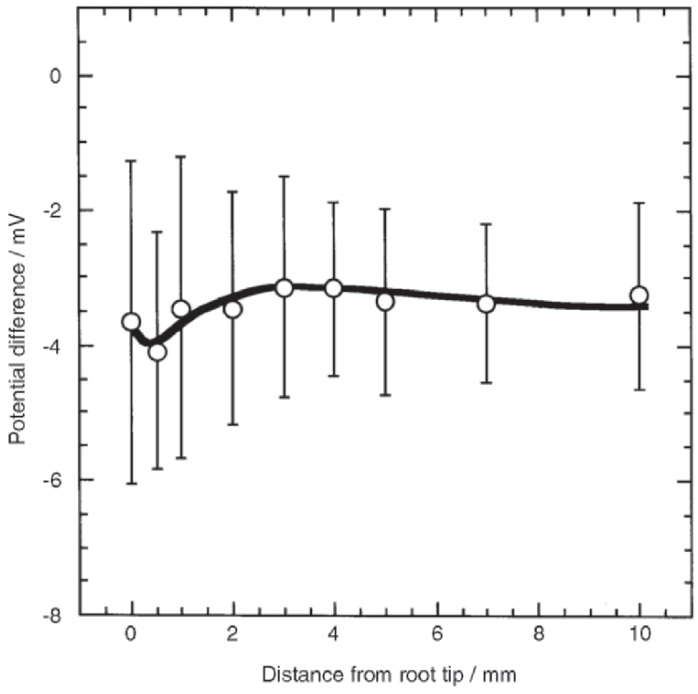

Fig. 15.16. Electrochemical potential measured near the root surface of a *Vigna mungo* seedling without cotyledon cultured in a 0.05 mM K_2HPO_4 solution. The potential was measured at the distance of 100 μm from the primary root surface with the same method shown in Fig. 15.3 (Tachizawa M 1995)

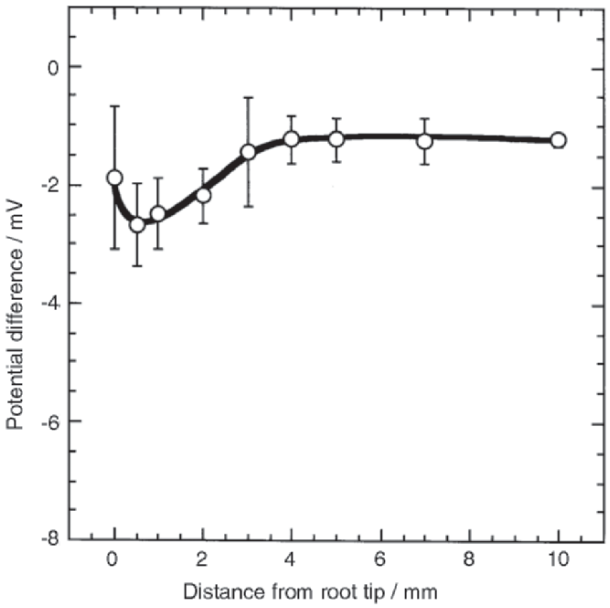

Fig. 15.17. Electrochemical potential measured near the root surface of a *Vigna mungo* seedling without cotyledon cultured in a 0.05 mM K_2HPO_4 + 0.2 mM $CaSO_4$ solution. The potential was measured at the distance of 100 μm from the primary root surface with the same method shown in Fig. 15.3 (Tachizawa M 1995)

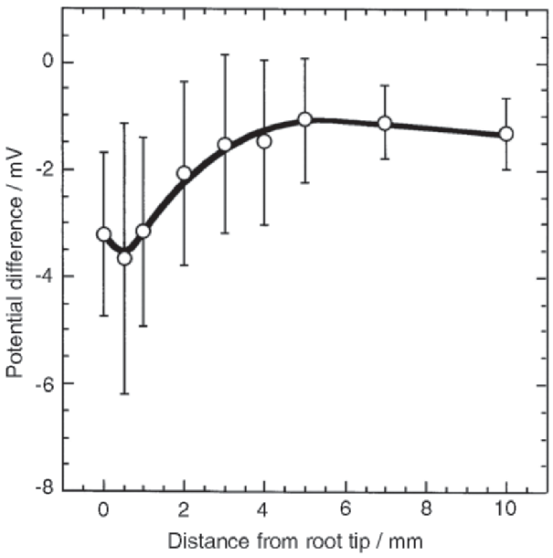

Fig. 15.18. Electrochemical potential measured near the root surface of a *Vigna mungo* seedling without cotyledon cultured in a solution containing full nutrients (MS Culturing Solution). The potential was measured at the distance of 100 μm from the primary root surface with the same method shown in Fig. 15.3 (Tachizawa M 1995)

15.5 Growth acceleration of dicotyledon seedlings by application of potential to the root in the culturing bath

15.5.1 Introduction

Green chemistry requires not exhausting any chemical substance that is an environmentally unfavorable substance and embraces to accelerate the growth rate of plants, including trees and vegetables. Rapid growing of plants enables the encroaching of harmful insects to be ignored. The use of an exterminator is unprofitable because of its unavoidable pollution.

For the purpose of plant growth rate acceleration, the most popular method adopted is to use some chemicals having the growth rate acceleration effect. Use of plant hormones including ethylene, auxin, cytokinin, gibberellin, etc. are the most popular (Richard et al. 2001; Scherer 2002) and recently salicylic acid (Rajasekaran and Blake 1998) and brassinosteroid (Grove et al. 1979; Noguchi et al. 1999; Zullo and Kohout 2004) have now been studied extensively. Use of chemical materials, however, appears not necessarily to ignore the pollution problem. For these purposes, the physical method is preferred. Application of magnetism, high tension electric field, centrifuging field, and artificial wind, etc. is proposed.

With regard to the effect of an electric field on plants, a number of papers have been reported. Fromm and Spanswick reviewed the use of action potentials (Fromm and Spanswick 1993) for many papers, but paid attention to the physiological standpoint, ignoring the effect on growth rate acceleration.

From sections 2–4, as a result of metabolism, an electrochemical potential profile settled around the root in culturing solution was shown. The action of the ion pump causes protons to be released as a result of the ATP–ADP cycle. The release of protons and uptake of nutrition is considered to proceed via root hair. This means that the amount of nutrition uptake is roughly proportional to the net surface area of the active portion of the root, so the number of lateral root shooting is considered to be a measure of the activity of the growing seedling.

The idea of the reverse process was that when a potential difference near the growing root is applied, it leads to the possibility to enhance the growth rate of the plant. Yamafuji and Toko are considered to be the pioneers on the research work of electric signal stimulation to the plant root cultured in a solution. They found interesting results on the root shape change and changes in the proton release rate and distribution etc. (Toko and Yamafuji 1988; Ezaki et al. 1990b). They began to apply electrical signals to the culturing plant root, and found that the number of the lateral root was increased by the signal stimuli. However, it appears they did not pay attention to the wave shape of the signal.

In the preliminary experiment, the present author and coworkers could find that the growth rate of bean sprout can be accelerated by the application of electrochemical voltage to the culturing bath, where an alternate current

wave was found more effective (Mizuguchi et al. 1994; Takeuchi et al. 1994). Since our findings are only with the preliminary experimental results obtained from the dicotyledonous plant, it is worthwhile to investigate in detail not only for dicotyledon, but also for monocotyledon, plants. In the present study, we would like to show the extended results on growth rate acceleration effect by potential application both for monocotyledon and dicotyledon plants together with a tentative elucidation of the mechanism.

As introduced in the preceding section, presence of the potential well around the root tip is a strong indication of the vivid growth of the plant. This led to the idea that application of an electrochemical potential to the seedling root growing in a culturing bath will affect the growth rate of the seeding.

Thus a study of the potential application to the root in the culturing bath was initiated. It is interesting to examine both dicotyledon and monocotyledon plants as in the case of H^+ releasing from the roots. In this section, the case of the dicotyledon seedling will be shown. Due to the ease of handling, *Vigna mungo* (L.) Hepper was chosen as the test sample. Since there is a lack of information detailing what type of the applying voltage source is the most preferable, various voltage sources such as direct current, sinusoidal, square, and spike waves, respectively, were examined. After culturing for 1 week, the seedlings were taken off from the bath and the growth amount was compared with that of the control sample.

15.5.2 Experimental

As the sample seedlings of *Vigna mungo* (L.) Hepper were examined, the bean seeds were sterilized, and swelled for 24 h in 0.5 mM $CaSO_4$ aqueous solution at 25 °C in the dark. The husk was than removed and planted on shallow agar gel medium in the dark. The grown seedlings, having 1.5–2.5 cm roots, were planted in a floating agar plate and cultured in 0.5 mM K_2SO_4 aqueous solution in acrylic polymer containers ($20 \times 7 \times 12$ cm) under controlled weather conditions (22 °C, 50% relative humidity, 70% daylight illumination). The container was divided into two equal compartments along the longer direction. In one of the compartments, two platinum (Pt) plate electrodes were mounted at both sides separated by 15 cm and electrochemical voltage was applied from a voltage source during the growth (Fig. 15.19).

The voltage distribution between the Pt electrodes were examined with a Ag/Ag probe electrode at a number of positions in the vessel and verified the voltage gradient was nearly linear throughout the vessel.

15.5.3 Results and discussion

The top view photograph for the case of a square wave application (30 Hz, 5 V amplitude) 5 days after culturing is shown in Fig. 15.20, where the top half (a) is for the case of voltage application, and the bottom (b) is for the

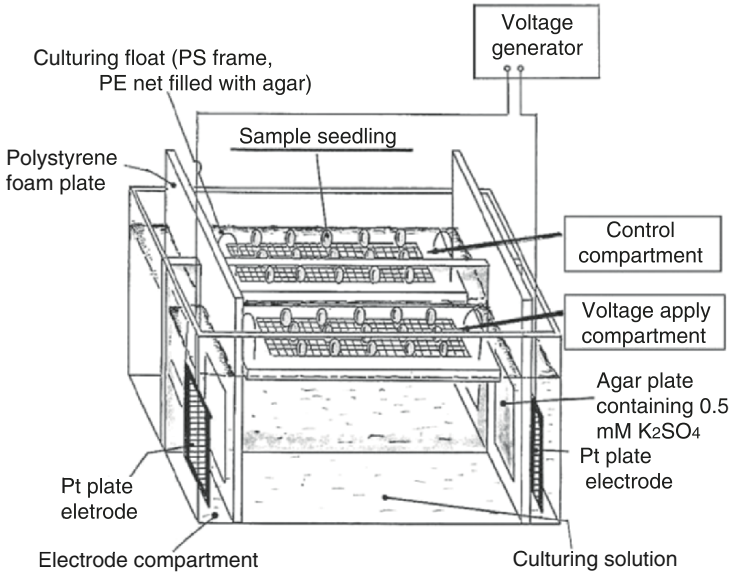

Fig. 15.19. Culturing bath (constructed with methyl methacrylate resin for seedling growth with and without voltage application to the roots (Mizuguchi et al. 1994)

control. As seen in the top part of the figure (a), the shooting of the lateral roots (white lines) is quite distinct as compared with those in (b). The growth ratio versus that of control was evaluated by comparing the seedling body length.

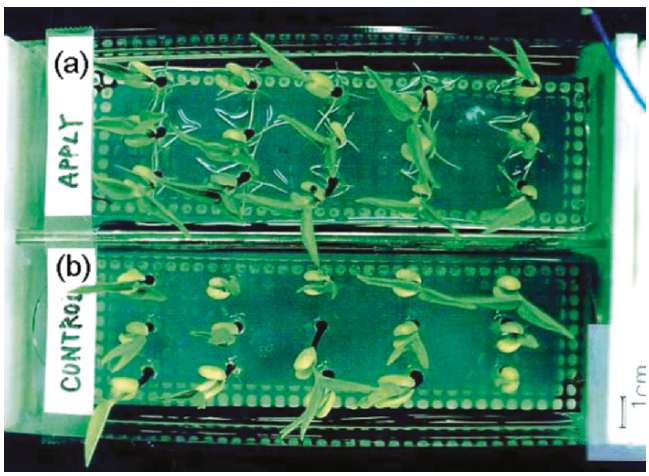

Fig. 15.20. Top view photograph of 5 days old seedlings of *Vigna mungo* (L.) Hepper cultured in 0.5 mM K_2SO_4 aqueous solution with (**a**) and without (**b**) square wave voltage application to the root (Mizuguchi et al. 1994)

The growth rate of *Vigna mungo* was found to accelerate as a result of the voltage application as shown in Fig. 15.20. Prior to the precise examination of the growth acceleration condition, it was necessary to settle the culturing condition, especially the daylight illumination. Since bean sprout is cultured in the dark without light illumination, it was postulated that the growth acceleration effect could be recognized in the dark. In order to examine whether this expectation is working or not, we measured the degree of the growth acceleration by changing the daylight illumination time. As a measure of the acceleration degree, the number of shooting of the lateral root during the voltage application was counted. The reason why this method of determining acceleration was chosen is roughly proportional to the uptake rate of nutrition, and the rate is proportional to the total active surface area of root, which may be roughly proportional to the number of the lateral root after an appropriate period from shooting. The results are shown in Fig. 15.21, where we see that the results are opposing to our expectation and the acceleration degree is strongly dependent on the daylight illumination time.

Therefore, the voltage application experiment was performed in a weather-controlling chamber under 75% day light illumination at 22 °C and relative humidity of 50%. At first, the acceleration effect was examined for different wave shape. Examples are shown in Fig. 15.22, where we see the growth acceleration effect is dependent on not only the wave shape but also the amplitude of the wave. Too high voltage is expected to cause electrolytic decomposition of the electrolyte, which is unfavorable to the growth. This results in the most favorable voltage (amplitude) range for the acceleration.

With respect to the wave shape, the weakest effect was by the sinusoidal wave, and the strongest one by the square wave. The acceleration effect was

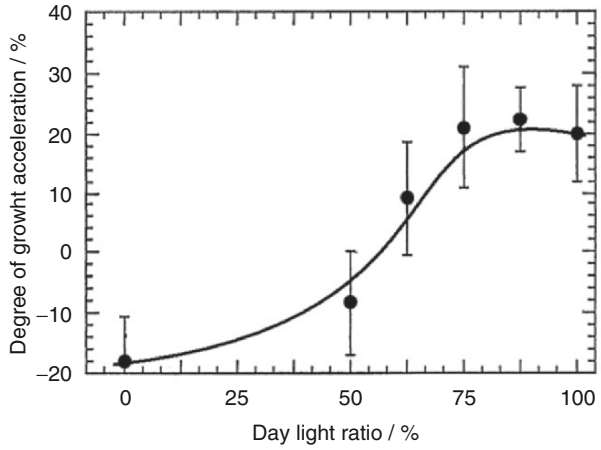

Fig. 15.21. Day light ratio (100% corresponds to 24 h illumination) dependency of the degree of the growth acceleration as measured by the number of lateral root shooting of *Vigna mungo* cultured in 0.5 mM K_2SO_4 solution for 5 days by application of 30 Hz square wave whose amplitude was 3 V (Matsuzaki H 1995)

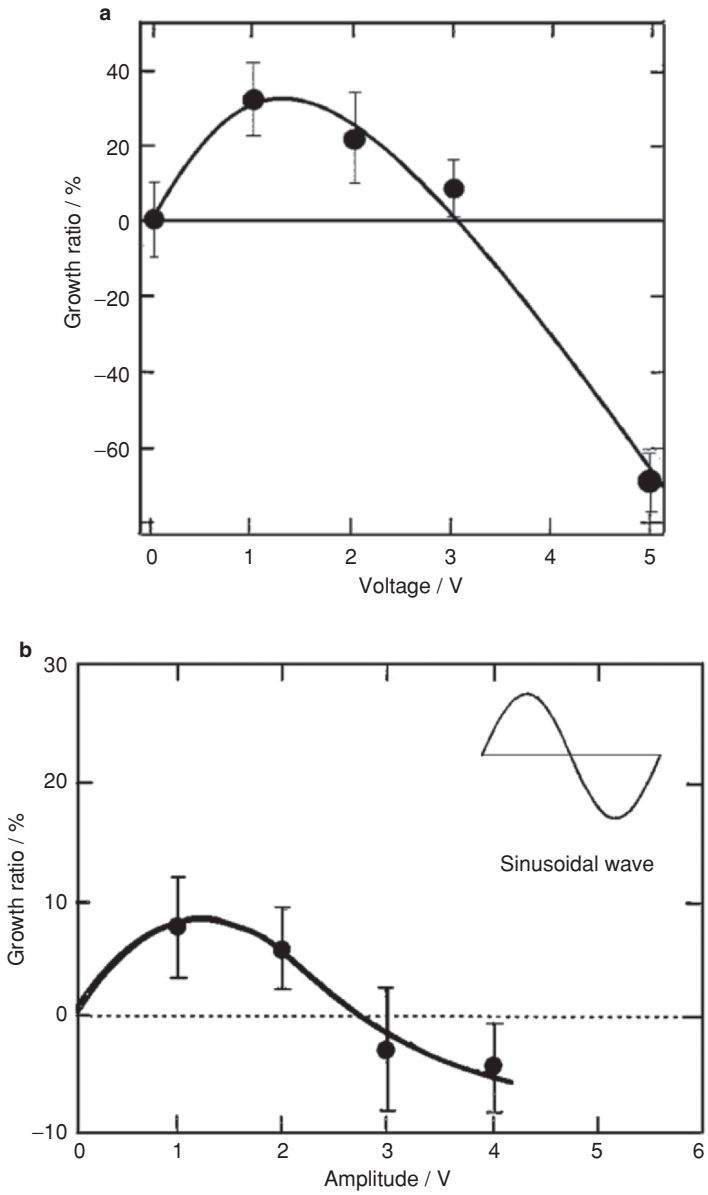

Fig. 15.22. Voltage (amplitude) dependency of the growth acceleration degree for *Vigna mungo* seedling cultured in 0.5 mM K_2SO_4 solution at 22 °C for 5 days with three different wave shapes. **a** Direct current; **b** sinusoidal wave 20 Hz (Mizuguchi et al. 1994)

found dependent on the frequency as well. The frequency dependence of the growth accelerating effect was examined for the most effective wave shape, the square wave, by keeping the amplitude to be constant at 3.5 V. The results are shown in Fig. 15.23, where the most effective frequency is shown around

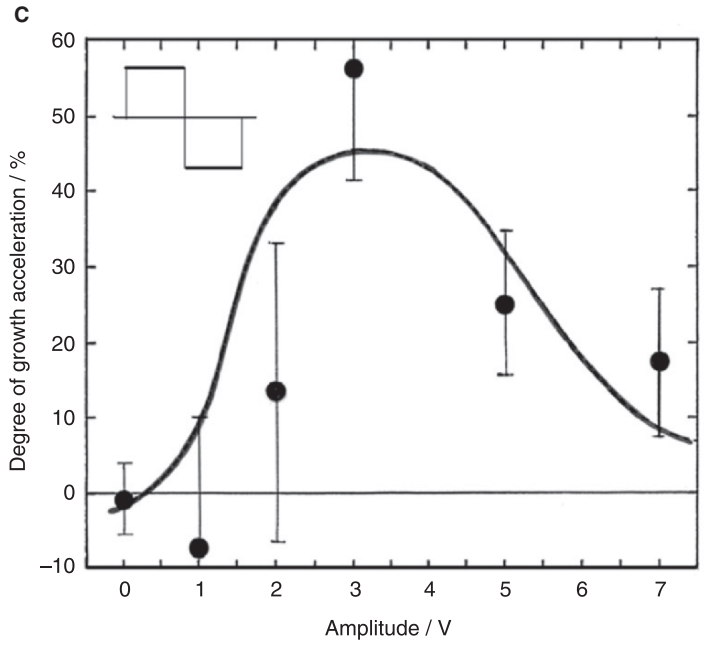

Fig. 15.22. (*Continued*) **c** square wave 20 Hz (Mizuguchi et al. 1994)

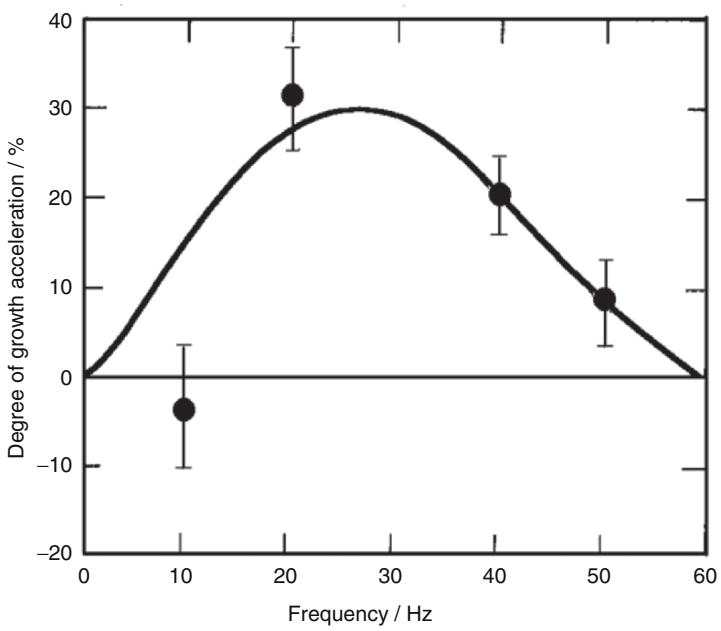

Fig. 15.23. Frequency dependency of the growth acceleration effect on 5 days old seedling of *Vigna mungo* cultured in 0.5 mM K_2SO_4 solution at 22 °C under the application of square wave whose amplitude was 3.5 V (Mizuguchi et al. 1994)

30 Hz. The reason why 30 Hz is the most effective will be discussed after examining the monocotyledon plant.

15.6 Growth acceleration of a monocotyledon seedling by application of potential in culturing bath

15.6.1 Introduction

In the preceding section, the growth acceleration effect on the dicotyledon seedling due to voltage application to the roots in a culturing bath was examined. It is interesting to examine that such can be found for the monocotyledon plant, as shown in this section. As the examining sample, *Zea Mays* was chosen, since this is one of the typical species and is easy to handle.

15.6.2 Experimental

After the sample seedlings of *Zea Mays* (L.) var everta Sturt were examined, the seeds were sterilized, and swelled for 25 h in 0.5 mM $CaSO_4$ aqueous solution at 25 °C in the dark. The seeds were then planted in the 0.3% agar culture ground. At the time when the radicle grew to 1 cm in length, they were planted on the net floating raft in the culturing vessel containing an aqueous solution of 7.35% KH_2PO_4 and 0.35% KOH. The vessel was kept in a weather controlling chamber at 22 °C and relative humidity 60% under 75% daylight illumination for 180 h. Then, they were taken out from the vessel and the degree of growth was evaluated by the measurement of the total length of the upper part from the cotyledon and counting the number of the lateral root shooting.

15.6.3 Results and discussion

15.6.3.1 Growing acceleration by square wave application

The degree of growth of seedlings exposed to voltage application was accelerated remarkably as shown in Fig. 15.24. The photograph to the right shows not only the leaf length but also how the number and length of the lateral root shooting are emphasized remarkably as compared to the control sample shown to the left. Since the square wave has been recognized to be the most effective for acceleration, the effect of the square wave for different frequencies and amplitudes was examined with summarizing results in Fig. 15.25. The results are summarized in Fig. 15.25. The most effective frequency and amplitude were 20 Hz and 5 V which are somewhat different from the data obtained with *Vigna Mungo,* viz, 30 Hz and 3 V, but falling within the range of the same category if we take the difference in culturing solution and culturing period into consideration.

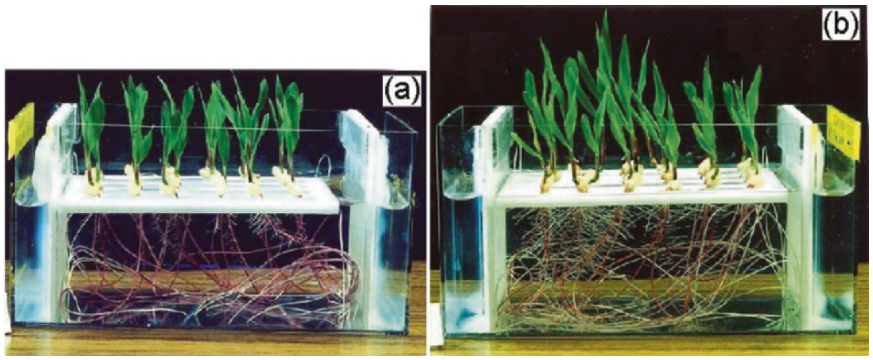

Fig. 15.24. Photograph of 180 h old *Zea Mays* seedlings cultured in an aqueous solution of 7.35% KH_2PO_4 and 0.35% KOH at 22 °C and relative humidity 60% under 75% daylight illumination. **a** Control without voltage application; **b** cultured by the application of 20 Hz square wave of 3.5 V amplitude during growth (Abe T 1994)

15.6.3.2 Mechanism analysis

At first the magnitude of the amplitude will be examined in relation to the field strength in the culturing bath during voltage application. Since the distance of the two facing Pt electrodes are 170 mm, the applied voltages of 5 V

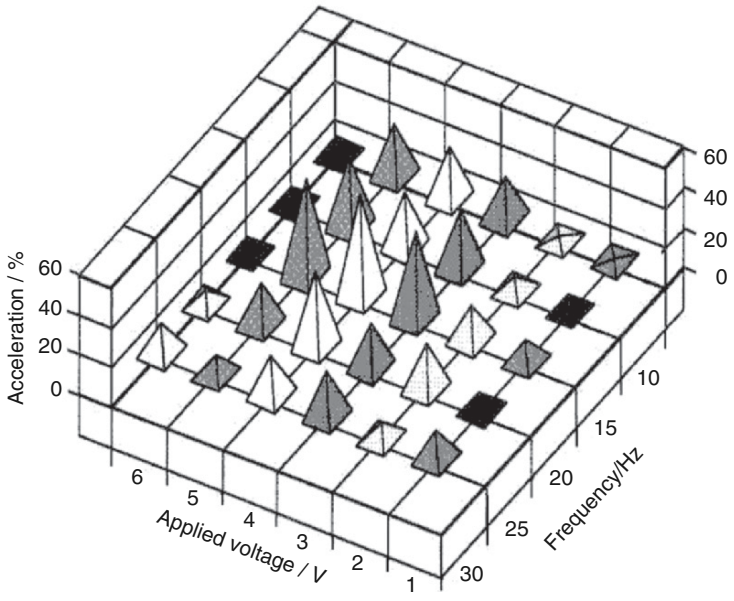

Fig. 15.25. Frequency and amplitude dependency of the growth acceleration of *Zea Mays* seedlings by the voltage application of square wave cultured in an aqueous solution of 7.35% KH_2PO_4 and 0.35% KOH at 22 °C and relative humidity 60% under 75% daylight illumination. The acceleration effect was evaluated based on the number of lateral root shooting (Abe T 1994)

and 3 V results in the electric field strength of 29 and 18 mV mm^{-1}, respectively. If the pulse potential strength of 30 mV mm^{-1} is applied between the two sides of the 1 mm thick root, the magnitude is nearly the same as that of the action potential amplitude reported by Abe et al. (1980), Abe and Takeda (1986), and Fromm and Spanswick (1993).

The applied voltage having the same order of magnitude as the action potential can assist to stimulate the action of the proton pump as far as the voltage stimulation program is similar to the change in action potential. The wave shape of a square wave where the voltage change is instantaneous is similar to that of an action potential change. The importance is the rapidity of the motion, since the motion of the proton pump entirely depends on the motion of the pump protein. A number of studies have been performed on the rapidity of the pump and the repetition rapidity has been reported to be around several tens of milliseconds (Danysza and Parsons 1998; Ostedgard et al. 2001).

A frequency of 20–30 Hz corresponds to several tens of milliseconds, which coincides with the repetition rate of the ion pump action. The coincidence appears not to be fortuitous since the repetition of the square wave with the same voltage magnitude to the action potential likely gives rise to resonance with the pump cell motion. The accelerated motion of the ion pump causes acceleration the metabolism, resulting in the acceleration of growth.

15.7 Control of lateral root shooting position

15.7.1 Introduction

In sections 5 and 6, it was shown that the application of a square wave voltage accelerates the growth of seedlings, but in these cases, the voltage application was performed homogeneously throughout the culturing solution, resulting in the homogeneous acceleration effect throughout the root. It is interesting to examine when only a specified portion of the seedling root is applied with square wave voltage and the rest of the root is alone. It is expected that the acceleration effect will be seen only where the voltage is applied. In this section, the results of this examination will be shown.

15.7.2 Experimental

The hand made experimental set up, mostly made with polymethylmetacrylate resin except for the glass Luggin capillaries, is shown in Fig. 15.26. At the bottom of the culturing compartment, the sample seedling was laid down and fixed with fixing nets. The culturing solution was 0.5 mM K_2SO_4 aqueous solution and two Pt electrodes were mounted in two Luggin capillaries whose tips were set facing near the seedling primary root. A 30 Hz square wave having an amplitude of 3 V was applied between the two Pt electrodes.

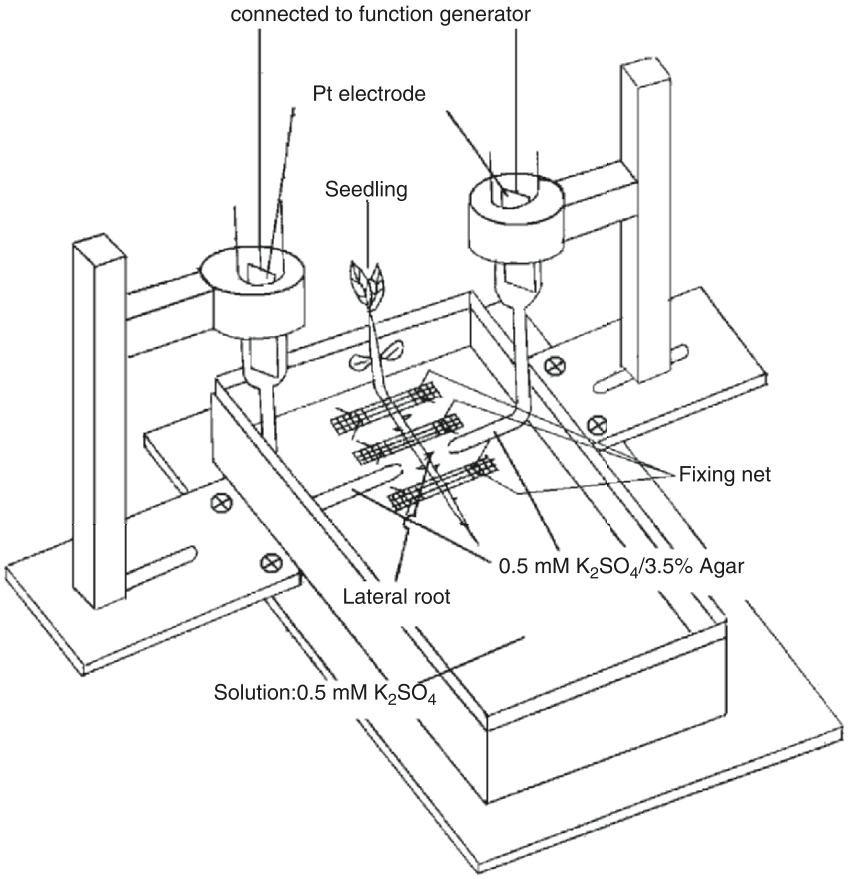

Fig. 15.26. Experimental set up for examining the effect of voltage application at the specified portion of the primary root (Kusunoki T 1995)

15.7.3 Results and discussion

15.7.3.1 Acceleration of lateral root shooting at voltage applied position

The number of lateral root shoots 6 days of culturing with applied voltage is shown as a function of the distance along with the primary root in Fig. 15.27. As shown in this figure, the number of shot lateral roots at the position of 0 mm, which corresponds to the voltage applied position, is increased as compared with those of its surroundings. This is the indication of acceleration of the shooting of lateral roots at the position where the square wave voltage is applied. The effect, however, faded away for long term culturing

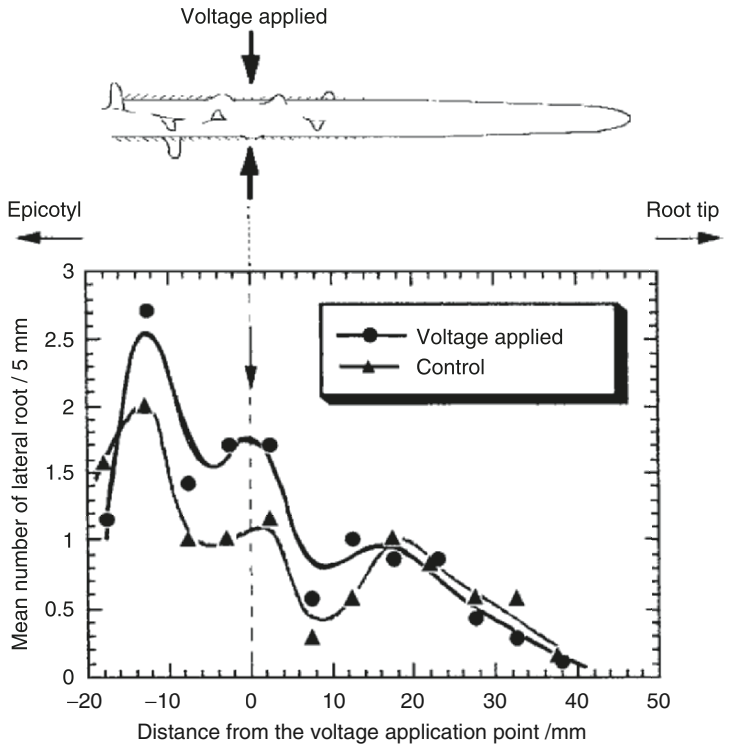

Fig. 15.27. Number of lateral root shot in each range of 5 mm length along the primary root during 6 days culturing in 0.5 mM K_2SO_4 at 22 °C. The seedling was set in the special vessel shown in Fig. 15.23 (Kusunoki T 1995)

where the nutrient supply from the cotyledon became decreased. The effect of nutrient supply will be shown more distinctly in the next section.

15.7.3.2 Wave shape and degree of acceleration

As already shown, the degree of acceleration is dependent on the shape of the applied wave, schematically shown in Fig. 15.28. The alternate wave and the direct current voltage application were found all effective, although the effectiveness depends on the wave shape. It is difficult to elucidate that the sinusoidal wave is less effective as compared to the direct current. The most effective wave was the square wave followed by the pulse wave, which implies that the sudden change in voltage is important for stimulation. The sudden voltage change is likely to accelerate the rotation of ion pumps, causing the acceleration of metabolism.

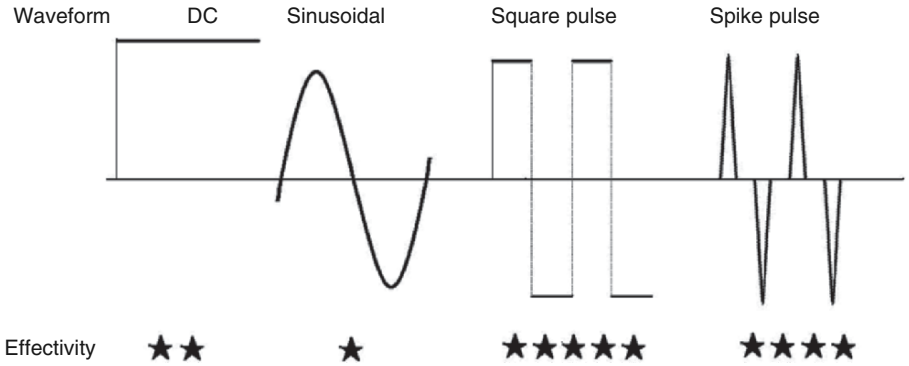

Fig. 15.28. Degree of the stimulating effect to the growth rate of mono- and dicotyledon plant seedlings due to application voltage to the root for several wave shapes. The magnitude is indicated with the number of stars

15.8. Effect of Ca^{2+} and phosphate ions for the growth acceleration by voltage application

15.8.1 Introduction

In section 4, absence of the cotyledon was shown to depress the metabolism activity of the seedling causing it to be worthwhile to investigate a seedling without cotyledon for the purpose of examining what types of ions are taking part in the acceleration mechanism. The acceleration effect due to the application of voltage, however, has been examined for seedlings having cotyledon alone in the preceding sections. Therefore, in this section, the results obtained with seedlings having no cotyledon in relation to the effect of presenting ions in the solution are shown.

15.8.2 Experimental

As the test specimen, seedlings of *Vigna mungo* (L.) Hepper of 1 day maturity were used after removing all the cotyledons from the seedling body.

Effects of the presence of Ca^{2+} was first examined by using a culturing solution containing only 0.05 mM K_2SO_4. Test culturing solutions containing different concentrations of calcium sulfate were prepared. In each test solution, the seedling were planted similar to the case shown in the preceding section, and a 30 Hz square wave having amplitude of 2.5 V was applied in the culturing solution at 22 °C with 70% daylight illumination.

15.8.3 Results and discussion

The growing feature in the absence of Ca^{2+} in the culturing solution is illustrated in Fig. 15.29 for the seedlings with and without cotyledon during 1 week.

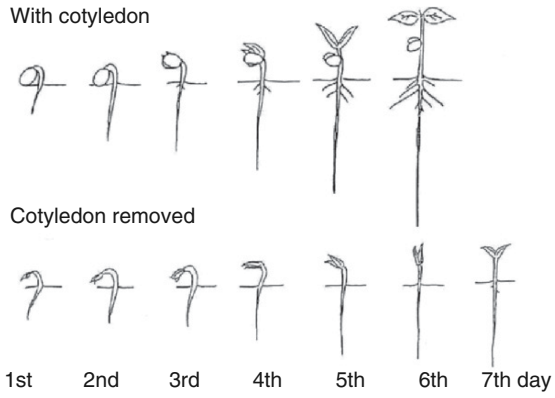

Fig. 15.29. Illustration of growing feature of *Vigna mungo* seedlings with and without cotyledon during culturing in a solution containing only 0. 5 mM K_2SO_4 under application 30 Hz square wave having amplitude of 2.5 V at 22 °C. The indicated date is the one after the planting on the culturing bed (Matsuzaki H 1995)

The seedlings lacking cotyledons grew slowly; the first leaves and the length of the radicle are poor as compared with those of seedlings having cotyledon, implying the cotyledon is very important to supplying nutrients for the metabolism of the seedling growth. Also, the application of voltage could not support enough accelerated rate to grow for the seedling having no cotyledon.

In the case of the Ca^{2+} ion, the growth rate was dependent on the Ca^{2+} concentration, which can be seen in Fig. 15.30 for a bean seedling having cotyledon. The growth rate was increased with the increase in Ca^{2+} concentration in both cases, with and without a square wave application, but it tended to be

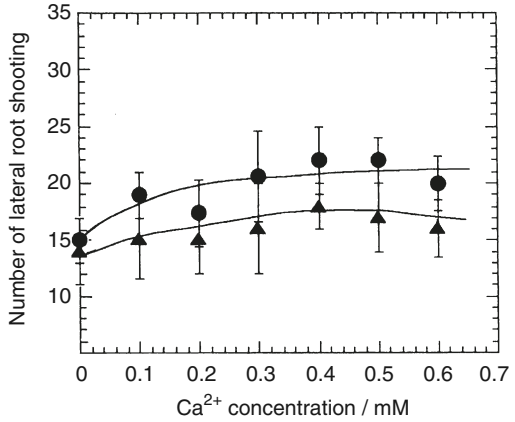

Fig. 15.30. Number of lateral root shooting of been seedling having cotyledon as a function of Ca^{2+} concentration in the culturing solution with (*circle*) and without (*triangle*) square wave applied (Matsuzaki H 1995)

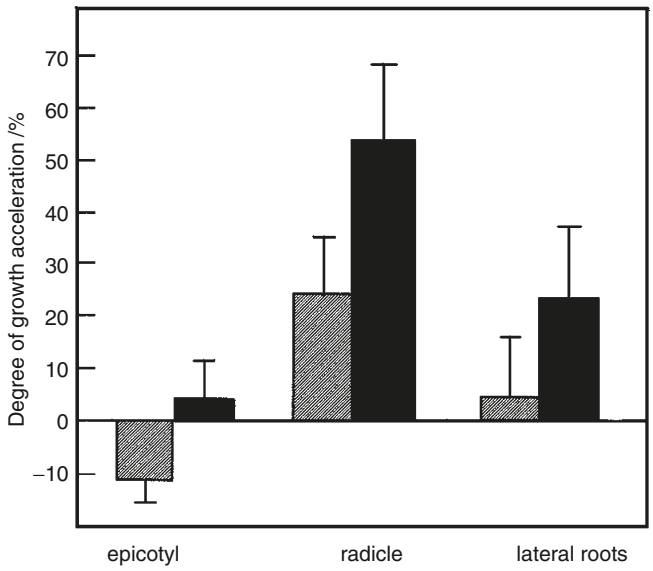

Fig. 15.31. Comparison of the growth amount of bean seedling (whose cotyledon was fully removed) within 6 days with (*black*) and without (*mesh*) square wave application in 0.05 mM K_2SO_4 containing 0.3 mM Ca^{2+} (Matsuzaki H 1995)

saturated at the concentration of 0.3 mM. This amount may be sufficient to support the cell activity of the ion-pump cell.

As clearly seen in Fig. 15.30, the voltage application could accelerate the growing rate of bean seedlings in the presence of Ca^{2+} added, even though the seedling has cotyledon from which some amount of Ca^{2+} is supposed to be supplied.

In the case without cotyledon, the effect of Ca^{2+} was remarkable, as shown in Fig. 15.31, where *Vigna* mungo, whose cotyledons were fully removed, are compared in cases with and without square wave applied for 6 days. Not only the lengths of epicotyl and radicle but also the number of lateral root shooting is quite enhanced by the square wave application. This shows the real effect of the square wave combined with the effect of Ca^{2+}.

15.9 Conclusions

Electrochemistry is useful not only for perusing the living mechanisms of plants but also to assist the plants to survive vividly. Due to the space limitation, an analysis of the ATP–ADP cycle could not be written in detail. According to Onoki's analysis (Onoki 1995) the amount of the two important substances did not show any remarkable change in the amount in the body of

growing *Vigna mungo* seedling during voltage application, in spite of the growth rate enhancement and enlarged amount of released proton. This implies that the ATP-ADP cycle reaction rate was accelerated by the enhanced action of ATPase during voltage application. The reason why the cycle was accelerated by the action of voltage application is not clear yet, which is an interesting future task to examine.

For the purpose of growth acceleration by the voltage application, a convenient practical method for the plant growing in nature has to be determined, which is another future task. Spreading the conductive carbon powder (black ash) combined with ferrite powder near the root will be helpful.

Acknowledgements. First of all, I would like to express my deep appreciation to Professor Alexander George Volkov for his kindness to provide me an opportunity to commit as one of the authors in this book. Without his invitation, almost all the materials will not have an opportunity to be opened to the public as an authorized form.

I extend my sincere thanks to the graduate students of my laboratory at the Department of Chemistry, Rikkyo University (Tokyo, Japan) for their hard work to accomplish all of this research, which ended at the time of my retirement from the university in 1995.

Pioneering work to establish the potential measuring system is due to Mr. S. Takeuchi, who also obtained Figs 15.1–15.5, and 15.8. Another pioneering work of growth rate acceleration is due to Mr. Y. Mizuguchi, who obtained Figs 15.19–15.23. Elegant observation and proof of Figs 15.6, 15.7, 15.13 and 15.14 was done by Miss Y. Watanabe (now Mrs. Y. Nakajima). The beautiful experiment on *Oryza* was done by Mr. M. Ashisada. Initiation of the research without cotyledons was done by Miss M. Tachizawa (now Mrs. M. Kawai) for obtaining Figs 15.15–15.18. Interesting results following local application of voltage were obtained by Mr. T Kusunoki (Figs 15.26 and 15.27). Elaborate work on the effect of Ca^{2+} was succeeded by Mr. H. Matsuzaki (Figs 15.21, 15.29–15.31). Mr. T. Onoki carried out precise determination of ATP and ADP by HPLC for the analysis of the proton pump action together with obtaining Fig. 15.11. The author's deep thanks are due to Mrs. C. Nakahara for her kindness to settle all the equipments.

The financial support by Mitsubishi Zaidan was most helpful in purchasing the expensive equipment.

Finally, my deep appreciation is due to my wife, Kiyoko, for her persistent encouragement throughout the preparation process of this article.

References

Abe S, Takeda J (1986) The membrane potential of enzymatically isolated *Nitella expansa* protoplasts as compared with their intact cells. J Exp Bot 37:238–252

Abe S, Takeda J, Senda M (1980) Resting membrane potential and action potential of *Nitella expansa* protoplasts. Plant Cell Physiol 21:537–546

Abe T (1994) Effect of potential application to the growth of grasses cultured in water. Thesis for bachelor degree, Department of Chemistry, Rikkyo University, Tokyo, Japan

Ashisada M (1995) Ion concentration on the surface of radicle during the metabolizm and the potential distribution. Thesis for master degree, Department of Chemistry, Rikkyo University, Tokyo, Japan

Bibikova T, Gilroy S (2003) Root hair development. J Plant Growth Regul 21:383–415

Danysza W, Parsons CG (1998) Glycine and N-methyl-D-aspartate receptors: physiological significance and possible therapeutic applications. Pharmacol Rev 50:597–664

Dubrovsky JG, Rost TL, Colón-Carmona A, Doerner P(2001) Early primordium morphogenesis during lateral root initiation in *Arabidopsis* thaliana. Planta 214:30–36
Ezaki S, Toko K, Yamafuji K, Irie F (1988) Electric potential patterns around a root of the higher plant. Trans IEICE E71:965–967
Ezaki S, Toko K, Yamafuji K (1990a) Electrical control of growth of the higher plant. Memoirs of the Faculty of Engineering Kyushu Univ 50:379–393
Ezaki S, Toko K, Yamafuji K (1990b) Electrical stimulation on the growth of root of the higher plant. Trans IEICE E73:922–927
Fromm J, Spanswick R (1993) Characteristics of action potentials in willow (*Salix communis* L.). J Exp Bot 44:1119–1125
Grove MD, Spencer FG, Rohwededer WK, Mandava NB, Worley JF, Warthen JD Jr, Steffens GL, Flippen-Anderson JL, Cook JC Jr (1979) Brassinolide, a plant growth promoting steroid isolated from *Brassica napus* pollen. Nature 281:216–217
Henderson P(1907) Zur Thermodynamik der Flüssigkeitsketten. Z Physik Chem 59:118–128
Iwabuchi A, Yano M, Shimizu H (1989) Development of extracellular electric pattern around *Lepidium* roots: its possible role in root growth and gravitropism. Protoplasma 148:94–100
Kusunoki T (1995) Topological potential application to the root of bean radicle and the shooting of the rateral root. Bachelor Degree Thesis, Department of Chemistry, Rikkyo University, Tokyo, Japan
Matuzaki H (1995) Mechanism of the growth acceleration of plant in the electric fields. Master Degree Thesis, Department of Chemistry, Rikkyo University, Tokyo, Japan
Miwa Y, Kushihashi Y (1992) Study of information field in morphognensis of plans (1st report, measurement of bioelectric potential distribution on callus surface and around primary root). Nihon Kikaigakkai Rep (C) 58:216–221
Mizuguchi Y, Watanabe Y, Matsuzaki H, Ikezawa Y, Takamura T (1994) Growth acceleration of bean sprouts by the application of electrochemical voltage in culturing bath. Denki Kagaku 62:1083–1085
Noguchi T, Fujioka S, Choe S, Takatsuto S, Yoshida S, Yuan H, Feldmann KA, Tax FE (1999) Brassinosteroid-insensitive dwarf mutants of Arabidopsis accumulate brassinosteroids. Plant Physiol 121:743–752
Onoki T(1995) HPLC analysis of the amount of ATP and ADP in the seedling body *of Vigna mungo* (L.) Hepper during growth with the square wave application to the root. Master Degree Thesis, Department of Chemistry, Rikkyo University
Ostedgard LS, Baldursson O, Welsh MJ (2001) Regulation of the cystic fibrosis transmembrane conductance regulator Cl^- channel by its R domain. J Biol Chem 276: 7689–7692
Rajasekaran LR, Blake TJ (1998) Early growth invigoration of jack pine seedlings by natural plant growth regulators. Trees Struct Funct 12:420–423
Richard DE, King KE, Ait-ali T, Harberd NP (2001) How gibberellin regulates plant growth and development: a molecular genetic analysis of gibberellin signaling. Annu Rev Plant Physiol Plant Mol Biol 52:67–88
Scherer GFE (2002) Secondary messengers and phospholipase Az in auxin signal transduction. Plant Mol Biol 49:357–372
Tachizawa M (1995) Potential distribution near the root of bean radicle in a culturing bath containing integral nutrients. Bachelor Degree Thesis, Department of Chemistry, Rikkyo University, Tokyo, Japan
Takeuchi S, Watanabe Y, Ikezawa Y, Takamura T (1994) Potential distribution and ionic concentration near the radicle surface of growing bean sprouts. Denki Kagaku 62:352–353
Toko K, Yamafuji K (1988) Spontaneous formation of the spatial pattern of electric potential in biological systems. Ferroeletrics 86:269–279
Watanabe Y, Takeuchi S, Ashisada M, Ikezawa Y, Takamura T (1995) Potential distribution and ionic concentration at the bean root surface of the crowing tip and lateral root emerging points. Plant Cell Physiol 36:691–698
Zullo MAT, Kohout L (2004) Semisystematic nomenclature of brassinosteroids. Plant Growth Regul 42:15–28

16 Electrophysiology of Turgor Regulation in Charophyte Cells

MARY J. BEILBY,[1] MARY A. BISSON,[2] VIRGINIA A. SHEPHERD[1]

16.1 Turgor regulation

16.1.1 What is turgor pressure?

Turgor pressure is the difference in hydrostatic pressure between the inside and outside of a plant cell. A positive turgor pressure is generated when an osmotic gradient draws water into the cell, but cell expansion is limited by the ability of the cell wall to expand. The pressure that results is a function of the elastic modulus of the cell wall:

$$dP = \varepsilon * (dV/V) \tag{16.1}$$

[See Nobel (1974) for a discussion of water relations in plants, and Findlay (2001) for a recent review of water movement and turgor regulation.] A positive pressure is generally seen as a good thing for plants, particularly by those who work with terrestrial plants. Turgor drives the expansion growth of walled cells. It has a primary responsibility for generating form in non-woody tissues, as the positive pressure inflates the cell, constrained by the often asymmetrically strengthened cell wall. Loss of turgor is considered a bad thing, as environmental factors that reduce turgor cause damage to the plant and loss of agricultural yield (Boyer 1982; Bartels and Nelson 1994). This can be due to a number of factors, such as the inability of cells to grow, of roots to penetrate through the soil, of leaves to expand to optimize photon capture, etc. Turgor is lost when water is withdrawn; shrinkage of the cell results in loss of turgor, again determined by the volumetric elastic modulus (ε; Eq. 16.1). Water is withdrawn from the cell when the water potential outside the cell becomes lower than that inside the cell; this is referred to as hypertonic stress. This term is preferable to the term "hyperosmotic stress", since osmotic pressure is not the only determinant of water movement. Water potential, defined as the chemical potential of water divided by the partial molar volume of water, is affected by a number of different factors, such as hydrostatic pressure, dissolved solutes (osmotic pressure), and the presence of surfaces (matric potential, capillary force, or colloid osmotic pressure).

[1] Department of Biophysics, School of Physics, University of New South Wales, Sydney NSW Australia

[2] Department of Biological Sciences, University at Buffalo, Buffalo NY 14260 USA

Plant Electrophysiology – Theory & Methods (ed. by Volkov)

Those working on aquatic plants, however, particularly marine plants, need to keep in mind that an increase in turgor has greater potential danger than a decrease. A decrease in turgor is often reversible and non-lethal, particularly if it is small and transient enough that plasmodesmata are not disrupted or cytoplasm markedly dehydrated. An increase in turgor results from an influx of water due to hypotonic stress. (Note that in plant cells, the medium is typically hypo-osmotic even when it is isotonic, because of the effect of turgor on the cells' water potential. "In this case the term 'hypo-osmotic'" to describe the stress is particularly misleading.) Turgor that is sufficient to exceed the mechanical strength of the cell wall results in rupture, which is irreversible and inevitably fatal. Aquatic plants adapted to high salinity often respond to hypotonic stress more rapidly than to hypertonic stress (Bisson and Kirst 1980b; Hoffmann and Bisson 1990; Stento et al. 2000).

16.1.2 How do plant cells regulate turgor?

In order to regulate its turgor in response to environmental challenges, a cell must first be able to determine when its turgor has been perturbed. The mechanism by which a cell measures its turgor is not known in any case. Numerous hypotheses have been proposed (Coster and Zimmermann 1976; Gutknecht et al. 1978; Pickard and Ding 1992, 1993; Bisson and Kirst 1995; Heidecker et al. 1999; Shepherd et al. 2002; Kacperska 2004). They generally invoke physical differences that occur as a result of pressure on or differential pressure across the membrane. This might include proximity between elements of the membrane and cell wall, curvature of the membrane globally or locally, compression of the membrane, and tension within the membrane. Communication of these changes to the cell may occur by alteration in the activity of membrane proteins, particularly ion transporters, and hence may have electrophysiological consequences. For instance, stretch-activated or -inactivated channels within the membrane could change membrane conductance (G) and electrical potential difference across the membrane (PD). These channels themselves could admit calcium into the cytoplasm, or the alteration of PD could activate calcium channels. Calcium could alter the activity of various transporters or enzymes directly or indirectly through the activation of various signal transduction factors. In order to affect turgor, these changes need to result in an alteration of cytoplasmic osmotic pressure that reverses the movement of water and restores the desired turgor. If these processes involve the transport of charged species, they are likely to have electrophysiological consequences.

16.1.3 Other consequences of turgor stress

Survival of osmotic stress involves more than regulating turgor. For instance, if rapid turgor regulation results in a disruption of normal ion ratios, these may need to be restored over the long term, or ionic solutes replaced with

non-ionic ones (Kirst 1977; Bisson and Gutknecht 1980). Osmotic stress may have a number of pathological effects, often related to oxidative stress, and response to these may have electrophysiological consequences (Smirnoff 1998; Hasegawa and Bressan 2000). These are not, strictly speaking, turgor regulation, but may be confused with it, and may cause alterations of electrophysiological parameters after turgor itself has been restored to normal.

16.2 Why study giant-celled algae?

16.2.1 Advantages of aquatic systems

We study responses to osmotic stress in algae that have extraordinarily large cells. There are a number of reasons to study these so-called "giant-celled" algae. Higher plants in terrestrial systems are not uniform. Different parts of the plant experience different kinds and different degrees of water stress, and water stress from soil (with large matric potential) or air (dehydration stress) is difficult to control. Water is often not in equilibrium, but rather there is net water flow through the plant. Growing plants under hydroponic conditions can alleviate some of these problems, but generates its own stresses.

In aquatic environments, on the other hand, water potential of the medium is dominated by its osmotic pressure, which is generated by dissolved solutes:

$$\pi = RT\,\Sigma\gamma\,[X] \tag{16.2}$$

where R and T have their usual meanings, [X] is the concentration of each solute, and γ is the osmotic coefficient which takes into account the non-ideality of that solute, that is, the degree to which the solute interacts chemically with other molecules, rather than just physically displacing water molecules. γ is generally less than or equal to one, lower for ions than for non-ionic solutes, and lower for divalent ions than for monovalent. Osmotic pressure reduces the water potential of the solution, so that, in the absence of other influences on water potential,

$$\psi = -\pi \tag{16.3}$$

In aquatic systems, when cells are bathed in a uniform solution, and the membranes are highly permeable to water, water is in equilibrium across biological membranes, and the internal water potential is equal to the external water potential:

$$\psi^{out} = \psi^{in} \tag{16.4}$$

If the internal osmotic pressure is not equal to the external, water will move until the resultant hydrostatic pressure difference (see Eq. 16.1) increases the internal water potential and balances the osmotic difference, and internal and external water potentials are equal:

$$\psi^{out} = -\pi^{out} = \psi^{in} = \Delta P - \pi^{in} \tag{16.5}$$

Hence, at equilibrium,

$$\Delta P = \pi^{in} - \pi^{out} = \Delta\pi \tag{16.6}$$

External osmotic stress can therefore be delivered in a simple, quantitative fashion, by altering natural ions or other solutes. Turgor can be estimated as $\Delta\pi$, and regulation of turgor achieved by manipulating π^{in}. The cells can be studied in a situation that is very close to their natural condition.

The situation is not always quite that simple, however. Equation 16.6 is true only for simple solutes and ideally semipermeable membranes, that is, membranes that have a much higher permeability to water than to solutes. If solutes can pass the membrane, this movement will tend to dissipate differences in concentration and hence in osmotic pressure. Just as the non-ideality of the solute is accounted for by the osmotic coefficient γ, the non-ideality of the membrane is described by the reflection coefficient σ. σ is usually between 0 and 1. As σ decreases from 1, ΔP decreases from $\Delta\pi$, so that at steady state

$$\Delta P = \sigma\Delta\pi \tag{16.7}$$

In addition, if colloidal substances are present in solution, they will also decrease the water potential. This is sometimes described as colloid osmotic pressure, although a more correct term is matric potential. This component of water potential is usually neglected, even in the cytoplasm, where filamentous proteins and membranes can generate a significant matric potential. The osmotic relations of most cells, however, are controlled by the vacuole, whose contents are often a simple salt solution. However, colloidal substances may be associated with cell walls and sometimes in the vacuole, at least in the case of the salt-tolerant Charophyte *Lamprothamnium* (Shepherd and Beilby 1999; see Fig. 16.1).

16.2.2 Advantages of studying algae

Complex plants have numerous cell types with different functions and potentially different responses to turgor changes. One must therefore either study a complex response due to contributions from numerous sources of uncertain similarity, or isolate individual cell types, with resultant risk of altering their physiological activities. The algae we describe here have relatively few cell types, with turgor regulatory responses dominated by a single cell type. In angiosperms, moreover, cells communicate with one another via plasmodesmata with variable transcellular conductance (Roberts and Oparka 2003). Thus, ion transport processes in one cell will cause alterations in membrane potential of adjacent cells, dependent on the unknown conductivity of the intercellular connections, and it is difficult to disentangle the effects of transport in neighboring cells. While cells in some of the algae we study are

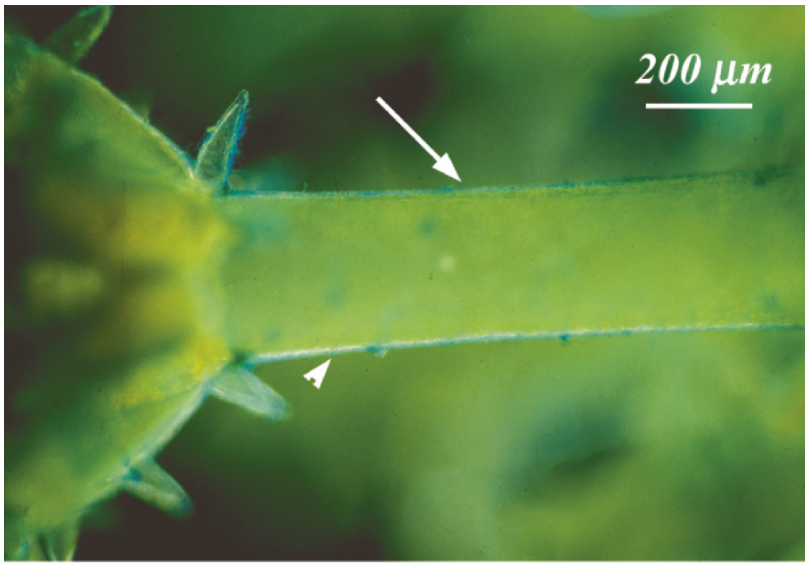

a

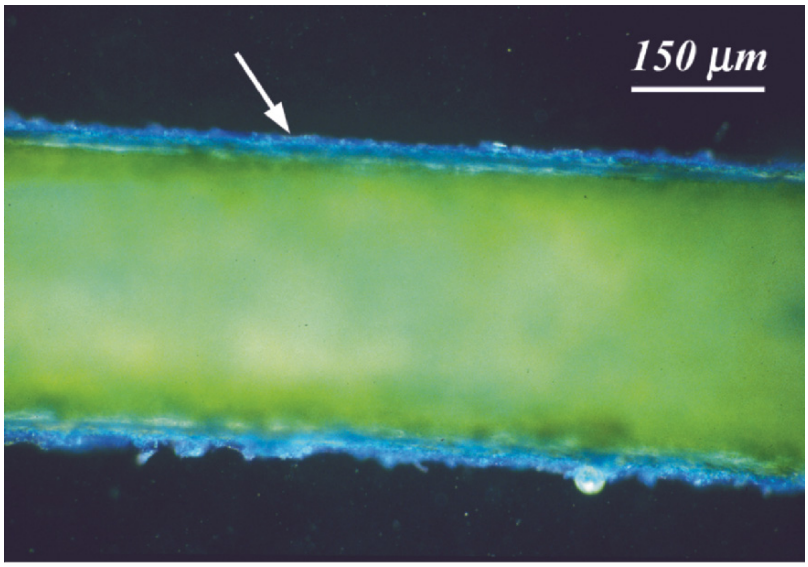

b

Fig. 16.1. a, b The extracellular sulphated polysaccharide mucilage layer secreted by *Lamprothamnium* cells becomes progressively thicker with increasing age of cells. This correlates with a change from a "fast-regulating" response to hypotonic treatment (young cells, with thin mucilage) to a "slow-regulating" response (older cells with thick mucilage). Both figures show cells from a *Lamprothamnium* plant growing in a mesohaline ditch (salinity of ~1/2 seawater). Cells were stained with an Alcian Blue cationic stain at low pH. Sulphated polysaccharides appear bright blue. Cells were photographed using dark-field optics. **a** Internodal cell close to the apex of the plant. The mucilage layer is thin (~7 µm) and small areas of the mucilage are lightly staining (large arrow), whilst other areas are unstained (*arrowhead*). **b** Internodal cell from the central region of the plant (5th internode from the apex). The mucilage (*arrow*) is thicker (~22 µm), and heavily stained, indicating the presence of substantial amounts of sulphated polysaccharides

plasmodesmatally connected, the giant cells in which measurements are made dominate the overall electrophysiological characteristics.

16.2.3 Advantages of studying algae with giant cells

Electrophysiological measurements present particular constraints. In early experiments, they could only be made by impaling the cell with microelectrodes, an act that could result in damage that was inversely related to the size of the cell. Advances in technology have enabled measurements on smaller cells using patch clamp techniques, but these present their own difficulties, particularly in plant cells. Patch clamp methodology requires an intimate interaction between the membrane and the patch pipette, and this requires removal of the cell wall. This presents a number of difficulties, from the use of fungal enzymes that induce anti-pathogen responses with their own electrophysiological consequences (Gelli et al. 1997), to the elimination of turgor itself. While such techniques can provide useful information about the activity of particular transport systems, processes that involve complex relationships between different systems will inevitably be disrupted. Marked differences have been noted between the activity of individual transporters, as determined by patch clamp techniques, and the integrated electrophysiological characteristics of intact cells (Tyerman and Skerrett 1999). Since wall-less cells have no turgor, impalement of intact, walled cells is the only way to assess electrophysiological parameters related to turgor regulation processes.

Given that one must impale turgid cells, the advantage of large cells is clear. If a smaller fraction of the surface area of the cell is perturbed by the intruding microelectrode, damage is less likely to impair cellular activity. Large cells can often be impaled by a number of probes simultaneously, to measure voltage, inject current, measure pressure, etc. However, the cells are not infinitely robust, and multiple impalements may cause damage that can affect turgor regulation.

Large cells can also be perfused, that is, the internal contents can be removed and replaced with a controlled solution of choice (Gutknecht 1967; Fujii et al. 1979; Smith and Walker 1981; Clint and MacRobbie 1987; Shimmen et al. 1994; Beilby et al. 1997). This gives the experimenter greater ability to control parameters when trying to understand the causes and significance of electrophysiological changes. Even turgor can be controlled in a perfused cell (Hastings and Gutknecht 1974). Of course, physiological alterations due to damage to the cell and removal of critical components will also ensue.

Finally, different parts of a single cell can be physically or electrically isolated. This is the basis of the "K-anesthesia" method of measuring PD without impalement (Shimmen et al. 1994) and also for measuring Ca^{2+} and Na^{+} fluxes (Clint and MacRobbie 1987; Reid and Smith 1993; Whittington and Bisson 1994), which are often important for turgor regulation, and necessary to explain the ionic basis of the electrophysiological responses measured.

16.3 Charophyte algae

Of all the algae, Charophytes have been best studied using electrophysiological techniques. Their phylogenetic relations are briefly summarized here

16.3.1 Phylogeny

The "green plants" or Viridiplantae are now viewed as containing two evolutionary lineages or clades, the Charophyta and the Chlorophyta (Fig. 16.2; Karol et al. 2001). The charophyte clade contains the charophyte algae and embryophytes (land plants), whilst the chlorophyte clade contains essentially the rest of the green algae.

Charales. Of the five orders within the charophyte clade, only members of the Charales have been the subjects of sustained research into turgor regulation. The Charales are regarded as a sister group to land plants (Graham and Gray 2001; Karol et al. 2001; Turmel et al. 2001; Lewis and McCourt 2004; McCourt et al. 2004). This conclusion has been reached on the basis of morphological and ultrastructural data, including the presence in both land plants and Charales of "true" plasmodesmata, as well as molecular characteristics, including genes (the 18 s and 26 s rRNA nuclear genes, actin nuclear genes, rbcL and atpB plastid genes, nad5 mitochondrial genes) and whole genome characteristics, such as presence of introns, and the whole plastid and mitochondrial genomes (see Fig. 16.1, and Lewis and McCourt 2004).

The Charales are closer relatives of land plants than they are of the chlorophyte green algae. For example, the sequenced cDNA for the vacuolar H^+-pump in *Chara corallina* is 71% identical to V-ATPases of land plants, but less than 46% identical to that of *Acetabularia* (Nakanishi et al. 1999). The mitochondrial genomes of *Chara vulgaris* and the liverwort *Marchantia* are strikingly similar, apart from diversity of introns. The mitochondrial genome of the ancestor common to both Charales and land-plants was then ". . . tightly packed, gene-rich, and relatively intron poor. . ." (Turmel et al. 2001).

The capacity to regulate turgor pressure is closely related to salinity tolerance of extant Charales (see below). A search for the aetiology of turgor regulatory mechanisms thus provokes the question of whether the charophytes had a marine or a freshwater ancestry.

The earliest fossil spores of liverwort-like land plants date from the Ordovician, 475 million years ago (Graham and Gray 2001). The Charales diverged from land plants before then, but the fossil record is unfortunately incomplete, and definite charophyte fossils of the Ordovician, or earlier, are lacking. The earliest (Paleozoic) fossils of charophytes suggest that these lived in a marine environment. However, it is likely that ancestors of the Paleozoic charophytes migrated from freshwater into the sea, radiated there, and subsequently remigrated back into both brackish waters, and fresh water. The

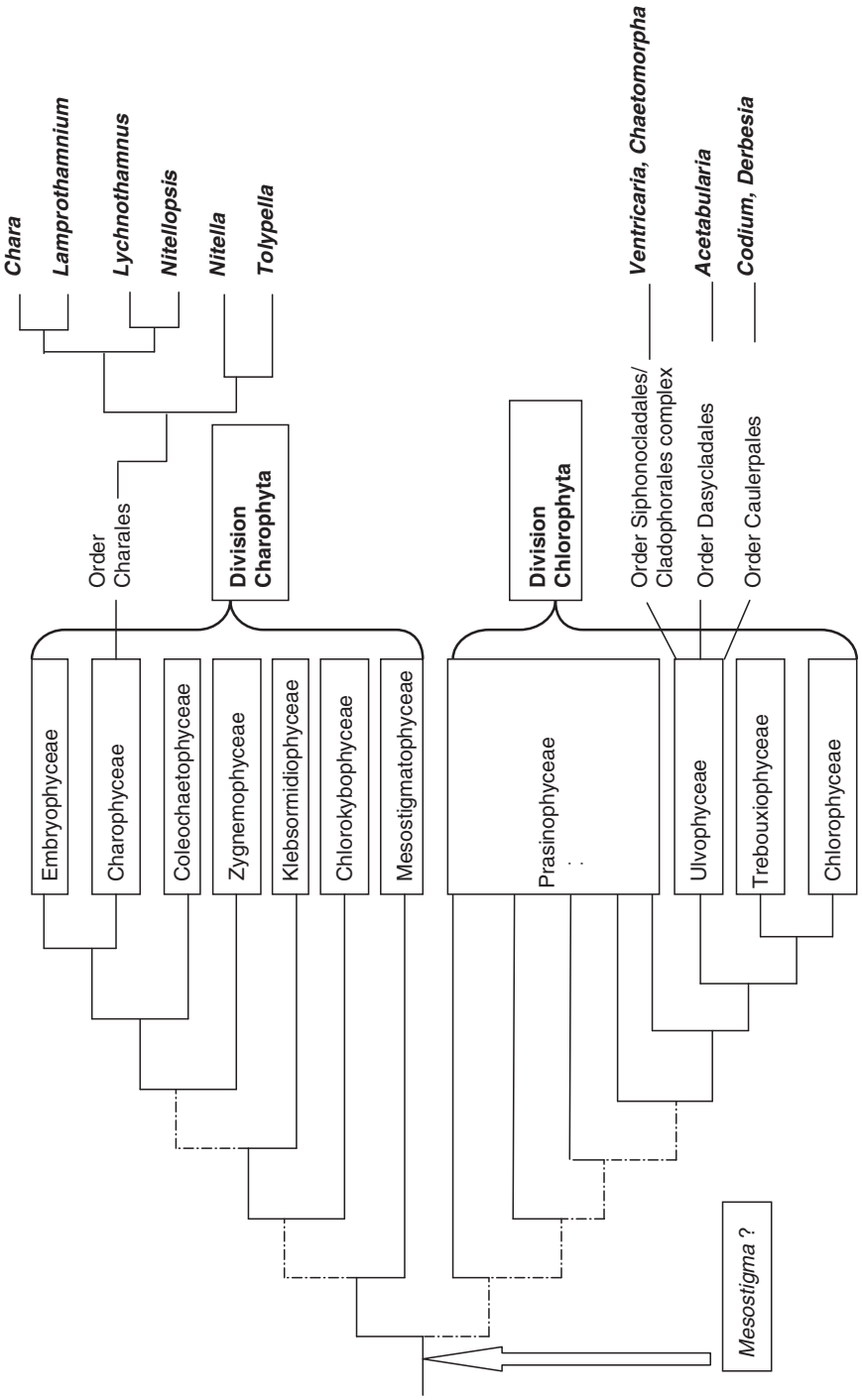
Chara
Lamprothamnium
Lychnothamnus
Nitellopsis
Nitella
Tolypella
Ventricaria, Chaetomorpha
Acetabularia
Codium, Derbesia
Order Charales
Division Charophyta
Division Chlorophyta
Order Siphonocladales/ Cladophorales complex
Order Dasycladales
Order Caulerpales
Embryophyceae
Charophyceae
Coleochaetophyceae
Zygnemophyceae
Klebsormidiophyceae
Chlorokybophyceae
Mesostigmatophyceae
Prasinophyceae
Ulvophyceae
Trebouxiophyceae
Chlorophyceae
Mesostigma ?

predominance of freshwater Charales supports this concept of an ultimately freshwater ancestry. That so many extant members of the Charales do inhabit brackish environments points to a more recent ancestor inhabiting a saline environment.

Of extant salt-tolerant forms, some *Tolypella*, some *Chara*, and *Lamprothamnium* species completely regulate their turgor pressure through accumulation of K^+, Cl^-, Na^+ and occasionally sucrose. These organisms inhabit a wide range of saline environments, up to and sometimes exceeding marine levels of salinity. Complete turgor regulators include *Tolypella nidifica* and *T. glomerata* (Winter et al. 1996), *Chara buckelli* (now *C. longifolia*) (Hoffmann and Bisson 1986), and *Lamprothamnium* (*papulosum* or *succinctum*) (Bisson and Kirst 1980a; Okazaki et al. 1984). Some *Tolypella* and *Chara* species are found in moderately saline Australian lakes (up to 50 g/l), whilst *Lamprothamnium* species can live in fully marine or ~150 g/l hypersaline environments (Williams 1998). The extraordinary *Lamprothamnium* can reproduce sexually in highly saline environments, and species bearing oogonia were observed in Australian saline lakes at 1–2 times the salinity of seawater (Burne et al. 1980).

Some Charales are capable of partially regulating turgor pressure, using K^+ and Cl^- fluxes, but these fluxes do not keep pace with the increased Na^+ at higher salinities. These partial turgor-regulators include the brackish dwellers *Chara canescens* (Winter and Kirst 1991) and *Chara aspera* (Winter and Kirst 1992). Some of the Charales, such as *Nitellopsis obtusa* and *Chara vulgaris* inhabit mildly brackish environments. *Nitellopsis obtusa* lacks the ion transport mechanisms of both the complete and partial turgor-regulators, and does not survive for longer than a week in brackish media above 15 $mOsmol.kg^{-1}$ (Winter et al. 1999). *Chara vulgaris* partially regulates turgor with Na^+ and Cl^- fluxes, but long-term salinity stress results in loss of K^+ from the vacuole (Winter and Kirst 1990).

Obligate inhabitants of freshwater, such as *Chara corallina* and *Nitella flexilis,* do not regulate turgor pressure. Instead, they regulate internal osmotic pressure through K^+ concentration in their cell vacuoles (Gutknecht et al. 1978; Sanders 1981; Bisson and Bartholomew 1984).

Tolypella belongs on a different phylogenetic branch to both *Chara* and *Lamprothamnium* (Fig. 16.2). The two species investigated by Winter et al.

Fig. 16.2. A schematic diagram of the major relationships between the green algae, showing only the orders from which organisms have been selected for experiments into turgor-regulation. Mechanisms of turgor regulation differ in the two Divisions Charophyta and Chlorophyta, but turgor regulation within the Orders of these Divisions shows many similarities. Figure based on molecular systematic data (Fig. 1, Karol et al. 2001; Table 2 and Fig. 18, Lewis and McCourt 2004) and nuclear DNA data (Kapraun 2005). The branch lengths are not quantitative. Note that the Class Prasinophyceae is currently undergoing revision; it may be polyphyletic, as indicated

(1996) completely regulate turgor pressure by adjusting K^+ and Cl^- concentrations, and to some extent sucrose. In these aspects, the turgor-regulating mechanism is essentially the same as that found in *Lamprothamnium* (See section 16.3.2.3). These authors conclude that the ancestor common to *Chara*, *Lamprothamnium* and *Tolypella* was salt-tolerant. However, in contrast to *Lamprothamnium*, these *Tolypella* species cannot sexually reproduce in the high salinity environment. This may be the reason that they occupy brackish environments up to 550 $mOsmol.kg^{-1}$, although their vegetative bodies can tolerate the more saline environment.

The wide range of salinity tolerances within the Charales and their close relationship to land plants makes them ideal experimental material for studying turgor pressure regulation and salinity tolerance of the higher plants. In particular, in the genus *Chara*, where some species are salt-tolerant turgor regulators, some can partially regulate turgor pressure, and others are obligate freshwater species, we have a unique opportunity to seek what it is that has been gained or lost when the transition was made to the terrestrial, and largely salt-sensitive, lifestyles of land plants. Thus, the capacity for turgor regulation in land plants, which has been particularly well studied in guard cells and phloem loading, may well be an elaboration of the primal capacities found within the charophytes.

16.3.2 Advantages to study

Charophytes have long been the subject of electrophysiological studies, and as a result, there is an extensive body of information about them (Hope and Walker 1975; Tazawa et al. 1987). The elongated cylindrical shape of the large internodal cells is particularly suited to the "K-anesthesia" method of measurement of PD and the flux measurements mentioned above. This shape can also generate problems in assessing conductance because of its cable properties, but these are easily remedied by computational methods.

Like most large plant cells, the bulk of the volume of the cell is occupied by the vacuole. In most cases, the microelectrodes are placed into the vacuole, and the electrophysiological measurements are made on two membranes in series. Measurements can be made across the plasma membrane only, however, by careful placement of the microelectrode (Spanswick and Williams 1964), by eliminating the vacuole by centrifugation and ligation (Beilby and Shepherd 1989), or by perfusion (Fujii et al. 1979; Smith and Walker 1981; Beilby et al. 1997). These experiments indicate that the tonoplast has a small PD and high conductance, so that the properties of the plasma membrane dominate those of the two membranes in series. To interpret these electrophysiological responses in terms of ion fluxes, however, it is critical to know the ion concentrations of all three compartments: vacuole, cytoplasm, and external medium. Sampling of the vacuole is simplified by its large volume, and direct measurements of vacuolar ion concentrations are therefore easy to

make [see Hope and Walker (1975) and Raven (1975, 1985) for examples]. Estimates of cytoplasmic concentrations can be made by a combination of computational methods and physical separation (Hope and Walker 1975; Reid and Smith 1992; Whittington and Bisson 1994). Optical methods have been used to estimate cytoplasmic calcium activity (Williamson and Ashley 1982).

Cytoplasmic streaming is a well studied property of charophyte cells (Williamson and Ashley 1982; Reid and Walker 1983; reviewed in Shimmen and Yokata 1994). This plays two significant roles in physiological studies. One is that healthy cells show vigorous streaming, and this can therefore be used to assess the health of the cell during experiments. The other is that elevated calcium inhibits streaming, so that an abrupt, transient cessation of streaming is a good indication of a transient increase in cytoplasmic calcium.

As mentioned above, charophytes are evolutionarily most closely allied to the green algal line that gave rise to higher plants (Graham 1993; Karol et al. 2001), and therefore make good models for them. They show electrophysiological similarities, in particular a hyperpolarized membrane potential due to a vanadate-sensitive H^+-pumping ATPase (Spanswick 1972, 1980, 1981; Smith and Raven 1979; Sze et al. 1999). The strongly negative membrane potential affects the driving force for any passive ion movement. Moreover, many active transport systems are due to symport or antiport with protons, and are therefore dependent on the electrochemical driving force for $H^+\left(\Delta\overline{\mu}_H\right)$ generated by this pump.

16.3.2.1 Ionic species likely to have an effect on electrophysiological properties during turgor regulation

The primary solutes playing a role in osmotic adjustment of turgor are the ions K^+ and Cl^-. These are accumulated or removed from the vacuole to alter osmotic pressure and restore normal turgor (Okazaki et al. 1984; Hoffmann and Bisson 1986). There must be two transport steps to accomplish this, one at the plasma membrane and one at the tonoplast.

Potassium. We can quickly describe the driving force on ion movement by comparing the Nernst potential of ions to the PD. The Nernst potential (E_X) is determined by the following equation:

$$E_X = -\frac{RT}{z_X F} \ln \frac{[X]^{in}}{[X]^{out}} \tag{16.8}$$

The Nernst potential is the membrane potential at which a given ion concentration ratio is at equilibrium. If the PD is more negative than E_X, positive ions will be driven into the cell and negative ions driven out. No net driving force occurs when the PD=E_X. When PD is more positive than E_X, positive ions will be driven out of the cell and negative ions drawn in.

Under normal circumstances (moderate K^+ and neutral pH), the cytoplasm of charophytes is negative to the Nernst potential for K^+. In low salt

medium, the external K^+ is typically 0.1–0.2 mM, and cytoplasmic [K^+] is about 115 mM; hence, E_K is about −150 to −175 mV. The PD is strongly dependent on pH (Bisson and Walker 1982; Beilby 1989), but at neutral pH is about –220 mV. In this case, K^+ may be taken up passively into the cytoplasm by a variety of transport mechanisms (Beilby 1986b).

In salt culture, the external K^+ is elevated, but cytoplasmic K^+ increases only slightly (Hoffmann and Bisson 1986). This decreases E_K to −60 to −80 mV, and at neutral to slightly alkaline pH, both salt-tolerant charophytes *Lamprothamnium* and *C. longifolia* are usually more negative than this, so the same overall forces on K^+ pertain. Again, alterations in the membrane potential that normally occur during turgor regulation (see below) may alter this circumstance—if the membrane depolarizes to a value less than E_K, passive uptake will diminish and export can occur passively.

The energetics of movement from the cytoplasm to the vacuole are more variable between species and conditions, because the vacuolar concentrations of ions are more variable, as would be expected in a compartment that is not highly metabolically active. In freshwater, vacuolar K^+ concentrations range from 40 to 80 mM, and therefore E_K is around 9–25 mV, vacuole positive. The potential difference across the tonoplast is about 10 mV, vacuole positive (Spanswick and Williams 1964), probably due to inwardly directed H^+ pumps (Shimmen and MacRobbie 1987). K^+ is therefore likely to be close to equilibrium across this membrane, and will move easily across this membrane through a variety of K^+ channels (Lühring 1986; Laver and Walker 1987; Tyerman and Findlay 1989) in a direction that will shift with slight changes in the driving force. In salt-acclimated charophytes, vacuolar K^+ is strongly correlated with external osmotic pressure, and can be as high as 400 mM (Bisson and Kirst 1980a; Okazaki et al. 1984; Hoffmann and Bisson 1986). E_K at this extreme would be around −30 mV. Whether the PD across the tonoplast shifts under these conditions is not known, so what the driving forces are on K^+ at this membrane is not clear.

Chloride. The cytoplasm of charophytes is always negative to the Nernst potential for Cl^- in freshwater media, typically about +40 to +75 mV, with cytoplasmic concentrations 10–20 mM and external concentrations 1–2 mM (Hope and Walker 1975). Therefore, Cl^- is lost to the external medium by passive transport and must be taken up actively. The active uptake of Cl^- has been characterized as a $2H^+$:Cl^- symport (Beilby and Walker 1981; Sanders et al. 1985). This means that Cl^- influx generates a positive inward current, and that it is influenced by the driving force for $H^+\left(\Delta\overline{\mu}_H\right)$ which is generated by the H^+-pumping ATPase, which has distinctive I–V characteristics (Beilby 1984) (see section 16.3.2.3). In saline media, on the other hand, external concentrations of Cl^- of 150–250 mM mean that E_{Cl} is much more negative, –40 to –80 mV. Plasma membrane PD is typically more negative than this, so that the same driving forces described above apply, but depolarization of the membrane during turgor regulation can reverse these relations.

The energetics of movement from the cytoplasm to the vacuole is again variable. In freshwater, vacuolar Cl^- concentrations are 110–150 mM (Hope and Walker 1975), and therefore E_{Cl} is around 45–70 mV, vacuole positive. This is more positive than the tonoplast PD of 10 mV, and Cl^- therefore is lost passively from the vacuole and must be actively transported in, by an unknown mechanism. In salt-acclimated charophytes, Cl^- is strongly correlated with external osmotic pressure, and can be as high as 600 mM (Bisson and Kirst 1980a; Okazaki et al. 1984; Hoffmann and Bisson 1986). E_{Cl} at this extreme would be around +100 mV. Whether the PD across the tonoplast shifts under these conditions is not known, but it seems unlikely to become that positive.

16.3.2.2 Turgor regulation

Hypotonic stress. The decrease in osmolarity of the medium due to concentration drop of ionic or non-ionic solutes increases the water potential, driving water into the cell to regain equilibrium (Eq. 16.6). If the medium change is a step function, the water inflow occurs within seconds (Steudle and Zimmermann 1974; Zimmermann and Steudle 1974). Such an event can occur in nature when salt-tolerant charophytes growing in brackish shallow ponds experience a sudden downpour that dilutes the pond surface. In this case the main constituent diluted is NaCl. In the laboratory the dilution can be rapid or gradual, achieved by reducing ionic concentrations or neutral osmolytes such as sorbitol or mannitol. The advantage of applying the rapid (step) change in medium osmolarity is that the subsequent cell response can be clearly resolved.

Table 16.1. Experimental hypotonic steps used in studying Charophytes, SW-seawater

Reference	Initial medium, $mOsmol \cdot kg^{-1}$	Hypotonic step, $mOsmol \cdot kg^{-1}$	Material
Wichmann and Kirst (1989)	260	150 and 250	*Lamprothamnium succinctum*
Stento et al. (2000)	225	100	*Chara longifolia*
Hoffmann and Bisson (1990); Bisson et al. (1995)	370	150	*Chara longifolia*
Okazaki et al. (1984); Okazaki and Tazawa (1986a,b, 1987); Okazaki and Iwasaki (1992); Beilby and Shepherd (1996); Beilby et al. (1999); Okazaki et al. (2002)	370 (~1/3 SW)	150 (to ~1/6 SW)	*Lamprothamnium succinctum*
Reid et al. (1984)	750 (~3/4 SW)	250 (to ~1/2 SW)	*Lamprothamnium succinctum*
Shepherd et al. (1999); Shepherd and Beilby (1999)	1072 (full SW)	268 (to 3/4 SW)	*Lamprothamnium succinctum*

A number of labs have studied a number of different species under a range of conditions, as summarized in Table 16.1. As described below, responses of cells may vary with species, age and size of cells, and the conditions to which they are subjected. Care must therefore be taken in comparing different experiments.

Changes in PD, conductance and streaming rate. Bisson and Kirst (1980b) found that *L. succinctum* showed a mixed response of resting PD to hypotonic step of 200–300 mOsmol.kg^{-1}. Cells in a depolarized state prior to hypotonic challenge generally hyperpolarized, while cells with more negative initial PDs hyperpolarized, depolarized or remained steady in about equal proportion.

Subsequent studies all found resting PD going more positive upon hypotonic exposure. Reid et al. (1984) found in *L. succinctum* rapid membrane depolarization from −170 mV to about −80 mV. The membrane repolarized after about 30 min to an intermediate level between −110 and −100 mV. Okazaki et al. (1984) measured a similar change in PD in *L. succinctum*, which lasted for more than 60 min. They also monitored the membrane resistance and found a transient drop from about 0.75 ohm.m^2 to less than 0.1 ohm.m^2 within 5 min of hypotonic exposure (1/3 SW to 1/6 SW). Further, they showed that a drop in ionic concentration alone, achieved by isosmotic substitution of sorbitol for NaCl, did not result in PD or resistance change.

Okazaki and Tazawa (1986a,b), using *L. succinctum*, demonstrated Ca^{2+} involvement in the hypotonic regulation. The cytoplasmic streaming was inhibited for up to 20 min after hypotonic exposure. The increase in $[Ca^{2+}]^{cyt}$ was implicated as the cause, because $[Ca^{2+}]^{cyt}$ greater than 1 μM inhibited streaming in *Lamprothamnium* tonoplast-free cells. The decrease of $[Ca^{2+}]^{o}$ from 1 mM to 0.01 mM (or exposure to Ca^{2+} antagonist nifedipine at concentration greater than 25 μM) inhibited turgor regulation, and prevented both cessation of streaming and the large conductance increase in first 10 min, but did not prevent membrane depolarization. Thus, influx of Ca^{2+} from the medium seemed necessary for hypotonic regulation. However, the story was complicated by the finding of Okazaki and Tazawa (1987) that tonoplast-free cells of *L. succinctum* did not regulate turgor, despite sufficient Ca^{2+} in the perfusion medium. The authors assumed that some other cytoplasmic factor is required. Using intact cells, Okazaki et al. (1987) used aequorin to measure the increase in $[Ca^{2+}]^{cyt}$ during hypotonic regulation. In SW with normal Ca^{2+}, light emission increased after about 1 min, indicating an increase in $[Ca^{2+}]^{cyt}$. If the hypotonic stress was given in low Ca^{2+} SW, light emission did not increase. Subsequent to addition of more external Ca^{2+} an increase in light emission occurred within seconds. The authors reasoned that opening of the Ca^{2+} channel mediated by turgor increase occurred with delay of about 1 min. Once the channels were opened and Ca^{2+} was supplied, the influx into the cytoplasm was instantaneous.

Hoffmann and Bisson (1990) exposed *Chara longifolia* to a decrease in external osmolality from 375 to 225 mOsmol.kg^{-1}, and found a similar shift of

the membrane PD from about −125 to −75 mV, lasting for more than 60 min. The conductance increased from about 2 $S.m^{-2}$ to up to 29 $S.m^{-2}$ in first 10 min of hypotonic stress.

Okazaki and Iwasaki (1992) utilized a similar hypotonic step and found a depolarization from about −200 mV to −80 mV, lasting at least 20 min, with conductance rising from about 2 to 19 $S.m^{-2}$ in first 10 min and remaining at about 5 $S.m^{-2}$ at 20 min. They also measured cytoplasmic streaming rate and Cl^- efflux. They found a good correlation between increased conductance, increased Cl^- efflux and streaming inhibition, demonstrating the involvement of Ca^{2+}-activated Cl^- channel.

Bisson et al. (1995) discovered more complexities about the hypotonic regulation in *C. longifolia*. One complexity is a size dependence of the rate of turgor regulation: small cells (less than 10 mm in length) regulated turgor within 60 min, while cells longer than 30 mm required 3 days. Another complexity is that Ca^{2+} is not required for all phases of turgor regulation. Turgor regulation in small cells proceeded in two phases: the first reduced turgor by about 25% in 5 min, the second returned turgor to steady state level in 40 min. The second phase of regulation was inhibited by low Ca^{2+} concentration in the medium (decrease from 4.6 mM to 0.01 mM). The low Ca^{2+} SW also inhibited the streaming stoppage and the transient conductance increase (from 5 to 15 $S.m^{-2}$) in the initial 20 min of hypotonic exposure. The influx of $^{45}Ca^{2+}$ was measured and increased influx was found in cells less than 7 mm in length. The initial depolarization was inhibited by passage of hyperpolarizing current pulses after the cell was exposed to hypotonic medium. The cells regulated turgor in low ionic strength medium (APW with sorbitol added to 375 $mOsmol.kg^{-1}$ and subsequently removed to produce hypotonic step to 225 $mOsmol.kg^{-1}$), with only minimal Ca^{2+} (0.1 μM). The authors reasoned that the initial depolarizing agent is unknown and acts with or without Ca^{2+} in the medium. This depolarization subsequently activated the K^+ channels. The opening of the Ca^{2+}-activated Cl^- channels was assumed to follow in the second phase of the turgor regulation, which was inhibited by low Ca^{2+} medium.

Beilby and Shepherd (1996) applied current-voltage (I/V) analysis to the hypotonic effect in *L. succinctum,* and these results will be discussed in more detail in the next section. They blocked the K^+ channels with 20 mM TEA and the Ca^{2+} channels with 0.5 mM $LaCl_3$ (consequently preventing the activation of the Cl^- channels). They found that the Cl^- channel activation preceded (with some overlap) the K^+ channel opening. They confirmed that the initial depolarizing mechanism is independent of Ca^{2+} concentration and is not inhibited by TEA. Similarly to Bisson et al. (1995), Beilby et al. (1999) found that cells vary in their ability to regulate turgor (as measured by changes in vacuolar concentrations of K^+, Cl^- and Na^+). Young apical *Lamprothamnium* internodes responded to hypotonic shock with the canonical response described above, i.e. depolarization, cessation of streaming, and transient increase of conductance. These cells achieved more than 90% regulation in 1 h, and were referred to as FR (fast regulating) cells. Older, more basipetal

cells responded to hypotonic shock with much smaller depolarizations (~20 mV), unchanged streaming speed, and small or no change in conductance. The vacuolar concentrations of K^+, Cl^- and Na^+ hardly changed within 1 h, but continued to decrease over 24 h. Na^+ participated less in the regulation. These cells were coated with extracellular mucilage more than 10 μm thick (see Fig. 16.1a, b) and were called SR (slow regulating) cells. The extracellular mucilage was identified by histochemical staining (Toluidine Blue and Alcian Blue at low pH) as a sulphated polysaccharide (Shepherd et al. 1999). Its thickness was a direct function of both the salinity of the environment where the plants were growing, and of cell age. Cells from plants growing in SW had thicker mucilage than those growing in 1/2 SW. However, in both environments, the mucilage progressively increased in thickness, proceeding from cells at the apex of a plant to those at its base. This was coupled, in cells from a single plant, with a change from FR (apical cells) to SR (basal cells) behavior.

Treating mucilaginous cells with heparinase enzyme both removed the capacity of the mucilage for staining with cationic dyes at low pH, and converted SR behavior to an extreme form of FR behavior (Shepherd and Beilby 1999). Heparinased cells depolarized, cytoplasmic streaming halted, and cell conductance increased 4-fold. These features are consistent with recovery of Ca^{2+} activation of Cl^- channels, which is absent or reduced in SR cells. However, the PD remained at close to zero, or even at positive values, and the cells retained their elevated conductances for at least 1 h. Removal of heparinase led to an overnight recovery of normal electrophysiology, restoration of staining with cationic stains at low pH, and a restoration of the canonical SR response to hypotonic treatment.

Patch clamp experiments were performed on the tonoplast membrane surrounding cytoplasmic droplets on both types of cells. FR cells have two types of K^+ channel, 150 pS and 35 pS, and a small conductance Cl^- channel of 35 pS. SR cells also have two similar types of K^+ channel, 90 pS and 35 pS. The small conductance Cl^- channels displayed greater degree of activity.

The FR and SR cells also differed in how they sequestered the fluorochrome 6-carboxyfluorescein (6CF): FR cells accumulated 6CF in cytoplasm, SR cells in the vacuole. We speculated that the vacuolar system in FR cells has complex topology of canalicular elements, whereas large central vacuole has formed in SR cells.

Stento et al. (2000) performed elegant experiments with two adjacent *C. longifolia* cells to measure turgor and electrical characteristics simultaneously. They found that membrane depolarization, increased conductance and cessation of cytoplasmic streaming indicated fast turgor regulation. Cells that showed small depolarization, no streaming stoppage and small increase in conductance, were slow regulators. They did not systematically determine whether mucilage was present or whether differences in the cell structure similar to those described above occurred. The Ca^{2+} antagonists verapamil and nifedipine were applied at the time of hypotonic exposure. The verapamil effects were too variable to show any trend. At concentrations 25–50 μM,

nifedipine irreversibly inhibited the Ca^{2+} entry and thus subsequent streaming stoppage and conductance increase due to Cl^- outflow. The turgor regulation on a short time scale (80 min) was inhibited. At a lower concentration of nifedipine (5 μM), the cells regulated turgor, but the response was delayed. Cytoplasmic streaming rate remained constant throughout the experiment. The influx of $^{45}Ca^{2+}$ was measured in steady state and under hypotonic stress. There was no significant difference $^{45}Ca^{2+}$ influx in steady state and hypotonic stress. However, the steady state flux was insensitive to nifedipine, while hypotonic flux was reduced by 54%. The authors suggested that the steady state flux declined as hypotonic stress-induced flux increased.

Okazaki et al. (2002) injected Fura-dextran into cytoplasm of *L. succinctum* to correlate the increase in $[Ca^{2+}]^{cyt}$ with the membrane conductance and the streaming rate at the time of hypotonic regulation. The increase in $[Ca^{2+}]^{cyt}$ commenced about 50 s after hypotonic step from 360 to 210 $mOsmol.kg^{-1}$. $[Ca^{2+}]^{cyt}$ increased from steady state value of 100 nM to about 500 nM in about 60 s. The conductance peaked at 300 nM $[Ca^{2+}]^{cyt}$. The total streaming stoppage required around 600 nM $[Ca^{2+}]^{cyt}$. Thus the streaming as indicator of $[Ca^{2+}]^{cyt}$ has to be viewed with caution, as small $[Ca^{2+}]^{cyt}$ increase may not be reflected in changes of streaming rate. One of us (M.A.B.), working with N. Allen and E. Johansson, noted that in rhizoids of *Chara,* fura-dextran was rapidly accumulated in the endoplasmic reticulum. Some care must therefore be taken in assuming that the fluor is uniformly distributed in the cytoplasm.

16.3.2.3 I/V profiles and modeling

Many transport processes across the cell membrane involve movement of charge and can be modeled by electrical circuit of parallel conductances (see Fig. 16.3). The circuit in Fig. 16.3a illustrates only a small fraction of the charophyte plasma membrane transporters, but these contribute most of the total membrane conductance. In the large charophyte cell the transmembrane PD, V, can be controlled by the voltage clamp method.

In the current–voltage (I/V) protocol, the membrane, or membranes, are voltage-clamped to a bipolar staircase command. Starting with the voltage-clamp at the resting level, the membrane PD is stepped up and down until preset limits are reached. The PD is returned to resting level in between the depolarizing and hyperpolarizing pulses. The I/V data can be easily analyzed only if the conductances turn on and off within the pulse period and RP (resting potential) reset time, respectively (Beilby 1989, 1990).

The total current, I_{Total}, flows through populations of transporters that are opened at that membrane PD. Fortunately, the I/V characteristics are very distinct for each type of transporter. Inward rectifier channels are activated as V approaches some negative PD level (around −250 mV in Fig. 16.3b,c). The current due to the inward rectifier, I_{irc}, (long-dashed line, Fig. 16,3b, c) then contributes to the I_{Total} at more negative PDs. Similarly, the outward rectifier

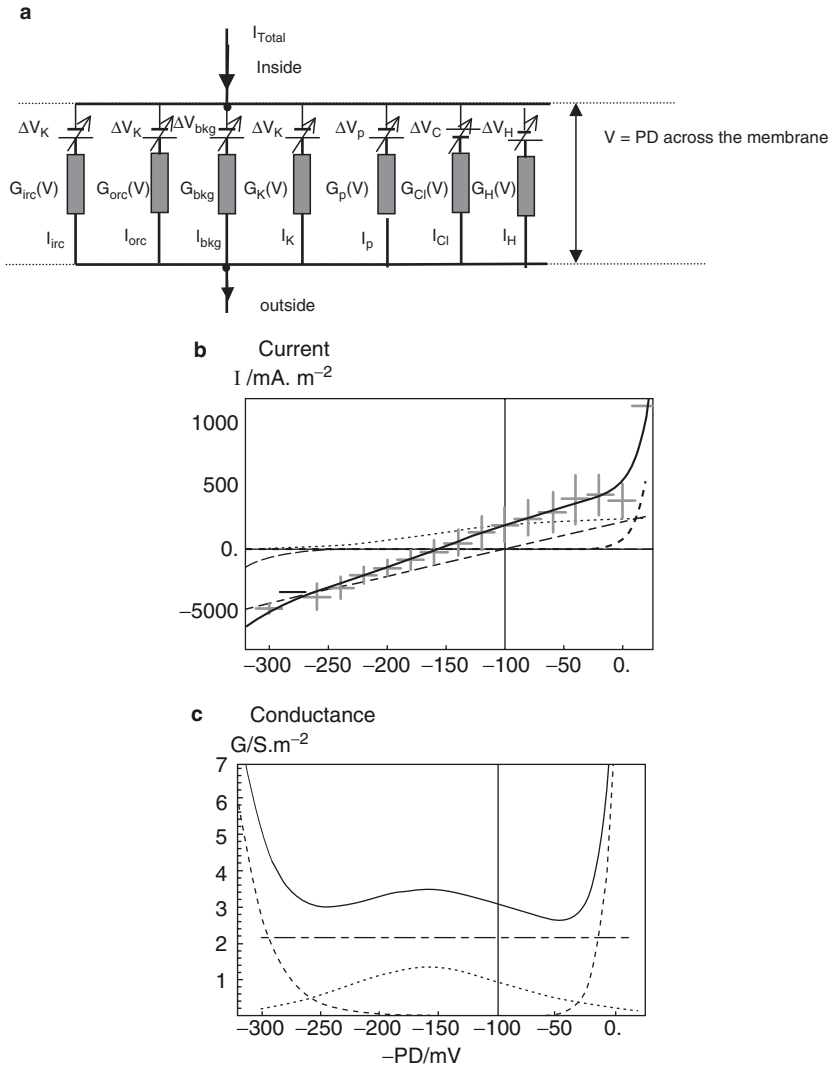

Fig. 16.3. a The circuit model of the membrane, see text for detailed explanation. **b** Data from six *Lamprothamnium* cells in 0.4 SW were gathered into 20 mV slots (*horizontal error bars*) with standard error shown as *vertical error bars*. The total current (*continuous dark line*) was fitted as sum of I_p (*dotted line*), I_{bkg} (*uneven dashed line*), I_{orc} (*short dashed line*) and I_{irc} (*long dashed line*). **c** Conductance, types of lines as in **b**

current, I_{orc}, activates at about −25 mV (short-dashed line, Fig. 16.3b, c). The free-running membrane PD is kept negative by the action of the proton pump current I_p (dotted line, Fig. 16.3b, c). The ubiquitous background current, I_{bkg}, is revealed (unequal-dashed line, Fig. 16.3b, c) when the cell is subjected to a metabolic blockade. The other three types of transporters, Ca^{2+}-activated Cl^-

channels, large conductance K^+ channels and H^+ channels, are activated when the proton pump is inactivated (see Beilby 1989, for review).

The transporters in Fig. 16.3a are of two kinds, ion channels and a pump (ATPase). For most channels, the motive force, ΔV_X, is the difference between the membrane PD and E_X (Eq. 16.8). As described in section 16.3.2.2., if V (the PD) is more negative than E_X and the channel is open, the efflux of cations or influx of anions will result in a negative current. No net current will flow if $V=E_X$. When V is more positive than E_X, the efflux of cations or influx of anions will result in a positive current. The potential energy for the ion transport comes from the unequal concentrations of the ions on each side of the membrane, and from the imposed membrane PD. The conductances of the various transporters depend on the PD in complex ways. These can be modeled by the Goldman–Hodgkin–Katz (GHK) equation, supplemented by Boltzmann statistics. The nature of the "background conductance", G_{bkg}, is not clear at present. G_{bkg} is independent of PD. The reversal PD, E_{bkg}, is found near −100 mV in both *Chara* and *Lamprothamnium*. It cannot be attributed to the Nernst potential of any particular ion that is abundant in the cells and in their habitat. However, we have evidence that at least some of the channels contributing to G_{bkg} are mechanosensory or stretch-activated channels (SA channels: Shepherd et al. 2002).

The nature of the motive force for the pump, ΔV_p, is different, and comes from the hydrolysis of ATP. In the free running state, the proton pump moves protons against their electrochemical gradient and hyperpolarizes the membrane PD by more than 100 mV. The dependence of the pump current, I_p, on membrane PD has been fitted by the HGSS (Hansen, Gradmann, Sanders and Slayman) model (Beilby 1984; Blatt et al. 1990).

The model. The background current, I_{bkg}, with PD-independent conductance, G_{bkg}, and reversal PD, E_{bkg}, near −100 mV is always present. The background current was fitted by an empirical equation

$$I_{bkg} = G_{bkg}\,(V - E_{bkg}) \tag{16.9}$$

The identity of the I_{bkg} carriers is not clear at present, but there is an experimental evidence for such a linear profile 'background state' in both *Chara* and *Lamprothamnium* (Beilby 1985; Beilby and Shepherd 2001a). For cells in hyperpolarized state the pump current, I_p, dominates:

$$I_p = zFN\,\frac{k_{io}\kappa_{io} - k_{oi}\kappa_{oi}}{k_{io} + k_{oi} + \kappa_{io} + \kappa_{oi}} \tag{16.10}$$

$$k_{io} = k_{io}^0 e^{\frac{zFV}{2RT}} \tag{16.10a}$$

$$k_{oi} = k_{oi}^0 e^{-\frac{zFV}{2RT}} \tag{16.10b}$$

F, R, T symbols have their usual meanings; z is the pump stoichiometry, which has been set to 1. *N* is a scaling factor (2×10^{-8}) and *V* is the PD across

the membrane or membranes. The number of carrier states was reduced to two with a pair of PD-dependent constants, κ_{io} and κ_{oi}, with a symmetric Eyring barrier; and PD-independent rate constants, k_{io} and k_{oi} (Beilby 1984; Blatt et al. 1990 and references therein).

The I_{irc}, I_{orc}, I_K, I_H and I_{Cl} are fitted by the Goldmann–Hodgkin–Katz (GHK) equation, multiplied by the Boltzmann distribution of open probabilities, P_{o-} and P_{o+} (Beilby and Walker 1996; Amtmann and Sanders 1999). This simulates the channel closure as the PD is clamped beyond the positive or the negative closing threshold:

$$I_X = \frac{P_{o+} P_{o-} N_X P_X (zF)^2 V \left([X]_i - [X]_o e^{-\frac{zFV}{RT}} \right)}{RT \left(1 - e^{-\frac{zFV}{RT}} \right)} \tag{16.11}$$

$$P_{o-} = 1 - \frac{1}{1 + e^{-\frac{z_g F (V - V_{50})}{RT}}} \tag{16.12}$$

$$P_{o+} = \frac{1}{1 + e^{-\frac{z_g F (V - V_{50})}{RT}}} \tag{16.13}$$

where z is the valence of the transported ion, $[X]^o$ and $[X]^i$ are the ion concentrations in the medium, and in the cytoplasm, respectively. $N_X P_X$ stands for the number of X ion channels and their permeability, and it is treated as a single parameter; z_g is the number of gating charges, V_{50-} and V_{50+} are the half activation potentials, V_{50}, at the negative and positive PDs of channel closure.

The inward and outward rectifiers, I_{irc} and I_{orc}, are both carried by K^+ in *Lamprothamnium,* and in *Chara*. They have been modeled by Eq. 16.11, with a single probability distribution P_{o-} Eq. 16.12 for I_{irc} and P_{o+} Eq. 16.13 for I_{orc}. The conductances, G_{irc}, G_{orc}, G_{Cl}, G_K and G_H are calculated as differentials of the appropriate currents, with respect to the membrane PD (see Fig. 16.3c). The G/V (conductance–voltage) characteristics are instructive when considering the whole system, since the multiple parallel channel conductances are directly additive.

Different membrane states of salt-tolerant charophytes. If the medium contains more than about 1 mM K^+ and the membrane PD is sufficiently depolarized, the K^+ current, I_K, flows through the large conductance K^+ channels and cell enters K^+ state. The K^+ channels dominate the membrane conductance near the resting PD and the PD follows the predictions of the Nernst equation for potassium (Eq. 16.8). The K^+ state was recognized by Oda (1962) in *Chara* and was studied mainly in salt-sensitive charophytes. The I/V curve in this state has a typical appearance with negative conductance regions as the K^+ channels close rapidly if the membrane PD is clamped too positive or too negative (Smith 1984; Beilby 1985, 1986a,b; Tester 1988a,b). In salt-sensitive charophytes, the K^+ channels are blocked once Na^+ concentration in the medium rises above about 20

mM for K^+ concentration of about 5 mM (Beilby 1986a,b; Tester 1988a,b). High Ca^{2+}/K^+ concentration ratio also decreases I_K (Beilby 1986b). The I_K is abolished by tetraethylammonium (TEA) of similar concentration to K^+ (Beilby 1986b; Tester 1988a,b). The exposure to 0.1 mM $LaCl_3$ inhibited excitation irreversibly, but K^+ channels re-activate upon washout (Beilby 1986b; Tester 1988a). Bisson and Kirst (1980a) observed K^+ state in *L. succinctum*. Beilby and Shepherd (2001b) fitted the I/V profile of K^+ channel-dominated state in *L. succinctum* by Eqs 16.11–16.13. The medium contained 170 mM NaCl and the K^+ concentration was changed from zero to 45 mM (see Fig. 16.4). Further, we observed that K^+ state can be activated even in full SW. This may be an important difference between the transporters of salt-sensitive and salt-tolerant charophytes. However, *C. longifolia* does not easily go into the K-state (Yao et al. 1992). This may be because *C. longifolia* lives in high Mg^{2+} concentrations, which may block the K^+ channels.

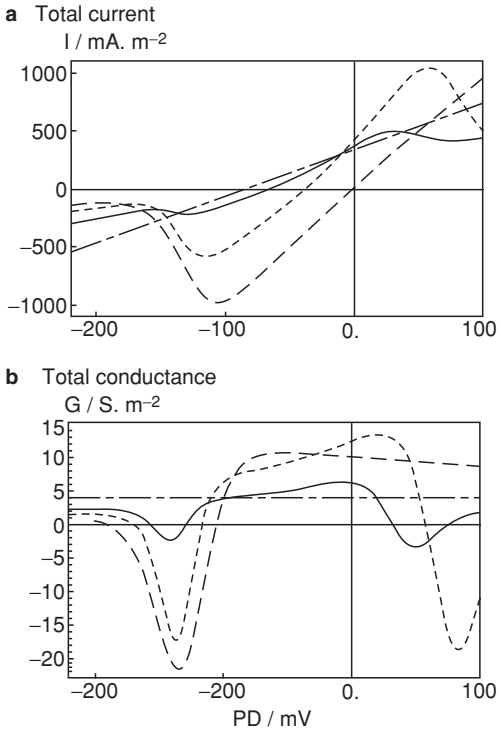

Fig. 16.4. The K^+ state I/V curves of *Lamprothamnium succinctum* acclimated to medium containing in mM: 170 NaCl, 4.5 KCl, 3.3 $CaCl_2$, 0.73 $NaHCO_3$, osmolarity 530 mOsM. **a** Total currents: the K^+ concentration was varied from 0 (*uneven-dashed line*) to 4.5 mM (*continuous line*), 9 mM (*short-dashed line*), 45 mM (*long-dashed line*). The profiles are generated by the fit parameters from Table 1 of Beilby and Shepherd (2001b). The inward and outward rectifiers were omitted. **b** The conductances calculated from currents in **a**

Once the pH of the medium rises above 9.0, the membrane conductance becomes dominated by the H^+ (or OH^-) channels (Bisson and Walker 1980). The H^+ state was observed in *L. succinctum* by Bisson and Kirst (1980a). *Chara corallina* and *C. longifolia* display banding where regions of the cell are dominated by the H^+ pump (acid bands) or by H^+ channels (alkaline bands) (Walker and Smith 1977; Yao et al. 1992). *L. succinctum* was not observed to band.

IV profiles as function of salinity. The first I/V profile of *L. succinctum* was measured by Kishimoto and Tazawa (1965). They found that the conductance increased greatly with higher NaCl concentration in the medium. Yao and co-workers (Yao et al. 1992; Yao and Bisson 1993), working on *C. longifolia*, suggested that the rise of conductance with salinity is due to an increase in the passive (background) conductance as well as higher rate of proton pumping, which keeps the membrane PD negative. They observed that the alkaline bands cover greater cell area at higher salinity and suggested that the increase in passive conductance is due to rise in G_H. Beilby and Shepherd (2001a), working on *L. succinctum*, also found an increase in pump conductance from ~1 $S.m^{-2}$ in 1/5 SW to 5 $S.m^{-2}$ in full SW. However, a greater conductance increase arises from the

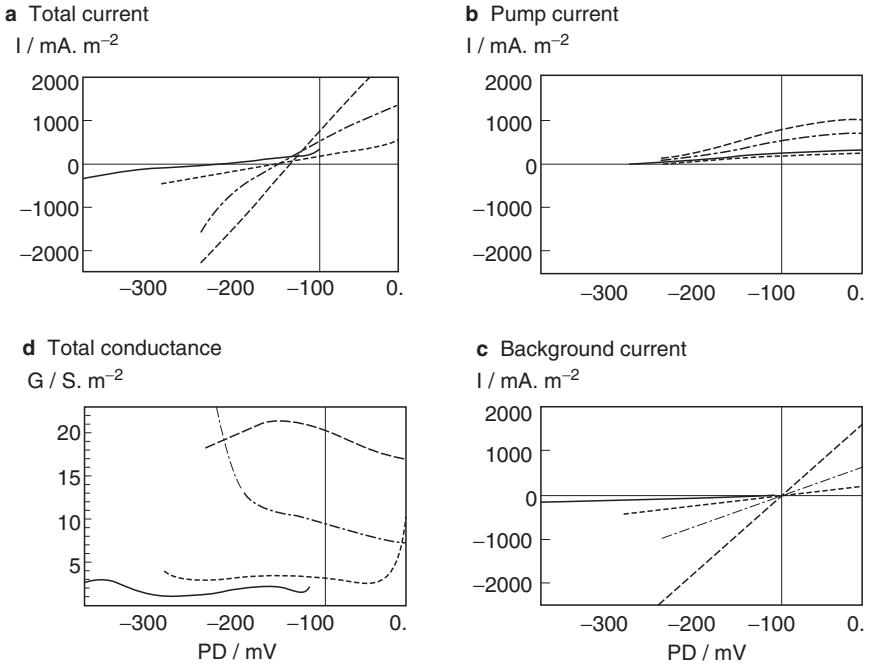

Fig. 16.5. The I/V characteristics of *Lamprothamnium* as function of medium salinity. **a** Total currents: 0.2 SW, continuous line, fitted to data from six cells; 0.4 SW, *short-dashed line*, fitted to data from six cells; 0.5 SW, *uneven dashed line*, fitted to data from six cells; full SW, *long-dashed line*, fitted to data from eight cells. **b** Fitted pump current, line types as in **a**. **c** Fitted background current, line types as in **a**. **d** Total conductance obtained by differentiation of I/V curves in **a**. The figure is based on fit parameters from Table 2 of Beilby and Shepherd (2001a)

change in G_{bkg} (see Eq. 16.9) from 0.5 S.m^{-2} at 1/5 SW to ~20 S.m^{-2} in full SW (see Fig. 16.5). E_{bkg} remains at –100 mV in this salinity range. The correlation of the data from these two charophytes is yet to be done, as the ions carrying I_{bkg} have not been identified.

IV profiles of hypotonic regulation. The I/V analysis at the time of hypotonic effect in *L. succinctum* (Beilby 1986b; Beilby and Shepherd 1996; Shepherd and Beilby 1999; Shepherd et al. 1999) showed that three types of currents participate: I_{Cl}, I_K and I_{bkg}. In young cells with thin mucilage (FR), all three currents can be observed (see Fig. 16.6d). In older cells with thicker mucilage (SR), I_{Cl} magnitude decreases progressively with mucilage thickness until it disappears. I_K magnitude also decreases with mucilage thickness. In some cells with thick mucilage only I_{bkg} responds to hypotonic shock; E_{bkg} goes more positive and G_{bkg} increases transiently (Shepherd et al. 1999, 2002). As outlined above

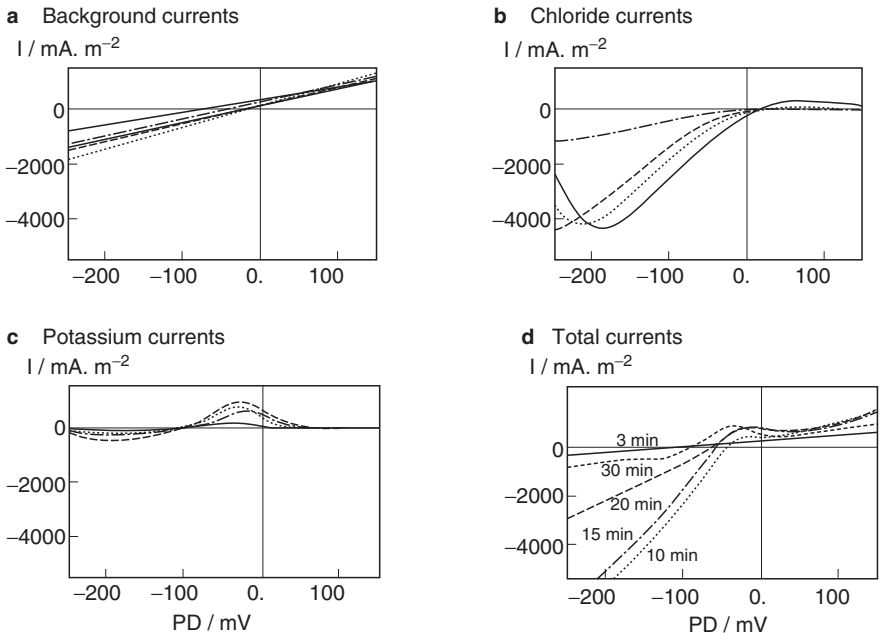

Fig. 16.6. The transporters active in the hypotonic regulation of *Lamprothamnium succinctum*. The transporters are shown at different times after the hypotonic exposure: 3 min (*continuous line*); 10 min (*dotted line*); 15 min (*long dashed line*); 20 min (*unequally dashed line*); 30 min (*short-dashed line*). **a** Background current: the fitted parameters from FR cell exposed to 20 mM TEA (Table 2a, Beilby and Shepherd 2006a). **b** Chloride current: the fitted parameters from the same cell as in **a**. **c** Potassium current: fitted parameters from a "lanthanized" cell (Table 2, Beilby and Shepherd 2001b). This cell was already in K^+ state, when the hypotonic medium was introduced. Cells no in K^+ state initially, enter this state with a delay of about 10 min after hypotonic exposure. **d** Total current: the different currents put together as they would be in a normal FR cell. The inward and outward rectifiers have been omitted, as their role in the hypotonic regulation is not well defined

eventually the E_{bkg} returns to about −100 mV and the G_{bkg} settles to lower value than in the higher NaCl medium.

The increase in G_K at the time of hypotonic effect was fitted for a FR cell treated with $LaCl_3$ to inactivate Ca^{2+} and Cl^- channels (Beilby 1986b) (Fig. 16.6c). The nature of the activation of the K^+ channel by the hypotonic stress is not known, but the model parameters suggest that the K^+ concentration in the cytoplasm rises before the increase in G_K. This can be achieved if the K^+ channels on the tonoplast are activated, allowing K^+ to move passively from the vacuole to the cytoplasm. In the "lanthanized" cells, the streaming does not stop, indicating that the tonoplast K^+ channels respond to a very small Ca^{2+} increase, or to some other change.

The Ca^{2+}-activated Cl^- channels were modeled at the time of hypotonic regulation in a FR cell treated with 20 mM TEA to inactivate K^+ channels (Beilby and Shepherd 2006a). The channels respond to changes in PD within ms, and show strong rectification, with the conductance maximum between 0 and −150 mV (see Fig. 16.6b). As $[Ca^{2+}]^{cyt}$ decreases after the initial hypotonic shock, the modeled parameter of combined channel number and permeability $N_{Cl}P_{Cl}$ decreases. However, using data from Okazaki et al. (2002), higher $[Ca^{2+}]^{cyt}$ is necessary to stop the streaming (~600 nM) than to activate all the Cl^- channels (~300 nM). Similarly to K^+ channels, the modeled membrane reversal PD suggests that the vacuolar Cl^- concentration equilibrates with the cytoplasmic Cl^- concentration by the time the I/V profiles are measured (6–9 min after hypotonic exposure, when the membrane PD showed less rapid change). In this case the signal is the increase in $[Ca^{2+}]^{cyt}$, as the vacuolar Cl^- channels are also Ca^{2+} activated (see Tester 1990, for review).

In the SR *Lamprothamnium* cells with thicker mucilage, only I_K and I_{bkg} are activated by the hypotonic challenge. Yet these cells also regulate turgor, but over much longer periods (several days; Beilby et al. 1999). The Cl^- efflux is thought to occur via the I_{bkg} pathway. Larger *C. longifolia* cells also exhibit slow regulation without the Ca^{2+}-activated Cl^- channels (Bisson et al. 1995).

Hypertonic stress. The increase in osmolarity of the medium due to concentration increase of ionic or non-ionic solutes decreases the water potential, driving water out of the cell. The turgor pressure falls and the cell has to increase ion concentration in the vacuole to attract water back in and to restore turgor.

Similar to hypotonic experiments, these experiments are usually performed using a step up in osmolarity by increase of ion concentrations (mainly NaCl) or uncharged solutes, such as sorbitol.

Changes in PD, conductance and streaming rate. Bisson and Kirst (1980b) subjected *Lamprothamnium succinctum* to an increase in salinity by 200–300 $mOsmol.kg^{-1}$. They found a variable response in cell PD. Of K-state cells (more positive than −90 mV), 74% depolarized further, 13% hyperpolarized and 13% did not change; of pump state cells (more negative than −130 mV) 33% depolarized, 44% hyperpolarized and 19% did not change.

Okazaki et al. (1984) transferred *L. succinctum* cells from 1/3 SW to 1/2 SW, an increase of about 160 mOsmol.kg^{-1}. They found membrane PD became more negative after a 10-min lag, reaching a peak after about 1 h of hypertonic stress. The resistance seems to decrease after 20 h, but error bars were too large for statistical significance.

Reid et al. (1984) increased external osmolarity by 300 mOsmol.kg^{-1}. They observed a transient depolarization of membrane PD for about 10 min, followed by hyperpolarization by 20 mV on average within 1 h of initiating hypertonic stress. They found a transient drop in ATP concentration in the first 10 min, paralleled by a rise in respiration. Streaming decreased briefly, but then increased (compared to steady state) for about 1 h. The influxes of Na^+, K^+ and Cl^- increased over 800 min.

Bisson and coworkers (Hoffmann and Bisson 1988; Hoffmann et al. 1989), working on *Chara longifolia*, found that the ratio of Na^+/Ca^{2+} is important for the regulation to occur and the cells to survive. In freshwater-acclimated cells, an increase of Na^+ from 1 to 70 mM caused 50% death rate within 6 days, if Na^+/Ca^{2+} was 700:1. Cells survived and regulated turgor with a similar stress if Na^+/Ca^{2+} was 10:1. With this increase in medium osmolarity of 150 mOsmol.kg^{-1}, cells transiently hyperpolarized by about 50 mV for about 10 min. The conductance transiently decreased over the same period. The regulation took between 95 and 144 h. Yao et al. (1992) showed that the rate of proton pumping increased for *C. longifolia* in more saline media to

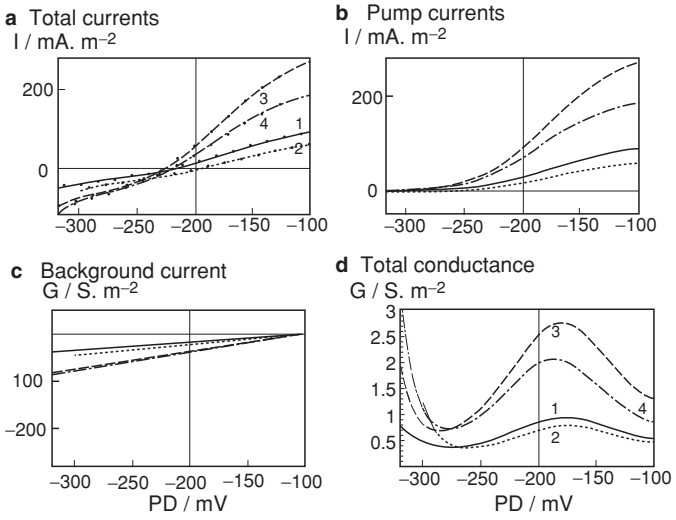

Fig. 16.7. The hypertonic regulation in *Lamprothamnium succinctum*. The cell was acclimated to 0.2 SW and hypertonic stress was produced by exposure to 0.4 SW (Beilby and Shepherd 2001a). **a** Total current in steady state (1, 0.2 SW, *continuous line*); 5 min in 0.4 SW (2, *dotted line*), maximal pump activation after 2 h and 34 min (3, *long-dashed line*); 3 h 30 min (4, *unequal dashed line*). **b** Fitted pump currents (same types of lines as in **a**). **c** Fitted background current. **d** Total conductance

compensate for increased background current (which was thought to increase due to greater area of alkaline bands and consequently G_H).

Beilby and Shepherd (2001a), working with *L. succinctum*, showed that the proton pumping rate is higher in cells acclimated to higher salinity (see Fig. 16.5b), but also transiently upon hypertonic stress (see Fig. 16.7). In hypertonic regulation there is an initial decrease in the pump rate (coinciding with the low ATP concentration found by Reid et al. (1984). The rate peaks at about 2 h of the hypertonic exposure.

The cells used in these experiments had very thin extracellular mucilage. The effect of mucilage thickness on the hypertonic regulation has not been investigated up to date. The slow rate of hypertonic regulation probably stems from the fact that energy has to be expended to move ions from the medium to the vacuole. The inward rectifier only opens at negative membrane PDs and the pump rate needs to increase to hyperpolarize the membrane. Cl^- is likely to be imported by a $Cl^-/2\ H^+$ symporter, studied in *Chara* by Beilby and Walker (1981). The symport uses the pH gradient (generated by the H^+ pump) and the rates are smaller than the channel mediated rate (Tester 1990).

16.4 Future avenues for study

While we are starting to understand which transporters are involved in both hypo- and hyper-tonic regulation and some of the signal cascades that turn them on and off, the detectors of both these stresses are still not known. For the hypotonic stress, the detectors are clearly SA channels and the detailed analysis of their operation will require experiments involving both electrophysiology, to assess function, and microscopy, to assess structural changes. The giant cells are the perfect system to perform these experiments. For the hypertonic stress, the detector could be the inward rectifier channels, which seem to activate at more positive PDs minutes after hypertonic exposure (Beilby and Shepherd 2001a), or the proton pump influenced via biochemical changes in the cytoplasm observed by Reid et al. (1984). The comparison of the transporter reaction to hypertonic regulation in salt-sensitive *Chara corallina* and salt-tolerant *Chara longifolia* and *Lamprothamnium succinctum* will illustrate the basic mechanisms which make plants salt-tolerant at cellular level (Beilby and Shepherd 2006b).

16.5 Summary

16.5.1 I/V curve technique

The resting PD of a cell results from interaction of many transporters. Their contributions can be resolved by perturbing the membrane PD away from equilibrium. The application of the I/V technique to charophytes and higher

plant cells under many conditions reveals considerable differences in PD dependencies of the major membrane conductances (transporters). The speed with which the membrane PD can be altered over hundreds of mV allows the experimenter to follow changes in transporter I/V profiles, while the cell is facing challenges such as metabolic inhibition or salinity stress. The availability of the raw data, both the clamp PD and the clamp current bipolar staircases, are vital for estimation of time dependencies of the response to PD change and artifact recognition. The analytic power of I/V technique increases as more data are acquired and modeled. The conductance-voltage (G/V) profiles, obtained as the derivatives of the I/V curves, provide an easily comprehensible record of parallel transporter combinations, as parallel conductances are directly additive. Similarly, the resistance-voltage (R/V, where R=1/G) profiles for transporters in series (on different membranes) are directly additive and more easily analyzed. With all these analytical techniques, much information can be gained on major transport systems, simultaneously responding to physical or chemical stresses.

16.5.2 "Giant" cells

The "giant" algal cells allow one to easily perform voltage clamp experiments, often in combination with other invasive experimental techniques such as turgor measurement, turgor clamping, and perfusion of cellular content to control intracellular concentration. What is more, these experiments can be performed in intact cells with normal cell walls and normal turgor pressures, or turgor pressures perturbed in a controlled way. Thus, these systems allow a degree of control of cells that is often not available in smaller cell types. The Charophytes are sufficiently similar to the embryophytes that results from these cells make good models for prediction of the activity in embryophytes. What they lack is good molecular characterization of the transport and regulatory mechanisms. However, as more information on these arise from work on embryophytes, physiological characterization of their actual activities must be done, and it is likely that the giant-celled algae will provide a good system, indeed, the only system, in which a clear characterization can be made. In particular, clear and convincing evidence concerning the nature and physical function of the turgor sensor itself (as contrasted to various downstream elements of turgor regulation such as various kinases and phosphatases activated by osmotic stress) is likely to be made only in a system where pressure itself can be sustained and manipulated in a precise fashion, as in the case of these giant cells.

References

Amtmann A, Sanders D (1999) Mechanisms of Na^+ uptake by plant cells. Adv Bot Res 29:76–112

Bartels D, Nelson D (1994) Approaches to improve stress tolerance using molecular genetics. Plant Cell Environ 17:659–667

Beilby MJ (1984) Current-voltage characteristics of the proton pump at *Chara* plasmalemma. I. pH dependence. J Membr Biol 81:113–125
Beilby MJ (1985) Potassium channels at *Chara* plasmalemma. J Exp Bot 163:228–239
Beilby MJ (1986a) Potassium channels and different states of *Chara* plasmalemma. J Membr Biol 89:241–249
Beilby MJ (1986b) Factors controlling the K^+ conductance in *Chara*. J Membr Biol 93:187–193
Beilby MJ (1989) Electrophysiology of giant algal cells. Methods Enzymol 174:403–442
Beilby MJ (1990) Current-voltage curves for plant membrane studies: a critical analysis of the method. J Exp Bot 41:165–182
Beilby MJ, Shepherd VA (1989) Cytoplasm-enriched fragments of *Chara* – structure and electrophysiology. J Exp Bot 41:168–182
Beilby MJ, Shepherd VA (1996) Turgor regulation in *Lamprothamnium papulosum*. I. I/V analysis and pharmacological dissection of the hypotonic effect. Plant Cell Environ 19:837–847
Beilby MJ, Shepherd VA (2001a) Modeling the current-voltage characteristics of charophyte membranes. II. The effect of salinity on membranes of *Lamprothamnium papulosum*. J Membr Biol 181:77–89
Beilby MJ, Shepherd VA (2001b) Modeling the current-voltage characteristics of charophyte membranes. III. K^+ of *Lamprothamnium*. Aust J Plant Physiol 28:541–550
Beilby MJ, Shepherd VA (2006a) The characteristics of Ca^{++}-activated Cl^- channels of salt-tolerant charophyte *Lamprothamnium*. Plant Cell Environ 29:764–777
Beilby MJ, Shepherd VA (2006b) The electrophysiology of salt tolerance in charophytes Cryptoganie Algologie (in press)
Beilby MJ, Walker NA (1981) Chloride transport in *Chara*. I. Kinetics and current-voltage curves for a probable proton symport. J Exp Bot 32:43–49
Beilby MJ, Walker NA (1996) Modelling the current-voltage characteristics of *Chara* membranes: I. The effect of ATP removal and zero turgor. J. Membrane Biol 149:89–101
Beilby MJ, Mimura T, Shimmen T (1997) Perfusion of charophyte cells: a critical analysis of the method. J Exp Bot 48:157–172
Beilby MJ, Cherry CA, Shepherd VA (1999) Dual turgor regulation response to hypotonic stress in *Lamprothamnium papulosum*. Plant Cell Environ 22:347–359
Bisson MA, Bartholomew D (1984) Osmoregulation or turgor regulation in *Chara?* Plant Physiol 74:252–255
Bisson MA, Gutknecht J (1980) Osmotic regulation in algae. In: Spanswick RM, Lucas WJ, Dainty J (ed). Plant membrane transport: current conceptual issues. Elsevier/North Holland Biomedical Press Amsterdam. pp 131–142.
Bisson MA, Kirst GO (1980a) *Lamprothamnium,* a euryhaline Charophyte. I. Osmotic relations and membrane potential at steady state. J Exp Bot 31:1223–1235
Bisson MA, Kirst GO (1980b) *Lamprothamnium,* a euryhaline Charophyte. II. Time course of turgor regulation. J Exp Bot 31:1237–1244
Bisson MA, Kirst GO (1995) Osmotic acclimation and turgor pressure regulation in algae. Naturwissenschaften 82:461–471
Bisson MA, Walker NA (1980) The *Chara* plasmalemma at high pH. Electrical measurements show rapid specific passive uniport of H^+ or OH^-. *J. Membrane Biol.* 56:1–7
Bisson MA, Walker NA (1982) Transitions between modes of behaviour (states) of the Charophyte plasmalemma. In: Marré E, Hertel R (eds) Plasmalemma and tonoplast: their functions in the plant cell. Elsevier Biomedical Press, Amsterdam, pp 35–40
Bisson MA, Kiegle E, Black D, Kiyosawa K, Gerber K (1995) The role of calcium in turgor regulation in *Chara longifolia*. Plant Cell Environ 18:129–137
Blatt M, Beilby M, Tester M (1990) Voltage dependence of the *Chara* proton pump revealed by current-voltage measurement during rapid metabolic blockade with cyanide. J Membr Biol 114:205–223
Boyer JS (1982) Plant productivity and environment. Science 218:443–448
Burne RV, Bauld J, de Dekker P (1980) Saline lake charophytes and their geological significance. J Sed Petrol 50:281–294

Clint GM, MacRobbie EAC (1987) Sodium efflux from perfused giant algal cells. Planta 171:247–253
Coster HGL, Zimmermann U (1976) Transduction of turgor pressure by cell membrane compression. Z Naturforsch 31:461–463
Findlay GP (2001) Membranes and the electrophysiology of turgor regulation. Aust J Plant Physiol 28:617–634
Fujii S, Shimmen T, Tazawa M (1979) Effect of intracellular pH on the light-induced potential change and electrogenic activity in tonoplast-free cells of *Chara australis*. Plant Cell Physiol 20:1315–1328
Gelli A, Higgins VJ, Blumwald E (1997) Activation of plant plasma membrane Ca^{2+}-permeable channels by race-specific fungal elicitors. Plant Physiol 113:269–279
Graham L (1993) Origin of land plants. Wiley, New York
Graham LE, Gray J (2001) The origin, morphology, and ecophysiology of early embryophytes: neontological and paleontological perspectives. In: Gensel PG, Edwards D (eds) Plants invade the land. Evolutionary and environmental perspectives. Columbia University Press, New York, pp 140–159
Gutknecht J (1967) Ion fluxes and short-circuit current in internally perfused cells of *Valonia ventricosa*. J Gen Phys 50:1821–1834
Gutknecht J, Hastings D, Bisson MA (1978) Ion transport and turgor pressure regulation in giant algal cells. In: Giebisch G, Tosteson D, Ussing G (eds) Membrane transport in biology, vol III. Transport across multimembrane systems. Springer, Berlin Heidelberg New York, pp 125–174
Hasegawa PM, Bressan RA (2000) Plant cellular and molecular responses to high salinity. Annu Rev Plant Physiol Plant Mol Biol 51:463–499
Hastings DF, Gutknecht J (1974) Turgor pressure regulation: Modulation of active potassium transport by hydrostatic pressure gradients. In: Zimmermann U, Dainty J (eds) Membrane transport in plants. Springer, Berlin Heidelberg New York, pp 79–83
Heidecker M, Wegner LH, Zimmermann U (1999) A patch-clamp study of ion channels in protoplasts prepared from the marine alga *Valonia utricularis*. J Membr Biol 172:235–247
Hoffmann R, Bisson MA (1986) *Chara buckellii,* a euryhaline charophyte from an unusual saline environment. I. Osmotic relations at steady state. Can J Bot 64:1599–1605
Hoffmann R, Bisson MA (1988) The effect of divalent cations on Na^+ tolerance in Charophytes. I. *Chara buckellii*. Plant Cell Environ 11:461–472
Hoffmann R, Bisson MA (1990) *Chara buckellii,* a euryhaline charophyte from an unusual saline environment. III. Time course of turgor regulation. Plant Physiol 93:122–127
Hoffmann R, Tufariello JM, Bisson MA (1989) Effect of divalent cations on Na^+ permeability of *Chara corallina* and freshwater grown *Chara buckellii*. J Exp Bot 40:875–881
Hope AB, Walker NA (1975) The physiology of giant algal cells. Cambridge University Press, London
Kapraun DF (2005) Nuclear DNA content estimates in multicellular green, red, and brown algae: phylogenetic considerations. Ann Bot 95:7–44
Kacperska A (2004) Sensor types in signal transduction pathways in plant cells responding to abiotic stressors: do they depend on stress intensity? Physiol Plant 122:159–168
Karol KG, McCourt RM, Cimino MT, Delwiche CF (2001) The closest living relatives of land plants. Science 294:2351–2353
Kirst GO (1977) Coordination of ionic relations and mannitol concentrations in the euryhaline unicellular alga, *Platymonas subcordiformis* after osmotic shocks. Planta 135:69–75
Kishimoto U, Tazawa M (1965) Ionic composition and electric response of *Lamprothamnium succinctum*. Plant Cell Physiol 6:529–536
Laver DR, Walker NA (1987) Steady-state voltage-dependent gating and conduction kinetics of single K^+ channels in the membrane of cytoplasmic drops of *Chara australis*. J Membr Biol 100:31–42
Lewis LA, McCourt RM (2004) Green algae and the origin of land plants. Am J Bot 91:1535–1556
Lühring H (1986) Recording of single K^+ channels in the membrane of cytoplasmic drop of *Chara australis*. Protoplasma 133:19–27

McCourt RM, Delwiche CF, Karol KG (2004) Charophyte algae and land plant origins. Trends Ecol Evol 19:661–2353

Nakanishi Y, Matsuda N, Aizawa K, Kashiyama T, Yamamoto K, Mimura T, Ikeda M, Maeshima M (1999) Molecular cloning and sequencing of the cDNA for vacuolar H^+-pyrophosphatase from *Chara corallina*. Biochim Biophys Acta 1418:245–250

Nobel PS (1974) Introduction to biophysical plant physiology. Freeman, San Francisco

Oda K (1962) Polarised and depolarised states of the membrane in *Chara braunii* with special reference to the transition between the two states. Sci Rep Tohoku Univ Ser IV Biol 28:1–16

Okazaki Y, Iwasaki N (1992) Net efflux of Cl^- during hypotonic turgor regulation in a brackish water alga *Lamprothamnium*. Plant Cell Environ 15:61–70

Okazaki Y, Tazawa M (1986a) Ca^{2+} antagonist nifedipine inhibits turgor regulation upon hypotonic treatment in internodal cells of *Lamprothamnium*. Protoplasma 135:65–66

Okazaki Y, Tazawa M (1986b) Involvement of calcium ion in turgor regulation upon hypotonic treatment in *Lamprothamnium succinctum*. Plant Cell Environ 9:185–190

Okazaki Y, Tazawa M (1987) Increase in cytoplasmic calcium content in internodal cells of *Lamprothamnium* upon hypotonic treatment. Plant Cell Env 10:619–621

Okazaki Y, Shimmen T, Tazawa M (1984) Turgor regulation in a brackish Charophyte, *Lamprothamnium succinctum*. II. Changes in K^+, Na^+ and Cl^- concentrations, membrane potential and membrane resistance during turgor regulation. Plant Cell Physiol 25:573–581

Okazaki Y, Yoshimoto Y, Hiramoto Y ,Tazawa M (1987) Turgor regulation and cytoplasmic free Ca^{2+} in the alga *Lamprothamnium*. Protoplasma 140:67–71

Okazaki Y, Ishigami M, Iwasaki N (2002) Temporal relationship between cytosolic free Ca^{2+} and membrane potential during hypotonic turgor regulation in a brackish water charophyte *Lamprothamnium succinctum*. Plant Cell Physiol 43:1027–1035

Pickard BG, Ding JP (1992) Gravity sensing by higher plants. Adv Comp Env Physiol 10:81–110

Pickard BG, Ding JP (1993) The mechanosensory calcium-selective ion channel: key component of a plasmalemmal control centre? Austr J Plant Physiol 20:439–459

Raven JA (1975) Algal cells. In: Baker D, Hall A (eds) Ion transport in plant cells and tissues. North Holland, Amsterdam, pp 125–160

Raven JA (1985) Energetics and transport in aquatic plants. Liss, New York

Reid RJ, Smith FA (1992) Measurement of calcium fluxes in plants using ^{45}Ca. Planta 186:558–566

Reid RJ, Smith FA (1993) Effects of salinity and turgor on ^{45}Ca influx in *Chara*. Plant Cell Environ 16:547–554

Reid RJ, Walker NA (1983) Adenylate concentrations in *Chara:* variability, effects of inhibitors and relationship to protoplasmic streaming. Austr J Plant Physiol 10:373–383

Reid RJ, Jefferies R, Pitman MG (1984) *Lamprothamnium,* a euryhaline charophyte IV. Membrane potential, ionic fluxes and metabolic activity during turgor adjustment. J Exp Bot 35:925–937

Roberts AG, Oparka KJ (2003) Plasmodesmata and the control of symplastic transport. Plant Cell Environ 26:103–124

Sanders D (1981) Physiological control of chloride transport in *Chara corallina*. I. Effects of low temperature, cell turgor pressure, and anions. Plant Physiol 67:1113–1118

Sanders D, Smith FA ,Walker NA (1985) Proton/chloride cotransport in *Chara:* mechanism of enhanced influx after rapid acidification. Planta 163:411–418

Shepherd VA, Beilby MJ (1999) The effect of an extracellular mucilage on the response to osmotic shock in the charophyte alga *Lamprothamnium papulosum*. J Membrane Biol 170:229–242

Shepherd VA, Beilby MJ, Heslop DJ (1999) Ecophysiology of the hypotonic response in the salt-tolerant charophyte alga *Lamprothamnium papulosum*. Plant Cell Environ 22:333–346

Shepherd VA, Beilby MJ, Shimmen T (2002) Mechanosensory ion channels in charophyte cells: the response to touch and salinity stress. Eur Biophys J 31:341–355

Shimmen T, Yokota E (1994) physiological and biochemical aspects of cytoplasmic streaming. Int Rev Cytol 155:97–139

Shimmen T, Mimura T, Kikuyama M, Tazawa M (1994) Characean cells as a tool for studying electrophysiological characteristics of plant cells. Cell Struc Funct 19:263–278
Shimmen T, MacRobbie EAC (1987) Characterization of two proton transport systems in the tonoplast of plasmalemma-permeabilized *Nitella* cells. Plant Cell Physiol 28:1023–1031
Smirnoff N (1998) Plant resistance to environmental stress. Curr Opin Biotech 9:214–219
Smith FA, Raven JA (1979) Intracellular pH and its regulation. Annu Rev Plant Physiol 30:289–311
Smith PT (1984) Electrical evidence from perfused and intact cells for voltage-dependent K^+ channels in the plasmalemma of *Chara australis*. Austr J Plant Physiol 11:303–318
Smith PT, Walker NA (1981) Studies on the perfused plasmalemma of *Chara corallina*. I. Current voltage curves: ATP and potassium dependence. J Membr Biol 60:223–236
Spanswick RM (1972) Evidence for an electrogenic ion pump in *Nitella translucens*. I. The effects of pH, K^+, Na^+, light and temperature on the membrane potential and resistance. Biochim Biophys Acta 288:73–89
Spanswick RM (1980) Biophysical control of electrogenic pumps in the *Characeae*. In: Spanswick RM, Lucas WJ, Dainty J (eds) Plant membrane transport: current conceptual issues. Elsevier/North Holland Biomedical Amsterdam, pp 305–315
Spanswick RM (1981) Electrogenic ion pumps. Annu Rev Plant Physiol 32:267–289
Spanswick RM, Williams EJ (1964) Electrical potentials and Na, K, and Cl concentrations in the vacuole and cytoplasm of *Nitella translucens*. J Exp Bot 15:193–200
Stento NA, Ryba NG, Kiegle EA, Bisson MA (2000) Turgor regulation in the salt-tolerant alga *Chara longifolia*. Plant Cell Environ 23:629–637
Steudle E, Zimmermann U (1974) Determination of the hydraulic conductivity and of reflection coefficients in *Nitella flexilis* by means of direct cell-turgor pressure measurements. Biochim Biophys Acta 332:399–412
Sze H, Li X, Palmgren MG (1999) Energization of plant cell membranes by H^+-pumping ATPases: regulation and biosynthesis. Plant Cell 11:677–689
Tazawa M, Shimmen T, Mimura T (1987) Membrane control in the Characeae. Annu Rev Plant Physiol 38:95–117
Tester M (1988a) Blockade of potassium channels in the plasmalemma of *Chara corallina* by tetraethylammonium, Ba^{2+}, Na^+ and Cs^+. J Membrane Biol 105:77–85
Tester M (1988b) Potassium channels in the plasmalemma of *Chara corallina* are multi-ion pores—voltage-dependent blockade by Cs+ and anomalous permeabilities. J Memb Biol 105:87–94
Tester M (1990) Plant ion channels: whole-cell and single-channel studies. New Phytol 114:77–85
Turmel M, Ehara M, Otis C, Lemieux C (2001) Phylogenetic relationships among streptophytes as inferred from chloroplast small and large subunit rRNA gene sequences. J Phycol 38:364–375
Tyerman SD, Findlay GP (1989) Current–voltage curves of single Cl^- channels which coexist with two types of K^+ channel in the tonoplast of *Chara corallina*. J Exp Bot 40:105–117
Tyerman SD, Skerrett IM (1999) Root ion channels and salinity. Sci Hort 78:175–235
Walker NA, Smith FA (1977) Circulating electric currents between acid and alkaline zones associated with HCO_3^- assimilation in *Chara*. J Exp Bot 28:1190–1206
Whittington J, Bisson MA (1994) Na^+ fluxes in *Chara* under salt stress. J Exp Bot 45:657–665
Wichmann F, Kirst GO (1989) Adaptation of the euryhaline Charophyte *Lamprothamnium papulosum* to brackish and freshwater: turgor pressure and vacuolar solute concentrations during steady-state culture and after hypo-osmotic treatment. J Exp Bot 40:135–141
Williams WD (1998) Salinity as a determinant of the structure of biological communities in salt lakes. Hydrobiology 381:191–201
Williamson RE, Ashley CC (1982) Free Ca^{2+} and cytoplasmic streaming in the alga *Chara*. Nature 296:647–651
Winter U, Kirst GO (1990) Salinity response of a freshwater charophyte, *Chara vulgaris*. Plant Cell Environ 13:123–134
Winter U, Kirst GO (1991) Partial turgor regulation in *Chara canescens* and its implications for a generalised hypothesis of salinity response in charophytes. Bot Acta 104:37–46

Winter U, Kirst GO (1992) Turgor pressure regulation in *Chara aspera* (Charophyta): the role of sucrose accumulation in fertile and sterile plants. Phycol 31:240–245

Winter U, Soulié-Märsche I, Kirst GO (1996) Effects of salinity on turgor pressure and fertility in *Tolypella* (Characeae). Plant Cell Environ 19:869–879

Winter U, Kirst GO, Grabowski V, Heinemann U, Plettner I ,Wiese S (1999) Salinity tolerance in *Nitellopsis obtusa*. Austr J Bot 47:337–346

Yao X, Bisson MA (1993) Passive proton conductance is the major reason for membrane depolarization and conductance increase in *Chara buckellii* in high-salt conditions. Plant Physiol 103:197–203

Yao X, Bisson MA, Brzezicki LJ (1992) ATP-driven proton pumping in two species of *Chara* differing in their salt tolerance. Plant Cell Env 15:199–210

Zimmermann U, Steudle E (1971) Effects of potassium concentration and osmotic pressure of sea water on the cell-turgor pressure of *Chaetomorpha linum*. Mar Biol 11:132–137

Zimmermann U, Steudle E (1974) The pressure-dependence of the hydraulic conductivity, the membrane resistance and membrane potential during turgor pressure regulation in *Valonia utricularis*. J Membr Biol16:331–352

17 Electrical Signals in Plants: Facts and Hypotheses

ERIC DAVIES

17.1 What is the context?

Electrical signals were first described over 200 years ago in both plants (Berthelon 1783) and animals (Galvani 1791), and had become an important line of study in plants over 140 years ago (Burdon-Sanderson 1873; Darwin 1875); thus they are far from being a novel phenomenon. Most of the earlier work (Burdon-Sanderson 1873; Darwin 1875), involved insect-trapping plants, which, like the sensitive plant, *Mimosa pudica*, have very rapid and visually striking responses to touch (reviewed in Simons 1981; Braam 2005) and were the preferred organisms for study for over a century. Until about 1880, there seemed to have been general acceptance of electrical signals as common to plants and animals; indeed, they were the only mechanism known for intercellular communication in any living system. However, shortly after his work on electrical signals, Darwin (1875) postulated the existence of chemical signals in plants (Darwin 1881), thus, plants were recognized as having both electrical and chemical signals, while animals had only electrical. Then, with the discovery of animal hormones and the emergence of the field of endocrinology at the turn of the (twentieth) century, it was accepted that both animals and plants had both types of signal.

Work on electrical signals in plants continued in the twentieth century, especially in India (e.g. Bose and Das, 1925), and to a lesser extent the USA (e.g. Pickard 1973), yet there seems to have been a paradigm shift, the existence of electrical signals, at least in "normal" plants was questioned. There are at least two reasons for this. First, almost concomitant with the publication of Pickard's (1973) review of action potentials in plants, there appeared a book (Tompkins and Bird 1973), aimed at the general public, which was based to a large extent on irreproducible results reported by an FBI lie detector expert (Backster 1968). This work caught the public's imagination (at least in the USA), but caused immense consternation among genuine plant scientists, since the entire field of plant electrophysiology was rendered suspect (Galston and Slayman 1979). Second, there was an underlying assumption that there was no real need for rapid signals in organisms as sluggish as

Botany Department, North Carolina State University, Raleigh NC 27695–7612, USA (e-mail: eric_davies@ncsu.edu)

Plant Electrophysiology – Theory & Methods (ed. by Volkov)

plants. Thus, research on electrical signals in plants hit an impasse, particularly in the USA, where funding effectively stopped for 2 decades. However (and despite this lack of funding), the field has opened up again over the last 25 years, and there is increasing consensus that electrical signals in plants do, indeed, exist, not only in those with rapid movements, but in all plants. This recognition has come about at least in part from the realization that "normal" plants can have very rapid systemic responses on fundamental processes such as gene expression (Davies and Schuster 1981a,b) and this requires the generation and transmission of even more rapid systemic signals (Davies 1987a,b). This recognition of the need for electrical signals in plants is also manifested by the very recent "First Symposium in Plant Neurobiology" (see: http//izmb.de/zellbio/volkmann/index.html) and the publication of a book with articles from that Symposium (Baluska et al. 2006) as well as the publication of this present textbook, the first ever devoted to plant electrophysiology. To summarize, the main "fact" emerging from the first section is that electrical signals do, indeed, occur in most, if not all organisms (including plants), not just those exhibiting rapid and visibly-obvious responses.

17.2 What are major definitions and types of signal?

For the purposes of this article, a stimulus is anything that evokes a response within the plant (termed "stimulus–response coupling" in the animal literature), while a signal is anything which is generated and transmitted by the plant in response to that stimulus. Thus the stimulus might be applied from outside the plant, while the signal *must* be generated within the plant. Further, the signal itself becomes a stimulus when it arrives at its destination and provokes its own response.

As an example to expound on this point (and references will be furnished later in the appropriate sections), when voltage is applied to a plant (electrical stimulation) it can evoke the generation of an electrical signal (action potential, or AP), which is transmitted through the plant. This traveling AP almost certainly involves calcium influx into the cytoplasm followed by chloride and potassium efflux. These sub-components of the AP signal, such as increased cytosolic calcium, become stimuli when they evoke responses further downstream, such as the activation of phospholipase C. Phospholipase C can be thought of a signal in the vicinity of the plasma membrane, where it becomes a stimulus and evokes the release of inositol phosphate metabolites. These metabolic signals (especially IP_3), can then act as stimuli to evoke release of more calcium from intracellular stores. Finally, these signals (IP_3, calcium and/or their associated protein phosphorylation events) can then act as stimuli to modulate gene expression (Davies and Stankovic 2006). This sequence of

$$\text{stimulus} \rightarrow \text{signal} = \text{stimulus} \rightarrow \text{signal} = \text{stimulus} \rightarrow \text{signal}$$

continues, and a major goal of research on electrical signals in plants is to decipher as many of the steps as possible.

The array of signals in plants for which the term "electrical" has been used includes: action potentials (AP), including spontaneous action potential (SAPS); variation potentials (VP), also called slow wave (SW; Stahlberg and Cosgrove 1996); voltage transients (VT) or voltage spikes (VS); and rhythmical electrical activity (REA). By definition, all of these electrical activities must involve changes in membrane potential (MP). However, this review will be restricted to those changes in MP which are transmitted long distances and which have known stimulus and response. The major reason behind this is that any flux of ions across the plasma membrane will elicit some change in MP, and since all cells (especially root cells involved in ion uptake) have ions traversing the plasma membrane virtually all the time, then almost all of metabolism would be linked to "electrical" signals.

Here, we define "signal" as having some aspect of transmission, and, depending on the distance transmitted, it might be systemic, i.e. throughout the plant (thus, by definition, long distance), intercellular, or intracellular. Here we will focus our attention on the two major long-distance signals, AP and VP, especially in "normal" vascular plants, i.e. those without obvious rapid visible manifestations, and limited consideration will be given to plants with rapid movements (Braam 2005), and to non-vascular plants, especially algae with very large cells and with which most of the early intracellular recordings were made (Wayne 1994). For more information on giant algal cells, I suggest reading the chapters in this text by Bisson et al. (this volume) and Shimmen (this volume). This review will also not deal with local changes in MP with little or no transmission, such as REA (Mitsumo and Sibaoka 1989; Antkowiak et al. 1991; Davies et al. 1991), or VT (Pickard 1984a,b; Krol and Trebacz 1999). Nor will it deal with changes in MP induced by symbionts (Assmann 1995; Felle et al. 1995), pathogens (Kurusu et al. 2005; Pike et al. 2005), insects (Volkov and Haack 1995; Maffei et al. 2004); gravity, or those involved in tip growth (Harold and Caldwell 1990). The role of biotic agents will be dealt with in this book by Maffei and Bossi (2006), gravity by Stankovic (2006) and in roots by Takamura (2006). This review will also not discuss the so-called "spontaneous" action potentials (SAPS), since they have no known stimulus or consequence (Zawadzki et al. 1995).

17.3 What are action potentials?

The AP is the only long distance signal that can be considered to be a "genuine" electrical signal (reviewed by Pickard 1973; Gradmann and Mummert 1980; Simons 1981; Wayne 1994; Ksenzhek and Volkov 1998; Davies 2004) The fundamental properties of a "pure" AP are that it be self-propagating,

all-or-nothing, and transmitted at essentially constant velocity and amplitude (Zawadzki et al. 1991; Dziubinska 2003). Since they are self-propagating, AP must depend on ion channels that respond (open) to changes in MP, i.e. voltage-gated channels (VGC), thus any cell containing voltage-gated channels can generate and transmit an AP. The primary VGC seems to be a plasma membrane-associated calcium channel that causes a sharp increase in the normally very low cytosolic calcium levels (Tester 1990; Wayne 1994, Fisahn et al. 2004). It has, however, been suggested that the increased cytosolic Ca^{2+} does not come through the plasma membrane, but is released from internal stores, perhaps triggered by IP3 (Plieth et al. 1998; Biskup et al. 1999; Wacke and Thiel 2001), but this view has been challenged recently (Tazawa and Kikuyama 2003). Nevertheless, there does seem to be cross-talk between PIP derivatives and K^+ channels (Liu et al. 2005) and the K^+ channel does appear to be a voltage sensing component of the membrane, at least in animal tissues (MacKimmon 2004; Horn 2005). In either case, the increase in calcium seems to trigger opening of a calcium-dependent chloride channel, which allows chloride efflux into the apoplast, and then the original (resting) MP is restored by an outward rectifying potassium channel. This sequence of ion fluxes has been described for giant algal cells (Wayne 1994; Shimmen 1997), a liverwort (Trebacz et al. 1994), the sensitive plant Mimosa (Samejima and Sibaoka 1980), and even trees such as willow (Fromm and Spanswick 1993), reviewed by Tester (1990). The transient change in MP causes the same sequence of events (Ca^{2+} influx, Cl^- efflux and K^+ efflux) to be repeated along the series of cells in the pathway.

In vascular plants, the primary location for long distance AP transmission is the phloem, especially the sieve tubes (Eschrich et al. 1988; Fromm and Spanswick 1993; Dziubinska et al. 2001; Dziubinska 2003), but there is no reason why lateral spread cannot occur through other cell types that contain VGC. In this case, all cells with symplastic connection to the phloem are likely to be "informed" by, and respond to, the passage of an AP. Indeed, in non-vascular plants such as algae (Wayne 1994) and liverworts (Trebacz et al. 1994). The AP must, by definition, be transmitted though non-phloem tissues.

The AP in plants seems to be very similar to the AP in animal cells such as heart, epithelium, etc, differing primarily in their rapidity (Sussman 1992), but they are very different from the AP in neurons, which rely on Na^+/K^+ exchange (Davies 1987b). The AP is made possible by the fact that the resting MP of plant cells is very negative (approximately 200 mV) to the inside. Calcium influx causes depolarization (less negative inside), this is enhanced by chloride efflux, but then neutralized by potassium efflux. Once an AP has passed, there is a period of delay (the refractory period) during which another AP cannot be generated or transmitted. This is most likely the result of temporary inactivation of one or other of the ion channels, most likely the calcium VGC.

17.4 What are variation potentials?

Unlike the AP which is a self-propagating, transmitted change in MP, the VP is a local change in MP resulting from the passage of some other signal (Malone 1994, 1996; Malone et al. 1994a,b; Stankovic et al. 1998; Mancuso 1999). Nevertheless, the local change in MP must again be the result of ion fluxes across the plasma membrane, but not through VGC, otherwise this would generate an AP. Further, long distance AP transmission occurs primarily in the phloem, primarily in the living but enucleate sieve tubes, whereas the VP is transmitted in the dead xylem (Davies et al. 1991; Malone 1994, 1996; Mancuso 1999).

There are two main candidates for the xylem-transmitted component: changes in pressure/tension and transport of chemicals. Both types of primary signal most likely exist and evidence for both of them is good. Since VP must depend on ion channels (but not VGC), the former explanation (pressure/tension changes) must be based on mechanosensitive channels (MSC), whereas the latter (chemicals in the xylem) must be based on ligand-activated channels (LAC). The evidence for rapid loss of tension in the xylem comes primarily from work using excision, heat wound and/or a pressure bomb as stimuli and employing electrodes, position sensing transducers and an analytical balance to assess changes in MP, tissue deformation and water uptake, respectively (Roblin and Bonnemain 1985; Davies et al. 1991; Stahlberg and Cosgrove 1995, 1996; Stankovic et al. 1997, 1998; Stankovic and Davies 1997b; Stahlberg et al. 2005). When one leaf is heat-wounded there is an essentially instantaneous relaxation of the entire stem, followed by changes in MP which appear both smaller and more delayed with increasing distance from the point of wounding (Davies et al. 1991; Stankovic et al. 1997; Stankovic and Davies 1997b; Mancuso 1999) These changes in MP and stem relaxation can be mimicked by transient or prolonged application of slight pressure to one leaf (Stankovic et al. 1997). Similar changes were also seen in wheat leaves (Malone and Stankovic 1991), who at that time evoked a mechanosensory explanation. More recently, Malone and co-workers have come to favor a role for chemicals transmitted in the xylem (Malone et al. 1994a; Malone 1996), which, by definition would have to involve LAC.

17.5 What stimuli evoke AP and VP and what are the consequences?

The brief answer to the first question is “non-damaging stimuli evoke AP, while damaging stimuli evoke VP” (Dziubinska 2003). Non-damaging stimuli that evoke AP include electrical stimulation, light/dark transitions (Trebacz and Zawadzki 1985), brief cooling (Pyatygin et al. 1992) and pollination

(Fromm et al. 1995), while damaging stimuli that evoke VP include severe wounding (reviewed in Dziubinska 2003). However, the distinction is not too clear. Sometimes excision results in AP (Pickard and Davies, unpublished results), while in the same organism excision is known to evoke a VP/SW (Stahlberg and Cosgrove 1995). The major consequences of electrical signals are provided in the chapter of this textbook (Fromm, this volume). Here I will briefly discuss the rapid responses, since it is the rapidity of response that necessitates a rapidly-generated and transmitted signal. These initial responses will be evoked by any of the primary events occurring as sub-components of the AP (or VP) including Ca^{2+} influx, Cl^- efflux, K^+ efflux, and the concomitant change in MP. As discussed earlier, these include changes in enzyme activity, gene expression, and in the status of the cytoskeleton (Davies 1987a,b, 1993).

Here I will emphasize responses at the level of gene expression, primarily transcription, but also translation, since it was the incredibly rapid changes in polyribosome formation and protein synthesizing capacity (Davies and Schuster 1981a) that led us to conclude that ultra-rapid signals must be involved (Davies and Schuster 1981b), and this led us to examine the potential role of electrical signals in systemic wound responses. We have focused our efforts on the putative role of elevated cytoplasmic Ca^{2+}, the channels through which it enters, their association with the cytoskeleton, and the effects of Ca^{2+} on modulating enzyme activity via phosphorylation. We showed early on that the *increase* in polyribosomes was accompanied by a paradoxical *reduction* in protein synthesis as well as a concomitant cessation of cytoplasmic streaming (Davies 1990). This reduction in protein synthesis along with formation of polysomes could be explained by phosphorylation of elongation factor, which would cause ribosomes to pile-up on mRNA (Davies 1993). Similarly, cessation of cytoplasmic streaming could result from phosphorylation of myosin and the simultaneous effect on both processes could be explained if polysomes were attached to the cytoskeleton (Davies et al. 1998; Davies and Stankovic 2006).

In addition to affecting translation, both kinds of electrical signal modify transcription. Both electrical stimulation (AP) and heat-wounding (VP), evoke systemic accumulation of protease inhibitor transcripts, but only flame-wounding (VP) induces calmodulin transcripts (Stankovic and Davies 1996, 1997a,b). The VP also causes accumulation of transcripts encoding a chloroplast mRNA binding protein (Vian et al. 1999), a leucine zipper transcription factor, bZIP (Stankovic et al. 2000), a vacuolar ATPase (Coker et al. 2003) and many others (Coker et al. 2005), including some that peak within 2 min in a leaf 5 cm distant from the wound site (Davies et al. 1997; Davies 2004). Again, Ca^{2+}-induced phosphorylation of a specific protein, in this case of RNA polymerase 2, could explain this very rapid systemic transcript accumulation (Davies and Stankovic 2006).

We have tried to understand how the different electrical signals might evoke the accumulation of different transcripts and our explanation is summarized in Fig. 17.1 and the pertinent references are cited in Davies (1993) and

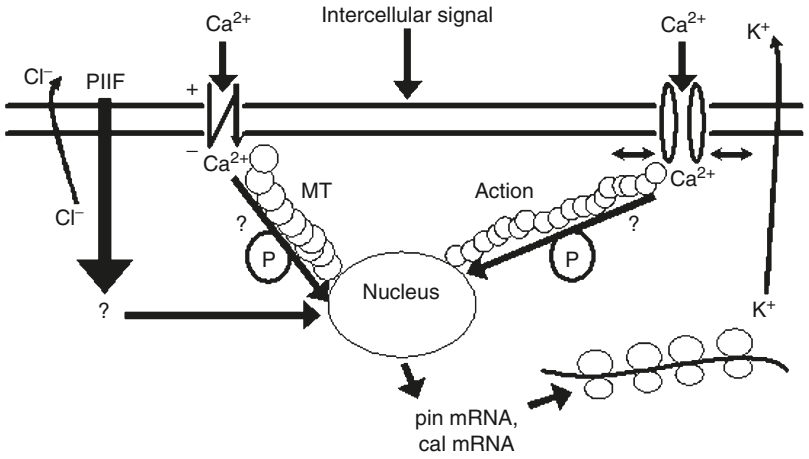

Fig. 17.1. Transduction of intercellular signals into cellular responses involving gene expression in tomato. In the case of an AP, voltage-gated channels associated with microtubules (MT) will allow calcium entry, while in the case of a VP, mechano-sensing channels associated with microfilaments will allow entry. Since the channels are associated with different cytoskeletal elements, are located in different parts of the cell, and are open for different durations, the downstream effects of calcium will be quite distinct. The encircled P denotes a phosphorylation wave, caused by cytoskeleton-associated protein kinases, and transmitted along the microtubules and microfilaments. With microfilaments, in particular (involved in the heat-wound-induced VP), this wave will continue to the nucleus where RNA synthesis will be enhanced and transcript accumulation will occur. This is because actin in the nucleus associates with RNA polymerase 2 which becomes activated on phosphorylation. These newly-synthesized transcripts might not be translated, either because potassium leaves the cell, lowering it to sub-optimal levels for translation, or because cytoskeleton-associated polysomes become non-functional because of phosphorylation (inactivation) of elongation factor. Finally, chloride passing into the cell wall might activate cell wall enzymes, including those that liberate PIIF (protease-inhibitor inducing factor). References in support of these events are elsewhere (Davies and Schuster 1981a,b; Davies 1987a,b, 1990, 1993, 2004; Davies et al. 1998; and especially Davies and Stankovic 2006). Figure from Stankovic and Davies (unpublished)

Davies and Stankovic (2006). Briefly, the hypothesis suggests that Ca^{2+} entering through a mechanosensitive channel (VP) will encounter Ca^{2+}-binding proteins, such as calcium-dependent protein kinases, associated with microfilaments, In the cytoplasm, these will phosphorylate myosin and thus inhibit cytoplasmic streaming, and elongation factor and thus inhibit ribosome movement on cytoskeleton-bound polysomes, while in the nucleus, phosphorylation of RNA polymerase 2 will enhance transcription. These phosphorylation responses can be extremely rapid (Bogre et al. 1996). In contrast, Ca^{2+} entering a voltage gated channel (AP) will encounter Ca^{2+}-binding proteins on the microtubules also possibly leading to enhanced transcription (Mori et al. 2004). Interestingly, in terms of changes in transcript accumulation, the transmitting tissue, although "informed", is unable to respond, thus making the

system more nerve-like. This is obvious with the VP, since it is transmitted in dead xylem cells, which are incapable of any metabolic response. However, it must also be true of the electrically stimulated AP, since it is transmitted in sieve tubes which have no nuclei, thus cannot synthesize RNA.

17.6 How do you measure AP and VP?

To measure any change in MP, some kind of electrode in contact with the plant must be attached to some kind of recording device. Since the electrical changes are small, the signals usually have to be amplified and the recording device must have high impedance, otherwise the electrical output from the plant is used to drive the recording device and the signal "disappears". The simplest electrodes to use are extracellular ones, which can either be surface contact electrodes or wire (piercing) electrodes. Surface contact electrodes (akin to the lie detector electrodes used by Backster 1968) have the advantage of not inflicting tissue damage, which is important when studying wound responses. However, since these electrodes contain KCl and they tend to dry out, this changes the ionic status of the region being measured, so these electrodes can be used for only short-term (a few hours) recordings. Piercing electrodes (silver, platinum) have the disadvantage of inflicting damage, but this problem can be circumvented by allowing the tissue to recover from the wound. They have the advantage of being usable for days and perhaps weeks and they do not appreciably alter the ionic status of the tissue (Zawadzki et al. 1995). Both electrodes measure the apoplastic ion concentration in the region of the electrode, and we have found essentially identical recordings with both types of electrodes placed close together on the same plant.

In order to take measurements, however, there must be a complete circuit, and so another electrode is needed. This may be a genuine ground electrode (i.e. in the soil), or a reference electrode at some other part of the plant. With a ground electrode, one measures the change in MP at the measuring electrode compared with (presumably) no change in the ground electrode, while with a reference electrode at some other point on the plant one measures the difference in MP between what is happening at the measuring electrode compared with what is happening at the reference. This is clearly seen in Fig. 17.2, where the signal going through successive measuring electrodes is upwards, but this gains the opposite sign when passing through the reference.

A more difficult type of electrode to use is a microelectrode (see Shabala 2006, this volume for details). The microelectrode must be inserted (with great care) into the cytoplasm of an individual cell making sure it is not in the much more voluminous vacuole. The reference electrode is put in the bathing medium, and so this method measures the actual MP of that individual cell, as well as any change in MP that results from an electrical signal. These electrodes were first used in giant algal cells even before they were used in animal cells

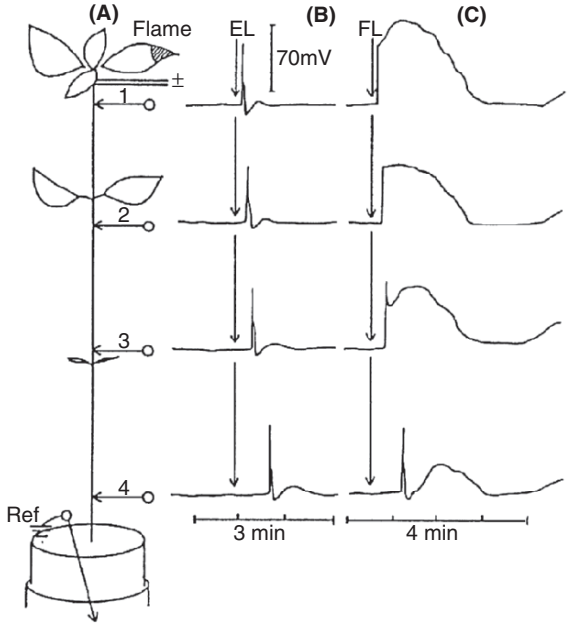

Fig. 17.2. Typical action potentials and variation potentials measured in sunflower. The plant diagrammed to the left (**A**) was stimulated electrically (5 V for 1 s) at a point about 5 cm below the lowest petiole (+/–) or heat wounded with a gentle flame applied to the tip of a leaf (*W*). Measuring electrodes (inserted silver wires) were placed along the stem, and a reference electrode was placed in the pot. The electrical responses to electrical stimulus are action potential that are shown in the middle (**B**). The electrical responses to the heat wounding stimulus are variation potentials that are shown to the right (**C**). From Davies et al. (1991), with permission. Note: electrical stimulation evoked a pure AP, while flame-wounding evoked a combined AP/VP, with the former "traveling" faster than the latter

(Wayne 1994). The main limitation of this method for vascular plants is that it is generally restricted to large, accessible cells, either epidermal or subepidermal, or individual cells such as root hairs or pollen tubes (Tester 1990). In such instances the tissue, organ, or intact plant has to be in the bathing medium, thus preventing their measurement in any but small seedlings. More recently, several workers have taken advantage of an aphid's ability to probe phloem sieve tubes. Generally, the aphid is allowed to penetrate the phloem sieve tube, its head is severed, leaving its mouthparts in the phloem, and then electrodes are (very carefully) inserted into the aphid's mouthparts giving the microelectrode direct access to the sieve tube (Koziolek et al. 2003) This permits the measurement of MP in phloem sieve tube cells of essentially any plant (attacked by aphids) growing under any condition, including trees such as poplar (Lautner et al. 2005). This technique has given unequivocal evidence

that the AP does travel in the phloem sieve tube, but has not ruled out its transmission in other tissues. Yet another electrode that can measure changes in MP is the vibrating probe electrode (see Feijo 2006, this volume for details), but it, too, needs to be in a bathing medium. Both of these techniques have the additional advantage of being able to measure specific ions, not just MP, thus the specific ion fluxes involved in AP and VP can be identified (in the accessible cell types).

The signal emerging from the electrode system needs to be converted into a visible representation, and for many years this was done using a chart recorder. These were satisfactory for most purposes, except they would suffer from baseline drift, an overly large signal, or some other factor that would cause the pen to go off-scale. Furthermore, rapid chart speeds could not be used or else entire rolls of chart paper would be consumed in minutes. In the past 15 years, there has been increasing use of computers especially equipped with data acquisition cards (analog/digital converters) and data manipulating programs such as LabView. Such programs store all the data, which can then be visualized (and printed) with the appropriate time intervals and voltage parameters. Furthermore, the number electrodes that can be used is limited only by computer memory rather than by the number of channels on the recorder(s). Recently, additional kinds of electrical activity in plants have been identified as result of taking exceedingly rapid (frequent) data sampling (Volkov 2000; Pickard 2001; Volkov et al. 2005).

17.7 How do you differentiate between AP and VP?

The most convenient way to differentiate between these signals is by their shape, velocity and constancy. The AP consists normally of a sharp rise, a brief peak, and sharp return to near baseline, whereas the VP (as its name suggests) is far more variable, normally appearing as a sharp rise followed by a lingering decline, often with spikes (AP?) superimposed and/or interspersed. In addition, the AP stays essentially the same as it passes through the plant, while the VP gets smaller and "slower". "Slower" is put in quotes, since it is not the VP itself that travels, but either a loss of tension (hydraulic signal) or perhaps chemicals in the xylem. In analogy to identification of "ducks" analogy, "If it looks like an AP, moves like an AP, and keeps going like an AP, it is most likely an AP".

There are reports in the literature (e.g. Wildon et al. 1992) claiming that flame-wounding evokes AP, even though the signals had shapes typical of VP, and a series of electrodes was not used to determine whether the signal diminished with passage. More recently others (Kozoliek et al. 2003; Lautner et al. 2005) have shown that flame-wounding evokes VP-like signals, but based on other evidence (cold blockage of signal) they called them AP. The situation is made very complex because a VP (resulting from a

hydraulic signal transmitted in the xylem) can evoke an AP in the phloem. Cold blocks would remove the phloem component, but not the xylem component. However, since the VP is fundamentally different from the AP it should be possible to differentiate between them quite clearly. This is because the VP results (usually) from a loss of tension in the xylem and, by using position sensing transducers (PST), this change in tension can be measured indirectly by changes in tissue deformation (contraction/relaxation) throughout the plant (Davies et al. 1991; Stahlberg and Cosgrove 1995; Mancuso 1999).

In our hands, these changes in stem length and diameter *always* precede changes in MP and are accompanied by almost immediate cessation of water uptake (Davies et al. 1991; Stankovic et al. 1998), whereas an AP is *never* preceded by tissue deformation (although it may be followed by very small fluctuations in stem length/diameter). To clearly distinguish between the AP and VP, experiments employing a combination of several electrodes in a row, PSTs, and balances (to measure water uptake), in conjunction with stripping the bark, phloem-girdling and/or applying a cold block (to prevent phloem AP), and/or under high humidity (to presumably reduce the VP) would be needed. I am unaware of any such "complete" reports, but such a study would be a welcome addition to the literature. The experiments will, however, need to be done carefully, since there is cross-talk between the VP and AP, insofar as any change in MP, including that evoked by a VP, can evoke an AP. Indeed, pressure, presumably detected by MSC and normally evoking a VP can be transduced to elicit an AP (Shimmen, this volume).

17.8 Why do plants have electrical signals and why are there two types?

The fundamental reason why plants have electrical signals is that they permit very rapid systemic information transmission, so that the entire plant is informed almost instantly even though only one region may have been perturbed. This is especially important for detection and response to danger, which is detected at one location, but where the entire plant needs to be warned so it can mount an essentially immediate response. Such an ultrarapid response is of particular importance with viruses, which can enter a wound and then launch a systemic invasion very rapidly, annihilating the plant unless it mounts an effectively rapid counter-attack. Not only do responses to putative viral attack need to be rapid and systemic, they also need to be highly coordinated, so that the appropriate cells exhibit the appropriate response. As described recently (Davies and Stankovic 2006), the wounded cells send a signal to both adjacent and distant cells, which respond by stopping cytoplasmic streaming, thereby slowing down intracellular flow and virus movement, clog plasmodesmata, thereby stopping cell-to-cell

transmission, inhibit translation elongation/termination, preventing ribosome movement along mRNA and translation of viral mRNA, and also by activating genes that can help in the defense response. Obviously, some of these responses cannot occur in the signal transmitting cells, since these are either dead (xylem) or lack nuclei and major cytoskeleton elements (sieve tubes). In contrast to these defense responses, insectivorous plants employ a pre-emptive strategy by making the first strike, although rapidity and coordinated activity of several cells are again essential, this time to prevent escape of the prey.

One plausible explanation for why there are two different electrical signals is that they provide back-up for each other, furnishing at least some overlap in the responses they elicit. Indeed, there may be cross-talk between the pressure-sensing VP and the voltage-sensing AP (Shimmen, this volume), especially if plants possess force/voltage sensors as have been described in prokaryotes (Bezanilla and Perozo 2002). Another reason could be that the two signals also evoke different responses, so that their effects can be additive and this might be why heat-wounding often evokes a combination of VP and AP (Stankovic et al. 1998). Another explanation is that since the VP is transmitted via the xylem, it will be more effective during the day, especially under conditions of high transpiration, whereas (at least in our hands with sunflower and tomato), the electrically-induced AP is more easily evoked at night. It is to be expected that any highly successful biological entity (and plants are undoubtedly that) will have developed back-up systems to cope with an immense diversity of threats and opportunities.

References

Antkowiak B, Mayer WE, Engelmann W (1991) Oscillations in the membrane potential of pulvinar motor cells in situ in relation to leaflet movements of *Desmodium motorium*. J Exp Bot 42:901–910

Assmann S (1995) Electrifying symbiosis. Proc Natl Acad Sci USA 92:1795–1796

Backster C (1968) Evidence of a primary perception in plant life. Int J Parapsychol 10:329–348

Baluska F, Mancuso S, Volkmann D (2006) Communications in plants. Neuronal aspects of plant life. Springer, Berlin Heidelberg New York

Bertholon ML (1783) De l'Electricité des Végétaux, Alyon, Paris

Bezanilla F, Perozo E (2002) Force and voltage sensors in one structure. Science 298:1562–1563

Biskup B, Gradmann D, Thiel G (1999) Calcium release from InsP3-sensitive internal stores initiates action potential in Chara. FEBS Lett 453:72–76

Bogre L, Ligterink W, Heberle-Bors E, Hirt H (1996) Mechanosensors in plants. Nature 383:489–490

Bose JC, Das GP (1925) Physiological and anatomical investigations on *Mimosa pudica*. Proc R Soc B 98:290–312

Braam J (2005) In touch: plant responses to mechanical stimuli. New Phytol 165:373–389

Burdon-Sanderson J (1873) Note on the electrical phenomena which accompany stimulation of a leaf of *Dionaea muscipula*. Trans R Soc Lond 21:495–496

Coker JS, Jones DA, Davies E (2003) Identification, conservation, and relative expression of V-ATPase cDNAs in tomato plants. Plant Mol Biol Rep 21:145–158
Coker JS, Vian A, Davies E (2005) Identification, accumulation, and functional prediction of novel tomato transcripts systemically up-regulated after flame-wounding. Physiol Plant 124:311–322
Darwin C (1875) Insectivorous plants. Murray, London
Darwin C (1881) The power of movements in plants. Murray, London
Davies E (1987a) Wound responses in plants. Biochem Plants 12:243–264
Davies E (1987b) Action potentials as multifunctional signals in plants: a hypothesis attempting to unify apparently disparate wound responses. Plant Cell Environ 10:623–631
Davies E (1990) Plant wound signals and translation. Proceedings of the 13th international congress on plant growth substances, pp 519–530
Davies E (1993) Intercellular and intracellular signals in plants and their transduction via the membrane–cytoskeleton interface. Semin Cell Biol 4:139–147
Davies E (2004) Commentary: new functions for electrical signals in plants. New Phytol 161:607–610
Davies E, Schuster A (1981a) Intercellular communication in plants: Evidence for a rapidly-generated, bidirectionally-transmitted wound signal. Proc Natl Acad Sci USA 78:2422–2426
Davies E, Schuster A (1981b) Wounding, action potentials and polysome formation. Plant Physiol 67:538
Davies E, Stankovic B (2006) Electrical signals, the cytoskeleton, and gene expression: a hypothesis on the coherence of the cellular responses to environmental insult. In: Baluska F, Mancuso S, Volkmann D (eds) Communication in plants. Neuronal aspects of plant life. Springer, Berlin Heidelberg New York
Davies E, Zawadzki T, Witters D (1991) Electrical activity and signal transmission in plants: how do plants know? In: Penel C, Greppin H (eds) Plant signaling, plasma membrane and change of state, University of Geneva Press, Geneva, Switzerland, pp 119–137
Davies E, Vian A, Vian C, Stankovic B (1997) Rapid systemic up-regulation of genes after heat-wounding and electrical stimulation. Acta Physiol Plant 19:571–576
Davies E, Abe S, Larkins BA, Clore AM, Quatrano RS, Weidner S (1998) The role of the cytoskeleton in plant protein synthesis. In: Bailey-Serres J, Gallie DR (eds) A look beyond transcription: mechanisms determining mRNA stability and translation in plants. ASPP, pp 115–124, Rockville, MD, USA
Dziubinska H (2003) Ways of signal transmission and physiological role of electrical potentials in plants. Acta Soc Bot Pol 72:309–318
Dziubinska H, Trebacz K, Zawadzki T (2001) Transmission route for action potentials and variation potentials in Helianthus annuus. L. J Plant Physiol 158:1167–1172
Eschrich W, Fromm J, Evert RF (1988) Transmission of electric signals in sieve tubes of zucchini plants. Bot Acta 101:327–331
Felle HH, Kondorosi E, Kondorosi A, Schultze M (1995) Nod signal-induced plasma membrane potential changes are differentially sensitive to structural modification of the lipochitooligosacchraride. Plant J 7:939–947
Fisahn J, Herde O, Willmitzer L, Pena-Cortes H (2004) Analysis of the transient increase in cytosolic Ca2+ during the action potential of higher plants with high temporal resolution: requirement of Ca2+ transients for induction of jasmonic acd biosynthesis and PINII gene expression. Plant Cell Physiol 45:456–459
Fromm J, Spanswick R (1993) Characteristics of action potentials in willow (*Salix viminalis* L.). J Exp Bot 264:1119–1125
Fromm J, Hajirezaei M, Wilke I (1995) The biochemical response of electrical signaling in the reproductive system of Hibiscus plants. Plant Phys 109:375–384
Galston AW, Slayman CL (1979) The not-so-secret life of plants. Bioscience 29:337–344
Galvani L (1791) De viribus electricitatis in motu musculari commentarius. Bononiae Instituti Scientiarum, Bologna

Gradmann D, Mummert H (1980) Plant action potentials. In: Spanswick RM, Lucas WJ, Dainty J (eds) Membrane transport: current conceptual issues. Elsevier/North-Holland Press, Amsterdam, pp 333–344

Harold FM, Caldwell JD (1990) Tips and currents: electrobiology of apical growth. In: Heath IB (ed) Tip growth in plant and fungal cells. Academic Press, San Diego, pp 59–89

Horn R (2005) How ions channels sense membrane potential. Proc Natl Acad Sci USA 102:4929–4930

Koziolek C, Grams TEE, Schreiber U, Matyssek R, Fromm J (2003) Transient knockout of photosynthesis mediated by electrical signals. New Phytol 161:715–722

Krol E, Trebacz K (1999) Calcium-dependent voltage transients evoked by illumination in the liverwort *Conocephalum conicum*. Plant Cell Physiol 40:17–24

Ksenzhek OS, Volkov AG (1998) Plant energetics. Academic Press, San Diego

Kurusu T, Yagala T, Miyao A, Hirochika H, Kuchitsu K (2005) Identification of a putative voltage-gated Ca^{2+} channel as a key regulator of elicitor-induced hypersensitive cell death and mitogen-activated protein kinase activation in rice. Plant J 42:798–809

Lautner S, Grams TEE, Matyssek R, Fromm J (2005) Characteristics of electrical signals in poplar and responses in photosynthesis. Plant Physiol 138:2200–2209

Liu K, Li L, Luan S (2005) An essential function of phosphatylinositol phosphates in activation of plant shaker-type K^+ channels. Plant J 42:433–443

MacKimmon R (2004) Voltage sensor meets lipid membrane. Science 306:1303–1305

Maffei M, Bossi S, Spiteller D, Mithofer A, Boland W (2004) Effects of feeding *Spodoptera littoralis* on lima bean leaves. I. Membrane potentials, intercellular calcium variations, oral secretions, and regurgitate components. Plant Physiol 134:1752–1762

Malone M (1994) Wound-induced hydraulic signals and stimulus perception in *Mimosa pudica* L. New Phytol 128:49–56

Malone M (1996) Rapid, long-distance signal transmission in higher plants. Adv Bot Res 22:163–228

Malone M, Stankovic B (1991) Surface potentials and hydraulic signals in wheat leaves following localized wounding by heat. Plant Cell Environ 14:431–436

Malone M, Alarcon J-L, Palumbo L (1994) A hydraulic interpretation of rapid, long-distance wound signalling in the tomato. Planta 193:181–185

Malone M, Palumbo L, Boari F, Monteleone M, Jones HG (1994) The relationship between wound-induced proteinase inhibitors and hydraulic signals in tomato seedlings. Plant Cell Environ 17:81–87

Mancuso S (1999) Hydraulic and electrical transmission of wound-induced signals in *Vitis vinifera*. Aust J Plant Physiol 26:55–61

Mitsumo T, Sibaoka T (1989) Rhythmic electrical potential change of motor pulvinus in lateral leaflet of *Codariocalyx motorius*. Plant Cell Physiol 30:1123–1127

Mori MX, Erickson MG, Yue DT (2004) Functional stoichiometry and local enrichment of calmodulin interacting with Ca^{2+} channels. Science 304:432–435

Pickard B (1973) Action potentials in higher plants. Botanical Reviews 39:172–201

Pickard B (1984a) Voltage transients elicited by sudden step-up of auxin. Plant Cell Environ 7:171–178

Pickard B (1984b) Voltage transients elicited by brief chilling. Plant Cell Environ 7:679–681

Pickard WF (2001) A novel class of fast electrical events recorded by electrodes implanted in tomato shoots. Aust J Plant Physiol 28:121–129

Pike SM, Zhang X-C, Gassmann W (2005) Electrophysiological characterization of the *Arabidopsis avrRpt2*-specific hypersensitive response in the absence of other bacterial signals. Plant Physiol 138:1009–1017

Plieth C, Sattelmacher B, Hansen U-P, Thiel G (1998) The action potential in Chara: Ca^{2+} released from internal stores visualized by Mn^{2+}-induced quenching of fura-dextran. Plant J 13:167–175

Pyatygin SS, Opritov VA, Khudyakhov VA (1992) Subthreshold changes in excitable membranes of *Cucurbita pepo* L stem cells during cooling-induced action potential generation. Planta 186:161–165

Roblin G, Bonnemain J-L (1985) Propagation in *Vicia faba* stem of a potential variation induced by wounding. Plant Cell Physiol. 26:1273–1283

Samejima M, Sibaoka T (1980) Changes in extracellular ion concentration in the main pulvinus of *Mimosa pudica* during rapid movement and recovery. Plant Cell Physiol 21:467–479

Shimmen T (1997) Studies on mechano-perception in Characeae: effects of external Ca^{2+} and Cl^{-}. Plant Cell Physiol 38:691–699

Simons PJ (1981) The role of electricity in plant movements. New Phytol 87:11–37

Stahlberg R, Cosgrove DJ (1995) Comparison of electric and growth responses to excision in cucumber and pea seedlings. II. Long distance effects are caused by the release of xylem pressure. Plant Cell Environ 18:33–41

Stahlberg R, Cosgrove DJ (1996) Induction and ionic basis of slow wave potentials in seedlings of *Pisum sativum* L. Planta 200:416–425

Stahlberg R, Cleland RE, van Volkenburgh E (2005) Decrement and amplification of slow wave potentials during their propagation in *Helianthus annuus* L. shoots. Planta 220:550–558

Stankovic B, Davies E (1996) Both action potentials and variation potentials induce proteinase inhibitor gene expression in tomato. FEBS Lett 390:275–279

Stankovic B, Davies E (1997a) Intercellular communication in plants: electrical stimulation of proteinase inhibitor gene expression in tomato. Planta 202:402–406

Stankovic B, Davies E (1997b) Wounding evokes rapid changes in tissue deformation, electrical potential, transcription, and translation in tomato. Plant Cell Physiol 39:268–274

Stankovic B, Zawadzki T, Davies E (1997) Characterization of the variation potential in sunflower. Plant Physiol 115:1083–1088

Stankovic B, Witters DL, Zawadzki T, Davies E (1998) Action potentials and variation potentials in sunflower: an analysis of their relationships and distinguishing characteristics. Physiol Plant 105:51–58

Stankovic B, Vian A, Henry-Vian C, Davies E (2000) Molecular cloning and characterization of a tomato cDNA encoding a systemically wound-inducible bZIP DNA-binding protein. Planta 212:60–66

Sussman MR (1992) Shaking *Arabidopsis thaliana.* Science 256:619

Tazawa M, Kikuyama M (2003) Is Ca^{2+} release from internal stores involved in membrane excitation in characean cells. Plant Cell Physiol 44:518–526

Tester M (1990) Plant ion channels: whole cell and single channel studies. New Phytol 114:305–340

Tompkins P, Bird C (1973) The secret life of plants. Harper and Row, New York

Trebacz K, Zawadzki T (1985) Light-triggered action potentials in the liverwort *Conocephalum conicum.* Physiol Plant 64:482–486

Trebacz K, Simonias W, Schonknecht G (1994) Cytoplasmic Ca^{2+}, K^{+}, Cl^{-}, and NO_3^{-} activities in the liverwort *Conocephalum conicum* L, at rest and during action potentials. Plant Phys 106:1073–1084

Vian A, Henry-Vian C, Davies E (1999) Rapid and systemic accumulation of chloroplast mRNA binding protein transcripts after flame stimulus in tomato. Plant Physiol 121:517–524

Volkov AG, Haack RA (1995) Insect induced bioelectrochemical signals in potato plants. Bioelectrochem Bioenerg 35:55–60

Volkov AG (2000) Green plants/electrochemical interfaces. J Electroanal Chem 483:150–156

Volkov AG, Dunkley TC, Labady AJ, Brown C (2005) Phototropism and electrified interfaces in green plants. Electrochim Acta 504241–4247

Wacke M, Thiel G (2001) Electrically-triggered all-or-none liberation during action potential in the giant alga, Chara. J Gen Physiol 118:11–21

Wayne R (1994) The excitability of plant cells: with a special emphasis on characean internodal cells. Bot Rev 60:265–367

Wildon DC, Thain JF, Minchin PEH, Gubb IR, Reilly AJ, Skipper YD, Doherty HM, O'Donnell PJ, Bowles DJ (1992) Electrical signaling and systemic proteinase inhibitor induction in the wounded plant. Nature 360: 62-65.

Zawadzki T, DaviesE, Dziubinska H, Trebacz K (1991) Characteristics of action potentials in *Helianthus annuus* L. Physiol Plant 83:601–604

Zawadzki T, Dziubinska H, Davies E (1995) Characteristics of action potentials generated spontaneously in *Helianthus annuus*. Physiol Plant 93:291–297

18 Electrophysiology of Plant Gravitropism

Bratislav Stanković

18.1 Introduction

Earth's gravitational field influences plant growth, morphology, and development. The vector of the gravity force is powerful enough to largely dominate the other directional tropic stimuli to which plants respond. Both roots and shoots respond to gravistimulation with differential, directional growth, through processes known as positive and negative gravitropism, respectively (Darwin 1896). Some of the cellular events that underlie gravitropic responses are known (recently reviewed by Morita and Tasaka 2004); the completion of a mechanistic model of plant gravity responses remains an elusive objective.

In roots, the gravity-sensing cells are the columella cells located in the root cap. These cells, known as stacocytes, contain starch-filled amyloplasts that sediment in the direction of gravity (Masson 1995). In shoots, the gravity-perceptive tissue is the endodermis, which contains sedimentable amyloplasts (Tasaka et al. 1999). In both roots and shoots, the perceived gravitropic stimulus is transduced to cells that start exhibiting differential growth, resulting in organ bending and reorientation. Little is known about the signaling pathway linking gravity perception to differential growth responses, either in the root, or in the shoot.

Plant cells exhibit a spectrum of bioelectric characteristic including electrical potentials, conductance, impedance, and permeability. Plant physiological functions are closely intertwined with cells' electric properties, through processes that involve energy maintenance and ion exchange with the environment. Steady-state electrical potentials can be measured across the plasma membrane, using microelectrodes and patch-clamping techniques. On the external plant surface, electrical potentials and ion fluxes are monitored using surface-contact electrodes and vibrating probes.

A variety of abiotic stimuli induce electrical activity in plants. The best-characterized electrical signals in plants are the action potentials and the variation potentials ("slow waves"). Voltage-gated, mechanosensitive, and ligand-activated ion channels, as well as proton pumps, are involved in

Brinks Hofer Gilson & Lione, 455 North Cityfront Plaza Drive, Chicago, IL 60611, USA

Plant Electrophysiology – Theory & Methods (ed. by Volkov)

generation and maintenance of these bioelectric potentials. Action potentials and variation potentials are both local and intercellularly propagated electrical signals. Transmitted to distant regions, these signals trigger an array of systemic molecular and cellular responses (reviewed by Davies and Stanković 2005). The information that the electrical signals carry and the responses that they evoke depend on either the ions traversing the membrane, the change in membrane potential, or both.

Despite the long-documented existence of gravity-induced electrical activity in plants, this field is marked with a surprising dearth of investigation. Discovered a century ago in the petioles of *Tropaeolum* as a differential change in extracellular electric potential (Bose 1907), the phenomenon of gravielectricity has been rarely studied by either electrophysiologists or by researchers studying gravitropism. Therefore, coming forth with a hypothesis to describe gravielectrical responses in plants is a speculative endeavor.

This review summarizes the state of knowledge related to the role of extra- and intra-cellular electrical activity in gravistimulated higher plants. The seminal studies concerning the electrophysiology of plant gravitropism are highlighted. A few ideas on the correlation of electrical activity with responses to gravity are presented. In conclusion, a prospect for future research on the electrophysiology of gravitropism is suggested.

18.2 Extracellular gravielectric potentials

The early studies on involvement of electrical potentials in plant gravitropism involved measurements of extracellular electric potentials. In the heroic age of discovery of plant electrical activity, measurements were done using extracellular, surface contact electrodes, using ionic bridges typically consisting of diluted potassium chloride. Following the studies of Bose (1907), pioneering investigations in the field were conducted by Brauner (1927), Clark (1937), and Schrank (1947). These studies provided evidence that reorientation of plants induces transient electrical activity, a phenomenon that was dubbed "geolectric effect". Decades had to pass before that phenomenon received further attention from plant biologists.

18.2.1 Shoots

Plants are electrically active. They generate characteristic steady-state transmembrane potential differences and extracellular ionic current patterns. Bioelectricity may be involved in the establishment of plant cell and organ polarity (Nechitailo and Gordeev 2001). For example, electrical current flows along the surface of upright-growing epicotyls (Toko et al. 1989, 1990). On the physically lower end of the organ, the plasma membrane is hyperpolarized by

1–2 mV. This hyperpolarization is presumably correlated to spatial information (Etherton and Dedolph 1972).

Horizontal reorientation induces electrical activity in both lower and higher plants (reviewed by Weisenseel and Meyer 1997). Gravistimulation alters the patterns of extracellular ionic currents, causing current asymmetry. Gravistimulation also changes the patterns of electrical potential along roots and shoots. For example, within minutes of horizontal reorientation of maize coleoptiles, the electrical potential became more positive on the lower side than on the upper side. The maximal change in potential was 20–25 mV, and it was reversible when the coleoptiles were rotated back to vertical (Grahm and Hertz 1962).

In soybean hypocotyls, directional change in the gravity vector induced fast electrical field changes (Tanada and Vinten-Johansen 1980). These changes were reflected as increase in positive electrical potential in the lower side of the hypocotyl, occurring rapidly, approximately one minute after horizontal placement. The increase in positive electrical potential was maximal in the region undergoing gravity-induced curvature, in a zone 1–2 cm below the hook. The maximal amplitude of the transient change in electrical potential was about 17 mV (Tanada and Vinten-Johansen 1980).

Similarly, in bean epicotyls, electrical potential on the lower side increased, whereas the potential on the upper side decreased for about one hour after gravistimulation (Imagawa et al. 1991; Fig. 18.1). The electrical activity was monitored as soon as the plants were rotated. The amplitudes of

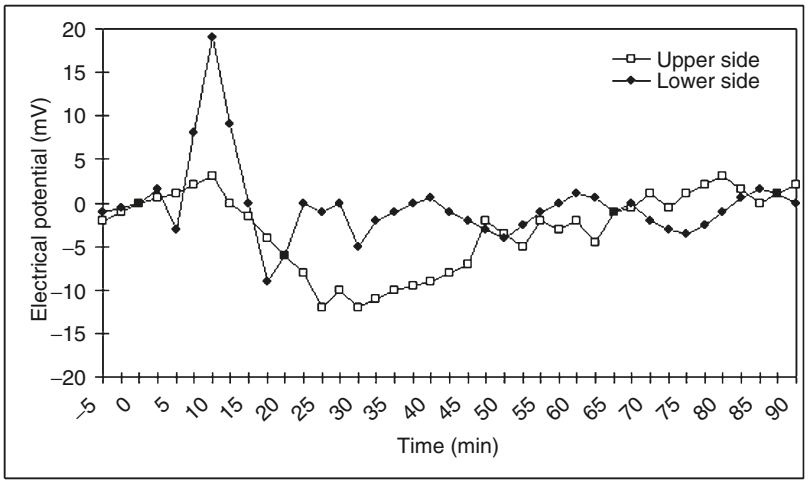

Fig. 18.1. Changes in extracellular potentials in gravistimulated shoots (approximate data are redrawn from Imagawa et al. 1991). Kinetics of the change in surface electrical potential in the upper and lower sides of gravistimulated adzuki bean (*Phaseolus angularis*) epicotyl is shown. The measured area was approximately 20 mm from the base of the first leaves. At zero time, the epicotyl was rotated to horizontal position

the electrical potential changes were 10–25 mV, and were dependent on the position of the electrodes attached to the epicotyls (Imagawa et al. 1991).

More recently, Shigematsu et al. (1994) monitored rapid surface potential changes in gravistimulated bean epicotyls. In a limited region on the upper side of the epicotyl, surface electrical potential decreased soon after gravistimulation. The magnitude of the transient potential change was about 10 mV, and it occurred 30–120 s following gravistimulation. At the same time, the surface potentials on the lower side of the epicotyls scarcely changed. The rapid change in potential on the upper side was highly correlated to the early downward curvature (transient positive gravitropic response) that was simultaneously monitored (Shigematsu et al. 1994).

It has been suggested that the electrical asymmetry across the epicotyl is related to asymmetric auxin distribution and contributes to induction of H^+ secretion, which is thought to initiate differential growth in shoot gravitropism (Wright and David 1983). Indeed, because the electrical changes occur prior to the plausible movement of auxin, it was postulated that the signals mediate the asymmetric auxin distribution or asymmetric Ca^{2+} distribution during gravitropism (Imagawa et al. 1991).

18.2.2 Roots

The growing root tip also exhibits strong electrical activity. Detailed measurements of endogenous currents surrounding roots were reported over 40 years ago (Scott and Martin 1962). Since then, several related studies have indicated that the pattern of endogenous ionic currents around vertically growing roots is consistent across species. Ionic currents typically enter the meristem and the younger parts of the elongation zone, and leave the remainder of the elongation zone and the more mature parts of the root (Behrens et al. 1982; Weisenseel et al. 1992). An area of variable current exists around the root cap; an area of large inward current is present around the meristem and apical part of the elongation zone; and an area of moderate outward current is present in the remainder of the elongation zone and the mature root tissue (Collings et al. 1992).

Horizontal reorientation of plants induces changes in the current pattern around the root. The change in current pattern is rapid, and is initiated at the root cap; it also appears at the meristem and the elongation zone. Along cress roots, differential current pattern was monitored within just 3–5 min of reorientation (Behrens et al. 1982; Iwabuchi et al. 1989). Also in cress roots, the shifts in electrical current pattern were correlated to changes in the growth rate following gravistimulation (Iwabuchi et al. 1989).

Using a vibrating probe, Björkman and Leopold (1985, 1987) studied the gravistimulus-induced electrophysiological asymmetry in maize roots. They discovered that gravistimulus induced a transient increase in current flow on the upper side of the root. The increase began 2–6 min following

gravistimulation, had a magnitude of approximately 1 μA cm^{-2}, and lasted approximately 10 min. A consistent change in current was observed only in the region adjacent to the statocytes (columella cells). Gravistimulation had little effect on currents in the elongation zone and at the tip of the root cap (Björkman and Leopold 1985).

Gravity-induced current changes along maize roots were also monitored by Collings et al. (1992). Within 10–15 min upon reorientation, currents above the root changed from inward to outward, resulting in asymmetries of up to 1.5 μA cm^{-2}. That asymmetry is significant, considering that the maximum average current density in vertical roots was approximately 1.62 μA cm^{-2}. In similar studies, the lag of the onset of current change occurred prior to the initiation of bending. This lag has been correlated to the so-called presentation time for gravity sensing (Behrens et al. 1982; Monshausen and Sievers 2002).

18.3 Intracellular gravielectric potentials

Despite the suggested role for cytosolic ions in responses to gravity, the nature of membrane potential changes in response to gravistimulation is not well understood. Different types of ion fluxes have been correlated to gravitropism and to the concomitant electrical responses. Most frequently, the gravity-induced fluxes of Ca^{2+} and H^+ have been investigated. A few studies have suggested that calcium may not be involved, or may not be necessary in gravitropism. Examining the gravity-induced bending of maize roots, Collings et al. (1992) discovered that lanthanum had little effect on either the current asymmetry or the growth response. Even a thorough imaging study failed to identify a change in cytosolic Ca^{2+} in gravistimulated roots (Legue et al. 1997). Some researchers have opined that much of the differential electric current upon gravistimulation may be carried by protons instead of Ca^{2+} (Behrens et al. 1982; Collings et al. 1992).

18.3.1 Shoots

Adding to the controversy as to the possible role of Ca^{2+}, several pharmacological studies using Ca^{2+} inhibitors suggest involvement of Ca^{2+} in gravitropism (Lee et al. 1983a; Belyavskaya 1996; Philosoph-Hadas et al. 1996). For example, maize roots cultured in EDTA and EGTA lost their ability to respond to gravity; the response was restored by addition of $CaCl_2$ but not $MgCl_2$. Furthermore, asymmetric application of Ca^{2+} solution to vertical roots induced curvature toward the side of high Ca^{2+} concentration (Hepler and Wayne 1985).

Significant trans-organ fluxes of Ca^{2+} are triggered by gravitropic stimulation. In oat coleoptiles, Ca^{2+} fluxes were monitored within 10 min following

gravistimulation, preceding the initiation of organ bending (Roux et al. 1983). Calcium ions were asymmetrically distributed in oat coleoptiles during and after gravistimulation (Daye et al. 1984). Calcium redistribution was also monitored in the graviresponding pulvini of *Mimosa* (Roblin and Fleurat-Lessard 1987). Studying transgenic Arabidopsis expressing aequorin, a role for cytoplasmic Ca^{2+} was recently affirmed in the gravity transduction mechanism. In these plants, distinct calcium signaling was observed in response to gravistimulation, with kinetics of increases in intracellular Ca^{2+} being very different from Ca^{2+} transients evoked by other abiotic stimuli. The cytoplasmic Ca^{2+} transients had duration of many minutes, and were correlated to the strength of the displacement stimulus (Plieth and Trewavas 2002).

Extracellular Ca^{2+} is also needed for gravitropism (Björkman and Cleland 1991). Oat coleoptiles incubated in 1 mM EGTA did not exhibit a gravitropic response. However, when the EGTA solution was displaced with a solution containing Ca^{2+}, gravitropism was restored (Daye et al. 1984). Similarly, elevated concentration of apoplastic Ca^{2+} was observed in the slower growing parts of gravistimulated organs (Lee et al. 1983b). Thus, increases in apoplastic Ca^{2+} concentration are correlated with the gravitropic response.

In addition to calcium, fluxes of other ions occur upon reorientation. Redistribution of other ions such as potassium and phosphorus was observed during gravity-induced curvature in sunflower hypocotyls and maize coleoptiles (Goswami and Audus 1976). Redistribution of K^+ and Cl^- was also monitored during the gravitropic response of *Mimosa* pulvini (Roblin and Fleurat-Lessard 1987). These findings are particularly interesting, because the current belief is that both action potentials and variation potentials in plants involve calcium influx followed by chloride and potassium efflux. Transient fluxes of Ca^{2+}, Cl^-, and K^+, and the concomitant electrical signals, might play a significant role in transducing the change in the gravity vector into a cellular response leading to differential growth. Earlier, it was suggested that, even if the same ions are involved in transducing the information about a multitude of abiotic stimuli, the downstream signaling events might not be the same, since the flux of any ion will depend on the kind, location, number, activity, connections, and other properties of the channel through which it passes (Davies and Stanković2005). Therefore, different channel and pump properties might create selectivity and specificity of the cellular responses.

18.3.2 Roots

Rapid changes in membrane potential in gravistimulated root cap cells have been monitored in several model systems (Behrens et al. 1985; Björkman and Leopold 1987; Sievers et al. 1995). Where transient depolarization of columella cells on the lower side of cress roots was observed, the initial changes in membrane potential were measured within a few seconds

following gravistimulation. At the same time, statocytes on the upper side of the root cap gradually became hyperpolarized (Behrens et al. 1985).

In roots of mung beans, gravistimulation changed the intracellular potentials of the elongating cells. Differential membrane potentials between upper and lower flanks of the root cap were recorded within 30 s following gravistimulation (Ishikawa and Evans 1990; Fig. 18.2). The rapidity of such gravistimulus-induced changes in electrical parameters has been used as an argument for assigning a role to electrical potentials as possible signal transmitters or transducers in the gravity response.

Distinct spatial and temporal patterns of pH fluxes are also correlated with gravistimulation. These include both apoplastic proton fluxes, as well as cytoplasmic pH changes. Gravity was found to induce rapid pH changes in Arabidopsis columella cells, causing rapid acidification of the apoplast (Scott and Allen 1999). In *Arabidopsis*, Fasano et al. (2001) observed that the root cap apoplast acidified from pH 5.5 to 4.5 within 2 min of gravistimulation. Furthermore, cytoplasmic pH increased only in the columella cells from 7.2 to 7.6, but was unchanged elsewhere in the root. Similar gravity-induced changes in cytoplasmic pH occurred in the maize pulvinus, shoot tissue that

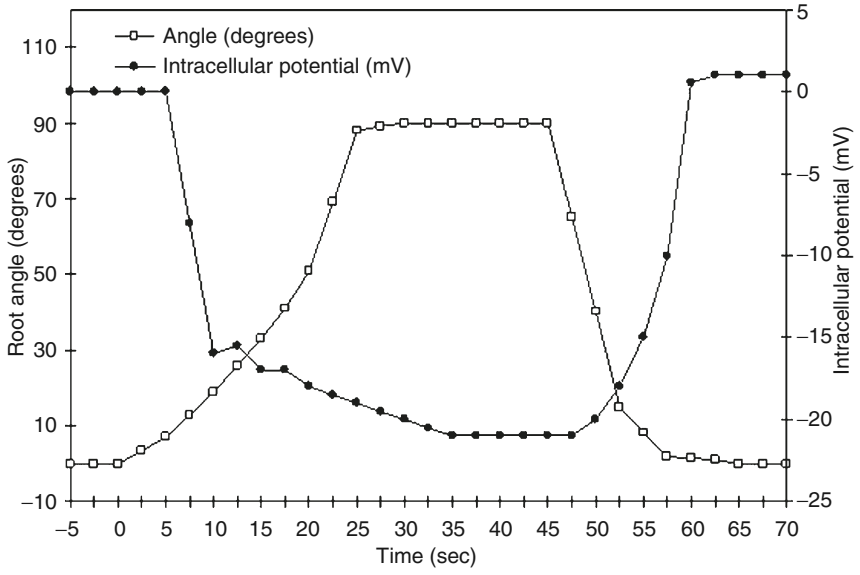

Fig. 18.2. Changes in curvature and intracellular potential in gravistimulated mung bean root (approximate data are redrawn from Ishikawa and Evans 1990). Kinetics of the change in intracellular potential of an upper cortical cell within the elongation zone upon reorientation from 0° (vertical) to 90° (horizontal) and back to 0°. The cell position was 2 mm from the root tip, and 0.15 mm from the upper surface in horizontal orientation. When the root was in vertical orientation, the intracellular potential value was approximately −115 mV. The root was turned horizontally at zero time, and turned vertically at approximately 45 s

is specialized in gravity perception (Johannes et al. 2001). Such pH changes may be a component of the changes in membrane potential that occur during gravitropism.

18.4 Physiology of the gravielectric phenomena

The bioelectric polarity of plants begins at the molecular level. Cells contain a multitude of structural and functional molecules that electrically behave as dipoles. These molecules exhibit defined reactive capacities. In addition, cells contain highly conductive aqueous electrolytes that are separated by low-conductivity membranes populated with electrically active macromolecules. The plant's bioelectric cellular heterogeneity and polarity are intrinsic features of an organism that is evolutionary adapted to gravity.

Microgravity causes abnormal plant development and abnormal plant morphology (Nechitailo and Gordeev 2001; Link, Stanković et al., unpublished data). However, establishing causal relationships between the changes in electrical activity and the known gravitropic responses is a challenging and speculative task. The heterogeneity of resistance and capacitance, as well as the existence of both passive and active transmembrane ion channels and pumps, creates considerable macromolecular complexity.

The Cholodny–Went theory of plant gravitropism is alive and well. According to this theory, a lateral gradient of auxin induces differential growth leading to organ curvature. The upward growth of horizontally positioned stems occurs due to asymmetric auxin distribution, and its increased concentration in the lower side. Inhibitors that prevent polar auxin transport also inhibit gravitropic responses (Katekar and Geissler 1980). Half a century ago, the then-discovered gravistimulus-induced positive electrical potential in cells of the lower side of plant tissue was viewed as the driving force leading to differential auxin accumulation (Wilkins 1966; Woodcock and Wilkins 1971).

The differential changes in auxin might be correlated with gravistimulus-induced proton fluxes. Recent elegant studies suggest that the H^+ dynamics in the root cap during gravistimulation is highly complex (Scott and Allen 1999). Protons are known carriers of current. In plant cells, the plasma membrane H^+-ATPase is primarily responsible for generating the membrane potential (Assmann and Haubrick 1996). The H^+-ATPases on the lower side of gravistimulated shoots transport protons into extracellular space. These positive charges might attract auxin, leading to differential growth. Indeed, auxin movement has been correlated to amyloplast sedimentation.

In an electrophysiological context, intracellular increase in positive charge could lead to accelerated influx and accumulation of negatively charged growth substance, resulting in increased differential growth during the gravitropic response. Exactly how these changes in electrical activity might signal differential growth is unclear. The electrical asymmetry may provide positional (up/down) information, intracellularly, or trans-organ. The

overall scheme might be complex beyond our current understanding, as different ion fluxes might be counterbalanced. For instance, while H^+ secretion results in membrane hyperpolarization, simultaneous K^+ uptake of positive charge via a H^+/K^+ symporter (Philippar et al. 1999) will lead to acidification of the apoplast at unchanged membrane potential.

Components of the plasmalemma may be sensing the changes in the force of gravity, and may be subsequently regulating the activity of plasmalemmal ion channels and pumps. Actin (microfilament) networks could be absorbing the force of sedimentation of amyloplasts, and could be used to amplify the signal via connected ion channels (Fig. 18.3). Feedback regulation might be involved. It has been suggested that extended, perhaps continuous signaling

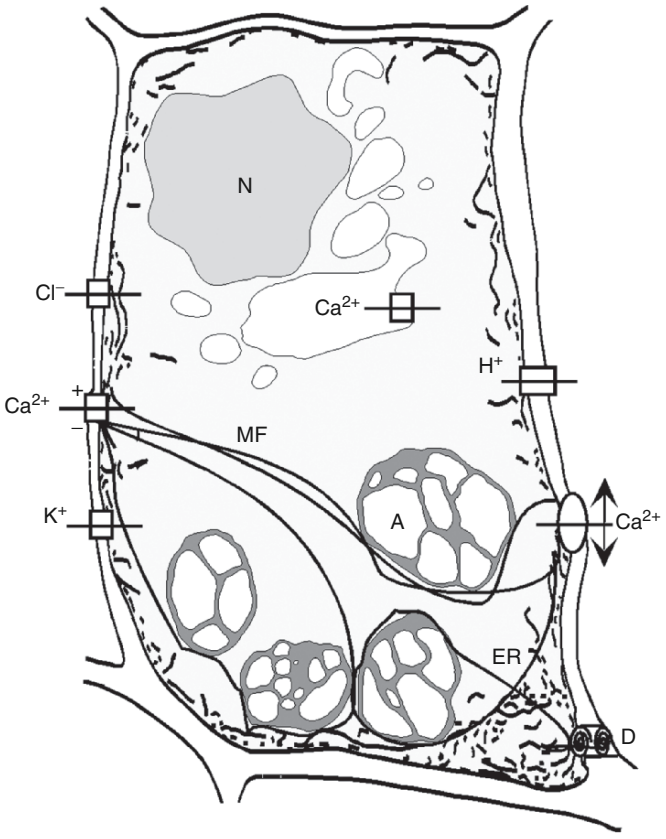

Fig. 18.3. Structural overview of a columella cell showing the known subcellular components that might be involved in gravielectric responses. Note the presence of both voltage-activated (+/−) and mechanosensitive (*double arrow*) ion channels. Microfilaments (*MF*) are in contact with these channels and with proton pumps (H^+), and with sedimenting amyloplasts (*A*). Mature columella cells exhibit distinct polarity, with the nucleus (*N*) being positioned at the upper end of the cell. The endoplasmic reticulum (*ER*) is particularly dense at the lower end of the cell. Desmotubules (*D*) might also be involved in communication with adjoining columella cells

occurs between the root cap area and the root elongation zone through active maintenance of the resting membrane potential in statocytes (Monshausen et al. 1996).

Alternatively, the electrical responses could be merely causal effects of other subcellular responses that act as primary transducers of the gravitropic stimulus. For instance, changes in cytoskeletal tension upon reorientation of the cells might induce the activity of mechanosensitive ion channels. The resulting changes in membrane potential could thus be secondary consequences of some primary signaling mechanism that functions during gravitropism.

The purpose of signal transduction is conductance of information and control. Nature uses electrical signals as convenient means for information transfer, amplification, and control in biological systems. In cellular context, electrical transducers are coupled to actuators that stimulate other transducers, becoming integrated into a myriad of control processes that constitute cellular homeostasis.

Upon gravistimulation, ion channels, ion pumps, H^+-ATPases, actin microfilaments, amyloplasts, and other molecular components create a network that may use electrical transients as a means of transducing the information about the perceived reorientation (gravity stimulus). Such a network can be likened to an electronic circuit, where changes in ionic amplitudes, frequency, and duration of transients will translate into a physiological response to gravity. This cellular network (circuit) might be characterized with cardinal design principles such as feedback stabilization, where the precise characteristics of the individual transducers and actuators are relegated to secondary importance. A design where the variations are compensated by the feedback received would allow the reliability of the transduction process to be inherent in the circuit design rather in the exactitude of its components. That circuit would exhibit tolerance regarding variations in the transducers, actuators, and communication links.

If cytosolic ions are involved as electrical signals in transduction of the gravistimulus intro graviresponse, their precise conduction pathways remain elusive. Hejnowicz et al. (1991) proposed a signaling pathway via an intrasymplasmic system composed of desmotubules and the endoplasmic reticulum. This is a plausible proposition; some studies suggest involvement of the endoplasmic reticulum in the response to gravity. Further studies, particularly in relation to sedimentation of amyloplasts onto the endoplasmic reticulum, are required to test this hypothesis.

Early workers postulated that the gravielectric effect is a consequence of auxin distribution in shoots curving upward after gravistimulation (Grahm 1964; Wilkins and Woodcock 1965). Support for that hypothesis does exist. Gravistimulated cress roots exhibit different surface acidification in the root cap (Monshausen and Sievers 2002). Through the use of proton-selective microelectrodes, gravity-induced surface pH changes were monitored across all root zones. The differential surface acidification progressed toward the

elongation zone at a rate similar to the rate of auxin transport (250–350 μm min^{-1}). The kinetics suggests a correlation of the gravity-induced pH changes (also correlated to changes in membrane potential) and the development of a lateral auxin gradient in the root gravitropic response (Monshausen and Sievers 2002).

18.5 Prospects

The phenomenon of plant gravielectricity is understudied, and consequently poorly understood. Discrepancies exist in the reporter parameters of electrical activity following gravistimulation, and in interpretation of the results obtained. These discrepancies can be attributed to the heterogeneity of use of different model systems, measurements of potentials at incorrect locations, absence of uniform techniques, etc.

Molecular genetics keeps providing substantial evidence to support the two fundamental hypotheses of gravitropism: the Cholodny–Went hypothesis and the starch-statolith hypothesis. Transgenic plants open the doors for dissecting the role of electrical potentials in gravitropism. Interesting discoveries have already been made. Using transgenic maize overexpressing K^+ channels, it was discovered that the auxin-induced K^+ channel expression is an essential step in the gravitropic responses of maize coleoptiles (Philippar et al. 1999). Upon gravistimulation of coleoptiles, differential expression between the upper and the lower halves of K^+ channel was observed. This differential expression closely followed the gravitropic-induced auxin redistribution; it preceded any detectable bending of the coleoptile (Philippar et al. 1999). More recently, it was also shown using transgenic plants that auxin activates KAT1 and KAT2, two K^+-channel genes (Philippar et al. 2004). These observations led to the hypothesis that in maize coleoptiles transcriptional regulation of K^+ channels represents a key step in response to physiological growth stimuli such as gravitropism (Philippar et al. 1999, 2004). Studies similar to these will help decipher the molecular bases underlying the nature and the significance of the electrophysiological responses during gravitropism.

A dose of cautious optimism is in order, as interesting work awaits those interested in studying plant gravitropism and the related plant space biology questions (Stanković 2001). At present, there is no data about the effects of microgravity on plant electrophysiology. Measurements of electrical potentials and ion fluxes in microgravity will help reveal the influence of gravity on ion fluxes and electrical potentials. It was already postulated that microgravity-grown plants might become hypersensitive to gravity, having more activated Ca^{2+} channels that might fire action potentials upon return from orbit (Weisenseel and Meyer 1997).

Back on Earth, the process of signal transduction in plant gravitropism needs to be dissected. The molecular identity of the mechanosensing receptor (channel/pump?) that senses changes in the gravity vector is unknown. The timing, duration, amplitude, and frequency of electrical potentials associated with graviresponses need to be determined. The ions involved in the process need to be precisely identified in terms of a signaling cascade triggered by gravistimulation. Causal relationships of the electrophysiological activity with known molecular, cellular, and organ responses to gravity need to be established. Combined methodological approaches using electrophysiology, microscopy, and transgenic plants will yield new information that will advance our understanding of the role of electrical signals in plant gravitropic responses.

References

Assmann SM, Haubrick LL (1996) Transport proteins of the plant plasma membrane. Curr Opin Cell Biol 8:458–467

Behrens HM, Weisenseel MH, Sievers A (1982) Rapid changes in the pattern of electric current around the root tip of *Lepidium sativum* L. following gravistimulation. Plant Physiol 70:1079–1083

Behrens HM, Gradmann D, Sievers A (1985) Membrane-potential responses following gravistimulation in roots of *Lepidium sativum* L. Planta 163:463–472

Belyavskaya NA (1996) Calcium and graviperception in plants: inhibitor analysis. Int Rev Cytol 168:123–185

Björkman T, Leopold AC (1985) Gravistimulation-induced changes in current patterns around root caps. Physiologist 28:S99–S100

Björkman T, Leopold AC (1987) An electric current associated with gravity sensing in maize roots. Plant Physiol 84:841–846

Björkman T, Cleland RE (1991) The role of extracellular free-calcium gradients in gravitropic signaling in maize roots. Planta 185:379–384

Bose JC (1907) Comparative electro-physiology, a physico-physiological study. Longmans Green, London

Brauner L (1927) Untersuchungen über das geoelektrische Phänomen. Jahrb Wiss Bot 66:381–428

Clark WG (1937) Polar transport of auxin and electrical polarity in coleoptile of *Avena*. Plant Physiol 12:409–440

Collings DA, White RG, Overall RL (1992) Ionic current changes associated with the gravity-induced bending response in roots of *Zea mays* L. Plant Physiol 100:1417–1426

Darwin C (1896) The power of movement in plants. Appleton, New York

Davies E, Stanković B (2006) Electrical signals, the cytoskeleton, and gene expression: current hypotheses. In: *Communication in Plants – Neuronal Aspects of Plant Life*. Baluška F, Mancuso S, Dieter V, eds., Berlin, New York, Springer Verlag, pp 309–320

Daye S, Biro RL, Roux SJ (1984) Inhibition of gravitropism in oat coleoptiles by the calcium chelator, ethyleneglycol-bis-(α-aminoethyl ether)-N,N′-tetraacetic acid. Physiol Plant 61:449–454

Etherton B, Dedolph RR (1972) Gravity and intracellular differences in membrane potentials of plant cells. Plant Physiol 49:1019–1020

Fasano JM, Swanson SJ, Blancaflor EB, Dowd PE, Kao T, Gilroy S (2001) Changes in root cap pH are required for the gravity response of the Arabidopsis root. Plant Cell 13:907–921

Goswami KKA, Audus LJ (1976) Distribution of calcium, potassium and phosphorus in *Helianthus annuus* hypocotyls and *Zea mays* coleoptiles in relation to tropic stimuli and curvatures. Ann Bot 40:49–64

Grahm L, Hertz CH (1962) Measurement of the geoelectric effect in coleoptiles by a new technique. Physiol Plant 15:96–114
Grahm L (1964) Measurement of geoelectric and auxin-induced potentials in coleoptiles with a refined vibrating electrode technique. Physiol Plant 17:231–261
Hejnowicz Z, Krause E, Glebicki K, Sievers A (1991) propagated fluctuations of the electric potential in the apoplasm of *Lepidium sativum* L. roots. Planta 186:127–134
Hepler PK, Wayne RO (1985) Calcium and plant development. Annu Rev Plant Physiol 36:416–419
Imagawa K, Toko K, Ezaki S, Hayashi K, Yamafuji K (1991) Electrical potentials during gravitropism in bean epicotyls. Plant Physiol 97:193–196
Ishikawa H, Evans M (1990) Gravity-induced changes in intracellular potentials in elongating cortical cells of mung bean roots. Plant Cell Physiol 31:457–462
Iwabuchi A, Yano M, Shimizu H (1989) Development of extracellular electric pattern around *Lepidium* roots: its possible role in root growth and gravitropism. Protoplasma 148:98–100
Johannes S, Collings DA, Rink JC, Allen NS (2001) Cytoplasmic pH dynamics in maize pulvinal cells induced by gravity vector changes. Plant Physiol 127:119–130
Katekar GF, Geissler AE (1980) Auxin transport inhibitors. IV. Evidence of a common mode of action for a proposed class of auxin transport inhibitors: the phytotropins. Plant Physiol 66:1190–1195
Lee JS, Mulkey TJ, Evans ML (1983a) Reversible loss of gravitropic sensitivity in maize roots after tip application of calcium chelators. Science 220:1375–1377
Lee JS, Mulkey TJ, Evans ML (1983b) Gravity induces polar transport of calcium across root tips of maize. Plant Physiol 73:874–876
Legue V, Blancaflor E, Wymer C, Perbal G, Fantin D, Gilroy S (1997) Cytoplasmic free Ca^{2+} in *Arabidopsis* roots changes in response to touch but not gravity. Plant Physiol 114:789–800
Masson PH (1995) Root gravitropism. BioEssays 17:119–127
Morita MT, Tasaka M (2004) Gravity sensing and signaling. Curr Opin Plant Biol 7:712–718
Monshausen GB, Sievers A (2002) Basipetal propagation of gravity-induced surface pH changes along primary roots of *Lepidium sativum* L. Planta 215:980–988
Monshausen GB, Zieschang HE, Sievers A (1996) Differential proton secretion in the apical elongation zone caused by gravistimulation is induced by a signal from the root cap. Plant Cell Environ 19:1408–1414
Nechitailo G, Gordeev A (2001) Effect of artificial electric fields on plants grown under microgravity conditions. Adv Space Res 28:629–631
Philippar K, Fuchs I, Lüthen H, Hoth S, Bauer CS, Haga K, Thiel G, Ljung K, Sandberg G, Böttger M, Becker D, Hedrich R (1999) Auxin-induced K^+ channel expression represents an essential step in coleoptile growth and gravitropism. Proc Natl Acad Sci USA 96:12186–12191
Philippar K, Ivashikina N, Ache P, Christian M, Lüthen H, Palme K, Hedrich R (2004) Auxin activates KAT1 and KAT2, two K^+-channel genes expressed in seedlings of *Arabidopsis thaliana*. Plant J 37:815–827
Philosoph-Hadas S, Meir S, Rosenberger I, Halevy AH (1996) Regulation of the gravitropic response and ethylene biosynthesis in gravistimulated snapdragon spikes by calcium chelators and ethylene inhibitors. Plant Physiol 110:301–310
Plieth C, Trewavas AJ (2002) Reorientation of seedlings in the Earth's gravitational field induces cytosolic calcium transients. Plant Physiol 129:1–11
Roblin G, Fleurat-Lessard P (1987) Redistribution of potassium, chloride and calcium during the gravitropically induced movement of *Mimosa pudica* pulvinus. Planta 170:242–248
Roux SJ, Biro RL, Halle CC (1983) Calcium movements and the cellular basis of gravitropism. Adv Space Res 3:221–227
Schrank AR (1947) Bioelectric fields and growth. Lund EJ (ed). University of Texas Press, Austin, Tex.
Scott AC, Allen NS (1999) Changes in cytosolic pH within Arabidopsis root columella cells play a key role in the early signaling pathway for root gravitropism. Plant Physiol 121:1291–1298
Scott BIH, Martin DW (1962) Bioelectric fields of bean roots and their relation to salt accumulation. Aust J Biol Sci 15:83–100

Shigematsu H, Toko K, Matsuno T, Yamafuji K (1994) Early gravi-electrical responses in bean epicotyls. Plant Physiol 105:875–880
Sievers A, Sondag C, Trebacz K, Hejnowicz Z (1995) Gravity induced changes in intracellular potentials in statocytes of cress roots. Planta 197:392–398
Stanković B (2001) 2001: a plant space odyssey. Trends Plant Sci 6:591–593
Tasaka M, Kato T, Fukaki H (1999) The endodermis and shoot gravitropism. Trends Plant Sci 4:103–107
Tanada T, Vinten-Johansen C (1980) Gravity induces fast electrical field change in soybean hypocotyls. Plant Cell Environ 3:127–130
Toko K, Fujiyoshi T, Tanaka C, Iiyama S, Yoshida T, Hayashi K, Yamafuji K (1989) Growth and electric current loops in plants. Biophys Chem 33:161–176
Toko K, Tanaka C, Ezaki S, Iiyama S, Yamafuji K (1990) Growth and electric current flowing at the surface of stems. Protoplasma 154:71–73
Weisenseel MH, Meyer AJ (1997) Bioelectricity, gravity and plants. Planta 203:S98–S106
Weisenseel M.H, Becker HF, Ehlogötz JG (1992) Growth, gravitropism, and endogenous ion currents of cress roots (*Lepidium sativum* L.). Plant Physiol 100:16–25
Wilkins MB, Woodcock AER (1965) Origin of the geoelectric effect in plants. Nature 208:990–992
Wilkins MB (1966) Geotropism. Annu Rev Plant Physiol 17:379–408
Woodcock AER, Wilkins MB (1971) The geoelectric effect in plant shoots. IV. Inter-relationship between growth, auxin concentration and electrical potentials in *Zea* coleoptiles. J Exp Bot 22:512–525
Wright LZ, David LR (1983) Evidence for a relationship between H^+ excretion and auxin in shoot gravitropism. Plant Physiol 72:99–104

19 Electrochemistry of Plant Life

Alexander G. Volkov, Courtney L. Brown

19.1 Green plants: electrochemical interfaces

All processes of living organisms examined with suitable and sufficiently sensitive measuring techniques generate electric fields (Volkov 2000). The conduction of electrochemical excitation must be regarded as one of the most universal properties of living organisms (Bertholon 1783; Bois-Reymond 1848; Burdon-Sanderson 1873, 1888; Burdon-Sanderson and Page 1876; Bose 1914, 1925, 1926, 1927). It arose in connection with a need for the transmission of a signal about an external influence from one part of a biological system to another. The study of the nature of regulatory relations of the plant organism with the environment is a basic bioelectrochemical problem. It has a direct bearing on the tasks of controlling the growth and development of plants (Mizuguchi et al. 1994).

According to Goldsworthy (1983), bioelectrochemical signals resemble nerve impulses, and they exist in plants at all levels of evolution. The inducement of non-excitability after excitation and the summation of subthreshold irritations were developed in the vegetative and animal kingdoms in protoplasmatic structures prior to morphological differentiation of nervous tissues. These protoplasmatic structures merged into the organs of a nervous system and adjusted the interfacing of the organism with the environment.

Action potentials in plants have been studied in detail in the giant cells of *Chara* and *Nitella*. These plants possess many of the properties associated with action potentials of animal cells such as the all-or-nothing law, threshold potential, and a refractory period (Abe et al. 1980). Action potentials have been researched with detail in many species of higher plants, and these same electrophysiological properties have been found (Ksenzhek and Volkov 1998; Volkov et al. 2002c).

Action potentials are signals caused by the depolarization of the cellular membrane (Volkov and Jovanov 2002; Lautner et al. 2005). The plasma membrane allows for cells, tissues, and organs to transmit electrochemical signals over short and long distances. According to Gunar and Sinyukhin (1963), excitation waves or action potentials in higher plants are possible mechanisms for

Department of Chemistry, Oakwood College, 7000 Adventist Boulevard, Huntsville, AL 35896, USA

Plant Electrophysiology – Theory & Methods (ed. by Volkov)

intercellular and intracellular communication in the presence of environment changes.

Plants respond to irritants at the site of the applied stimulus, but excitation can be dispersed throughout the entire plant (Sinyukhon and Britikov 1967; Pickard 1973; Volkov 2000). Waves of excitation travel from the top of the stem to the root and from the root to the top of the stem, but not at identical rates (Zavadzki 1980; Zavadzki et al. 1991). The speed of propagation is dependent on factors such as the chemical treatment, intensity of the irritation, mechanical wounding, previous excitations, or temperature (Volkov and Mwesigwa 2001a).

Conductive bundles of vegetative organisms support the movement of material, and they trigger the transfer of bioelectrical impulses (Sinyukhin and Gorchakov 1966, 1968, 1996). This feature motivates the harmonization of processes pertaining to the fundamental activity of vegetative organisms. Electrical impulses arise under the impact of various chemical compounds such as herbicides, plant growth stimulants, salts, and water (Volkov et al. 2001a, 2002a,b). Physical factors such as electromagnetic or gravitational fields, mechanical wounding, and temperature effects also elicit electrical impulses (Sibaoka 1962; Abe 1981; Eschrich et al. 1988; Eschrich and Fromm 1989, 1994; Fromm and Eschrich 1989; Pyatygin and Opritov 1990; Fromm 1991; Fromm and Spanswick 1993; Fromm and Bauer 1994).

Bioelectrochemical signaling is the most rapid technique of long distance signal transmission between plant tissues and organs. Plants respond quickly to changes in luminous intensity, osmotic pressure, and temperature. They also rapidly respond to cutting, mechanical stimulation, water availability, and wounding (Davies and Schuster 1981; Davies 1983; Davies et al. 1991). These responses can be discovered in distant parts of the plant directly after the stimulus occurs. Action potentials activate the membrane enzymatic systems. These systems realize biochemical reactions, accelerate the production of ethylene, increase the concentration of the proteinase inhibitor, and modify the rate of production of polysomes and proteins (Stankovich and Davies 1996).

The physiological aspect of rapid, electrochemical long-distance communication between plant tissues and organs is poorly understood (Siomons 1981). Traditionally, the translocation of phytohormones and other endogenous compounds is recognized as the principal means of signaling between stimulated and specific remote tissues in the plant where physiological responses are observed. Slow response kinetics limit the communication system utilizing the transport of chemical compounds. Many physiological responses in higher plants occur within seconds of the application of a stimulus: gravitropic responses, thigmotropic responses in *Mimosa pudica* L. and *Dionaea muscipula* Ellis, growth responses to salinity, and stomatal closure following treatment of *Salix* roots with abcisic acid.

The speed of propagation of action potentials depends upon the varying types of induced stress (Volkov et al. 2000). The speed of propagation of bioelectrical signals ranges from 0.05 cm/s to 40 m/s and it adequately sustains

swift long-distance communication. This also allows for the rapid response feature to be observed in plants.

Action potentials in higher plants may be the information carriers in intercellular and intracellular communication in response to environmental changes. A potential pathway for transmission of this electrical signal might be the phloem sieve-tube system, which represents a continuum of plasma membranes. Phloem is an electrical conductor of bioelectrochemical impulses over long distances. Phloem consists of two types of conducting cells: the characteristic type known as sieve-tube elements and another type called companion cells. Sieve-tube elements are elongated cells that have end walls perforated by numerous minute pores through which dissolved materials can pass. Such sieve-tube elements are connected in vertical series, known as sieve tubes. Although their nuclei disintegrate before the element begins its conductive function, sieve-tube elements are alive at maturity. The companion cells are generally smaller. They have nuclei at maturity, and they are alive. They are adjacent to the sieve-tube elements, and are believed to control conduction in the sieve tubes. This sieve-tube apparatus, representing a continuum of plasma membranes, is a potential pathway for electrical pulses to travel.

Electrical potentials have been measured at the tissue and whole plant level. At the cellular level, electrical potentials exist across membranes, and thus between cellular and specific compartments. Electrolytic species such as K^+, Ca^{2+}, H^+, and Cl^- are actively involved in the establishment and modulation of electrical potentials.

Differences in electrical potentials are expressed spatially within biological tissue, and are modulated over time. Many investigators have postulated that electrical potentials participate in intercellular and intracellular communication, and thus in the regulation of phloem unloading. Specificity of communication can be accomplished through modulation of the amplitude, duration, direction of the change in polarity, and rate of propagation of the electrical potential signal.

The generation of electrochemical responses induced by blue and red photosensory systems was observed in soybean plants (Fig. 19.1). A phototropic response is a sequence of the four following processes: reception of the directional light signal, signal transduction, transformation of the signal to a physiological response, and the production of directional growth response. Experimentation reveals that the irradiation of soybean plants at 450 ± 50 nm, 670 nm, and 730 nm induces action potentials with duration times of about 0.3 ms and amplitudes around 60 mV (Volkov et al. 2004a,b, 2005).

The physiological condition of the plant and the plant species influences the ability of a given stimulus to elicit electrical signals in plants, and perhaps even to the extent of receptor tissue response. According to Davies et al. (1991) and Zawadski et al. (1991), many electrophysiological parameters are highly variable within higher plants, including the excitability state, the excitability threshold, the velocity of impulse movement, and the length of the refractory period. The propagation of each impulse is followed by the

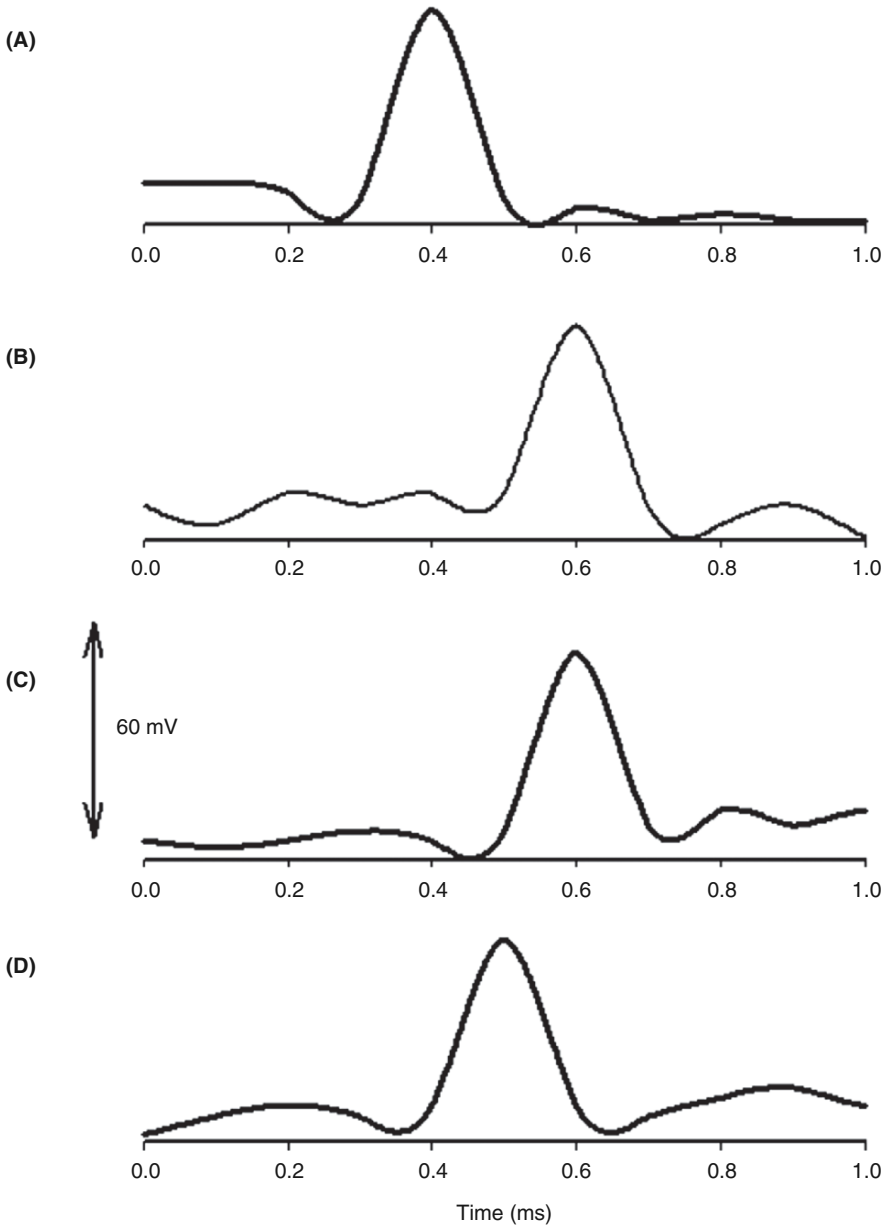

Fig. 19.1. Action potentials in soybean induced by irradiation at 450 nm (**A**), 470 nm (**B**), 671 nm (**C**), and 730 nm (**D**) in the direction B as shown on Fig. 19.7. Irradiance was 8.5 μE/m^{2}s

absolute refractory period, during which the fiber cannot transmit a second impulse (Volkov et al. 2002c). The integral organism of a plant can be maintained and developed in a continuously varying environment only if all cells, tissues and organs function in concordance.

19.2 Effects of environmental conditions on the electrochemistry of plants

Plants are constantly responding with the external world in order to maintain homeostasis. Internal biological processes and their concomitant responses to the environment are closely associated with the phenomenon of excitability in plant cells. The extreme sensitivity of the protoplasm to chemical effects is the foundation for excitation. The excitable cells, tissues and organs alter their internal condition and external reactions under the influence of environmental factors, referred to as irritants; this excitability can be monitored. Plants generate different types of extracellular electrical events in connection to environmental stress (Fensom 1958; Fensom and Spanner 1969; Volkov and Mwesigwa 2001a,b; Volkov et al. 2001a,b, 2002a,b).

19.2.1 Atmospheric electrochemistry: effects of the electric double layer of the Earth and acid rains

The existence of ions in the atmosphere is the fundamental reason for atmospheric electricity. The voltage between Earth's surface and the ionosphere is approximately 40 kV, with an electrical current of approximately 2000 A, and a current density around 5 pA/m^2. The Earth is an electrode immersed in a weak gaseous electrolyte, the naturally ionized atmosphere. The earth's surface has a negative charge. The electrostatic field strength at the earth's surface is around 110–220 V/m, and depends on time of day. It is approximately it is 110 V/m, however at 7 p.m. GMT the electrostatic field strength is nearly 220–250 V/m. Oceans, lakes, and rivers cover a significant part of the Earth, and their surfaces are also charged negatively against the atmosphere. Electrical polarity in soybeans, potatoes, tomatoes, and cacti coincides with the electrical field of the electric double layer of the Earth: negative in roots and positive on the top of the plants (Volkov 2000). Atmospheric change of the electrostatic field strength at 7 p.m. GMT does not induce action potentials or change in the variation potential of soybean or potato plants.

Acid rain is the most serious environmental problem, impacting agriculture, forestry, and human health (Shvetsova et al. 2002). Chemical reactions involving aerosol particles in the atmosphere are derived from the interaction of gaseous species with water. These reactions are associated with aerosol particles and dissolved electrolytes. For example, the generation of HONO from nitrogen oxides takes place at the air/water interface of seawater aerosols or in clouds. Clouds convert between 50% and 80% of SO_2 to H_2SO_4. This process contributes to the formation of acid rain. Acid rain exerts a variety of influences on the environment by greatly increasing the solubility of different compounds, thus directly or indirectly affecting many forms of life.

Acid rain has a pH below 5.6. Sulfuric and nitric acids are the two predominant acids in acid rain. Roughly 70% of the acid in acid rain is sulfuric acid, and nitric acid contributes about 30%. Spraying the soybean with an

aqueous solution of H_2SO_4, in a pH region of 5.0–5.6, does not induce action potentials or deviations in the resting potential. However, spraying the leaves of the plant with 0.1 ml of an acidic solution or depositing 10 µl drops of aqueous solution of H_2SO_4 or HNO_3 in the pH region from 0 to 4.9 induce action potentials in the soybean (Fig. 19.2). The duration of single action potentials after treatment by HNO_3 and H_2SO_4 was 0.2 s and 0.02 s, respectively

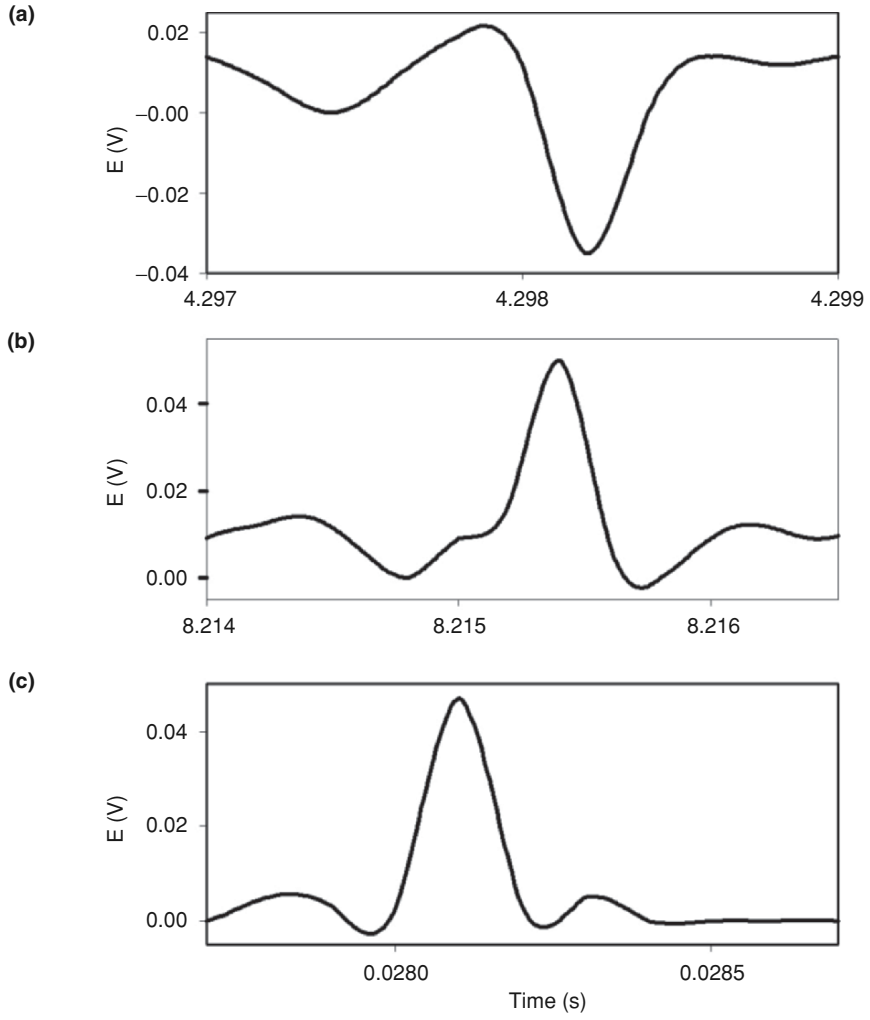

Fig. 19.2. Potential difference between two Ag/AgCl electrodes in the stem of soybean 1 (**a**), 15 (**b**), and 48 (**c**) h after spraying 1 ml of 0.1 N H_2SO_4 onto the plant. Distance between Ag/AgCl electrodes was 5 cm. Frequency of scanning was 10,000 samples per second. Volume of soil was 0.5 l. The soil around the plant was treated with water daily. Room temperature was 22 °C. Humidity was 45–50%

(Shvetsova et al. 2001; Volkov and Mwesigwa 2001a,b; Volkov et al. 2001a,b, 2002a,b).

The cells of many biological organs generate an electric potential that may result in the flow of an electric current. Electrical impulses may arise spontaneously, or result from stimulation. Once initiated, they can propagate to the adjacent excitable cells. The change in transmembrane potential creates a wave of depolarization, or action potential. It affects the adjoining, resting membrane. When the phloem is stimulated at any point, the action potential is propagated with a constant voltage over the entire length of the cell membrane and along the phloem (Volkov et al. 2002c).

19.2.2 Effects of pesticides, pollutants, uncouplers, and protonophores

In photosynthetic pathways, the radiation from the sun excites photosynthetic pigments. This excitement compels the pigments to donate electrons to the electron acceptors in the electron transport chain. Pheophytin is the first structure to receive this energized electron. The proton transport in the electron transport chain, associated with sequential redox reaction, help to establish proton gradients across the thylakoid membrane. The energy produced from this gradient is used to drive ATP synthesis. It is at this stage where uncouplers have the ability to separate the flow of electrons in the electron transport chain and the H^+ pump in ATP synthesis. Uncouplers prevent the energy transfer from electron transport chain to ATPase. They are thought to uncouple oxidative phosphorylation.

Uncouplers are generally weak acids. These chemicals are often used to inhibit photosynthetic water oxidation due to their ability to become oxidized by the manganese cluster of the O_2-evolving complex of photosystem II (PSII) and chloroplast. Most protonophoric uncouplers, widely used in photosynthesis research, are oxidized by the manganese cluster of the PSII O_2-evolving complex in chloroplasts and inhibit photosynthetic water oxidation. Oxidized uncouplers can be reduced by the membrane pool of plastoquinone, leading to formation of an artificial cyclic electron transfer chain around PSII involving uncouplers as redox carriers. Protonophores such as carbonylcyanide m-chlorophenylhydrazone (CCCP), 2,3,4,5,6-pentachlorophenol (PCP), and 4,5,6,7-tetrachloro-2-trifluoromethylbenzimidazole (TTFB) inhibit the Hill reaction with $K_3Fe(CN)_6$ in chloroplast and cyanobacterial membranes. Inhibition of the Hill reaction by uncouplers reaches maximum when the pH corresponds to the pK values of these compounds.

Uncouplers promote auto-oxidation of the high-potential form of cytochrome b559 and partially convert it to lower potential forms. Protonophores uncouple electron transport, accelerate the deactivation of the S-2 and S-3 states on the donor side, and facilitate the oxidation of cytochrome b559 on the acceptor side of PSII.

Once oxidized, uncouplers can then be reduced by plastoquinone, thereby facilitating the formation of artificial cyclic electron transport chain around photosystem II involving uncouplers as redox carriers. Auto-oxidation of high potential cytochrome b559 is enhanced by the presence of uncouplers. Cytochrome b559 is also converted to low potential forms in the presence of chemical uncouplers.

Protonophores: (1) uncouple electron transport and H^+ pump in ATP synthesis, (2) accelerate the deactivation of the S-2 and S-3 states on the donor side, and (3) facilitate oxidation of cytochrome b559 on the acceptor side of photosystem II. Although the interaction of proton-conducting ionophores with photosynthetic electron transport has been extensively studied during the past decade, the mode of action of protonophores remained uncertain. Electrochemical measurements in real time are required for a better understanding of the molecular mechanism of action of protonophores (Labady et al. 2002).

Pesticides PCP, (2,4-dinitrophenol) DNP, CCCP, and (carbonylcyanide-4-trifluoromethoxyphenyl hydrazone) FCCP act as insectides and fungicides. PCP is the primary source of dioxins found in the environment. This pollutant is a defoliant and herbicide. PCP is utilized in termite control, wood preservation, seed treatment, and snail control. The pesticide DNP is used to manufacture dye and wood preservative. DNP is often found in pesticide runoff water. The electrochemical effects of CCCP, PCP, DNP, and FCCP have been evaluated on soybean plants (Volkov and Mwesigwa 2001b).

Aqueous CCCP caused the variation potentials of soybeans to decrease from 80–90 mV to 0 mV after 20 h. CCCP induced fast action potentials in soybeans with an amplitude of 60 mV (Volkov et al. 2001a). The maximum speed of propagation was 25 m/s. Exudation is a manifestation of the positive root pressure in the xylem. After treatment with CCCP, the exudation from cut stems of the soybean remains the same. Therefore, the addition of CCCP did not cause a change in the pressure, although it may influence the zeta potential due to depolarization (Labady et al. 2002).

The addition of aqueous PCP also causes the variation potential in soybeans to stabilize at 0 mV after 48 h. Rapid action potentials are induced. These action potentials last for 2 ms, and have amplitudes of 60 mV. The speed of propagation is 12 ms^{-1}; after 48 h, the speed increased to 30 ms^{-1}.

DNP decreases the variation potential to zero in soybeans (Mwesigwa et al. 2000; Volkov 2000). The addition of aqueous DNP to the soil induces fast action potentials in soybeans. After treatment with an aqueous solution of DNP, the variation potential, measured between two Ag/AgCl microelectrodes in a stem of soybean, slowly decreases from 80–90 mV (negative in a root, positive on the top of the soybean) to 0 during a 48-h time frame. The duration of single action potentials, 24 h after treatment by DNP, varies from 3 s to 0.02 s (Fig. 19.3). The amplitude of action potentials is about 60 mV. The maximum speed of action potential propagation is 1 m/s. After 2 days,

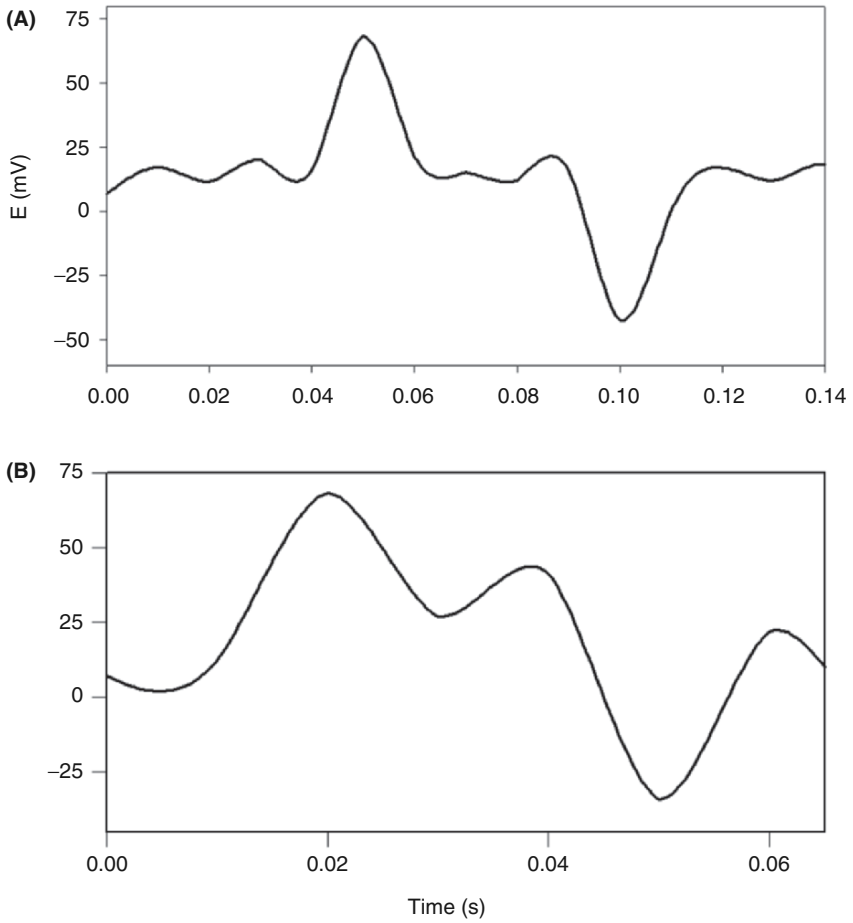

Fig. 19.3. Potential difference between two Ag/AgCl electrodes in the stem of soybean 25 (**A**) and 75 (**B**) h after adding 50 ml of 10^{-3} M 2,4-dinitrophenol to soil. Distance between electrodes was 6 cm. The soil was preliminary treated by water every other day. Room temperature was 24 °C. Volume of soil was 0.5 l. Frequency of scanning was 5000 samples per second

the variation potential stabilized at 0. Fast action potentials were generated in a soybean, with amplitude of about 60 mV, 0.02 s duration time, and a speed of 2 m/s, after treatment. Fromm and Spanswick (1993) studied the inhibiting effects of DNP on the excitability of willow by recording the resting potential in the phloem cells. In willow, 10^{-4} M DNP rapidly depolarized the membrane potential by about 50 mV.

The FCCP also induced action potentials. The maximum speed of these action potentials after 20 h was 10 ms^{-1}. After 100 h, the action potentials were still being produced. The amplitude of 60 mV remained constant.

19.2.3 Insect-induced bioelectrochemical signals in potato plants

Volkov and Haack (1995) were the first to afford a unique opportunity not only to investigate the role of electrical signals induced by insects in long-distance communication in plants but also to confirm the mechanism by which electrical signals can directly influence both biophysical and biochemical processes in remote tissues. Plant responses to herbivore attack are complex and involve an array of signals, leading to activation of multiple defenses (Maffei et al. 2004).

Action and variation potentials were measured in potato plants (*Solanum tuberosum* L.) in the presence of leaf-feeding larvae of the Colorado potato beetle (*Leptinotarsa decemlineata* (Say); Coleoptera: Chrysomelidae). The larvae consumed the upper leaves of the potato plants. After 6–10 h, action potentials with amplitudes of 40 ± 10 mV were recorded every 2 ± 0.5 h during a 2-day test period. The insect induced action potentials traveled down the stem at 0.05 cm/s. The variation potential decreased from 30 mV to a steady state level of 0 ± 5 mV. Figure 19.4 shows the positive spikes and negative humps that appear during measurement of electrical potential difference between two reversible silver chloride electrodes of the potential difference. The action potential induced by the Colorado potato beetle in potato plants propagates slowly; hence, the speed of propagation can be measured with two Ag/AgCl electrodes. The action potential propagates from plant leaves with Colorado potato beetles down the stem, and to the potato tuber (Fig. 19.4). The speed of propagation of the action potential does not depend on the location of a working electrode in the stem of the plant or tuber, or the distance between the working and reference electrodes (Fig. 19.5). The speed of propagation of the action potential, induced by the Colorado potato beetle, can be determined from the slope of the dependence of the time interval between peaks of the distance between electrodes (Fig. 19.5); in this case, it is approximately 0.05 cm/s.

19.3 Electrical activity of excitable membranes

Nerve cells in animals and phloem cells in plants share one fundamental property: they possess excitable membranes through which action potentials can propagate (Hille 2001). These propagating excitations are modeled theoretically as traveling wave solutions of certain parameter dependant nonlinear reaction-diffusion equations coupled with nonlinear ordinary differential equations. These traveling wave solutions can be classified as single loop pulse, multiple loop pulses, fronts and backs, or periodic waves of different wave speed. This classification is matched by the classification of the electrochemical responses observed in plants. The experimental observations also show that under the influence of various pathogens, the shapes and wave

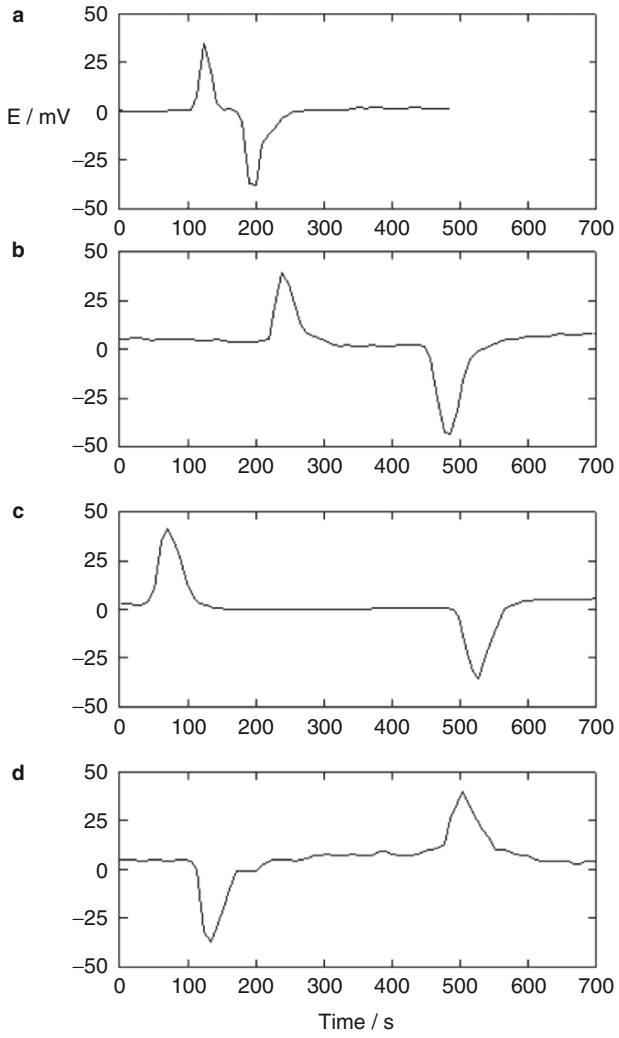

Fig. 19.4. Action potentials in the stem of a potato plant with Colorado beetles on the young terminal leaves. Distance between electrodes: **a** 3.5 cm; **b** 12 cm; **c** 22 cm; **d** 20 cm. The reference Ag/AgCl electrode was inserted in the stem between the cotyledons. The working Ag/AgCl electrode was inserted into the stem (**a**, **b**, **c**) or the tuber (**d**)

speeds of the electrochemical responses undergo changes. From the theoretical perspective, the changes in the shapes and wave speeds of the traveling waves can be accounted for by appropriate changes in parameters in the corresponding nonlinear differential equations (Volkov and Mwesigwa 2001a).

Hodgkin and Huxley (1952) formulated a membrane model that accounts for K^+, Na^+ and ion leakage channels in squid giant axons (Fig. 19.6A). The

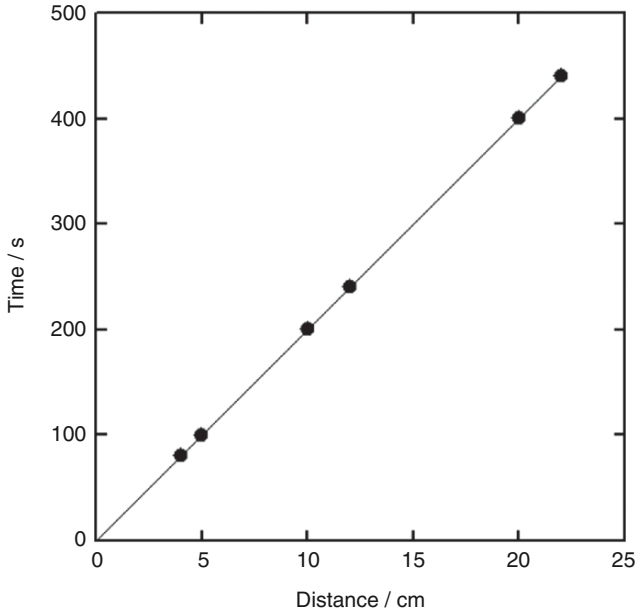

Fig. 19.5. The dependence of the time interval between the positive and negative peaks of action potential induced by Colorado potato beetles on the distance between electrodes. The electrodes were inserted in the potato tubers and different parts of the plant stem 2 h before the potential difference was measured

membrane resting potential for each ion species is treated like a battery. A variable resistor models the degree to which the channel is open.

Fromm and Spanswick (1993) found that electric stimulation of the plant is followed by ion shifts that are most striking in the phloem cells. While the content of potassium and chloride was diminished after stimulation, the amount of cytoplasmic calcium increased slightly. These displacements lead to the conclusion that Ca^{2+} influxes, as well as K^+ and Cl^- efflux are involved in the propagation of action potentials. The main difference between propagation of action potentials in animals and plants is that in an axon there is the K^+/Na^+ transmembrane transport, but in phloem cells the K^+/Ca^+ channels are involved in this process (Fig. 19.6B) (Brown et al. 2005).

19.4 Measuring of action and variation potentials in plants

Figure 19.7 is an example of the experimental configuration for the measuring of extracellular action and variation potentials. All electrochemical measurements are conducted at constant temperature inside a Faraday cage mounted on a vibration-stabilized table in a laboratory. An IBM-compatible

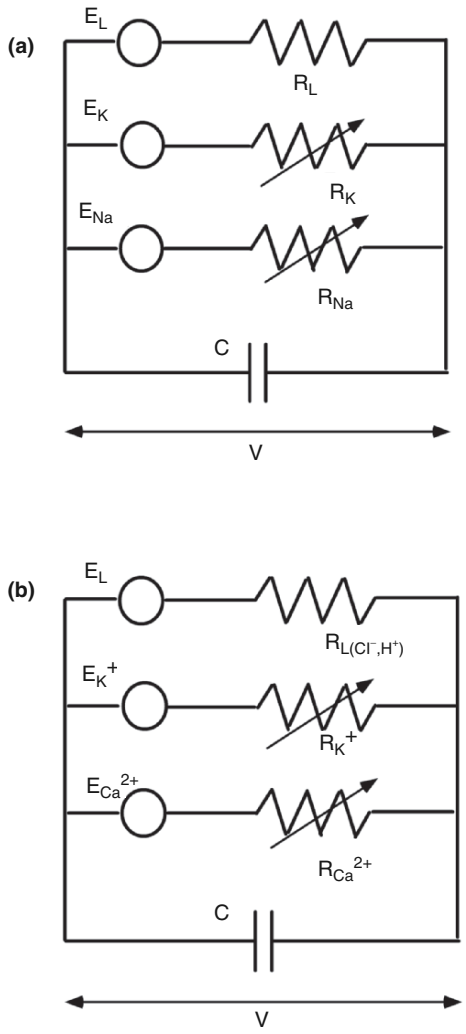

Fig. 19.6. The Hodgkin–Huxley (HH) equivalent circuit for an axon (**a**) and the modified HH circuit for sieve tubes in phloem (**b**)

microcomputer with multi I/O plug-in data acquisition board NI 6052E DAQ (National Instruments) is interfaced, through a NI SC-2040 Simultaneous Sample and Hold (National Instruments), with non-polarizable, reversible Ag/AgCl electrodes to record the digital data. The multifunction NI 6052E data acquisition board provides high resolution and a wide gain range. The NI 6052E features continuous, high-speed data acquisition; a single channel can be sampled at any gain up to 333 kSamples/s. Each analog input channel of the SC-2040 has its own instrumentation amplifier with differential inputs. The

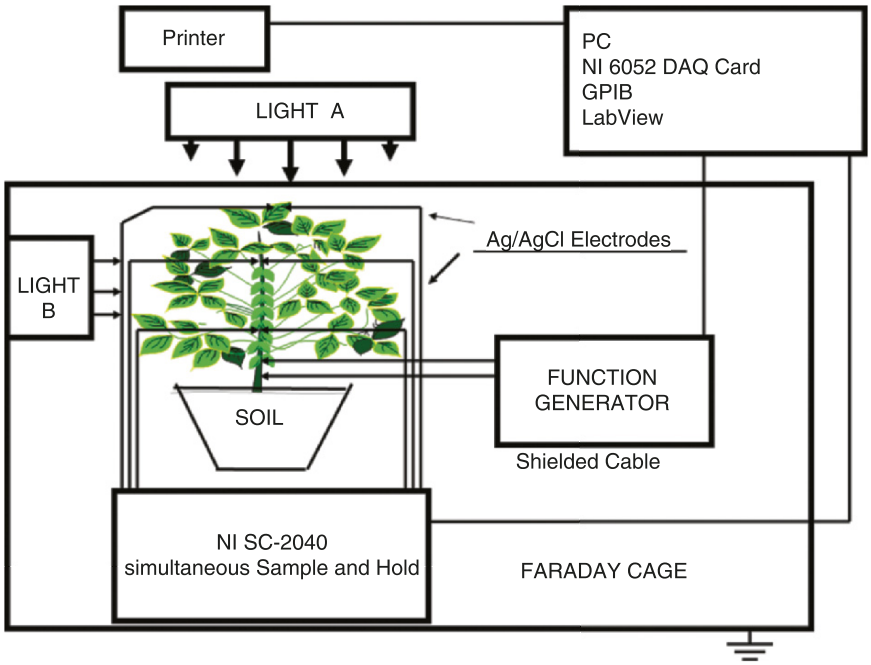

Fig. 19.7. Experimental set-up for measuring electrical signals in green plants

output of every instrumentation amplifier is routed to a track-and-hold amplifier. In track mode, the outputs of the track-and-hold amplifiers follow their inputs. When put into hold mode, the track-and-hold amplifier outputs simultaneously freeze, holding the signal levels constant. The digitized data includes negligible time skew (less than 50 ns) between channels. Measurements are recorded as ASCII files using Labview (National Instruments) software.

As a fundamental rule of sampled data systems, the input signal must be sampled at a rate greater than twice the highest frequency component in the signal; that is, $f_s/2>f_a$, where f_s is the sampling frequency and f_a is the maximum frequency of the signal being sampled. This rule is known as the Shannon sampling theorem, and the critical sampling rate is called the Nyquist rate. A violation of the Nyquist criterion is considered undersampling, resulting in aliasing. Theoretically, the recovery of information about signals with frequencies at or below the Nyquist frequency is impossible. Due to this limitation, all data presented in this paper were collected on high-speed data acquisition system.

Ksenzhek and Volkov (1998) described the preparation of Ag/AgCl electrodes from Teflon coated silver wire. Ag/AgCl electrodes are sensitive to changes in the temperature; therefore, the temperature should remain constant. Both Ag/AgCl electrodes are identical; they are referred to as reference and working electrodes. The reference electrode (–) is generally inserted in

the stem or in a root of a soybean. On the other hand, the upper working electrode (+) is inserted in the stem or a leaf. Following insertion of the electrodes, the plants should be allowed to rest until a stable potential difference was obtained between the working and reference electrodes. The insertion of the electrodes in plants induces action potentials across the stem and slow fluctuations of the variation potential. After approximately 1–2 h, the variation potential stabilizes.

The automatic measurements of the extracellular and intracellular electrical potential difference can be effectively used in plant electrophysiology to study the molecular interfacial mechanisms of ion transport, the influence of external stimuli on plants, and for investigating the bioelectrochemical aspects of the interaction between insects and plants (Volkov et al. 2001a).

19.5 Electrochemistry of photosynthetic systems

Annually, mankind consumes about 4×10^{17} kJ of energy. This rate is rising rapidly; in fact, it is doubling every 20 years. At present, the known fossil fuel reserves can only yield approximately 5×10^{19} kJ of energy. This deficiency makes exploring alternative sources of energy fundamentally important. Harvesting solar energy is an obvious possibility. On Earth, the sun contributes nearly 5×10^{21} kJ of energy per year; however, 3×10^{18} kJ of this energy is converted into chemical energy by photosynthetic plants and microorganisms. In water-oxidizing photosynthesis, photosystems I (PSI) and PSII are utilized in a series (Fig. 19.8). The electron transfer starts in both photosystems vectorially across the membrane. Light energy is harvested by the photosynthetic pigment systems where the electronic structure of excited-state chlorophyll donates an electron to a primary acceptor pheophytin, the first component of an electron transport chain. The electron is enriched with the energy from the original photon of light that was absorbed. In the process of electron transport the energy is captured in two ways. The first involves coupling a proton pump mechanism that is coupled to the sequential redox reactions in one part of the electron transport chain, establishing a proton gradient across the thylakoid membrane. The electrochemical energy of the proton gradient is then drives ATP synthesis via the ATP synthase enzymes embedded in the membrane. The second energy capture occurs when an acceptor molecule such as NADP is reduced to NADPH, which in turn, is used to reduce carbon dioxide in the Calvin cycle (see Volkov 2002).

19.5.1 Structure and composition of the oxygen-evolving complex in vivo

The redox map of photosynthesis in green plants can be described in terms of the well-known *Z*-scheme proposed by Hill and Bendall (1960). The main advantage of the currently accepted *Z*-scheme, depicted in Fig. 19.9, lies in the

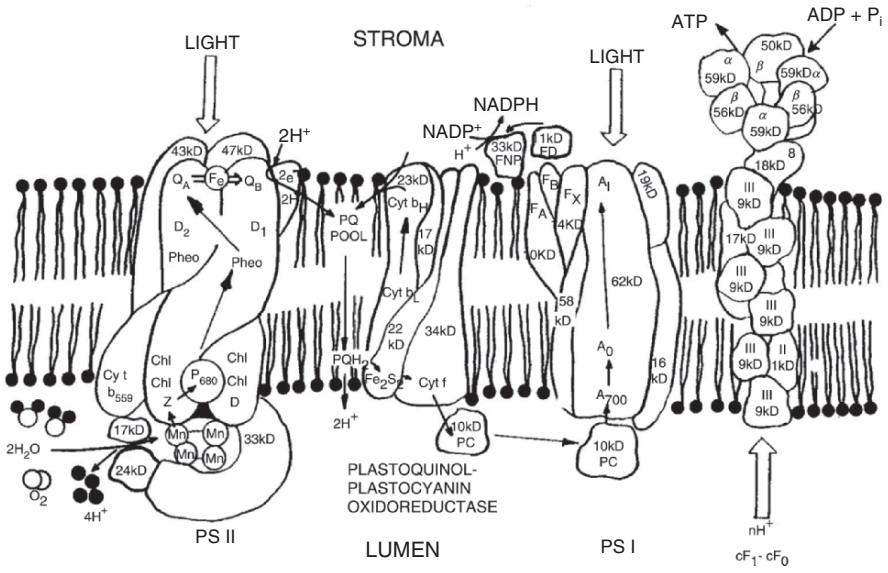

Fig. 19.8. Electron transfer during photosynthesis in higher plants. The abscissa shows the midpoint redox potential at pH 7.0. Light quanta (hν) are absorbed in two sets of antenna chlorophyll molecules, and the excitation energy is transferred to the reaction center chlorophyll *a* molecules of photosystem II (P680) and photosystem I (P700) forming $(P680)^*$ and $(P700)^*$. The latter two initiate electron transport. Abbreviations: *LHC* light harvesting complex; *Z* and *D* are tyrosine residues; *Cyt* b_{559} is cytochrome b_{559} of unknown function; *Pheo* is pheophytin; Q_A, Q_B and *PQ* are plastoquinone molecules; Fe_2S_2 represents the Rieske iron-sulphur center, *Cyt f* stands for cytochrome f, *PC* is plastocyanin; A_o is suggested to be a chlorophyll molecule, A_1 is possibly vitamin K; *FNR* is ferredoxin NADP oxidoreductase;(x): inhibitors (DBMIB: dibromo-3-methyl-6-isopropyl-p-benzo-quinone; *DCMU* 3-(3′,4′-dichlorophenyl)-1,1-dimethylurea)

specific mechanism of charge transfer at the stage of water oxidation. It is a multielectron reaction mechanism without unknown intermediates (Volkov et al. 1998).

The molecular organization of a thylakoid membrane is shown in Fig. 19.8. The spectral characteristics of PSII indicate that the primary electron donor is the dimer of chlorophyll P680 with absorption maxima near 680 and 430 nm. Water can be oxidized by an oxygen-evolving center (OEC) composed of several chlorophyll molecules, two molecules of pheophytin, plastoquinol, several plastoquinone molecules and a manganese–protein complex containing four manganese ions. The oxygen-evolving complex is a highly ordered structure in which polypeptides interact to provide the appropriate environment for cofactors such as manganese, chloride, and calcium, as well as for electron transfer within the complex. Figure 19.10 shows the electronic equivalent circuit of PSI and PSII.

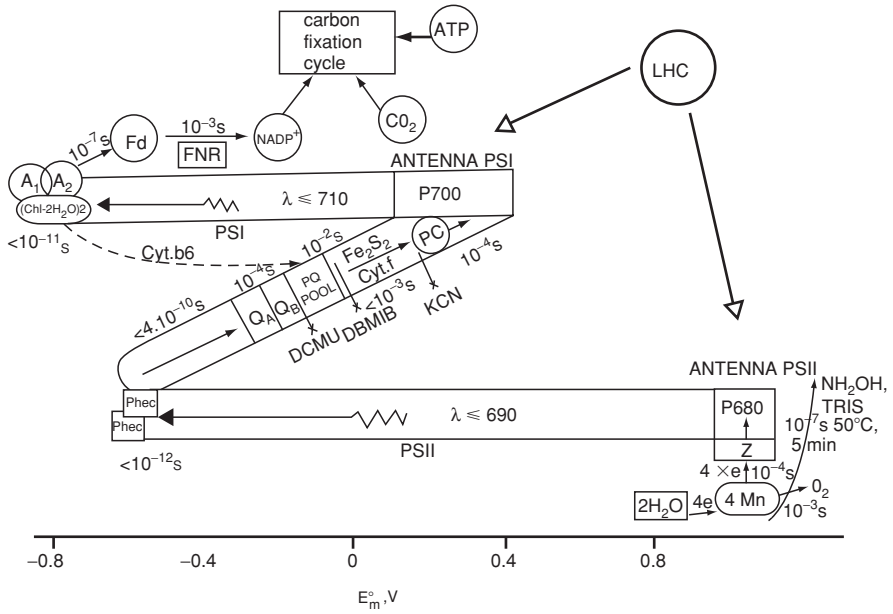

Fig. 19.9. A schematic model of the electron transport chain with most of the light-harvesting pigment-protein complexes omitted

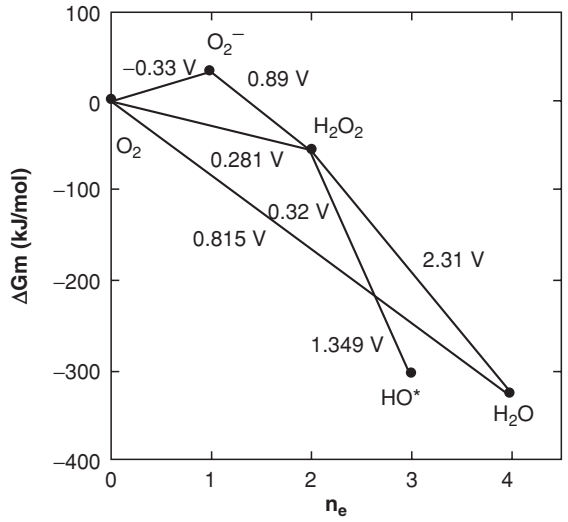

Fig. 19.10. Energy diagram for possible routes of reaction $2\ H_2O \Leftrightarrow O_2 + 4H^+ + 4e^-$. G_m is the reaction Gibbs free energy at pH 7

Manganese binding centers were first revealed in thylakoid membranes by EPR methods, and it is now understood that four manganese ions are essential for oxygen evolution during water photo-oxidation. Plastoquinone (PQ) acts as a transmembrane carrier of electrons and protons between reaction centers of two photosystems in the case of non-cyclic electron transfer and may also serve as a molecular "tumbler" that rotates between one-electron reactions and two-electron reactions. Pheophytin is an intermediate acceptor in PSII. The direct formation of P680 pheophytin ion radical pairs was revealed by experiments on magnetic interactions between Pheo- and PQ-in the EPR spectra.

PSII uses light energy to split water into protons, electrons and molecular oxygen. Nature has solved the difficult chemical problem of efficient four-electron oxidation of water to yield oxygen without significant amounts of reactive intermediate species. In order to use Nature's solution for the design of artificial catalysts that split water, it is important to understand the mechanism of the reaction. Water oxidation to molecular oxygen is a multielectron process that proceeds with surprisingly high quantum efficiency (Volkov 1989). The water oxidation reaction can proceed upon illumination at 680 nm, a wavelength of light that excludes one-electron mechanisms using hydroxyl and oxygen radicals (Fig. 19.11). For a three-electron reaction, an oxidant stronger than the cation-radical $P680^+$ is needed. A synchronous 2:2-electron pathway of the reaction is thermodynamically possible if the standard free energy of the binding of the two-electron intermediate is about −40 kJ/mol. This value corresponds to the energy of two hydrogen bonds forming between H_2O_2 and the catalytic center. For this case a molecular mechanism proposed (Fig. 19.12), and is discussed below. The synchronous

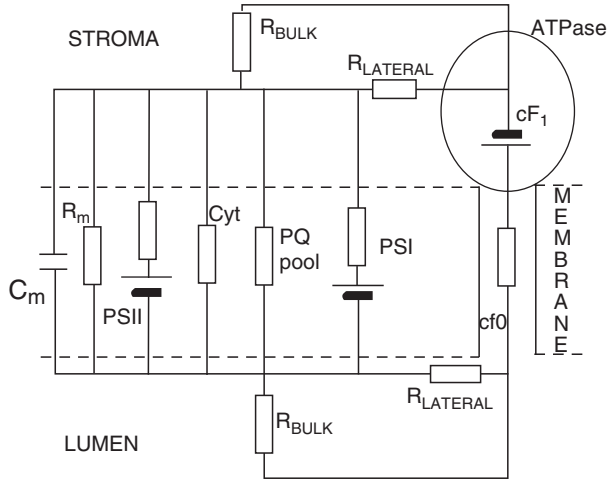

Fig. 19.11. Electronic equivalent circuit of photosystems II and I

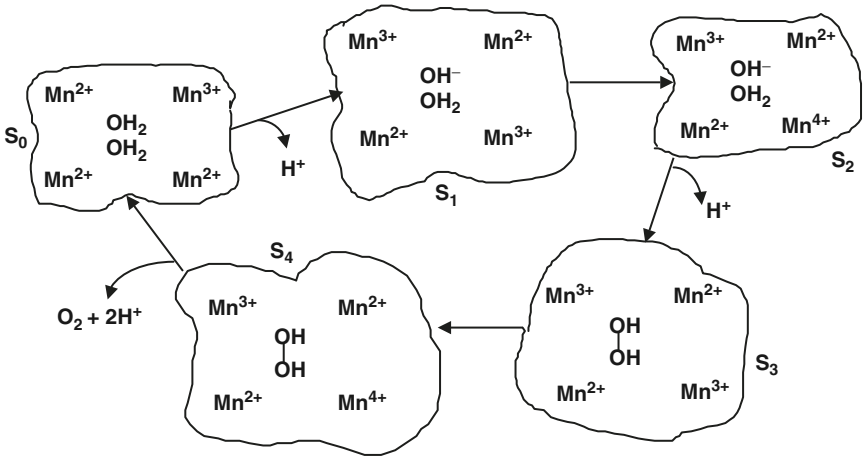

Fig. 19.12. Proposed 2:2-electron mechanism of water photo-oxidation

four-electron oxidation of water to molecular oxygen is also thermodynamically possible (Volkov 1989).

One-electron mechanisms of water oxidation are likely to be operative in some model systems with a low quantum efficiency, but two- or four-electron reactions cannot occur due to kinetic limitations. The intermediates formed in these systems would be highly reactive and could enter into side reactions of hydroxylation, oxidation, and destruction of chlorophyll and other components of the reaction center (Volkov et al. 1998).

19.5.2 Molecular mechanism of oxygen evolution in vivo

Membrane-bound P680 enters an excited state upon illumination. In dimers and other aggregated forms of chlorophyll the quantum efficiency of triplet states is low, and it is the singlet-excited states that undergo photochemical transformations. In several picoseconds, an electron is first transferred to pheophytin, and then to plastoquinone Q_A. From plastoquinone Q_A, the electron transfers to another polypeptide-bound plastoquinone Q_B, in thylakoid membrane (Fig. 19.9). This electron transfer results in an oxidized pigment and a reduced acceptor. The cation radical $P680^+$ successively oxidizes four manganese ions, which drives the production of molecular oxygen. Formation of a cation radical of chlorophyll or oxidation of manganese ions is accompanied by dissociation of water bound to the reaction center and ejection of protons. The synchronous multielectron process that describes all four oxidizing states of the oxygen-evolving complex was proposed earlier. The transfer of electrons in a 1:1:1:1 series from a manganese cluster to the electron-transport chain is accompanied by the ejection of 1:0:1:2 protons and the evolution of molecular oxygen.

Protons are released from reaction centers either by regulators of proton distribution, or by a hydrogen bond transfer analogous to a Grotthus mechanism through the hydration shell of manganese ions (Volkov 1989). The hydration sphere of manganese is known to contain water molecules that rapidly exchange protons with bulk water. The presence of divalent cations at the interface between two immiscible electrolyte solutions facilitates strong adsorption of water molecules belonging to the second hydration shell of ions. Thus, a portion of coordinatively bound water enters the compact part of the electric double layer which changes its differential capacity at the interface. In the case of multivalent ions with small radii, the electric field near a cation is large. This can disturb the microstructure of the adjacent intrathylakoid space and bring about dielectric saturation effects.

Manganese ions play a particularly important role in the evolution of dioxygen during photosynthesis. Although there are several manganese pools in chloroplasts, only one is involved in water oxidation. The manganese ions associated with OEC of the chloroplast can perform a number of functions:

- Mn-polypeptide complex is a redox intermediate that protects the reaction center from redox and radical destruction.
- Mn-clusters are redox buffers facilitating accumulation of four holes in the reaction center of PSII, which are needed to ensure water photooxidation.
- Hydrated multivalent manganese cations bring water to the reaction center so that rapid proton exchange and transport through the hydration shell of manganese ions in the zone of water oxidation.
- Multivalent manganese ions induce dielectric saturation effects in the polar region of the reaction center of photosystem II, which reduces the reorganization energy of the medium during charge transfer.

19.6 Conclusions and future perspectives

Green plants interfaced with a computer through data acquisition systems can be used as fast biosensors to: monitor the environment; detect effects of pollutants, pesticides, and defoliants; predict and monitor of climate changes; and facilitate the direct and fast control of conditions influencing the agricultural harvest. The use of new computerized methods provides opportunities for detection of fast action potentials in green plants in real time.

Studying the electrochemistry in green plants allows electrophysiologists to learn more about the processes of life through the observation of excitation waves. Green plants are a unique canvas for studying signal transduction, the foundation to discovering and improving biosensors, and essential to the development of alternative sources of energy. The evolution of oxygen is the most vital chemical reaction on earth. The photosynthetic process in plants contributes life-sustaining oxygen to the atmosphere. The investigation of the

effects of acid rain and other pollutants on vegetative organisms is crucial to maintaining life on earth.

References

Abe S, Takeda J, Senda M (1980) Resting membrane potential and action potential of *Nitella expansa* protoplasts. Plant Cell Physiol 21:537–546

Abe T (1981) Chloride ion efflux during an action potential in the main pulvinus of *Mimosa pudica*. Bot Mag 94:79–383

Bertholon M (1783) De l'electricite des vegetaux : ouvrage dans lequel on traite de l'electricite de l'atmosphere sur les plantes, de ses effets sur l'economie des vegetaux, de leurs vertus medicaux. Didotjeune, Paris

Bois-Reymond DE (1848) Untersuchungen über Thierische Elektricität, Erster Band. Reimer, Berlin, pp 7–10

Bose JC (1914) An automatic method for the investigation of velocity of transmission of excitation in mimosa. Philos Trans B 204:63–97

Bose JC (1925) Transmission of stimuli in plants. Nature 115:457–457

Bose JC (1926) The nervous mechanism of plants. Longmans Green, New York

Bose JC (1927) Plant autographs and their revelations. Macmillan, New York

Brown CL, Mbyirurukira G, Osei AJ, Volkov AG (2005) Effects of ion channel blockers on signal transduction in green plants. Biophys J 88:430a–430a

Burdon-Sanderson J (1873) Note on the electrical phenomena which accompany stimulation of the leaf of *Dionaea muscipula*. Proc R Soc Lond 21:495–496

Burdon-Sanderson J (1888) On the electromotive properties of *Dionaeva* in the excited and unexcited states. Philos Trans 179:417–449

Burdon-Sanderson J, Page FJM (1876) On the mechanical effects and on the electrical disturbance consequent on excitation of the leaf of *Dionaeva muscipula*. Proc R Soc Lond 25:411–434

Davies E (1983) Action potentials as multifunctional signals in plants: a unifying hypothesis to explain apparently disparate wound responses. Plant Cell Environ 10:623–631

Davies E, Shuster A (1981) Intercellular communication in plants: evidence for rapidly generated, bidirectionally transmitted wound signal. Proc Natl Acad Sci USA 78:2422–2426

Davies E, Zawadzki T, Witters D (1991) Electrical activity and signal transmission in plants: how do plants know? Plant signaling, plasma membrane and change of state. Universite de Geneve, Geneve, pp 119–137

Eschrich W, Fromm J (1989) Correlation of ionic movements with phloem unloading and loading in barley leaves. Plant Physiol Biochem 25:577–585

Eschrich W, Fromm J (1994) Evidence for two pathways of phloem loading. Physiol Plant 90:699–707

Eschrich W, Fromm J, Evert RF (1988) Transmission of electrical signals in sieve tubes of zucchini plants. Bot Acta 101:327–331

Fensom DS (1958) The bioelectric potentials of plants and their functional significance II: The patterns of bioelectric potential and exudation rate in excised sunflower roots and stems. Can J Bot 36:367–383

Fensom DS, Spanner DC (1969) Electro-osmotic and biopotential measurement on phloem strands of nymhoides. Planta 88:321–331

Fromm J (1991) Control of phloem unloading by action potentials in Mimosa. Physiol Plant 83:529–533

Fromm J, Bauer T (1994) Action potentials in maize sieve tubes change phloem translocation. J Exp Bot 45:463–469

Fromm J, Eschrich W (1989) Electric signals released from roots of Willow (*Salix viminalis* L.) Change transpiration and photosynthesis. J Plant Physiol 141:673–680

Fromm J, Spanswick R (1993) Characteristics of action potentials in willow (*Salix viminalis* L.). J Exp Bot 44:1119–1125
Goldsworthy A (1983) The evolution of plant action potentials. J Theor Biol 103:645–648
Gunar II, Sinyukhin AM (1963) Functional significance of action currents affecting the gas exchange of higher plants. Sov Plant Physiol 10:219–226
Hille B (2001) Ion channels of excitable membranes. Sinauer Associates, Sunderland, Mass
Hill R, Bendal P (1960) Function of the two cytochrome components in chloroplasts: a working hypothesis. Nature 186:136–137
Hidgkin AL, Huxley AF (1952) A quantitative description of membrane current and its application to conduction and excitation in nerve. J Physiol 117:500–544
Ksenzhek OS, Volkov AG (1998) Plant energetics. Academic Press, San Diego
Labady A, Thomas D'J, Shvetsova T, Volkov AG (2002) Plant electrophysiology: excitation waves and effects of CCCP on electrical signaling in soybean. Bioelectrochem 57:47–53
Lautner S, Grams TEE, Matyssek R, From J (2005) Characteristics of electrical sifnals in poplar and responses in photosynthesis. Plant Physiol 138:2200-2209
Maffei M, Bossi S, Spiteller D, Mithofer A, Boland W (2004) Effects of feeding *Spodoptera littoralis* on lima bean leaves. I. Membrane potentials, intercellular calcium variations, oral secretions, and regurgitate components. Plant Physiol 134:1752–1762
Mizuguchi, Watanabe Y, Matsuzaki H, Ikezawa Y, Takamura T (1994) Growth acceleration of bean sprouts by the application of electrochemical voltage in a culturing bath. Denki Kagaku 62:1083–1085
Mwesigwa J, Collins DJ, Volkov AG (2000) Electrochemical signaling in green plants: effects of 2,4-dinitrophenol on resting and action potentials in soybean. Bioelectrochem 51:201–205
Pickard BC (1973) Action potentials in higher plants. Bot Rev 38:172–201
Pyatygin SS, Opritov VA (1990) Effect of temperature on action potentials generating in higher plant excitable cells. Biophysics 35:444–449
Shvetsova T, Mwesigwa J, Volkov AG (2001) Plant electrophysiology: FCCP induces fast electrical signaling in soybean. Plant Sci 161:901–909
Shvetsova T, Mwesigwa J, Labady A, Kelly S, Thomas D'J, Lewis K, Volkov AG (2002) Soybean electrophysiology: effects of acid rain. Plant Sci 162:723–731
Sibaoka T (1962) Excitable cells in mimosa. Science 137:226–228
Sinukhin AM, Britikov EA (1967) Action potentials in the reproductive system of plant. Nature 215:1278–1280
Sinukhin AM, Gorchakov VV (1966) Characteristics of the action potentials of the conducting systems of pumpkin stems evoked by various stimuli. Sov Plant Physiol 13:727–733
Sinukhin AM, Gorchakov VV (1968) Role of the vascular bundles of the stem in long-distance transmission of stimulation by means of bioelectric impulses. Sov Plant Physiol 15:400–407
Sinukhin AM, Gorchakov VV (1996) Action potentials of higher plants not possessing motor activity. Biophysics 11:966–975
Siomons PJ (1981) The role of electricity in plant movements. New Physiologist 87:11–37
Stankovic B, Davies E (1996) Both action potentials and variation potentials induce proteinase inhibitor gene expression in tomato. FEBS Lett 390:275–279
Volkov AG (1989) Oxygen evolution in the course of photosynthesis. Bioelectrochem Bioenerg 21:3–24
Volkov AG (2000) Green plants: electrochemical interfaces. J Electroanal Chem 483:150–156
Volkov AG (2002) Biocatalysis: electrochemical mechanisms of respiration and photosynthesis. In: Volkov AG (ed) Interfacial catalysis. Dekker, New York, pp 1–22
Volkov AG, Haack RA (1995) Insect induced bioelectrochemical signals in potato plants. Bioelectrochem Bioenerg 35:55–60
Volkov AG, Jovanov E (2002) Electrical signaling in green plants: action potentials. In: Jan J, Kozumplik J, Provaznik J (eds) Analysis of biomedical signals and images. Vutum Press, Brno, pp 36–38

Volkov AG, Mwesigwa J (2001a) Interfacial electrical phenomena in green plants: action potentials. In: Volkov AG (ed) Liquid interfaces in chemical, biological, and pharmaceutical applications. Dekker, New York, pp 649–681
Volkov AG, Mwesigwa J (2001b) Electrochemistry of soybean: effects of uncouplers, pollutants, and pesticides. J Electroanal Chem 496:153–157
Volkov AG, Deamer DW, Tanelian DL, Markin VS (1998) Liquid interfaces in chemistry and biology. Wiley, New York
Volkov AG, Collins DJ, Mwesigwa J (2000) Plant electrophysiology: pentachlorophenol induces fast action potentials in soybean. Plant Sci 153:185–190
Volkov AG, Labady A, Thomas D'J, Shvetsova T (2001a) Green plants as environmental biosensors: electrochemical effects of carbonyl cyanide 3-chlorophenylhydrazone on soybean. Anal Sci 17 [Suppl]:i359–i362
Volkov AG, Mwesigwa J, Shvetsova T (2001b) Soybean as an environmental biosensor: action potentials and excitation waves. In: Butler M, Vanysek P, Yamazoe N (eds) Chemical and biological sensors and analytical methods II. Electrochemical Society, Pennington, pp 229–238
Volkov AG, Mwesigwa J, Jovanov E, Labady A, Thomas DJ, Lewis K, Shvetsova T (2002a) Acid rain induces action potentials in green plants. In: Cerutti S, Akay M, Mainardi LT, Sato S, Zywietz C (eds) Proceedings of the IVth international workshop on biosignal interpretation BSI2002, Milan, Polytechnic University Press, pp 513–517
Volkov AG, Mwesigwa J, Labady A, Kelly S, Lewis K, Shvetsova T (2002b) Soybean electrophysiology: effects of acid rain. Plant Sci 162:723–731
Volkov AG, Shvetsova T, Markin VS (2002c) Waves of excitation and action potentials in green plants. Biophys J 82:18a–218a
Volkov AG, Dunkley TC, Labady AJ, Ruff D, Morgan SA (2004a) Electrochemical signaling in green plants induced by photosensory systems: molecular recognition of the direction of light. In: Bruckner-Lea C, Hunter G, Miura K, Vanysek P, Egashira M, Mizutani F (eds) Chemical sensors VI: chemical and biological sensors and analytical methods. Electrochemical Society, Pennington, pp 344–353
Volkov AG, Dunkley TC, Morgan SA, Ruff D II, Boyce Y, Labady A J (2004b) Bioelectrochemical signaling in green plants induced by photosensory systems. Bioelectrochemistry 63:91–94
Volkov AG, Dunkley TC, Labady AJ, Brown C (2005) Phototropism and electrified interfaces in green plants. Electrochim Acta 50:4241–4247
Zavadzki T (1980) Action potentials in *Lipinus angustifolius* L. shoots. V. Spread of excitation in the stem, leaves and root. J Exp Bot 31:1371–1377
Zavadzki T, Davis E, Dziubinska H, Trebacz K (1991) Characteristics of action potentials in *Helianthus-Annus*. Physiol Planet 83:601–604

20 Electrophysiology and Plant Responses to Biotic Stress

Massimo Maffei, Simone Bossi

Plants respond actively to biotic stress by sensing and triggering cascades of signals that lead to the production of toxic compounds, spreading from secondary metabolites to reactive oxygen species. Here, we show that the evaluation of plasma transmembrane potential (V_m) is a powerful tool for the deciphering of earlier events following biotic attacks. After a short introduction and definition of abiotic and biotic stress, we describe how plants react to herbivore attack by changing V_m and how this can be measured using electrophysiology.

20.1 Abiotic and biotic stress

20.1.1 What is an abiotic stress?

One important feature distinguishing plants from other complex multicellular organisms is that plants are static organisms and thus cannot escape environmental challenges. Abiotic stresses are caused by physical Earth's forces such as salt, water, light, heat and cold stresses. Although clearly different from each other in their physical nature, each of them elicit specific plant responses as well as activate some common reactions in plants (Zhu 2001). Abiotic stresses, such as drought, salinity, extreme temperatures, chemical toxicity and oxidative stress are serious threats to agriculture and result in the deterioration of the environment (Wang et al. 2003). Abiotic stress is the primary cause of crop loss worldwide (more than 50% yield reduction for most major crop plants; Boyer 1982; Bray et al. 2000). Abiotic stress often leads to morphological, physiological, biochemical and molecular changes affecting plant growth and productivity (Wang et al. 2001). Abiotic stresses may activate cell signaling pathways (Knight and Knight 2001; Zhu 2001, 2002) and cellular responses (Wang et al. 2003) that can lead to alteration of the transmembrane potential (V_m). In general, V_m variations depend on unbalanced ion distribution across the plasma membrane and depolarization occurs

Department of Plant Biology and Centre of Excellence CEBIOVEM, University of Turin, Viale P.A. Mattioli, 25 10125 Turin, Italy (e-mail: massimo.maffei@unito.it)

Plant Electrophysiology – Theory & Methods (ed. by Volkov)

when cations (such as K^+ and Ca^{2+}) are allowed to enter the cell or upon anion efflux. On the other hand, hyperpolarization mainly depends on the activity of the plasma membrane H^+-ATPase or when inward anion channels (or outward cation channels) are opened. The primary candidate for intercellular signaling in higher plants is the stimulus-induced change in V_m and excitation waves transmit information from one part of the plant to another with a speed of propagation of the action potential that in soybean can reach 40 m s^{-1} (Shevstova et al. 2001). Since ion fluxes through channels directly influence V_m, it seems reasonable to assume that molecules able to act on channel activity might be considered as important factors inducing electrical signals (Maffei et al. 2004). Under abiotic stress, the up-regulation of free radical scavenging systems is a common component of the response (Pasternak et al. 2005), as are heat stress (Dat et al. 1998; Larkindale and Knight 2002), UV-radiation stress (Brosche and Strid 2003), photoinhibition (Muller-Moule et al. 2003), heavy metal stress (Pinto et al. 2003) and anoxia (Blokhina et al. 2001). All of them may have consistent repercussions on the balance of ions across the plasma membrane, and hence on V_m. Emerging evidence suggests a broader role for common signals (such as reactive oxygen species) that mediate responses to abiotic environment, developmental cues, infection and the programmed cell death in different cell types (Torres and Dangl 2005) making tools to detect abiotic stress responses useful to quantify other plant responses. While trying to balance water deficits and carbon assimilation, plants must integrate additional information on light quality, nutrient status and temperature to make "informed decisions" to add to the pressure posed by the presence of biotic stress.

20.1.2 What is a biotic stress?

As primary producers in the food chain, plants are the source of carbon, protein, vitamins and minerals for all heterotrophic organisms, from bacteria to humans. Thus we can define biotic stress as the pressure posed on plants by living organisms. In recent years, the molecular basis of biotic stress responses in plants (Maleck et al. 2000) has been identified (reviewed by Karpinski et al. 2003). Among biotic stress, the most studied are microbial infections and herbivore attack. Based on their effects on the plant, microbes interacting with plants can be classified as pathogenic, saprophytic and beneficial. Pathogens can attack leaves, stems or roots. Current models of the mechanisms of plant defense against pathogen infection are based on animal models, and have been recently linked to the light-sensing network and to the oxygen-evolving complex in photosystem II (PSII) (Abbink et al. 2002). Much progress has been made in understanding the mechanisms by which plants detect and defend themselves against pathogens (Kunkel and Brooks 2002). Progress has been done in cloning and characterization of plant disease resistance genes that govern the recognition of specific pathogen strains

(Staskawicz et al. 2001; Dangl and Jones 2001), the deciphering of signal transduction pathways for the activation of defense responses (Feys and Parker 2000; Glazebrook 2001), and the characterization of endogenous plant signaling molecules involved in plant defense [salicylic acid (SA), jasmonic acid (JA) and ethylene (ET) (Dong 1998; Thomma et al. 2001)]. The current advances of the roles of the SA, JA and ET signaling pathways in pathogen defense has been summarized in several recent reviews (Kunkel and Brooks 2002 and references therein). There is also a growing body of literature that reports that the JA, SA and ET defense signaling pathways do not function independently, but show an active crosstalk (Kunkel and Brooks 2002). Recent studies indicate that defense signaling may be even more complex than expected, and that additional plant signaling pathways are likely to be involved in regulating pathogen defense, most of them involving ion fluxes and then variations in V_m.

Recognition is considered to be the initial key event in the response of plants to microbes. Recognition can occur through physical interaction, such as through adhesins, fimbriae, flagella, and type III and type IV secretion systems, or through signaling by small molecules (Lugtenberg et al. 2002). Early events during pathogen attack, before gene expression, involve the release of cell wall oligosaccharides (so-called elicitors) which can be recognized by specific receptors able to trigger signaling cascades involving ion fluxes and activation of reactive oxygen species (ROS) forming enzymes (Kombrink and Somssich 1995). One of the two of the earliest occurrences following recognition are a calcium flux across the plasmalemma and the generation of O_2^- and H_2O_2, the so-called "oxidative burst" (Mur et al. 2005) with these two events appearing to be mutually regulated (Grant et al. 2000). The generation of the plant oxidative burst has been linked to the initiation of electron flow across the plasmalemma via a NADPH oxidase complex, analogous to that found in mammalian neutrophils (Mur et al. 2005).

The evolution of plant secondary compounds is often considered to be tightly associated with defense against biotic stress, and it has recently been proposed that plant chemical defense could also be involved in abiotic stress responses, such as photodamage (Holopainen 2004). Thus, plants possess biochemical defense mechanisms which prevent or reduce further damage from both abiotic and biotic stress. The defense includes the induction of both de novo biosynthesis and rapid accumulation of secondary metabolites, referred to as phytoalexins (Mithöfer et al. 2004). These compounds are low molecular weight organic molecules not present in all plants that may also exhibit antibiotic activities (Mithöfer et al. 2004). Regardless of the plant species, major classes of secondary metabolites are phenylpropanoids, terpenoids, and nitrogen-containing organic compounds. Secondary plant compounds are present both as constitutive as well as inducible plant defenses. Volatile organic compounds (VOCs) emitted by plants can form as by-products of plant processes and can be emitted to the atmosphere owing to their volatility (Holopainen 2004). Some volatile compounds appear to behave like

signals for plant protection and communication. Herbivore induced plant volatiles (HIPV) are VOCs emitted from aerial and underground plant organs after herbivore damage (Kessler and Baldwin 2001; Holopainen 2004). HIPV may act as an indirect plant defense by repelling non-specific herbivores or by attracting predators and parasitoids of herbivores (Heil 2004). Evidence for trade-offs between resistance to pathogens and herbivores were reported (Felton and Korth 2000).

20.2 Plant responses to herbivore attack

Plant responses to herbivore attack are complex and involve an array of signals, leading to activation of multiple defenses. Feeding herbivores cause extensive and irreversible wounding along with an introduction of salivary secretions. Both, wounding and components from the insects' secretions have an obvious, but clearly different impact on the plants response (Schittko et al. 2001 and references cited therein). In the model system *Nicotiana attenuata* and its specialist herbivore *Manduca sexta*, feeding elicits a JA burst, a large transcriptional reorganization of the plant host and, after hours, a systemic release of VOCs (Halitschke et al. 2003). Principally the same sequence is passed through in the interaction between Lima bean and spider mites (Arimura et al. 2000), and in the interaction of corn plants (*Zea mays*) with the beet armyworm (*Spodoptera exigua*) (see also Gatehouse 2002).

Recently, Maffei, Bossi and co-workers of the Max Planck Institute of Jena (Maffei et al. 2004) presented novel facets to the previously known sequence and demonstrated that herbivore attack onto a Lima bean leaf is associated with: a) a strong V_m depolarization at the bite zone causing a wave of V_m depolarization spreading throughout the entire attacked leaf and; b) a consistent influx of Ca^{2+}, at the very edge of the bite, which is halved by application of the Ca^{2+} channel blocker verapamil. Regurgitants (R) and *N*-acyl-amino acid conjugates interact with the plasma membrane and alter V_m. R from Lima bean reared larvae altered V_m in a concentration-independent fashion and its effect is clearly different from that observed in V_m studies with the individual compounds (Maffei et al. 2004). A non-linear response of V_m to the concentration of R and R-factors was observed. Possibly the effects are related to different modes of membrane V_m depolarization by either micellar transport of ions or pore formations by the conjugates and other components of R (Abramson and Shamoo 1979). Volicitin (*N*-[17-hydroxylinolenoyl]-L-glutamine), which was isolated from the oral secretions of beet armyworm (*Spodoptera exigua*) larvae and increases the emission of VOCs when applied to maize, was the first reported herbivore-specific elicitor. Unfortunately, volicitin was completely inactive on lima bean V_m (Maffei et al. 2004), moreover, neither enantiomer of volicitin was active in the induction of VOCs (Felton and Korth 2000). The

time-course and distance-dependence spreading of the V_m depolarization upon herbivore attack in intact leaves is probably associated with a molecule able to disperse within tissues at a relatively high speed. Recent results from perfusing leaves with H_2O_2 (Maffei et al. 2006) and Ethephon (the ethylene releasing agent) (unpublished data) indicate a V_m depolarizing effect of these molecules. Another interesting target is the analysis of the early events in the interaction of volatiles (including VOCs, ethylene, hydrogen peroxide and NO) emitted from wounded plants and/or perceived by neighboring healthy plants. Preliminary results already indicate compound-specific variations in V_m (Maffei et al., unpublished data). Using spider mites (*Tetranychus urticae*) and predatory mites (*Phytoseiulus persimilis*) (Takabayashi and Dicke 1996), it has been shown that not only the attacked plant but also neighboring plants are affected, becoming more attractive to predatory mites and less susceptible to spider mites (Bruin et al. 1992). The mechanism involved in such interactions, however, remains elusive. Arimura et al. (2000) showed that uninfested lima bean leaves activate five separate defense genes when exposed to volatiles from conspecific leaves infested with *T. urticae*, but not when exposed to volatiles from artificially wounded leaves. These data indicate that gene activation is preceded by perception of VOCs and signal transduction; all involving the plant cell plasma membrane. Both wounding and the introduction of herbivore-specific elicitors appear to be essential for the full induction of defense responses. Recent studies applying a continuous rather than a single instance of mechanical damage (pattern wheel) to Lima bean leaves clearly resulted in the emission of volatile blends resembling those that occur after herbivore damage (Mithöfer et al. 2005). In accordance with Arimura and co-workers (2005), we can conclude that early and secondary cell signaling for herbivore-induced plant responses comprise: (1) the reception of an extracellular signal(s) such as high- or low-molecular weight factors from the herbivore (e.g. fatty acid–amino acid conjugates), (2) V_m depolarization and an intracellular calcium influx, (3) the activation of protein kinase/phosphatase cascades, and (4) the release of linolenic acid from the cell membrane and subsequent activation of the octadecanoid pathway which leads finally to the synthesis of JA and other oxylipins.

Until recently, herbivore-induced indirect defenses have largely been a laboratory phenomenon, but a recent study of *N. attenuata* plants growing in natural populations demonstrated, by manipulating the release of single compounds in the herbivore-induced VOC bouquet, that VOC emission resulted in increased predation rate of *Manduca* eggs by a generalist predator and decreased oviposition rate by the adult moths (Baldwin et al. 2001).

Recent physiological studies have linked the plant signal transduction pathways that result in induction of direct defenses in leaves to indirect defences that act through the production of volatiles that attract natural enemies of herbivores (Agrawal 2000).

20.3 Plant responses to plant attack

VOCs are also emitted by plants to cope with other plants for nutrition in what is called allelopathy. Allelopathy is the negative effect of chemicals released by one plant species on the growth or reproduction of another (Inderjit and Callaway 2003). Plants synthesize a great variety of terpenoid natural products, which can be involved in allelopathic interactions. The ability of allelochemicals to alter membrane permeability and affect V_m (thus inhibiting mineral absorption) has been investigated since the 1970s (Balke 1985).

Many phenolic compounds induce efflux of anions and cations, and inhibition of uptake may depend on alterations and perturbations induced in the inner membrane by specific binding or by prevention of the development of an electrochemical V_m (Moreland and Novitzky 1987). Isosakutranetin (ISK; 5,7-dihydroxy 4′-methoxy flavanone) is a plant exudate with known cytotoxic and fungicide properties. When tested on wheat roots it inhibited K^+-dependent H^+ extrusionand net K^+ uptake. ISK acts on wheat roots as an inhibitor of K^+ permeation suggesting a major role of ISK as an allelopathic molecule (Sacco and Maffei 1997).

Monoterpenoids are the major components of some essential oils: they have toxic effects on seed germination (Robinson 1983; Rice 1984), growth of some bacterial strains (Knobloch et al. 1989; Economou and Nahrstedt 1991), development and growth of some insects (Lee et al. 1999), growth of pathogenic fungi (Adam et al. 1998). Increasing the concentration of peppermint essential oil from 100 up to 900 ppm caused an increasing depolarization of cucumber root V_m (from 5 to 110 mV) (Maffei et al. 2001). A plot of log of octanol–water partition coefficient (K_{ow}) against their depolarizing effect showed a significant negative correlation, suggesting that among all monoterpenoids increased membrane depolarization depends on lower K_{ow} (Maffei et al. 2001). Recent findings have shown that monoterpenes affect biological membranes by damaging their structure and changing their lipid packing density which increases ion permeability and perturbs membrane-bound enzyme function (Griffin et al. 2000). Maffei et al. (2001) found that decreasing water solubility of monoterpenes increases the possibility for terpenoids to interact with and disrupt membrane integrity, thus causing a rapid and reversible membrane V_m depolarization.

Another important allelopathic molecule is juglone. Significant inhibition of transpiration and stomatal conductance reported by Jose and Gillispie (1998) in hydroponically grown corn and soybeans exposed to juglone suggests that this phytotoxin may interfere with normal water transport. Furthermore, a decrease in H^+-ATPase activity was positively correlated with increasing juglone concentration in corn and soybean root microsomal membranes (Hejl and Koster 2004). These data support the hypothesis that juglone-mediated reductions in growth arise from the decreased ability of the roots to translocate water secondary to inhibition of plasma membrane H^+-ATPase activity. These data also were corroborated by observations that seedlings appeared wilted, like drought-affected plants, and the roots

appeared flaccid, even though submerged in nutrient solution. Since the plant cell plasma-membrane H^+-ATPase and associated membrane proteins play an essential role in the maintenance of cell turgor and uptake of components essential for growth (Babakov et al. 2000), significant reduction in mineral and water uptake by roots subsequent to H^+-ATPase inhibition in root cells would lead to closing of stomata and have a strong indirect effect on numerous essential plant functions, such as respiration, photosynthesis, and protein synthesis, resulting in decreased growth (Hejl and Koster 2004).

20.4 Methods in plant electrophysiology following herbivore attack

20.4.1 Our model system for electrophysiology

The system developed to measure V_m in leaves is the result of many technical tests which gave at the end a useful set of both electrical, electronic and hydraulic instrumentations, with the aim of on-line (or real-time) recording of electrical variations through the plant plasma membrane.

This system was initially developed to measure membrane potential variations of the aquatic plant *Elodea densa* (Bellando et al. 1995). It consists mainly of a home-made Plexiglas block, a polymethyl methacrylate (PMMA) polymer, or even Teflon, a more inert polymer of polytetrafluoro ethylene (PTFE), unfortunately not transparent; some wells and sockets which were made and dug, as shown in Fig. 20.1. The main use of this block is to perfuse

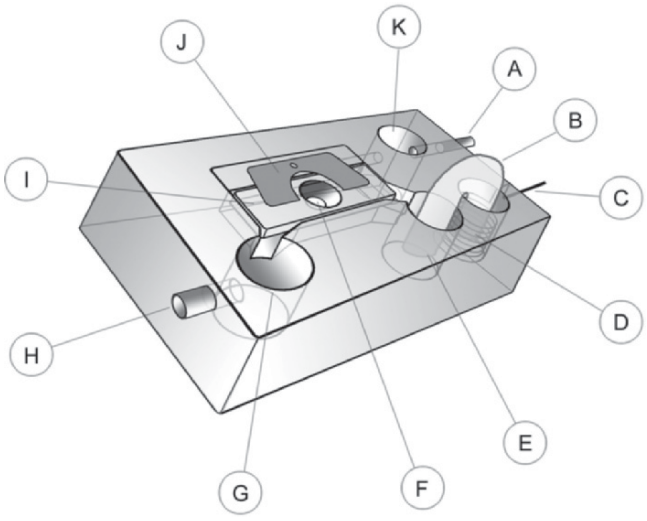

Fig. 20.1. Schematic representation of the system used for the evaluation of V_m. See description in the text

buffers or specific chemical through a leaf segment, allowing electrophysiological measurements. A small squared part of a leaf, following incubation in a fresh buffer, is placed in the central socket (Fig. 20.1F) of the block and then fixed on top (Fig. 20.1J) with a plastic holed lid (Fig. 20.1F). The hole in the lid allows the operator to reach the leaf fragment and directly measure V_m. As previously reported (Maffei et al. 2004, 2006) an external tubing system managed by a eight barrel multi channel peristaltic pump allows perfusion of buffer. Pump speed is normally 1 ml/min, flowing through the port shown as Fig. 20.1A; different other molecules could also flow through the same port (Fig. 20.1A), in this case a special setting of two-three way valves between the pump and the aperture (Fig. 20.1A) allows a convenient switching from the normal buffer to a new chemical, without stopping the V_m evaluation. The buffer driven through [A] by the peristaltic pump, reaches the first well (Fig. 20.1 K) where bubbles, if present in the perfusion liquid or in tubes, can easily emerge and dissolve. Then the perfusion medium runs directly in the central socket (Fig. 20.1F) where the leaf piece is posed and fixed and where molecules, if present in the liquid, can act on plant tissues. This central socket is in communication with two other wells (Fig. 20.1G, E); both wells are deeper than the central socket, thus allowing buffers or other liquids to flow in continuously from the central part. The well marked with [E] serves to contain one of the two ends of the salt bridge (Fig. 20.1B) and from the well [G] liquids flow out through the exhaust tube (Fig. 20.1H), to be collected or sent to waste. The well [G] is quite useful in those cases where an overflow from [A] occurs: in this situation liquids can be removed directly from the well [G] with a pipette quickly and safely. There is a last well marked with [D] in Fig. 20.1: it serves to contain the other end of the salt bridge, and, more importantly, contains a silver wire solenoid which is directly connected to the outside of the well with a male plug (Fig. 20.1C), allowing electrical connections to the circuit (see below for the electrical settings).

The core of the entire system is the electrical circuit which allows V_m measurement. In order to measure V_m we used very thin tip (2–3 μm) borosilicate glass capillaries (WPI Inc., model 1B150F-4) which are obtained with a capillary puller (Narishige model PE-21) and filled with a 3 M KCl solution prepared in ultra-pure water (Millipore). Due to the very thin tip, the 3 M KCl solution in the inner part of the glass electrode permits an efficient electrical conductance with a very low (fM) loss on ions from the electrode to the cellular matrix. Fig. 20.2 shows the glass electrode on its way to the plant cell to be impaled.

Glass microelectrodes are directly connected to a probe (WPI inc.) by means of an electrode holder (WPI Inc.); this probe does the first step of the signal cleaning up and stabilization, and is connected to a signal amplifier (WPI inc. model Electro 705). The amplifier takes the electrical signal coming from the cell and brings it amplified, cleaned and stabilized to an oscilloscope (Tektronics model TDS 210), for further digital elaboration and data storage. The signal is measured and recorded in mV. The oscilloscope also allows

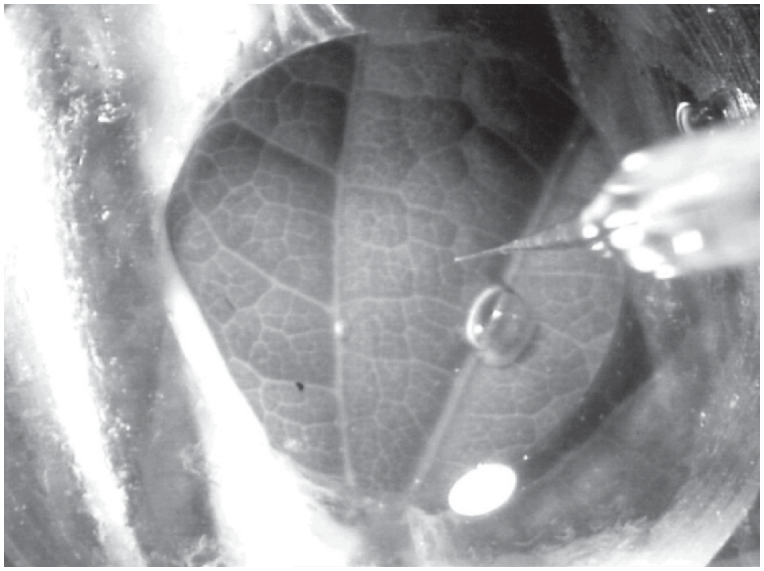

Fig. 20.2. Microcapillary made of borosilicate is used as an electrode in order to impale plant cells and detect V_m

seeing the wave of the electrical signal, the shape of which gives important information about cell condition, electrode integrity and, in general, the electrical conditions of the entire system. The oscilloscope is also plugged to the ground, to complete the electrical circuit; ground is represented by the silver wire solenoid in the well (Fig. 20.1D). The ground is a special silver–silver chloride electrode which acts as signal transducer by converting ionic currents in solution to an electric current within a wire, the same operation done by the probe attached to the glass electrode. The silver wire is plated with chlorine by electroplating, which ensures stability and good conductibility to the silver wire. The well where the ground is present is filled with a 3 M KCl^+ saturated $AgCl_3$ solution which allows electrical communication with the salt bridge (Fig. 20.1B). The salt bridge is the electric link between the ground and the buffer solution in which the plant material is immersed; it is a curled glass pipe filled with agarose jellified solution containing 3 M KCl. The entire system, set up as explained, gives a signal with a wave shape quite near to a square wave; in fact parts of system acts as an electrical capacitor. To solve this problem, a special device, a variable resistance connected in parallel, is mounted between the silver–silver chloride electrode and the oscilloscope, resulting in straight line electrical signal more convenient for measuring and recording. Figure 20.3 depicts the scheme of how this variable resistance is working. “IN” represents the wire coming from the ground, “OUT” is the wire connected to the oscilloscope, 1 is a switch, the general ground is marked with 2 and the variable resistance is marked with 3.

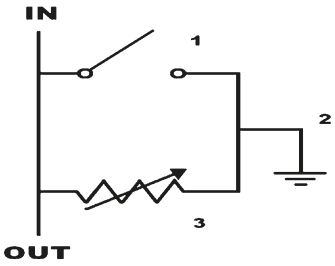

Fig. 20.3. Scheme of the circuit used to trigger the signal

Finally, Fig. 20.4 shows a simplified scheme of the electrical circuit.

All instruments and electrical devices are very sensitive to both physical vibration and environmental electrical noises, thus all the equipment is mounted on a stable work table, electrically grounded and kept under a Faraday cage; all cables and wires, when not shielded properly, are wrapped with aluminum foil in order to reduce noise. Obtaining a good V_m is a very delicate operation and the use of a micromanipulator, which can move in three directions, is fundamental. A stereo microscope or a special video camera is also needed in order to see exactly where to position the electrode onto the leaf tissue. Data recording is performed mainly with two different systems: data or electrical signals from the V_m are simply directed to a normal paper recorder which plots an immediate graphical image of what is going on during an experiment. The second is represented by the oscilloscope's signal that can go directly to a computer: the oscilloscope takes the analogical electrical signals and transform them into digital data, transferred by a serial

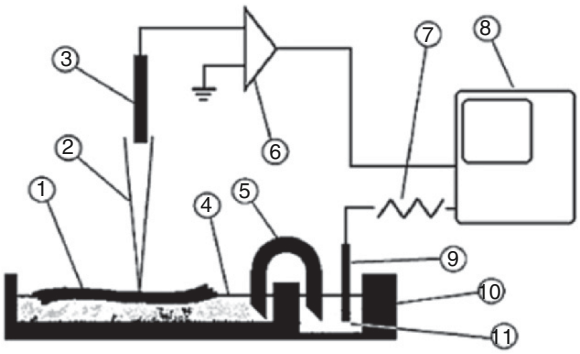

Fig. 20.4. General simplified representation of the system used to detect V_m. *1*, leaf; *2*, borosilicate capillary electrode; *3*, probe; *4*, perfusion liquid; *5*, 3 M agarose/KCl salt bridge; *6*, amplifier; *7*, variable resistance; *8*, oscilloscope; *9*, $Ag/AgCl_3$ electrode; *10*, plexiglas block; *11*, 3 M $KCl/AgCl_3$ saturated solution

cable to the computer; a special software (WaveWork v 4.2a Scope K&S Elecktronik) can draw these data in graphics and can transform them in text tables.

All the system described above is useful for experiments in which V_m variations, if present, are depending on the kind of solution perfused to the plant and on the molecules of interest present in the medium. For this reason, experiments can only be carried out with the treatment with molecules easily miscible in aqueous media. Many compounds are dissolved in organic solvents, like methanol, and then dissolved in the aqueous buffer, but some of them may have a very low polarity. These molecules are also volatile, making difficult to keep their concentration at a constant value during the experiment. To overcome problems linked to molecule solubility, we developed a new system, mainly based on the above described system. Figure 20.5 shows how a plant cutting can be analyzed. A plastic block (Fig. 20.5G) in which an entire aerial part of a plant (Fig. 20.5A) is positioned and immersed in buffer (Fig. 20.5H). The membrane potential is captured with a glass electrode (Fig. 20.5B) directly over an entire leaf fixed on a stative (Fig. 20.5C); the other parts of the electric devices are similar to those described above, silver–silver chloride ground and salt bridge (Fig. 20.5F) operate in the same way as above. The novelty of the system is mainly represented by the plastic chamber (Fig. 20.5D) which hosts both the plant leaf and the electrode, allowing evaluation of gaseous treatment over the plant; the plant and the electrode are gently sealed with rubber in order to allow small movements of the electrode and to maintain the plant into a closed environment. Special ports (Fig. 20.5E, I) are made in order to drive in and out a volatile compound allowing a real-time recording of a V_m induced by a controlled gaseous treatment of a particular molecule.

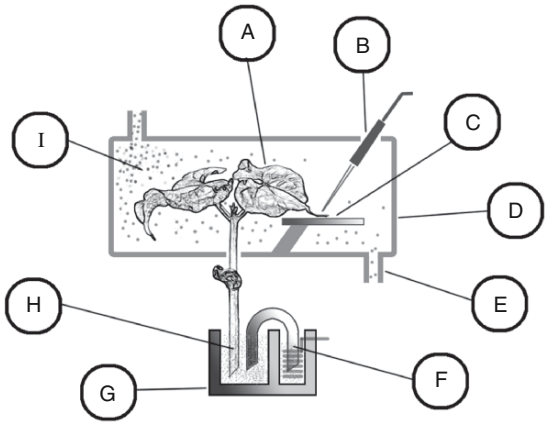

Fig. 20.5. Scheme of the new system used for the detection of V_m in intact leaves. See text for description

20.4.2 Bite and wounds: is there any difference?

The results of the measurement of membrane potential after mechanical wounding and herbivore attack indicate a specific response of the leaf tissue. Lima bean leaf V_m varies according to the cell type. Preliminary tests on intact leaves allowed evaluating the average V_m of epidermal, guard cell, palisade and spongy parenchyma cells. Epidermal cells have an average V_m of −50 mV (± 5.7 mV), guard cells have an average V_m of −200 mV (± 12.2 mV), palisade cells have an average V_m of −140 mV (± 9.8 mV), and spongy parenchyma cells have an average V_m of −100 mV (± 10.5 mV). Different trials demonstrated that Lima bean palisade cells are the most responsive cells, when leaf tissues are attacked by larvae of *S. littoralis* (Maffei et al. 2004).

To study the early effects at the bite zone and subsequent signal spreading, V_m was evaluated at increasing distances from the site of damage. The response was a strong V_m depolarization in the bite zone, followed by a transient V_m hyperpolarization and, finally, a constant V_m depolarization throughout the rest of the attacked leaf. Figure 20.6 shows the V_m variations superimposed on the wounded Lima bean leaf tissue. The ordinates represent V_m expressed in mV, while in the abscissa the bands (and the corresponding histogram bars) represent different distances (and the corresponding V_m values) from the bite zone. The V_m of the mechanically wounded leaf (control) is represented by the dashed line. Exponential interpolation shows the trend of V_m variation. A strong V_m depolarization was found up to about 1.5 mm from the bite zone, whereas a V_m hyperpolarization was found at ~2.5–3 mm from the bite zone, immediately followed by a second strong V_m depolarization. V_m differences from control in the zone from 3.5 to ~6 mm from the bite zone were not significant, but V_m displayed depolarized values from 6 mm throughout all the attacked leaf (Fig. 20.6).

The trend of the V_m variation prompted a series of experiments aimed to better understand the nature and the reasons for this effect. The first attempt was to probe whether the feeding activity of the herbivore was perceived as a V_m variation even at considerable distances from the bite zone in the same leaf. An intact leaf from a potted plant was fixed to the V_m apparatus and the V_m determined. When V_m reached a constant value *S. littoralis* was allowed to start its feeding activity. Figure 20.7 depicts V_m variations as a function of time and distance from mechanically wounded (MW) Lima bean leaf tissue, starting with a potential of about −137 mV, and V_m from a leaf under attack by *S. littoralis*. It is evident that feeding activity starts a series of V_m variations eventually leading to V_m depolarization within the first 15 min after the onset of the feeding activity. In particular when V_m was taken from palisade cells at an average distance of 5 mm a strong and transient hyperpolarization occurred within 5 min after the herbivore bite, followed by a constant depolarization. The same pattern was observed when V_m palisade cell was measured at a distance of 30 mm from the bite zone, but depolarization was higher than in cells at 5 mm distance. Finally in palisade cells which were 60 mm

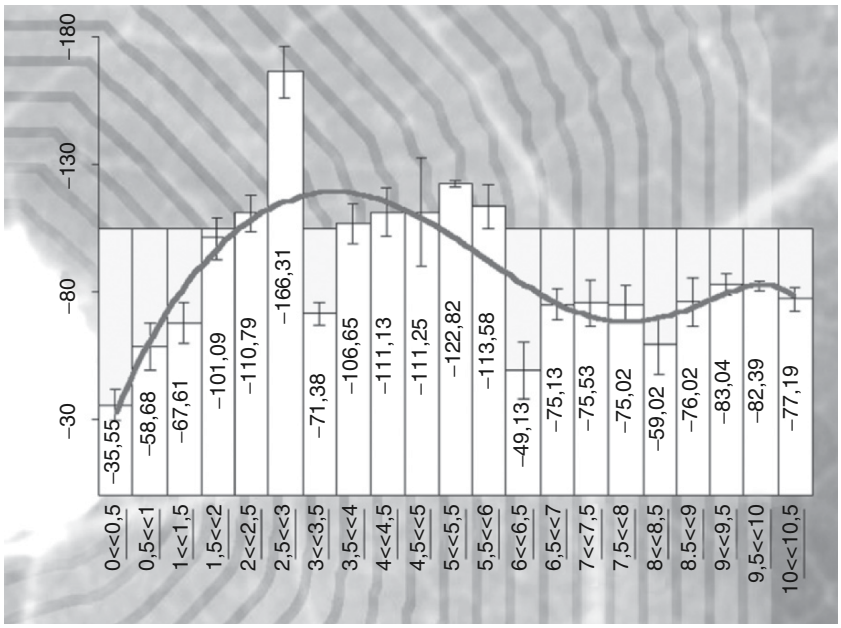

Fig. 20.6. Lima bean (*Phaseolus lunatus*) leaf V_m values as a function of distance from the bite zone 15 min after herbivore damage. The histogram superimposed on Lima bean leaf wounded by a larva of *Spodoptera littoralis* represents V_m values (and standard deviations) measured at increasing distances from the bite zone. *Upper bars* represents the average V_m value from a mechanically wounded Lima bean leaf. In the close vicinity of the bite zone (up to 1.5 mm) there is a strong drop in the V_m (depolarization), whereas at about 2.5–3 mm from the bite zone an increase of V_m is observed (hyperpolarization). About 6 mm from the bite zone throughout all leaf there is a constant V_m depolarization

distant from the bite zone V_m depolarization occurred within 2–3 min from the bite event and no hyperpolarization was observed (Fig. 20.7). From Fig. 20.7, it is evident that the recognition of the bite activity of *S. littoralis* is quickly perceived in the same leaf at increasing distances from the bite area. However, the attempt to find variations in neighboring leaves (OL) resulted in no obvious variations as did mechanical wounding (MW) on the same leaf (Fig. 20.7).

20.4.3 Action potentials and membrane potentials: continuous recording

In general, cells are electrically coupled by plasmodesmata to provide signal conduction, thus, application of mechanical or chemical damage to intact plants (e.g. connected to the V_m detector in rooted plants in pot) results in fast action potentials which can propagate up to several cm per second (Fromm et al. 1995; Volkov et al. 2001). Usually, after signal transmission the resting

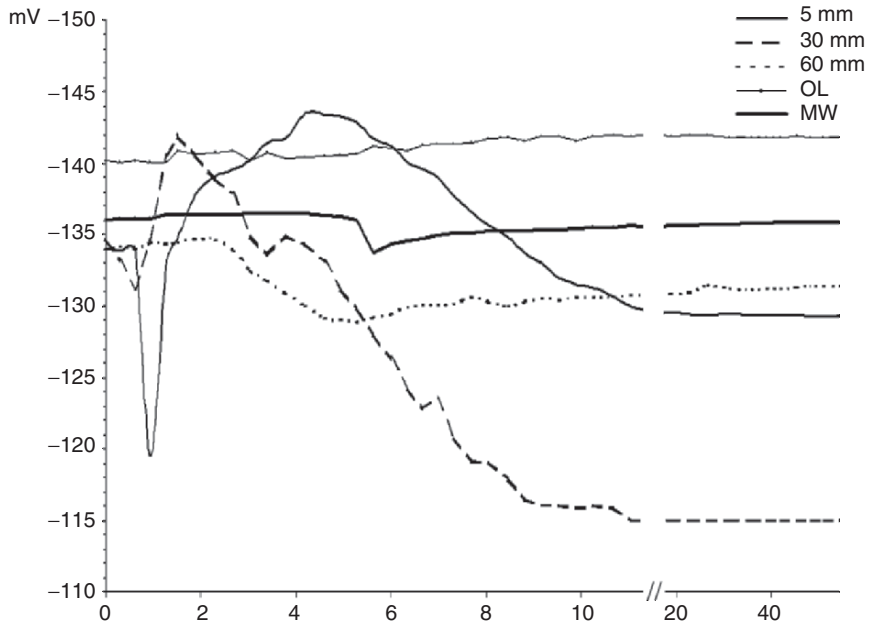

Fig. 20.7. Time-course of the V_m variations in palisade cells distant 5, 30 and 60 mm from the bite activity of *S. littoralis*. The feeding larva induces a series of V_m variations leading to V_m depolarization after about 15 min from the onset of the feeding activity. In particular, when V_m was taken at an average distance of 5 mm, a strong and transient hyperpolarization occurred within 5 min after the herbivore bite, followed by a constant depolarization. The same pattern was observed when V_m was measured at a distance of 30 mm from the bite zone, but depolarization was higher than in cells at 5 mm distance. In cells 60 mm distant from the bite zone, V_m depolarization occurred within 2–3 min after the bite, and no hyperpolarization was observed. MW=V_m value after mechanical wounding; OL=V_m value of the opposite leaf

potential remains stable. In order to evaluate the speed of depolarization in an intact leaf we grounded the basal part of the Lima bean stem and impaled a palisade cell with a micropipette. When the V_m was stable (around –140 mV), a mechanical damage was done with a small forceps at different distances from the impaled cell on the same leaf. An immediate action potential was recorded and when V_m was again stable a drop of a strong oxidant was applied at the wounded zone. After the application of the oxidant a small action potential was also recorded. After a few seconds a significant V_m depolarization was recorded and the original resting potential was not re-established, indicating that the voltage change was not an action potential. The V_m was then allowed to reach a stable value. The new value was a V_m hyperpolarized value with respect the beginning of the experiment. A second damage was then performed in another part of the leaf and an action potential was recorded, once

again a drop of a strong oxidant was applied and a V_m depolarization was observed after a longer period (Fig. 20.8).

In Lima bean the speed of the fastest V_m depolarization after a strong oxidant application was found to be about 1 mm s^{-1}, and the speed of the slowest V_m depolarization was 4 mm s^{-1}, that is 0.1 cm s^{-1} and 0.4 cm s^{-1}, respectively. In a putative isotropic and constant system, given these transmission rates, the diffusion coefficient *(D)* of a putative chemical signal would be (according to the Einstein random walk equation):

$$D_{fast} = d^2/2t = (0.1)^2/2\,(1) = 5\times 10^{-3}\,\mathrm{cm}^2/\mathrm{s} = 5\times 10^{-7}\,\mathrm{m}^2\,\mathrm{s}^{-1}$$

$$D_{slow} = d^2/2t = (0.4)^2/2\,(1) = 8\times 10^{-2}\,\mathrm{cm}^2/\mathrm{s} = 8\times 10^{-6}\,\mathrm{m}^2\,\mathrm{s}^{-1}$$

where t is time, and where fast and slow represent the speed of propagation after the first and the second strong oxidant application. Using the Stokes–Einstein equation, the radius *(r)* of a spherical molecule that has such a diffusion coefficient is:

$$\mathrm{D} = kT/6\pi r\eta \text{ or } \mathrm{r} = k\mathrm{T}/\mathrm{D}6\pi\eta$$

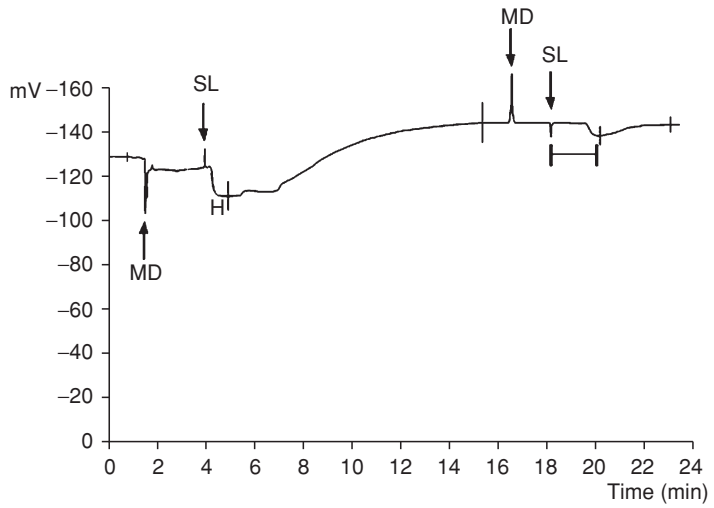

Fig. 20.8. Action potentials and membrane potentials (V_m) in Lima bean intact leaves in response to mechanical wounding and application of a strong oxidant (*SL*). V_m was measured in a palisade cell and mechanical damage (MD) was performed at different distances from the impaled cell. Actions potentials are evidenced by a fast potential change that returns to the same value. After the application of a strong oxidant a small action potential was recorded. After a few seconds a significant V_m depolarization was recorded and the original resting potential was not re-established, indicating that the voltage change was not an action potential. After some minutes the V_m is stable, but at higher (hyperpolarized) values. A second MD was then applied in another part of the leaf and an action potential was recorded, once again a drop of a strong oxidant was applied and a V_m depolarization was observed after a longer period. Metric bars indicate standard deviation

where k is Boltzmann's constant, T is absolute temperature, and η is viscosity (Pa s). If T=298 K, η=0.001 Pa s, and k=1.38×10^{-23} J/K, then r_{fast}=4.37×10^{-13} m, and r_{slow}=2.73×10^{-14} m.

Since this is about or less than the radius of a single carbon ion, it is unlikely that in this hypothetical system any molecule can diffuse so quickly. If we consider that the leaf mesophyll is not a constant environment and considering the various resistances to the spread of a signal it is reasonable to argue that the measured message might travel from the wound site by electrical signals.

20.4.4 Much more than a bite: the effect of larvae regurgitates

In order to evaluate which molecule may be responsible of V_m variations a series of experiments was carried out using regurgitate (R) collected from larvae previously feeding on Lima bean leaves for 24 h (Maffei et al. 2004).

Perfusion with R caused a V_m depolarization, however the effect was found not to be linearly linked to concentration. In fact, perfusion with 100 µg ml^{-1} R depolarized V_m more than perfusion with 250 µg ml^{-1}, but less than perfusion with 500 µg ml^{-1}. Interestingly, when R was washed out with fresh buffer, palisade V_m experienced a hyperpolarization for all concentrations, with an opposite trend as observed during depolarization (Fig. 20.9).

Since previous studies have demonstrated that R of *S. littoralis* contains several surface active, amphiphilic compounds, especially *N*-acyl glutamine conjugates (Spiteller and Boland 2003a,b) these compounds were used to study V_m variations.

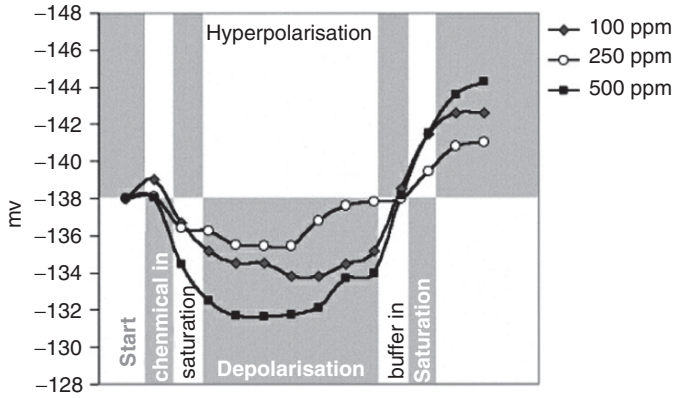

Fig. 20.9. Effect of *S. littoralis* oral secretions and regurgitants (*R*) on the V_m of Lima bean palisade cells. At the lowest concentration (100 µg ml^{-1}) R caused an intermediate V_m depolarization when compared to concentrations of 250 and 300 µg ml^{-1}. After washing the tissues with fresh buffer V_m was hyperpolarized at all concentrations, and once again R at 100 µg ml^{-1} had an intermediate value (modified from Maffei et al. 2004)

The effect of racemic volicitin (Alborn et al. 1997, 2000) and that of the naturally occurring (17*S*)-*N*-(17-hydroxylinoleoyl)-L-glutamine (Spiteller et al. 2001) on V_m was low (Maffei et al. 2004). In order to assess whether fatty acid chain length and degree of saturation have an impact on V_m, leaves were perfused with *N*-palmitoleoyl-L-glutamine and *N*-linolenoyl-L-glutamine. Perfusing cells with *N*-palmitoleoyl-L-glutamine caused a V_m depolarization at the lowest concentration used (25 μg ml^{-1}), but a V_m hyperpolarization when higher concentrations (100–300 μg ml^{-1}) were applied (Maffei et al. 2004). Removal of conjugates with fresh buffer had no effect on 25 and 300 μg ml^{-1} concentrations. A V_m depolarization was, however, observed in perfusion with 100 μg ml^{-1} (Maffei et al. 2004). Perfusion with *N*-linolenoyl-L-glutamine caused no V_m variation when used at 50 and 500 μg ml^{-1}, whereas the strongest V_m depolarization was observed at 100 μg ml^{-1} (Maffei et al. 2004).

To study the impact of the fatty acid and amino acid building blocks of the conjugates, Lima bean leaves were individually treated with linolenic acid and glutamine. Linolenic acid caused no obvious effect on V_m at low concentrations (10 and 50 μg ml^{-1}), while a weak V_m depolarization was observed when leaf tissues were perfused with L-glutamine (Maffei et al. 2004).

Because of their molecular architecture, *N*-acyl glutamines are amphiphilic compounds with a pronounced ability to form micelles, similar to known detergents such as sodium dodecyl sulfate (SDS). In order to test whether a detergent has an effect on V_m, increasing concentrations of SDS were applied to Lima bean leaves. Low concentrations had no effect, whereas at high concentration (500 mM) a clear V_m depolarization was observed, even after washing with fresh buffer (Maffei et al. 2004).

Application of the fatty acid or amino acid components of the conjugates shows virtually no effect for linolenic acid but a clear V_m depolarization for glutamine. The latter effect could play a role during larval feeding after enzymatic cleavage of the conjugates and may rely on transport processes (e.g. symport) of the amino acid (Delrot et al. 2001) and/or interaction of free glutamine with receptors. However, as yet, nothing is known about the stability of *N*-acyl amino acids in the plant cells.

20.5 Conclusions

Millions of years of continuous interaction between plants and herbivores/pathogens allowed the evolution of defense mechanisms from both sides, granting an equal and co-evoluted fitness to stress conditions. On the one side, plants have evolved the ability to respond to herbivores/pathogens by producing toxic weapons (such as many secondary metabolites) and refining the capability to detect and respond quickly to tissue damage by activating cascade signals and gene activation or to attract predators of the attacking biota. On the other hand, herbivores and pathogens evolved the ability to detoxify

poisons and to reduce plant responses by inhibiting signal transduction and/or gene activation. In all of this, the first barrier between a plant and its invader is the plasma membrane. Alteration of the balanced flux of different ions and organic acids/molecules generates a quick response that can be defined as one of the early events following a biotic attack. Depolarization of the V_m is one of the first responses of the plasma membrane and is mainly depending on anion efflux followed by calcium release from internal stores or influx from the apoplast (Hammond-Kosack and Jones 2000; Maffei et al. 2006). Thus electrophysiology is indeed a valuable tool to study and understand what is going on at the very beginning of plant interaction with other organisms (including other plants) and V_m evaluation, more that the single patch analysis, gives a tissue image of cooperative interplay among wounded and unwounded cells. Much more has to be done in this field, but the promising results obtained in intact rooted plants following biotic and abiotic stress may lead to interesting new discoveries.

References

Abbink TEM, Peart JR, Mos TNM, Baulcombe DC, Bol JF, Linthorst HJM (2002) Silencing of a gene encoding a protein component of the oxygen-evolving complex of photosystem II enhances virus replication in plants. Virology 295:307–319

Abramson JJ, Shamoo AE (1979) Anionic detergents as divalent-cation ionophores across black lipid-membranes. J Membr Biol 50:241–255

Adam K, Sivropoulou A, Kokkini S, Lanaras T, Arsenakis M (1998) Antifungal activities of *Origanum vulgare* subsp. Hirtum, *Mentha spicata*, *Lavandula angustifolia* and *Salvia fruticosa* essential oils against human pathogenic fungi. J Agric Food Chem 46:1739–1745

Agrawal AA (2000) Mechanisms, ecological consequences and agricultural implications of tritrophic interactions. Curr Opin Plant Biol 3:329–335

Alborn HT, Jones TH, Stenhagen GS, Tumlinson JH (2000) Identification and synthesis of volicitin and related components from beet armyworm oral secretions. J Chem Ecol 26:203–220

Alborn HT, Turlings TCJ, Jones TH, Stenhagen G, Loughrin JH, Tumlinson JH (1997) An elicitor of plant volatiles from beet armyworm oral secretion. Science 276:873–949

Arimura GI, Ozawa R, Shimoda T, Nishioka T, Boland W, Takabayashi J (2000) Herbivory-induced volatiles elicit defence genes in lima bean leaves. Nature 406:512–515

Arimura GI, Kost C, Boland W (2005) Herbivore-induced, indirect plant defences. Biochim Biophys Acta 1734:91–111

Babakov AV, Chelysheva VV, Klychnikov OI, Zorinyanz SE, Trofimova MS, De Boer AH (2000) Involvement of 14-3-3 Proteins in Osmotic Regulation of H^+-ATPase in Plant Plasma Membrane. Planta, 211:446–448

Baldwin IT, Halitschke R, Kessler A, Schittko U (2001) Merging molecular and ecological approaches in plant-insect interactions. Curr Opin Plant Biol 4:351–358

Balke NE (1985) Effects of allelochemicals on mineral uptake and associated physiological processes. In: Thompson AC (ed) The chemistry of allelopathy. Biochemical interactions among plants. America Chemical Society, Washington, D.C., pp 161–178

Bellando M, Marrè MT, Sacco S, Talarico A, Venegoni A, Marrè E. (1995) Transmembrane potential-mediated coupling between H^+ pump operation and K^+ fluxes in *Elodea densa* leaves hyperpolarized by fusicoccin, light or acid load. Plant Cell Environ 18:963–976

Blokhina OB, Chirkova TV, Fagerstedt KV (2001) Anoxic stress leads to hydrogen peroxide formation in plant cells. J Exp Bot 52:1179–1190
Boyer JS (1982) Plant productivity and environment. Science 218:443–448
Bray EA, Bailey-Serres J, Weretilnyk E (2000) Responses to abiotic stresses. In: Gruissem W, Buchannan B, Jones R (eds) Biochemistry and molecular biology of plants. American Society of Plant Physiologists, Rockville, MD, pp 1158–1249
Brosche N, Strid A (2003) Molecular events following perception of ultraviolet-B radiation by plants. Physiol Plant 17:1–10
Bruin J, Dicke M, Sabelis MW (1992) Plants are better protected against spider-mites after exposure to volatiles from infested conspecifics. Experientia 48:525–529
Dangl JL, Jones JD (2001) Plant pathogens and integrated defense responses to infection. Nature 411:826–833
Dat JF, Foyer CH, Scott IM (1998) Changes in salicylic acid and antioxidants during induction of thermotolerance in mustard seedlings. Plant Physiol 118:1455–1461
Delrot S, Atanassova R, Gomès E, Coutos-Thévenot P (2001) Plasma membrane transporters: a machinery for uptake of organic solutes and stress resistance. Plant Sci 161:391–404
Dong X (1998) SA, JA, ethylene, and disease resistance in plants. Curr Opin Plant Biol 1:316–323
Economou D, Nahrstedt A (1991) Chemical, physiological, and toxicological aspects of the essential oil of some species of the genus *Bystropogon*. Planta Med 57:347–351
Felton GW, Korth KL (2000) Trade-offs between pathogen and erbivore resistance. Curr Opin Plant Biol 3:309–314
Feys BJ, Parker JE (2000) Interplay of signaling pathways in plant disease resistance. Trends Genet 16:449–455
Fromm J, Hajirezaei M, Wilke L (1995) The biochemical response of electrical signaling in the reproductive system of *Hibiscus* plants. Plant Physiol 109:375–384
Gatehouse JA (2002) Plant resistance towards insects herbivores: a dynamic interaction. New Phytol 156:145–169
Glazebrook J (2001) Genes controlling expression of defense responses in *Arabidopsis*—2001 status. Curr Opin Plant Biol 4:301–308
Grant JJ, Yun BW, Loake GJ (2000) Oxidative burst and cognate redox signalling reported by luciferase imaging: identification of a signal network that functions independently of ethylene, SA and Me-JA but is dependent on MAPKK activity. Plant J 24:569–582
Griffin S, Markham JL, Dennis G, Grant Wyllie S (2000) Using atomic force microscopy to view the effects of terpenoids on the stability and packing of phosphatidylcholine supported lipid bilayers. Proceedings of the 31st international symposium on essential oils, Hamburg, 10–13 September 2000
Halitschke R, Gase K, Hui D, Schmidt DD, Baldwin IT (2003) Molecular interactions between the specialist herbivore *Manduca sexta* (Lepidoptera, Sphingidae) and its natural host *Nicotiana attenuata*. VI. Microarray analysis reveals that most herbivore-specific transcriptional changes are mediated by fatty acid-amino acid conjugates. Plant Physiol 131:1894–1902
Hammond-Kosack K, Jones JDG (2000) Responses to plant pathogens. In: Buchanan B, Gruissem W, Jones R (eds) Biochemistry and molecular biology of plants. American Society of Plant Physiologists, Rockville, MD, pp 1102–1156
Hejl AM, Koster KL (2004) Juglone disrupts root plasma membrane H^+-ATPase activity and impairs water uptake, root respiration, and growth in soybean (*Glycine max*) and corn (*Zea mays*). J Chem Ecol 30:453–471
Heil M (2004) Direct defense or ecological costs: responses of herbivorous beetles to volatiles released by wild Lima bean (*Phaseolus lunatus*). J Chem Ecol 30:1289–1295
Holopainen JK (2004) Multiple functions of inducible plant volatiles. Trends Plant Sci 9:529–533
Inderjit, Callaway RM (2003) Experimental designs for the study of allelopathy. Plant Soil 256:1–11

Jose S, Gillispie AR (1998) Allelopathy in black walnut (*Juglans nigra* L.) alley cropping. II. Effects of juglone on hydroponically grown corn (*Zea mays* L.) and soybean (*Glycine max* L. Merr.) growth and physiology. Plant Soil 203:199–205

Karpinski S, Gabrys H, Karpinska B, Mullineaux, P (2003) Light perception in plant disease defence mechanisms. Curr Op Plant Biol 6:390–396

Kessler A, Baldwin IT (2001) Defensive function of herbivoreinduced plant volatile emissions in nature. Science 291:2141–2144

Knight H, Knight MR (2001) Abiotic stress signalling pathways: specificity and cross-talk. Trends Plant Sci 6:262–267

Knobloch K, Pauli A, Iberl B, Weigand H, Weis N (1989) Antibacterial and antifungal properties of essential oil components. J Essent Oil Res 1:119–128

Kombrink E, Somssich IE (1995) Defense responses of plants to pathogens. Adv Bot Res 21:1–34

Kunkel BN, Brooks DM (2002) Cross talk between signaling pathways in pathogen defense. Curr Opin Plant Biol 5:325–331

Larkindale J, Knight MR (2002) Protection against heat stress-induced oxidative damage in *Arabidopsis* involves calcium, abscisic acid, ethylene and salicylic acid. Plant Physiol 128:682–695

Lee S, Tsao R, Coats JR (1999) Insecticidal activity of monoterpenoids to western corn rootworm (Coleoptera: Chrisomelidae), twospotted spider mite (Acari: Tetranychidae) and house fly (Diptera: Muscidae). J Econ Entomol 92:56–67

Lugtenberg BJJ, Chin-A-Woeng TFC, Bloemberg GV (2002) Microbe-plant interactions: principles and mechanisms. Antonie van Leeuwenhoek 81:373–383

Maffei M, Camusso W, Sacco S (2001) Effects of *Mentha* x *piperita* essential oil and monoterpenes on cucumber root membrane potential. Phytochemistry 58:703–707

Maffei M, Bossi S, Spiteller D, Mithoefer A, Boland W (2004) Effects of feeding *Spodoptera littoralis* on lima bean leaves. I. Membrane potentials, intracellular calcium variations, oral secretions, and regurgitate components. Plant Physiol 134:1752–1762

Maffei ME, Mithöfer A, Arimura G-I, Uchtenhagen H, Bossi S, Bertea CM, Starvaggi Cucuzza L, Novero M, Volpe V, Quadro S, Boland W (2006) Effects of feeding *Spodoptera littoralis* on Lima bean leaves. III. Membrane Depolarization and Involvement of Hydrogen Peroxide. Plant Physiol 140:1022–1035

Maleck K, Levine A, Eulgem T, Morgan A, Schmidt J, Lawton KA, Dangl JL, Dietrich RA (2000) The transcriptome of *Arabidopsis thaliana* during systemic acquired resistance. Nat Genet 26:403–409

Mithöfer A, Schulze B, Boland W (2004) Biotic and heavy metal stress response in plants: evidence for common signals. FEBS Lett 566:1–5

Mithöfer A, Wanner G., Boland W (2005) Effects of feeding *Spodoptera littoralis* on Lima Bean leaves. II. Continuous mechanical wounding resembling insect feeding is sufficient to elicit herbivory-related volatile emission. Plant Physiol 137:1160–1168

Moreland DE, Novitzky WP (1987) Effects of phenolic acids, coumarins, and flavonoids on isolated chloroplasts and mitochondria. In: Walzer GR (ed) Allelochemicals: role in agricolture and forestry. American Chemical Society, Washington D.C., pp 247–261

Muller-Moule P, Havaux M, Niyogi KK (2003) Zeaxanthin deficiency enhances the high light sensitivity of an ascorbate-deficient mutant of *Arabidopsis*. Plant Physiol 133:748–760

Mur L, Kenton P, Draper J (2005) *In planta* measurements of oxidative bursts elicited by avirulent and virulent bacterial pathogens suggests that H_2O_2 is insufficient to elicit cell death in tobacco. Plant Cell Environ 28:548–561

Pasternak T, Rudas V, Potters G, Jansen MAK (2005) Morphogenic effects of abiotic stress: reorientation of growth in *Arabidopsis thaliana* seedlings. Environ Exp Bot 53:299–314

Pinto E, Sigaud-Kutner TCS, Leitao MAS, Okamoto OK, Morse D, Colepicolo P (2003) Heavy metal-induced oxidative stress in algae. J Phycol 39:1008–1018

Rice EL (1984) Allelopathy, 2nd edn. Academic Press, Orlando

Robinson T (1983) The organic constituents of higher plants, 5th edn. Cordus Press, North Amherst, Mass.

Sacco S, Maffei M (1997) The effect of isosakuranetin (5,7-dihydroxy 4′-methoxy flavanone) on potassium uptake in wheat root segments. Phytochemistry 46:245–248
Schittko U, Hermsmeier D, Baldwin IT (2001) Molecular interactions between the specialist herbivore *Manduca sexta* (lepidoptera, Sphingidae) and its natural host *Nicotiana attenuata*. II. Accumulation of plant mRNAs in response to insect-derived cues. Plant Physiol 125:701–710
Shvetsova T, Mwesigwa J, Volkov AG (2001) Plant electrophysiology: FCCP induces action potential and excitation waves in soybean. Plant Sci 161:901–909
Spiteller D, Boland W (2003a) *N*-(15,16-dihydroxylinoleoyl)-glutamine and *N*-(15,16-epoxylinoleoyl)-glutamine isolated from oral secretions of lepidopteran larvae. Tetrahedron 59:135–139
Spiteller D, Boland W (2003b) Identification and synthesis of *N*-(17-acyloxyacyl)-glutamine conjugates from oral secretion of lepidopteran larvae. J Org Chem 68:8743–8749
Spiteller D, Pohnert G, Boland W (2001) Absolute configuration of volicitin; an elicitor of plant volatile biosynthesis from Lepidopteran larvae. Tetrahedron Lett 42:1483–1485
Staskawicz BJ, Mudgett MB, Dangl JL, Galan JE (2001) Common and contrasting themes of plant and animal diseases. Science 292:2285–2289
Takabayashi J, Dicke M (1996) Plant-carnivore mutualism through herbivore-induced carnivore attractants. Trends Plant Sci 1:109–113
Thomma BP, Penninckx IA, Broekaert WF, Cammue BP (2001) The complexity of disease signaling in *Arabidopsis*. Curr Opin Immunol 13:63–68
Torres MA, Dangl JL (2005) Functions of the respiratory burst oxidase in biotic interactions, abiotic stress and development. Curr Opin Plant Biol 8:397–403
Volkov AG, Dunkley TC, Morgan SA, Ruff D II, Boyce YL, Labady AJ (2001) Bioelectrochemical signalling in green plants induced by photosensory systems. Bioelectrochemistry 63:91–94
Wang W, Vinocur B, Shoseyov O, Altman A (2001) Biotechnology of plant osmotic stress tolerance: physiological and molecular considerations. Acta Hort 560:285–292
Wang W, Vinocur B, Altman A (2003) Plant responses to drought, salinity and extreme temperatures: towards genetic engineering for stress tolerance. Planta 218:1–14
Zhu JK (2001) Cell signaling under salt, water and cold stresses. Curr Opin Plant Biol 4:401–406
Zhu JK (2002) Salt and drought stress signal transduction in plants. Annu Rev Plant Biol 53:247–73

21 Control of Plant Development by Hydro-Electrochemical Signal Transduction: a Means for Understanding Photoperiodic Flower Induction

EDGAR WAGNER, LARS LEHNER, JUSTYNA VEIT, JOHANNES NORMANN, MARCO VERVLIET-SCHEEBAUM, JOLANA T.P. ALBRECHTOVÁ

21.1 Introduction: photoperiodic flower induction

The hypothesis that flowering involves a specific stimulus is based upon the demonstration that (a) in photoperiodism the flowering response depends upon the day length conditions given to the leaves, whereas the response occurs in the apices, and that (b) a floral stimulus can be transmitted via a graft union from an induced partner (donor) to a non-induced one (receptor). Transmission of the floral stimulus by grafting has been demonstrated within various photoperiodic response types, as well as between different photoperiodic response types in interspecific and intergeneric grafts. The physiological evidence for a floral stimulus is clear-cut, but up to now the nature of the stimulus has remained obscure (Bernier 1988).

The specific kind of photoperiodic behavior depends very much on the exact environmental conditions, as was shown for four different North American ecotypes of *Chenopodium rubrum* (Tsuschiya and Ishiguri 1981). The southern ecotypes display an obligate short-day behavior under white (W), red (R) and blue (B) light. The most northern ecotype is day neutral in B and W and has an amphiphotoperiodic response in R light. Another northern ecotype has an amphiphotoperiodic response in B and a short-day response in W and R light. The amphiphotoperiodic response in B is modified to day neutral by changing the temperature from 20 to 12 °C. These data clearly indicate that photoperiodic behavior is extremely flexible in adapting to specific environmental conditions.

Irrespective of the flexibility of plants in modifying their photoperiodic behavior in adapting to specific environmental conditions as just mentioned, the following essentials of the photoperiodic reaction have to be kept in mind as a basis for further considerations:

(a) Short-day (SDP) and long-day plants (LDP) show opposite reactions to a given photoperiod.
(b) Reactions result from coincidence or non-coincidence of light and dark phases of the photoperiod with corresponding phases of an endogenous circadian rhythm and the main photoreceptors are the plant sensory

University of Freiburg, Institute of Biology II, Schänzlestr. 1, 79104 Freiburg, Germany

Plant Electrophysiology – Theory & Methods (ed. by Volkov)

pigment systems phytochrome and cryptochrome. Circadian rhythm and photoreceptors have the same properties in SDP and LDP.

(c) Critical photoperiodic induction produces irreversible changes in the leaves of SDP and LDP leading to a common state both in SDP and LDP, as proven by grafting experiments. There is no difference between SDP and LDP in their response towards a common inductor from a grafted leaf from an induced short- or long-day plant.

Analyzing the kinetics of change at the shoot apical meristem (SAM) during flower initiation can give hints on the mechanism(s) of signal transduction from leaves to SAM during photoperiodic flower induction.

21.2 Model system *Chenopodium*: induction of flowering from physiology to molecular biology

The model system *Chenopodium spec*. had been established to study photoperiodic control of flowering on the physiological, the biochemical and molecular level.

First *Chenopodium* was developed as a "Petri-dish plant" by Cumming (1959) for large scale screening of photoperiodic flower induction with several latitudinal ecotypes showing short-day, long-day and day-neutral responses (Cumming 1967; Tsuschiya and Ishiguri 1981).

Subsequent studies demonstrated that phytochrome photoreversibility could not act as an hour glass timer in photoperiodism, but was gated in its light sensitivity by an endogenous (circadian) rhythm presenting photophile and skotophile phases in daily 24-h light:dark cycles (Cumming et al. 1965). Following Bünning's (1942) and Hendricks' (1963) early concepts on metabolic control of timing in photoperiodism, *C. rubrum* has been used to establish an analysis of energy metabolism demonstrating a circadian rhythm in redox state and energy charge as macroparameters timing photoperiodic behavior (Wagner et al. 1975). Recently, *C. rubrum* was also used in molecular studies on signal transduction in photoperiodic flower induction. An ortholog of *LEAFY*, a transcription factor involved in a signaling cascade leading to flowering in *Arabidopsis* (Nilsson et al. 1998), was identified in *C. rubrum*. Expression kinetics of *LEAFY* ortholog *CrFL* at SAM is related to photoperiod (Veit et al. 2004). Transgenic plants were produced using RNA interference in order to analyse function of *CrFL* in signal transduction in *C. rubrum*.

With studies on the hydro-electrochemical integration of communication in *Chenopodium* plants, we could demonstrate that action potentials precede turgor mediated leaf movements and changes in stem extension rate (Wagner et al., 2005) (Fig. 21.1). Molecular and physiological studies at SAM of *C. rubrum* in transition to flowering presented evidence of changes in turgor and in aquaporin expression (Albrechtová and Wagner 2004;

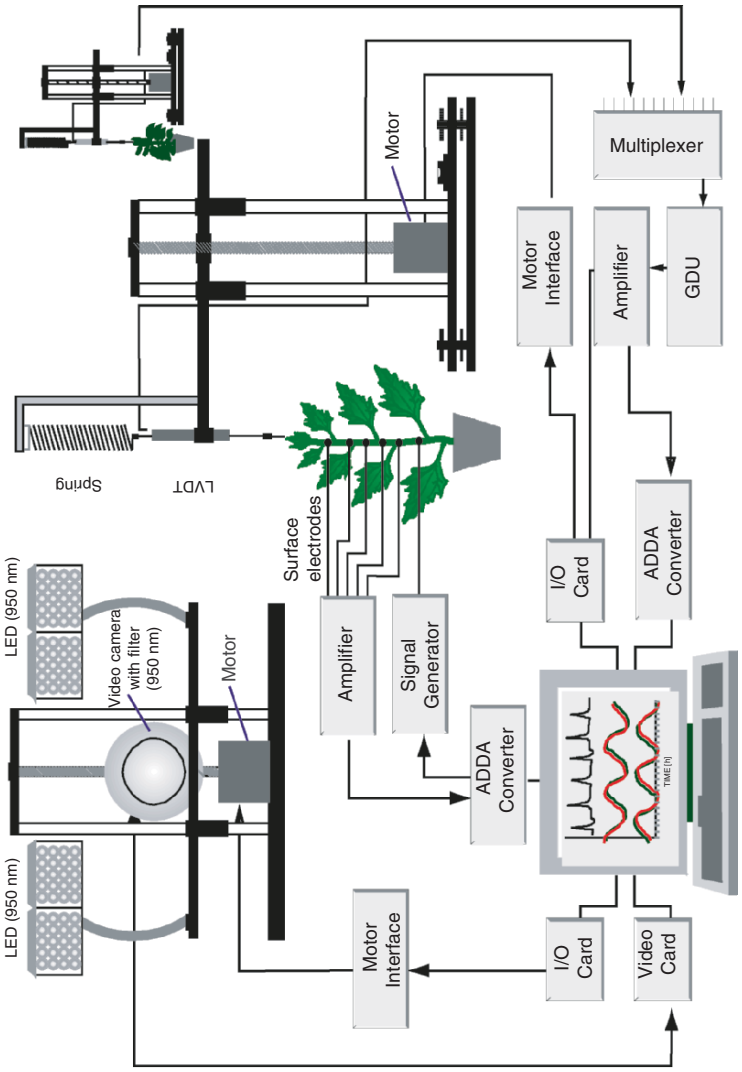

Fig. 21.1. Experimental setup. Measuring device for long term recording of changes in electric surface membrane potential, leaf movements (LM) and stem elongation rate (SER). Video imaging at 950 nm for continuous monitoring of leaf movements in light–dark cycles. Linear voltage differential transformers (LVDTs) hooked to the plant stem with a spring loaded constant pull of 1.5 g. Optimal measuring conditions for video imaging and SER registration are maintained via software controlled step motors positioning the devices according to the growth of the plants. Platinum electrodes are used together with a commercial contact gel for measuring and stimulation. Additional sensors monitor electromagnetic noise, temperature, light intensity and humidity. From Wagner et al. (2005)

Albrechtová et al. 2004) which are most likely triggered by APs traveling along the stem axis as a line of communication between leaves, roots and SAM. A rapid communication between roots and SAM is inferred from a reduction of O^{15}-water uptake by the roots after cutting off apical meristems (Ohya et al. 2005).

The recording of the frequency distribution of spontaneous APs moving basipetal and acropetal on the stem axis resulted in electrophysiograms (EPGs) which could be used to characterize the flowering and vegetative state in *C. rubrum* and *C. murale*. In addition to the characterization of such phase changes, the information from EPGs has been used for the electrogenic initiation of flowering (Lehner 2002) opening a new field for applications in horticulture, agriculture and silviculture (Wagner et al. 2004).

21.3 Electrophysiology and plant behavior

Chenopodium is very well characterized with respect to the kinetics of photoperiod controlled flower induction in a whole series of latitudinal ecotypes (Cumming 1959, 1967; King 1975). In *C. rubrum*, the circadian rhythmic organization of energy metabolism has been analyzed in detail (Wagner et al. 1975, 2004).

In view of demonstrated rhythmic and photoperiod mediated surface potential phenomena, we suggested that the flowering stimulus might be an electrical or electrochemical signal (Wagner et al. 1996, 1997). A similar concept was advanced in relation to systemic effects from wound responses; it was suggested that action potentials could be involved as signaling mechanisms in chilling injury, mechanical perturbation and invasion by pathogens (Davies 1987; Wildon et al. 1989, 1992), as well as for the influence of light and gravity (Davies et al. 1991). Application of direct current, i.e. electrical stimulation, induced proteinase inhibitor II Pin2 gene expression and modulation of photosynthetic activity in the leaves (Herde et al. 1995). Induction of proteinase inhibitor gene expression involved both action potentials and variation potentials in another set of experiments (Stankovic and Davies 1996). Systemic Pin2 gene expression in wild type and ABA-deficient tomato plants was triggered by mechanical wounding, current application and heat treatment (Herde et al. 1998a,b). Mechanical wounding of *Chenopodium rubrum* leaves induced changes in membrane potential, as seen by using a fluorescent probe as indicator (Albrechtová and Wagner 1998).

In sunflower plants, electrical activities could be evoked in response to various external stimuli or were generated spontaneously. Action potentials, graded potentials, changes in resting potential and rhythmic electrical activity were observed. Large graded potentials were paralleled by a decrease in

growth rate and in the rate of water uptake. Spontaneous action potentials along the stem axis were generated only at night in vegetative plants but they were generated during the day as well as during the night in flowering plants (Davies et al. 1991). Flower induction in *Spinacia* was correlated to the light-stimulated bioelectric response from the leaves (Greppin et al. 1973; Greppin and Horwitz 1975).

As suggested by some previous experiments on the control of flowering (Adamec and Krekule 1989a,b; Adamec et al. 1989), endogenous electrical activities of plants can be manipulated by electric current from outside; specifically in the long-day plant *Spinacia oleracea* (Montavon and Greppin 1983, 1986), as well as in the short-day plant *Chenopodium rubrum* (Adamec et al. 1989; Machackova et al. 1990; Machackova and Krekule 1991), photoperiodic flower induction could be inhibited by the application of direct electric current (DC) via felt-tipped electrodes. It was concluded that DC probably interfered with the translocation of a floral stimulus from induced leaves to SAM (Adamec and Krekule 1989a,b; Adamec et al. 1989).

There is controversial evidence concerning transport of the flower inducing stimulus in the phloem (see Bernier 1988 and references therein), which would be the transport path for the stimulus in florigenic and multicomponental theories. Phloem has been considered as a pathway for signal spreading: but a general symplast/apoplast interaction might be involved as well, as evidenced from studies on fast electric transients induced by electric stimulation in the apoplast of tomatoes (Herde et al. 1998a,b). Temporal changes in plasmodesmal patterning might be involved in modulating electric signal transduction (Wright and Oparka 1997; Liarzi and Epel 2005).

Bearing in mind the circadian rhythm in transcellular current in *Acetabularia* (Novak and Sironval 1976) and the diurnal rhythm in resting membrane potential in *Chenopodium* as shown previously (Wagner et al. 1998), it seems possible that a circadian rhythm in bioelectricity may be of great significance in the circadian rhythmic coordination of the whole plant responsible for sensitivity changes in membrane-bound activities (Vigh et al. 1998). The circadian rhythm in transcellular current probably arises from a circadian rhythm in energy metabolism and rhythmicity of transport processes at the plasma membrane (Mayer and Fischer 1994; Mills et al. 1994; Pickard 1994).

In *C. rubrum,* a detailed analysis of the occurrence of surface sum APs revealed electric activity in all organs (root, stem, leaves) of the plant. With a series of electrodes along the stem axis the basipetal or acropetal propagation of APs was recorded. Under quite different experimental condition, so-called reflected APs occasionally could be observed, i.e.APs were propagating basipetal and than seemed to be reflected acropetal (Fig. 21.2). They have not been studied in detail so far but might be very relevant for analyzing the importance of the communication between root meristems and SAM in control of growth and development.

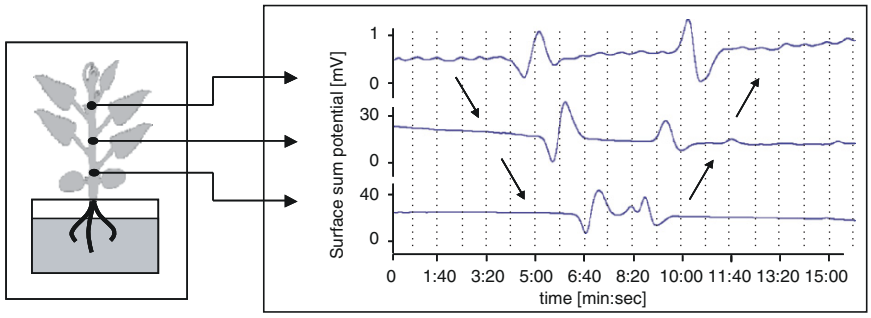

Fig. 21.2. "Reflection" of an action potential (AP) at the basal section of a stem axis of *C. rubrum*. The recordings of the surface sum potential are presented after a light to dark transition of a 5-week-old plant of *C. rubrum* at time 0. The AP is moving basipetal from the apical part of the stem axis, is successively passing three bipolar surface electrodes. Below the basal electrodes it is either reflected immediately and is moving acropetal, or, alternatively, the basipetal moving AP might trigger a new AP moving acropetal. Growing conditions: 20°C, 70% rh; photosynthetic active radiation (PAR): 120 mol/m^{2}s. The mirror image pattern of basipetal, acropetal propagating APs is due to the measuring principle which is using bipolar (+; –) electrodes and a differential amplifier (see also Zawadzki et al. 1991)

21.4 Circadian rhythms as metabolic bases for hydro-electrochemical signal transduction

Rhythmicity is one of the characteristics of life which expresses itself at all levels of organization from unicellular systems to humans. Rhythmic phenomena in physiology, development and behavior of all living systems show period lengths ranging from fractions of a second to hourly, daily and even annual cycles.

The most conspicuous rhythm is the so-called circadian oscillation. The length of exactly 24 h when the organisms are synchronized by the daily light-dark cycle of the earth. In constant conditions, however, its period length is only approximately 24 h, i.e. circadian. In contrast to biological rhythms showing other frequencies, circadian rhythms are temperature compensated and almost unsusceptible to chemical manipulation. It is this stability or homeo-dynamics of period length which qualifies the circadian rhythm as a precise physiological timer and thus is the essence of Bünning's (1973, 1977) theory of the physiological clock.

From an evolutionary point of view, circadian rhythmicity has been considered to be an adaptation of pro- and eukaryotic energy conservation and transformation to optimize energy harvesting by photosynthesis in the daily cycle of energy supply from the environment (Cumming and Wagner 1968; Wagner and Cumming 1970; Wagner 1977; Wagner et al. 1998). It was also assumed that this adaptation is dependent on the division of energy transformation within different compartments of the cell, such as chloroplasts,

mitochondria and the glycolytic space involving redox mediated transcriptional controls (Bauer et al. 1999). In photosynthetic prokaryotes, lacking cell organelles, a metabolic micro-compartmentation allows for a similarly sophisticated regulatory network as in eukaryotes.

High-frequency oscillations in energy-transducing metabolic sequences could give rise to low-frequency oscillations of energy flow in the metabolic network of the whole system, providing a basis for the evolution of a temperature-compensated circadian rhythm (Wagner and Cumming 1970). The clock's periodicity is genetically determined and provides the temporal frame for physiological and behavioral patterns that are necessary for adaptation of organisms and populations to environmental constraints. Thus the circadian rhythmic cell is a hydro-electrochemical oscillator driven or synchronized by the daily dark/light cycle with a temporal compartmentation of metabolism and a network of metabolic sequences to compensate for oxidative stress tin adapting to their light environment. This is best shown in the adaptation of photosynthetic machineries from bacteria (Joshi and Tabita 1996; Zeilstra-Ryalls et al. 1998; Bauer et al. 1999; Sippola and Aro 2000) to higher plants (Anderson et al. 1988; Asada 1999), which respond to changing light quality and quantity with coordinated changes of pigmentation, electron transport components, membrane composition, organization and function (Anderson et al. 1988). The acclimation of plants at the cellular level requires interaction between the nucleus, mitochondria and chloroplasts in a regulatory network involving several photoreceptors such as phytochromes, blue light receptors and chlorophyll.

The existence of circadian rhythmicity is dependent on the living cell and suggests that metabolic compartmentation spatial and/or temporal is of significance for its generation (Barbier-Brygoo et al. 1997; Flügge 2000). Furthermore, circadian rhythms in photosynthesis, respiration and chloroplast shape suggest that investigation of the metabolic controls may be fruitful for the elucidation of the mechanism of biological rhythms. Interrelations between cellular compartments have already been shown. For example, Könitz (1965) has shown reciprocal changes in the ultrastructure of chloroplasts and mitochondria in daily light–dark cycles. Murakami and Packer (1970) demonstrated that, within the same cell, mitochondria swell and chloroplasts contract upon illumination and the reverse occurs in the dark. The importance of the entire metabolic network for the display of circadian oscillations is underlined by the fact that, in contrast to the temperature-compensated circadian oscillations of the intact system, isolated organelles display high frequency oscillations (Gooch and Packer 1974; Gylkhandanyan et al. 1976) which are temperature dependent. Similarly in photosynthetic bacteria, cellular signal transduction integrates micro-compartmentation of photosynthesis, carbon dioxide assimilation and nitrogen fixation (Joshi and Tabita 1996). From a detailed analysis of rhythms in enzyme activities involved in compartmental energy metabolism with and without feeding of sugars (cf. Wagner et al. 1983; Jang and Sheen 1994) and on changes of nucleotide pool size levels

in the short-day plant *Chenopodium rubrum* L., we compiled evidence in favor of circadian rhythmicity in overall energy transduction. Our observations lead us to suggest that circadian rhythmicity, as the timer in photoperiodism, should be based on a circadian rhythm in energy metabolism. This rhythm would be the result of a compensatory control oscillation between glycolysis and oxidative phosphorylation, coupled to photophosphorylation in cyanobacteria (Huang et al. 1990), photosynthetic bacteria and green plants (Wagner and Cumming 1970; Wagner et al. 1974a,b; Wagner 1976a–c). This mechanism of circadian rhythmicity could involve energy control of ion transport processes at the membranes of cells and organelles. The membrane's physical state, e.g. modulated by temperature, could control transcription (Vigh et al. 1998) or via frequency coded calcium oscillations leads to differential gene activation and expression (Dolmetsch et al. 1998; Li et al. 1998).

Taking into account the symplastic organization of higher plants, the concept of compartmental feedback becomes even more attractive in view of bioelectric phenomena. The symplastic organization of higher plants might be the basis for translocation of electric, photoperiodic and morphogenetic stimuli (Genoud and Métraux 1999). The energetic integration of the entire system could be based on the same symplastic organization, so that proton translocation (Mitchell 1976) and concomitant ion movements would give rise to a circadian rhythm in electric potential paralleled by circadian leaf movements and stem extension rates (Aimi and Shibasaki 1975; Wagner et al. 1998).

The circadian rhythm in transcellular current of a single cell, as observed by Novak and Sironval (1976) in *Acetabularia*, probably arises from the compartmental feedback between mitochondria, chloroplasts and glycolysis, as suggested in our concept for a mechanism of circadian rhythmicity. The vacuole could be involved in this control net by acting as a reservoir for metabolites as in the case of oscillations in Crassulacean acid metabolism. A similar concept might hold true for photosynthetic active bacteria in general and their temporal organization of metabolism, but certainly for circadian rhythmic behavior of the cyanobacterium *Synechococcus* (Huang et al. 1990; Ishiura et al. 1998).

21.5 Hydraulic-electrochemical oscillations as integrators of cellular and organismic activity

The symplast of higher plants is probably not only the network for rapid electrical integration of metabolic activities but also the route for the translocation of sucrose and the transfer of the flowering stimulus. An observation that may have some bearing on the significance of changes in membranes during signal transduction is the detection of alterations in the distribution of the endoplasmic reticulum in cells of SAM of *Chenopodium album* after photoperiodic stimulation (Gifford and Stewart 1965). In spinach, the plasma membrane of

apical cells is modified during flower induction (Penel et al. 1988; Crèvecoeur et al. 1992). Changes in pH and Ca^{2+} patterning as measured with fluorescent dyes can be observed between the earliest events of photoperiodically inductive conditions in flower initiation in *C. rubrum* (Walczysko et al. 2000; Albrechtová et al. 2001, 2003). In the case of flower induction, the temporal organization of development at SAM might involve rhythmic symplastic transport of metabolites and the interaction of rhythmic (bioelectric) signals originating in the leaves (Novak and Greppin 1979) leading to a frequency-coded electrochemical communication between leaves and SAM (Wagner et al. 1998).

Communication by surface membrane action or variation potentials in higher plants has been observed for a series of systemic responses (Wagner et al. 1997).Changes in action potentials triggered by light to dark or dark to light transitions can be related to changes in photosynthetic electron transport (Trebacz and Sievers 1998). Observations on phytochrome action in the moss *Physcomitrella patens* are indicative of activation of plasma membrane anion channels (Ermolayeva et al. 1997), leading to membrane depolarization as a very first step in signal transduction.

Bearing in mind the circadian rhythm in transcellular current reported in *Acetabularia* (Novak and Sironval 1976), it seems possible that a circadian rhythm in proton flow, of action and variation potentials, may be of great significance in the circadian coordination of the whole plant, and the communication between plant organs such as the leaves and SAM in photoperiodic flower induction (Wagner et al. 1998; Elowitz and Leibler 2000; Smith and Morowitz 2004).

The display of circadian rhythms in energy charge and reduction charge favor the concept that the many non-linear oscillators of cell metabolism are coupled such as to evolve the circadian frequency of the system as a whole (Wagner et al. 2000; Smith and Morowitz 2004).

An interplay between oscillating enzymatic reactions and contractile elements of the structural proteins of the cell has even been used to design a mechanochemical model of the biological clock (Sorensen and Castillo 1980; Kung 2005), and most significant, with protoplasts from *Phaseolus* pulvinar motor cells a circadian rhythm in volume oscillations could be shown (Mayer and Fischer 1994). This "electrochemical" view of metabolic control could be very relevant in relation to the mechanism of growth and differentiation. Numerous experimental findings show the involvement of stable electric fields in growing and differentiating cells. The experimental evidence indicates the possibility that the chemical reaction network is controllable by electric fields. This could open up a way to visualize the synchronization of circadian rhythms by electric and magnetic fields and thus could allow for synchronizing inputs from so called subtle geophysical factors (Olcese 1990).

It is very likely that physiological rhythms are based on the same structural and functional principles underlying Mitchell's (1976) chemiosmotic hypothesis of energy transduction. Allosteric enzymes could function as molecular

high frequency oscillators as in glycolysis while compartmental feedback between organelles with vectorially organized metabolic reactions in their enclosing membranes could give rise to a circadian rhythm in energy transduction by proton flow through the entire cell. Thus the coupling between compartmented metabolic sequences is possibly achieved through cycles in nucleotide ratios and ionic balances via transport mechanisms and redox shuttles in the different energy-transducing biomembranes, which could act as coupling elements and frequency transformers. The membranes themselves could act as high-frequency oscillators (Morré and Morré 1998; Morré et al. 1999). Such high-frequency membrane oscillators could be the basis for perception and transduction of high-frequency signals from the environment (Novak and Greppin 1979).

The ratios of coupling nucleotides would be relatively temperature independent and the nucleotides themselves could thus, as rate effectors in compartmental feedback, fulfill the requirements for precise temperature-compensated time keeping. Proton flow and concomitant ion movement through the symplast could be the basis of rhythmic electrochemical integration of the whole plant (Wagner et al. 1997, 2000; Igamberdiev and Kleczkowski 2003; Stelling et al. 2004).

The circadian pacemaker oscillation expresses itself by temperature compensated phosphorylation/dephosphorylation or reduction/oxidation cycles as the time standard for the control of transcription and translation controlled ~24 h cycles of protein synthesis turnover (Elowitz and Leibler 2000; Richly et al. 2003; Tomita et al. 2005).

21.6 Local hydraulic signaling: the shoot apex in transition

Photoperiodic flower induction involves a reorganization of organogenesis at SAM from vegetative phylotaxis to floral development. Floral transition includes molecular signaling and physiological and physical changes. Each step in molecular signal transduction is influenced by feedback from sequences of events from other pathways. In this way, the "physiological state" of a plant controls signal transduction, and vice versa. Very little is yet known regarding relationships between the molecular and physiological level of the control of organogenesis. To analyze the change from the vegetative to the flowering apex, we studied kinetics of molecular and physiological changes at SAM of *C. rubrum* during floral transition in order to elucidate the kinetic relationships between the events.

Electric and hydraulic long-distance signals are anticipated to be involved in flower induction. The perception of a flower inducing dark span by phytochrome possibly leads to a change in the electrochemical signaling between leaves and SAM to allow flower initiation to occur (Wagner et al. 1998). Turgor dependent volume changes, stretch-activated membrane channels

(Kung 2005) and correlated changes in membrane potential might be an essential part of the "hardware" for signal transduction at the cellular and organismic level. The "software" could involve frequency-coded signals at the cellular, the tissue and organismic level.

Membrane potentials are ubiquitous in all living cells and provide the energy for the active transport of substances. The depolarization of the cellular membrane potential can generate APs which in higher plants can be propagated over long distances via the phloem and plasmodesmata. Localized strain of the plasma membrane can elicit electric signals via mechanosensitive ion channels. Such signals can stimulate turgor loss and may even activate genes (Banes et al. 1995; Lang and Waldegger 1997). Due to its mechanisms of action, hydraulic and electric signaling is always coupled.

Physical strain at the surface of SAM was previously suggested to play a key role in the patterning of organogenesis (Green 1994). The distribution of local forces is a result of the upward pressure given by the expanding inner cell layers (corpus) to the sheet on the surface (tunica), and from the local extensibility of cell walls at the surface. A signaling network regulates organogenesis, involving molecular, biophysical and biochemical pathways of signal transduction. Based on crosstalk between all pathways, the "physiological state" of a plant controls signal transduction, and vice versa.

Our studies aim at understanding local water transport and turgor changes as related to changing organogenesis at SAM of *Chenopodium* plants under photoperiodic flower induction. We could show that size of SAM increases during flower inducing treatment (Fig. 21.3) (Albrechtová et al. 2004). The expansion of the meristem results from cell enlargement rather than changes in cell division, and therefore is presumably based on water uptake. The phyllotactic spiral changes to a circular pattern, visible as local differences in optical properties of cell walls. The results suggest that organogenesis changes long before flower induction is completed. We therefore conclude that the change of organogenesis at SAM during floral transition is initiated by an increased movement of water into SAM leading to its expansion and to the redistribution of the forces at its surface.

A change in water movement could involve aquaporins, which in consequence have been studied in SAM of *C. rubrum*. Aquaporins (AQPs) are highly selective water channels facilitating transport of water across the membrane (Baiges et al. 2002). We identified in *Chenopodium rubrum* a gene with high homology to aquaporins from other plants, CrAQP (Fig. 21.4). Its expression differs significantly in leaves and in SAM between vegetative and flower induced plants (Albrechtová and Wagner 2004). Involvement of aquaporins at SAM in flower initiation was proven using application of an inhibitor of aquaporin activity HgCl directly to SAM. HgCl partially inhibited flowering, if applied before or during the dark span.

A comparison of the kinetics of parameters studied revealed that the increase in SAM size is accompanied by an increase in calcium concentration and average pH value at SAM (Walczysko et al. 2000; Albrechtová et al. 2001,

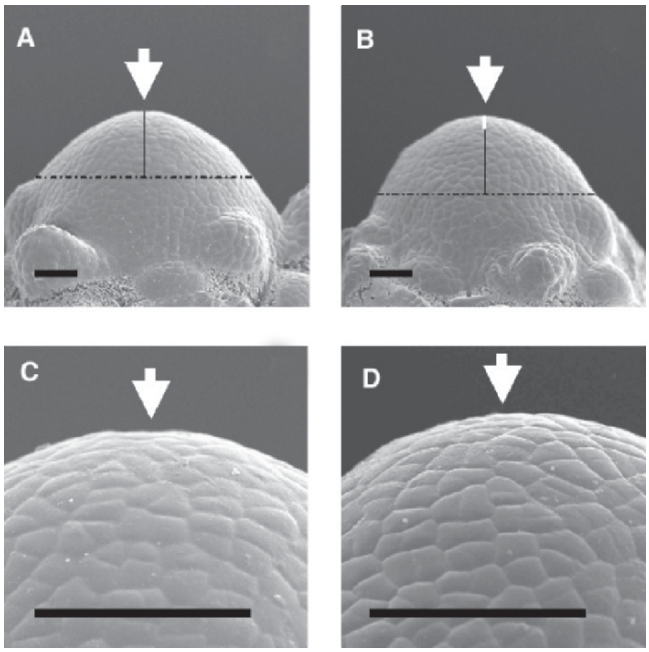

Fig. 21.3. Changes in geometry of SAM during flower inducing treatment. Cryo SEM. **A**, **C**, control plant, **B**, **D**, plant at the end of 12 h inductive dark span. The difference is mostly pronounced on the top (*arrows*): A subtle depression is visible at SAM of control plant (**A**, **C**), the SAM of the plant after inductive treatment is well rounded (**B**, **D**). Both apices have the same diameters of 250 Fm (*dotted lines*), but different heights (*full lines*, the difference is shown with a *thick white line* in **B**). The ratio height to diameter quantifies the typical difference between both treatments. *Bars* represent 50 Fm. From Albrechtová et al. (2004)

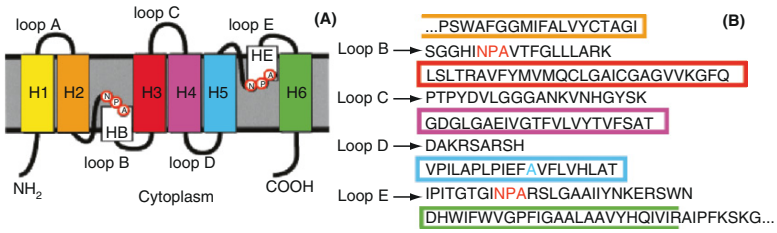

Fig. 21.4. The typical structure of aquaporins (**A**) and the putative protein sequence of a fragment of the aquaporin *CrAQP*, identified in *Chenopodium rubrum* (**B**). Helices are indicated by different colors identical in the putative sequence and on the scheme. The typical highly conserved motifs are indicated as red (NPA motif in loops B and E) and blue (alanine in helix H5, typical for plant aquaporins) letters in the sequence. Both C-terminus and N-terminus are missing in the identified fragment

2003). Further studies should reveal, if intracellular pH and calcium concentration can influence water transport by regulating activity of *CrAQP* (Tournaire-Roux et al. 2003). Our further observations confirmed a putative increase of free sucrose at SAM during floral transition, shown in other model plants (Albrechtová and Wagner 2004). The increase in sucrose concentration could lead to an increase in the osmotic pressure in the cells of SAM and thus produce together with a redistribution of ions a driving force for water transport.

A central role in the shift of organogenesis during floral transition is thus played by water status, local physical properties of cell walls and distribution of local forces at the surface of the meristem. Altogether, the results support the hypothesis about the involvement of hydraulic signals in organogenesis at SAM. It is anticipated that hydraulic changes at SAM leading to flower initiation are mediated by a specific hydro-electrochemical communication between (roots), leaves and SAM.

21.7 Summary and perspectives: electrophysiology and primary meristems

The hypothesis of a hydraulic electrochemical communication between plant organs prompted studies on the influence of local water transport and turgor changes on organogenesis at SAM of *Chenopodium* plants. Specific changes in shape and size of SAM were found to precede reorganization of organogenesis under photoperiodic flower induction. Optical properties of cell walls at the surface of SAM were found to precede reorganization of organogenesis under photoperiodic flower induction. Expression of the aquaporin *CrAQP* increased at SAM during an early phase of flower induction and the application of an inhibitor of aquaporin activity partially inhibited flowering. Changes in ion balance and carbohydrate levels in the cells seem also to be involved in the process. Altogether, the results support a hypothesis on the involvement of hydraulic signals in organogenesis at SAM. It is anticipated that hydraulic changes at SAM leading to flower initiation are mediated by a specific hydro-electrochemical communication between roots, leaves and SAM.

Studies on the uptake of O^{15} labeled water are indicative of a rapid communication between SAM and root meristems (Ohya et al. 2005). Water uptake was strongly reduced after removal of shoot apices, but was not affected, if roots were removed before removal of the apices. The root and shoot primary meristems might be centers of AP generation (Fig. 21.5) as a basis for coordination of physiological processes, such as water uptake and transpiration. Structure and function of both meristems is at present under intensive investigation (Schoof et al. 2000; Bäurle and Laux 2003; Baluska et al. 2004). Their hydro-electrochemical analysis should be most rewarding for an understanding of growth and differentiation.

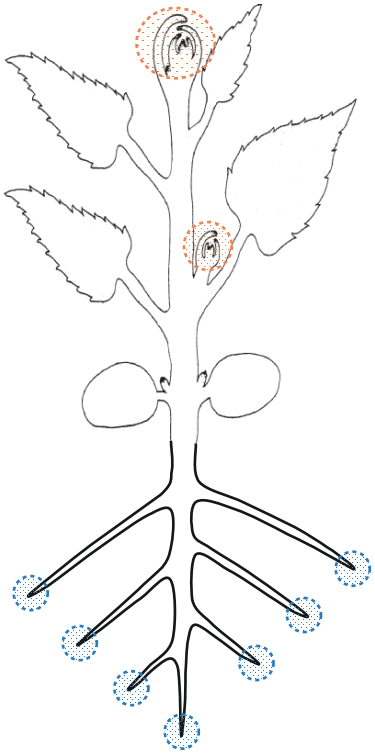

Fig. 21.5. Schematic drawing of a higher plant emphasizing elongating meristems as "centres" for root–shoot coordination. From the data reported so far it is concluded that in daily light dark cycles the rhythmic activity of the various plant organs [shoot apical meristem(s), leaves, stem (internodes), roots] is synchronized to 24 h with specific phase relationships between organ systems. Hydraulic and electric signals (APs, VPs) and their temporal structure are coordinating the developmental adaptation of the system to endogenous and environmental constraints. APs are predominantly generated at the root and shoot apical meristems. Leaf movements, rhythmic stem elongation (Wagner et al. 1996) and rhythmic root water transport (Lopez et al. 2003) are the main components of the hydraulic system. Changes in turgor are transduced via mechanotransductive ion channels into electric signals (APs). Plant systems can be considered as hydraulic–electrochemical oscillators. They display both circadian and higher frequency oscillations that are obviously taking part in the integration of the plant as a whole in its metabolic and developmental adaptation to the environmental conditions

Leaf movements, rhythmic stem elongation and rhythmic root exudation are components of the hydraulic system. Changes in turgor are transduced via mechanotransductive ion channels into electric signals (APs). Plant systems thus can be considered as hydraulic–electrochemical oscillators displaying both circadian and high frequency oscillations involved in the integration of the plant in its metabolic and developmental adaptation to the environmental conditions.

Further studies will monitor in detail the generation and propagation of APs in parallel to physiological and molecular studies to elucidate the patterns of cooperation between plant organs in response of the plant to seasonal changes in photoperiod as well as biotic and abiotic stress conditions.

References

Adamec L, Krekule J (1989a) Changes in membrane potential in *Chenopodium rubrum* during the course of photoperiodic flower induction. Biol Plant 31:336–343

Adamec L, Krekule J (1989b) Changes in transorgan electric potential in *Chenopodium rubrum* during the course of photoperiodic flower induction. Biol Plant 31:344–353

Adamec L, Machackova I, Krekule J, Novakova M (1989) Electric current inhibits flowering in the short-day plant *Chenopodium rubrum* L. J. Plant Physiol 134:43–46

Aimi R, Shibasaki S (1975) Diurnal change in bioelectric potential of *Phaseolus* plant in relation to the leaf movement and light conditions. Plant Cell Physiol 16:1157–1162

Albrechtová JTP, Wagner E (1998) Measurement of membrane potential using a fluorescent probe: "nerves" in plants? Abstracts of the symposium of the 11th international workshop on plant membrane biology, Cambridge, UK, p 318

Albrechtová JTP, Wagner E (2004) Mechanisms of changing organogenesis at the apex of *Chenopodium rubrum* during photoperiodic flower induction. Flowering Newslett 38:27–33

Albrechtová JTP, Metzger C, Wagner E (2001) pH-patterning at the shoot apical meristem as related to time of day during different light treatments. Plant Physiol Biochem 39:115–120

Albrechtová JTP, Heilscher S, Leske L, Walczysko P, Wagner E (2003) Calcium and pH patterning at the apical meristem are specifically altered by photoperiodic flower induction in *Chenopodium spp*. Plant Cell Environ 26:1985–1994

Albrechtová JTP, Dueggelin M, Dürrenberger M, Wagner E (2004) Changes in geometry of the apical meristem and concomitant changes in cell wall properties during photoperiodic induction of flowering in *Chenopodium rubrum*. New Phytol 163:263–269

Anderson JM, Chow WS, Goodchild DJ (1988) Thylakoid membrane organisation in sun/shade acclimation. Aust J Plant Physiol 15:11–26

Asada K (1999) The water–water cycle in chloroplasts: scavenging of active oxygens and dissipation of excess photons. Annu Rev Plant Physiol Plant Mol Biol 50:601–639

Baiges I, Schaffner AR, Affenzeller MJ, Mas A (2002) Plant aquaporins. Physiol Plant 115:175–182

Baluska F, Mancuso S, Volkmann D, Barlow PW (2004) Root apices as plant command centres: the unique "brain-like" status of the root apex transition zone. Biologia 59 [Suppl 13]:7–19

Banes AJ, Tsuzaki M, Yamamoto J, Fischer T, Brigman B, Brown T, Miller L (1995) Mechanoreception at the cellular level: the detection, interpretation, and diversity of responses to mechanical signals. Biochem Cell Biol 73:349–365

Barbier-Brygoo H, Joyard J, Pugin A, Ranjeva R (1997) Intracellular compartmentation and plant cell signalling. Trends Plant Sci 2:214–222

Bauer CE, Elsen S, Bird TH (1999) Mechanisms for redox control of gene expression. Annu Rev Microbiol 53:495–523

Bäurle I, Laux T (2003) Apical meristems: the plant's fountain of youth. BioEssays 25:961–970

Bernier G (1988) The control of floral evocation and morphogenesis. Annu Rev Plant Physiol Plant Mol Biol 39:175–219

Bünning E (1942) Untersuchungen über den physiologischen Mechanismus der endogenen Tagesrhythmik bei Pflanzen. Z Bot 37:433–486

Bünning E (1973) The physiological clock. Springer, Berlin Heidelberg New York

Bünning E (1977) Die physiologische Uhr. Springer, Berlin Heidelberg New York

Crèvecoeur M, Crespi P, Lefort F, Greppin H (1992) Sterols and plasmalemma modification in spinach apex during transition to flowering. J Plant Physiol 139:595–599

Cumming BG (1959) Extreme sensitivity of germination and photoperiodic reaction in the genus *Chenopodium* (Tourn.) L. Nature 184:1044–1045
Cumming BG (1967) Early-flowering plants. In: Wilt F, Wessels N (eds) Methods in developmental biology. Crowell, New York, pp 277–299
Cumming BG, Wagner E (1968) Rhythmic processes in plants. Annu Rev Plant Physiol 19:381–416
Cumming BG, Hendricks SB, Borthwick HA (1965) Rhythmic flowering responses and phytochrome changes in a selection of Chenopodium rubrum. Can J Bot 43:825–853
Davies E (1987) Action potentials as multifunctional signals in plants: a unifying hypothesis to explain apparently disparate wound responses. Plant Cell Environ 10:623–631
Davies E, Zawadzki T, Witter JD (1991) Electrical activity and signal transmission in plants: how do plants know? In: Penel C, Greppin H (eds) Plant signalling plasma membrane and change of state. University of Geneva, Geneva, pp 119–137
Dolmetsch RE, Xu K, Lewis RS (1998) Calcium oscillations increase the efficiency and specificity of gene expression. Nature 392:933–936
Elowitz MB, Leibler S (2000) A synthetic oscillatory network of transcriptional regulators. Nature 403:335–338
Ermolayeva E, Sanders D, Johannes E (1997) Ionic mechanism and role of phytochrome-mediated membrane depolarisation in caulonemal side branch initial formation in the moss *Physcomitrella patens*. Planta 201:109–118
Flügge U-I (2000) Transport in and out of plastids: does the outer envelope membrane control the flow? Trends Pharmacol Sci 5:135–137
Genoud T, Métraux J-P (1999) Crosstalk in plant cell signaling: structure and function of the genetic network. Trends Pharmacol Sci 4:503–507
Gifford EM, Stewart KD (1965) Ultrastructure of vegetative and reproductive apices of *Chenopodium album*. Science 149:75–77
Gooch D, Packer L (1974) Oscillatory states of mitochondria. Studies on the oscillatory mechanism of liver and heart mitochondria. Arch Biochem Biophys 163:759–768
Green PB (1994) Connecting gene and hormone action to form, pattern and organogenesis: biophysical transductions. J Exp Bot 45:1775–1788
Greppin H, Horwitz B (1975) Floral induction and the effect of red and far-red preillumination on the light-stimulated bioelectric response of spinach leaves. Z Pflanzenphysiol 75:243–249
Greppin H, Horwitz BA, Horwitz LP (1973) Light-stimulated bioelectric response in spinach leaves and photoperiodic induction. Z Pflanzenphysiol 68:336–345
Gylkhandanyan AV, Evtodienko YV, Zhabotinsky AM, Kondrashova MN (1976) Continuous Sr^{2+}-induced oscillations of the ionic fluxes in mitochondria. FEBS Lett 66:44–47
Hendricks SB (1963) Metabolic control of timing. Science 141:1–7
Herde O, Fuss H, Pena-Cortés H, Fisahn J (1995) Proteinase inhibitor II gene expression induced by electrical stimulation and control of photosynthetic activity in tomato plants. Plant Cell Physiol 36:737–742
Herde O, Pena-Cortés H, Willmitzer L, Fisahn J (1998a) Time-resolved analysis of signals involved in systemic induction of Pin2 gene expression. Bot Acta 111:383–389
Herde O, Pena-Cortés H, Willmitzer L, Fisahn J (1998b) Remote stimulation by heat induces characteristic membrane-potential responses in the veins of wild-type and abscisic acid-deficient tomato plants. Planta 206:146–153
Huang TC, Tu J, Chow TJ, Chen TH (1990) Circadian rhythm of the prokaryote *Synechococcus* Sp. RF-1. Plant Physiol 92:531–533
Igamberdiev AU, Kleczkowski LA (2003) Membrane potential, adenylate levels and Mg^{2+} are interconnected via adenylate kinase equilibrium in plant cells. Biochim Biophys Acta 1607:111–119
Ishiura M, Kutsuna S, Aoki S, Iwasaki H, Andersson CR, Tanabe A, Golden SS, Johnson CH, Kondo T (1998) Expression of a gene cluster *kaiABC* as a circadian feedback process in cyanobacteria. Science 281:1519–1523
Jang J-C, Sheen J (1994) Sugar sensing in higher plants. Plant Cell 6:1665–1679

Joshi HM, Tabita FR (1996) A global two component signal transduction system that integrates the control pf photosynthesis, carbon dioxide assimilation, and nitrogen fixation. Proc Natl Acad Sci USA 93:14515–14520

King RW (1975) Multiple circadian rhythms regulate photoperiodic flowering responses in *Chenopodium rubrum*. Can J Bot 53:2631–2638

Könitz W (1965) Elektronenmikroskopische Untersuchungen an *Euglena gracilis* im tagesperiodischen Licht-Dunkel-Wechsel. Planta 66:345–373

Kung C (2005) A possible unifying principle for mechanosensation. Nature 436:647–654

Lang F, Waldegger S (1997) Regulating cell volume. Am Sci 85:456–463

Lehner L (2002) Elektrophysiologische Untersuchungen zur Steuerung der Blütenbildung bei Kurz-und Langtagpflanzen. PhD Thesis, University of Freiburg

Li W, Llopis J, Whitney M, Zlokarnik G, Tsien RY (1998) Cell-permeant caged $InsP_3$ ester shows that Ca^{2+} spike frequency can optimize gene expression. Nature 392:936–940

Liarzi O, Epel BL (2005) Development of a quantitative tool for measuring changes in the coefficient of conductivity of plasmodesmata induced by developmental, biotic and abiotic signals. Protoplasma 225:67–76

Lopez F, Bousser A, Sissoëff I, Gaspar M, Lachaise B, Hoarau J, Mahé A (2003) Diurnal regulation of water transport and aquaporin gene expression in maize roots: contribution of PIP2 proteins. Plant Cell Physiol 44:1384–1395

Machackova I, Krekule J (1991) The interaction of direct electric current with endogenous rhythms of flowering in *Chenopodium rubrum*. J Plant Physiol 138:365–369

Machackova I, Pospiskova M, Krekule J (1990) Further studies on the inhibitory action of direct electric current on flowering in the short-day plant *Chenopodium rubrum* L. J Plant Physiol 136:381–384

Mayer W-E, Fischer C (1994) Protoplasts from *Phaseolus occineus* L. pulvinar motor cells show circadian volume oscillations. Chronobiol Int 11:156–164

Mitchell P (1976) Vectorial chemistry and the molecular mechanics of chemiosmotic coupling: power transmission by proticity. Biochem Soc Trans 4:399–430

Mills JW, Lazaro J, Mandel J (1994) Cytoskeletal regulation of membrane transport events. FASEB J 8:1161–1165

Montavon M, Greppin H (1983) Effet sur le développement de l'épinard de l'application d'un potentiel électrique sur le pétiole d'une feuille. Saussurea (Genève) 14:79–85

Montavon M, Greppin H (1986) Développement apical de l'épinard et application d'un potentiel électrique de contrainte. Saussurea (Geneve) 17:85–91

Morré JD, Morré DM (1998) NADH oxidase activity of soybean plasma membranes oscillates with a temperature compensated period of 24 min. Plant J 16:277–284

Morré JD, Morré DM, Penel C, Greppin H (1999) NADH oxidase periodicity of spinach leaves synchronized by light. Int J Plant Sci 160:855–860

Murakami S, Packer L (1970) Light-induced changes in the conformation and configuration of the thylakoid membrane of *Ulva* and *Porphyra* chloroplasts in vivo. Plant Physiol 45:289–299

Nilsson O, Lee I, Blázquez MA, Weigel D (1998) Flowering-time genes modulate the response to *LEAFY* activity. Genetics 149:403–410

Novak B, Greppin H (1979) High-frequency oscillations and circadian rhythm of the membrane potential of *Spinach* leaves. Planta 144:235–240

Novak B, Sironval C (1976) Circadian rhythms of the transcellular current in regenerating enucleated posterior stalk segments of *Acetabularia mediterranea*. Plant Sci Lett 6:273–283

Ohya T, Hayashi Y, Tanoi K, Rai H, Suzuki K, Albrechtova JTP, Nakanishi TM, Wagner E (2005) Root-shoot-signalling in *Chenopodium rubrum* L. as studied by ^{15}O labeled water uptake. Abstracts of the Symposium of the XVIIth International Botanical Congress, Vienna, Austria, 17–23 July 2005, p 313

Olcese JM (1990) The neurobiology of magnetic field detection in rodents. Prog Neurobiol 35:325–330

Penel C, Auderset G, Bernardini N, Castillo FJ, Greppin H, Morré J (1988) Compositional changes associated with plasma membrane thickening during floral induction in spinach. Physiol Plant 73:134–146

Pickard BG (1994) Contemplating the plasmalemmal control center model. Protoplasma 182:1–9

Richly E, Dietzmann A, Biehl A, Kurth J, Laloi C, Apel K, Salamini F, Leister D (2003) Covariations in the nuclear chloroplast transcriptome reveal a regulatory master-switch. EMBO Rep 4:491–498

Schoof H, Lenhard M, Haecker A, Mayer KFX, Jürgens G, Laux T (2000) The stem cell population of *Arabidopsis* shoot meristems is maintained by a regulatory loop between the *CLAVATA* and *WUSCHEL* genes. Cell 100:635–644

Sippola K, Aro E-M (2000) Expression of *psbA* genes is regulated at multiple levels in the cyanobacterium *Synechococcus* sp. PCC 7942. Photochem Photobiol 71:706–714

Smith E, Morowitz HJ (2004) Universality in intermediary metabolism. Proc Natl Acad Sci 101:13168–13173

Sørensen TS, Castillo JL (1980) Spherical drop of cytoplasm with an effective surface tension influenced by oscillating enzymatic reactions. J Colloid Interface Sci 76:399–417

Stankovic B, Davies E (1996) Both action potentials and variation potentials induce proteinase inhibitor gene expression in tomato. FEBS Lett 390:275–279

Stelling J, Gilles ED, Doyle FJ III (2004) Robustness properties of circadian clock architectures. Proc Natl Acad Sci 101:13210–13215

Tomita J, Nakajima M, Kondo T, Iwasaki H (2005) No transcription-translation feedback in circadian rhythm of KaiC phosphorylation. Science 307:251–254

Tournaire-Roux C, Sutka M, Javot H, Gout E, Gerbeau P, Luu DT, Bligny R, Maurel C (2003) Cytosolic pH regulates root water transport during anoxic stress through gating of aquaporins. Nature 425:393–397

Trebacz K, Sievers A (1998) Action potentials evoked by light in traps of *Dionaea muscipula* Ellis. Plant Cell Physiol 39:369–372

Tsuschiya T, Ishiguri Y (1981) Role of the quality of light in the photoperiodic flowering response in four latitudinal ecotypes of *Chenopodium rubrum* L. Plant Cell Physiol 22:525–532

Veit J, Wagner E, Albrechtová JTP (2004) Isolation of a *FLORICAULA/LEAFY* putative orthologue from *Chenopodium rubrum* and its expression during photoperiodic flower induction. Plant Physiol Biochem 42:573–578

Vigh L, Maresca B, Harwood JL (1998) Does the membrane's physical state control the expression of heat shock and other genes? Trends Biochem Sci 23:369–374

Wagner E (1976a) Endogenous rhythmicity in energy metabolism: Basis for timer-photoreceptor-interactions in photoperiodic control. In: Hastings JW, Schweiger HG (eds) Dahlem Konferenzen. Aabkon Verlagsgesellschaft, Berlin, pp 215–238

Wagner E (1976b) Kinetics in metabolic control of time measurement in photoperiodism. J Interdiscipl Cycle Res 7:313–332

Wagner E (1976c) The nature of photoperiodic time measurement: energy transduction and phytochrome action in seedlings of *Chenopodium rubrum*. In: Smith H (ed) Light and plant development. Proceedings of the 22nd Nottingham Easter School in Agricultural Sciences, Butterworth, London

Wagner E (1977) Molecular basis of physiological rhythms. In: Jennings DH (ed) Integration of activity in the higher plant, Society for Experimental Biology, Symposium 31. Cambridge University Press, Cambridge, pp 33–72

Wagner E, Cumming BG (1970) Betacyanine accumulation, chlorophyll content and flower initiation in *Chenopodium rubrum* as related to endogenous rhythmicity and phytochrome action. Can J Bot 48:1–18

Wagner E, Frosch S, Deitzer GF (1974a) Membrane oscillator hypothesis of photoperiodic control. In: De Greef JA (ed) Proceedings of the Annual European Symposium on Plant Photomorphogenesis. Campus of the State University Centre, Antwerpen, pp 15–19

Wagner E, Frosch S, Deitzer GF (1974b) Metabolic control of photoperiodic time measurements. J Interdiscipl Cycle Res 5:240–246

Wagner E, Deitzer GF, Fischer S, Frosch S, Kempf O, Stroebele L (1975) Endogenous oscillations in pathways of energy transduction as related to circadian rhythmicity and photoperiodic control. BioSystems 7:68–76

Wagner E, Haertle U, Kossmann I, Frosch S (1983) Metabolic and developmental adaptation of eukaryotic cells as related to endogenous and exogenous control of translocators between subcellular compartments. In: Schenk H, Schwemmler W (eds) Endocytobiology II. De Gruyter, Berlin, pp 341–351

Wagner E, Bonzon M, Normann J, Albrechtová JTP, Greppin H (1996) Signal transduction and metabolic control of timing in photoperiodism. In: Greppin H, Degli Agosti R, Bonzon M (eds) Vistas on biorhythmicity. Geneva University Press, Geneva, pp 3–23

Wagner E, Normann J, Albrechtová JTP, Bonzon M, Greppin H (1997) Photoperiodic control of flowering: electrochemical-hydraulic communication between plant organs—"florigen" a frequency-coded electric signal? In: Greppin H, Penel C, Simon P (eds) Travelling shot on plant development. University of Geneva, Geneva, pp 165–181

Wagner E, Normann J, Albrechtová JTP, Walczysko P, Bonzon M, Greppin H (1998) Electrochemical-hydraulic signalling in photoperiodic control of flowering: is "florigen" a frequency-coded electric signal? Flowering Newslett 26:62–74

Wagner E, Albrechtová JTP, Normann J, Greppin H (2000) Redox state and phosphorylation potential as macroparameters in rhythmic control of metabolism—a molecular basis for seasonal adaptation of development. In: Vanden Driessche T, Guisset JL, Petiau-De Vries GM (eds) The redox state and circadian rhythms. Kluwer Academic Press, Dordrecht

Wagner E, Lehner L, Normann J, Albrechtová JTP (2004) Electrogenic flower initiation—perspectives for whole plant physiology and for applications in horticulture, agriculture and silviculture. Flowering Newslett 38:3–9

Wagner E, Lehner L, Normann J, Veit J, Albrechtová J (2005) Hydro-electrochemical integration of the higher plant—basis for electrogenic flower induction. In: Baluska F (ed) Communication in plants. Neuronal aspects of plant life. Springer, Berlin Heidelberg New York

Walczysko P, Wagner E, Albrechtová JTP (2000) Application of co-loaded Fluo-3 and Fura Red fluorescent indicators for studying the spatial Ca^{2+} distribution in living plant tissue. Cell Calcium 28:23–32

Wildon DC, Doherty HM, Eagles G, Bowles DJ, Thain JF (1989) Systemic responses arising from localized heat stimuli in tomato plants. Ann Bot 64:691–695

Wildon DC, Thain JF, Minchin PEH, Gubb IR, Reilly AJ, Skipper YD, Doherty HM, O'Donnell PJ, Bowles DJ (1992) Electrical signalling and systemic proteinase inhibitor induction in the wounded plant. Nature 360:62–65

Wright KM, Oparka KJ (1997) Metabolic inhibitors induce symplastic movement of solutes from the transport phloem of *Arabidopsis* roots. J Exp Bot 48:1807–1814

Zawadzki T, Davies E, Dziubinska H, Trebacz K (1991) Characteristics of action potentials in *Helianthus annuus*. Physiol Plant 83:601–604

Zeilstra-Ryalls J, Gomelsky M, Eraso JM, Yeliseev A, O'Gara J, Kaplan S (1998) Control of photosystem formation in *Rhodobacter sphaeroides*. J Bacteriol 180:2801–2809

Index